



ISSN 1580-3155

Pages 1–172 ■ Year 2023, Vol. 70, No. 1

Slovensko kemijsko društvo
Slovenian Chemical Society



Acta *Chimica Slo*
Acta Chimica Slo
Slovenica *Acta C*

1

70/2023



<http://acta.chem-soc.si>

EDITOR-IN-CHIEF

FRANC PERDIH

University of Ljubljana, Faculty of Chemistry and Chemical Technology, Večna pot 113, SI-1000 Ljubljana, Slovenija
E-mail: ACSi@fkk.uni-lj.si, Telephone: (+386)-1-479-8514

ASSOCIATE EDITORS

Alen Albreht, National Institute of Chemistry, Slovenia
Aleš Berlec, Jožef Stefan Institute, Slovenia
Janez Cerkovnik, University of Ljubljana, Slovenia
Mirela Dragomir, Jožef Stefan Institute, Slovenia
Krištof Kranjc, University of Ljubljana, Slovenia
Matjaž Kristl, University of Maribor, Slovenia
Aleš Ručigaj, University of Ljubljana, Slovenia

Jernej Stare, National Institute of Chemistry, Slovenia
Helena Prosen, University of Ljubljana, Slovenia
Irena Vovk, National Institute of Chemistry, Slovenia

ADMINISTRATIVE ASSISTANT

Eva Mihalinec, Slovenian Chemical society, Slovenia

EDITORIAL BOARD

Wolfgang Buchberger, Johannes Kepler University, Austria
Alojz Demšar, University of Ljubljana, Slovenia
Stanislav Gobec, University of Ljubljana, Slovenia
Marko Goličnik, University of Ljubljana, Slovenia
Günter Grampp, Graz University of Technology, Austria
Wojciech Grochala, University of Warsaw, Poland
Danijel Kikelj, University of Ljubljana
Janez Košmrlj, University of Ljubljana, Slovenia
Blaž Likozar, National Institute of Chemistry, Slovenia
Mahesh K. Lakshman, The City College and
The City University of New York, USA

Janez Mavri, National Institute of Chemistry, Slovenia
Friedrich Sreenc, University of Minnesota, USA
Walter Steiner, Graz University of Technology, Austria
Jurij Svete, University of Ljubljana, Slovenia
David Šarlah, University of Illinois at Urbana-Champaign, USA;
Università degli Studi di Pavia, Italy
Ivan Švancara, University of Pardubice, Czech Republic
Jiri Pinkas, Masaryk University Brno, Czech Republic
Gašper Tavčar, Jožef Stefan Institute, Slovenia
Ennio Zangrando, University of Trieste, Italy

ADVISORY EDITORIAL BOARD

Chairman

Branko Stanovnik, Slovenia

Members

Udo A. Th. Brinkman, The Netherlands
Attilio Cesaro, Italy
Vida Hudnik, Slovenia
Venčeslav Kaučič, Slovenia

Željko Knez, Slovenia
Radovan Komel, Slovenia
Stane Pejovnik, Slovenia
Anton Perdih, Slovenia
Slavko Pečar, Slovenia
Andrej Petrič, Slovenia
Boris Pihlar, Slovenia
Milan Randić, Des Moines, USA

Jože Škerjanc, Slovenia
Đurđa Vasić-Rački, Croatia
Marjan Veber, Slovenia
Gorazd Vesnaver, Slovenia
Jure Zupan, Slovenia
Boris Žemva, Slovenia
Majda Žigon, Slovenia

Acta Chimica Slovenica is indexed in: *Academic Search Complete*, *Central & Eastern European Academic Source*, *Chemical Abstracts Plus*, *Chemical Engineering Collection (India)*, *Chemistry Citation Index Expanded*, *Current Contents (Physical, Chemical and Earth Sciences)*, *Digitalna knjižnica Slovenije (dLib.si)*, *DOAJ*, *ISI Alerting Services*, *PubMed*, *Science Citation Index Expanded*, *SciFinder (CAS)*, *Scopus* and *Web of Science*. Impact factor for 2021 is IF = 1.524.



Articles in this journal are published under the
Creative Commons Attribution 4.0 International License

Izdaja – Published by:

SLOVENSKO KEMIJSKO DRUŠTVO – SLOVENIAN CHEMICAL SOCIETY
Naslov redakcije in uprave – Address of the Editorial Board and Administration
Hajdrihova 19, SI-1000 Ljubljana, Slovenija
Tel.: (+386)-1-476-0252; Fax: (+386)-1-476-0300; E-mail: chem.soc@ki.si

Izdajanje sofinancirajo – Financially supported by:

National Institute of Chemistry, Ljubljana, Slovenia
Jožef Stefan Institute, Ljubljana, Slovenia
Faculty of Chemistry and Chemical Technology, University of Ljubljana, Slovenia
Faculty of Chemistry and Chemical Engineering, University of Maribor, Slovenia
University of Nova Gorica, Slovenia

Slovensko kemijsko društvo
Slovenian Chemical Society



Acta Chimica Slovenica izhaja štirikrat letno v elektronski obliki na spletni strani <http://acta.chem-soc.si>. V primeru posvečenih številk izhaja revija tudi v tiskani obliki v omejenem številu izvodov.

Acta Chimica Slovenica appears quarterly in electronic form on the web site <http://acta.chem-soc.si>. In case of dedicated issues, a limited number of printed copies are issued as well.

Transakcijski račun: 02053-0013322846 Bank Account No.: SI56020530013322846-Nova Ljubljanska banka d. d., Trg republike 2, SI-1520 Ljubljana, Slovenia, SWIFT Code: LJBA SI 2X

Oblikovanje ovitka – Design cover: KULT, oblikovalski studio, Simon KAJTNA, s. p. Grafična priprava za tisk: OSITO, Laura Jankovič, s.p.



Seventy Years of Acta Chimica Slovenica

Acta Chimica Slovenica, the journal of the Slovenian Chemical Society, is celebrating in 2023 its 70th anniversary. In 1954 the editorial board decided to publish the *Vestnik Slovenskega kemijskega društva* (*Bulletin of the Slovenian Chemical Society*) as a constituent of the *Documenta Chemica Yugoslavica* together with *Croatica Chemica Acta* and *Glasnik Srpskog hemijskog društva*. *Vestnik* was published for a quarter of a century sporadically, sometimes with a big delay.

In 1978 (vol. 25) a new editorial board (Drago Kolar editor, Marko Razinger technical editor and Branko Stanovnik chairman of editorial board) decided to improve the journal in many aspects: to publish 4 issues per year regularly, to publish review articles, plenary lectures delivered at the congresses and symposia organized by the Slovenian Chemical Society, special issues to celebrate the anniversaries of prominent chemists, to give the information about the research activities and development in chemical and pharmaceutical industry.

Editorial board wanted to change the name of *Vestnik* already in 1978. However, since the *Vestnik* was part of the *Documenta Chemica Yugoslavica*, it was not possible

until 1992, when Slovenia became an independent state. After the Slovenian Chemical Society was admitted to the Federation of European Chemical Societies in 1992, the Slovenian Chemical Society changed, by suggestion of the editor and editorial board, the name of the journal into *Acta Chimica Slovenica* (ACSi) starting in 1993 with vol. 40. Over the years ACSi has gained reputation within the international community. The editorial board was taken over by younger colleagues, who reorganized and digitised it accordingly, and within a few years ACSi became an internationally renowned journal. In the meantime, Drago Kolar 1993–1996, Ljubo Golič 1997–1998 were editors for a short period. Since 1999–2003 Andrej Petrič was the editor, followed by Janez Košmrlj 2004–2005 (Vol. 51–52), Alekander Pavko 2006–2017 (Vol. 53–64), Ksenija Kogej 2018–2022 (Vol. 65–69), and Franc Perdih 2023– (Vol. 70–).

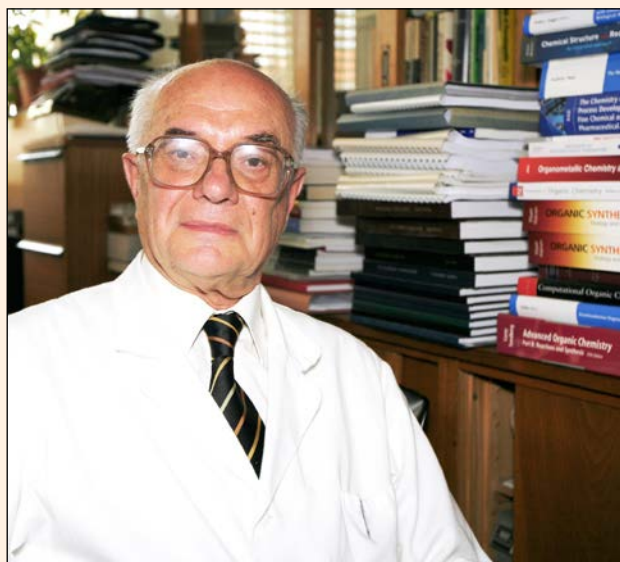
ACSi is extracted by *Chemical Abstracts*, *Current Contents*, *PubMed*, *Science Citation Index Expanded* and *Scopus*. In 2002 the ACSi obtained IF for the first time, in 2021 IF = 1.524.

Acta Chimica Slovenica demonstrates the enthusiasm, creativity and vitality of Slovenian scientific community and represents a permanent genuine contribution to Slovenian culture.

I would like to congratulate and express my sincere thanks and gratitude to authors for their contributions, to reviewers, members of editorial boards, guest and associated editors and editors and to all those who have in any way contributed to the success of our journal.

Best wishes for the future.

Branko Stanovnik
Chairman of the advisory editorial board



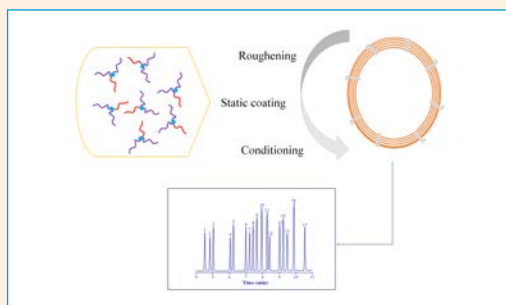
SCIENTIFIC PAPER

1–11

Analytical chemistry

An Amphiphilic Star-Shaped Polymer (Star-PEG-PCL₂) used as a Stationary Phase for GC

Ruo-nan Chen, Zhi-qiang Cai, Wei Zhang, Qiu-chen Huang, Wei Li,
Ke-yun Jin, Yi Zhao, Ge Feng and Tao Sun

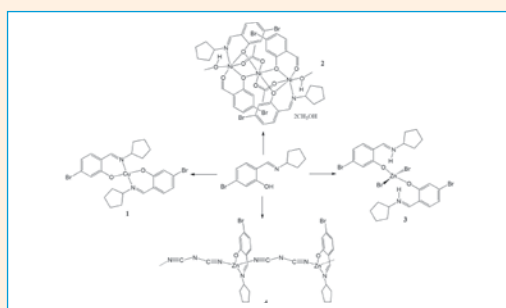


12–20

Inorganic chemistry

Syntheses, Characterization, Crystal Structures and Antimicrobial Activity of Copper(II), Nickel(II) and Zinc(II) Complexes Derived from 5-Bromo-2- ((cyclopentylimino)methyl)phenol

Li Zhang, Xiao-Yang Qiu and Shu-Juan Liu

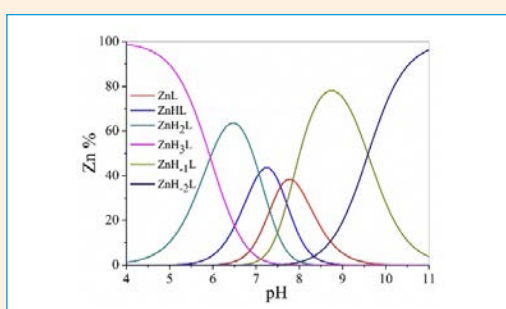


21–28

Inorganic chemistry

Potentiometric Study of the Dissociation and the Metal Complex-formation Competence of 5-(3,3-dimethyl-1- triazeno)-imidazole-4-carboxamide (Dacarbazine)

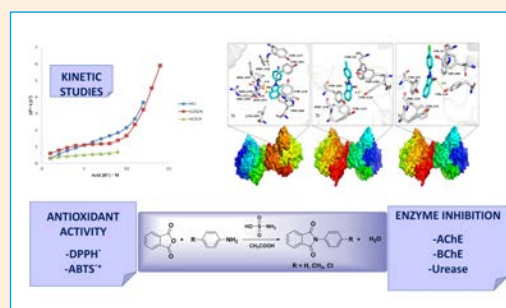
Hasan Atabey, Faisal Naji Al-Obaidi and Hayati Sari



29–43 General chemistry

Kinetic Studies, Antioxidant Activities, Enzyme Inhibition Properties and Molecular Docking of 1,3-Dihydro-1,3-Dioxoisindole Derivatives

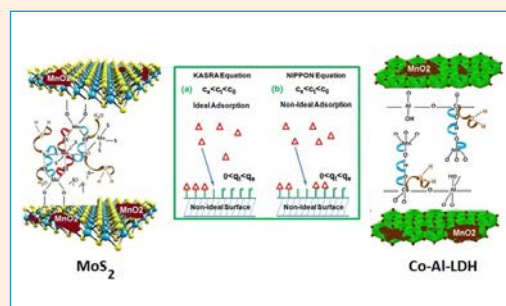
Hasan Yakan, Seyhan Ozturk, Elvan Uyar Tolgay, Semiha Yenigun, Sarmad Marah, Tugrul Doruk, Tevfik Ozen and Halil Kutuk



44–58 Chemical, biochemical and environmental engineering

Comparison of Kinetics of Adsorption of Permanganate on Co-Al-Layered Double Hydroxide and MoS_2 Nanocompounds

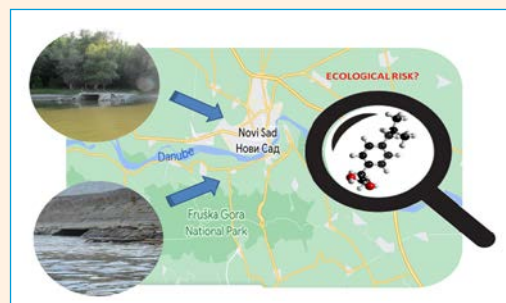
Shahin Ghobadi, Babak Samiey, Enis Esmaili and Chil-Hung Cheng



59–64 Chemical, biochemical and environmental engineering

Ibuprofen as an Organic Pollutant in the Danube and Effects on Aquatic Organisms

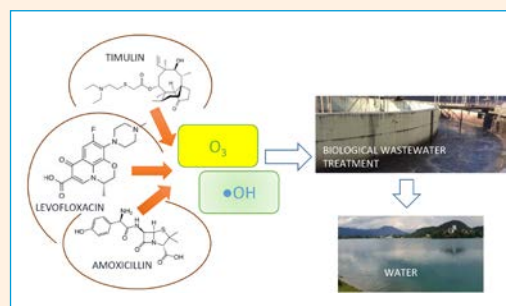
Nevena Grujić-Letić, Emilia Gligorić, Branislava Teofilović, Milan Vraneš and Slobodan Gadžurić



65–73 Chemical, biochemical and environmental engineering

Biotreatability Improvement of Antibiotic-Contaminated Waters: High Efficiency of Direct Ozonation in Comparison to Hydroxyl Radical Oxidation

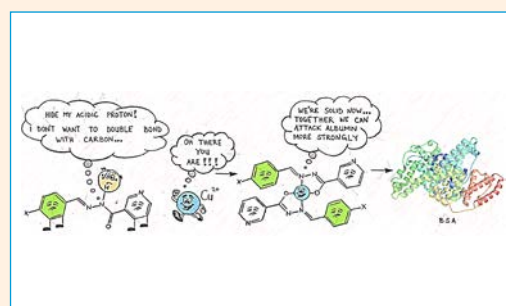
Igor Boševski and Andreja Žgajnar Gotvajn



74–85 Inorganic chemistry

Interaction of Copper(II) Complexes of Bidentate Benzaldehyde Nicotinic Acid Hydrazones with BSA: Spectrofluorimetric and Molecular Docking Approach

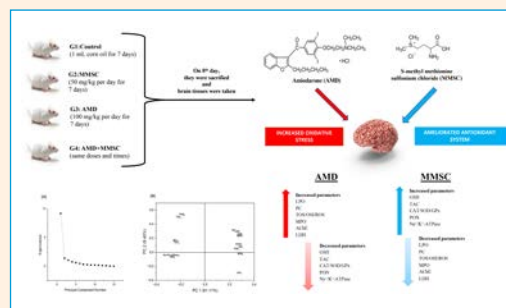
Adnan Zahirović, Irnesa Osmanković, Amar Osmanović, Aleksandar Višnjevac, Amina Magoda, Selma Hadžalić and Emira Kahrović



131–138 Biochemistry and molecular biology

Oxidative Brain Injury Induced by Amiodarone in Rats: Protective Effect of S-Methyl Methionine Sulfonium Chloride

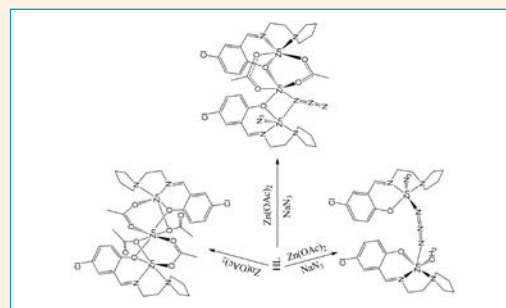
Ismet Burcu Turkyilmaz



139–147 Inorganic chemistry

Synthesis, Crystal Structures and Urease Inhibition of Zinc Complexes Derived from 4-Chloro-2-(((2-(pyrrolidin-1-yl)ethyl)imino)methyl)phenol

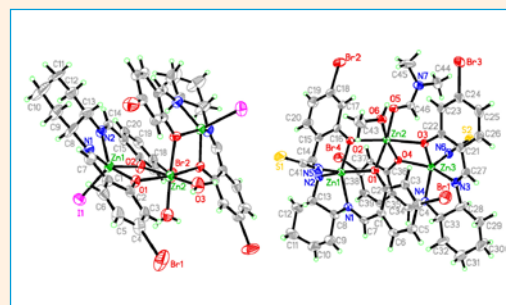
Jian Jiang, Yao Liu, Bo Liu, Yijin Wang and Zhonglu You



148–154 Inorganic chemistry

Trinuclear Zinc(II) Complexes Derived from N,N'-Bis-(5-bromosalicylidene)-1,2-cyclohexanediamine: Syntheses, Crystal Structures and Antimicrobial Activity

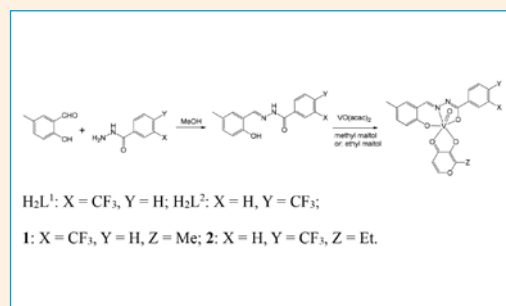
Guo-Xu He, Xue-Yao Guo and Ling-Wei Xue



155–162 Inorganic chemistry

Methyl Maltolate and Ethyl Maltolate Coordinated Oxidovanadium(V) Complexes with N'-(2-Hydroxy-5-methylbenzylidene)-4-trifluoromethylbenzohydrazide: Synthesis, Crystal Structures and Catalytic Epoxidation Property

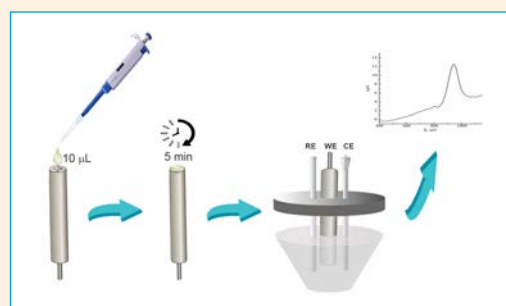
Zhongduo Xiong and Ping Zhang



163–171 Analytical chemistry

Carbon-Paste Electrode Modified by β -Cyclodextrin as Sensor for Determination of Sunset Yellow FCF and Ponceau 4R in Soft Drinks

Konstantin Pliuta and Denys Snigur



Scientific paper

An Amphiphilic Star-Shaped Polymer (Star-PEG-PCL₂) used as a Stationary Phase for GC

Ruo-nan Chen,¹ Zhi-qiang Cai,^{1,*} Wei Zhang,¹ Qiu-chen Huang,¹ Wei Li,¹ Ke-yun Jin,² Yi Zhao,² Ge Feng² and Tao Sun^{2,*}

¹ Liaoning Province Professional and Technical Innovation Center for Fine Chemical Engineering of Aromatics Downstream, School of Petrochemical Engineering, Shenyang University of Technology, Liaoyang 111003, P. R. China.

² College of Chemistry and Chemical Engineering, Henan Key Laboratory of Function-Oriented Porous Materials, Luoyang Normal University, Luoyang 471934, P. R. China.

* Corresponding author: E-mail: kahongzqc@163.com
suntao2226@163.com

Received: 01-30-2022

Abstract

A star-shaped polymer (Star-PEG-PCL₂) was synthesized to with PCL and PEG, and used as a stationary phase for gas chromatography. The statically coated Star-PEG-PCL₂ column exhibited an efficiency of 2260 plates/m determined by naphthalene at 120 °C and moderate polarity. The Star-PEG-PCL₂ column showed high resolution performance for isomers of a wide ranging polarity, including methylnaphthalenes, halogenated benzenes, nitrobenzene, phenols, and anilines, and displayed dual-nature selectivity for a mixture of 17 analytes. Also, the Star-PEG-PCL₂ column exhibited good separation performance and column inertness for Grob test mixture and a series of *cis/trans*-isomers. In addition, it exhibited advantageous separation performance over the commercial HP-35 and PEG-20M columns for chloroaniline and bromoaniline isomers through its unique three-dimensional framework. In conclusion, it has good potential as a new stationary phase for separating a variety of analytes because of its special structure and excellent separation performance.

Keywords: Stationary phase; capillary gas chromatography; star-shaped polymer; separation performance

1. Introduction

Capillary gas chromatography (GC) has been widely used in petrochemical, pharmaceutical, environmental, biochemistry, food and other fields, while the stationary phase is the key of GC analysis because the separation performance and retention behavior of a capillary GC column mostly depend on the chromatographic features of its stationary phase.^{1–4} Currently, polymers,^{5–8} macrocyclics,^{9–12} ionic liquids,^{13,14} metal-organic frameworks (MOFs),^{15,16} and covalent organic frameworks (COFs)^{17,18} have been reported as stationary phases for GC separations. It is worth noting that polymers are the most popular chromatographic stationary phases because of their excellent physicochemical properties such as good film-forming properties, chemical stability and easy modification.

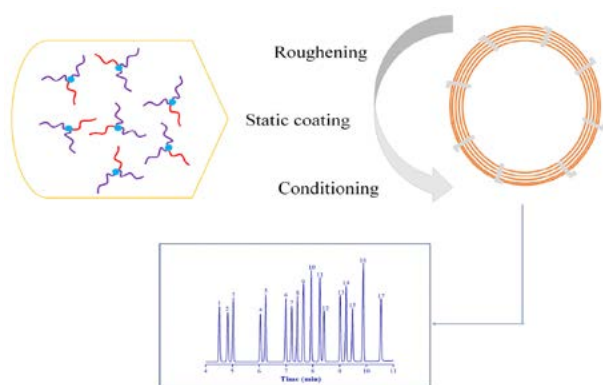
Poly(ethylene)glycol (PEG) is widely used in the fields of medicine, cosmetics, plastics and biology because of its non-toxic, non-volatile and hydrophilic properties.¹⁹ It is well known that PEG is one of the commonly used

stationary phases in GC, which is suitable for the separation of polar analytes. With the development of PEG-based materials, the researchers found that the selectivity of the stationary phase could be improved by PEG-derivatization.^{20–22} Poly(ϵ -caprolactone) (PCL) has the advantages of biocompatibility, biodegradability and good film-forming ability, and is easily soluble in common organic solvents such as aromatic compounds, ketones and polar solvents.^{23–25} It is a hydrophobic and flexible polymer with five nonpolar methylene groups and one polar ester group in the structurally repeating unit, which can be a selector in chromatographic separations.²⁶

Star-shaped polymer is a kind of polymer with characteristic shape, which is a star shape with linear chain as the core and three or more than three branched chains as the arms. Moreover, it is the simplest branched polymer and can be obtained by two polymerization approaches: core-first and arm-first.²⁷ For the application of GC stationary phase, compared with linear polymers, the star-shaped

polymer has unique 3D network structure, which can increase the interaction areas between the stationary phase and analytes, play the role of 3D molecular recognition interactions of the stationary phase, and then improve the selectivity and chromatographic separation performance of the stationary phase. Based on these features, star-shaped polymer is a promising candidate for GC stationary phase.²⁸

Herein, the star-shaped polymer (Star-PEG-PCL₂) was synthesized and characterized, and coated on the inner wall of capillary column (Scheme 1). Subsequently, we investigated the separation performance of the Star-PEG-PCL₂. Firstly, we measured its column efficiency through the Golay curve and obtained its polarity by McReynolds constants. Secondly, we investigated the chromatographic retention behavior of the Star-PEG-PCL₂ column with the Grob test mixture, a mixture of 17 analytes of various polarities, and challenging halogenated anilines as analytes.



Scheme 1. The Star-PEG-PCL₂ capillary column for GC separation.

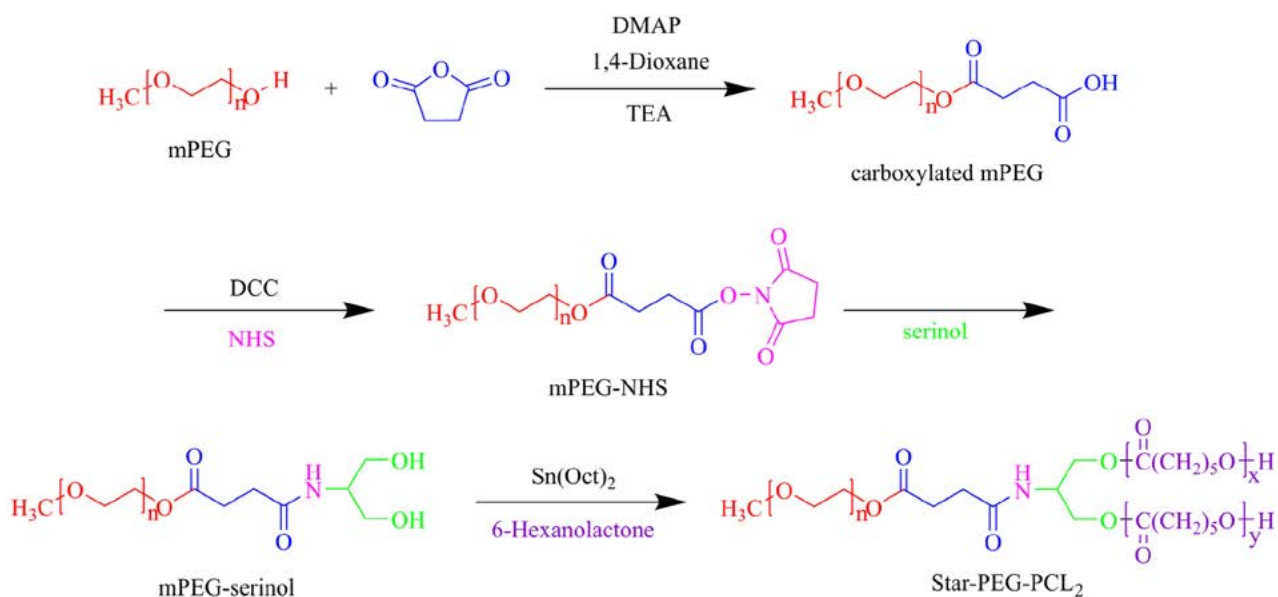
Additionally, we also explored its separation performance for a variety of positional and *cis-/trans*-isomers with different polarities. To our knowledge, this is the first report on the use of Star-PEG-PCL₂ as a GC stationary phase.

2. Experimental

2. 1. Materials and Methods

N,N'-Dicyclohexylcarbodiimide (DCC) was purchased from Heowns Biochemical Technology Co., Ltd. (Tianjin, China). 4-Dimethylaminopyridine (DMAP) was purchased from Sinopharm Chemical Reagent Co., Ltd. (Shanghai, China). Succinic anhydride, triethylamine (TEA), 2-amino-1,3-propanediol (serinol), poly(ethylene glycol) methyl ether (Mn.2000), tin(II) 2-ethylhexanoate, 6-hexanolactone and *N*-hydroxysuccinimide (NHS) were purchased from Sun Chemical Technology Co., Ltd. (Shanghai, China). The analytical samples and standards were obtained from Energy Chemical and used without further purification. All the analytes in this work were analytical grade and dissolved in dichloromethane (DCM). Fused-silica capillary column (0.25 mm i.d.) was purchased from Yongnian Ruifeng Chromatogram Apparatus Co., Ltd (Hebei, China). The HP-35 (15 m × 0.25 mm i.d., 0.25 μm film thickness) and PEG-20M (15 m × 0.25 mm i.d., 0.25 μm film thickness) capillary commercial columns were purchased from Agilent Technologies Co., Ltd. (Palo Alto, California, USA) for comparison.

The synthesized polymers were characterized by FT-IR and ¹H NMR. The IR spectra were obtained by a Tensor II FT-IR spectrometer (Bruker, Karlsruhe, Germany) and the ¹H NMR were recorded on a Bruker Biospin 400 MHz instrument (Bruker Biospin, Rheinstetten, Germany).



Scheme 2. The synthesis of Star-PEG-PCL₂.

Thermal gravimetric analysis (TGA) was done on a DTG-60AH instrument (Shimadzu, Japan).

GC separations were performed on an Agilent 7890A system (Palo Alto, USA) with a flame ionization detector (FID). All the GC separations were performed under the following conditions: nitrogen of high purity (99.999%) as carrier gas, injection port at 300 °C, split injection mode at a split ratio of 100 : 1 and FID detector at 300 °C. The specific temperature program and flow rate of carrier gas are indicated in the caption of each figure.

2. 2. Synthesis

Synthesis route is shown in Scheme 2. The synthesis according to the method in the reference.²⁹

2. 2. 1. Synthesis of the mPEG-serinol

Firstly, the carboxylated mPEG and mPEG-NHS were synthesized following the procedure described in reference.²⁹ And then, mPEG-NHS (0.720 g, 0.334 mmol) and serinol (0.222 g, 2.338 mmol) were added into DMSO (15 mL). The mixture was stirred at room temperature for 36 h. After the reaction, the deionized water was added into the crude product, and extracted with DCM. The organic phase was concentrated in vacuo and the product was precipitated with cold diethyl ether. The solid was filtered and dried in vacuo at 40 °C (48.89% yield). m. p. 46.9–54.1 °C; ¹H NMR (400 MHz, CDCl₃) δ 3.65 (s, H_b), 3.38 (s, H_a), 2.62 (s, H_c, H_d and H_e). IR (KBr, cm⁻¹): 1060.34 (C-O-C), 1087.18 (C-O-C), 1728.76 (C=O), 2849.42 (CH₂), 2891.68 (CH₂), 2926.83 (CH₃), 3322.35 (OH).

2. 2. 2. Synthesis of the Star-PEG-PCL₂

The mPEG-serinol (0.479 g, 0.224 mmol), PCL (1.437 g, 12.590 mmol) and Sn(Oct)₂ (0.012 g, 0.0311 mmol) were added to a round-bottom flask and stirred at 120 °C for 18 h. After the reaction, the mixture was slowly cooled down at room temperature. Then, the reaction mixture was added into cold diethyl ether and stirred to obtain white solid, then the solid was filtered and dried in vacuo at 40 °C (39.23% yield). m. p. 49.9–56.4 °C; ¹H NMR (400 MHz, CDCl₃) δ 4.23 (t, *J* = 5.2 Hz, H_c and H_f), 4.06 (t, *J* = 6.8 Hz, H_i), 3.65 (s, H_b), 3.38 (s, H_a), 2.63 (s, H_e and H_d), 2.31 (t, *J* = 7.6 Hz, H_g), 1.67–1.63 (m, H_j and H_k), 1.44–1.33 (m, H_l). IR (KBr, cm⁻¹): 1062.95 (C-O-C), 1104.39

(C-O-C), 1720.77 (C=O), 2862.56 (CH₂), 2891.11 (CH₂), 2944.04 (CH₃).

2. 3. Fabrication of the Star-PEG-PCL₂ Capillary Column

The capillary column was made by static coating method. After rinsing, the inner surface of the capillary column was roughened with saturated sodium chloride methanol solution. Then, the column was filled with coating solution (Star-PEG-PCL₂ dissolved in DCM). At last, after the solvent was evaporated, the column was conditioned by temperature program. The specific process is referred to in the previous literature of our research group.^{30,31}

3. Results and Discussion

3. 1. Column Efficiency and McReynolds Constants of Star-PEG-PCL₂ Stationary Phase and Capillary Column

The column efficiency of Star-PEG-PCL₂ stationary phase was determined through plotting the height equivalent to a theoretical plate (HETP) of naphthalene at 120 °C. According to the measured data, the Golay curve in Fig.1 was drawn, and the results showed that the measured minimum HETP was 0.44 mm, corresponding to a column efficiency of 2260 plates/m at flow rate of 0.3 mL/min.

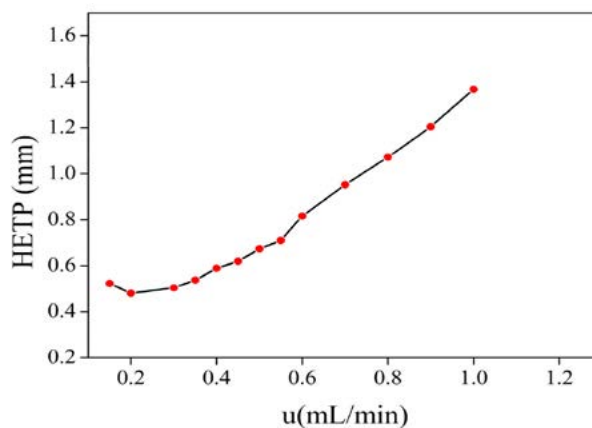


Fig. 1 Golay curve of the Star-PEG-PCL₂ column.

Table 1. McReynolds constants of the Star-PEG-PCL₂, HP-35 and PEG-20M columns

Stationary phase	X'	Y'	Z'	U'	S'	General polarity	Average
Star-PEG-PCL ₂	194	379	251	409	342	1575	315
HP-35	96	149	142	226	176	790	158
PEG-20M	303	520	351	557	484	2215	443

X', benzene; Y', 1-butanol; Z', 2-pentanone; U', 1-nitropropane; S', pyridine. Temperature: 120 °C.

Moreover, the polarity of the stationary phase was characterized by McReynolds constants, and its measurement was determined by the five probe solutes of benzene, 1-butanol, 2-pentanone, 1-nitropropane, and pyridine.^{32,33} Table 1 shows that the average value of Star-PEG-PCL₂ stationary phase was 315, indicating its moderate polarity. Also, the polarity of the Star-PEG-PCL₂ column is between that of the HP-35 and PEG-20M columns, in particular the lower polarity than that of the PEG-20M stationary phase may be due to the introduction of two PCL chains as polymer arms.

3. 2. Separation Performance and Retention Behaviours

In order to explore the separation performance of Star-PEG-PCL₂ stationary phase, the Grob test mixture, a

mixture of 17 analytes, positional and *cis*-/*trans*-isomers were used as the analytes.

3. 2. 1. Grob Test Mixture

Grob test mixture is a commonly used diagnostic reagent for GC stationary phase evaluation, which can evaluate the separation performance of the stationary phase and the inertness of the chromatographic column. Fig. 2 revealed the separation performance of Star-PEG-PCL₂, PCL-PEG-PCL, HP-35 and PEG-20M columns. PCL-PEG-PCL stationary phase has a linear structure, which has been reported by our group.³⁰ As shown, the Star-PEG-PCL₂ column can separate almost all analytes except 2,6-dimethylphenol/2-ethylhexanoic acid (peaks 9/10) and dicyclohexylamine/methyl dodecanoate (peaks 11/12), showing its excellent resolving capability for the

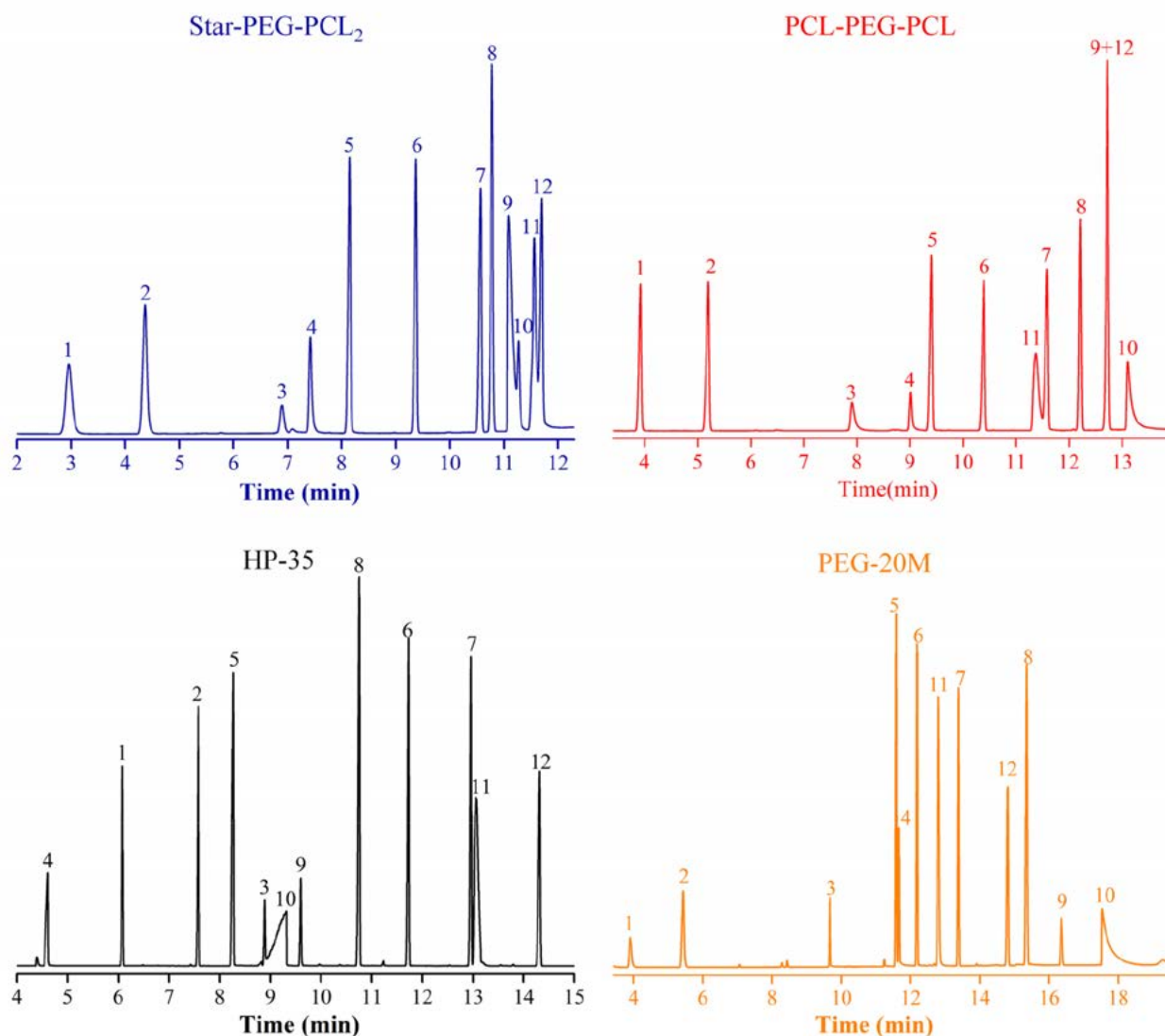


Fig. 2 Separations of Grob test mixture on the Star-PEG-PCL₂, PCL-PEG-PCL, HP-35, and PEG-20M columns. Peaks: (1) *n*-decane, (2) *n*-undecane, (3) nonanal, (4) 2,3-butanediol, (5) 1-octanol, (6) methyl decanoate, (7) methyl undecanoate, (8) 2,6-xylydine, (9) 2,6-dimethylphenol, (10) 2-ethylhexanoic acid, (11) dicyclohexylamine, (12) methyl laurate. Oven program: 40 °C (1min) to 160 °C at 10 °C/min. Flow rate at 0.6 mL/min.

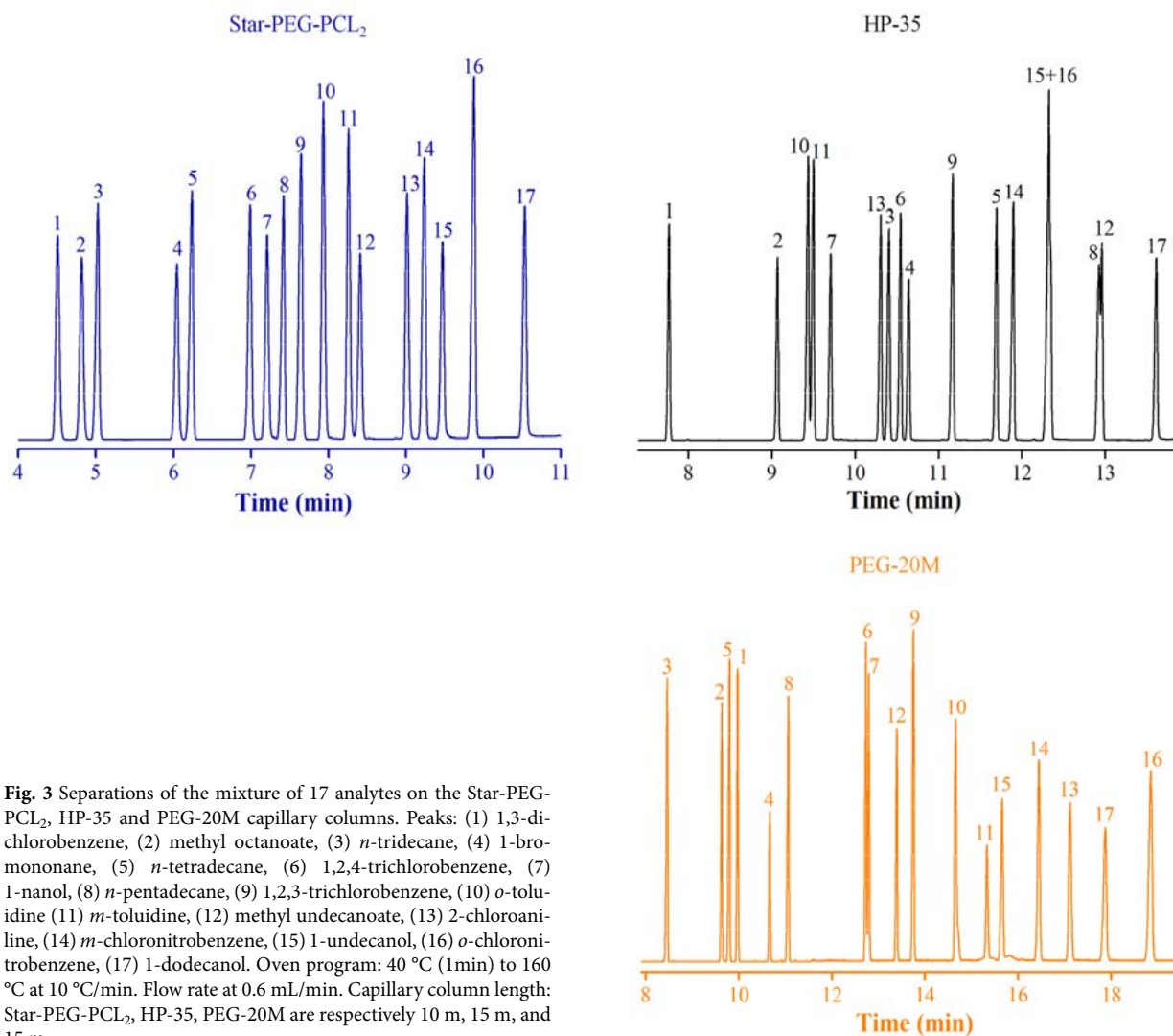


Fig. 3 Separations of the mixture of 17 analytes on the Star-PEG-PCL₂, HP-35 and PEG-20M capillary columns. Peaks: (1) 1,3-dichlorobenzene, (2) methyl octanoate, (3) *n*-tridecane, (4) 1-bromononane, (5) *n*-tetradecane, (6) 1,2,4-trichlorobenzene, (7) 1-nanol, (8) *n*-pentadecane, (9) 1,2,3-trichlorobenzene, (10) *o*-toluidine (11) *m*-toluidine, (12) methyl undecanoate, (13) 2-chloroaniline, (14) *m*-chloronitrobenzene, (15) 1-undecanol, (16) *o*-chloronitrobenzene, (17) 1-dodecanol. Oven program: 40 °C (1min) to 160 °C at 10 °C/min. Flow rate at 0.6 mL/min. Capillary column length: Star-PEG-PCL₂, HP-35, PEG-20M are respectively 10 m, 15 m, and 15 m.

complex mixture. Regarding the retention behavior, the Star-PEG-PCL₂ column exhibited distinct elution order compared to other comparative columns. Star PEG-PCL₂ stationary phase had strong retention for polar analytes such as 2,3-butanediol and 2-ethylhexanoic acid (peaks 4 and 10) due to its PEG-group, and its retention behavior was similar to that of PCL-PEG-PCL and PEG-20M stationary phases. Specifically, weakly polar analytes including dicyclohexylamine and methyl laurate (peaks 11 and 12) exhibited prolonged retention times on the Star PEG-PCL₂ stationary phase, similar to the polysiloxane HP-35 stationary phase. This may be due to the star-shaped structure of Star-PEG-PCL₂, which had stereo recognition interaction with analytes, and the dispersion interaction between them was enhanced. In addition, all the components had good chromatographic peak shapes on the Star-PEG-PCL₂ column, including 2-ethylhexanoic acid and dicyclohexylamine which are easy to tail in chromatographic analysis. The above results showed that the Star-PEG-PCL₂ column had good chromatographic separation perfor-

mance and column inertness which originated from its unique chemical structure and properties.

3. 2. 2. A Mixture of 17 Analytes

To further investigate the separation performance and retention behavior of Star-PEG-PCL₂ column, a mixture of 17 analytes containing different types, including *n*-alkanes, anilines, halogenated benzenes, alcohols, and esters, was used as the analytes. The HP-35 and PEG-20M columns were employed for reference. As shown in Fig. 3, the Star-PEG-PCL₂ column presented excellent chromatographic separation performance over the HP-35 and PEG-20M columns. It can be observed from Fig. 3 that the mixture of 17 analytes was baseline separated ($R > 1.5$), while some components of them were overlapped or co-eluted on the two commercial columns, *i.e.*, *n*-pentadecane/methyl undecanoate (peaks 8/12), *o*-toluidine/*m*-toluidine (peaks 10/11) and 1-undecanol/*o*-chloronitrobenzene (peaks 15/16) on HP-35 column, 1,2,4-trichlorobenzene/1-nanol

(peaks 6/7) on PEG-20M column. For some pairs of the analytes, such as methyl octanoate/*n*-tridecane, 1-bromononane/*n*-tetradecane, 1-nanol/*n*-pentadecane, *m*-toluidine/methyl undecanoate, *m*-chloronitrobenzene/1-unde-

canol, *o*-chloronitrobenzene/1-dodecanol (peaks 2/3, 4/5, 7/8, 11/12, 14/15, 16/17), the elution order on the Star-PEG-PCL₂ column was consistent with that on the HP-35 column with weaker polarity, and was opposite to that on

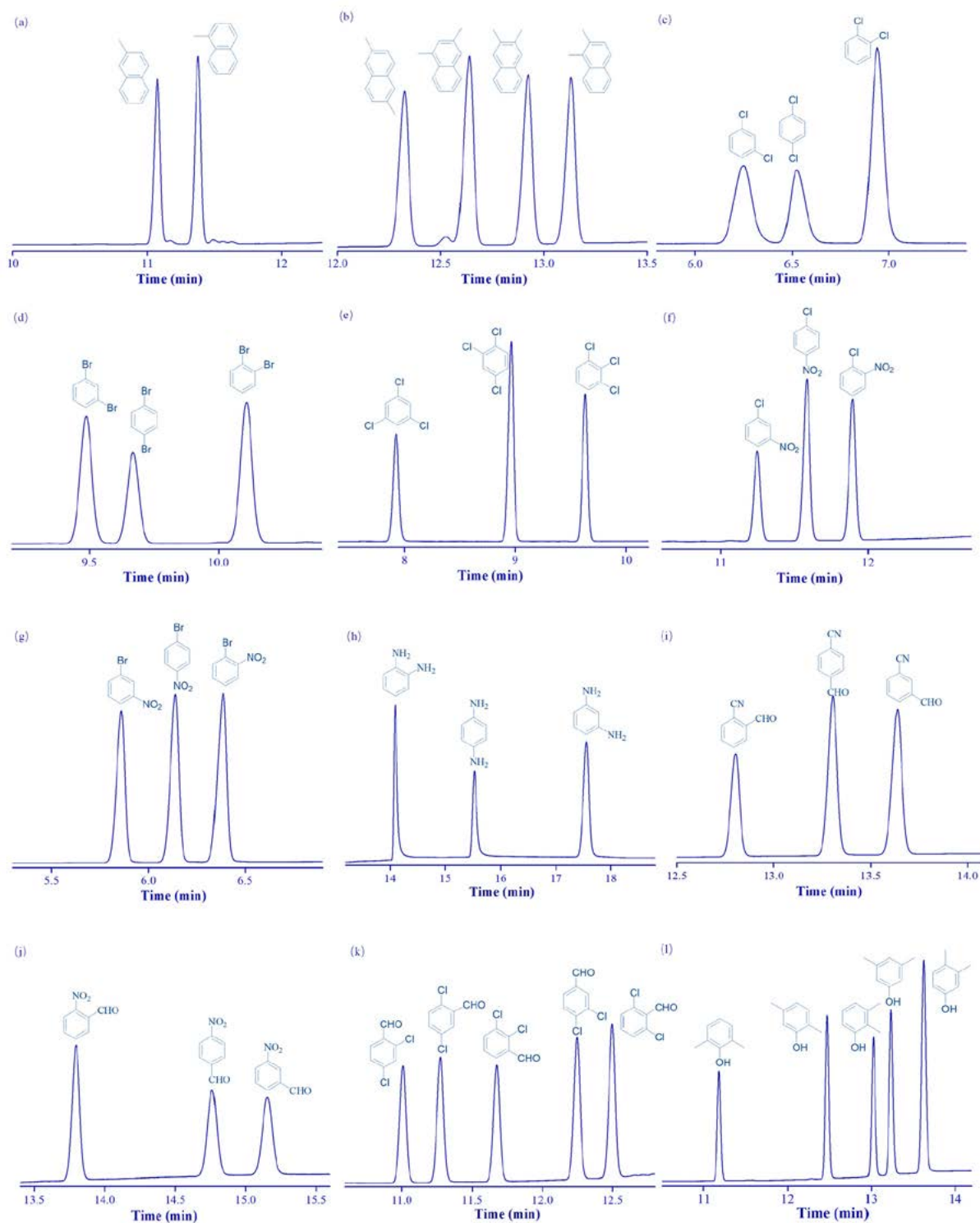


Fig. 4 GC separation of (a) methyl-naphthalene, (b) dimethyl-naphthalene, (c) dichlorobenzene, (d) dibromobenzene, (e) trichlorobenzene, (f) chloronitrobenzene, (g) bromonitrobenzene, (h) phenylenediamine, (i) cyanobenzaldehyde, (j) nitrobenzaldehyde, (k) dichlorobenzaldehyde, and (l) dimethylphenol isomers on Star-PEG-PCL₂ column. Temperature program: 40 °C for 1 min to 160 °C at 10 °C/min, flow rate at 0.6 mL/min.

the PEG-20M column with stronger polarity. This may be due to the Star-PEG-PCL₂ containing two PCL blocks where the apolar methylene (-CH₂-) units had stronger dispersion interactions with the weakly polar analytes (peaks 3, 5, 8, 12, 15, 17). Besides, for some other pairs of analytes, such as *n*-tetradecane/1,2,4-trichlorobenzene, *n*-pentadecane/1,2,3-trichlorobenzene, methyl undecanoate/2-chloroaniline (peaks 5/6, 8/9, 12/13), the elution order on the Star-PEG-PCL₂ column was consistent with that on the PEG-20M column, and was opposite to that on the HP-35 column. Using Star-PEG-PCL₂ stationary phase

allowed for prolonged retention time for some polar components (peaks 6, 9, 13), indicating stronger H-bonding and dipole-dipole interactions between them through the PEG chains. The above results demonstrated that Star-PEG-PCL₂ was suitable for the separation of analytes with a wide range of polarity and had dual-nature selectivity.

3. 2. 3. Positional Isomers

Isomers often exist as by-products during synthesis, which are close in nature and structure. Separation capa-

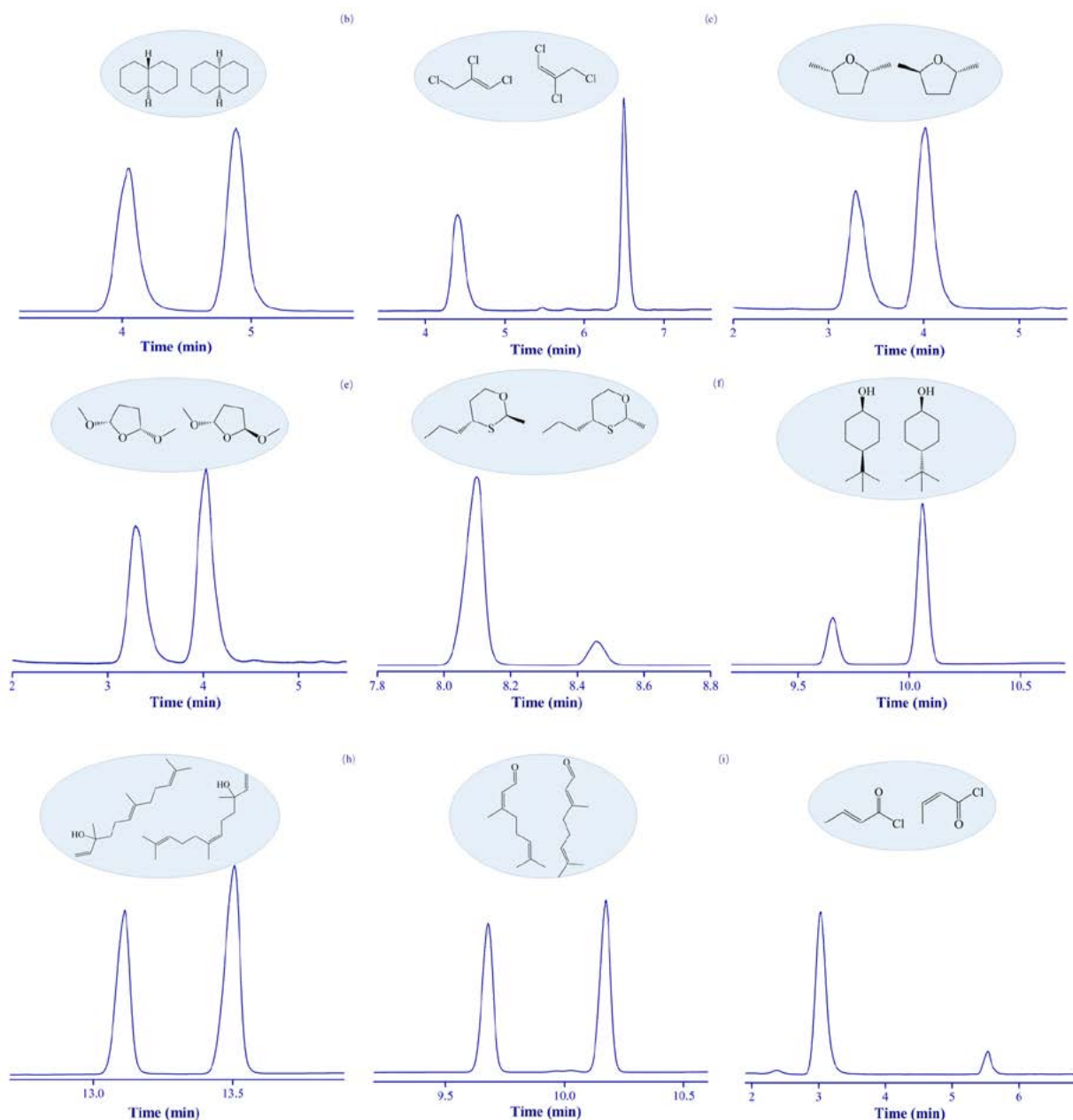


Fig. 5 Chromatogram of *cis*-/*trans*-isomers of (a) decahydronaphthalene, (b) 1,2,3-trichloropropene, (c) 2,5-dimethyltetrahydrofuran, (d) 2,5-dimethoxytetrahydrofuran, (e) 2-methyl-4-propyl-1,3-oxathiane, (f) 4-*tert*-butylcyclohexanol, (g) nerolidol, (h) citral, and (i) crotonyl chloride on the Star-PEG-PCL₂ column. Oven program: 40 °C (1 min) to 160 °C at 10 °C/min. Flow rate at 0.6 mL/min.

bility for isomers is also an indicator to evaluate the performance of a stationary phase. Therefore, dozens of positional isomer mixtures were selected to investigate the capability of the Star-PEG-PCL₂ column. Fig. 4 illustrates the resolving capacity of Star-PEG-PCL₂ stationary phase for 12 positional isomers from non-polar to polar, exhibiting that Star-PEG-PCL₂ stationary phase achieved baseline resolution and good peak shapes. Methylnaphthalene and dimethylnaphthalene (Fig. 4a-b) were well separated on the Star-PEG-PCL₂ column, and the dispersion interaction between them played an important role. The observations of Fig. 4c-g revealed high distinguishing ability of dichlorobenzene, dibromobenzene, trichlorobenzene, chloronitrobenzene, and bromonitrobenzene on the Star-PEG-PCL₂ column. Especially, *m/p*-dichlorobenzene whose boiling point difference is less than 1 °C were completely separated, suggesting there may be C-H... π interaction and halogen bonds between the analytes and the Star-PEG-PCL₂ stationary phase. The outstanding separation performance of Star-PEG-PCL₂ column for phenylenediamine (Fig. 4h) can be described with the existence of H-bonding interaction. In GC analyses, the peaks of benzaldehydes and phenols are prone to tail but the indicating analytes in Fig. 4i-l (cyanobenzaldehyde, nitrobenzaldehyde, dichlorobenzaldehyde and dimethylphenol isomer) displayed sharp and symmetrical peak shapes on the Star-PEG-PCL₂ column, revealing the Star-PEG-PCL₂ column had good column inertness and appropriate H-bonding interaction with the analytes.

3. 2. 4. *Cis-/trans*-isomers

Cis-/trans-isomers were used to further determine the distinguishing performance of Star-PEG-PCL₂ column, and the analytes included decahydronaphthalene, 1,2,3-trichloropropene, 2,5-dimethyltetrahydrofuran, 2,5-dimethoxytetrahydrofuran, 2-methyl-4-propyl-1,3-oxathiane, 4-*tert*-butylcyclohexanol, nerolidol, citral, and crotonyl chloride. As can be clearly seen from Fig. 5, analytes with highly similar structures could be completely resolved. This is perhaps derived from the unique structure of the stationary phase as previously stated, which endows the 3D molecular recognition and multiple molecular interactions involving van der Waals, H-bonding, dipole-dipole, C-H... π , halogen bonds, and dispersion interactions with solutes. Accordingly, the combination of the above-mentioned interactions can be capable of improving separation capability.

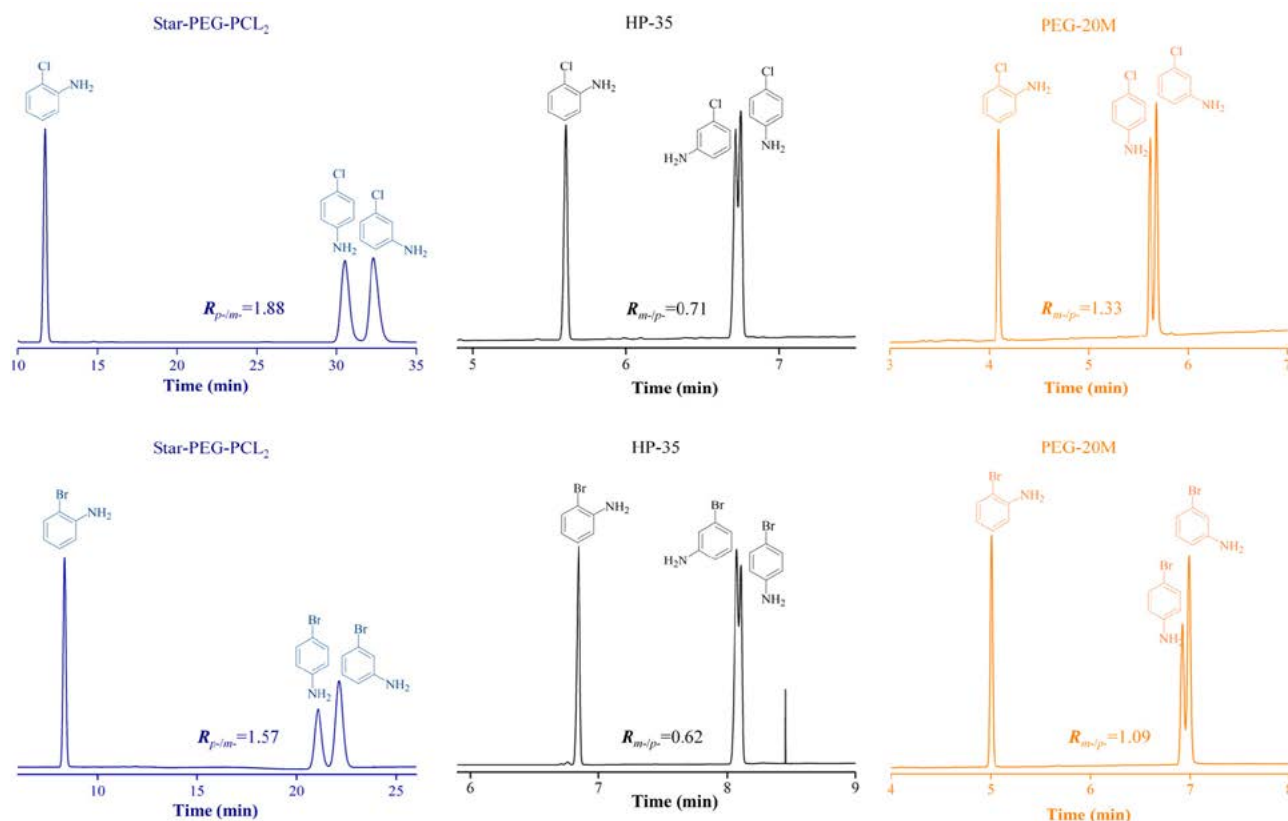


Fig. 6 Separations of the chloroaniline and bromoaniline isomers on the Star-PEG-PCL₂, HP-35, and PEG-20M columns. Temperature program on Star-PEG-PCL₂ capillary column for chloroaniline and bromoaniline: keep 100 °C and 120 °C, respectively. Temperature program on HP-35 capillary columns: 40 °C (1 min) to 160 °C at 10 °C/min. Temperature program on PEG-20M capillary column: 160 °C (1 min) to 220 °C at 10 °C/min. Flow rate of all at 0.6 mL/min.

3. 2. 5. Halogenated Aromatic Amines

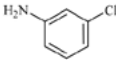
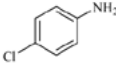
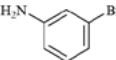
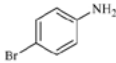
The high toxicity and carcinogenicity of aromatic amines pose a great threat to humans and the environment, so the separation of aromatic amine isomers is extremely important.^{34–36} The separation of aromatic amines is a challenge in the field of GC analysis. Fig. 6 showed the separation performance of Star-PEG-PCL₂, HP-35 and PEG-20M columns for chloroaniline and bromoaniline isomers. The Star-PEG-PCL₂ column attained the baseline separation of all the analytes and the isomers ($R > 1.5$) in contrast to the overlapping peaks that took place on the commercial columns such as the co-eluting peaks including *m/p*-chloroaniline ($R = 0.71$) and *m/p*-bromoaniline ($R = 0.62$) on the HP-35 column, and *m/p*-chloroaniline ($R = 1.33$) and *m/p*-bromoaniline ($R = 1.09$) on PEG-20M column, despite of these critical pairs of isomers having high similarity in their structure and physicochemical properties, including boiling points and dipolar moment (Table 2). The higher resolution of Star-PEG-PCL₂ column compared with the weakly polar HP-35 and polar PEG-20M columns, can be attributed to the unique architecture with branched chains that endow Star-PEG-PCL₂ more abundant and stronger retention interactions including dipole-dipole and H-bonding interactions with the isomers of different conformation.

umn exhibited good separation performance for Grob test mixture and a mixture of 17 analytes containing different types. Moreover, the Star-PEG-PCL₂ column exhibited high resolving capability for a series of positional and *cis/trans*-isomers with different polarities. Remarkably, the chloroaniline and bromoaniline isomers were completely separated by the Star-PEG-PCL₂ column, and the resolution was better than the two commercial columns. In addition, we found that the Star-PEG-PCL₂ stationary phase has dual-nature selectivity and high distinguishing capability for different analytes. This work shows that star-shaped materials have great potential as a new type of GC stationary phase.

Acknowledgements

The work was supported by the Scientific Research Foundation of the Education Department of Liaoning Province (LJGD2020015), the Training Project for Youth Backbone Teachers in Colleges and Universities of Henan Province (No. 2018GGJS127), the Henan Province Science and Technology Attack Plan Foundation (No. 202102310485), and the Training Project for Youth Backbone Teachers in Colleges and Universities of Luoyang Normal University.

Table 2. Structure and properties of the analytes in Fig. 6

Compound	CAS	Structure	Boiling point	Dipole
<i>o</i> -chloroaniline	95-51-2		209 °C	1.77 Debye
<i>m</i> -chloroaniline	108-42-9		230 °C	2.82 Debye
<i>p</i> -chloroaniline	106-47-8		232 °C	3.20 Debye
<i>o</i> -bromoaniline	615-36-1		229 °C	1.73 Debye
<i>m</i> -bromoaniline	591-19-5		251 °C	2.86 Debye
<i>p</i> -bromoaniline	106-40-1		250 °C	3.27 Debye

4. Conclusion

Here we present a star-shaped polymer Star-PEG-PCL₂ as a GC stationary phase for the first time. Star-PEG-PCL₂ column was composed of one PEG chain and two PCL chains, with star-shaped structure and amphiphilic nature. The results showed that the Star-PEG-PCL₂ col-

5. References

- J. X. Yin, M. F. Wu, R. M. Lin, X. Li, H. Ding, L. F. Han, W. Z. Yang, X. B. Song, W. L. Li, H. B. Qu, H. S. Yu, Z. Li, *Microchem. J.* **2021**, *168*, 106527. DOI:10.1016/j.microc.2021.106527
- C. Xu, L. R. Gao, M. H. Zheng, L. Qiao, K. R. Wang, D. Huang, S. Wang, *Environ. Sci. Technol.* **2021**, *55*, 109–119.

- DOI:10.1021/acs.est.0c02290
3. S. Belarbi, M. Vivier, W. Zaghouani, A. D. Sloovere, V. Agasse-Peulon, P. Cardinael, *Food Chem.* **2021**, 359, 129932. DOI:10.1016/j.foodchem.2021.129932
 4. J. D. Pavlica, Č. Podlipnik, M. Pompe, *Acta Chim. Slov.* **2021**, 68, 728–735. DOI:10.17344/acsi.2021.6817
 5. X. Li, J. C. Bai, A. Q. Du, Z. X. Yang, B. Wu, *New J. Chem.* **2020**, 44, 695–703. DOI:10.1039/C9NJ04918E
 6. T. Sun, Q. C. Huang, R. N. Chen, W. Zhang, Q. L. Li, A. P. Wu, G. X. Wang, S. Q. Hu, Z. Q. Cai, *New J. Chem.* **2021**, 45, 20459–20467. DOI:10.1039/D1NJ03893A
 7. J. L. Peng, Y. G. Shi, Z. S. Yang, M. L. Qi, F. Wang, *J. Chromatogr. A* **2016**, 1466, 129–135. DOI:10.1016/j.chroma.2016.08.070
 8. P. Delmonte, A. Milani, J. K. G. Kramer, *J. AOAC Int.* **2021**, 104, 288–299. DOI:10.1093/jaoacint/qsaa147
 9. X. M. Shuai, Z. Q. Cai, Y. J. Chen, X. Y. Zhao, Q. Q. Song, K. X. Ren, X. X. Jiang, T. Sun, S. Q. Hu, *Microchem. J.* **2020**, 157, 105124. DOI:10.1016/j.microc.2020.105124
 10. X. M. Shuai, Z. Q. Cai, X. Y. Zhao, Y. J. Chen, Q. Zhang, Z. W. Ma, J. J. Hu, T. Sun, S. Q. Hu, *Chromatographia* **2021**, 84, 325–333. DOI:10.1007/s10337-021-04018-x
 11. P. Zhang, S. J. Qin, M. L. Qi, R. N. Fu, *J. Chromatogr. A* **2014**, 1334, 139–148. DOI:10.1016/j.chroma.2014.01.083
 12. Y. Zhang, Q. Lv, M. L. Qi, Z. Q. Cai, *J. Chromatogr. A* **2017**, 1496, 115–121. DOI:10.1016/j.chroma.2017.03.054
 13. H. Nan, J. L. Anderson, *TrAC, Trends Anal. Chem.* **2018**, 105, 367–379. DOI:10.1016/j.trac.2018.03.020
 14. H. Nan, C. Zhang, R. A. O'Brien, A. Benchea, J. H. Davis Jr, J. L. Anderson, *J. Chromatogr. A* **2017**, 1481, 127–136. DOI:10.1016/j.chroma.2016.12.032
 15. J. Zhang, Z. L. Chen, *J. Chromatogr. A* **2017**, 1530, 1–18. DOI:10.1016/j.chroma.2017.10.065
 16. W. Q. Tang, S. S. Meng, M. Xu, Z. Y. Gu, *Chin. J. Chromatogr.* **2021**, 39, 57–68. DOI:10.3724/SPJ.1123.2020.06028
 17. Y. C. Zheng, M. J. Wan, J. Q. Zhou, X. M. Dai, H. L. Yang, Z. N. Xia, L. J. Wang, *J. Chromatogr. A* **2022**, 1662, 462731. DOI:10.1016/j.chroma.2021.462731
 18. L. Y. Zhao, W. J. Lv, X. Y. Niu, C. J. Pan, H. L. Chen, X. G. Chen, *J. Chromatogr. A* **2020**, 1615, 460722. DOI:10.1016/j.chroma.2019.460722
 19. R. Rashidi, S. Khakpour, S. Masoumi, Y. Jafarzadeh, *Chem. Eng. Res. Des.* **2022**, 177, 815–825. DOI:10.1016/j.cherd.2021.11.021
 20. R. B. Greenwald, A. Pendri, D. Bolikal, C. W. Gilbert, *Bioorg. Med. Chem. Lett.* **1994**, 4, 2465–2470. DOI:10.1016/S0960-894X(01)80411-X
 21. E. Cristóbal-Lecina, D. Pulido, P. Martín-Malpartida, M. J. Macias, F. Albericio, M. Royo, *ACS Omega* **2020**, 5, 5508–5519. DOI:10.1021/acsomega.0c00130
 22. T. Öztürk, A. Kılıçlıoğlu, B. Savaş, B. Hazer, *J. Macromol. Sci. A* **2018**, 55, 588–594. DOI:10.1080/10601325.2018.1481344
 23. F. Lu, L. Lei, Y.-Y. Shen, J.-W. Hou, W.-L. Chen, Y.-G. Li, S.-R. Guo, *Int. J. Pharm.* **2011**, 419, 77–84. DOI:10.1016/j.ijpharm.2011.07.020
 24. G. Kravanja, M. Globočnik, M. Primožič, Ž. Knez, M. Leitgeb, *Acta Chim. Slov.* **2019**, 66, 337–343. DOI:10.17344/acsi.2018.4822
 25. V. Ocelic Bulatovic, M. Jakić, D. Kučić, *Acta Chim. Slov.* **2020**, 67, 651–665. DOI:10.17344/acsi.2019.5676
 26. J. Cao, F. R. Cheng, H. Cao, A. J. Lu, M. T. Cai, Y. W. Chen, B. He, Z. W. Gu, X. L. Luo, *Colloids Surf. B* **2015**, 125, 213–221. DOI:10.1016/j.colsurfb.2014.11.040
 27. K. Khanna, S. Varshney, A. Kakkar, *Polym. Chem.* **2010**, 1, 1171–1185. DOI:10.1039/c0py00082e
 28. A. Vora, K. Singh, D. C. Webster, *Polymer.* **2009**, 50, 2768–2774. DOI:10.1016/j.polymer.2009.03.054
 29. K. Yoon, H. C. Kang H, L. Li, H. Cho, M.-K. Park, E. Lee, Y. H. Bae, K. M. Huh, *Polym. Chem.* **2015**, 6, 531–542. DOI:10.1039/C4PY01380H
 30. T. Sun, X. M. Shuai, K. X. Ren, X. X. Jiang, Y. J. Chen, X. Y. Zhao, Q. Q. Song, S. Q. Hu, Z. Q. Cai, *Molecules* **2019**, 24, 3158. DOI:10.3390/molecules24173158
 31. T. Sun, X. M. Shuai, Y. J. Chen, X. Y. Zhao, Q. Q. Song, K. X. Ren, X. J. Jiang, S. Q. Hu, Z. Q. Cai, *RSC Adv.* **2019**, 9, 38486–38495. DOI:10.1039/C9RA07798G
 32. W. O. McReynolds, *J. Chromatogr. Sci.* **1970**, 8, 685–691. DOI:10.1093/chromsci/8.12.685
 33. C. Ragonese, C. Sciarbone, P. Q. Tranchida, P. Dugo, L. Mondello, *J. Chromatogr. A* **2012**, 1255, 130–144. DOI:10.1016/j.chroma.2012.04.069
 34. H. Kataoka, *J. Chromatogr. A* **1996**, 733, 19–34. DOI:10.1016/0021-9673(95)00726-1
 35. T. C. Schmidt, R. Haas, K. Steinbach, E. vonLow, *Fresenius' J. Anal. Chem.* **1997**, 357, 909–914. DOI:10.1007/s002160050273
 36. M. M. Chen, G. H. Zhu, S. S. Wang, K. Z. Jiang, J. X. Xu, J. S. Liu, J. X. Jiang, *J. Sep. Sci.* **2018**, 41, 440–448. DOI:10.1002/jssc.201700786

Povzetek

V tem prispevku smo iz PCL in PEG sintetizirali zvezdasti polimer Star-PEG-PCL₂ in ga uporabili kot stacionarno fazo za plinsko kromatografijo. Statično prevlečena kolona Star-PEG-PCL₂ ima učinkovitost 2260 teoretskih prekatov/meter za naftalen pri 120 °C in je zmerno polarna. Pokazala je visoko ločljivost za izomere v širokem območju polarnosti, vključno z metilnaftaleni, halogeniranimi benzeni, nitrobenzenom, fenoli in anilini, ter izkazala dva tipa selektivnosti za zmes 17 analitov. Prav tako je izkazala dobro ločbo in inertnost za Grobovo testno mešanico ter serijo *cis-/trans*-izomerov. Dodatno je zaradi svojega edinstvenega tridimenzionalnega ogrodja pokazala prednosti pri ločbi kloroanilinov in bromoanilinov v primerjavi s komercialnima kolonama HP-35 in PEG-20M. Star-PEG-PCL₂ polimer ima dober potencial kot nova stacionarna faza za ločbo različnih analitov zaradi svoje posebne strukture in odličnih separacijskih lastnosti.



Except when otherwise noted, articles in this journal are published under the terms and conditions of the Creative Commons Attribution 4.0 International License

Scientific paper

Syntheses, Characterization, Crystal Structures and Antimicrobial Activity of Copper(II), Nickel(II) and Zinc(II) Complexes Derived from 5-Bromo-2-((cyclopentylimino)methyl)phenol

Li Zhang, Xiao-Yang Qiu* and Shu-Juan Liu

College of Science & Technology, Ningbo University, Ningbo 315315, P. R. China

* Corresponding author: E-mail: xiaoyang_qiu@126.com

Received: 08-12-2022

Abstract

Four new complexes of copper(II), nickel(II) and zinc(II), $[\text{CuL}_2]$ (**1**), $[\text{Ni}_3\text{L}_2(4\text{-BrSal})_2(\text{CH}_3\text{COO})_2(\text{CH}_3\text{OH})_2]\cdot 2\text{CH}_3\text{OH}$ (**2**), $[\text{ZnBr}_2(\text{HL})_2]$ (**3**) and $[\text{ZnL}(\text{dca})]_n$ (**4**), where L is 5-bromo-2-((cyclopentylimino)methyl)phenolate, HL is the zwitterionic form of 5-bromo-2-((cyclopentylimino)methyl)phenol, 4-BrSal is the monoanionic form of 4-bromosalicylaldehyde, dca is dicyanamide anion, were synthesized and characterized by elemental analysis, IR and UV-Vis spectroscopy. The structures of the complexes were further confirmed by single crystal X-ray structure determination. Complex **1** is a mononuclear copper(II) compound, with a crystallographic two-fold rotation axis symmetry. The Cu atom is in distorted square planar coordination. Complex **2** is a trinuclear nickel(II) compound, with an inversion center symmetry. The Ni atoms are in octahedral coordination. Complex **3** is a mononuclear zinc(II) compound, while complex **4** is a dca bridged polymeric zinc(II) compound. The Zn atoms are in tetrahedral coordination. The compounds were assayed for their antimicrobial activities.

Keywords: Schiff base, copper complex, nickel complex, zinc complex, antimicrobial activity

1. Introduction

The synthesis of new metal complexes with biological activities is a hot topic in coordination chemistry and bioinorganic chemistry. Among the complexes, those with Schiff base ligands have received particular attention due to their facile preparation, interesting structural diversity, and the possibility of the presence of various electron-donating or electron-withdrawing substituents.¹ Schiff base copper, nickel and zinc complexes have been extensively studied and are considered as excellent alternatives for classic organic antibacterial, antifungal and antitumor.² Despite the presence of a large number of studies on the antibacterial activities of such complexes, it is still necessary to explore new complexes with more effective activities. It has been proved that the compounds with electron-withdrawing substituent groups can improve their antimicrobial ability.³ Rai *et al.* reported some compounds with fluoro, chloro, bromo, and iodo-substituted groups, and their remarkable antimicrobial property.⁴ Schiff base complexes of copper, nickel and zinc have potential antibacterial activities.⁵ Recently, our research group has re-

ported some Schiff base complexes with biological properties.⁶ The platinum complexes with cyclopentylamine exhibited considerable cytotoxicity against cancer cell lines.⁷ Moreover, the complexes with cyclopentylamine Schiff base ligands have interesting antibacterial activity.⁸ In pursuit of new Schiff base complexes with potential antimicrobial activity, four new complexes $[\text{CuL}_2]$ (**1**), $[\text{Ni}_3\text{L}_2(4\text{-BrSal})_2(\text{CH}_3\text{COO})_2(\text{CH}_3\text{OH})_2]\cdot 2\text{CH}_3\text{OH}$ (**2**), $[\text{ZnBr}_2(\text{HL})_2]$ (**3**) and $[\text{ZnL}(\text{dca})]_n$ (**4**), where L is 5-bromo-2-((cyclopentylimino)methyl)phenolate, HL is the zwitterionic form of 5-bromo-2-((cyclopentylimino)methyl)phenol, 4-BrSal is the monoanionic form of 4-bromosalicylaldehyde, dca is dicyanamide anion, and their antimicrobial activities are present.

2. Experimental

2.1. Materials and Methods

4-Bromosalicylaldehyde, cyclopentylamine, copper acetate, nickel acetate, zinc bromide, zinc nitrate and sodi-

um dicyanamide were obtained from Sigma-Aldrich. All other chemicals were commercial obtained from Xiya Chemical Co. Ltd. Elemental analyses of C, H and N were carried out in a Perkin-Elmer automated model 2400 Series II CHNS/O analyzer. FT-IR spectra were obtained on a Perkin-Elmer 377 FT-IR spectrometer with samples prepared as KBr pellets. UV-Vis spectra were obtained on a Lambda 35 spectrometer. Single crystal structural X-ray diffraction was carried out on a Bruker APEX II CCD diffractometer. ^1H NMR data were recorded on a Bruker 500 MHz instrument. Molar conductivities of the complexes in DMSO solutions (10^{-3} M) at room temperature were measured using a Systronic model 303 direct reading conductivity meter.

2. 2. Synthesis of 2-bromo-6-((2-(isopropylamino)ethylimino)methyl)phenol (HL)

4-Bromosalicylaldehyde (1.0 mmol, 0.20 g) and cyclopentylamine (1.0 mmol, 0.085 g) were mixed and stirred in methanol (30 mL). The mixture was refluxed for 30 min, and with the solvent removed by distillation. The solid product was re-crystallized from methanol to give yellow product. Yield 93%. Anal. calc. for $\text{C}_{12}\text{H}_{14}\text{BrNO}$: C, 53.75; H, 5.26; N, 5.22; found: C, 53.62; H, 5.35; N, 5.31%. Characteristic IR data (cm^{-1}): 1637 ($\text{C}=\text{N}$). UV-Vis data (MeOH, λ_{max} , nm): 233, 272, 335. ^1H NMR (d_6 -DMSO, δ , ppm): 12.11 (s, 1H, OH), 8.63 (s, 1H, $\text{CH}=\text{N}$), 7.51 (d, 1H, ArH), 7.45 (s, 1H, ArH), 6.92 (d, 1H, ArH), 3.27 (m, 1H, CH), 1.89 (m, 2H, CH_2), 1.73 (m, 2H, CH_2), 1.50 (m, 2H, CH_2), 1.43 (m, 2H, CH_2).

2. 3. Synthesis of $[\text{CuL}_2]$ (1)

HL (0.10 mmol, 27 mg) and copper acetate monohydrate (0.10 mmol, 20 mg) mixed in methanol (15 mL) were stirred at room temperature for 30 min to give a clear blue solution. Block blue single crystals suitable for X-ray diffraction were grown from the solution upon slowly evaporation within 5 days. The crystals were isolated by filtration. Yield 41%. Anal. calc. for $\text{C}_{24}\text{H}_{26}\text{Br}_2\text{CuN}_2\text{O}_2$: C, 48.22; H, 4.38; N, 4.69; found: C, 48.03; H, 4.47; N, 4.57%. Characteristic IR data (cm^{-1}): 1621 ($\nu_{\text{C}=\text{N}}$). UV-Vis data (MeOH, λ_{max} , nm): 227, 248, 274, 361. Molar conductance (10^{-3} M in DMSO): $22 \Omega^{-1} \text{cm}^2 \text{mol}^{-1}$.

2. 4. Synthesis of $[\text{Ni}_3\text{L}_2(4\text{-BrSal})_2(\text{CH}_3\text{COO})_2(\text{CH}_3\text{OH})_2]\cdot 2\text{CH}_3\text{OH}$ (2)

HL (0.10 mmol, 27 mg), 4-bromosalicylaldehyde (0.10 mmol, 20 mg) and nickel acetate tetrahydrate (0.10 mmol, 25 mg) mixed in methanol (15 mL) were stirred at room temperature for 30 min to give a clear green solution. Block green single crystals suitable for X-ray diffraction were grown from the solution upon slowly evaporation within 3

days. The crystals were isolated by filtration. Yield 53%. Anal. calc. for $\text{C}_{46}\text{H}_{56}\text{Br}_4\text{N}_2\text{Ni}_3\text{O}_{14}$: C, 40.73; H, 4.16; N, 2.06; found: C, 40.87; H, 4.05; N, 1.97%. Characteristic IR data (cm^{-1}): 1646 ($\nu_{\text{C}=\text{O}}$), 1632 ($\nu_{\text{C}=\text{N}}$), 1586 ($\nu_{\text{as-acetate}}$), 1405 ($\nu_{\text{s-acetate}}$). UV-Vis data (MeOH, λ_{max} , nm): 227, 245, 267, 362. Molar conductance (10^{-3} M in DMSO): $17 \Omega^{-1} \text{cm}^2 \text{mol}^{-1}$.

2. 5. Synthesis of $[\text{ZnBr}_2(\text{HL})_2]$ (3)

HL (0.10 mmol, 27 mg) and zinc bromide (0.10 mmol, 23 mg) mixed in methanol (15 mL) were stirred at room temperature for 30 min to give a clear colorless solution. Block colorless single crystals suitable for X-ray diffraction were grown from the solution upon slowly evaporation within 8 days. The crystals were isolated by filtration. Yield 45%. Anal. calc. for $\text{C}_{24}\text{H}_{28}\text{Br}_4\text{N}_2\text{O}_2\text{Zn}$: C, 37.85; H, 3.71; N, 3.68; found: C, 37.71; H, 3.65; N, 3.77%. Characteristic IR data (cm^{-1}): 1628, 1633 ($\nu_{\text{C}=\text{N}}$). UV-Vis data (MeOH, λ_{max} , nm): 215, 260, 313, 370. Molar conductance (10^{-3} M in DMSO): $26 \Omega^{-1} \text{cm}^2 \text{mol}^{-1}$.

2. 6. Synthesis of $[\text{ZnL}(\text{dca})]_n$ (4)

HL (0.10 mmol, 27 mg), sodium dicyanamide (0.10 mmol, 8.9 mg) and zinc nitrate hexahydrate (0.10 mmol, 30 mg) mixed in methanol (15 mL) were stirred at room temperature for 30 min to give a clear colorless solution. Block colorless single crystals suitable for X-ray diffraction were grown from the solution upon slowly evaporation within 4 days. The crystals were isolated by filtration. Yield 52%. Anal. calc. for $\text{C}_{14}\text{H}_{13}\text{BrN}_4\text{OZn}$: C, 42.19; H, 3.29; N, 14.06; found: C, 42.37; H, 3.40; N, 13.93%. Characteristic IR data (cm^{-1}): 2371, 2281, 2195 (ν_{dca}), 1618 ($\nu_{\text{C}=\text{N}}$). UV-Vis data (MeOH, λ_{max} , nm): 221, 245, 279, 360. Molar conductance (10^{-3} M in DMSO): $33 \Omega^{-1} \text{cm}^2 \text{mol}^{-1}$.

2. 7. X-ray Crystallography

X-ray diffraction was carried out at a Bruker APEX II CCD area diffractometer equipped with MoK α radiation ($\lambda = 0.71073 \text{ \AA}$). The collected data were reduced with SAINT,⁹ and multi-scan absorption correction was performed using SADABS.¹⁰ The structures of the complexes were solved by direct method, and refined against F^2 by full-matrix least-squares method using SHELXTL.¹¹ All of the non-hydrogen atoms were refined anisotropically. The H6 atom in complex 2, and H1 and H2 atoms in complex 3 were located from difference Fourier maps and refined isotropically, with O-H and N-H distances restrained to 0.85(1) and 0.90(1) \AA , respectively. The remaining hydrogen atoms were placed in calculated positions and constrained to ride on their parent atoms. The cyclopentyl group in complex 2 is disordered over two sites, with occupancies of 0.45(3) and 0.55(3), respectively. The crystallographic data and refinement parameters for the complexes are listed in Table 1.

Table 1. Crystallographic and refinement data for the complexes

Complex	1	2	3	4
Formula	C ₂₄ H ₂₆ Br ₂ CuN ₂ O ₂	C ₄₆ H ₅₆ Br ₄ N ₂ Ni ₃ O ₁₄	C ₂₄ H ₂₈ Br ₄ N ₂ O ₂ Zn	C ₁₄ H ₁₃ BrN ₄ OZn
Formula weight	597.83	1356.69	761.49	398.56
Crystal system	Triclinic	Monoclinic	Monoclinic	Orthorhombic
Space group	<i>P</i> -1	<i>P</i> 2 ₁ / <i>c</i>	<i>P</i> 2 ₁ / <i>n</i>	<i>Cmca</i>
<i>a</i> (Å)	9.4221(12)	11.2785(12)	17.6493(13)	7.4850(11)
<i>b</i> (Å)	10.0407(12)	12.2231(13)	8.8618(14)	19.0531(10)
<i>c</i> (Å)	12.6190(13)	20.7738(16)	18.0178(13)	22.4816(13)
α (°)	91.7950(10)	90	90	90
β (°)	91.5060(10)	93.9970(10)	99.451(2)	90
γ (°)	102.3690(10)	90	90	90
<i>V</i> (Å ³)	1164.9(2)	2856.9(5)	2779.8(5)	3206.2(5)
<i>Z</i>	2	2	4	8
<i>D</i> _{calc} (g cm ⁻³)	1.704	1.577	1.820	1.651
μ (Mo Ka) (mm ⁻¹)	4.391	3.834	6.656	4.027
<i>F</i> (000)	598	1364	1488	1584
Measured reflections	6293	14712	14377	8412
Unique reflections	4306	5317	5167	1619
Observed reflections (<i>I</i> ≥ 2σ(<i>I</i>))	3140	2039	2902	1119
Parameters	280	365	304	115
Restraints	0	94	2	0
GOOF	1.006	0.972	1.012	1.027
<i>R</i> ₁ , <i>wR</i> ₂ [<i>I</i> ≥ 2σ(<i>I</i>)] ^a	0.0385, 0.0878	0.0825, 0.2402	0.0473, 0.1001	0.0409, 0.0982
<i>R</i> ₁ , <i>wR</i> ₂ (all data) ^a	0.0603, 0.0962	0.1966, 0.3189	0.1039, 0.1230	0.0709, 0.1118

$$^a R_1 = \frac{\sum ||F_o| - |F_c||}{\sum |F_o|}, wR_2 = \frac{\{\sum [w(F_o^2 - F_c^2)^2]\}}{\sum [w(F_o^2)]}^{1/2}$$

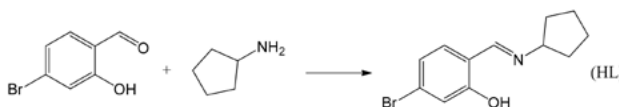
2. 8. Antimicrobial Assay

The antibacterial activity of the complexes was tested against *Bacillus subtilis*, *Staphylococcus aureus*, *Escherichia coli*, and *Pseudomonas fluorescens* using MH (Mueller–Hinton) medium. The antifungal activities of the compounds were tested against *Candida albicans* and *Aspergillus niger* using RPMI-1640 medium. The MIC values of the tested compounds were determined by a colorimetric method using the dye MTT.¹² A stock solution of the compound (150 μg mL⁻¹) in DMSO was prepared and graded quantities (75 μg mL⁻¹, 37.5 μg mL⁻¹, 18.8 μg mL⁻¹, 9.4 μg mL⁻¹, 4.7 μg mL⁻¹, 2.3 μg mL⁻¹, 1.2 μg mL⁻¹, 0.59 μg mL⁻¹) were incorporated in specified quantity of the corresponding sterilized liquid medium. A specified quantity of the medium containing the compound was poured into micro-titration plates. Suspension of the microorganism was prepared to contain approximately 1.0 × 10⁵ cfu mL⁻¹ and applied to microtitration plates with serially diluted compounds in DMSO to be tested and incubated at 37 °C for 24 h and 48 h for bacteria and fungi, respectively. Then the MIC values were visually determined on each of the micro-titration plates, 50 μL of PBS (phosphate buffered saline 0.01 mol L⁻¹, pH = 7.4) containing 2 mg of MTT mL⁻¹ was added to each well. Incubation was continued at room temperature for 4–5 h. The content of each well was removed and 100 μL solution of isopropanol (95%) and 1 mol L⁻¹ HCl (5%) was added to extract the dye. After 12 h of incubation at room temperature, the optical density was measured with a microplate reader at 550 nm.

3. Results and Discussion

3. 1. Synthesis and Characterization

The Schiff base HL was readily prepared by the reaction of equimolar quantities of 4-bromosalicylaldehyde and cyclopentylamine in methanol. The complexes 1–4 were prepared by the reaction of HL with copper acetate, nickel acetate, zinc bromide, and zinc nitrate and sodium dicyanamide, respectively in methanol (Scheme 1). Single crystals of the complexes were obtained by slow evaporation of their methanolic solution. Elemental analyses of the complexes are in accordance with the molecular structures determined by the single crystal X-ray analysis.



Scheme 1. The synthetic procedure for HL and the complexes.

3. 2. Spectroscopic Studies

The typical and strong absorptions at 1637 cm⁻¹ for HL and 1618–1632 cm⁻¹ for the complexes are generated by the vibrations of the C=N bonds, indicating the formation of the Schiff bases from the condensation reaction of the 4-bromosalicylaldehyde and cyclopentylamine during the coordination.¹³ The strong band at 1646 cm⁻¹ for com-

plex 2 can be assigned to the C=O absorption of the 4-bromosalicylaldehyde ligand. Complex 2 exhibit two bands at 1586 cm^{-1} for $\nu_{\text{as-acetate}}$ and 1405 cm^{-1} for $\nu_{\text{s-acetate}}$.¹⁴ The separation between the two bands is 181 cm^{-1} , which can be correlated to the bidentate acetate groups.¹⁴ The characteristic bands at 2371 , 2281 and 2195 cm^{-1} in the spectrum of complex 4 can be assigned to the vibrations of the dicyanamide ligands.¹⁵

In the UV-Vis spectra of HL and the complexes, the bands at $360\text{--}370\text{ nm}$ are attributed to the azomethine chromophore $\pi\rightarrow\pi^*$ transition.¹⁶ The bands at higher energies ($210\text{--}230$ and $245\text{--}280\text{ nm}$) are associated with the benzene $\pi\rightarrow\pi^*$ transition.¹⁶

3. 3. Structure Description of Complex 1

Selected bond lengths and angles for complex 1 are listed in Table 2. Molecular structure of the complex is shown in Figure 1. The Cu atom is coordinated in square planar geometry, with two phenolate O and two imino N

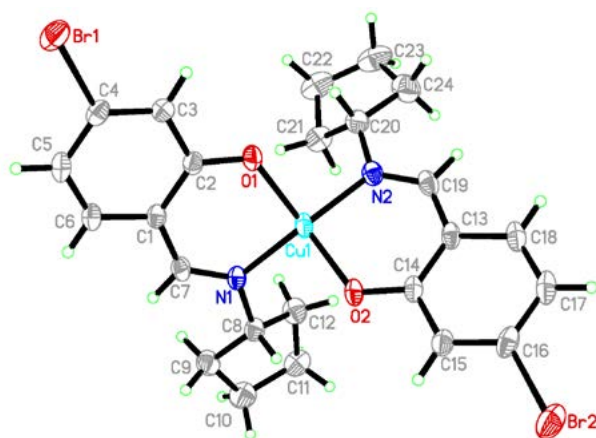


Figure 1. A perspective view of complex 1 with the atom labeling scheme. Thermal ellipsoids are drawn at the 30% probability level.

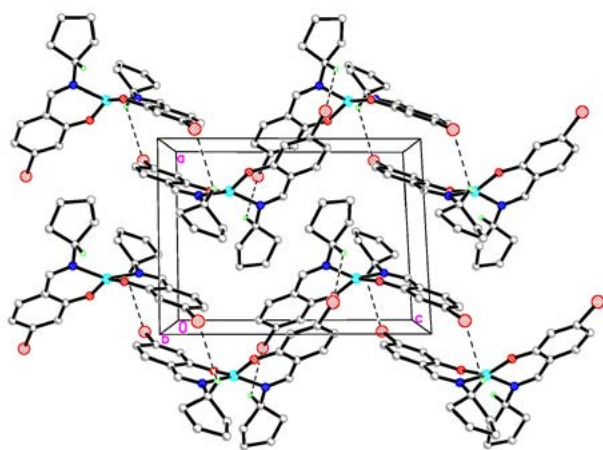


Figure 2. The crystal structure of complex 1, viewed along the *b* axis. Hydrogen bonds are shown as dashed lines.

atoms from two Schiff base ligands. The Schiff base ligands, act as bidentate ligands, chelate the Cu atom by generating two six-membered rings with bite angles of $94.20(11)^\circ$ and $94.61(12)^\circ$. The *trans* angles are $147.92(12)^\circ$ and $151.50(12)^\circ$, indicating the coordination is tetrahedrally distorted. The dihedral angle between the O1-Cu1-N1 and O2-Cu1-N2 planes is $41.8(2)^\circ$. The coordinate bond lengths and angles are comparable to those in the reported Schiff base copper complexes.¹⁷ The dihedral angle between the two benzene rings of the two Schiff base ligands is $35.7(3)^\circ$.

In the crystal structure of the complex, molecules are linked through intermolecular C-H...Br hydrogen bonds (Table 3), to form chains running along the *c* axis (Figure 2).

3. 4. Structure Description of Complex 2

Selected bond lengths and angles for complex 2 are listed in Table 2. Molecular structure of the complex is shown in Figure 3. The compound contains a centrosymmetric trinuclear nickel complex molecule and two methanol molecules of crystallization. The inversion center is located at the site of Ni2 atom. There are three bridges across the Ni...Ni atom pairs, involving two phenolate O atoms from a Schiff base ligand and a 4-bromosalicylaldehyde ligand, and an O-C-O moiety of a $\mu_2\text{-}\eta^1\text{:}\eta^1\text{-OAc}$ group. The acetate bridges linking the central and terminal nickel atoms are mutually *trans*. The trinuclear nickel complex molecule consists of two NiL units connected to each other by a completely encapsulated third metal atom, Ni2. The adjacent Ni1...Ni2 distance is $3.070(1)\text{ \AA}$.

The cage of Ni2 is formed by phenolate bridges, O1 and O2, from the Schiff base and 4-bromosalicylaldehyde ligands, and by two O atoms from two $\mu_2\text{-}\eta^1\text{:}\eta^1\text{-OAc}$ ligands that furthermore connect the central metal with the two outer metal atoms resulting in an octahedral environment. The coordination around Ni2 atom displays only slight distortion. The bond distances Ni-O are relatively similar and range from $2.063(7)$ to $2.089(7)\text{ \AA}$. The greatest deviation of the bond angles from those expected for an ideal octahedral geometry is found for O1-Ni2-O2 with $76.6(3)^\circ$, and O1-Ni2-O2A with $103.4(3)^\circ$. The remaining bond angles are close to the ideal values for the octahedral coordination.

The coordination around the inversion-related terminal Ni atoms, Ni1 and Ni1A, is also octahedral, with one imino N and one phenolate O atoms of a Schiff base ligand, and one carbonyl O and one phenolate O atoms of a 4-bromosalicylaldehyde ligand, defining the equatorial plane, and with two O atoms respectively from a methanol and a $\mu_2\text{-}\eta^1\text{:}\eta^1\text{-OAc}$ ligand occupying the axial positions. The coordination around the terminal metal atoms also displays slight distortion. The greatest deviation of the bond angles from those expected for an ideal octahedral geometry is O1-Ni1-O2 ($79.9(3)^\circ$), which is caused by the strain created by the four-membered chelate ring Ni1-O1-Ni2-O2.

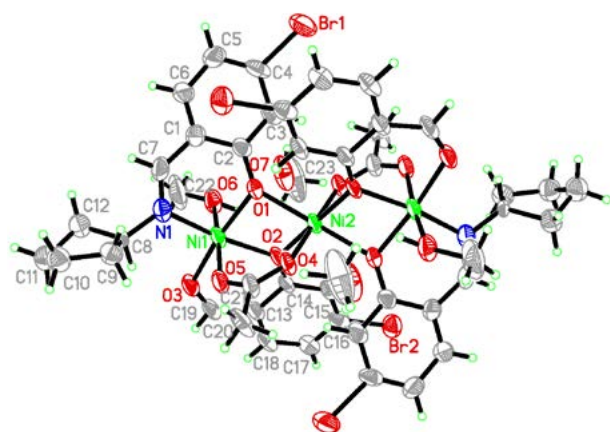


Figure 3. A perspective view of complex 2 with the atom labeling scheme. Thermal ellipsoids are drawn at the 30% probability level. The unlabeled atoms are related to the symmetry operation $1 - x, 1 - y, 1 - z$.

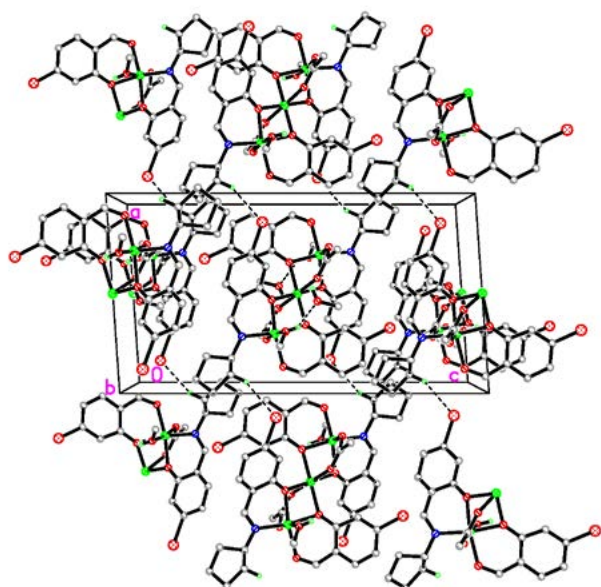


Figure 4. The crystal structure of complex 2, viewed along the b axis. Hydrogen bonds are shown as dashed lines.

The coordinate bond lengths and angles are comparable to those in the reported Schiff base nickel complexes.¹⁸ The NiL units in the complex are butterfly-shaped, with the dihedral angle formed by the two benzene rings of the Schiff base ligand and 4-bromosalicylaldehyde ligand of $34.5(4)^\circ$.

In the crystal structure of the complex, molecules are linked through intermolecular C-H...Br hydrogen bonds (Table 3), to form chains running along the a axis (Figure 4).

3. 5. Structure Description of Complex 3

Selected bond lengths and angles for complex 3 are listed in Table 2. Molecular structure of the complex is

shown in Figure 5. The Zn atom is coordinated in tetrahedral geometry, with two phenolate O atoms from two zwitterionic Schiff base ligands. The coordinate bond angles are $102.33(12)$ – $119.46(4)^\circ$, indicating it is deviated from ideal tetrahedral geometry. The coordinate bond lengths and angles are comparable to those in the reported Schiff base zinc complexes.¹⁹ The dihedral angle between the two benzene rings of the two Schiff base ligands is $59.4(5)^\circ$.

In the crystal structure of the complex, molecules are linked through intermolecular C-H...Br hydrogen bonds (Table 3), to form chains running along the b axis (Figure 6).

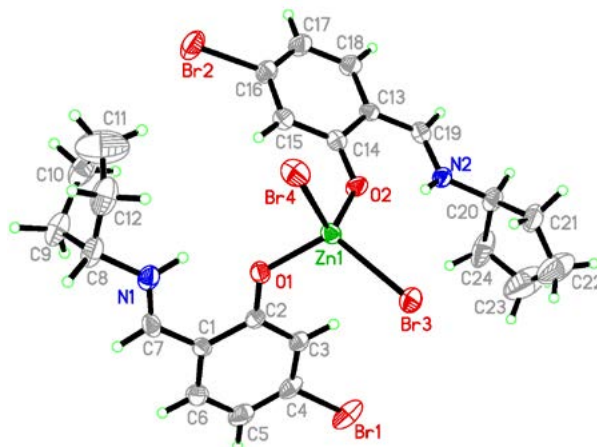


Figure 5. A perspective view of complex 3 with the atom labeling scheme. Thermal ellipsoids are drawn at the 30% probability level.

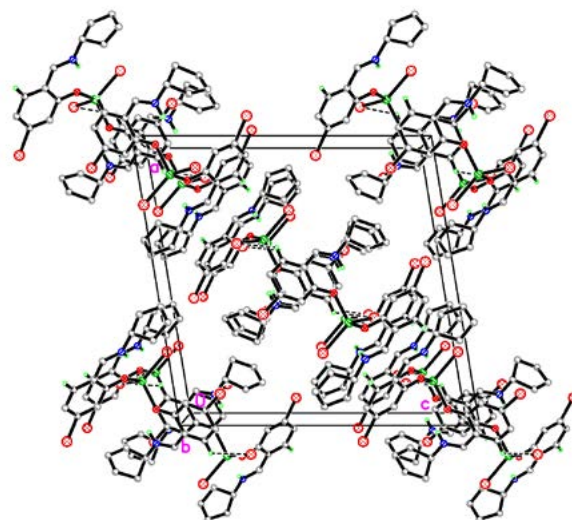


Figure 6. The crystal structure of complex 3, viewed along the b axis. Hydrogen bonds are shown as dashed lines.

3. 6. Structure Description of Complex 4

Selected bond lengths and angles for complex 4 are listed in Table 2. Molecular structure of the complex is

shown in Figure 7. The compound is a dicyanamide bridged polymeric zinc complex. Each Zn atom is coordinated in tetrahedral geometry, with one phenolate O and one imino N atoms of the Schiff base ligand, and two N atoms of dicyanamide ligand. The coordinate bond angles are 99.12(18)–115.32(13)°, indicating it is deviated from ideal tetrahedral geometry. The coordinate bond lengths and angles are comparable to those in the reported Schiff base zinc complexes with dicyanamide bridges.²⁰

In the crystal structure of the complex, the [ZnL] units are linked through dicyanamide ligands, to form an infinite one-dimensional chain along the *a* axis. The chains are further linked through intermolecular C–H...N hydrogen bonds (Table 3) at the axis-*b* direction, to form two dimensional sheet parallel to the *ab* plane (Figure 6).

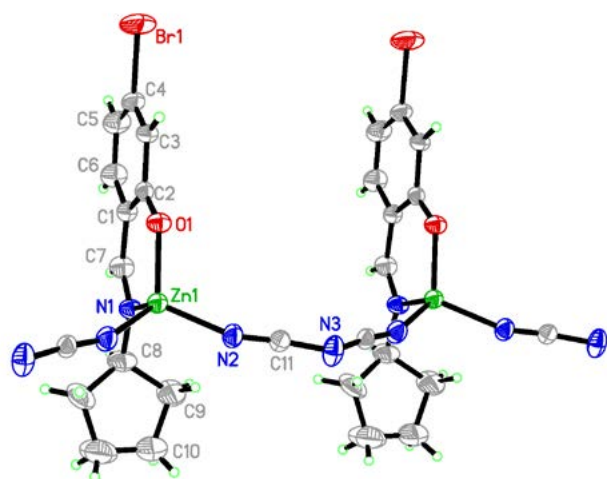


Figure 7. A perspective view of complex 4 with the atom labeling scheme. Thermal ellipsoids are drawn at the 30 % probability level. The unlabeled atoms are related to the symmetry operation $1 - x, y, z$.

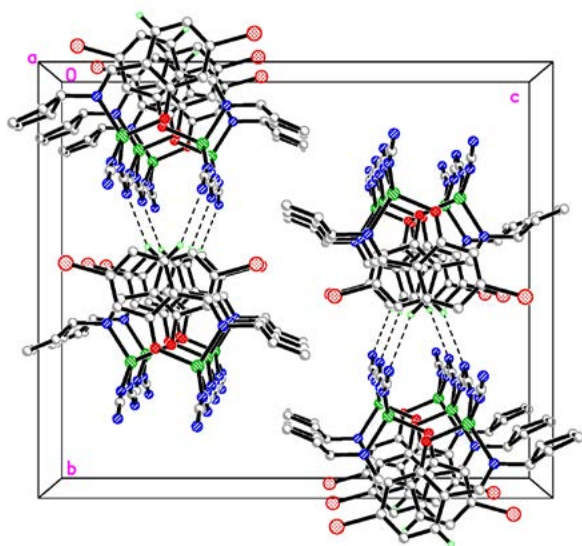


Figure 8. The crystal structure of complex 4, viewed along the *a* axis. Hydrogen bonds are shown as dashed lines.

Table 2. Selected bond distances (Å) and angles (°) for the complexes

1			
Cu1–O1	1.886(3)	Cu1–O2	1.883(3)
Cu1–N1	1.961(3)	Cu1–N2	1.950(3)
O2–Cu1–O1	147.92(12)	O2–Cu1–N2	94.61(12)
O1–Cu1–N2	93.42(12)	O2–Cu1–N1	93.36(11)
O1–Cu1–N1	94.20(11)	N2–Cu1–N1	151.50(12)
2			
Ni1–O1	2.002(7)	Ni1–O2	2.006(7)
Ni1–O3	2.026(8)	Ni1–N1	2.003(10)
Ni1–O5	2.039(8)	Ni1–O6	2.103(8)
Ni2–O1	2.063(7)	Ni2–O4	2.075(7)
Ni2–O4	2.075(7)	Ni2–O2	2.089(7)
N1–Ni1–O1	91.0(4)	N1–Ni1–O2	170.7(4)
O1–Ni1–O2	79.9(3)	N1–Ni1–O3	97.7(4)
O1–Ni1–O3	170.7(3)	O2–Ni1–O3	91.5(3)
N1–Ni1–O5	90.1(4)	O1–Ni1–O5	97.4(3)
O2–Ni1–O5	88.8(3)	O3–Ni1–O5	86.0(3)
N1–Ni1–O6	91.5(4)	O1–Ni1–O6	90.2(3)
O2–Ni1–O6	90.8(3)	O3–Ni1–O6	86.2(3)
O5–Ni1–O6	172.2(4)	O1–Ni2–O1A	180
O1–Ni2–O4A	91.8(3)	O1–Ni2–O4	88.2(3)
O1–Ni2–O4A	91.8(3)	O4–Ni2–O4A	180
O1–Ni2–O2A	103.4(3)	O4–Ni2–O2A	89.2(3)
O1–Ni2–O2	76.6(3)	O1–Ni2–O2A	103.4(3)
O4–Ni2–O2A	89.2(3)	O4–Ni2–O2	90.8(3)
O2–Ni2–O2A	180		
3			
Zn1–Br3	2.3629(10)	Zn1–Br4	2.3546(10)
Zn1–O1	1.954(4)	Zn1–O2	1.942(4)
O2–Zn1–O1	107.36(18)	O2–Zn1–Br4	111.25(12)
O1–Zn1–Br4	102.33(12)	O2–Zn1–Br3	103.42(12)
O1–Zn1–Br3	112.70(13)	Br4–Zn1–Br3	119.46(4)
4			
Zn1–O1	1.907(4)	Zn1–N2	1.966(4)
Zn1–N1	1.980(5)		
O1–Zn1–N2	111.45(12)	O1–Zn1–N2A	111.45(12)
N2–Zn1–N2A	104.4(2)	O1–Zn1–N1	99.12(18)
N2–Zn1–N1	115.32(13)		

Symmetry code for A: $1 - x, y, z$.

3. 4. Antimicrobial Activity

The complexes as well as HL and related inorganic metal salts were screened for antibacterial activities against two Gram (+) bacterial strains (*Bacillus subtilis* and *Staphylococcus aureus*) and two Gram (–) bacterial strains (*Escherichia coli* and *Pseudomonas fluorescense*) by MTT method. The MIC (minimum inhibitory concentration, $\mu\text{g mL}^{-1}$) values of the compounds against four bacteria are listed in Table 4. Penicillin G was used as the standard drug. As a result, the complexes have better activities

Table 3. Hydrogen bond distances (Å) and angles (°) for the complexes

D–H...A	d(D–H)	d(H...A)	d(D...A)	Angle (D–H...A)
1				
C8–H8...Br1 ^{#1}	0.98	3.04(3)	3.723(5)	128(6)
2				
C12–H12D...Br1 ^{#2}	0.97	2.79(4)	3.694(6)	155(7)
3				
C6–H6...Br4 ^{#3}	0.93	3.05(4)	3.671(7)	125(6)
4				
C6–H6...N3 ^{#4}	0.93	2.51(3)	3.379(1)	156(3)

Symmetry codes: #1: 2 – x, 1 – y, – z; #2: 1 + x, y, z; #3: 1 – x, 2 – y, 1 – z; #4: 1/2 + x, –1/2 + y, z.

against all the bacteria than the free Schiff base HL and the related inorganic metal salts. Complexes **1** and **3** show strong activity against *B. subtilis*, *S. aureus* and *E. coli*, while weak activity against *P. fluorescence*. Complex **2** shows medium activity against *B. subtilis*, and weak activity against *S. aureus*, *E. coli* and *P. fluorescence*. Complex **4** shows strong activity against *B. subtilis* and *S. aureus*, medium activity against *E. coli*, while weak activity against *P. fluorescence*. Complexes **1**, **3** and **4** have stronger activity against all the bacteria than Penicillin G. Complex **2** has stronger activity against *E. coli* and *P. fluorescence*, while weaker activity against *B. subtilis* and *S. aureus* than Penicillin G. However, all the complexes have no activity on the fungal strains *Candida albicans* and *Aspergillus niger*.

Table 4. Antibacterial activities of the assayed compounds with minimum inhibitory concentrations ($\mu\text{g mL}^{-1}$)

Tested material	<i>B. subtilis</i>	<i>S. aureus</i>	<i>E. coli</i>	<i>P. fluorescence</i>
1	1.2	2.3	4.7	18.8
2	9.4	18.8	18.8	37.5
3	2.3	4.7	4.7	37.5
4	4.7	2.3	9.4	75
HL	18.8	37.5	37.5	> 150
Copper acetate	9.4	4.7	9.4	37.5
Nickel acetate	37.5	37.5	> 150	> 150
Zinc bromide	18.8	18.8	75	> 150
Zinc nitrate	18.8	18.8	75	> 150
Penicillin G	2.3	4.7	>150	> 150

4. Conclusion

Four new copper, nickel and zinc complexes derived from the Schiff base 5-bromo-2-((cyclopentylimino)methyl)phenol were synthesized and characterized by infrared and electronic spectra. The detailed structures of the complexes have been confirmed by single crystal X-ray structure determination. The complexes have strong activities against the bacteria *B. subtilis*, *S. aureus* and *E. coli*, which deserve further study.

Acknowledgments

This work was financially supported by Ningbo Public Welfare Funds (Project No. 2021S142), and College of Science & Technology Ningbo University (Project No. hx2022010).

Supplementary Data

CCDC 2192715 (**1**), 2192716 (**2**), 2192718 (**3**) and 2192719 (**4**) contain the supplementary crystallographic data for the compounds. These data can be obtained free of charge via <http://www.ccdc.cam.ac.uk/conts/retrieving.html>, or from the Cambridge Crystallographic Data Centre, 12 Union Road, Cambridge CB2 1EZ, UK; fax: (+44) 1223-336-033; or e-mail: deposit@ccdc.cam.ac.uk.

5. References

- (a) A. Jurowska, W. Serafin, M. Hodorowicz, K. Kruczala, J. Szklarzewicz, *Polyhedron* **2022**, *222*, 115903; DOI:10.1016/j.poly.2022.115903
(b) Y. Yuan, X. K. Lu, G. Q. Zhou, X.-Y. Qiu, *Acta Chim. Slov.* **2021**, *68*, 1008–1015; DOI:10.17344/acsi.2021.7070
(c) S. Han, Y. Wang, *Acta Chim. Slov.* **2021**, *68*, 961–969; DOI:10.17344/acsi.2021.6965
(d) W.Y. Shen, C.P. Jia, L.Y. Liao, L.L. Chen, C. Hou, Y.H. Liu, H. Liang, Z.F. Chen, *J. Med. Chem.* **2022**, *65*, 5134–5148. DOI:10.1021/acs.jmedchem.2c00133
- (a) M.S. Ragab, M.H. Soliman, M.R. Shehata, M.M. Shoukry, M.A. Ragheb, *Appl. Organomet. Chem.* **2022**, e6802;
(b) M. Bencela, S.S. Kumari, *Polyhedron* **2022**, *219*, 115788; DOI:10.1016/j.poly.2022.115788
(c) H. Goudarziafshar, S. Yousefi, Y.A. Tyula, M. Dusek, V. Eigner, *RSC Advances* **2022**, *12*, 13580–13592; DOI:10.1039/D2RA00719C
(d) S. Esmaielzadeh, E. Zarenezhad, *Acta Chim. Slov.* **2018**, *65*, 416–428; DOI:10.17344/acsi.2018.4159
(e) D.L. Peng, N. Sun, *Acta Chim. Slov.* **2018**, *65*, 895–901; DOI:10.17344/acsi.2018.4543
(f) C.L. Zhang, X.Y. Qiu, S.J. Liu, *Acta Chim. Slov.* **2019**, *66*,

- 484–489; DOI:10.17344/acsi.2019.5019
- (g) S.F. Yu, X.Y. Qiu, S.J. Liu, *Acta Chim. Slov.* **2020**, *67*, 1301–1308; DOI:10.17344/acsi.2020.6321
- (h) A.S. Hossain, J.M. Mendez-Arriaga, C.K. Xia, J.M. Xie, S. Gomez-Ruiz, *Polyhedron* **2022**, *217*, 115692. DOI:10.1016/j.poly.2022.115692
3. (a) G. Paraskevopoulos, S. Monteiro, R. Vosatka, M. Kratky, L. Navratilova, F. Trejtnar, J. Stolarikova, J. Vinsova, *Bioorg. Med. Chem.* **2017**, *25*, 1524–1532; DOI:10.1016/j.bmc.2017.02.053
- (b) M. Zhang, D.-M. Xian, H.-H. Li, J.-C. Zhang, Z.-L. You, *Aust. J. Chem.* **2012**, *65*, 343–350; DOI:10.1071/CH11424
- (c) H.-F. Guo, Y. Pan, D.-Y. Ma, P. Yan, *Chinese J. Inorg. Chem.* **2013**, *29*, 1447–1453.
4. N. P. Rai, V. K. Narayanaswamy, T. Govender, B. K. Manuprasad, S. Shashikanth, P. N. Arunachalam, *Eur. J. Med. Chem.* **2010**, *45*, 2677–2682. DOI:10.1016/j.ejmech.2010.02.021
5. (a) H. Kargar, M. Fallah-Mehrjardi, R. Behjatmanesh-Ardakani, H.A. Rudbari, A.A. Ardakani, S. Sedighi-Khavidak, K.S. Munawar, M. Ashfaq, M.N. Tahir, *Inorg. Chim. Acta* **2022**, *530*, 120677; DOI:10.1016/j.ica.2021.120677
- (b) T. Vijayan, J. Kim, M. Azam, S.I. Al-Resayes, A. Stalin, B.S. Kannan, A. Jayamani, A. Ayyakannu, S. Nallathambi, *Appl. Organomet. Chem.* **2022**, *36*, e6542; DOI:10.1002/aoc.6542
- (c) J.L. Hou, H.Y. Wu, C.B. Sun, Y. Bi, W. Chen, *Acta Chim. Slov.* **2020**, *67*, 860–865; DOI:10.17344/acsi.2020.5824
- (d) L.W. Xue, X. Fu, G.Q. Zhao, Q.B. Li, *Acta Chim. Slov.* **2021**, *68*, 17–24. DOI:10.17344/acsi.2020.5817
6. (a) C.-L. Zhang, X.-Y. Qiu, S.-J. Liu, *Acta Chim. Slov.* **2019**, *66*, 719–725; DOI:10.17344/acsi.2019.5241
- (b) L.-Y. He, X.-Y. Qiu, J.-Y. Cheng, S.-J. Liu, S.-M. Wu, *Polyhedron* **2018**, *156*, 105–110; DOI:10.1016/j.poly.2018.09.017
- (c) S. M. Wu, X. Y. Qiu, J. C. Wang, S. J. Liu, L. Y. He, *Russ. J. Coord. Chem.* **2019**, *45*, 378–384. DOI:10.1134/S1070328419040109
7. (a) C. Marzano, S. M. Sbovata, V. Gandin, D. Colavito, E. Del Giudice, R. A. Michelin, A. Venzo, R. Seraglia, F. Benetollo, M. Schiavon, R. Bertani, *J. Med. Chem.* **2010**, *53*, 6210–6227; DOI:10.1021/jm1006534
- (b) J. Zhao, S. H. Gou, G. Xu, *Inorg. Chim. Acta* **2014**, *409*, 310–314. DOI:10.1016/j.ica.2013.09.034
8. X. Zhou, X.-F. Meng, W.-N. Li, C. Li, J.-J. Ma, *Synth. React. Inorg. Met.-Org. Nano-Met. Chem.* **2016**, *46*, 202–205. DOI:10.1080/15533174.2014.963241
9. Bruker, SMART (Version 5.625) and SAINT (Version 6.01). Bruker AXS Inc., Madison, Wisconsin, USA, 2007.
10. G. M. Sheldrick, SADABS. Program for Empirical Absorption Correction of Area Detector, University of Göttingen, Germany, 1996.
11. G. M. Sheldrick, SHELXTL V5.1 Software Reference Manual, Bruker AXS, Inc., Madison, Wisconsin, USA, 1997.
12. J. Meletiadis, J. F. G. M. Meis, J. W. Mouton, J. P. Donnelly, P. E. Verweij, *J. Clin. Microbiol.* **2000**, *38*, 2949–2954. DOI:10.1128/JCM.38.8.2949-2954.2000
13. (a) S. Manna, E. Zangrando, H. Puschmann, S.C. Manna, *Polyhedron* **2019**, *162*, 285–292; DOI:10.1016/j.poly.2019.01.057
- (b) P. Chakraborty, S. Majumder, A. Jana, S. Mohanta, *Inorg. Chim. Acta* **2014**, *410*, 65–75. DOI:10.1016/j.ica.2013.10.013
14. (a) B. Sarkar, M.G.B. Drew, M. Estrader, C. Diaz, A. Ghosh, *Polyhedron* **2008**, *27*, 2625–2633; DOI:10.1016/j.poly.2008.05.004
- (b) U. Kumar, J. Thomas, N. Thirupathi, *Inorg. Chem.* **2010**, *49*, 62–72; DOI:10.1021/ic901100z
- (c) B.-H. Ye, X.-Y. Li, I.D. Williams, X.-M. Chen, *Inorg. Chem.* **2002**, *41*, 6426–6431. DOI:10.1021/ic025806+
15. (a) P. Talukder, S. Shit, A. Sasmal, S.R. Batten, B. Moubaraki, K.S. Murray, S. Mitra, *Polyhedron* **2011**, *30*, 1767–1773; DOI:10.1016/j.poly.2011.03.049
- (b) K. Bhar, S. Chattopadhyay, S. Khan, R.K. Kumar, T.K. Maji, J. Ribas, B.K. Ghosh, *Inorg. Chim. Acta* **2011**, *370*, 492–498; DOI:10.1016/j.ica.2011.02.055
- (c) A. Ray, G. Pilet, C.J. Gomez-Garcia, S. Mitra, *Polyhedron* **2009**, *28*, 511–520. DOI:10.1016/j.poly.2008.11.054
16. (a) M. F. Iskander, T. E. Khalil, R. Werner, W. Haase, I. Svoboda, H. Fuess, *Polyhedron* **2000**, *19*, 949–958; DOI:10.1016/S0277-5387(00)00340-5
- (b) S. Chandra, A. K. Sharma, *J. Coord. Chem.* **2009**, *62*, 3688–3700. DOI:10.1080/00958970903121305
17. (a) X.W. Dong, Y.G. Li, Z.W. Li, Y.M. Cui, H.L. Zhu, *J. Inorg. Biochem.* **2012**, *108*, 22–29; DOI:10.1016/j.jinorgbio.2011.12.006
- (b) C. Senol, Z. Hayvali, H. Dal, T. Hokelek, *J. Mol. Struct.* **2011**, *997*, 53–59. DOI:10.1016/j.molstruc.2011.04.037
18. (a) L.-W. Xue, Q.-L. Peng, P.-P. Wang, H.-J. Zhang, *Acta Chim. Slov.* **2019**, *66*, 694–700; DOI:10.17344/acsi.2019.5151
- (b) H. Adams, D.E. Fenton, P.E. McHugh, *Inorg. Chem. Commun.* **2004**, *7*, 147–150. DOI:10.1016/j.inoche.2003.09.026
19. R.-H. Hui, P. Zhou, Z.-L. You, *Synth. React. Inorg. Met.-Org. Nano-Met. Chem.* **2008**, *38*, 464–467. DOI:10.1080/15533170802255476
20. Q. Shi, L. Sheng, K. Ma, Y. Sun, X. Cai, R. Liu, S. Wang, *Inorg. Chem. Commun.* **2009**, *12*, 255–258. DOI:10.1016/j.inoche.2008.12.024

Povzetek

Sintetizirali smo štiri nove komplekse bakra(II), niklja(II) in cinka(II), $[\text{CuL}_2]$ (**1**), $[\text{Ni}_3\text{L}_2(4\text{-BrSal})_2(\text{CH}_3\text{COO})_2(\text{CH}_3\text{OH})_2]\cdot 2\text{CH}_3\text{OH}$ (**2**), $[\text{ZnBr}_2(\text{HL})_2]$ (**3**) in $[\text{ZnL}(\text{dca})]_n$ (**4**), pri čemer je L = 5-bromo-2-((ciklopentilimino)metil)fenolat, HL je 5-bromo-2-((ciklopentilimino)metil)fenol v zwitterionski obliki, 4-BrSal je monoanionska oblika 4-bromosalicilaldehida, dca je dicianamidni anion. Produkte smo karakterizirali z elementno analizo, IR in UV-Vis spektroskopijo. Strukture kompleksov smo določili z monokristalno rentgensko difrakcijo. Kompleks **1** je enojedrna spojina bakra(II) z dvoštevno rotacijsko simetrijo in atomom Cu v popačeni kvadratno planarni koordinaciji. Kompleks **2** je trijedrna spojina niklja(II) s centrom inverzije in atomi Ni v oktaedrični koordinaciji. Kompleks **3** je enojedrna spojina cinka(II), kompleks **4** pa polimerna spojina cinka(II) z mostovnimi ligandi dca. Cinkovi atomi so v tetraedrični koordinaciji. Preiskovali smo antimikrobno aktivnost dobljenih produktov.



Except when otherwise noted, articles in this journal are published under the terms and conditions of the Creative Commons Attribution 4.0 International License

Scientific paper

Potentiometric Study of the Dissociation and the Metal Complex-formation Competence of 5-(3,3-dimethyl-1-triazeno)-imidazole-4-carboxamide (Dacarbazine)

Hasan Atabey,¹ Faisal Naji Al-Obaidi^{2,*} and Hayati Sari³¹ Mersin National Education Directorate, Department of Analytical Chemistry, Mersin, Turkey.² Retired Associate Professor at the University of Al-Mustansiryia, Faculty of Science, Baghdad, Iraq.³ Faculty of Science and Arts, Department of Chemistry, Gaziosmanpasa University, 60250 Tokat, Turkey.

* Corresponding author: E-mail: faisalnaji@hotmail.com; fkhedher@hotmail.com

Tel: 44 7982600368

Received: 08-20-2022

Abstract

A potentiometric investigation has been carried out to disclose the coordination properties of Dacarbazine, 5-(3,3-dimethyl-1-triazeno)-imidazole-4-carboxamide (abbreviated DTIC) with particular transition metal ions (Zn^{2+} , Cu^{2+} , Ni^{2+} and Co^{2+}). The coordination of DTIC with these metal ions results in several complexes emerging in solution. The aim of this work is to determine the protonation constants of the DTIC and to show the extent of its coordination with (Zn^{2+} , Cu^{2+} , Ni^{2+} and Co^{2+}), in other words, establish the stability of the complexes formed between the DTIC and these metal ions by the determination of their stability constants. Experimental environments were organized to attain the coordination and measurements in aqueous solutions at 25 ± 0.1 °C and an ionic background of 0.1 mol dm^{-3} NaCl. The HYPERQUAD computer program was used to determine both the protonation and stability constants for the ligand and metal-ligand complexes respectively. DTIC has five protonation constants that can be obtained under experimental conditions used; 10.54, 20.15, 26.99, 32.02 and 36.01. The results are interpreted in terms of the basicity of the donor atoms and structural composition of the ligand. All the complexes produced in the solution are exhibited in speciation diagrams.

Keywords: DTIC; Stability constants; Protonation constants; Potentiometric titration; distribution diagram; HYPERQUAD.

1. Introduction

DTIC is renowned for its antitumor activity^{1–5} and as such is a drug utilised in chemotherapy for treating, specifically, malignant melanoma.^{6–8} This is the most devastating form of skin cancer and its rate is increasing globally, particularly among the white population who are highly exposed to sunlight.^{9,10} Malignant melanoma can also be located in other parts of the body, such as in the eye, the digestive tract and mucosal surfaces of lymph nodes.¹⁰ But it is plausibly treatable through surgical removal after diagnosis at initial phases.¹¹ DTIC can also be used to treat numerous types of cancer, namely Hodgkin lymphoma, Sarcoma, and Islet Cell Carcinoma of the pancreas.¹² DTIC is presumed to attack and eliminate cancer cells by adding alkyl groups to their DNA.^{10,13}

DTIC can be used in combination with various chemotherapy drugs for more effective treatment of ade-

nocarcinoma and soft tissue sarcoma.^{14–16} The anticancer properties of DTIC are boosted when introduced as a complex with certain metals such as copper (II), zinc (II), nickel(II) and Cobalt (II).^{6,12, 16–19} Therefore the coordination of DTIC with metal ions is an immediately relevant topic in medicine as these types of interactions have gained traction in the medical field. The antitumor properties of DTIC is manifested in its triazene group is responsible for the chemical and physical properties of the molecule.^{20,21}

The intention behind this investigation is to evaluate the coordination potential of the ligand DTIC by determining its dissociation constants and the stability of its complexes with some divalent ions, namely; Zn^{2+} , Cu^{2+} , Ni^{2+} , and Co^{2+} . DTIC has seven donor atoms so it is assumed to possess a variety of coordination sites.

2. Experimental

2.1. Reagents

All the reagents used in this investigation were of analytical grade. The transition metals and NaCl were purchased from (Merck), potassium hydrogen phthalate (KHF) and Borax ($\text{Na}_2\text{B}_4\text{O}_7$) from (Fluka). DTIC and 0.1 mol dm⁻³ NaOH and 0.1 mol dm⁻³ HCl as standard from Aldrich. CO₂ free double distilled deionized water was utilized in all experiments and prepared by means of an aqua MAX™ – Ultra water purification system (Young Linst); its resistivity was 18.2 M Ω cm⁻¹. Potentiometric titration was operated by using the Molspin pH meter™ with an Orion 8102BNUWP ultra combination pH electrodes. The temperature in the double-walled glass titration vessel was continuously controlled using a thermostat (DIGITERM 100, SELECTA) and kept at 25.0 ± 0.1 °C. The cell contents were stirred at a constant rate.

Solutions of metal (2×10^{-3}) mol.dm⁻³ were prepared from ZnCl₂, CuCl₂, NiCl₂, and CoCl₂, and the exact concentration was determined analytically by means of ethylene-diamine-tetra acetic acid (EDTA).²² Less diluted solution can be attained by volumetric dilution.

2.2 Potentiometric Measurements

The glass electrode was calibrated by means of two buffer solutions with pH of 4.005 (KHP) and pH = 9.018 (Borax) at 25.0 ± 0.1 °C following the guidelines of the Molspin manual.²³ NaOH was standardized with primary standard (KHP) solution by pH metric titration. HCl solution was prepared from concentrated HCl and its concentration was determined with standardized NaOH. All potentiometric titrations were undertaken in 100 mL double-walled glass vessel using combination electrode and the temperature was controlled as it mentioned in section 2.1 above. Atmospheric CO₂ was excluded from the titration vessel by pumping nitrogen gas (99.9%) through the titration vessel and to keep an inert atmosphere. The vessel was equipped with a small magnetic stirrer, and a securely fitting cap containing three holes to accommodate the combined electrode, combined nitrogen gas inlet and outlet ports and an automatic burette to deliver the alkali solution. The system was maintained at a fixed ionic strength of 0.1 mol.dm⁻³ by means of NaCl as background electrolyte. All potentiometric titrations took place in solution, in a 100 mL double – walled glass vessel using the Molspin automatic titration system as mentioned previously.

Approximately 0.01 mmol of DTIC was placed in the reaction cell to which the needed quantity of the supporting electrolyte 0.1 mol.dm⁻³ NaCl and 0.1 mol dm⁻³ HCl were added, followed by doubly distilled deionized water to bring the total volume to 50 mL pH measurements of the solution were taken after the addition of 0.03 cm³ of the standardized NaOH. Other solutions include the same

quantities as above in addition to about 0.01 mmol of transition metal ions of Zn²⁺, Cu²⁺, Ni²⁺ and Co²⁺ in each iteration, followed by adding doubly distilled deionized water to make up the total volume 50 mL as before.

The potentiometric titrations were arranged so that the ratio ligand to metal ion is 1:1 throughout the whole investigation, with each titration repeated three times. The pK_w value used in the calculations is 13.41. The data obtained from potentiometric titration were used to calculate the protonation constants of the ligand and stability constants of the metal complexes using the HYPERQUAD computer program.²⁴

3. Results and Discussion

3.1. Dissociation Constants of DTIC

The protonation and deprotonation properties of the ligand DTIC Figure 1 are studied potentiometrically in this investigation. Figure 2 and Figure 3 demonstrate the titration curve and the species distribution diagram of DTIC ligand respectively. Both protonation and deprotonation (dissociation) constants of this ligand are determined through a sequence of numerous separated potentiometric measurements. The distribution diagram Figure 3 displays various ligand species concentration depending on pH. Six species have been observed during the potentiometric titration course; L, HL, H₂L, H₃L, H₄L and H₅L, which are governed by five dissociation constants. The five

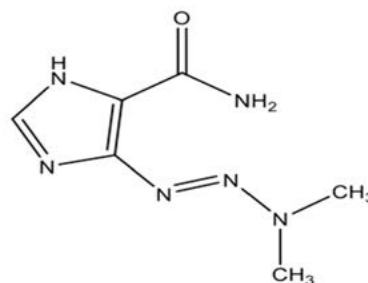


Figure 1. Chemical structure of DTIC

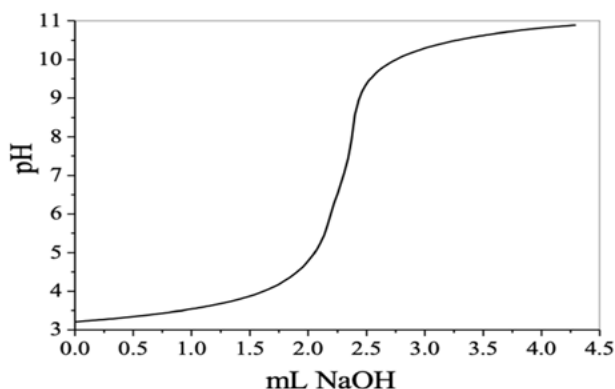


Figure 2. Titration curve of DTIC

values of the protonation and dissociation constants of the DTIC ligand are listed in Table 1. Figure 4 shows the fully protonated ligand, where the three nitrogen atoms in the Triazenyl group and oxygen atom of carbonyl group are protonated. DTIC can also exist in two tautomeric forms; a and b Figure 5. Tautomer b has a higher stability than tautomer a due to the formation of two intramolecular hydrogen bonds.^{25,26}

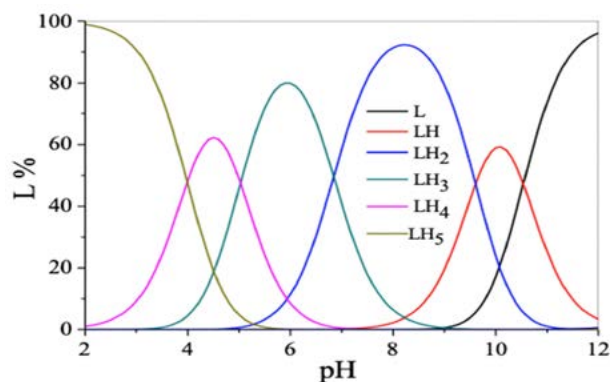


Figure 3. The species distribution diagram of DTIC

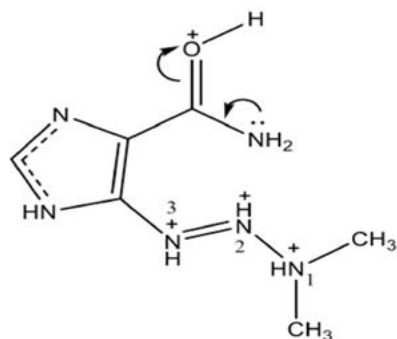


Figure 4. fully protonated DTIC

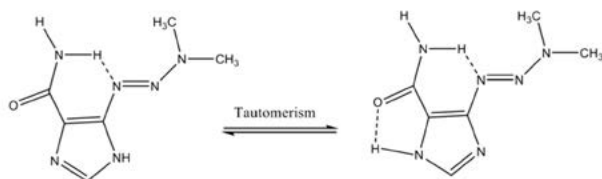


Figure 5. Tautomeric forms (a and b) of DTIC

The following equation represents the deprotonation equilibrium (charges are omitted for simplicity):



and the dissociation constants (K_n) are given as:

$$K_n = \frac{[\text{LH}_{n-1}][\text{H}]}{[\text{LH}_n]}$$

The species distribution diagram Figure 3 shows the pH range where all species of the ligand are formed and its concentration at any specific pH, represented as a percentage. The distribution diagram provides the requirements for the experimental conditions needed for the coordination between any species of the ligand with metal ions.

Table 1. Dissociation constants of the ligand (25.0 ± 0.1 °C, $I = 0.1$ mol dm⁻³ NaCl in aqueous solution)

Ligand	Species	Log ₁₀ β	pK _a values
DTIC	H ₅ L	10.54	3.99
	H ₄ L	20.15	5.03
	H ₃ L	26.99	6.84
	H ₂ L	32.02	9.61
	HL	36.01	10.54

Theoretical calculations were used to determine the protonation order of the three nitrogen atoms in DTIC. The proton affinity (PA) of each donor atom engaged in the protonation process, can be calculated from the following equation:²⁷

$$\text{PA}(\text{B}) = 367.2 + \Delta H_f(\text{B}) - \Delta H_f(\text{HB}^+)$$

PA (B) is the proton affinity of molecule B, $\Delta H_f(\text{B})$ and $\Delta H_f(\text{HB}^+)$ are the heat of formation of molecule B and protonated BH^+ respectively, and 367.2 is the heat formation of H^+ .

Table 2. The calculated $\Delta_f H$ of TE and PA values for DTIC ligand and its mono-protonated forms using the PM3 method.

Species	PM3		
	T.E. (kcal/mol)	Hf (kcal/mol)	PA
DTIC	-49127,38	42.68	-
1 N-H ⁺	-49318,84	194.28	205.09
2 N-H ⁺	-49309,58	155.27	195.82
3 N-H ⁺	-49319,66	142.21	205.95

The protonation order in Table 2 displays the extent of the basicity of the donor atoms in the ligand. This is significant in demonstrating the coordination between the ligand and the proton or metal ion as well as the expectation of the coordination positions. The protonation constant of a ligand is essential to measuring its basicity.^{28,29}

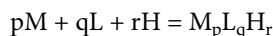
N#3 in Figure 4 is more basic than the other nitrogen donor atoms in the triazenyl group, and a probable intra-hydrogen bonding is presumed to develop with the hydrogen of the amide group. Intra-hydrogen bonding is also possible between the oxygen of the carbonyl group and the proton of the nitrogen in the imino group of the imidazole

moiety Figure 5.²⁵ This bonding will not be expected to preclude the coordination process between the ligand and metal ion; this is due to the tenuous construction of this bonding.^{30,31} The existence of a C=O dipole and, to a smaller degree, an N-C dipole in the DTIC, allows it to operate as a hydrogen bond acceptor. The C=O dipole consists of a π -bonding structure and its oxygen atom has higher electronegativity than nitrogen in the N-C group, giving the carbonyl group greater electronegativity. DTIC can engage in hydrogen bonding with water molecules thus increasing the water solubility of the ligand in aqueous solutions. The high electron withdrawing environment of the carbonyl group through resonance is due to the delocalization of the lone pair of electrons on the nitrogen of amide moiety, thereby decreasing the basicity of the nitrogen atom. In other words, the electron withdrawal environment produced by this conjugated system will constrain the capability of the lone pair of electrons in the amide group to coordinate with electrophiles.

The ligand distribution diagram Figure 3 identifies the initial experimental conditions of the coordination between the ligand and metal ion.^{31,32} Six species exist in solution within the pH range between above 2 to just lower than 12, the above mentioned diagram Figure 3 shows clearly the pH range and the amount of each species exists in the solution. Five protonation and five deprotonation (dissociation) constants are obtained in this study. pK_a of value 3.99 Table 1 is associated with the nitrogen N#2, where values are reported in literature 2.33 and 2.30 for monocyclic and bicyclic diazine respectively.^{33,34} The pK_a value of 5.03 is related to the oxygen in carbonyl group, while pK_a of 6.84 is associated with pyridine like nitrogen atom in the imidazole moiety.³⁵ The other two pK_a values 10.54 and 9.61 are associated with N#3 and N#1 respectively.

3. 2. Stability Constants

The stability constants of mono-binary complexes of Dacarbazine with some divalent metal ions in aqueous solution were determined with the HYPERQUAD²⁴ computer program. The overall stability (β_{pqr}) constants for the complex formed from the metal ion (M), ligand (L) and acid (H):



can be represented by:

$$\beta_{pqr} = [M_pL_qH_r]/[M]_p[L]_q[H]_r$$

where p, q and r are the respective stoichiometric coefficients. Various probable species form in the solution depending on pH; with only mono-binary complexes are formed for all the metal ions and possible existence of hydroxyl complexes at a high pH. The hydrolysis process

which leads to the formation of the hydroxyl species in our system involves the water molecules bound to the metal ion and pH.^{36,37} This happens as a result of the increase in acidity of the attached water molecules due to the formation of the coordinated bond.³⁶ The formation of coordinated bonds will induce the whole electronic charge distribution and increase the charge withdrawal environment towards the metal ion.^{36,37} There is no indication of the chloro-complexes existing in the solution. Data in Table 3 represent values of stability constants for all species formed in the solution at the experimental conditions set.

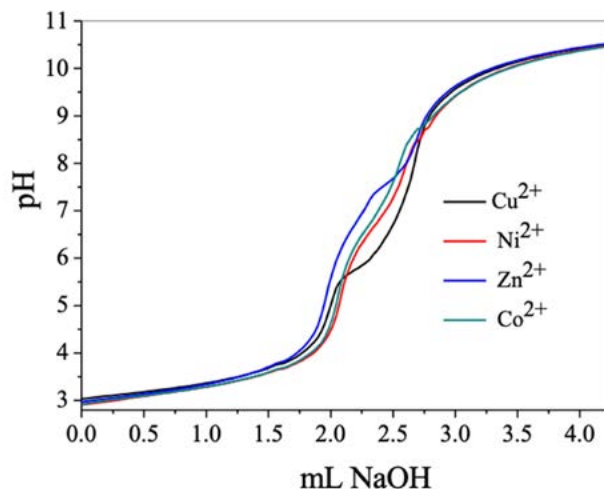


Figure 6. Titration curves of DTIC with Zn(II), Cu(II), Ni(II) and Co(II) at (298 K, $I=0.1 \text{ mol dm}^{-3}$ NaCl in aqueous solution.

Table 3. Stability constants of DTIC complexes with some divalent metal ions (25.0 ± 0.1 °C, $I=0.1 \text{ mol dm}^{-3}$ NaCl in aqueous solution).

Species	Cu ²⁺	Ni ²⁺	Zn ²⁺	Co ²⁺
<i>mhl</i>	$\log_{10}\beta$			
101	19.61 (1)	18.30 (2)	19.10(6)	18.57 (1)
111	26.74 (3)	25.81 (6)	26.66 (4)	26.36 (6)
121	32.04 (4)	32.45 (9)	33.73 (6)	33.09 (7)
131	38.49 (5)	38.53 (9)	39.77 (8)	39.25 (8)
1–11	10.23 (4)	9.31 (9)	11.25 (6)	9.14 (8)
1–21	0.16 (3)	0.09 (5)	1.66 (7)	0.35 (1)
σ (sigma)	0.79	1.51	1.40	1.28

Conditions were organised as a 1:1 ligand to metal ratio throughout all experiments. Owing to substantial basicity and the bi-dentate mode of the DTIC ligand, mono-binary complexes were formed in solution at this ratio. All complexes of the ligand with all metal ions were present in the solution at early stages of coordination. This is additional evidence of DTIC's basicity strength.

The chemical, physical and anti-tumour properties are due to the existence of triazenyl group in the DTIC li-

gand.²⁰ The more basic nitrogen atom in this group is N#3 (see Table 2), so it can be assumed that the coordination of the DTIC ligand will take place through this nitrogen atom. Since the DTIC is of bi-dentate nature, the most appropriate donor atoms to coordinate with the metal ions are the nitrogen N#3 in the triazenyl group and the nitrogen atom of the amido group, where the six membered ring is formed. Possible intra-hydrogen bonding is expected to formulate between the oxygen of the carbonyl group and hydrogen of the imine group in the imidazole moiety.²⁵

The size and structure of the ligand might develop the possibility of steric hindrance when coordinating with a metal ion to form a complex. But the reasonably high stability constants of the complexes in all metal ions used in this study (Table 3) reveal that steric hindrance has less impact than would be expected. This might be justified on the basis that the DTIC ligand is efficient in modifying its shape when the coordination process takes place, keeping steric hindrance at its minimum.³⁸

Comparing titration curves of the free ligand Figure 2 with that of the metal-ligand complexes Figure 6 reveal that the latter half of the curves (of the metal ligand complexes) will shift downwards towards a lower pH. This is due to the liberation of protons during the formation of hydroxyl complexes. This complies with the species distribution curves Figure 7 a-d as they indicate the formation hydroxyl complexes at a high pH. The quantity of protons liberated varies with the strength of the metal-bond.

All species of Zn-DTIC are higher in stability than the corresponding Cu^{2+} , Ni^{2+} and Co^{2+} (except Cu-HL and Cu-L species) Table 3. This might indicate that the Zn-DTIC complex is susceptible in modifying its structure from octahedral $[\text{Zn}(\text{H}_2\text{O})_6]^{2+}$ to a tetrahedral $[\text{Zn}(\text{DTIC})(\text{H}_2\text{O})_2]^{2+}$ when the complex is formed.³⁶ The extra stability is due to an increase in entropy as a result of the alteration in structure.³⁷ Zn-DTIC species forms in solution throughout a broad range of pH 4 – 11 Figure 7-a. At pH range 4.5–5.5 the only species that exist in solution are Zn-H₃L and Zn-H₂L, with a maximum percentage of Zn-H₃L over 90% of the total concentration of the metal ions at pH 4, while the species Zn-H₂L forms just above pH 5 and reaches its maximum percentage of 65% of the metal ions at pH 6.5. Zn-HL forms initially at pH just above 6 and attains a maximum percentage of 40% of the metal ion at pH 7.25. Zn-L starts to form in an appreciable amount at pH just above 7 and reaches maximum percentage of 35% at pH 7.75. At higher pH values, between 8 and 11, the main constituents in the solution are Zn-H₁L and ZnH₂L. The Zn-H₁L species reaches a peak of 75% at pH 9 while ZnH₂L starts to form at pH just after 9 and achieves a peak at 95% with pH 11.

The mono-binary Zn-DTIC system (and also other systems of other metal ions) subsists with numerous species mentioned earlier, with each species initiated from its predecessor as a consequence of proton release. The de-

protonation process, which is ongoing during the coordination progression, occurs as a consequence of the coordinated bond formation, which yields electron withdrawal in the direction of the metal ion. This leads to an increase to the dissociation of water molecules attached to the metal ions to produce hydroxyl groups. For this reason, the coordination between the metal ion and ligand will increase the dissociation of these water molecules, and any another acidic hydrogen in the complex, as a result of electron density shifted from the ligand towards the metal ion.

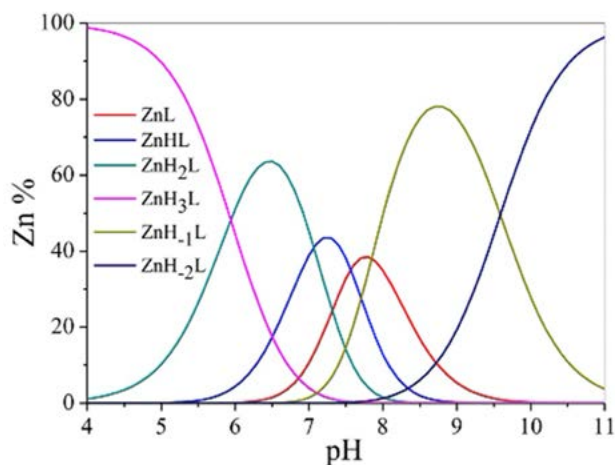


Figure 7-a. Species distribution diagram for Zn-DTIC system.

Figure 7-b displays all the probable species from the coordination of Cu^{2+} with the DTIC; six species of Cu-DTIC complex can be traced by means of our computer program when produced in detectable quantities. The complexes formed at pH levels between 4 and 6 are Cu-H₃L, Cu-H₂L and Cu-HL. The dominant species under pH 5 is Cu-H₃L, and at pH 5.75, the species Cu-H₂L, which comprises 10% of all of the metal ions at its peak. The species Cu-HL forms at just above pH 5, and at pH 6.5 reaches its maximum proportion of 70% of all of metal ions. The

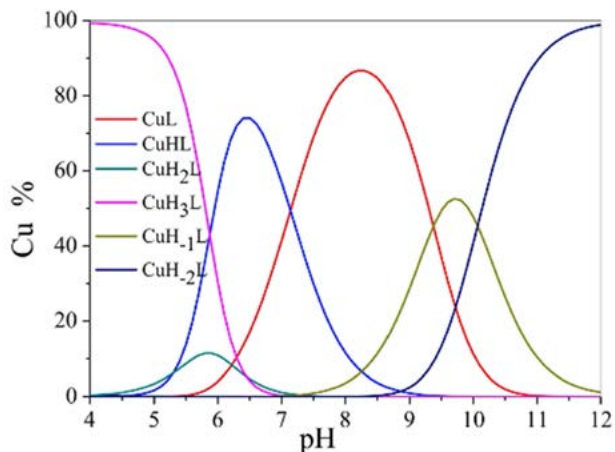


Figure 7-b. Species distribution diagram for Cu-DTIC system.

species Cu-L starts to form at pH just above 6 and at pH 8.5 reaches its maximum of 85% of all of the metal ions. At a high pH, there is a possibility that the hydrated Cu(II) ion would hydrolyse, forming hydrolysed species.³⁵ When the pH value exceeds 8, Cu-H₁L (hydrolysis species) starts to form and reaches its maximum of about 50% of all metal ions at pH approximately 9.75, followed by the formation of the second hydrolysed species CuH₂L at just about pH 9 and reaches its maximum at pH above 11 (Figure 7-b). The formation of the hydrolysed species in the solution also depends on the presence of water molecules on the solvated metal ion and type of metal ion.³⁶

Figure 7-c displays the distribution diagram for a Ni-DTIC system which shows resemblance to the cases of both Cu-DTIC system and Zn-DTIC system. All the species of the Ni-DTIC system formed almost in the same pH range as that of Cu(II)-DTIC system. This indicates that the species of both Ni-DTIC and Cu-DTIC are similar in strength (Table 3). Ni-H₃L, Ni-H₂L and Ni-HL formed in perceptible amounts in the pH range of 4 to 6.5, which is almost the same range as that of the Cu(II) species. The maximum percentage of Ni-H₃L occurs in the solution at pH 4, while the maximum percentage of Ni-H₂L is at 45%, formed at pH around 6.5. The Ni-HL species starts to form at pH just above 6 and reaches its maximum of 55% at pH 7.25. The maximum percentage composition of Ni-L is 75% of the total metal ions at pH 8.25. At pH just above 8 the hydrolysed species Ni-H₁L started to form and reached its maximum at 35% of the total metal ions at pH 9.25, Ni-H₂L starts at pH just above 8.5 and rises to above 10.5.

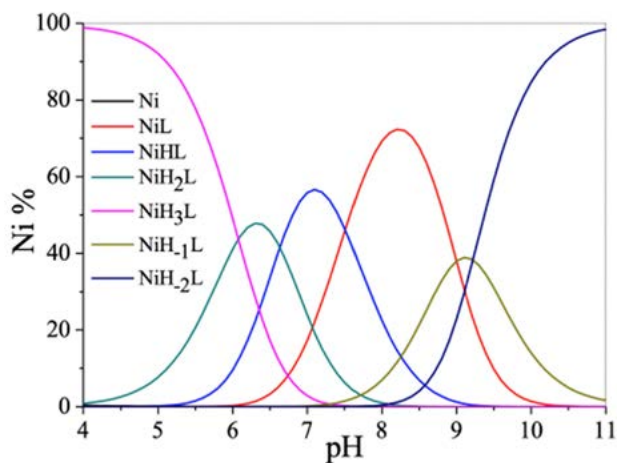


Figure 7-c. Species distribution diagram for Ni-DTIC system

Similarly, Co(II) also forms 6 species as a result of coordination between the metal ion and DTIC Figure 7d. The coordination starts at a low pH to form the Co-H₃L species followed by the species Co-H₂L as it starts to form just above pH 5 and reaches maximum of 50% at pH 6.5. Another species presents in the solution is Co-HL which reaches a maximum of about 60% at pH 7.25. Co-L species

forms at pH just over pH 7 and exists and attains a maximum percentage of 70% at about pH 8.5 and fades away at approximately pH 10.

Hydrolysed species start to occur in significant amounts at pH exceeding 8 as a result of the dissociation of water molecules attached to the partially complexed metal ion in the basic medium as mentioned above. Only two hydrolysed species occur in the experimental conditions used, Co-H₁L and the Co-H₂L, with the first species existing at a maximum of about 15% at pH 9 whilst the latter becomes the dominant species at pH above 10 Fig 7-d.

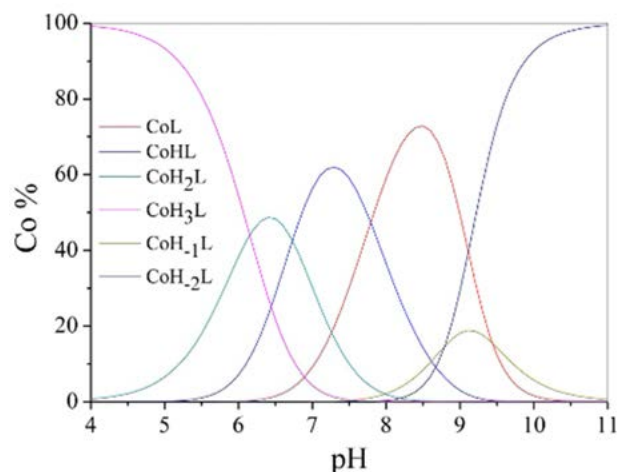


Figure 7-d. Species distribution diagram for Co-DTIC system.

4. Conclusion

The importance of DTIC is due to its anticancer properties, used on its own and combined with other drugs in chemotherapy treatments. These properties are enhanced when DTIC is present as a complex with certain metals. The coordination between the DTIC ligand and some selected di-valent transition metal ions are achieved potentiometrically, yielding numerous complexes including hydroxyl complexes in the solution depending on pH. This investigation was aimed to determine the dissociation constants of the ligand and the stability constants of the ligand-metal complexes. Experimental conditions were arranged for 1:1 ligand to metal ratio, so only mono-binary complexes were expected to form in the solution. Intra-hydrogen bonding is presumed to occur in both, the free ligand and complexed ligand *via* the oxygen of the carbonyl group and hydrogen in imidazole moiety. All metal-ligand species formed in the solution are exhibited in the speciation diagrams provided.

Acknowledgement

The authors would like to gratefully acknowledge the financial support of the Scientific Research Council of Gaziosmanpaşa University for our research.

Declarations

Conflict of interest The authors declare that they have no conflict of interest.

5. References

1. T. Kan, S. Takahagi, M. Kawal, D. Matsubara, A. Tanaka, M. Hide, *J. Dermatol.* **2020**, *47*, 907–910. DOI:10.1111/1346-8138.15408
2. K. Maktia, H. Hara, E. Sano, Y. Okamoto, Y. Ochiai, T. Ueda, T. Nakayama, S. Aizawa, A. Yoshino, *Int. J. Oncol.* **2019**, *54*, 1864–1874. DOI:10.3892/ijo.2019.4743
3. S. Bhatia, S. S. Tykodi, J. A. Thompson, *Oncology* **2009**, *23*, 488–496.
4. M. Respondek, A. Beberok, Z. Rzepka, J. Rok, *Fundam. Clin. Pharmacol.* **2020**, *34*, 20–31. DOI:10.1111/fcp.12503
5. S. Kakumanu, J. B. Tagne, T. A. Wilson, R. J. Nicolosi, *Nanomedicine* **2011**, *7*, 277–283. DOI:10.1016/j.nano.2010.12.002
6. C. G. Hartinger, M. G. Ferri-Mendoza, A. A. Nazarov, B. K. Keppler, *Polyhedron* **2006**, *25*, 1971–1978. DOI:10.1016/j.poly.2005.12.022
7. M. L. Benitz, C. B. Bender, T. L. Oliveria, K. M. Schachneider, T. Collares, F. K. Seixas, *Appl. Microbiol. Biotechnol.* **2019**, *103*, 7903–7916. DOI:10.1007/s00253-019-10057-0
8. E. Eskin, D. Polat, A. Erdem, *Electroanalysis* **2019**, *31*, 2012–2019. DOI:10.1002/elan.201900284
9. C. Garbe, U. Leiter, *Clin. Dermatol.* **2009**, *27*, 3–9. DOI:10.1016/j.clindermatol.2008.09.001
10. H. Asiabi, Y. Yamini, M. Alipour, S. Shamasayei, S. Hosseinkhani, *J. Mater. Sci.* **2019**, *97*, 96–102. DOI:10.1016/j.msec.2018.12.017
11. A. Piotrowska, J. Wierzbička, A. Rybarczyk, R. C. Tuckey, A. T. Slominski, M. A. Zmiewski, *Int. J. Oncol.* **2019**, *54*, 1481–1495. DOI:10.3892/ijo.2019.4725
12. T. Kumari, J. Shukla, S. Joshi, *Int. J. Chem. Sci.* **2011**, *9*, 1751–1762.
13. S. L. Safgren, J. M. Reid, R. Rios, M. M. Ames, *J. Chromatogr. B* **2001**, *754*, 91–96. DOI:10.1016/S0378-4347(00)00586-7
14. D. C. Lev, A. Onn, V. O. Melinkova, C. Miller, V. Stone, M. Ruiz, E. C. McGary, H. N. Ananthaswamy, J. E. Price, M. Bar-Eli, *J. Clin. Oncol.* **2004**, *22*, 2092–2100. DOI:10.1200/JCO.2004.11.070
15. Y. M. Temerk, M. M. Kamal, M. S. Ibrahim, H. S. M. Ibrahim, W. Schuhmann, *Electroanalysis* **2011**, *23*, 1638–1644. DOI:10.1002/elan.201100038
16. A. M. M. Eggermont, J. M. Kirkwood, *Eur. J. Cancer* **2004**, *40*, 1825–1836. DOI:10.1016/j.ejca.2004.04.030
17. Y. Temerk, H. Ibrahim, *J. Pharm. Biomed. Anal.* **2014**, *95*, 26–33. DOI:10.1016/j.jpba.2014.02.010
18. G. Swiderski, R. Lazny, M. Sienkiewicz, M. Kalinowska, R. Swislocka, A. O. Acar, A. Golonko, M. Matejczyk, W. Lewandowski, *Materials* **2021**, *14*, 1–21. DOI:10.3390/ma14123274
19. T. Iwamoto, Y. Hiraku, M. Okuda, S. Kawanishi, *Pharm. Res.* **2008**, *25*, 598–604. DOI:10.1007/s11095-007-9413-2
20. G. Roman, E. N. Grau, A. D. Company, A. Juan, S. Simonetti, *A Letters Journal Exploring the Frontiers of Physics* **2019**, *126*, P1–P6. DOI:10.1209/0295-5075/126/58002
21. F. Marchesi, M. Turriziani, G. Tortorelli, G. Avvisati, F. Torino, L. Vecchis, *Pharmacol. Res.* **2007**, *56*, 275–287. DOI:10.1016/j.phrs.2007.08.003
22. G. H. Jeffery, J. Bassett, J. Mendham, R. C. Denney: Vogel's Textbook of Quantitative Chemical Analysis sixth edition. Longman, London **1999**.
23. L. D. Pettit, : Molspin Software for Molspin pH Meter; Sourby Farm: Timble. Otley, LS21 2PW U. K **1992**.
24. P. Gans, A. Sabatini, A. Vacca, *Talanta* **1996**, *43*, 1739–1753. DOI:10.1016/0039-9140(96)01958-3
25. M. Amirmostofian, J. P. Jaktaji, Z. Soleimani, K. Tabib, F. Tanbakosazan, M. Omarani, F. Kobarfard, *Iran. J. of Pharm. Res.* **2013**, *12*, 255–265.
26. M. J. S. Dewar, K. M. Dieter, *J. Am. Chem. Soc.* **1986**, *108*, 8075–8086. DOI:10.1021/ja00285a033
27. H. Yu, R. Kuhne, R. Ebert, G. Schuurmann, *J. Chem. Inf. Model* **2010**, *50*, 1949–1960. DOI:10.1021/ci100306k
28. S. Spirtovic-Halilovic, D. Završnik, *J. Serb. Chem. Soc.* **2010**, *75*, 243–248. DOI:10.2298/JSC1002243S
29. S. A. Shteingolts, V. V. Davydova, M. A. Mar'yasov, O. E. Nasakin, R. R. Fayzullin, O. A. Lodochnikova, *J. Struct. Chem.* **2020**, *61*, 928–937. DOI:10.1134/S002247662006013X
30. F. N. Al-Obaidi, H. Sari, M. Macit, *J. Chem. Eng. Data* **2010**, *55*, 5576–5580. DOI:10.1021/je1003803
31. H. Atabey, H. Sari, F. N. Al-Obaidi, *J. Solution Chem.* **2012**, *41*, 793–803. DOI:10.1007/s10953-012-9830-7
32. H. J. S. Machado, A. Hinchliffe, *J. Mol. Struct. (Theochem)* **1995**, *339*, 255–258. DOI:10.1016/0166-1280(94)04108-5
33. A. O. Eseola, N. O. Obi-Egbedi, *Spectrochim. Acta A* **2010**, *75*, 693–701. DOI:10.1016/j.saa.2009.11.041
34. H. Sari, A. K. Covington, *J. Chem. Eng. Data* **2005**, *50*, 1425–1429. DOI:10.1021/je050091l
35. J. Burgess, Metal ions in Solution. Jon, Ellis Horwood Limited, Division of John Wiley & sons, Chichester **1978**.
36. J. E. Huheey, E. Keiter, R. L. Keiter, Inorganic chemistry, Principles of Structure and Reactivity 4th edition. Harper Collins, New York **1993**.
37. H. Sari, F. N. Al-Obaidi, M. Macit, H. Atabey, *J. Solution Chem.* **2011**, *40*, 1618–1628. DOI:10.1007/s10953-011-9733-z

Povzetek

Izvedli smo potenciometrično raziskavo koordinacijskih lastnosti dakarbazina, 5-(3,3-dimetil-1-triazeno)-imidazol-4-karboksamida (DTIC), z ioni nekaterih prehodnih kovin (Zn^{2+} , Cu^{2+} , Ni^{2+} in Co^{2+}). Koordinacija DTIC z omenjenimi ioni povzroči nastanek večjega števila kompleksov v raztopinah. Namen dela je določiti konstante protonacije DTIC in pokazati obseg njegove koordinacije z ioni Zn^{2+} , Cu^{2+} , Ni^{2+} in Co^{2+} oziroma določiti stabilnosti kompleksov med DTIC in temi ioni z določitvijo njihovih konstant stabilnosti. Meritve smo izvedli v vodnih raztopinah pri 25 ± 0.1 °C v 0.1 mol dm^{-3} NaCl. Za izračun konstant protonacije in stabilnosti za ligand in komplekse smo uporabili program HYPERQUAD. DTIC ima pet konstant protonacije, katerih vrednosti znašajo pod eksperimentalnimi pogoji 10.54, 20.15, 26.99, 32.02 in 36.01. Rezultate smo interpretirali glede na bazičnost donorskih atomov in strukture liganda. Vsi kompleksi, nastali v raztopinah, so prikazani na speciacijskih diagramih.



Except when otherwise noted, articles in this journal are published under the terms and conditions of the Creative Commons Attribution 4.0 International License

Scientific paper

Kinetic Studies, Antioxidant Activities, Enzyme Inhibition Properties and Molecular Docking of 1,3-Dihydro-1,3-Dioxoisindole Derivatives

Hasan Yakan,^{1,*} Seyhan Ozturk,² Elvan Uyar Tolgay,² Semiha Yenigun,² Sarmad Marah,² Tugrul Doruk,³ Tevfik Ozen^{2,*} and Halil Kutuk²

¹ Ondokuz Mayıs University, Faculty of Education, Department of Chemistry Education, 55139, Atakum-Samsun, Turkey.

² Ondokuz Mayıs University, Faculty of Sciences, Department of Chemistry, 55139, Atakum-Samsun, Turkey.

³ Ondokuz Mayıs University, Faculty of Sciences, Department of Molecular Biology and Genetics, 55139, Atakum-Samsun, Turkey.

* Corresponding author: E-mail: E-mail:hasany@omu.edu.tr; tevfkoz@omu.edu.tr

Received: 11-18-2022

Abstract

The acid catalyzed hydrolysis of the *N*-(*p*-substitutedphenyl) phthalimides in three different acids was investigated at 50.0 ± 0.1 °C. Two different antioxidant activity tests as DPPH* and ABTS** scavenging activities, and three various enzyme inhibition activity tests as urease, acetylcholinesterase (AChE), and butyrylcholinesterase (BChE) inhibition activities, were applied. Compound **3c** (2.03 µg/mL) has higher antioxidant activity than other compounds and standards according to DPPH test. In AChE assay, compounds **3a** and **3b** (13.13 and 9.59 µg/mL) has higher enzyme inhibition activity than the standard Galantamine (14.37 µg/mL). In BChE and urease tests, all compounds (6.84-13.60 and 10.49-17.73 µg/mL) have higher enzyme inhibition activity than the standard Galantamine (49.40 µg/mL) and thiourea (26.19 µg/mL), respectively. The molecule interaction for each of the three compounds with the active sites of AChE, BChE, and urease enzymes was examined via molecular docking simulations.

Keywords: Arylphthalimides; Kinetic Studies; Acid-Catalyzed Hydrolysis; Antioxidant Activity; Enzyme Inhibitor; Molecular Docking.

1. Introduction

Phthalimides (1,3-dihydro-1,3-dioxoisindoles) are a significant class of drugs showing antimicrobial,¹ antibacterial,² antituberculosis,³ cytotoxicity,⁴ anticancer,⁵ analgesic,⁶ acetylcholinesterase inhibitors,⁷ an inhibitor of nitric oxide synthase to human neuronal,⁸ and antiproliferative.⁹ These compound's derivatives showed various biological activities, were substantiated as an exciting pharmacophore and could interact with the peripheral anionic site of the enzymes. Some phthalimides synthesize as multi-function compounds and are determined to be a stabled multi-target active molecule that showed strong and stable activities against urease and cholinesterase inhibitors.¹⁰

They have recently attracted a noticeable amount of attention due to their interesting anti-inflammatory,¹¹ and anti-angiogenic specialties and their possible use in treating AIDS reasoned by HIV.¹² Because of its pharmaceuti-

cal, biological, and industrial importance, the synthesis of *N*-arylphthalimides has attracted considerable interest in the literature.¹³ *N*-Arylphthalimides have been commonly prepared with a phthalic acid anhydride and primary amines. This is the most known method in the literature.¹⁴

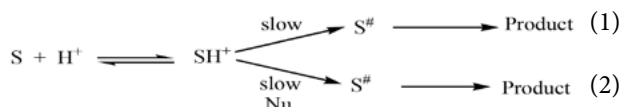
Antioxidants are the reducing agents that have been used to balance many free radicals. Free radicals are groups of atoms or atoms with a single number of electrons. They can be composed that oxygen molecules interacting with specific molecules in drugs, atmospheric pollutants, and mitochondrial respiratory chain reactions. Free radicals are dangerous to persons and harm all fundamental components of cells, with the inclusion of proteins, cell membranes, and DNA, and reason for various pathological statuses such as myocardial infarction, diabetes mellitus, atherosclerosis, asthma, arthritis, inflammation, neurodegenerative, carcinogenesis, and anemia diseases.¹⁵ Non-enzymatic and enzymatic antioxidants may avoid this oxidative damage in the human body. Still, it

may disrupt these protective mechanisms and the various pathological processes and, therefore, the reason for damage.¹⁶

Acetylcholinesterase (AChE) is cared for with the growth of cells and aids the development of regeneration of nerves and neurons.¹⁷ AChE is a significant member of the nervous system; therefore, adverse effects on AChE activity can induce neurotoxicity.¹⁸ Butyrylcholinesterase (BChE) is connected to physical factors such as the hydrolysis of noncholine and choline esters. Consequently, it has an essential role in neurotransmission and anesthesia.¹⁹ A significant rise in acetylcholinesterase activity is spied in Alzheimer's disease (AD) early phase, yet, the butyrylcholinesterase activity progressively advances in Alzheimer's late grades. Therefore, both BChE and AChE are pretty medicinal aims to improve the cholinergic explicit and idea the AD.²⁰ Urease enzyme inhibitors can enter into a vital to against the negative effect of urease in living organisms. These inhibitors are efficient against a few crucial infections induced by the secretion of urease by *Helicobacter pylori*.²¹ This bacteria releases urease, and the excretion of ammonia defends it from the acidic medium of the stomach.²²

In recent years, molecular docking techniques were performed upon massive enzyme numbers, including urease and cholinesterase. This study is used to understand and provide important information about the powerful binding of the inhibitor and enzymes through a set unlike protein-ligand interactions.²³ It is also repeatedly used to anticipate the binding orientation of ligands to the target protein/s and assess the candidate inhibitor's binding affinity, activity, and stability.²⁴

Acid-catalysed reactions as general and specific acid catalysis come off the two distinct ways.²⁵ Generally, acidic kinds catalyse the reaction according to their own characteristics. The substrate protonation becomes the rate-determining step, and the conjugate acid of the substrate reaction products in a quick step.²⁵ The only source of protonation is H_3O^+ in specific reactions that are acid-catalysed, which can occur in two distinct processes. A unimolecular mechanism A-1, a protonated substrate formed in the rate-limiting step and afterward transforms quickly into products (Eq.1 in Scheme 1). If the nucleophile attacks the protonated substrate (Nu; e.g., always water) in the rate-limiting step, a bimolecular mechanism A-2 is described (Eq.2 in Scheme 1).²⁵ Since the reaction mechanism is firmly specified under low acidity and high acidity conditions, a series of standards that meet the kinetic data, such as the order of acid catalytic efficiency,²⁶ shapes of profiles,²⁷ excess acidity treatment,²⁸ thermodynamic data,²⁹ and affection of substituent³⁰ are available.



Scheme 1. Specific acid-catalysed reactions. (1) Unimolecular reaction A-1, (2) Bimolecular reaction A-2

A bimolecular mechanism at low acidity is indicated by substituent effect, entropy effects and excess acidity method, with analysis of the data by the Cox–Yates.³¹ A unimolecular mechanism is observed at higher acidities. A unimolecular mechanism has ΔS^\ddagger of about 0 to $-41.7 \text{ JK}^{-1} \text{ mol}^{-1}$, while the reaction with a bimolecular mechanism has ΔS^\ddagger of -62.8 to $-125.6 \text{ JK}^{-1} \text{ mol}^{-1}$ in the acid-catalyzed hydrolysis of compounds proceeding.²⁹ The kinetic studies of amidosulfites,³² *N*-(4-substitutedarylsulfonyl) phthalimides,³³ (4-methoxybenzoyl)-4-tolueniminosulfonate,³⁴ and *N*-(4-substitutedarylthio) phthalimides³⁵ have been reported in the literature. There are no kinetic studies, and biological evaluations have been conducted on the *N*-(4-substitutedaryl) phthalimides. This work, it was aimed to obtain more information about kinetic studies and acidic hydrolysis activity of a series of *N*-(4-substitutedaryl) phthalimides **3a-c**. Moreover, antioxidant activities of the compounds were determined with two specific tests as DPPH· and ABTS·⁺ scavenging methods and were investigated three various enzyme inhibition activities as urease, acetylcholinesterase, and butyrylcholinesterase. Molecular docking simulations was used for the molecule interaction for each of the three compounds with the active sites of acetylcholinesterase, butyrylcholinesterase, and urease enzymes.

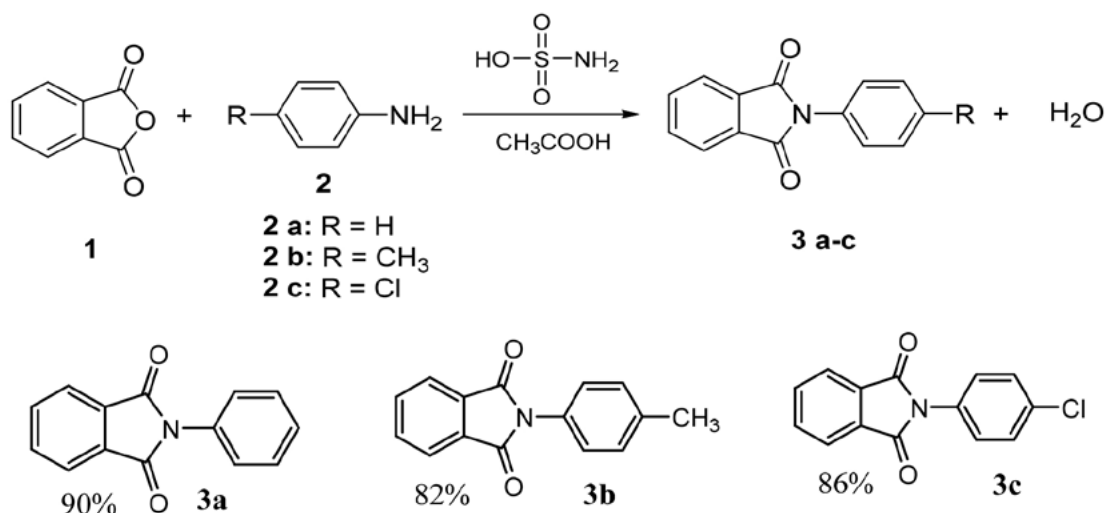
2. Experimental

2.1. General Remarks

Sigma, Riedel-de Haën, and Merck, what provide the all reagents used. The 1H and ^{13}C NMR spectra were determined on a Bruker Avance 300 MHz Spectrometer (Germany) at 300 MHz and 75 MHz, respectively, in $CDCl_3$ using tetramethylsilane as the internal calibration standard. IR spectra were saved with a Vertex 80v FT-IR (Germany). Melting point measurements were made by Electrothermal 9100 Melting Point Apparatus (China). Kinetic measurements of all compounds were obtained with a GBC Cintra 20 model Ultraviolet-Visible (UV-VIS) Spectrophotometer (Australia).

2.2. Synthesis

A mixture of phthalic anhydride (5 mmol) and aniline (5 mmol) was dissolved in acetic acid (25 mL). Also, sulphamic acid (10 mol%) was added as a catalyst. The reaction mixture was refluxed at $110 \text{ }^\circ\text{C}$ for 10 minutes. After that, the reaction mixture was poured into water. The solid was collected by filtration under vacuum, washed with ethyl acetate, and recrystallized in ethanol to give **3a-c** as white crystals in Scheme 2. The products were prepared with minor modifications according to a reported procedure³⁶.



N-(Phenyl) phthalimide (**3a**) *N*-(4-Methylphenyl) phthalimide (**3b**) *N*-(4-Chlorophenyl) phthalimide (**3c**)

Scheme 2. Synthesis of 1,3-dihydro-1,3-dioxisoindoles (**3a-c**)

N-(Phenyl)phthalimide (**3a**): White solid (0.98 g, 90%); m.p. 207 °C; Lit.³⁷ m.p. 206 °C; IR (KBr) (ν_{max} , cm⁻¹): 3088, (Ar. CH), 1745–1708 (C=O), 1160 (C-N); ¹H NMR (300 MHz, CDCl₃) (δ , ppm): 8.01–7.78 (4H, m, Arom.), 7.56–7.40 (5H, m, Arom.); ¹³C NMR (75 MHz, CDCl₃) (δ , ppm): 167.3 (C=O), 134.3, 133.2, 131.6, 129.7, 127.4, 124.6, 121.8 (Arom.C); found C, 75.23; H, 4.14; N, 6.27; calc. for C₁₄H₉NO₂ C, 75.33; H, 4.06; N, 6.27%.

N-(4-Methylphenyl)phthalimide (**3b**): White solid (0.97 g, 82%); m.p. 202–203 °C; Lit.³⁷ m.p. 204 °C; IR (KBr) (ν_{max} , cm⁻¹): 3064, (Ar. CH), 2958 (-CH₃), 1734–1713 (C=O), 1153 (C-N); ¹H NMR (300 MHz, CDCl₃) (δ , ppm): 7.99–7.94 (4H, m, Arom.), 7.84–7.79 (4H, m, Arom.), 2.38 (3H, s, -CH₃); ¹³C NMR (75 MHz, CDCl₃) (δ , ppm): 166.4 (C=O), 136.8, 135.1, 133.6, 131.3, 129.7, 127.9, 122.8 (Arom. C), 21.3 (-CH₃); found C, 76.31; H, 4.68; N, 6.00; calc. for C₁₅H₁₁NO₂ C, 75.94; H, 4.67; N, 5.90%.

N-(4-Chlorophenyl)phthalimide (**3c**): White solid (1.10 g, 86%); m.p. 196 °C Lit.³⁸ m.p. 194–195 °C; IR (KBr) (ν_{max} , cm⁻¹): 3043, (Ar. CH), 1731–1718 (C=O), 1159 (C-N), 873 (C-Cl); ¹H NMR (300 MHz, CDCl₃) (δ , ppm): 8.01–7.79 (4H, m, Arom.), 7.55–7.41 (4H, m, Arom.); ¹³C NMR (75 MHz, CDCl₃) (δ , ppm): 168.4 (C=O), 135.6, 133.4, 132.8, 131.3, 129.7, 128.9, 127.7, 123.0. (Arom.C); found C, 64.51; H, 3.11; N, 5.42; calc. for C₁₄H₈ClNO₂ C, 65.26; H, 3.13; N, 5.44%.

2. 3. Kinetic Procedure

The hydrolysis rate of the substrate **3a-c** were measured at a wavelength of 231–241 nm at 50.0 ± 0.1 °C. The kinetic run was started for all compounds by injecting 20

μL of 1.0 × 10⁻² M substrate stock solution in acetonitrile into the 3.0 mL acid solution equilibrated at 50.0 ± 0.1 °C in a quartz cuvette. The course of reactions was monitored over (at least) up to three half-lives and the absorbance values at infinity were acquired after ten half lives in all cases. Good first-order behaviour was observed with clean isosbestic points. The values of pseudo first-order rate constants (k_1) were calculated from the plots of $\ln(A-A_\infty)$ against time using the least squares procedure, where A is the absorbance at time t and A_∞ is the absorbance at infinity.³⁹ All kinetic runs were duplicated and the average deviation from the mean was less than < 3%. Deionized water, HPLC grade acetonitrile, and analytical grade concentrated acid were used to prepare all acid reaction solutions, making appropriate allowance for the water content of the acid.

2. 4. Product Analysis

Analysis of the product performed resulting from acid-catalyzed hydrolysis of *N*-(4-chlorophenyl) phthalimide was determined using the melting point comparison and spectroscopic (IR, NMR) methods. The products were thought of as phthalic acid and 4-chloroaniline. To determine products at the end of the reaction, we studied the same condition of the kinetic procedure. For this, 0.4 g of *N*-(4-chlorophenyl) phthalimide was allowed to react with 15 mL, 7.00 M HCl at 50.0 ± 0.1 °C for 6 hours. After the completion of the reaction, the solid white product was filtered and purified. The solid was crystallized from ethyl alcohol to give the expected products (phthalic acid). The melting point of the crystalline solid was found at 207–208 °C. The melting point of phthalic acid is 210–211 °C.⁴⁰ IR (KBr) (ν_{max} , cm⁻¹): 3093–2686 (-COOH, including Arom.

CH and Aliph.CH), 1721–1695 (C=O), 1283 (C-O). ¹H NMR (400 MHz, CDCl₃) (δ, ppm): 13.1–12.7 (2H, s, COOH), 8.02–7.75 (4H, m, Ar). ¹³C NMR (75 MHz, CDCl₃) (δ, ppm): 169.1 (C=O), 132.5, 131.2, 129.3 (Ar C). Finally, it was determined by IR, NMR, and melting point comparisons that these values are consistent with data in the literature.

2. 5. Antioxidant Evaluation

Free Radical Scavenging Activity (DPPH[•])

DPPH[•] activity of the samples was determined using the DPPH[•] (1,1-diphenyl-2-picryl-hydrazil) method⁴¹. 150 μL of distinct concentrations of samples or standards (TBHQ, α-tocopherol, and BHA), and 50 μL of 0.1 mM DPPH[•] have homogeneously mixed in a 96-well plate. The samples have waited in the dark at room temperature for 30 min. The absorbance values of each mixture were measured at 517 nm using the BIOTEK (Epoch2) microplate reader and determined the results by calculating the IC₅₀ (μg/mL) values. The activity for DPPH[•] scavenging was calculated by the following equation⁴¹:

$$\text{The percentage activity,} \\ \% = [(A_{\text{control, 517 nm}} - A_{\text{sample, 517 nm}}) / A_{\text{blank, 517 nm}}] \times 100.$$

ABTS^{••} Radical Scavenging Activity

ABTS^{••} radical scavenging activity of the samples was performed using the ABTS-K₂SO₈ method⁴². 2.45 mM K₂SO₈ and 7 mM ABTS (1:2) were mixed and incubated for 12–16 hours at room temperature in the dark. The mixture was diluted with ethanol so that the absorbance value was 0.700 ± 0.020. 20 μL of different concentrations of samples or standards (BHA, TBHQ, and α-tocopherol), and 180 μL of ABTS^{••} solution were mixed homogeneously in a 96-well plate. The absorbance value of each mixture was measured after 6 min at 734 nm using the BIOTEK (Epoch2) microplate reader, and the results were determined by calculating the IC₅₀ (μg/mL) values.

$$\text{ABTS}^{\bullet\bullet} \text{ scavenging activity (\%)} = [1 - (\text{absorbance of sample} / \text{absorbance of blank})] \times 100$$

2. 6. Enzyme Inhibition Activity

Urease Inhibition Activity

The urease inhibition activity of the samples was determined using the indophenol method⁴³. In a 96-well plate, 10 μL of samples or thiourea at different concentrations, 25 μL of 1 U urease (in 100 mM pH 8.2 sodium-potassium buffer), and 50 μL of 17 mM urea were mixed homogeneously. The samples were incubated for 15 minutes at 30°C. Mixture is homogeneously mixed with 45 μL of phenol reagent (0.1% (w/v) sodium nitroprusside and 8% (w/v) phenol) and 70 μL of alkaline reagent (4.7% (v/v) NaOCl and 2.5% (w/v) NaOH) solutions mixed. The samples were kept at 30 °C for 50 min. The absorbance values

of each mixture were measured at 630 nm using a BIOTEK (Epoch2) microplate reader, and presented the IC₅₀ (μg/mL) values of the results by calculated.

AChE and BChE Inhibition Activity

AChE and BChE inhibition activities of the samples were determined by using the Ellman method⁴⁴. 20 μL of samples or galantamine at different concentrations in a 96-well plate, 20 μL of 0.03 U AChE or BChE (in 100 mM pH 8.0 sodium-potassium buffer), 20 μL of 3.3 mM DTNB, and 140 μL of 100 mM pH 8.0 sodium-potassium buffer mixed homogeneously. The samples have incubated for 15 min at room temperature. The mixture has combined homogeneously by adding 10 μL of 1 mM acetylcholine iodide or butyrylcholine chloride. The absorbance values of each mix were measured at 412 nm using a BIOTEK (Epoch2) microplate reader and found the results by calculating the IC₅₀ (μg/mL) values.

2. 7. Molecules Preparation and Docking Protocol

All synthesized compounds were drawn in ChemDraw Ultra 18.0 and then by their geometry optimization (energy-minimized) with Chem3D 18.0. The optimized structures were saved in Mol2 format. The rotation ability for rotatable bonds in the flexible residues was detected automatically by the AutoDock Tools version 1.5.4 program. Then, synthesized compounds **3a–c** were optimized using AutoDock Tools software before the docking procedure.

All of the used protein 3D structure was retrieved from Protein Data Bank (RCSB PDB: an information portal to biological macromolecular structures), all enzymes' structure were selected due to their high resolution of 2 angstroms (Å) or less, and the program generated satisfactory solutions with this range of resolution⁴⁵. The crystal structure of Jack bean urease with PDB-ID 4GY7 at 1.49 Å resolution. On the other hand, the crystal structure of the human enzyme had been selected for acetylcholinesterase and butyrylcholinesterase with PDB-ID 4M0E and 1P0I, respectively; both enzyme structures had resolution at 2 Å. We also used the AutoDock Tools software for the enzyme macromolecules preparation. After removing non-standard residues and water molecules from enzymes, polar hydrogens were added to the macromolecule to reach the protonation state; then, enzymes coordinate were adjusted using the same program.

AutoDock vina tool has been used to predict the most appropriate binding site of the synthesized compounds **3a–c** within target enzymes⁴⁶. Those results, the solution that reached the minimum estimated Gibbs binding energy, was saved as the top-scoring mode. The graphical representation of the docked poses was rendered in PyMOL version 2.5 software for the 3D. To obtain the 2D

structure of the interactions between compounds and target enzymes and the Ligplot+ 2.2.4 program was used⁴⁷.

2. 8. Statistical Analysis

The results of triplicate analysis obtained from *in vitro* biological activity studies were expressed as \pm standard deviation values for each parameter. All data were analysed in the IBM Statistical Package for Social Studies (SPSS) 20.0 program. One-way ANOVA has been used because the means of more than two independent groups between the analysis averages and the variances with normal distribution in the data were homogeneous. Tukey HSD^{a,b} was used for multiple comparisons with the data obtained. The statistical significance level of the values compared with the activity analysis result group and the significance level was expressed with $p < 0.05$ deals and considered statistically significant.

3. Results and Discussion

3. 1. Kinetic Studies

First-order rate coefficients, k_1 , in the hydrolysis of *N*-(phenyl) phthalimide **3a** in the studied acid solutions are given in Figure 1. Increasing the concentration of acids in the worked range raised the hydrolysis rates continuously in all cases. There is no sign of maximum rate even at pretty high acidity.

The order of catalytic effectiveness of the acids obtained for the hydrolysis of **3a** was $\text{HCl} \cong \text{H}_2\text{SO}_4 > \text{HClO}_4$ or $\text{H}_2\text{SO}_4 \cong \text{HCl} > \text{HClO}_4$ in the whole range of acidity. Bunton and his co-workers⁴⁸ put forward that such an order is characteristic of a bimolecular mechanism, for the transition states of positive character are preferably stabilized by anions of high charge density such as Cl^- , while the opposite is usually the case for a unimolecular mechanism^{26a,48}.

The kinetic data obtained using the Cox and Yates Excess Acidity method³¹ are shown in Table 1. Eq.3 is used in a simplified form of the equations for unprotonated substrates.

$$\log k_1 - \log C_{\text{H}^+} - [\log C_{\text{s}} / (C_{\text{s}} + C_{\text{SH}^+})] = m^* m^\# X + r \log a_{\text{Nu}} + \log (k_0 / K_{\text{SH}^+}) \quad (3)$$

In equation (3), k_1 is the pseudo-first-order rate constant in aqueous acid concentration C_{H^+} and of Excess Acidity X and $m^* m^\#$ are the slope parameter, where $m^\#$ is characteristic of the type of reaction (for an A-1 process $m^\# > 1$; an A-2 processes $m^\# \cong 1$) and m^* is obtained from protonation studies $r \log a_{\text{Nu}}$ for the bimolecular reaction

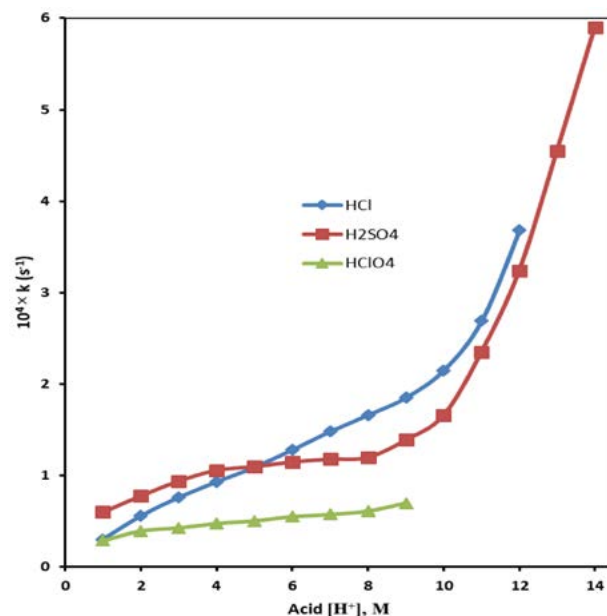


Figure 1. Plots of k_1 plots of different aqueous acid solutions for acid-catalyzed hydrolysis of **3a** at 50.0 ± 0.1 °C (●, HCl; ■, H_2SO_4 ; ▲, HClO_4)

Table 1. $10^4 k_1$ (s^{-1}) Values for the hydrolysis of the synthesized compounds at 50.0 ± 0.1 °C

[H ⁺]/M	3a			3b			3c		
	H ₂ SO ₄	HClO ₄	HCl	H ₂ SO ₄	HClO ₄	HCl	H ₂ SO ₄	HClO ₄	HCl
1	0.60	0.38	0.30	0.001	0.001	0.01	102	18.3	55.0
2	0.78	0.40	0.56	0.002	0.002	0.02	156	34.6	96.2
3	0.94	0.43	0.76	0.004	0.003	0.03	227	42.6	154.1
4	1.06	0.48	0.97	0.006	0.004	0.04	376	57.4	224.0
5	1.10	0.50	1.09	0.015	0.008	0.07	465	38.2	134.6
6	1.15	0.55	1.28	0.035	0.025	0.13	345	21.3	71.3
7	1.18	0.58	1.48	0.300	0.055	0.18	212	13.3	42.8
8	1.20	0.61	1.67	0.420	0.090	0.22	102	3.44	18.9
9	1.39	0.70	1.85	0.650	0.150	0.35	67	3.30	12.6
10	1.66	–	2.05	0.800	–	0.48	43	–	8.3
11	2.35	–	2.37	0.940	–	0.57	32	–	5.7
12	3.24	–	3.01	1.320	–	0.69	21	–	3.9
13	4.55	–	–	1.680	–	–	11.4	–	–
14	5.90	–	–	1.860	–	–	7.2	–	–

represents the activity of the nucleophile, where r is the number of water molecules involved in the formation of the transition state³¹.

Because of low basicity of the synthesized compounds, the protonation correction term $[\log C_s / (C_s + C_{SH}^+)]$ is negligible. X values were used for aqueous solution of the acid^{31b,49}.

The graph of $\log k_1 - \log C_{H^+}$ versus X for the hydrolysis of **3a** in HCl solution is shown in Figure 2. Similar plots were observed for **3b** and **3c** in HCl solution. In beginning, all such plots of arylphthalimide in the low acidity region showed downward curvature, which is a typical feature of A-2 reactions involving water²⁷.

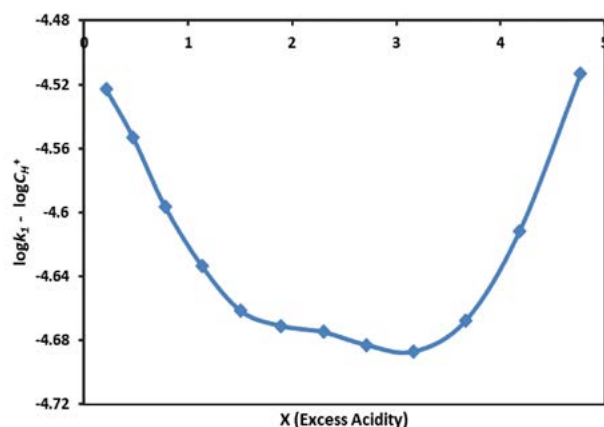


Figure 2. Plots of excess acidity versus $\log k_1 - \log C_{H^+}$ for the hydrochloric acid-catalysed hydrolysis of **3a** at $50.0 \pm 0.1^\circ\text{C}$

Show in Figure 2, in the 1.00–8.00 M region with increasing acid concentration, the plot shows that the rate of reaction was diminished, and there was no catalytic impact of the acids. Water activity decreases with acid concentration increases and the reaction rate decreases due to the decrease in water activity. After 8.00 M with acid concentration increases, the rate of hydrolysis increases, and there was consist of a catalytic effect of the acids. A curve was formed at 8.00–12.00 M acidity region. A straight line

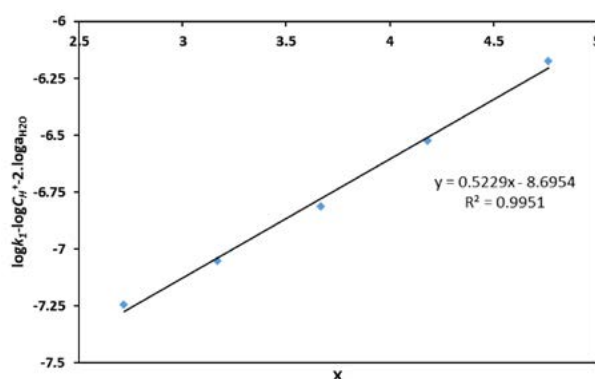


Figure 3. Plots of excess acidity versus $\log k_1 - \log C_{H^+} - 2 \log a_{H_2O}$ for the 8.00–12.00 M hydrochloric acid-catalyzed hydrolysis of **3a** at $50.0 \pm 0.1^\circ\text{C}$

was seen in the acidity region (8.00–12.00 M); values of $2 \log a_{H_2O}$ can be obtained from the left-hand side of Eq. (3), and the result was plotted against X . Straight-line correlation (Figure 3 and Table 1 where $r = 2$) was determined for aryl phthalimides. According to this evidence, two moles of water was detected in the reaction rate-determining step of the A-2 mechanism.

The relationship between temperature and rate constants was analyzed by a spreadsheet program (Eyring equation) using at least a square program. The values at different temperatures and Arrhenius parameters (Eq. 4) are shown in Tables 2 and 3, respectively.

$$k = \frac{k_B T}{h} \cdot \exp(-\Delta H^\ddagger / RT) \cdot (\Delta S^\ddagger / R) \quad (4)$$

Acid catalyzed hydrolysis of amides and esters²⁹ proceeding by an A-1 mechanism have ΔS^\ddagger of about 0 to $-41.8 \text{ Jmol}^{-1}\text{K}^{-1}$, while those proceeding by an A-2 mechanism have ΔS^\ddagger of -62.8 to $-125.5 \text{ Jmol}^{-1}\text{K}^{-1}$. For the hydrolysis of **3a** in 4.00 M and 8.00 M hydrochloric acid, the values of ΔS^\ddagger are -89.57 , $-71.69 \text{ Jmol}^{-1}\text{K}^{-1}$, respectively. Moreover, the values for the hydrolysis of **3b** and **3c** change similarly, as expected. Also, hydrolysis of **3a** in 4.00 M and 8.00 M sulfuric and perchloric acid, the values of ΔS^\ddagger are -93.84 , -71.69 , -101.63 , and $-99.51 \text{ Jmol}^{-1}\text{K}^{-1}$, respectively. In an A-2 mechanism, negative values of ΔS^\ddagger indicate that the water molecule behaves like a nucleophile. In the acidity range studied, electron-withdrawing substituents cause the highest rate of hydrolysis (**3c**>**3b**), and the substituent effects are well correlated by a satisfactory Hammett $\rho\sigma$ plot [at 8.00 M HCl, $\rho = 4.847$ (corr. 0.9987)] as shown in Figure 4. Noticeably at these acidities, the electron-withdrawing group enhances the nitrogen atom's positive charge. Therefore, the nucleophilicity of the water molecules becomes more effective on account of the positively charged nitrogen atom in the reaction rate-determining transition state for the A-2 mechanism.

However, [e.g. 4.00 M H_2SO_4 , $\rho = 13.11$ (corr. 0.9998)] as shown in Figure 5, **3c** hydrolysis was more rapid than **3b**. It is predominantly consistent with the bimolecular mechanism that substituent effects on the protonation and slow step operate in opposite directions. Similar behaviours have been observed for the hydrolysis of arylsulfonyl phthalimides³³ and substitutedarylthio phthalimides³⁵ an A-2 mechanism at lower acidities. 2.00 M HClO_4 , $\rho = 0.848$ (corr. 0.9997) for *N*-(4-bromophenylsulfonyl) phthalimides hydrolysis was more rapid than *N*-(4-methylphenylsulfonyl) phthalimides, and consistent with a predominantly an A-2 mechanism. Likewise, 1.00 M HClO_4 , $\rho = 0.803$ (corr. 0.996) for *N*-(4-chlorophenylthio) phthalimides hydrolysis was more rapid than *N*-(4-methylphenylthio) phthalimides. There is no direct evidence concerning the site of protonation of *N*-(4-substitutedaryl) phthalimides; however, *N*-(4-substitutedarylsulfonyl) phthalimides³³, *N*-(4-substitutedarylthio) phthalimides³⁵, and *N,N'*-diarylsulfamides³⁹ occurs pref-

entially at the nitrogen atom. In addition, m^*m^\ddagger are the combined slope parameters, where m^* gives information about the protonation site (for nitrogen m^* : 0.65–1.40; oxygen m^* : 0.13–0.60; sulfur m^* : 1.25–1.80; carbon m^* : 1.4–2.02)⁵⁰. For compound **3a**, m^*m^\ddagger slope parameters in various acids HCl (8.00–12.00 M), H₂SO₄ (8.00–12.00 M) and HClO₄ (6.00–9.00 M) are 0.52, 1.29, and 0.76, respectively (see at S11 and S13 in supplementary information). A value of $m^*=1.025$ is assumed for protonation on nitrogen. It was found that m^\ddagger is 0.51, 1.26, and 0.74 for HCl, H₂SO₄,

and HClO₄, respectively. According to the observations, the nitrogen atom is most likely the protonation site of all the compounds.

Based on the overall arguments available, we suggested the acid-catalyzed hydrolysis mechanism of the compounds improves with an A-2 mechanism in the whole range of acidity as given in Scheme 3. In the first, occur quick pre-equilibrium protonation of the arylphthalimide. It is assumed that protonation occurs on a nitrogen atom, and two water molecules attack the car-

Table 2. $10^4 k_1$ (s⁻¹) Values for the hydrolysis of the **3a-c** at varied temperatures (°C)

Acid (M)	Compounds	30.0	35.0	40.0	45.0	50.0	55.0	60.0
4.00 M HCl	3a			0.39	0.68	0.93	1.53	2.29
8.00 M HCl	3a			0.75	1.24	1.67	2.93	4.86
4.00 M H ₂ SO ₄	3a			0.44	0.70	1.06	1.54	2.51
8.00 M H ₂ SO ₄	3a			0.45	0.81	1.20	1.87	3.01
6.00 M HClO ₄	3a			0.20	0.35	0.55	0.74	1.13
8.00 M HClO ₄	3a			0.25	0.38	0.61	0.87	1.41
4.00 M HCl	3b			0.02	0.03	0.04	0.08	0.12
4.00 M HCl	3c	54	74	102	158	224		

Table 3. Values of ΔH^\ddagger and ΔS^\ddagger for the hydrolysis of the synthesized compounds

Compounds	Acid	[H ⁺] / M	ΔH^\ddagger (kJ/mol)	ΔS^\ddagger (J/molK)	Temperature Range (°C) ^a	R ²
3a	HCl	4.00	75.20	-89.57	40–60	0.995
		8.00	75.20	-71.69	40–60	0.995
	H ₂ SO ₄	4.00	73.61	-93.84	40–60	0.997
		8.00	73.90	-71.69	40–60	0.996
	HClO ₄	4.00	73.07	-101.63	40–60	0.991
		8.00	73.32	-99.51	40–60	0.997
3b	HCl	4.00	79.17	-102.1	40–60	0.998
3c	HCl	4.00	58.64	-95.92	30–50	0.994

^a The measurements were made at 5 °C intervals.

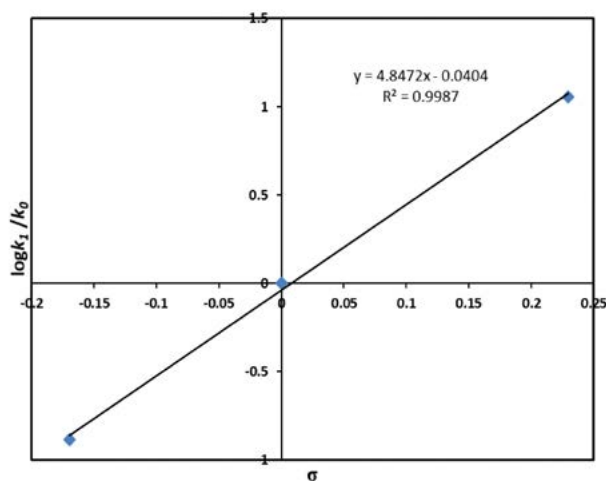


Figure 4. The plot of Hammett ρ versus $\log k$ values for acid-catalyzed hydrolysis (8.00 M HCl) of *N*-(4-substitutedaryl) phthalimides at 50.0 ± 0.1 °C

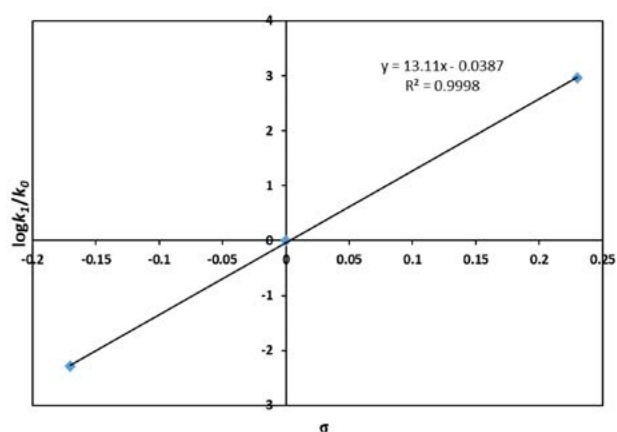
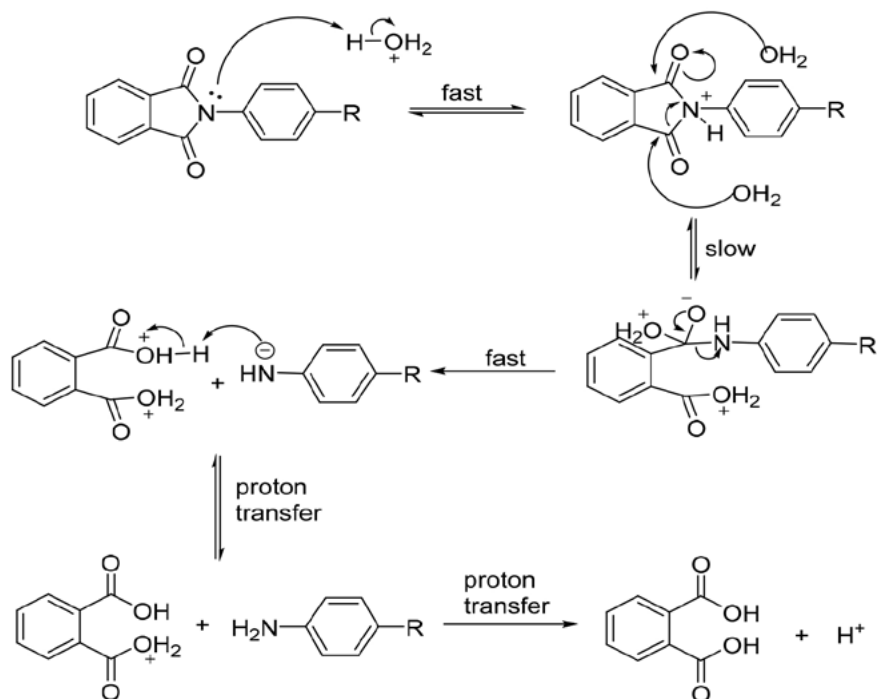


Figure 5. The plot of Hammett ρ versus $\log k$ values for acid-catalyzed hydrolysis (4.00 M H₂SO₄) of *N*-(4-substitutedaryl) phthalimides at 50.0 ± 0.1 °C



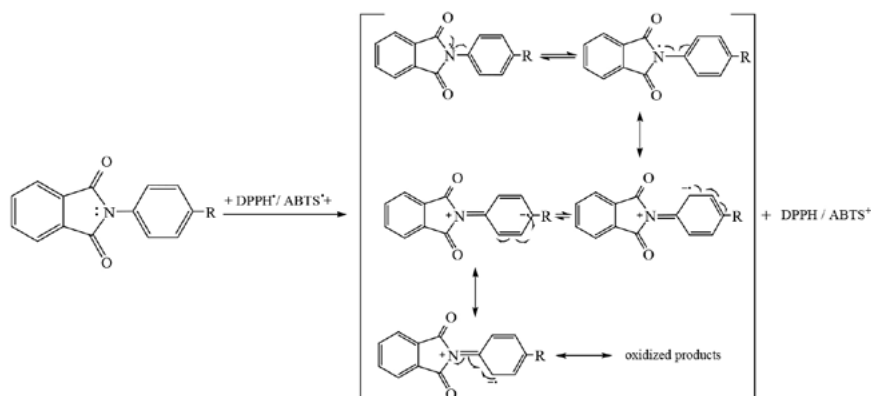
Scheme 3. A plausible acid-catalysed hydrolysis mechanism of the synthesized compounds

bonyl carbon atom as a nucleophile in the rate-determining step of the reaction. In intermediate step, aniline anion attack to protonated phthalic acid very fast. Then, the products of acid-catalyzed hydrolysis were observed to form phthalic acid and 4-chloroaniline.

3. 2. Antioxidant Evaluation

The DPPH \cdot and ABTS \cdot^+ scavenging activity results have shown in Table 4. Considering the molecules, compound **3c** is the most electronegative compound, then compound **3b** and then compound **3a** is electronegative. The N atom in the DPPH \cdot and ABTS \cdot^+ receives electrons from antioxidant compounds. The electronegativity of the N atom is higher than that of the Cl atom, the CH $_3$ molecule, and the H atom. Therefore, DPPH \cdot scavenging activ-

ities are ranked from highest to lowest as **3c** > **3b** > **3a**, while ABTS \cdot^+ radical scavenging activities are ordered as **3b** > **3c** > **3a** (Scheme 4). While there was a statistically significant difference between **3c**, α -tocopherol, BHA, **3b** and **3a** compounds in the DPPH \cdot scavenging activity test, there was no significant difference between TBHQ and **3c** and α -tocopherol ($p < 0.05$). Whereas there was a statistically significant difference between **3c**, α -tocopherol, BHA, **3b**, and **3a** compounds in the ABTS \cdot^+ scavenging activity test, there was no significant difference between BHA and TBHQ ($p < 0.05$). PerveenOrfali^[51] reported that the DPPH \cdot scavenging activity IC $_{50}$ values of the *N*-(phenyl)phthalimide, *N*-(4-methylphenyl)phthalimide, and *N*-(4-chlorophenyl)phthalimide as 87.40 ± 0.15 , 69.22 ± 0.12 , and 91.70 ± 0.05 μ M, respectively, and the BHA standard as 44.20 ± 0.06 μ M. Nayab, Pulaganti, Chit-



Scheme 4. The offer reactions of DPPH \cdot and ABTS \cdot^+ scavenging of the synthesized compounds

taOves^[52] studied that the DPPH[·] scavenging activity (IC₅₀) of the *N*-(4-methylphenyl)phthalimide, and *N*-(4-chlorophenyl)phthalimide as 1.30 ± 0.05 , and 1.40 ± 0.06 mg/mL, respectively, and the ascorbic acid standard as 0.10 ± 0.03 mg/mL. In our study, this assay observed *N*-(4-methylphenyl)phthalimide, and *N*-(4-chlorophenyl)phthalimide had lower activity.

inhibition activity test, there was no significant difference between **3a** and galantamine ($p < 0.05$). Also, the compound **3a** sample had the best BChE inhibition activity, while compounds **3b** and **3c** had the higher activity than the standard as well. The compounds from high to low activity; are shaped like **3a**, **3b**, **3c**, and galantamine. While there was a statistically significant difference between **3c**,

Table 4. The results of antioxidant and enzyme inhibition activities of the synthesized compounds

Compounds and standards	Antioxidant Activity IC ₅₀ (µg/mL)		Enzyme Inhibition Activity IC ₅₀ (µg/mL)		
	DPPH [·]	ABTS ^{·+}	AChE	BChE	Urease
3a	95.7 ± 0.8 ^e	79.9 ± 1.4 ^d	13.1 ± 0.2 ^b	6.8 ± 0.1 ^a	17.7 ± 0.6 ^b
3b	20.1 ± 0.0 ^d	6.4 ± 1.6 ^{ab}	9.6 ± 0.5 ^a	7.4 ± 0.4 ^a	17.3 ± 0.0 ^b
3c	2.0 ± 0.1 ^a	56.8 ± 1.5 ^c	29.6 ± 0.2 ^c	13.6 ± 0.6 ^b	10.5 ± 0.0 ^a
BHA	5.7 ± 0.5 ^c	3.8 ± 0.0 ^a	NU	NU	NU
TBHQ	3.2 ± 0.3 ^{ab}	4.0 ± 0.0 ^a	NU	NU	NU
α-tocopherol	3.9 ± 0.1 ^b	9.4 ± 0.2 ^b	NU	NU	NU
Galantamine	NU	NU	14.4 ± 0.0 ^b	49.4 ± 0.0 ^c	NU
Thiourea	NU	NU	NU	NU	26.2 ± 0.0 ^c
F-value	17512.1	1977.9	1604.3	5876.0	854.2

NU: Not use, The letters a, b, c, and d are statistical significant indicators. a; refers to statistical significance corresponding to high activity. b and c; represent statistical significance corresponding to moderate activity. d; refers to statistical significance corresponding to low activity. e; refers to statistical significance corresponding to very low activity. In all tests $p < 0.05$. F-values are based on one way ANOVA for individual instars

3. 3. Enzyme Inhibition Activity

The results of urease, AChE, and BChE inhibition activity have shown in Table 4. When comparing the activities of the samples with the standards and among themselves, it was observed that the compound **3c** had the best urease inhibition activity. It is possible that the reason **3c** sample was most effective against urease is that it has the chloride (negative ion) which in turn contributed to its stability at the active site of urease, that contain positively charged nickel atoms. In contrast, compounds **3a** and **3b** had higher activity than the standard as well. Ranking the compounds from high activity to low activity; are shaped like **3c**, **3b**, **3a**, and thiourea. While there was a statistically significant difference between **3c**, **3b** and thiourea compounds in urease inhibition activity test, there was no significant difference between **3a** and **3b** ($p < 0.05$). Besides, it was determined that the compound **3b** sample had the best AChE inhibition activity, whereas compound **3c** had the lowest activity. The compounds from high activity to low activity; are shaped like **3b**, **3a**, galantamine, and **3c**. While there was a statistically significant difference between **3c**, **3b**, **3a**, and galantamine compounds in AChE

3a, and galantamine compounds in BChE inhibition activity test, there was no significant difference between **3a** and **3b** ($p < 0.05$).

3. 4. Molecular Docking Analysis

The created docked complexes were analyzed based on the minimum affinity energy value (kcal/mol) and binding interaction patterns; the most stable poses with the lowest affinity energy value were taken for further analysis. So, we mainly focused our work on the ligands (synthetic compounds) interactions within these stable poses, which could inhibit the enzyme activity (Table 5). Docking results improved that **3b** showed the best binding among molecules at (−9.7 kcal/mol) affinity energy value within acetylcholinesterase, which was the best among samples. As for the remaining enzyme, **3b** and **3c** predict the same binding affinity energy value at (−9.0 kcal/mol) to butyrylcholinesterase. However, compound **3b** showed the minimum energy value (−8.6 kcal/mol). At the same time, **3a** gave (−7.8 kcal/mol) energy value which was somewhat lower than other compounds against urease. These poses with the lowest value (highest binding score) had been selected to analyze their interaction with enzyme residues.

As seen in Figure 6, the compounds (**3a-c**) have a significant interaction pose placed in the hollow at the AChE surface predicted interaction via hydrogen bonds and hydrophobic interactions with the amino acids surrounding it, as shown in the close-up part of the exact figure. Further, synthetic compounds demonstrate their ability to form potential hydrogen bonds within BChE at

histidine 438. Serine 198 amino acids also showed the possibility of attractive electrostatic interactions with the near amino acids Figure 7. Furthermore, as shown in Figure 8, **3a**, **3b**, and **3c** had bound to the urease enzyme via the same site. This linkage, as can be seen in the zoom-in part of Figure 8, it was done by a hydrogen bond between the

compounds' oxygen atom and the same atom from the tyrosine 32 from the enzyme for both **3b** and **3c** and with the second bond between the other oxygen of **3a** and lysine 716 amino acid.

We have also exported 2D interaction diagrams of ligands (using the Ligplot+) with the highest binding

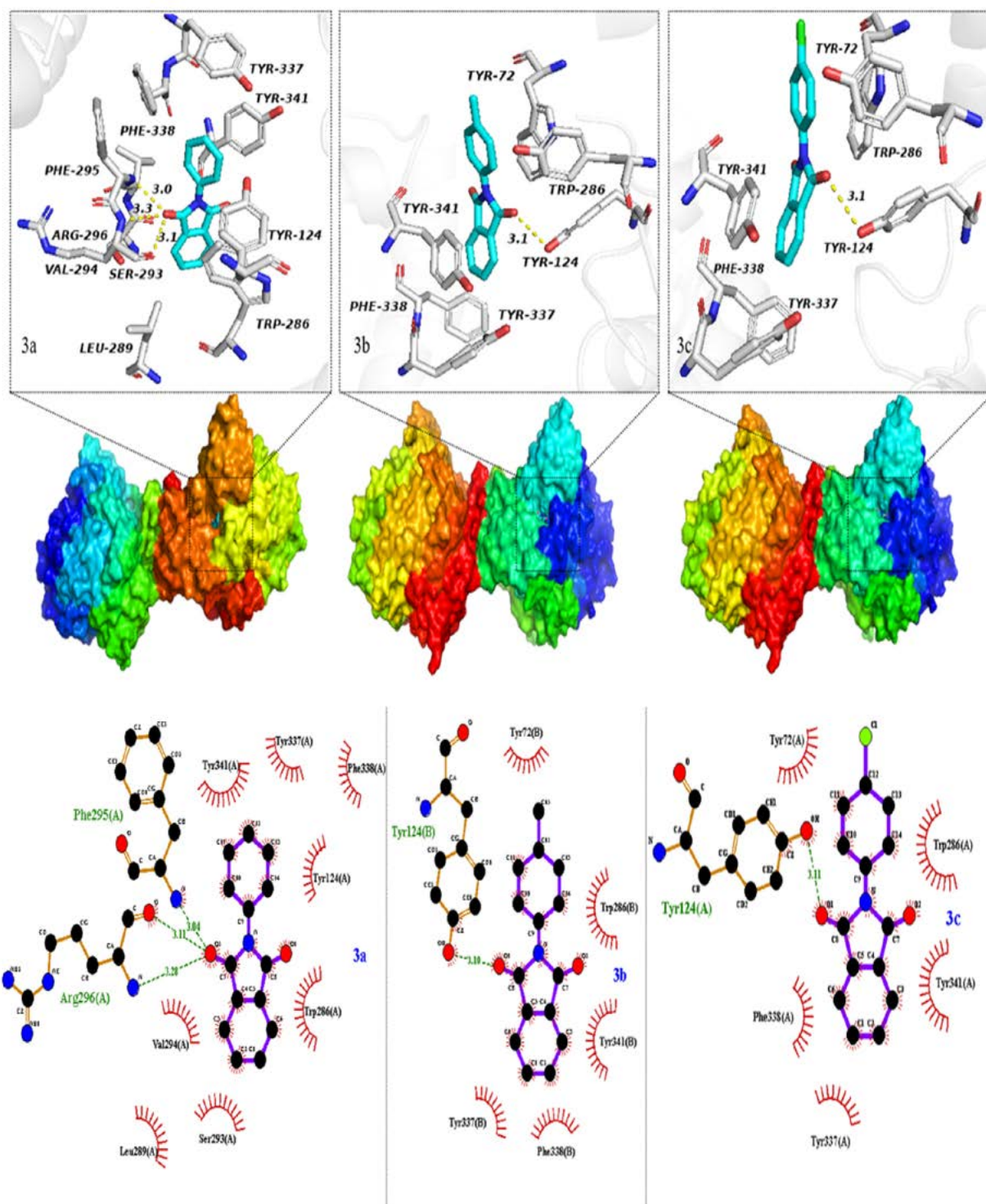


Figure 6. 3D and 2D detailed binding modes of the best pose of synthesized compounds into active catalytic site of AChE

scores and demonstrated that all compounds had succeeded in forming hydrogen bonds and hydrophobic interactions into the active sites of enzymes (Figures 6-8). These results were identical to what was obtained by the PyMOL program analyzing results and the 3D diagrams; the closed state of compound-AChE complexes in Figure 6 exposed

that **3a** compound, in addition to creating hydrogen bonds with two amino acids (Phe295 and Arg396), it can also develop kinds of hydrophobic interactions with (Val294, Leu289, Ser293, Trp286, Tyr124, Phe338, Tyr337, and Tyr341). However, **3b** and **3c** could be linked to AChE by a hydrogen bond at (Tyr124) and form a nonpolar attrac-

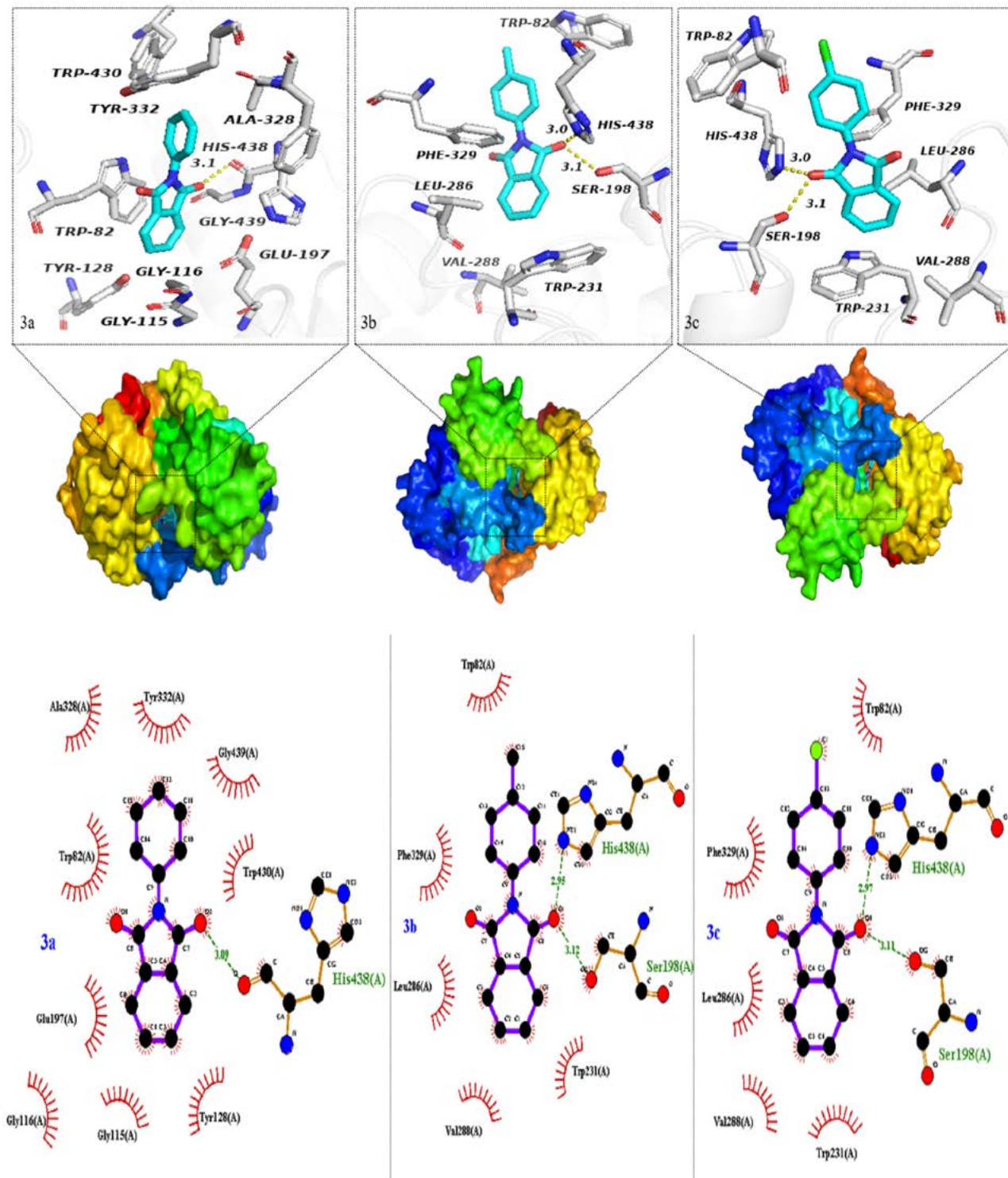


Figure 7. 3D and 2D detailed binding modes of the best pose of synthesized compounds into the active catalytic site of BChE

tion with (Tyr72, Trp286, Tyr341, Phe338, and Tyr337). For the BChE, as shown in Figure 7, **3a** compound is predicted to create a hydrogen bond with the His438 amino acid and been attracted by interaction with (Trp430, Gly439, Tyr332, Ala328, Trp82, Glu179, Gly116, Gly115 and Tyr128). At the same time, **3b** and **3c** compounds could form a hydrogen bond with (His438 and Ser198) and be hydrophobically affected by (Trp82, Phe329, Leu286, Val288, and Trp231) amino acids. As for the urease enzyme, **3a** is predicted to form an H-bond with (Tyr32 and Lys716) and form hydrophobic interaction with (Val744, Thr33, Val36, Glu742, Phe712, Asp730, and

Table 5. Binding scores for synthesized compounds with target enzymes

Compounds	Affinity (kcal/mol)		
	AChE	BChE	Urease
3a	-8.3	-8.7	-7.8
3b	-9.7	-9.0	-8.6
3c	-9.5	-9.0	-8.5

Glu718), whereas **3b** and **3c** are more likely to be bonded to (Tyr32) via H-bond and attracted by hydrophobic interaction to (Val744, Thr33, Val36, Ala37, Glu742, Phe712, Asp730, Lys716, and Glu718) simultaneously (Figure 8).

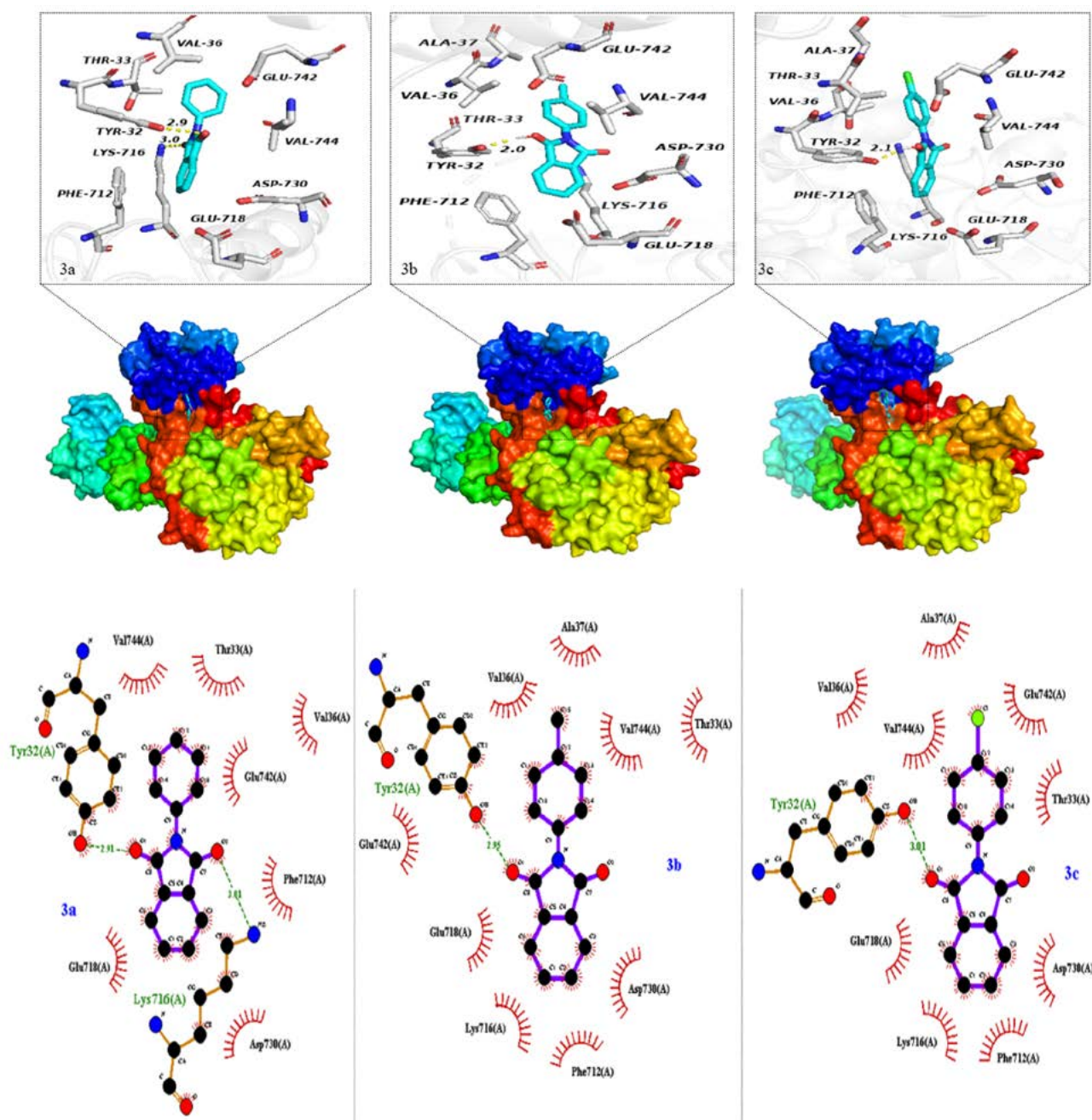


Figure 8. 3D and 2D detailed binding mode of the best-pose of synthesized compounds into the active catalytic site of urease

4. Conclusions

The acid-catalysed hydrolysis mechanism of *N*-(4-substituedphenyl) phthalimides **3a–c** was examined. Analyses of the data by the Excess Acidity treatment, entropy of activation, and substituent effect are consistent with an A-2 mechanism in the whole range of acidity. Catalytic order of strong acids for the acid catalyzed hydrolysis of the compounds studied were as $\text{HCl} \cong \text{H}_2\text{SO}_4 > \text{HClO}_4$ in all acidity ranges. These are the characteristics of an A-2 mechanism. Furthermore, two moles of water were involved as a nucleophile in the reaction rate-determining step of the A-2 mechanism.

When the antioxidant activities of the phthalimides; it was observed that the compound **3c** sample had the best DPPH[·] scavenging activity. Ranking the compounds from high to low activity; are shaped like **3c**, TBHQ, α -tocopherol, BHA, **3b**, **3a**. Besides, it was determined the compound **3b** sample had the best ABTS^{·+} radical scavenging activity. Ranking the compounds from high activity to low activity; are shaped like BHA, TBHQ, **3b**, α -tocopherol, **3c**, **3a**. As for the enzyme inhibition activities of the phthalimides; it was observed that the compound **3c** sample had the best urease inhibition activity. In contrast, compounds **3b** and **3a** were determined higher activities from thiourea. Thus, these compounds can be used as urease inhibitors. It was determined that compound **3b** sample had the best AChE inhibition activity, whereas compound **3a** was determined to have higher activities from galantamine. Thereby, compounds **3b** and **3a** can be used as acetylcholinesterase inhibitors. Also, it was observed the compound **3a** sample had the best BChE inhibition activity, while the compounds **3b** and **3c** were determined to have higher activities from galantamine. So, compounds **3b** and **3c** can be used as butyrylcholinesterase inhibitors.

All synthesized compounds successfully docked to urease, acetylcholinesterase, and butyrylcholinesterase binding sites. Among these molecules, **3b** has the best binding score (−9.7 kcal/mol) with acetylcholinesterase; further, simulation results were harmonious with *in-vitro* inhibition activity results for the same enzymes.

Declarations

Ethics approval

No permissions are required for this work.

Competing interests

The authors declare that they have no conflict of interest.

Funding

We would like to thank Ondokuz Mayıs University (Grant No. PYO.FEN.1904.12.027) for its financial support of this work.

Availability of data and materials

If data is requested, the relevant author will share it with you or reviewer.

Author Contributions

Hasan Yakan: Synthesis, Characterization, Kinetic Studies, Writing–Review. **Seyhan Ozturk:** Synthesis, Characterization, Writing–Review, Visualization & Editing. **Elvan Uyar Tolgay:** Synthesis, Characterization, Kinetic Studies. **Semiha Yenigun:** Antioxidant Activity and Enzyme Inhibitor Studies, Writing–Review. **Sarmad Marrah:** Molecular Docking Studies, Writing–Review. **Tugrul Doruk:** Molecular Docking Studies, Writing–Review. **Tevfik Ozen:** Biologic Studies, Writing–Review, Supervision. **Halil Kutuk:** Kinetic Studies, Writing–Review, Supervision.

Acknowledgments

The synthesis, structure elucidation, and kinetic-acidic hydrolysis assay parts of this study belong to Elvan Uyar Tolgay master thesis at Ondokuz Mayıs University. The authors thank Dr. Mohammad Maher Jerry for checking and proofreading the article.

Supplementary Material

Kinetic data of the compounds are given in the supporting information.

5. References

1. A. Khalil, M. Berghot, M. Gouda, *European journal of medicinal chemistry* **2010**, *45*, 1552–1559. DOI:10.1016/j.ejmech.2009.12.064
2. L. d. M. Lima, P. Castro, A. L. Machado, C. A. M. Fraga, C. Lugnier, V. L. G. de Moraes, E. J. Barreiro, *Bioorganic & medicinal chemistry* **2002**, *10*, 3067–3073. DOI:10.1016/S0968-0896(02)00152-9
3. S. H. L. Kok, R. Gambari, C. H. Chui, M. C. W. Yuen, E. Lin, R. S. M. Wong, F. Y. Lau, G. Y. M. Cheng, W. S. Lam, S. H. Chan, *Bioorganic & medicinal chemistry* **2008**, *16*, 3626–3631. DOI:10.1016/j.bmc.2008.02.005
4. F. A. Santos, M. L. Almeida, V. A. Silva, D. C. Viana, M. C. Pereira, A. S. Lucena, M. G. Pitta, M. R. Galdino-Pitta, M. J. de Melo Rêgo, I. da Rocha Pitta, *Med. Chem. Res.* **2022**, *31*, 108–119. DOI:10.1007/s00044-021-02821-7
5. J. L. Santos, P. R. Yamasaki, C. M. Chin, C. H. Takashi, F. R. Pavan, C. Q. Leite, *Bioorganic & medicinal chemistry* **2009**, *17*, 3795–3799. DOI:10.1016/j.bmc.2009.04.042
6. J. Singh, T. Singha, A. Naskar, M. Kundu, R. K. Harwansh, A. Mondal, T. Ghosh, T. Maity, *Pharmacologyonline* **2011**, *2*, 976–987.
7. S. C. Annedi, J. Ramnauth, S. P. Maddaford, P. Renton, S. Ra-

- khait, G. Mladenova, P. Dove, S. Silverman, J. S. Andrews, M. D. Felice, *Journal of medicinal chemistry* **2012**, *55*, 943–955. DOI:10.1021/jm201564u
8. P. Appelbaum, P. Hunter, *International journal of antimicrobial agents* **2000**, *16*, 5–15. DOI:10.1016/S0924-8579(00)00192-8
9. a) A. Aliabadi, A. Foroumadi, A. Mohammadi-Farani, M. G. Mahvar, *Iranian journal of basic medical sciences* **2013**, *16*, 1049;
b) C.-L. Chi, L. Xu, J.-J. Li, Y. Liu, B.-Q. Chen, *Med. Chem. Res.* **2022**, *31*, 120–131. DOI:10.1007/s00044-021-02823-5
10. Z. Sang, K. Wang, H. Wang, L. Yu, H. Wang, Q. Ma, M. Ye, X. Han, W. Liu, *Bioorganic & medicinal chemistry letters* **2017**, *27*, 5053–5059. DOI:10.1016/j.bmcl.2017.09.055
11. X. Collin, J.-M. Robert, G. Wielgosz, G. Le Baut, C. Bobin-Dubigeon, N. Grimaud, J.-Y. Petit, *Eur. J. Med. Chem.* **2001**, *36*, 639–649. DOI:10.1016/S0223-5234(01)01254-5
12. W. D. Figg, S. Rajee, K. S. Bauer, A. Tompkins, D. Venzon, R. Bergan, A. Chen, M. Hamilton, J. Pluda, E. Reed, *J. Pharm. Sci.* **1999**, *88*, 121–125. DOI:10.1021/js980172i
13. E. Atra, E. I. Sato, *Clin. Exp. Rheumatol.* **1993**, *11*, 487–493.
14. a) H. R. Lobo, B. S. Singh, G. S. Shankarling, *Green Chemistry Letters and Reviews* **2012**, *5*, 487–533; DOI:10.1080/17518253.2012.669500
b) M. Sani, G. Fossati, F. Huguenot, M. Zanda, *Angew. Chem.* **2007**, *119*, 3596–3599. DOI:10.1002/ange.200604557
15. a) L. Wang, Z. Kuang, D. Zhang, Y. Gao, M. Ying, T. Wang, *Biomed. Pharmacother.* **2021**, *133*, 110978; DOI:10.1016/j.biopha.2020.110978
b) Z. Zhou, X. Yuan, D. Long, M. Liu, K. Li, Y. Xie, *Spectrochimica Acta Part A: Molecular and Biomolecular Spectroscopy* **2021**, *246*, 118927. DOI:10.1016/j.saa.2020.118927
16. a) N. Kaushik, N. Kumar, A. Kumar, *Int. J. Pharm. Pharm. Sci.* **2015**, *7*, 120–123; b) S. Oyedemi, G. Bradley, A. Afolayan, *African Journal of pharmacy and pharmacology* **2010**, *4*, 070–078.
17. C. Zhang, D. Chen, X. Liu, *Molecular & Cellular Toxicology* **2016**, *12*, 45–52. DOI:10.1007/s13273-016-0007-0
18. M. Mrdaković, L. Ilijin, M. Vlahović, D. Matić, A. Gavrilović, A. Mrkonja, V. Perić-Mataruga, *Chemosphere* **2016**, *159*, 565–569. DOI:10.1016/j.chemosphere.2016.06.059
19. P. Taslimi, C. Caglayan, V. Farzaliyev, O. Nabiyevev, A. Sujayev, F. Turkan, R. Kaya, İ. Gulçin, *Journal of biochemical and molecular toxicology* **2018**, *32*, e22042. DOI:10.1002/jbt.22042
20. G. Zengin, I. Senkardes, A. Mollica, C. M. N. Picot-Allain, G. Bulut, A. Dogan, M. F. Mahomoodally, *Computational biology and chemistry* **2018**, *75*, 111–119. DOI:10.1016/j.compbiolchem.2018.05.005
21. Z. Amtul, R. Siddiqui, M. Choudhary, *Current medicinal chemistry* **2002**, *9*, 1323–1348. DOI:10.2174/0929867023369853
22. M. Amin, M. S. Iqbal, R. W. Hughes, S. A. Khan, P. A. Reynolds, V. I. Enne, Sajjad-ur-Rahman, A. S. Mirza, *Journal of Enzyme Inhibition and Medicinal Chemistry* **2010**, *25*, 383–390. DOI:10.3109/14756360903179518
23. a) S. Kumar, S. M. Lim, K. Ramasamy, M. Vasudevan, S. A. A. Shah, M. Selvaraj, B. Narasimhan, *Chemistry Central Journal* **2017**, *11*, 1–16; DOI:10.1186/s13065-017-0322-0
b) S. Zhang, B. Qiu, J. Zhu, M. Khan, X. Liu, *Spectrochimica Acta Part A: Molecular and Biomolecular Spectroscopy* **2018**, *203*, 13–18. DOI:10.1016/j.saa.2018.05.077
24. a) M. Hanif, K. Shoaib, M. Saleem, N. Hasan Rama, S. Zaib, J. Iqbal, *International Scholarly Research Notices* **2012**, *2012*; DOI:10.5402/2012/928901
b) N. Yayli, G. Kılıç, G. Celik, N. Kahriman, Ş. Kanbolat, A. Bozdeveci, Ş. A. Karaoğlu, R. Aliyazıcıoğlu, H. E. Sellitepe, İ. S. Doğan, *Turk. J. Chem.* **2021**, *45*, 788–804; DOI:10.3906/kim-2012-25
c) A. M. S. Mascarenhas, R. B. M. de Almeida, M. F. de Araujo Neto, G. O. Mendes, J. N. da Cruz, C. B. R. Dos Santos, M. B. Botura, F. H. A. Leite, *Journal of Biomolecular Structure and Dynamics* **2021**, *39*, 6021–6030; DOI:10.1080/07391102.2020.1796791
d) N. Yayli, G. Kılıç, N. Kahriman, Ş. Kanbolat, A. Bozdeveci, Ş. A. Karaoğlu, R. Aliyazıcıoğlu, H. E. Sellitepe, İ. S. Doğan, A. Aydın, *Bioorg. Chem.* **2021**, *115*, 105183; DOI:10.1016/j.bioorg.2021.105183
e) H. Yakan, Ü. M. Koçyiğit, H. Muğlu, M. Ergül, S. Erkan, E. Güzel, P. Taslimi, İ. Gülçin, *Journal of Biochemical and Molecular Toxicology* **2022**, *36*, e23018; DOI:10.1002/jbt.23018
f) Ü. M. Koçyiğit, P. Taslimi, B. Tüzün, H. Yakan, H. Muğlu, E. Güzel, *Journal of Biomolecular Structure and Dynamics* **2022**, *40*, 1–11;
g) Y. V. Martynenko, O. M. Antypenko, O. A. Brazhko, I. B. Labenska, S. I. Kovalenko, *Acta Chimica Slovenica* **2019**, *66*, 145–154. DOI:10.17344/acsi.2018.4731
25. a) B. Garcia, F. Hoyuelos, S. Ibeas, J. Leal, *The Journal of organic chemistry* **2006**, *71*, 3718–3726; DOI:10.1021/jo052561k
b) T. H. Lowry, K. S. Richardson, *Mechanism and theory in organic chemistry*, Harper & Row New York, **1987**, p.
26. a) C. Bunton, J. Fendler, *The Journal of Organic Chemistry* **1966**, *31*, 3764–3771; DOI:10.1021/jo01349a064
b) D. Jacewicz, J. Pranczk, A. Dąbrowska, L. Chmurzyński, *Reaction Kinetics, Mechanisms and Catalysis* **2010**, *100*, 11–20.
27. K. Yates, R. A. McClelland, *Journal of the American Chemical Society* **1967**, *89*, 2686–2692. DOI:10.1021/ja00987a033
28. K. K. Ghosh, S. Ghosh, *The Journal of Organic Chemistry* **1994**, *59*, 1369–1374. DOI:10.1021/jo00085a028
29. L. L. Schaleger, F. Long, *Adv. Phys. Org. Chem.* **1963**, *1*, 1–33. DOI:10.1016/S0065-3160(08)60276-2
30. R. A. Y. Jones, *Physical and mechanistic organic chemistry*, Cambridge University Press, Cambridge, **1979**, p.
31. a) R. A. Cox in *Excess acidities*, Vol. 35 Elsevier, **2000**, pp. 1–66; DOI:10.1016/S0065-3160(00)35011-0
b) R. A. Cox, K. Yates, *Journal of the American Chemical Society* **1978**, *100*, 3861–3867; DOI:10.1021/ja00480a033
c) R. A. Cox, K. Yates, *Can. J. Chem.* **1979**, *57*, 2944–2951. DOI:10.1139/v79-479
32. H. Kutuk, Y. Bekdemir, N. Turkoz, *Phosphorus, Sulfur, and Silicon and the Related Elements* **2006**, *181*, 931–937.

- DOI:10.1080/10426500500272186
33. H. Kutuk, S. Ozturk, *Phosphorus, Sulfur, and Silicon* **2009**, *184*, 332–340. DOI:10.1080/10426500802119655
34. H. Kutuk, J. Tillett, *Phosphorus, Sulfur, and Silicon and the Related Elements* **1993**, *85*, 217–224. DOI:10.1080/10426509308038201
35. H. Kutuk, H. Yakan, *Phosphorus, Sulfur, and Silicon and the Related Elements* **2011**, *186*, 1460–1469. DOI:10.1080/10426507.2010.517584
36. M. M. Langade, *Der Pharm Chem* **2011**, *3*, 283–286.
37. H. Asefi, J. G. Tillett, *Journal of the Chemical Society, Perkin Transactions 2* **1979**, 1579–1582. DOI:10.1039/p29790001579
38. B. Bujnicki, J. Drabowicz, M. Mikołajczyk, A. Kolbe, L. Stefaniak, *The Journal of organic chemistry* **1996**, *61*, 7593–7596. DOI:10.1021/jo960205j
39. Y. Bekdemir, A. Gediz Erturk, H. Kutuk, *J. Phys. Org. Chem.* **2014**, *27*, 94–98. DOI:10.1002/poc.3242
40. Z. Mei-Yun, L. Yi-Qun, X.-m. Xu, *Synth. Commun.* **2003**, *33*, 3777–3780. DOI:10.1081/SCC-120025187
41. a) M. S. Blois, *Nature* **1958**, *181*, 1199–1200; DOI:10.1038/1811199a0
 b) H. Muğlu, H. Yakan, A. G. A. Misbah, M. S. Çavuş, T. K. Bakır, *Res. Chem. Intermed.* **2021**, *47*, 4985–5005; DOI:10.1007/s11164-021-04576-7
 c) H. Muğlu, M. Akın, M. S. Çavuş, H. Yakan, N. Şaki, E. Güzel, *Computational Biology and Chemistry* **2022**, *96*, 107618; DOI:10.1016/j.compbiolchem.2021.107618
 d) H. Yakan, *Res. Chem. Intermed.* **2020**, *46*, 3979–3995; DOI:10.1007/s11164-020-04185-w
 e) H. Yakan, M. S. Çavuş, B. Z. Kurt, H. Muğlu, F. Sönmez, E. Güzel, *J. Mol. Struct.* **2021**, *1239*, 130495; DOI:10.1016/j.molstruc.2021.130495
 f) H. Yakan, T. K. Bakır, M. S. Çavuş, H. Muğlu, *Res. Chem. Intermed.* **2020**, *46*, 5417–5440. DOI:10.1007/s11164-020-04270-0
42. a) R. Re, N. Pellegrini, A. Proteggente, A. Pannala, M. Yang, C. Rice-Evans, *Free radical biology and medicine* **1999**, *26*, 1231–1237; DOI:10.1016/S0891-5849(98)00315-3
 b) B. Dechayont, P. Ruamdee, S. Poonnaimuang, K. Mokmued, J. Chunthorng-Orn, *Journal of Botany* **2017**, *2017*. DOI:10.1155/2017/8310275
43. L. Zhang, S. B. Mulrooney, A. F. Leung, Y. Zeng, B. B. Ko, R. P. Hausinger, H. Sun, *Biomaterials* **2006**, *19*, 503–511. DOI:10.1007/s10534-005-5449-0
44. a) G. L. Ellman, K. D. Courtney, V. Andres Jr, R. M. Featherstone, *Biochemical pharmacology* **1961**, *7*, 88–95; DOI:10.1016/0006-2952(61)90145-9
 b) A. B. Özçelik, M. Gökçe, I. Orhan, M. F. Sahin, *FABAD Journal of Pharmaceutical Sciences* **2010**, *35*, 153.
45. H. M. Berman, J. Westbrook, Z. Feng, G. Gilliland, T. N. Bhat, H. Weissig, I. N. Shindyalov, P. E. Bourne, *Nucleic acids research* **2000**, *28*, 235–242.
46. O. Trott, A. J. Olson, *Journal of computational chemistry* **2010**, *31*, 455–461.
47. R. A. Laskowski, J. Jabłońska, L. Pravda, R. S. Vařeková, J. M. Thornton, *Protein science* **2018**, *27*, 129–134. DOI:10.1002/pro.3289
48. C. A. Bunton, J. H. Crabtree, L. Robinson, *Journal of the American Chemical Society* **1968**, *90*, 1258–1265. DOI:10.1021/ja01007a027
49. J. Liang, J. Lv, J.-c. Fan, Z.-c. Shang, *Synthetic Communications* **2009**, *39*, 2822–2828. DOI:10.1080/00397910802474966
50. A. Bagno, G. Scorrano, R. M. O’Ferrall, *Reviews of chemical intermediates* **1987**, *7*, 313–352. DOI:10.1007/BF03155656
51. S. Perveen, R. Orfali, *Journal of Chemistry* **2018**, *2018*. DOI:10.1155/2018/5198325
52. P. S. Nayab, M. Pulaganti, S. K. Chitta, M. Oves, *Bangladesh Journal of Pharmacology* **2015**, *10*, 703–713. DOI:10.3329/bjp.v10i3.23637

Povzetek

Kislinsko katalizirano hidrolizo N-(p-substituiranih fenil) ftalimidov v treh različnih kislinah smo proučili pri 50,0 ± 0,1 °C. Uporabljena sta bila dva različna testa antioksidativne aktivnosti, in sicer določitev DPPH• in odstranjevanje DPPH•, ter trije različni testi inhibitorne aktivnosti encimov, in sicer inhibicija ureaze, acetilholinesteraze (AChE) in butilholinesteraze (BChE). Spojina 3c (2,03 µg/ml) je imela večjo antioksidativno aktivnost kot druge spojine in standardi glede na test DPPH. Pri testu AChE sta imeli spojini 3a in 3b (13,13 in 9,59 µg/ml) večjo inhibitorno aktivnost encima kot standard galantamin (14,37 µg/ml). Pri testih BChE in ureaze so imele vse spojine (6,84-13,60 in 10,49-17,73 µg/ml) večjo inhibitorno aktivnost encimov kot standard galantamin (49,40 µg/ml) oz. tiourea (26,19 µg/ml). S simulacijami molekularnega sidranja smo proučili interakcijo vsake od treh spojin z aktivnimi mesti encimov AChE, BChE in ureaze.



Except when otherwise noted, articles in this journal are published under the terms and conditions of the Creative Commons Attribution 4.0 International License

Comparison of Kinetics of Adsorption of Permanganate on Co-Al-Layered Double Hydroxide and MoS₂ Nanocompounds

Shahin Ghobadi,¹ Babak Samiey,^{1,*} Enis Esmaili¹ and Chil-Hung Cheng²

¹ Department of Chemistry, Faculty of Science, Lorestan University, Khoramabad 68137-17133, Lorestan, Iran

² Department of Chemical Engineering, Toronto Metropolitan University, Toronto, Ontario, M5B 2K3, Canada

* Corresponding author: E-mail: babsamiey@yahoo.com, samiey.b@lu.ac.ir

Received: 11-29-2022

Abstract

Permanganate (MnO₄⁻) ions were adsorbed on carbonate intercalated Co-Al-layered double hydroxide (Co-Al-LDH) and MoS₂ and after a while the adsorbed MnO₄⁻ ions were reduced to MnO₂. Reduction of adsorbed MnO₄⁻ ion was catalyzed on the surface of carbonate intercalated Co-Al-LDH but MnO₄⁻ ions reacted with MoS₂ surface. Adsorption kinetic tests were carried out at different temperatures, ionic strengths, pH, initial adsorbate concentrations and shaking rates. The adsorption kinetics was studied by the kinetics of adsorption study in the regions with constant adsorption acceleration (KASRA) model and KASRA, ideal-second-order (ISO), intraparticle diffusion, Elovich and (non-ideal process of adsorption) kinetics (NIPPON) equations.

In this work, a new equation called NIPPON equation was introduced. In this equation, it was assumed that during a non-ideal process, adsorbate species molecules were adsorbed simultaneously on the same type adsorption sites with different activities. Indeed, the average values of adsorption kinetic parameters were calculated by the NIPPON equation. Also, the character of boundaries of regions obtained from the KASRA model can be determined by this equation.

Keywords Co-Al-LDH, MoS₂, potassium permanganate, adsorption, NIPPON equation, KASRA model

1. Introduction

Industrial wastewaters, especially produced by chemical and pharmaceutical, leather, cosmetics, fabrics factories often include substances like organic synthetic substances, inorganic compounds and heavy metals that need to be treated before being discharged into the environment. There are different methods for treatment of these wastewaters such as coagulation and flocculation, filtration, sludge drying, sedimentation and adsorption. Among them, adsorption process is commonly used in industry for compound separation and wastewater treatment. This technology is especially featured by cost effectiveness and ease of design and operation.

Potassium permanganate (KMnO₄) is a strong oxidizing agent and there were a few work in relation to its adsorption from aqueous media. In continuation of our earlier works,^{1,2} mechanisms of adsorption kinetics of MnO₄⁻ on Co-Al-LDH and MoS₂ nanocompounds were studied by the KASRA model and the KASRA, ISO, NIPPON, Elovich and intraparticle diffusion equations. MnO₄⁻

ion was adsorbed on the surface of Co-Al-LDH and MoS₂ and then was reduced to MnO₂ and the reaction obeyed ARIAN-Hinshelwood mechanism.^{1,2} Layered double hydroxides (LDHs) have a general formula of [M²⁺_{1-x}M³⁺_x(OH)₂]^{x+}(A)ⁿ⁻_{x/n} · mH₂O and consist of highly ordered two-dimensional hydroxide layers where M²⁺ and M³⁺ are divalent and trivalent cations respectively and Aⁿ⁻ is the interlayer anion of valence *n* like carbonate, nitrate and so on,³⁻⁵ Fig. S1(a). LDHs are used in artificial photosynthesis,⁶ biomedical sectors,⁷ oxygen evolution reaction towards efficient hydrogen generation,⁸ controlled drug release and delivery⁹ and as adsorbent,¹⁰ corrosion inhibitors,¹¹ supercapacitors¹² and inorganic flame-retardant fillers.¹³ In this work, Co-Al-LDH was used for adsorption of MnO₄⁻ ions and catalyzed their reduction to MnO₂. As reported before, Co-Al-LDH was used as catalyst for reduction of dyes,¹⁴ CO₂ reduction in aqueous media,¹⁵ efficient superoxide dismutase-like nanozyme,¹⁶ enhanced catalyst for carbon-carbon coupling¹⁷ and as one of components of a photocatalyst.¹⁸

MoS₂ is a natural or synthetic compound and has a layered structure. In its structure, a plane of molybdenum atoms is sandwiched by two planes of sulfide ions which form a layer. These three planes stack on top of each other with strong covalent bonds between the Mo and S atoms and weak van der Waals forces hold these layers together,^{2,19–21} Fig. S1(b). MoS₂ shows polytypism and has three various configurations like 1T,²² 2H²³ and 3R²⁴ that represent its trigonal, hexagonal and rhombohedral arrangements, respectively and among them 2H is the most stable thermodynamic form of MoS₂.²³ MoS₂ possesses many applications such as solid lubricant,²⁵ biosensor,²⁶ gas sensor,²⁷ catalyst,²⁸ supercapacitor²⁹ and for tissue engineering,³⁰ electronic and optoelectronic devices,³¹ energy storage,³² solar energy storage,³³ and biomedical applications.³⁴

Potassium permanganate (KMnO₄), known as “Condy’s Crystal”, is a strong oxidizing inorganic compound and has many applications like medical uses,³⁵ water treatment process³⁶, analytical uses³⁷ and synthesis of organic compounds³⁸ in laboratories and industry.

In this study, as-synthesized carbonate intercalated Co-Al-LDH and MoS₂ were used as highly efficient adsorbents for MnO₄⁻. In our previous works,^{1,2} both Co-Al-LDH and MoS₂ were characterized by various techniques such as FTIR (Fourier transfer infrared spectroscopy), BET (Brauner-Emmett-Teller), FESEM (field emission scanning electron micrograph), EDS (energy dispersive X-ray spectroscopy), XPS (X-ray photoelectron spectroscopy) and XRD (X-ray diffraction). Here, we studied effects of different variables like pH, initial MnO₄⁻ concentration, temperature, shaking rate, contact time and ionic strength on adsorption capacity of Co-Al-LDH and MoS₂ for MnO₄⁻. Also, in this work, NIPPON equation was introduced for analysis of adsorption kinetic process. The kinetics of adsorption of MnO₄⁻ on Co-Al-LDH and MoS₂ were analyzed by the KASRA model and the KASRA, Elovich, intraparticle diffusion, ISO and NIPPON equations to give more information about the mechanism of these processes. In this study, using information obtained from carrying out kinetic tests and our previous works,^{1,2} mechanism of adsorption kinetics of MnO₄⁻ on Co-Al-LDH and MoS₂ were investigated.

2. Materials and Methods

2.1. Chemicals

Aluminum nitrate (Al(NO₃)₃·9H₂O) (>98.5%), cobalt nitrate (Co(NO₃)₂·6H₂O) (>99%), sodium carbonate (99.9%), sodium molybdate (Na₂MoO₄·2H₂O) (>99.5%), thioacetamide (>99%), hydrochloric acid (37%), concentrated sulfuric acid (98%), oxalic acid (>99%), sodium hydroxide (>98%), sodium chloride (>99.5%) and potassium permanganate (>99%) were purchased from Merck. All chemicals were used without further purification.

2.2. Synthesis of Co-Al-LDH and MoS₂

Synthesis of carbonate intercalated Co-Al-LDH was carried out according to the procedure for preparation of carbonate intercalated Mg-Al-LDH (Mg₆Al₂(OH)₁₆CO₃·4H₂O)³⁹ in our previous works.^{1,40} The MoS₂ was prepared according to the published procedure.^{2,41}

2.3. Characteristics of As-synthesized Co-Al-LDH and MoS₂

The synthesized Co-Al-LDH and MoS₂ were characterized by XRD, SEM, EDS, FTIR, BET and XPS techniques which confirmed their formation^{1,2} and were used for studying thermodynamics^{1,2} and kinetics of adsorption of MnO₄⁻ on Co-Al-LDH and MoS₂. It was shown that MnO₄⁻ ions were adsorbed on the mesopore and micropore adsorption sites of Co-Al-LDH and micropore adsorption sites of MoS₂ nanocompounds. Mesopore and micropore adsorption sites were abbreviated as ME and MI sites, respectively.

2.4. Adsorption Kinetic Tests

In adsorption kinetic tests, 0.002 g of Co-Al-LDH or 0.0015 g of MoS₂ samples were added to 10 ml of MnO₄⁻ solutions. Initial concentrations of MnO₄⁻ solutions were 2 × 10⁻⁵, 5 × 10⁻⁴ or 7 × 10⁻⁴ M in the case of Co-Al-LDH and 2.5 × 10⁻⁴, 5 × 10⁻⁴ or 0.75 × 10⁻⁴ M for MoS₂. The solutions were shaken at 40, 70 and 100 rpm in a temperature controlled water bath shaker (Fater electronic Co., Persian Gulf model) at 308, 318 and 328 K and different ionic strengths and pHs. The residual concentrations of MnO₄⁻ in the solutions were measured at different contact times during the course of adsorption, through photometry at their λ_{max} values by a UV mini 1240V Shimadzu spectrophotometer. The λ_{max} values of MnO₄⁻ in neutral water, acidic and alkaline media were 527 and 546 nm and that of MnO₄²⁻ in alkaline media was 437 nm. The relation used to calculate MnO₄⁻ adsorption capacity on the Co-Al-LDH or MoS₂, q_t (mg g⁻¹), was as follows

$$q_t = \frac{(c_0 - c_t)Mv}{1000w} \quad (1)$$

where q_t is adsorption capacity at time t (mg g⁻¹), c₀ and c_t are the initial concentration of adsorbate in each solution and adsorbate concentration at time t (M) respectively, v is the volume of solution (ml), M is the molecular weight of adsorbate (mg mole⁻¹) and w is the weight of the used adsorbent (g).

2.5. Adsorption Model and Isotherms

In our previous works,^{1,2} the adsorption thermodynamic isotherms of MnO₄⁻ on the surface of Co-Al-LDH and MoS₂ were analyzed by “*adsorption isotherm regional analysis model*” that is abbreviated as the ARIAN model

and their adsorption mechanism were explained by analysis of their adsorption isotherm and other experimental evidence. Here, we explained about this model because we used some results of it along with results of adsorption kinetic tests. The ARIAN model was explained in Supplementary material,^{42–46} Fig. S2. Briefly, this model is composed from four regions. Region I is related to adsorption of adsorbate on the most active adsorption sites. Region II is the result of interaction of adsorbate with a group of less active adsorption sites. If there are two or more adsorption sites, the sub-regions of region II are denoted by IIA, IIB, etc. Region III appears in the case of formation of aggregates of adsorbates on the surface like micelles and in region IV plateau appears or in some cases reverse desorption is observed. Adsorption kinetic tests of MnO_4^- on the Co-Al-LDH and MoS_2 were carried out within regions I and II of their isotherms and compared with each other.^{1,2}

2. 6. Adsorption Kinetic Equations and Model

The kinetic curves were studied by several equations. The intraparticle diffusion equation⁴⁷ is given by

$$q_t = k_{dif} t^{0.5} + I \quad (2)$$

where I is the boundary layer thickness and k_{dif} is the rate constant for intraparticle diffusion.

Another equation used for analysis of adsorption kinetics is the Elovich equation⁴⁸ that is written as

$$q_t = \frac{1}{\beta} \ln(\alpha\beta) + \frac{1}{\beta} \ln t \quad (3)$$

where α is initial adsorption rate and β is the Elovich constant.

Also, the KASRA model and KASRA equation^{49–51} were used to analyze the adsorption kinetics. KASRA is an abbreviation for “*kinetics of adsorption study in the regions with constant adsorption acceleration*”. KASRA is a Persian word meaning king. The KASRA model is based on the three assumptions for adsorption of an adsorbate species on an adsorption site: (1) each time range that adsorption acceleration in it is constant, is named a “*region*”, (2) there are two regions before reaching the plateau region, and (3) the boundary between the first and second regions is called *starting second region* (abbreviated as *ssr*) point and that of between the second and third regions is called *starting third region* (abbreviated as *str*) point that of between the third and fourth (plateau) regions is called *kinetics of adsorption termination* (abbreviated as *kat*) point. All of these points are determined by the KASRA equation^{49,50} given as follows:

$$q_t = \frac{1}{2} a_i t^2 + (v_{oi} - a_i t_{oi}) t + q_{oi} - \frac{1}{2} a_i t_{oi}^2 - (v_{oi} - a_i t_{oi}) t_{oi} \quad (4)$$

where q_{oi} , v_{oi} and t_{oi} are q_t , velocity and time at the beginning of the i th region, respectively and a_i is the acceleration

of adsorption kinetics in the i th region whereas $i = 1–4$. In these works, due to lack of the third region and thus *str* point, the point between the second and fourth regions was called *kat* point and thus $i = 1–3$. Each a_i is a negative value because during adsorption process the adsorbate concentration decreases. In the first region, t_{o1} and q_{o1} are equal to zero. The second region begins from *ssr* point which is assigned with the coordinates t_{o2} and q_{o2} . Finally, plateau (third) region starts at the equilibrium time, t_e and equilibrium adsorption capacity, q_e which are coordinates of *kat* point. In this region, $v_{o3} = a_3 = 0$, $t_{o3} = t_e$ and $q_{o3} = q_e$ and Eq. (4) is simplified to $q_t = q_e$. Due to different characteristics of the first and second regions, parameters obtained for these two regions such as rate constants are different from each other.

In this work, to avoid confusion in relation to the regions in isotherms and kinetic curves, kinetic regions are shown using numbers like region 1, etc. Typical adsorption kinetic curves of MnO_4^- on Co-Al-LDH and MoS_2 according to the KASRA model were shown in Fig. 1.

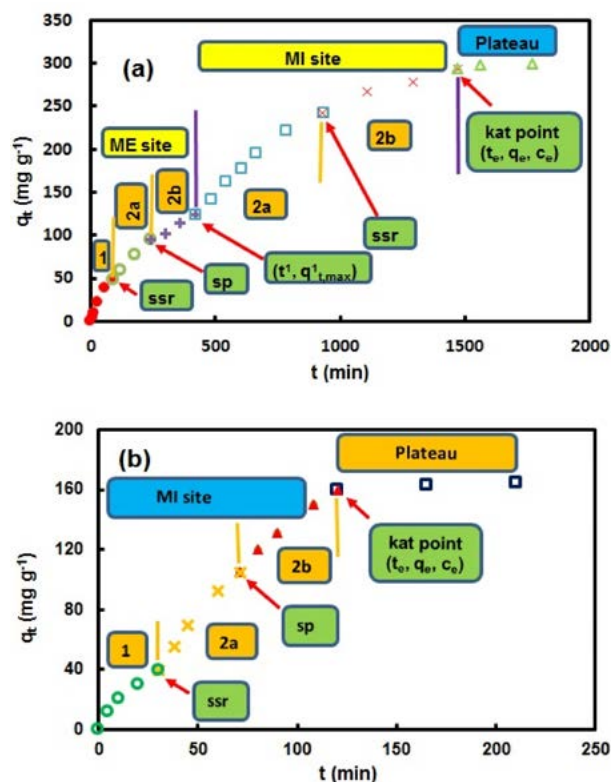


Fig. 1 Typical adsorption kinetic diagrams of MnO_4^- on (a) Co-Al-LDH and (b) MoS_2 based on the KASRA model

The *ideal-second-order* (or abbreviated as ISO) equation⁵⁰ is written as

$$\ln \left(\frac{q_e - q_t}{ac_i} \right) = - \frac{k_I c_e}{q_e} t + A' \quad (5)$$

where $k_I = k_1^2 q_e$ and k_1^2 are the first- and second-order adsorption rate constants of the ISO equation in each region

and are in $M^{-1} \text{ mg g}^{-1} \text{ min}^{-1}$ and $M^{-1} \text{ min}^{-1}$, respectively and $A' = \ln \left(\frac{q_e}{a c_e} \right) \cdot a = \frac{M \nu}{1000 w}$, where ν is the volume of solution (ml), w is the weight of the used adsorbent (g) and M is the molecular weight of adsorbate (mg mole^{-1}). A number of adsorbents have m different adsorption sites and adsorption occurs in sequence on their first, then second, ..., $(m - 1)$ th and m th sites, respectively. In these cases, there are m kinetic curves and in Eq. (5), q_e and c_e are used for m th site and for $m - 1$ other sites and these symbols are replaced with $q_{i,\max}^i$ and $c_{i,\max}^i$, where $i = 1, \dots, m - 1$. $q_{i,\max}^i$ and $c_{i,\max}^i$ are the maximum adsorption capacity of adsorbent and adsorbate concentration after adsorption completion on the i th adsorption site, respectively. Thus, the ISO equation is used m times to analyze these m kinetic curves.⁴⁶

As referred before, in this work due to lack of the third region, based on the KASRA model there are two regions in adsorption kinetic curves before reaching the plateau which result from non-ideality in adsorption process. In the first one, completely ideal adsorption occurs on the bare surface of adsorbent. The progressively changes happened on the surface of adsorbent in region 1 finally result in emerging another ideal region (region 2) in which adsorption carries out on a partly adsorbate-covered surface.

But, using the ISO equation shows that region 2 is composed of two another ideal parts that are named 2a and 2b. The first part of the second region, 2a, starts after *ssr* point and the second one, 2b, starts after *starting second part* (or abbreviated as *sp*) point and ends at the *kat* point.⁴⁹

The ISO first-order rate constant of region 1 is shown with k_{11} and those of the second region are shown with k_{12a} and k_{12b} , respectively. Also, the ISO second-order rate constant of region 1 is shown with k_{11}^2 and those of the second region are shown with k_{12a}^2 and k_{12b}^2 , respectively. Due to decrease in adsorbate concentration with time, the ISO rate constant of region 1 is greater than part a of region 2 or part 2a, i.e. $k_{11} > k_{12a}$ and in part b of region 2 (or part 2b), adsorption ends to plateau and due to this sudden change k_{12b} is greater than both k_{11} and k_{12a} , thus we have $k_{12b} > k_{11} > k_{12a}$. Similarly, for the ISO second-order rate constants we have $k_{12b}^2 > k_{11}^2 > k_{12a}^2$.

If the ISO rate constant of a step obeys the Arrhenius equation, that step is adsorption- or reaction-controlled and otherwise it is called diffusion-controlled. As referred above, in some adsorbents, there are two or more different adsorption sites which result in observing two or more successive adsorption kinetic curves in an adsorption kinetic diagram. In these cases, region 1, (completely ideal) is only observed in the first adsorption kinetic curve,⁴⁶ Fig. 1.

Sometimes, due to braking effect⁵⁰ an interval is observed between two successive adsorption kinetic curves or between regions 1 and 2 of the first adsorption curve. The “*time range of interval between two successive adsorption kinetic curves*” (abbreviated as TRAK) is used to compare this effect in different cases.^{46,51} On the other hand, the initial concentration of adsorbate has an important role in

appearing the TRAK in an adsorption kinetic curve. Thus, for comparing kinetic curves including TRAK(s) with together and other kinetic curves, their first-order rate constants obtained from the ISO equation are used.

If adsorption results in a TRAK, $q_{i,\max}^i$ and $c_{i,\max}^i$ are replaced by c_T^i and c_T^i , respectively. q_T^i and c_T^i are adsorption capacity of adsorbent and adsorbate concentration at the beginning of the TRAK between n th and $(n + 1)$ th kinetic curves, respectively. In these cases, $k_i = k_T^i q_T^i$ and subscript T is an abbreviation for TRAK.^{46,51}

2. 7. Introducing the NIPPON Equation

Adsorption on heterogeneous surface of adsorbents in liquid phase happens through different kinds of interactions, like hydrogen bonding, between adsorbate species and some parts (and not whole) of adsorbents surface. Also, at first, most active sites and then other less active sites of adsorbent surface interact with adsorbate species. Thus, adsorption thermodynamics and kinetics in liquid phase are intrinsically non-ideal. As explained in the KASRA model and ISO equation, adsorption on the most active and less active adsorption sites of the same type or adsorption on different types of adsorption sites on an adsorbent are separately studied as ideal cases and have different adsorption kinetic parameters.^{46,49,50} In the KASRA model, adsorption capacity was written as a three-term polynomial function of time. But, as in physics higher derivatives of position with respect to time are used for non-ideal situation,^{52,53} we can use higher derivatives of adsorption capacities with respect to time to analyze the non-ideal adsorption kinetic data to find average parameters of the same type adsorption sites that have different activities. By considering a time range of adsorption kinetics belonging to one average type of adsorption site as a continuous non-ideal process, the time function of non-ideal adsorption capacity, q_b , changes with time as $\sum_{n=0}^{\infty} (-1)^n t^n$ which is the Taylor series of $\frac{1}{1+t}$. Here, N is an abbreviation for “*non-ideal adsorption*”. In spite of the KASRA equation, in non-ideal adsorption it was assumed that in each time range adsorbate species were simultaneously adsorbed on adsorption sites with different activities. Thus, changes in q_i with time was written as

$$\frac{dq_i^N}{dt} = k(1 - t + t^2 - t^3 + t^4 - \dots) \quad (6)$$

By using the relation $\frac{1}{1+t} = 1 - t + t^2 - t^3 + t^4 - \dots$, Eq. (6) can be written as

$$\frac{dq_i^N}{dt} = k \left(\frac{1}{1+t} \right) \quad (7)$$

where k is the rate constant of the equation (6). By integration of Eq. (7) we have

$$\int dq_i^N = k \int \frac{dt}{1+t} \quad (8)$$

$$q_t^N = k \ln(1+t) + cte \quad (9)$$

where $cte = q_{ts}^N + k \ln(1 + t_s)$. q_{ts}^N and t_s are adsorption capacity and time in the starting point of the assumed time range, respectively. When $t \ll 1$ we have $\ln(1 + t) \approx t$ and then

$$q_t^N = kt \quad (10)$$

Dimension of natural logarithm argument, $1 + t$, is in $\frac{\text{time}}{\text{unit of time}}$. Equation (9) was derived and introduced by one of authors, Babak Samiey, and was called “*non-ideal process of adsorption kinetics equation*” or abbreviated as the NIPPON equation, Fig. 2.

NIPPON is a Japanese name of Japan and means the sun's origin. By taking the first and second derivatives of the NIPPON equation, non-ideal velocity and non-ideal acceleration adsorption kinetic equations, Eqs. (11) and (12), were obtained respectively. These equations are as follows

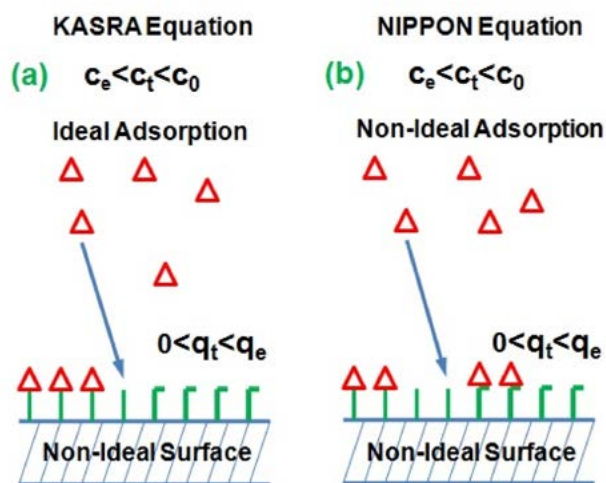


Fig. 2 Schematic comparison of adsorption kinetics by the (a) KASRA and (b) NIPPON equations. One type of functional group as adsorption site with two different types of activities was shown in green and adsorbate species were shown in red

Table 1. Adsorption acceleration and velocity parameters for the first and second region and related t_{ssr} and q_{ssr} values obtained from analysis of some adsorption processes by the KASRA model

Sym- bol	Adsorption process	First region				Second region		Ref.
		a_{01}	v_{01}	t_{ssr}	q_{ssr}	a_{02}	v_{02}	
A	Adsorption of oxalic acid on animal charcoal at 308 K	0	9.0×10^{-3}	10	0.02	-2.0×10^{-5}	2.0×10^{-2}	54
B	Adsorption of natural dissolved organic matter (in terms of DOC) by multiwalled carbon nanotubes at 5 °C	0	0.33	5.3	1.4	-6.7×10^{-5}	8.7×10^{-3}	55
C	Adsorption of natural dissolved organic matter (in terms of AOC) by multiwalled carbon nanotubes at 5 °C	-2.0×10^{-4}	5.2×10^{-3}	20.3	0.08	-1.2×10^{-5}	9.2×10^{-4}	55
D	Adsorption of direct yellow12 on coconut shell activated carbon	-0.02	1.46	10	14.9	-1.4×10^{-4}	1.49	56
E	Adsorption of basic blue 3 onto sphagnum agellanicum peat	0	9.75	1.2	11.7	-3.6×10^{-2}	0.54	57
F	Adsorption of reactive red 239 from aqueous solution by chitosan 8B	-0.17	0.61	10	9.6	-4.0×10^{-3}	0.24	58
G	Adsorption of methylene blue on activated carbon obtained from waste Elaeagnus stone	0	13.90	10.3	143.4	-3.8×10^{-2}	2.88	59
H	Adsorption of malachite green on activated carbon obtained from waste Elaeagnus stone	0	20.90	9.6	200.7	-5.6×10^{-2}	4.75	59
I	Adsorption of rhodamine B on activated carbon obtained from waste Elaeagnus stone	0	14.27	10.3	147.0	-2.4×10^{-2}	2.30	59
J	Adsorption of methyl orange on banana peel*	0	0.16	5	0.8	-4.0×10^{-3}	0.27	60
K	Adsorption of methylene blue on orange peel*	0	0.30	5	1.5	-0.01	0.45	60
L	Adsorption of methylene blue on poly(acrylic acid) (PAA)-based super-adsorbent nanocomposite hydrogel	0	5.72	12.8	73.2	-8.4×10^{-2}	10.45	61
M	Adsorption of remazol Y onto steam-activated carbons developed from date pits at pH = 3 and 37 °C	0	24.52	1.7	41.7	-0.12	2.03	62
N	Adsorption of methylene blue onto steam-activated carbons developed from date pits at pH = 5 and 27 °C	0	88.58	1.2	106.3	-8.8×10^{-2}	2.95	62
O	Adsorption of acid red on corn stalks modified by cetylpyridinium bromide at 328 K	0	2.03	3.5	7.1	-4.0×10^{-3}	0.26	63
P	Adsorption of acid orange on corn stalks modified by cetylpyridinium bromide at 318 K	0	2.28	5.6	10.5	-2.0×10^{-3}	0.15	63
Q	Adsorption of malachite green on seeds of dates at 15 °C	-0.60	6.75	14.2	92.5	-0.39	12.64	64
R	Adsorption of methylene blue on nanocrystalline cellulose at 318 K and 80 rpm and 0.045 mM methylene blue	-4.4×10^{-2}	0.21	10	2.8	-8.7×10^{-4}	0.08	50

Units of a_{01} and a_{02} were in $\text{mg g}^{-1} \text{hour}^{-2}$, v_{01} and v_{02} were in $\text{mg g}^{-1} \text{hour}^{-1}$ and t_{ssr} and q_{ssr} were in hour and mg g^{-1} in example L and a_{01} and a_{02} were in $\mu\text{mol g}^{-1} \text{min}^{-2}$, v_{01} and v_{02} were in $\mu\text{mol g}^{-1} \text{min}^{-1}$ and t_{ssr} and q_{ssr} were in min and $\mu\text{mol g}^{-1}$ in example F, respectively. In other cases, a_{01} and a_{02} were in $\text{mg g}^{-1} \text{min}^{-2}$, v_{01} and v_{02} were in $\text{mg g}^{-1} \text{min}^{-1}$ and t_{ssr} and q_{ssr} were in min and mg g^{-1} , respectively. *In examples J and K, TD values were 2.5 and 2 min before starting adsorption process, respectively.

Table 2. Non-ideal adsorption acceleration and velocity parameters for the first and second NIPPON curves and related t_{sc} and q_{sc}^N values obtained from analysis of some adsorption processes by the NIPPON and KASRA equations

Sym- bol	Adsorption process	First curve		t_{sc}	q_{sc}^N	Second curve		Ref.
		a_{fc}^N	v_{fc}^N			a_{sc}^N	v_{sc}^N	
A	Adsorption of oxalic acid on animal charcoal at 308 K	-0.01	0.01	-	-	-	-	54
B	Adsorption of natural dissolved organic matter (in terms of DOC) by multiwalled carbon nanotubes at 5 °C	0	0.33	5.3	1.4	-0.005	0.03	55
C	Adsorption of natural dissolved organic matter (in terms of AOC) by multiwalled carbon nanotubes at 5 °C	0.035	-0.035	-	-	-	-	55
D	Adsorption of direct yellow12 on coconut shell activated carbon	0	1.49	20	30.2	-0.46	5.02	56
E	Adsorption of basic blue 3 onto sphagnum agellanicum peat	0	9.75	1.2	11.7	-0.59	1.29	57
F	Adsorption of reactive red 239 from aqueous solution by chitosan 8B	-4.18	4.18	-	-	-	-	58
G	Adsorption of methylene blue on activated carbon obtained from waste Elaeagnus stone	-17.88	17.88	-	-	-	-	59
H	Adsorption of malachite green on activated carbon obtained from waste Elaeagnus stone	-19.07	19.07	-	-	-	-	59
I	Adsorption of rhodamine B on activated carbon obtained from waste Elaeagnus stone	-17.54	17.54	-	-	-	-	59
J	Adsorption of methyl orange on banana peel*	0	0.16	5	0.8	-0.10	0.61	60
K	Adsorption of methylene blue on orange peel*	0	0.30	5	1.5	-0.15	0.88	60
L	Adsorption of methylene blue on poly(acrylic acid) (PAA)-based super-adsorbent a nocomposite hydrogel	0	5.72	12.8	73.2	-1.51	20.79	61
M	Adsorption of remazol Y onto steam-activated carbons developed from date pits at pH=3 and 37 °C	0	24.52	1.7	41.7	-1.47	3.96	62
N	Adsorption of methylene blue onto steam-activated carbons developed from date pits at pH=5 and 27 °C	0	88.58	1.2	106.3	-5.15	11.32	62
O	Adsorption of acid red on corn stalks modified by cetylpyridinium bromide at 328 K	0	2.03	3.5	7.1	-0.14	0.63	63
P	Adsorption of acid orange on corn stalks modified by cetylpyridinium bromide at 318 K	0	2.28	5.6	10.5	-0.05	0.31	63
Q	Adsorption of malachite green on seeds of dates at 15 °C	-56.61	56.61	-	-	-	-	64
R	Adsorption of methylene blue on nanocrystalline cellulose at 318 K and 80 rpm and 0.045 mM methylene blue	-1.34	1.34	-	-	-	-	50

Units of a_{fc}^N and a_{sc}^N were in $\text{mg g}^{-1} \text{hour}^{-2}$, v_{fc}^N and v_{sc}^N were in $\text{mg g}^{-1} \text{hour}^{-1}$ and t_{sc} and q_{sc}^N were in hour and mg g^{-1} in example L and a_{fc}^N and a_{sc}^N were in $\mu\text{mol g}^{-1} \text{min}^{-2}$, v_{fc}^N and v_{sc}^N were in $\mu\text{mol g}^{-1} \text{min}^{-1}$ and t_{sc} and q_{sc}^N were in min and $\mu\text{mol g}^{-1}$ in example F, respectively. In other cases, a_{fc}^N and a_{sc}^N were in $\text{mg g}^{-1} \text{min}^{-2}$, v_{fc}^N and v_{sc}^N were in $\text{mg g}^{-1} \text{min}^{-1}$ and t_{sc} and q_{sc}^N were in min and mg g^{-1} , respectively. *In examples J and K, TD values were 2.5 and 2 min, and thus for first curve, and min were used in Eqs. (11) and (12), respectively. Subscripts *fc* and *sc* are abbreviations for starting first curve and starting second curve, respectively.

$$v_t^N = \frac{k}{1+t} \quad (11)$$

$$a_t^N = -\frac{k}{(1+t)^2} \quad (12)$$

where v_t^N and a_t^N were non-ideal velocity and acceleration of adsorption of adsorbate, respectively. On the other hand, at $t = 0$, $v_0^N = k$ and $a_0^N = -k$ and $t = t_e$ we have

$$v_e^N = \lim_{t \rightarrow \infty} \frac{k}{1+t} = 0 \quad (13)$$

$$a_e^N = -\lim_{t \rightarrow \infty} \frac{k}{(1+t)^2} = 0 \quad (14)$$

where v_e^N and a_e^N were non-ideal velocity and acceleration of adsorption of adsorbate at $t = t_e$, respectively. In initial time ranges of adsorption, the process is ideal and may obey from the KASRA equation.

In some adsorption processes, depending on the nature of adsorbent or adsorbate, it is possible to observe more than one curve. A number of examples chosen from published papers^{50,54–64} were analyzed by the KASRA model, Table 1 and Fig. S3 and the NIPPON equation, Table 2 and Fig. S4. Here, to calculate non-ideal velocity and acceleration of adsorption of adsorbates by using equations (11) and (12), and were used for the first and second curves, respectively.

3. Results and Discussion

3.1. Characterization of Co-Al-LDH and MoS₂ Nanocompounds

Characterization of these two compounds by XRD, XPS, FTIR, SEM, BET and EDS techniques showed that in this work Co₆Al₂(OH)₁₆CO₃·4H₂O and hexagonal

2H-MoS₂ were synthesized.^{1,2} Analysis of products of adsorption of MnO₄⁻ on Co-Al-LDH verified that Co-Al-LDH catalyzed reduction of MnO₄⁻ ions to MnO₂ in the pH range of 1–13 and reacted with it at pH=14. Study of data showed that its adsorption sites are Co–OH groups located on ME and MI sites.¹

On the other hand, analysis of products of MnO₄⁻ adsorption on MoS₂ confirmed that MnO₄⁻ reacted with MoS₂ in the pH range of 1–12 and its adsorption sites were Mo–S pairs located on its micropore sites.²

3. 2. Kinetics of adsorption of MnO₄⁻ on Co-Al-LDH

As reported before,^{65–69} Co-Al-LDH was used as an adsorbent or one of components of an adsorbent and kinetics and thermodynamics of these processes were studied by researchers. As observed in our earlier work,¹ the boundary of regions of adsorption isotherms of MnO₄⁻ on Co-Al-LDH under different conditions were shown in Table S1. Based on these data, appropriate initial concentrations of MnO₄⁻ were used for doing adsorption kinetic tests.

The adsorption kinetics of MnO₄⁻ on Co-Al-LDH was studied using various initial MnO₄⁻ concentrations of 0.25, 0.5 and 0.7 mM, shaking rates of 40, 70 and 100 rpm at 308, 318 and 328 K in water (neutral water), 0.1 M NaCl and in acidic (pHs of 2.8, 3.8) and alkaline (pHs of 12, 13 and 14) solutions, shown in Tables 3–7 and Figs. 3, 4 and S5. Under different conditions, MnO₄⁻ ions were adsorbed on the surface of Co-Al-LDH after 10 h.

As seen in Tables 4 and 6, in water, at 100 rpm and in 0.25 mM MnO₄⁻ (in region I of the thermodynamic ARIAN model) MnO₄⁻ ions were adsorbed on ME adsorption sites. However, in initial MnO₄⁻ concentrations of 0.5 and 0.7 mM (in region II of the thermodynamic ARIAN model) in water and 0.1 M NaCl, MnO₄⁻ ions were adsorbed on both ME and MI adsorption sites. Tests showed that an increase in the initial MnO₄⁻ concentration, shaking rate, temperature or ionic strength (other parameters were constant) increased the values of k_{diff} adsorption acceleration, initial adsorption rates, k_{I1} and k_{I2b} (both for kinetic curve of adsorption on ME sites), and k_{I2a} (for kinetic curve of adsorption on MI sites). Region 2 for kinetic curve of adsorption on ME sites was composed of only one part and its value was greater than that of region 1 thus it was part 2b.

In 0.1 M NaCl solution, an increase in k_{diff} adsorption acceleration, initial adsorption rates and a vigorous increase in k_{I1} and k_{I2b} (both for adsorption on ME sites) and k_{I2a} (for adsorption on MI sites) was observed compared to those in water at 318 K was due to that CO₃²⁻ ions were surrounded by Na⁺ ions, which decreased electric repulsion between CO₃²⁻ and MnO₄⁻ ions. Also, an initial high adsorption capacity for MnO₄⁻ ions resulted in emerging a TRAK in its adsorption kinetic curve, Table 3. Activation energies of k_{I1} and k_{I2b} (both for the adsorption on

ME sites) and k_{I2a} (for the adsorption on MI sites) in water were 60.4, 75.1 and 49.1 kJ mole⁻¹, respectively which showed that these steps were adsorption-controlled.

In acidic solutions, adsorption process happened only on ME adsorption sites which was due to the formation of bigger neutral HMnO₄ molecules.⁷⁰ Because of a decrease in formal charge of MnO₄⁻ ions, k_{diff} adsorption acceleration, initial adsorption rates, k_{I1} and k_{I2b} decreased with a decrease in pH of solutions from 3.8 to 2.8.

In acidic solutions, due to the increase in ionic strength and the acidity of solution that promoted adsorption capacity,¹ we noticed that k_{diff} adsorption acceleration, initial adsorption rates, k_{I1} and k_{I2b} values increased compared with those in water at 318 K.

In alkaline environment, it was observed that with an increase in pH value to 12, k_{diff} adsorption acceleration, initial adsorption rates, k_{I1} and k_{I2b} (both on ME adsorption sites) highly increased due to an increase in the number of –OH groups of adsorbent surface and ionic strength of the solution. pH_{ZPC} (pH of zero point charge) of carbonate intercalated Co-Al-LDH is 10 and in pHs of higher than 10 its surface charge is negative and became more negative with an increase in pH value.⁷¹ Thus, further increase in pH to 13 yielded in a decrease in k_{diff} adsorption acceleration, initial adsorption rates, k_{I1} and k_{I2b} because of the neutralization of amphoteric Al–OH groups of adsorbent, and also changing large amount of MnO₄⁻ to MnO₄²⁻ Tables 4 and 5.

At pH=13, due to neutralization of some hydroxide groups and increasing adsorbent surface negative charge, MnO₄⁻ ions were adsorbed only on ME sites. Activation energies of k_{I1} (for adsorption on ME sites) was 46.3 kJ mole⁻¹ which showed that the kinetics of this step was adsorption-controlled, similar to that in water. However, k_{I2b} values did not obey Arrhenius equation that confirmed that kinetics of adsorption of MnO₄⁻ ions in this step was diffusion-controlled.

At pH=14, similar to pH of 13, MnO₄⁻ ions were adsorbed on ME sites and due to very fast adsorption and reaction of MnO₄⁻ ions with ME adsorption sites, q_t value of ME sites reached 112.2 mg g⁻¹ (about 50% of total adsorption capacity of adsorbent) within less than half minute after the adsorption test started.

Because of the consumption of MnO₄⁻ ions, a TRAK was observed in the range of less than 0.5 min to 180 min, Table 3. After about 2 hours, a gradual production of MnO₄⁻ ions from MnO₄²⁻ ions in solution¹ resulted in the continuation of adsorption process, Tables 3 and 4. Comparison of EDS spectra of adsorbent samples after 1.5 and 8 hours in 1 mM MnO₄⁻ solutions at pH of 14 showed that about 75% of manganese adsorption occurred after 1.5 h contact with adsorbate solution, Fig. S6.

Analysis of adsorption kinetic data of MnO₄⁻ on Co-Al-LDH by NIPPON equation showed that an excess ideal curve was observed in the beginning of adsorption kinetic diagrams of 2.5 mM MnO₄⁻ at 318 K, 0.5 mM MnO₄⁻ at 328 K, 0.7 mM MnO₄⁻ at 318 K in water and in 0.5 mM

MnO_4^- at pHs of 2.8, 3.8, 12 at 328 K and at pH of 13 at 308, 318 and 328 K at 100 rpm compared to analysis with the KASRA model. These observations showed that activities of the most active adsorption sites located in initial time ranges of first region obtained from the KASRA model were somehow bigger than activities of rest of this type of adsorption sites.

Analysis of adsorption kinetic diagrams of 0.5 mM MnO_4^- at 308 and 318 K at 100 rpm and 0.5 mM MnO_4^- at 318 K at 70 rpm by NIPPON equation showed that there were no excess ideal curve in the beginning of them compared to regions obtained from the KASRA model. In cases 0.5 mM MnO_4^- at 308 and 318 K at 100 rpm, second curves were bigger than those obtained from the KASRA model that showed that activities of boundary adsorption sites were more similar to those located in the second region obtained from the KASRA model. In the case of 0.5 mM MnO_4^- at 318 K at 70 rpm, it was observed that first curve obtained by NIPPON equation was bigger than that calculated by the KASRA model that showed that the activities of boundary adsorption sites were more similar to those of the first region obtained from the KASRA model.

Because MnO_4^- was adsorbed at first on ME sites of Co-Al-LDH, only adsorption of MnO_4^- on these sites were studied by the Elovich equation. As shown in Table 7, α

values in water increased with an increase in temperature and shaking rate.

On the other hand, as reported before,¹ the used Co-Al-LDH adsorbent was recycled successfully by NaBH_4 .

3. 3. Kinetics of adsorption of MnO_4^- on MoS_2

During recent years, researchers used MoS_2 and its composites as efficient adsorbents.^{72–76} As reported in our previous work,² the regions of adsorption isotherms of MnO_4^- on MoS_2 and their boundaries under different conditions were analyzed by the ARIAN model and were shown in Table S2. Using data of this Table, the appropriate initial concentrations of MnO_4^- were determined for carrying out adsorption kinetic tests.

The adsorption kinetic curves of MnO_4^- on MoS_2 were obtained using different initial MnO_4^- concentrations of 0.25, 0.5 and 0.75 mM, shaking rates of 40, 70 and 100 rpm, at 308, 318 and 328 K in water (neutral water), 0.1 M NaCl and in acidic and alkaline solutions at 318 K, Tables 8–11 and Figs. 5, 6 and S7. Under various conditions, MnO_4^- ions were adsorbed on the surface of MoS_2 during different time periods (20–180 min) and then reacted with it. Analysis of adsorption kinetics of this process by the KASRA model showed that MnO_4^- ions were adsorbed on

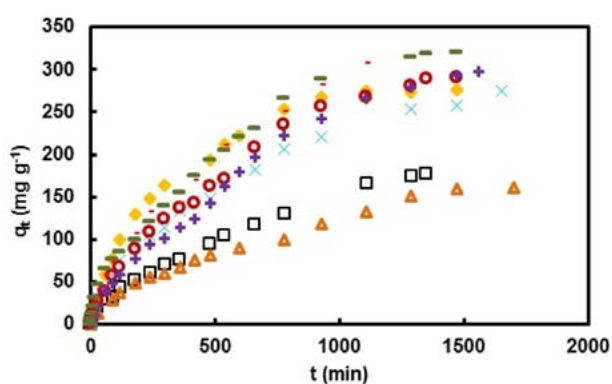


Fig. 3 Kinetic curves of adsorption of MnO_4^- on Co-Al-LDH in water in initial MnO_4^- concentrations of \square 0.25 mM \triangle at 318 K, 0.5 mM at Δ 308 K, \times 318 K and \blacklozenge 328 K and $-$ 0.7 mM at 318 K and $-$ 0.5 mM in 0.1 M NaCl at 318 K and 100 rpm and also tests were carried out in $[\text{MnO}_4^-]_0 = 0.5$ mM in water and 318 K at $+$ 40 rpm and \circ 70 rpm

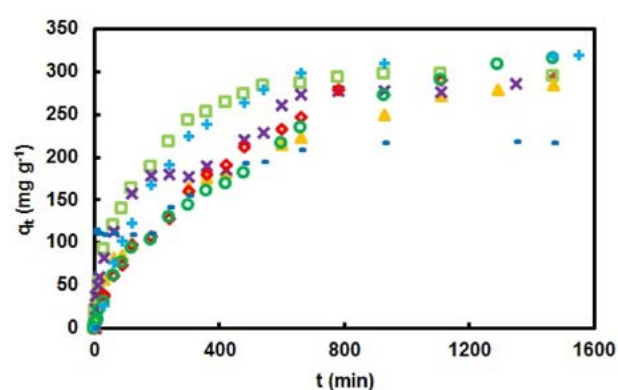


Fig. 4 Kinetic curves of adsorption of MnO_4^- on Co-Al-LDH in pHs of \blacktriangle 2.8, \square 3.8, \times 12 and $-$ 14 at 318 K and pH of 13 at \diamond 308 K, \circ 318 K and $+$ 328 K at 100 rpm and $[\text{MnO}_4^-]_0 = 0.5$ mM

Table 3. TRAKs for adsorption of MnO_4^- on Co-Al-LDH in 0.1 M NaCl and acidic and alkaline solutions at 308–328 K

Solvent	T (K)	$[\text{MnO}_4^-]_0$ (mM)	rpm	$\text{TRAK}_{C_1-C_2}$ (min–min)	$q_{\text{TRAK}_{C_1-C_2}}$ (mg g^{-1})	t_e (min)	q_e (mg g^{-1})
0.1 M NaCl*	318	0.5	100	300–360	141.4–141.7	1290	316.3
pH=2.8**	318	0.5	100	60–90	82.5–85.7	1290	278.3
pH=12*	318	0.5	100	180–420	178.3–185.4	660	273.6
pH=14**	318	0.5	100	> 0.5–180	112.2–110.1	930	216.6

$\text{TRAK}_{C_1-C_2}$ is the observed TRAKs between the first and second kinetic curves. *TRAK appeared at the end of ME sites range. **TRAK was in the time range of ME sites. t_e is the time of reaching equilibrium.

Table 4. Experimental t_e , q_e , t_{02} , q_{02} , t_{03} and q_{03} values and coefficients obtained from the KASRA equation and k_{diff} values of intraparticle diffusion equation for kinetics of MnO_4^- adsorption on Co-Al-LDH at different temperatures and in various shaking rates and initial MnO_4^- concentrations

Solvent	T (K)	[MnO_4^-]₀ (mM)	rpm	KASRA region I (1st curve)			KASRA region 2 (1st curve)			KASRA region 2 (2nd curve)							
				a_1	v_{01}	k_{diff}	(t_e, q_e)	(t_{02}, q_{02})	a_2	v_{02}	k_{diff}	(t_{03}, q_{03})	a_3	v_{03}	k_{diff}		
Corresponding to:				ARIAN region I (ME Site)			ARIAN section IIA (ME Site)			ARIAN section IIB (MI Site)							
Water	318	0.25	100	-2.0×10^{-2}	1.00	4.7	(30,20.9)	-9.9×10^{-5}	0.18	5.2	–	–	–	–	–	–	
	308	0.50	100	-1.3×10^{-3}	0.39	4.1	(300,59.7)	-1.9×10^{-4}	0.13	3.8	(780,100.3)	-8.5×10^{-5}	0.18	5.8			
	318	0.50	100	-2.3×10^{-2}	1.42	6.8	(60,43.7)	-2.1×10^{-3}	0.54	7.4	(300,113.2)	-1.4×10^{-4}	0.25	6.8			
	328	0.50	100	-4.2×10^{-2}	1.58	6.8	(30,27.3)	-3.6×10^{-3}	0.95	12.3	(240,148.0)	-2.3×10^{-4}	0.31	7.6			
	318	0.70	100	-6.8×10^{-2}	2.55	8.5	(30,46.3)	-3.2×10^{-3}	0.59	8.7	(180,99.5)	-2.9×10^{-4}	0.36	10.2			
	318 ^A	0.50	70	-1.6×10^{-2}	1.15	5.9	(60,38.6)	-1.0×10^{-3}	0.50	8.2	(420,142.6)	-3.6×10^{-4}	0.31	10.3			
	318 ^B	0.50	40	-4.2×10^{-3}	0.82	6.9	(120,58.7)	-6.1×10^{-4}	0.30	6.7	(420,123.8)	-2.9×10^{-4}	0.30	11.2			
	0.1M NaCl	318	0.50	100	-0.46	4.76	10.2	(10,25.0)	-1.7×10^{-3}	0.65	6.7	C(360,141.7)	-3.1×10^{-4}	0.33	11.3		
	pH=2.8	318	0.50	100	-2.9×10^{-2}	2.24	10.8	D(90,85.7)	-2.0×10^{-4}	0.29	7.3	–	–	–	–	–	–
	pH=3.8	318	0.50	100	-6.8×10^{-2}	4.03	18.3	(60,120.4)	-9.3×10^{-4}	0.55	11.2	–	–	–	–	–	–
	pH=12	318	0.50	100	-0.19	5.53	14.1	(30,82.6)	-8.2×10^{-3}	1.21	11.6	E(420,185.4)	-8.1×10^{-4}	0.46	16.8		
	pH=13	308	0.50	100	-6.3×10^{-3}	1.14	9.1	(180,107.2)	-4.8×10^{-4}	0.42	11.6	–	–	–	–	–	–
	pH=13	318	0.50	100	-6.6×10^{-3}	1.16	9.4	(180,103.8)	-2.2×10^{-4}	0.30	8.8	–	–	–	–	–	–
	pH=13	328	0.50	100	-8.2×10^{-3}	1.51	17.4	(120,122.7)	-1.0×10^{-3}	0.58	12.1	–	–	–	–	–	–
pH=14	318	0.50	100	Very fast (0.5 min <) ^F	–	–	(180,110.1)	-4.8×10^{-4}	0.31	7.7	–	–	–	–	–	–	

Units of a_1 , a_2 and a_3 are in $mg\ g^{-1}\ min^{-2}$ and those of v_{01} , v_{02} and v_{03} are in $mg\ g^{-1}\ min^{-1}$. Units of t_e , t_{02} and t_{03} are in min and those of q_e , q_{02} and q_{03} are in $mg\ g^{-1}$. In region 1, t_{01} and q_{01} are equal to zero. A and B refer to cases that there were TDs at 4 and 5 min before starting adsorption process, respectively. C, D, E and F refer to TRAKs in the range of 300–360, 60–90, 180–420 and >0.5–180 min, respectively

Table 5. Coefficients of region 1 and region 2 (parts 2a and 2b) of the ISO equation for kinetics of MnO_4^- adsorption on different sites of Co-Al-LDH at 308–328 K

Solvent	T (K)	[MnO_4^-]₀ (mM)	rpm	ARIAN region I and section IIA (ME Site)			ARIAN section IIB (MI Site)										
				(t_{ssr}, q_{ssr}) (min, $mg\ g^{-1}$)	k_{I2a}	(t_{sp}, q_{sp}) (min, $mg\ g^{-1}$)	k_{I2b}	$[MnO_4^-]_{I,max}$ ($mg\ g^{-1}$)	$q_{I,max}$ ($mg\ g^{-1}$)	k_{I2a}	(t_{sp}, q_{sp}) (min, $mg\ g^{-1}$)	k_{I2b}	$[MnO_4^-]_e$ ($mg\ g^{-1}$)	q_e ($mg\ g^{-1}$)			
Corresponding to:				ARIAN region I and section IIA (ME Site)			ARIAN section IIB (MI Site)										
Water	318	0.25	100	(30,20.9)	130	(360,76.7)	2803	(0.025,1350,177.7)	–	–	–	–	–	–	–	–	
	308	0.50	100	(300,59.7)	–	–	1075	(0.37,780,100.3)	1022	(1290,151.1)	3227	(0.30,1470,160.0)					
	318	0.50	100	(90,43.7)	–	–	3745	(0.36,300,113.2)	1743	(930,220.4)	3155	(0.15,1650,275.6)					
	328	0.50	100	(90,27.3)	–	–	6391	(0.31,240,148.0)	2188	(540,212.2)	7842	(0.15,1110,275.6)					
	318	0.70	100	(15,31.5)	–	–	2805	(0.5,180,99.5)	1317	(660,230.7)	4052	(0.31,1350,316.3)					
	318 ^A	0.50	70	(240,108.1)	–	–	5082	(0.32,420,142.6)	2729	(660,208.1)	6042	(0.14,1290,281.1)					
	318 ^B	0.50	40	(300,101.6)	–	–	2164	(0.34,420,123.8)	2155	(600,178.7)	5727	(0.13,1470,293.7)					
	0.1M NaCl	318	0.50	100	(180,106.9)	–	–	9031	C(0.32,300,141.4)	3176	(780,250.2)	14292	(0.10,1290,316.3)				
	pH=2.8	318	0.50	100	(30,56.7) ^P	2072	(660,223.4)	7156	(0.15,1290,278.3)	–	–	–	–	–	–	–	–
	pH=3.8	318	0.50	100	(60,120.4)	4557	(360,252.2)	9114	(0.13,780,293.3)	–	–	–	–	–	–	–	–
	pH=12	318	0.50	100	(60,112.9)	–	–	12461	E(0.29,180,178.3)	5550	(540,229.0)	31450	(0.15,660,273.6)				
	pH=13	308	0.50	100	(180,107.2)	–	–	3638	(0.13,1110,289.4)	–	–	–	–	–	–	–	–
	pH=13	318	0.50	100	(420,168.7)	–	–	18820	(0.04,1470,315.7)	–	–	–	–	–	–	–	–
	pH=13	328	0.50	100	(480,263.8)	–	–	18006	(0.11,930,309.5)	–	–	–	–	–	–	–	–
pH=14	318	0.50	100	(0.36,0.5<,112.2) ^F	3358	(540,194.4)	6427	(0.23,930,216.6)	–	–	–	–	–	–	–	–	

[MnO_4^-]_{I,max}^I and $q_{I,max}$ are MnO_4^- concentration, time and adsorption capacity at the end of the adsorption on ME site, respectively (corresponding to [MnO_4^-]_s, t_e and q_e are MnO_4^- concentration, time and adsorption capacity at the beginning of the plateau, respectively. Units of k_{I2a} , k_{I2b} and k_{I2c} are in $mg\ g^{-1}\ M^{-1}\ min^{-1}$. A and B refer to cases that there were TDs at 4 and 5 min before starting adsorption process, respectively. C, D, E and F refer to TRAKs in the range of 300–360, 60–90, 180–420 and >0.5–180 min, respectively.

Table 6. Non-ideal adsorption acceleration and velocity parameters for the first, second and third curves obtained from the NIPPON equation for kinetics of MnO_4^- adsorption on the surface of Co-Al-LDH at 308–328 K

Solvent	T (K)	[MnO_4^-] ₀ (mM)	rpm	(t _e , q _e)	NIPPON curve 1		NIPPON curve 2		NIPPON curve 3			
					a _{1c} ^N	v _{1c} ^N	a _{2c} ^N	v _{2c} ^N	a _{3c} ^N	v _{3c} ^N	(t _{1c} , q _{1c})	(t _{2c} , q _{2c})
Water	318	0.25	100	(1350,177.7)	-2.7×10 ⁻²	1.07	(16,12.6)	-5.9×10 ⁻²	1.01	(241,61.1)	-1.2×10 ⁻³	0.29
	308	0.50	100	(1470,160.0)	-4.0×10 ⁻³	0.49	(90,28.3)	-4.0×10 ⁻³	0.36	(780,100.3)	-1.6×10 ⁻⁴	0.12
	318	0.50	100	(1650,275.6)	-2.5×10 ⁻²	1.44	(30,31.4)	-4.7×10 ⁻²	1.45	(300,113.2)	-1.1×10 ⁻³	0.32
	328	0.50	100	(1110,266.7)	0	1.09	(5,5.5)	-0.38	2.29	(30,27.3)	-7.6×10 ⁻²	2.35
0.1M NaCl	318 ^A	0.70	100	(1350,319.3)	-0.25	3.41	(5,12.7)	-0.72	4.29	(180,99.5)	-3.4×10 ⁻⁴	0.06
	318 ^B	0.50	70	(1290,281.1)	-0.62	3.08	(60,38.9)	-1.5×10 ⁻²	0.91	(420,142.6)	-7.3×10 ⁻⁴	0.31
pH=2.8	318	0.50	100	(1470,293.7)	-8.8×10 ⁻³	0.97 ^B	(30,21.1)	-0.04	1.29	(420,123.8)	-7.8×10 ⁻⁴	0.33
	318	0.50	100	(1290,316.3)	-13.89	13.89	(60,58.6)	-1.4×10 ⁻²	0.88	(360,141.7)	-1.0×10 ⁻³	0.38
	318	0.50	100	(1290,278.3)	0	1.08	(2,2.2)	-2.92	8.77	(90,85.7)	-8.9×10 ⁻³	0.81
	318	0.50	100	(780,293.3)	-11.32	11.32	(5,20.4)	-1.25	7.50	(90,120.4)	-0.02	1.21
	318	0.50	100	(660,273.6)	-21.39	21.39	(15,59.6)	-0.20	3.13	(420,185.4)	-1.1×10 ⁻³	0.46
	308	0.50	100	(1110,289.4)	0	1.28	(30,38.2)	-4.1×10 ⁻²	1.28	(180,170.2)	-3.5×10 ⁻³	0.64
	318	0.50	100	(1470,315.7)	-4.35	4.35	(10,10.6)	-0.28	3.11	(180,103.8)	-3.3×10 ⁻³	0.59
	328	0.50	100	(930,309.5)	0	0.89	(30,26.8)	-0.10	2.99	-	-	-
pH=14	318	0.50	100	(930,216.6)	Very fast ^F	(180,110.1)	-2.2×10 ⁻³	0.41	-	-	-	-

A and B refer to cases that there are TDs at 4 and 5 min before starting adsorption process and thus for first curve 1, t = 4 and t = 5 min were used in Eqs. (11) and (12), respectively. C, D, E and F refer to TRAKs in the range of 300–360, 60–90, 180–420 and >0.5–180 min, respectively. Units of a_{1c}^N, a_{2c}^N and a_{3c}^N are in mg g⁻¹ min⁻² and those of v_{1c}^N, v_{2c}^N and v_{3c}^N are in mg g⁻¹ min⁻¹. Units of t_{1c}, t_{2c} and t_{3c} are in min and those of q_{1c}, q_{2c} and q_{3c} are in mg g⁻¹. Subscripts fc, sc and tc are abbreviations for starting first curve, starting second curve and starting third curve, respectively.

Table 7. Coefficients of the Elovich equation for adsorption of MnO_4^- adsorption on the surface of ME sites of Co-Al-LDH in various shaking rates and initial MnO_4^- concentrations and media at 308–328 K

Solvent	T (K)	[MnO_4^-] ₀ (mM)	rpm	α (mg g ⁻¹ min ⁻¹)	β (g mg ⁻¹)	R ²	
Water	318	0.25	100	3.11	0.23	0.99	
	308	0.50	100	1.16	0.06	0.98	
	318	0.50	100	3.88	0.09	0.99	
	328	0.50	100	3.67	0.08	0.98	
	318	0.70	100	8.33	0.10	0.98	
	318A	0.50	70	-	-	-	
318B	0.50	40	-	-	-		
0.1M NaCl	318	0.50	100	14.55	0.12	0.99	
	pH=2.8	318	0.50	6.60	0.09	0.99	
	pH=3.8	318	0.50	15.98	0.10	0.99	
	pH=12	318	0.50	29.13	0.05	0.99	
	pH=13	308	0.50	100	3.56	0.03	0.99
	pH=13	318	0.50	100	4.08	0.07	0.92
	pH=13	328	0.50	100	3.41	0.014	0.99
	pH=14	318	0.50	100	Very fast (0.5 min <)	-	-

A and B refer to cases that there were TDs at 4 and 5 min before starting adsorption process, respectively.

It was observed that k_{I1} and k_{I2b} values in water decreased with a decrease in shaking rate of solution or initial concentration of MnO_4^- . Also, it should be mentioned that 0.25 mM MnO_4^- (based on the KASRA model) had only region 1 (or in region I in its related isotherm based on the ARIAN model) and MnO_4^- ions were adsorbed on the most active adsorption sites without encountering hindrance of adsorbed MnO_4^- ions. Thus, its k_{I1} value was greater than k_{I1} values observed in other tests.

k_{I1} and k_{I2b} values in 0.1 M NaCl decreased compared with those in water at 318 K due to competitive adsorption of chloride ion with MnO_4^- .

In acidic pHs, because of interaction of H^+ with surface, k_{I1} and k_{I2b} values increased with decreasing pH but due to an increase in chloride ion concentration with a decrease in pH from 2 to 1 their values decreased a little.

At pH=11, k_{I1} value increased a little compared with that in water. This is due to interaction of OH^- ions with some adsorbent sites that decreased its adsorption capacity. Free MnO_4^- ions encountered less steric hindrance from the small amount of adsorbed ones and this resulted in a little faster interaction of MnO_4^- ions with adsorbent surface at pH=11 compared with that in water.

At pH=12, due to stronger reaction between MnO_4^- ions and MoS_2 and faster consumption of MnO_4^- ions, k_{I1} and k_{I2b} values in regions 1 and 2 increased drastically compared with those in pH ranges from 1 to 11.

Adsorption kinetics of MnO_4^- on MoS_2 were analyzed by NIPPON equation, Table 10. By this analysis, an excess ideal curve was observed at the beginning of adsorption kinetic diagrams of 0.5 mM MnO_4^- at 308 and 318 K and

0.75 mM MnO_4^- at 318 K in water and in 0.5 mM MnO_4^- in water, 0.1 M NaCl and at pHs of 2 and 11 at 318 K and 100 rpm compared to analysis with the KASRA model. These observations showed that activities of most active adsorption sites located in initial time ranges of first region obtained from the KASRA model were somehow bigger than activities of rest of this kind of adsorption sites.

On the other hand, the NIPPON equation analysis of adsorption kinetic diagrams of 0.25 mM MnO_4^- at 318, 0.5 mM MnO_4^- at 328 K, 100 rpm and 0.5 mM MnO_4^- at 70 and 40 rpm at 318 K and 0.5 mM MnO_4^- at pHs of 1 and 11 at 318 K and 100 rpm did not show any extra ideal curve at the beginning of them. These observations showed that in these cases the most active adsorption sites of adsorbent in the first region of the KASRA model were similar together.

Analysis of adsorption of MnO_4^- on adsorption sites of MoS_2 with the Elovich equation showed that α values changed randomly with an increase in pH, temperature and MnO_4^- concentration, Table 11.

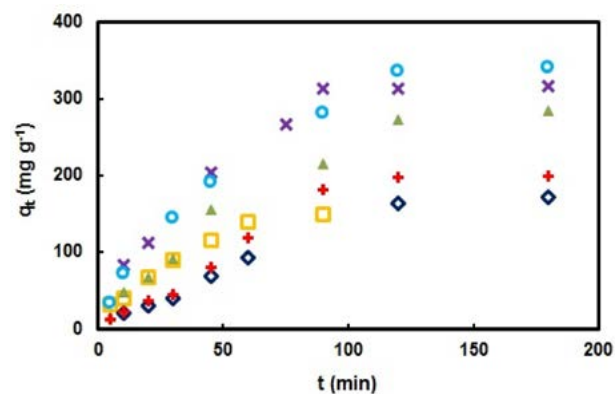


Fig. 5 Kinetic curves of adsorption of MnO_4^- on MoS_2 in water in initial MnO_4^- concentrations of \square 0.25 mM at 318 K, 0.5 mM at \blacktriangle 308 K, \diamond 318 K and \times 328 K and \circ 0.75 mM at 318 K and + 0.5 mM in 0.1 NaCl at 318 K and 100 rpm

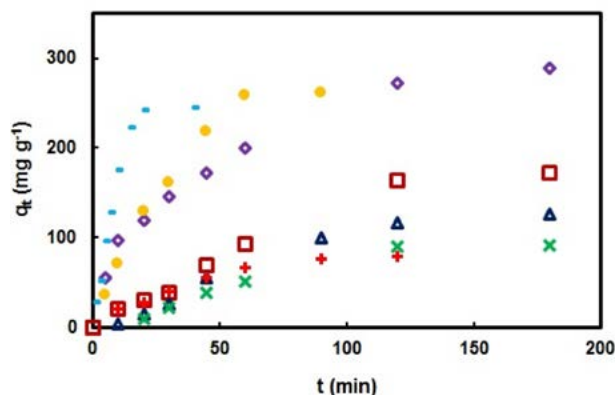
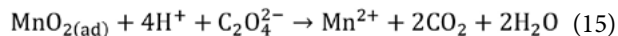


Fig. 6 Kinetic curves of adsorption of MnO_4^- on MoS_2 in water in initial MnO_4^- concentrations of 0.5 mM of MnO_4^- in \square water and pHs of \diamond 1, \bullet 2, + 11 and $-$ 12 and 100 rpm and at \times 40 rpm and Δ 70 rpm at 318 K

3. 3. 1. Recycling the used MoS_2

In this work, the used MoS_2 was recycled using a mixture of oxalic and sulfuric acids. In a series of tests, a mixture of 4 ml of 0.1 M oxalic acid and 1 ml of 0.5 M sulfuric acid were added to 0.01 g of the used MoS_2 at room temperature. Mixture was stirred for 10 minutes and the deposited MnO_2 into MoS_2 was reduced to Mn^{2+} according to the following reaction



Comparison of EDS spectra of the initial used MoS_2 sample and recycled MoS_2 showed there was a trace amount of manganese in the product of reaction (15) which verified recycling the used MoS_2 by this reaction, Figs. 7(a) and 7(b).

After three times recycling of the used MoS_2 , the adsorption capacity of the recycled MoS_2 was between 85% and 90% of that of as-synthesized adsorbent.

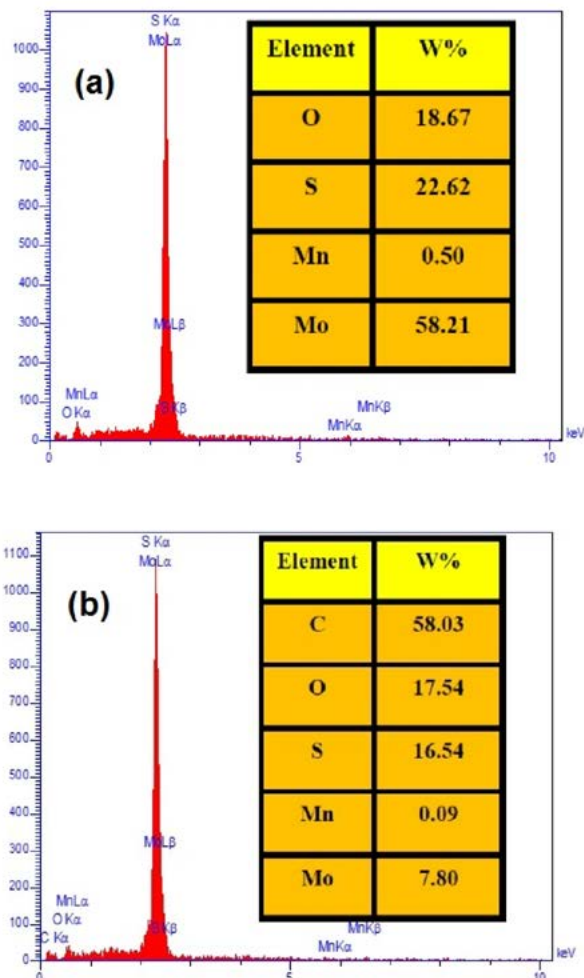


Fig. 7 EDS spectra of a sample of the used MoS_2 (a) before and (b) after recycling by using a mixture of 4 ml of 0.1 M oxalic acid and 1 ml of 0.5 M sulfuric acid solutions

Table 8. Experimental t_e , q_e , t_{02} and q_{02} values and coefficients obtained from the KASRA equation and k_{dif} values of intraparticle diffusion equation for kinetics of MnO_4^- adsorption on MoS_2 at different temperatures and in various shaking rates and initial MnO_4^- concentrations and media

Solvent	T (K)	[MnO_4^-] ₀ (mM)	rpm	(t_e, q_e)	KASRA region 1			KASRA region 2			
					a_1	v_{01}	k_{dif}	(t_{02}, q_{02})	a_2	v_{02}	k_{dif}
Corresponding to:				ARIAN region I			ARIAN region II				
Water	318	0.25	100	(90,149.6)	-0.04	3.57	21.0	-	-	-	
	308	0.50	100	(180,164.2)	-0.06	2.14	7.0	(30,39.1)	-2.0×10^{-2}	2.41	22.7
	318	0.50	100	(120,273.2)	-0.11	4.67	22.5	(30,91.9)	-1.2×10^{-2}	2.51	30.7
	328	0.50	100	(90,313.4)	-0.54	11.0	21.9	(20,119.9)	-2.2×10^{-2}	3.56	38.9
	318	0.75	100	(120,335.6)	-0.23	8.34	33.9	(30,145.1)	-1.2×10^{-2}	2.72	34.3
	318 ^A	0.50	70	(180,125.5)	-0.05	1.90	8.70	(20,15.0)	-1.0×10^{-2}	1.65	15.6
	318 ^B	0.50	40	(120,90.1)	-0.006	1.24	12.3	-	-	-	-
	0.1M NaCl	318	0.50	100	(120,196.9)	-0.07	2.52	9.80	(30,44.1)	-0.03	3.25
pH=1	318	0.50	100	(120,272.0)	-0.72	13.2	27.8	(20,119.6)	-1.4×10^{-2}	2.31	23.4
pH=2	318	0.50	100	(60,258.3)	-0.11	7.53	41.8	(20,128.9)	-2.6×10^{-2}	3.87	39.8
pH=11	318	0.50	100	(60,76.0)	-0.016	1.57	10.4	-	-	-	-
pH=12	318	0.50	100	(20,241.5)	0.00	18.0	62.2	(7, 128.3)	-1.27	16.9	62.5

Units of a_1 and a_2 are in $mg\ g^{-1}\ min^{-2}$ and those of v_{01} and v_{02} are in $mg\ g^{-1}\ min^{-1}$. Units of t_e and t_{02} are in min and those of q_e and q_{02} are in $mg\ g^{-1}$. In region 1, t_{01} and q_{01} are equal to zero. A and B refer to cases that there are TDs at 7.5 and 10 min before starting adsorption process, respectively.

Table 9. Coefficients of region 1 and region 2 (parts 2a and 2b) of the ISO equation for kinetics of MnO_4^- adsorption on MI sites of MoS_2 at 308–328 K

Solvent	T (K)	[MnO_4^-] ₀ (mM)	rpm	k_{I1}	(t_{ssr}, q_{ssr}) (min, $mg\ g^{-1}$)	k_{I2a}	(t_{sp}, q_{sp}) (min, $mg\ g^{-1}$)	k_{I2b}	$([MnO_4^-]_e, t_e, q_e)$ (mM, min, $mg\ g^{-1}$)
Water	318	0.25	100	27718	-	-	-	-	(0.11,90,149.6)
	308	0.50	100	2287	(30,39.1)	-	-	5363	(0.34,180,164.2)
	318	0.50	100	7623	(30,91.9)	-	-	16517	(0.22,120,273.2)
	328	0.50	100	9286	(20,111.9)	-	-	27857	(0.20,90,313.4)
	318	0.75	100	8558	(30,145.1)	-	-	13226	(0.43,120,335.6)
	318 ^A	0.50	70	1977	(20,15.0)	-	-	4284	(0.38,180,125.5)
	318 ^B	0.50	40	1522	-	-	-	-	(0.42,120,90.1)
	0.1M NaCl	318	0.50	100	2832	(30,44.1)	-	-	13454
pH=1	318	0.50	100	13499	(20,119.6)	-	-	14624	(0.24,120,272.0)
pH=2	318	0.50	100	25348	(20.0,128.9)	-	-	35488	(0.26,60,258.3)
pH=11	318	0.50	100	7993	-	-	-	-	(0.43,60,76.0)
pH=12	318	0.50	100	88376	(7,128.3)	-	-	239706	(0.20,20,241.5)

A and B refer to cases that there are TDs at 7.5 and 10 min before starting adsorption process, respectively. $[MnO_4^-]_e$, t_e and q_e are MnO_4^- concentration, time and adsorption capacity at the beginning of the plateau respectively. Units of k_{I2a} and k_{I2b} are in $mg\ g^{-1}\ M^{-1}\ min^{-1}$.

Table 10. Non-ideal adsorption acceleration and velocity parameters for the first, second and third curves obtained from the NIPPON equation for kinetics of MnO_4^- adsorption on the surface of MoS_2 at 308–328 K

Solvent	T (K)	[MnO_4^-] ₀ (mM)	rpm	(t_e, q_e)	NIPPON curve 1		NIPPON curve 2		NIPPON curve 3			
					a_{fc}^N	v_{fc}^N	(t_{sc}, q_{sc})	a_{sc}^N	v_{sc}^N	(t_{tc}, q_{tc})	a_{tc}^N	v_{tc}^N
Water	318	0.25	100	(90,149.6)	-17.02	17.02	(10,40.5)	-0.46	5.01	-	-	-
	308	0.50	100	(180,164.2)	0	3	(5,15.0)	-1.24	7.4	(30,91.9)	-0.13	3.99
	318	0.50	100	(120,273.2)	0	2.05	(10,20.5)	-0.15	1.61	(30,39.1)	-0.10	2.99
	328	0.50	100	(90,313.4)	-36.1	36.1	(20,111.9)	-0.30	6.27	-	-	-
	318	0.75	100	(120,335.6)	-6.64	6.64	(5,33.2)	-2.10	12.57	(45,191.0)	-0.07	3.18
	318	0.50	70	(180,125.5)	-0.21 ^A	1.76 ^A	(20,15.0)	-0.12	2.56	-	-	-
	318	0.50	40	(120,90.1)	-0.17 ^B	1.90 ^B	(30,22.3)	-0.05	1.61	-	-	-
	0.1M NaCl	318	0.50	100	(120,196.9)	-2.23	2.23	(10,22.3)	-0.17	1.92	(30,44.1)	-0.12
pH=1	318	0.50	100	(120,272.0)	-39.6	39.6	(20,119.6)	-0.19	3.97	-	-	-
pH=2	318	0.50	100	(60,258.3)	-7.17	7.17	(5,35.9)	-2.07	12.40	(20,138.9)	-0.28	5.85
pH=11	318	0.50	100	(60,76.0)	-2.76	2.76	(10,27.6)	-0.24	2.62	-	-	-
pH=12	318	0.50	100	(20,241.5)	-36.71	36.71	(3,50.9)	-7.46	29.85	-	-	-

A and B refer to cases that there are TDs at 7.5 and 10 min before starting adsorption process and thus for curve 1, $t = 7.5$ and $t = 10$ min were used in Eqs. (11) and (12), respectively. Units of a_{fc}^N , a_{sc}^N and a_{tc}^N are in $mg\ g^{-1}\ min^{-2}$ and those of v_{fc}^N , v_{sc}^N and v_{tc}^N are in $mg\ g^{-1}\ min^{-1}$. Units of t_e , t_{sc} and t_{tc} are in min and those of q_e , q_{sc} and q_{tc} are in $mg\ g^{-1}$. Subscripts fc , sc and tc are abbreviations for starting first curve, starting second curve and starting third curve, respectively.

Table 11. Coefficients of the Elovich equation for adsorption of MnO_4^- adsorption on the surface of MoS_2 in various shaking rates and initial MnO_4^- concentrations and media at 308–328 K

Solvent	T (K)	$[\text{MnO}_4^-]_0$ (mM)	rpm	α ($\text{mg g}^{-1} \text{min}^{-1}$)	β (g mg^{-1})	R^2
Water	318	0.25	100	28.68	0.08	0.96
	308	0.50	100	11.83	0.03	0.98
	318	0.50	100	5.53	0.06	0.98
	328	0.50	100	30.96	0.02	0.99
	318	0.75	100	2.28	0.05	0.98
	318 ^A	0.50	70	–	–	–
	318 ^B	0.50	40	–	–	–
0.1M NaCl pH=1 pH=2 pH=11 pH=12	318	0.50	100	6.09	0.05	0.99
	318	0.50	100	30.79	0.02	0.99
	318	0.50	100	21.73	0.01	0.98
	318	0.50	100	54.35	0.01	0.99
	318	0.50	100	5.36	0.06	0.90

A and B refer to cases that there are TDs at 7.5 and 10 min before starting adsorption process, respectively.

4. Conclusions

Reduction of MnO_4^- ions to MnO_2 by water molecules was catalyzed after its adsorption on the surface of carbonate intercalated Co-Al-LDH in the pH range of 1–13 and MnO_4^- reacted with MoS_2 in the pH range of 1–12. Adsorption kinetic tests were carried out at different temperatures, ionic strengths, pH, initial adsorbate concentrations and shaking rates. The adsorption kinetics was studied by the KASRA model and the KASRA, Elovich, ISO, intraparticle diffusion and NIPPON equations. Results showed that kinetic parameters like k_{dij} , k_{I1} , k_{I2b} , adsorption velocities and accelerations of MnO_4^- on Co-Al-LDH were increased with an increase in temperature, shaking rate, initial MnO_4^- concentration and decrease in pH. But, these parameters at pHs of 12 and 13, due to formation of MnO_4^- ions, were less than their values in neutral water and at pH = 14, due to a change in mechanism of reaction, MnO_4^- ions reacted with Co^{2+} ions of the adsorbent.

However, in the case of MoS_2 , MnO_4^- ions were adsorbed on MI sites of MoS_2 and then reacted with it and reduced to MnO_2 in the pH range of 1–12. Study of kinetic curves showed that they were composed from regions 1 and 2 and adsorption velocity and acceleration and k_{dij} , k_{I1} and k_{I2b} decreased from region 1 to region 2 and in region 1, these parameters increased with an increase in MnO_4^- initial concentration, temperature, shaking rate and acidic pHs and decreased in 0.1 M NaCl and pH = 11 compared to their values in water. At pH = 12, water molecules were replaced by hydroxide ions and MoS_2 reacted more rapidly with adsorbed MnO_4^- compared to that in water and changed it to MnO_2 .

k_{dij} , k_{I1} and k_{I2b} values of adsorption of MnO_4^- on MoS_2 were much greater than those for Co-Al-LDH and adsorption of MnO_4^- on MoS_2 was very faster than that on Co-Al-LDH.

In this work, the NIPPON equation was introduced. Based on this equation, compared to the KASRA model, an excess curve was observed in the beginning of some adsorption kinetic diagrams that showed some of the most active sites were a little more active than the other ones. Also, in some cases, change in boundary of some curves showed that sites of boundary of some regions are more similar to one of regions. Finally, in this work the used MoS_2 was recycled by using a mixture of oxalic and sulfuric acid solutions.

5. References

- E. Esmaili, B. Samiey, C.H. Cheng, *J. Clean. Prod.* **2022**, *351*, 131521. DOI:10.1016/j.jclepro.2022.131521
- S. Ghobadi, B. Samiey, A. Ghanbari, *JSSC* **2021**, *304*, 122588. DOI:10.1016/j.jssc.2021.122588
- L.P.F. Benício, R.A. Silva, J.A. Lopes, D. Eulálio, R.M.M. dos Santos, L.A. de Aquino, L. Vergütz, R.F. Novais, L.M. da Costa, F.G. Pinto, J. Tronto, *Revista Brasileira de Ciência do Solo* **2015**, *39*, 1–13. DOI:10.1590/01000683rbc2015081
- P. Nalawade, B. Aware, V.J. Kadam, R.S. Hirlekar, *JSIR* **2009**, *68*, 267–272.
- S. Velu, K. Suzuki, M.P. Kapoor, S. Tomura, F. Ohashi, T. Osaka, *Chem. Mater.* **2000**, *12*, 719–730. DOI:10.1021/cm9904685
- Y. Wang, D. Yan, S. El Hankari, Y. Zou, S. Wang, *Adv. Sci.* **2018**, *5*, 1800064. DOI:10.1002/advs.201800064
- A.K. Karmakara, Md. Saif Hasanb, A. Sreemanic, A. Das Jayantad, Md. Mehidi Hasane, N.A. Tithef, P. Biswasg, *Eur. Phys. J. Plus* **2022**, *137*, 801.
- X. Wan, Y. Song, H. Zhou, M. Shao, *Energy Mat. Adv.* **2022**, *2022*, 9842610. DOI:10.34133/2022/9842610
- Z. Tang, Z. Qiu, S. Lu, X. Shi, *Nanotechnology Reviews* **2020**, *9*, 800–819. DOI:10.1515/ntrev-2020-0065
- X. Bi, H. Zhang, L. Dou, *Pharmaceutics* **2014**, *6*, 298–332. DOI:10.3390/pharmaceutics6020298
- L. Shuhui, L. Bin, X. Dawei, L. Yu, C. Fanwei, L. Siqi, *J. Chin. Soc. Corros.* **2022**, *42*, 16–24.
- L. Zhang, P. Cai, Z. Wei, T. Liu, J. Yu, A.A. Al-Ghamdi, S. Wageh, *J. Colloid Interface Sci.* **2021**, *588*, 637–645. DOI:10.1016/j.jcis.2020.11.056
- B.W. Liu, H.B. Zhao, Y.Z. Wang, *Adv. Mater.* **2021**, 2107905.
- D. Kino, Y. Tokudome, P.D. Vaz, C.D. Nunes, M. Takahashi, *J. Asian Ceramic Societies* **2017**, *5*, 466–471. DOI:10.1016/j.jascer.2017.10.003
- K. Teramura, S. Iguchi, Y. Mizuno, T. Shishido, T. Tanaka, *Angew. Chem. Int. Ed.*, **2012**, *51*, 8008–8011. DOI:10.1002/anie.201201847
- S. Zhang, J. Chen, W-S Yang, X. Chen, *Nano Res.* **2022**, *15*, 7940–7950. DOI:10.1007/s12274-022-4479-z
- N.S. Ahmed, R. Menzel, Y. Wang, A. Garcia-Gallastegui, S.M. Bawaked, A.Y. Obaid, Basahel, M. Mokhtar, *JSSC* **2017**, *246*, 130–137. DOI:10.1016/j.jssc.2016.11.024
- J. Guo, H. Sun, X. Yuan, L. Jiang, Z. Wu, H. Yu, N. Tang, M.

- Yu, M. Yan, J. Liang, *Water Res.* **2022**, *219*, 118558. DOI:10.1016/j.watres.2022.118558
19. S. Balendhran, J.Z. Ou, M. Bhaskaran, S. Sriram, S. Ippolito, Z. Vasic, E. Kats, S. Bhargava, S. Zhuykov, K. Kalantar-zadeh, *Nanoscale* **2012**, *4*, 461–466. DOI:10.1039/C1NR10803D
20. X. Li, H. Zhu, *Journal of Materiomics* **2015**, *1*, 33e44. DOI:10.1016/j.jmat.2015.03.003
21. J. Sun, X. Li, W. Guo, M. Zhao, X. Fan, Y. Dong, C. Xu, J. Deng, Y. Fu, *Crystals* **2017**, *7*, 198. DOI:10.3390/cryst7070198
22. X. Gan, H. Zhao, T.W. Lo, K.H.W. Ho, L.Y.S. Lee, D.Y. Lei, K. Wong, *ACS Appl. Energy Mater.* **2018**, *1*, 4754–4765. DOI:10.1021/acsaem.8b00875
23. D. Gupta, V. Chauhan, R. Kumar, *Inorg. Chem. Commun.* **2020**, *121*, 108200. DOI:10.1016/j.inoche.2020.108200
24. R.M.A. Khalil, F. Hussain, A.M. Rana, M. Imran, G. Murtaza, *Nanostruct.* **2019**, *106*, 338–345. DOI:10.1016/j.physe.2018.07.003
25. Z. Chen, X. He, C. Xiao, S.H. Kim, *Lubricants* **2018**, *6*, 74. DOI:10.3390/lubricants6030074
26. K. Lu, J. Liu, X. Dai, L. Zhao, Y. Yang, H. Li, Y. Jiang, *RSC Adv.* **2022**, *12*, 798–809. DOI:10.1039/D1RA07962J
27. X. Liu, Z. He, S. Xu, J. Wu, J. Wu, *Sens. Actuators B: Chem.* **2022**, *367*, 132185. DOI:10.1016/j.snb.2022.132185
28. Y. Xiao, J. Yao, T. Zhang, X. Ma, D. Xu, H. Gao, *Dalton Trans.* **2022**, *51*, 638–644. DOI:10.1039/D1DT03411A
29. A. Kumar, S. Tyagi, R. Kumar, S. Sharma, M. Sharma, R. Adalat, Y. Kumar, R. Chandra, *Mater. Lett.* **2022**, *323*, 132576. DOI:10.1016/j.matlet.2022.132576
30. A. Kumar, A. Sood, S.S. Han, *J. Mater. Chem. B* **2022**, *10*, 2761–2780. DOI:10.1039/D2TB00131D
31. J. Yuan, F. Wang, S. Patel, Z.-L. Hu, M. Tang, J. Lou, *ACS Appl. Nano Mater.* **2021**, *4*, 8094–8100. DOI:10.1021/acsnm.1c01361
32. Y. Jia, G. Yin, Y. Lin, Y. Ma, *CrystEngComm* **2022**, *24*, 2314–2326. DOI:10.1039/D1CE01439K
33. G. Tian, R. Jervis, J. Briscoe, M. Titirici, A.J. Sobrido, *J. Mater. Chem. A* **2022**, *10*, 10484–10492. DOI:10.1039/D2TA00739H
34. B. Balasubramaniam, S.A. Kumar, K.A. Singh, S.B., Kartikey V.L. Tian, R.K. Gupta, A.K. Gaharwar, *Adv. NanoBiomed Res.* **2022**, *2*, 2100105. DOI:10.1002/anbr.202100105
35. R.A. Street, G.M. Kabera, C. Connolly, *S. Afr. Med. J.* **2018**, *108*, 187–189. DOI:10.7196/SAMJ.2017.v108i3.12606
36. K. Piezer, L. Li, Y. Jeon, A. Kadudula, Y. Seo, *Process Saf. Environ. Prot.* **2021**, *148*, 400–414. DOI:10.1016/j.psep.2020.09.058
37. H. Rahman, *Curr. Anal. Chem.* **2020**, *16*, 670–686. DOI:10.2174/1573411015666190617103833
38. A. Fawzy, S.A. Ahmed, I.I. Althagafi, M.H. Morad, K.S. Khairou, *Advances in Physical Chemistry* **2016**, *2016*, 4526578. DOI:10.1155/2016/4526578
39. E. Geraud, V. Prevot, F. Leroux, *J. Phys. Chem. Solids* **2006**, *67*, 903–908. DOI:10.1016/j.jpss.2006.01.002
40. N. Safar Beyranvand, B. Samiey, A. Dadkhah Tehrani, *Acta Chim. Slov.* **2019**, *66*, 443–454. DOI:10.17344/acsi.2018.4920
41. Z. Deng, Y. Hu, D. Ren, S. Lin, H. Jiang, C. Li, *Chem. Commun.* **2015**, *51*, 13838–13841. DOI:10.1039/C5CC05069C
42. B. Samiey, S. Golestan, *Cent. Eur. J. Chem.* **2010**, *8*, 361–369. DOI:10.2478/s11532-009-0135-7
43. B. Samiey, S. Abdollahi Jonaghani, *J. Pollut. Eff. Con.* **2015**, *3*, 2.
44. I. Langmuir, *J. Am. Chem. Soc.* **1918**, *40*, 1361–1403. DOI:10.1021/ja02242a004
45. M. Boudart, G. Djega-Mariadassou, *Kinetics of Heterogeneous Catalytic Reactions*, University Press, Princeton, NJ, 1984. DOI:10.1515/9781400853335
46. M. Rafi, B. Samiey, C.H. Cheng, *Materials* **2018**, *11*, 496. DOI:10.3390/ma11040496
47. M. Ozacar, I.A. Şengil, *Colloids Surf. A* **2004**, *242*, 105–113. DOI:10.1016/j.colsurfa.2004.03.029
48. F-C Wu, R-L Tseng, R-S Juang, *Chem. Eng. J.* **2009**, *150*, 366–373. DOI:10.1016/j.cej.2009.01.014
49. B. Samiey, S. Farhadi, *Acta Chim. Slov.* **2013**, *60*, 763–773.
50. B. Samiey, A. Dadkhah Tehrani, *J. Chin. Chem. Soc.* **2015**, *62*, 149–162. DOI:10.1002/jccs.201400093
51. N. Safar Beyranvand, B. Samiey, A. Dadkhah Tehrani, K. Soleimani, *J. Chem. Eng. Data* **2019**, *64*, 5558–5570. DOI:10.1021/acs.jced.9b00655
52. https://en.wikipedia.org/wiki/Fourth,_fifth,_and_sixth_derivatives_of_position
53. M. Visser, *Class. Quant. Grav.* **2004**, *21*, 2603–2616. DOI:10.1088/0264-9381/21/11/006
54. S. Lagergren, *Handlingar* **1898**, *24/II*, 1–39.
55. F. Su, C. Lu, *Environ. Sci. Health A* **2007**, *42*, 1543–1552. DOI:10.1080/10934520701513381
56. A.M. Aljeboree, A.N. Alshirifi, A.F. Alkaim, *Arab. J. Chem.* **2017**, *10*, S3381–S3393. DOI:10.1016/j.arabjc.2014.01.020
57. E.G. Contreras, B.E. Martinez, L.A. Sepúlveda, C.L. Palma, *Adsorp. Sci. Technol.* **2007**, *25*, 637–646. DOI:10.1260/026361707785082396
58. S. Karmaker, F. Sintaha, T. Kumar Saha, *Advances in Biological Chemistry* **2019**, *9*, 1–22. DOI:10.4236/abc.2019.91001
59. U. Geçgel, O. Üner, G. Gökara, Y. Bayrak, *Adsorp. Sci. Technol.* **2016**, *34*, 512–525. DOI:10.1177/0263617416669727
60. G. Annadurai, R.S. Juang, D.J. Lee, *J. Hazard. Mater. B* **2002**, *92*, 263–274. DOI:10.1016/S0304-3894(02)00017-1
61. X.S. Hu, R. Liang, G. Sun, *J. Mater. Chem. A* **2018**, *6*, 17612–17624. DOI:10.1039/C8TA04722G
62. S. Ashour, *J. Saudi Chem. Soc.* **2010**, *14*, 47–53. DOI:10.1016/j.jscs.2009.12.008
63. L. Soldatkina, M. Zavrichko, *Colloids Interfaces* **2019**, *3*, 4. DOI:10.3390/colloids3010004
64. K.M. Al-Ahmary, *Int. Res. J. Basic Appl. Sci.* **2013**, *2*, 27–37. DOI:10.7439/ijpc.v2i4.773
65. J.S. Calisto, I.S. Pacheco, L.L. Freitas, L.K. Santana, W.S. Fagundes, F.A. Amaral, S.C. Canobre, *Heliyon* **2019**, *5*, e02553. DOI:10.1016/j.heliyon.2019.e02553
66. Z. Huang, C. Xiong, L. Ying, W. Wang, S. Wang, J. Ding, J. Lu, *Chem. Eng. J.* **2022**, *449*, 137722. DOI:10.1016/j.cej.2022.137722

67. P. Wang, T. Song, C. Xie, P. Yang, *Appl. Surf. Sci.* **2022**, *580*, 152290. DOI:10.1016/j.apsusc.2021.152290
68. A. Kheradmand, M. Negarestani, S. Kazemi, H. Shayesteh, S. Javanshir, H. Ghiasinejad, *Sci. Rep.*, **2022**, *12*, 14623. DOI:10.1038/s41598-022-19056-0
69. H. Cheng, H. He, Z. Zhang, K. Xiao, Y. Liu, X. Kang, X. Li, *Sep. Purif. Technol.* **2022**, *303*, 122282. DOI:10.1016/j.seppur.2022.122282
70. S. Chatterjee, J. Qin, X. Li, F. Liang, D.K. Rai, Y.W. Yang, *J. Mater. Chem. B* 2020, *8*, 2238–2249. DOI:10.1039/D0TB00036A
71. Y. Zhang, J.R.G. Evans, *Colloids Surf. A: Physicochem. Eng. Asp.* 2012, *408*, 71–78. DOI:10.1016/j.colsurfa.2012.05.033
72. S. Verma, C. Mouli Pandey, D. Kumar, *New J. Chem.* **2022**, *46*, 21190–21200. DOI:10.1039/D2NJ04285A
73. W. Hu, Z. Chang, A. Tang, Y. Wei, D. Fang, X. Lu, P. Shao, H. Shi, K. Yu, X. Luo, L. Yang, *Environ. Res.* **2022**, *214*, 113969. DOI:10.1016/j.envres.2022.113969
74. I. Abouda, S. Walha, S. Bouattour, A.M. Botelhodo Rego, A.M. Ferrara, A.S.C. Sousa, N. Costa, S. Boufi, *J. Environ. Chem. Eng.* **2022**, *10*, 108583. DOI:10.1016/j.jece.2022.108583
75. W. Zhou, J. Deng, Z. Qin, S. Tong, R. Huang, Y. Wang, *J. Environ. Sci.* **2022**, *111*, 38–50. DOI:10.1016/j.jes.2021.02.031
76. J.S. Arya Nair, S. Saisree, K.Y. Sandhya, *Adv. Sustain. Syst.* **2022**, *6*, 2200039. DOI:10.1002/adsu.202200039
77. S. Han, K. Liu, L. Hu, F. Teng, P. Yu, Y. Zhu, *Sci. Rep.* **2017**, *7*, 43599. DOI:10.1038/srep43599
78. W. Li, Y. Li, Z. Li, Q. Wei, S. Xiao, S. Song, *Minerals* **2018**, *8*, 404. DOI:10.3390/min8090404

Povzetek

Permanganatni MnO_4^- ioni so bili adsorbirani na karbonatno interkaliranem Co-Al-slojenem dvojnem hidroksidu (Co-Al-LDH) in MoS_2 . Po določenem času so bili adsorbirani MnO_4^- ioni reducirani v MnO_2 . Redukcija adsorbiranega MnO_4^- iona je bila katalizirana na površini karbonatno interkaliranega Co-Al-LDH, MnO_4^- ioni pa so reagirali s površino MoS_2 . Kinetični testi adsorpcije so bili izvedeni pri različnih temperaturah, ionskih jakostih, pH, začetnih koncentracijah adsorbata in hitrostih stresanja. Adsorpcijsko kinetiko smo preučevali s študijo kinetike adsorpcije v regijah s konstantnim adsorpcijskim pospeškom modela KASRA, študijo idealnega drugega reda (ISO), difuzijo znotraj delcev, Elovich in z enačbo neidealnega procesa adsorpcijske kinetike (NIPPON).

V tem delu je bila predstavljena nova enačba, imenovana NIPPON enačba. V tej enačbi je bilo predpostavljeno, da so bile molekule adsorbatnih vrst med neidealnim procesom adsorbirane hkrati na adsorpcijskih mestih istega tipa z različnimi aktivnostmi. Povprečne vrednosti kinetičnih parametrov adsorpcije so bile izračunane z enačbo NIPPON. S to enačbo je mogoče določiti tudi značaj meja regij, pridobljenih iz modela KASRA.



Scientific paper

Ibuprofen as an Organic Pollutant in the Danube and Effects on Aquatic Organisms

Nevena Grujić-Letić,^{1*} Emilia Gligorić,¹ Branislava Teofilović,¹
Milan Vraneš,² Slobodan Gadžurić²

¹ University of Novi Sad, Faculty of Medicine, Department of Pharmacy, Hajduk Veljkova 3, 21000 Novi Sad, Serbia

² University of Novi Sad, Faculty of Sciences, Department of Chemistry, Biochemistry and Environmental Protection, Trg Dositeja Obradovića 3, 21000 Novi Sad, Serbia

* Corresponding author: E-mail: nevena.grujic-letic@mf.uns.ac.rs
Phone: +381 21 422 760 Fax: +381 21 422 760

Received: 10-15-2022

Abstract

The presence of emerging substances in surface water is of a great concern knowing they are the main source for community water supply needs. This study describes the development, optimization and application of an analytical method for the determination of ibuprofen in the Danube samples. Caffeine concentrations, as an indicator of human waste, were determined and maximum risk indexes for aquatic organisms were calculated. The Danube samples were collected from ten representative locations. A Solid-phase extraction was used for ibuprofen and caffeine separation and the analysis was performed by High-performance liquid chromatography method. Ibuprofen concentrations ranged (30.62–111.40) ng/L and caffeine (305.94–375.97) ng/L. Low risk on aquatic organisms was determined for ibuprofen and potential sublethal effect for caffeine was obtained. The results indicated that ibuprofen was effectively separated from other substances in the samples under defined chromatographic conditions for short period of time (4 minutes). Applied HPLC method showed good repeatability, accuracy, selectivity and robustness. Further studies including continuous monitoring of caffeine in the Danube are necessary in order to assess the real risks and possible prevention.

Keywords: Danube; ibuprofen; HPLC; maximum risk index

1. Introduction

Surface and groundwater are the main sources of drinking water worldwide, and purification processes that increase safety and quality of drinking water are of a crucial importance.¹ The presence of emerging substances (ESs) in the environment has become a subject of growing interest in recent decades. ESs are defined as materials present at low concentrations in the environment that have a potential or actual risk to the “One Health” trilogy – environment, human and animal.^{2,3} Pharmaceuticals, as one of the major classes of ESs, reach the environment mostly as a result of incomplete removal from municipal wastewater. Surface and groundwater purification processes cannot completely remove these substances, so traces can also be found in drinking water. Although the concentrations of these medicines in water are extremely low ($\mu\text{g/L}$ or ng/L), they are designed to have effects on human at low concentrations. Therefore, their continuous input into the

environment must be monitored, as they can lead to long-term negative consequences for the health of humans and aquatic organisms.^{2–5}

Ibuprofen, 2-(4-isobutylphenyl) propionic acid, is a non-steroidal anti-inflammatory drug (NSAID) that inhibits the synthesis of prostaglandins, compounds involved in inflammation, fever, blood pressure regulation, blood clotting, reproductive control and tissue growth by blocking cyclooxygenase (COX). As there are two isoforms of cyclooxygenase, it is important to note that ibuprofen is not a selective inhibitor of these isoenzymes, but inhibits both COX-1 and COX-2. It is believed that its positive therapeutic effects derived from the inhibition of COX-2, while the inhibition of COX-1 is responsible for its side effects and effects on the aggregation of platelets and mucous membranes of the digestive organs. It is also believed that antipyretic action is achieved by vasodilation and increased peripheral circulation.^{6,7}

Caffeine, 1,3,7-trimethylxanthine, is an odorless, slightly bitter-tasting substance found in natural products such as coffee, cocoa and tea leaves, but is also added to certain industrial foods and pharmaceuticals. It is a natural psychostimulant that has a stimulating effect on the body by acting on the central nervous system. It leads to dilation of the coronary arteries and better blood supply to the brain and dilates the renal vessels, increasing diuresis. Caffeine improves respiration and acts as a general analeptic by stimulating the work of all organs.^{8,9} It is often a part of combined analgoantipyretics. Scientific researchers showed that caffeine increases the effectiveness of these drugs by 40% when used together. Also, caffeine in such combinations not only increases the analgesic effect, but also eliminates possible sedative effects that certain analgesics can cause.^{10–12}

It is very difficult to extract and detect different analytes from surface water with acceptable yields and detection limits. Therefore, there is still a need for new, reliable analytical methods, which enable fast, sensitive and selective determination of drug residues in environmental samples.² The aim of this paper is the development and application of a new, fast and sensitive High-performance liquid chromatography (HPLC) analytical method for ibuprofen determination in surface water. The paper includes the development of procedures for efficient extraction and pre-concentration of analyte, optimization of chromatographic procedures and the establishment of protocols for the confirmation of the presence of ibuprofen. The developed method was applied to real samples of surface water, whereby a study on the state of water pollution was obtained. Also, the concentrations of caffeine, as an indicator of human pollution, in the same samples of the Danube were determined and the risk factors on aquatic organisms for both components were calculated. This is especially significant considering that the Western Balkans is a black box when it comes to the number of studies on the presence of drugs residues in the environment and data on the degree of water pollution.

2. Material and Methods

2. 1. Chemicals

The following HPLC grade compounds were used as standards for analysis by HPLC-DAD: ibuprofen (> 99%) and caffeine (> 99%) from Fluka. HPLC grade acetonitrile, methanol, chloroform and tetrahydrofuran were obtained from J.T. Baker. Sodium hydroxide, potassium dihydrogen phosphate, dipotassium hydrogen phosphate and tetrabutylammonium chloride were purchased from Sigma Aldrich. Distilled deionised water (dd H₂O) was used throughout the experiments.

2. 2. Sample Preparation

The Danube samples were collected during September 2020 from 10 locations in Novi Sad, Serbia, and stored

at 4 °C in dark bottles in a place protected from light until the beginning of the analysis. The samples were purified on an SPE column (Supelco, supelclean™ LC-18 SPE Tubes 6 ml (0,5 g)). Ibuprofen was eluted with 3 ml of methanol with TBACl (tetrabutylammonium chloride). The solution was evaporated to dryness and reconstituted in a mixture of water and methanol 30:70 (v/v). It was filtered through a 0.45 µm nylon membrane filter directly into the vial and 20 µl was injected into the HPLC system. Caffeine was extracted from the SPE column with chloroform (10 ml), and the solvent was removed by evaporation under reduced pressure. The dry residue was reconstituted in water pH = 8.0 (2.0 ml) and caffeine was analyzed by injecting 20 µl of the solution into the HPLC.¹³

2. 3. HPLC Analysis

The HPLC method¹³, using HPLC-DAD model Agilent HP 1100 system with autosampler injector (Waldbron, Germany) was applied for caffeine analysis.

For the analysis of ibuprofen in the Danube samples, the method of HPLC (HPLC-DAD model Agilent HP 1100, Waldbron, Germany) was developed and validated. The mobile phase was acetonitrile: phosphate buffer = 60:40 (v / v, pH 7.0) with flow rate 0.8 mL / min. Detection was performed at 260 nm, and the run time was 5 minutes.

3. Results

3. 1. HPLC method for Ibuprofen Determination in Surface Water

The standard stock solution of ibuprofen was prepared by dissolving 5 mg of the standard substance in 10 mL of the mobile phase (acetonitrile: phosphate buffer = 60:40 (v/v, pH 7.0)). The solution was stable approximately three days under refrigeration (4 °C). Working standard solutions were obtained by taking aliquots of (0.4–4) mL from the standard solution and dilution to 10 mL with mobile phase in a measuring flask. 20 µL of working solutions were injected into the HPLC system and the peak area responses were obtained. A method of the external standard calibration was used. Linear standard curve for ibuprofen was determined by plotting concentrations versus area responses and each calibration point was obtained as an average of three injections. The procedures used to validate the HPLC method for the determination of ibuprofen in surface water have been described in the literature^{14–16} and the results are presented in Tables 1-2. The linearity between ibuprofen concentrations and the areas under the curve was tested for concentration levels in the range (0.020–200) mg/L. Under defined HPLC conditions, working standard ibuprofen solutions were injected into the HPLC system and based on the areas under the curves, a regression equation was obtained. The high value of the

correlation coefficient $r = 0.99$ indicated that there is a good correlation between the concentrations and the areas under the curves. The limit of detection ($LOD-3.3 \cdot \sigma / S$) and quantification ($LOQ-10 \cdot \sigma / S$) were calculated using the standard deviation of the signal and slope, where S is the slope and σ is the standard deviation of the regression line. Calculations for accuracy and repeatability of this method are presented in Table 1.

Table 1. Accuracy and repeatability of analytical method

Accuracy		
Theoretical concentrations ($\mu\text{g/mL}$)	Experimental concentrations ($\mu\text{g/mL}$)	Recovery R (%)
20.08	19.98 ± 0.09	98.50
30.11	30.00 ± 0.14	99.63
50.20	51.08 ± 0.16	101.75
100.40	100.95 ± 0.22	100.54
200.80	201.33 ± 0.09	100.26
R \pm 2SD (%)		100.14 \pm 2.39
Repeatability		
Theoretical concentrations ($\mu\text{g/mL}$)	Retention time (min)	Area under a curve (AUC)
20.08	3.551 ± 0.009	49.85 ± 0.154
50.20	3.525 ± 0.006	62.93 ± 0.228
200.80	3.515 ± 0.009	117.13 ± 0.435
RSD (0.185–0.256) %		RSD (0.309–0.371) %

Data are presented as mean value of triplicate measurements \pm standard deviation.

The accuracy was tested by comparing measured and theoretical ibuprofen concentrations. According to the obtained values (98.50–101.75)%, the method showed good accuracy. The repeatability of the method was tested by analyzing three different concentrations of ibuprofen

standards in 6 replicates. The relative standard deviation (RSD) ranged from (0.185–0.256)% for retention time and (0.309–0.371)% for peak area, confirming excellent repeatability. By comparing the chromatograms obtained for the ibuprofen standard and the chromatograms for the samples, as well as checking the spectra of the obtained signals, it was determined that there are no signals in the samples whose retention time corresponds to the retention time of ibuprofen, which indicates that the method is selective. The yield (recovery) for the purification procedure was calculated by adding 300 μL of standard ibuprofen solution to the Danube samples and acceptable value for recovery was obtained (92.25 ± 1.55)%. Validation parameters and chromatogram of working standard solutions and UV spectrum of ibuprofen are presented in Table 2 and Figure 1.

Table 2. Validation parameters of analytical method for the determination of ibuprofen in surface water

Num-ber	Parameters	Acceptable values	Results
1	System convenience test		
	Asymmetry	< 2	1.11
	Theoretical plateaus	> 1800	11538.53
2	Limit of detection	–	0.007 mg/L
3	Limit of quantification	–	0.02 mg/L
4	Linearity	$r^2 = 0.995$ to 1	0.999
5	Repeatability	RSD < 2 %	(0.015–0.65) %
6	Selectivity	Without interference	Acceptable
7	Accuracy	Recovery: (98–102)%	(98.33–100.22) %
8	Robustness (reliability)	< 1%	(0.5–0.9) %

3. 2. Ibuprofen and Caffeine Determination in the Danube and Assessment of Potential Risk on Aquatic Organisms

Ibuprofen and caffeine amounts for each sampling site are presented in Table 3 and representative chromato-

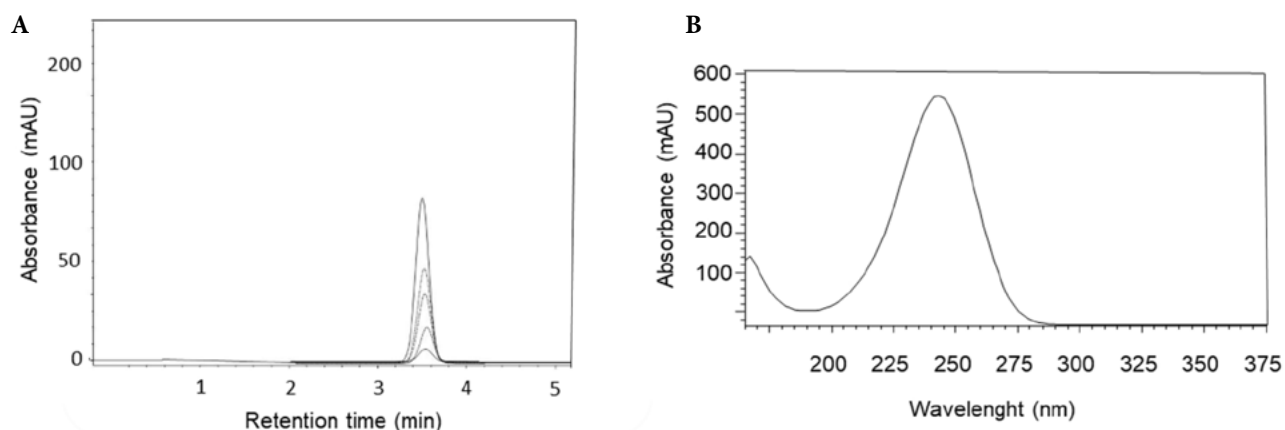


Figure 1. A) chromatogram of working standard solutions of ibuprofen; B) UV spectrum of ibuprofen

Table 3. Ibuprofen and caffeine concentrations with MaxRIs

Sample	Sampling site	GPS coordinate	Ibuprofen			Caffeine		
			Concentrations (ng/L)	MaxRI	Level of risk	Concentrations (ng/L)	MaxRI	Level of risk
1	VB us	4525498N	63.45±0.05	273.22	Class III	362.1±0.22	24.39	Class II
2	VB ds	1985616E	30.62±0.03	476.19	Class III	305.94±0.11	28.57	Class II
3	Beogradski kej us	4528327N	81.57±0.04	212.77	Class III	341.63±0.45	25.60	Class II
		1981049E						
4	Beogradski kej ds		111.40±0.12	156.25	Class III	325.97±0.62	25.64	Class II
5	Cepelin us	4525069N	48.26±0.04	357.10	Class III	321.34±0.77	27.03	Class II
6	Cepelin ds	1985648E	76.01±0.03	227.27	Class III	375.97±0.82	23.26	Class II
7	Štrand us	4523491N	53.62±0.04	322.58	Class III	345.62±0.55	25.00	Class II
8	Štrand ds	1984722E	80.31±0.02	217.39	Class III	358.84±0.77	24.39	Class II
9	DTD us	4528327N	66.62±0.04	263.16	Class III	349.29±0.33	25.00	Class II
10	DTD ds	1981049E	n.d.	–	–	354.45±0.45	25.00	Class II

Data are presented as mean value of triplicate measurements ± standard deviation; us – upstream; ds – downstream; n.d. not detected; MaxRI – maximum risk index; Class II ($10 < \text{MaxRI} < 100$) – sublethal effect on fish; Class III ($\text{MaxRI} > 100$) – low risk on fish.

grams are shown in Figure 2. Sampling site locations are highlighted in Figure 3.

Ibuprofen is considered to be one of the most frequently detected drugs in surface waters although the highest percentage is removed in the purification process.^{2,17,18} The significant presence in natural waters can be explained by the high consumption of ibuprofen and persistence in the aquatic environment.¹⁹ In our study ibuprofen concentrations ranged (30.62–111.40) ng/L with the highest value determined at sampling site No.4 and the lowest at No.2. These results can be explained by the fact that through the sewage system in Novi Sad, Serbia, all waste water without purification ends up in the Danube via two main pumping stations – GC1, which is located near Cepelin and GC2, located near Beogradski kej. Sampling site No.4 (Beogradski kej), where the highest concentration of ibuprofen was detected, is the closest to the GC2 discharge and it is located downstream. The other sampling site closest to GC2 (No.5) is upstream so lower ibuprofen concentrations were found which is in an agree-

ment with the literature.⁶ Compared to the research conducted in Madrid, Spain, on Henares-Jarama-Tajo river system (2784 ng/L)²⁰ a significantly lower value for ibuprofen was obtained in our study. Also, higher concentrations were found in the research analyzing Lis river (Portugal) samples (723 ng/L).⁶ Lower results in our work can be explained by the fact that more sensitive methods have been used in previous researches (HPLC-electrospray tandem mass spectrometry). The results of our study are similar to results obtained for Msunduzi river (South Africa) ranging 0.28–85 ng/L.²¹

Caffeine is found in relatively large quantities in surface waters and, along with carbamazepine and sucralose, has often been used as a detector of human pollution.^{22,23} According to our work, caffeine concentrations ranged (305.94–375.97) ng/L (Table 3). Highest value was determined at sampling site No.6 and the lowest at No.2. Sampling site No.6 (Cepelin) is near the place of discharge of wastewater (GC1) and it is located downstream which may explain the high concentration of caffeine. These results

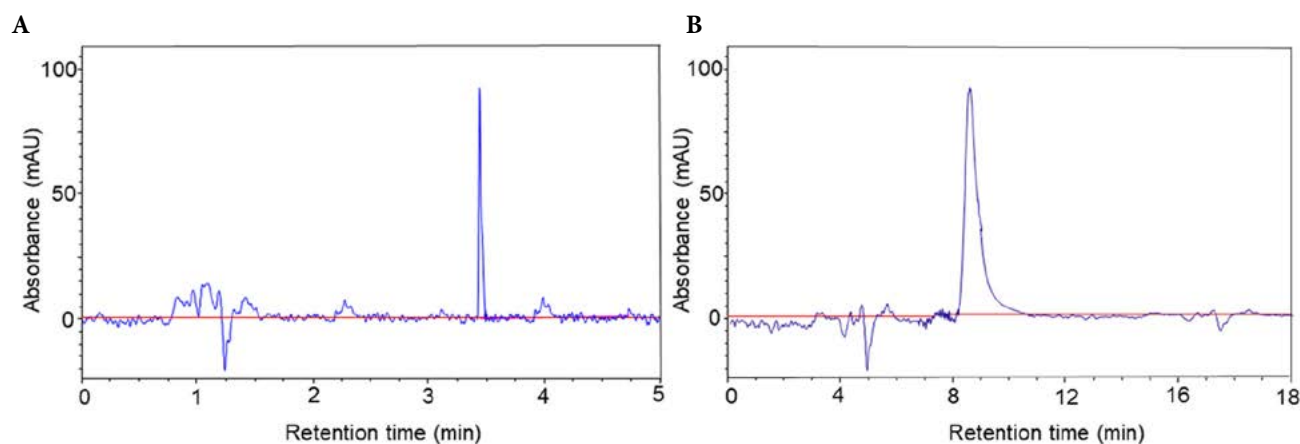


Figure 2. Representative chromatograms of samples: A) ibuprofen sample No. 4; B) caffeine sample No. 6



Figure 3. Sampling site locations

are slightly higher than in study analyzing the Danube samples during 2014¹³ where caffeine concentrations varied (15.91–306.12) ng/L, and lower than one obtained in Paquequer River, Brazil (0.16–47.25 µg/L) using analytical method (SPE-HPLC) with the same sensitivity.²⁴

MaxRIs of sublethal effects on fish for ibuprofen and caffeine are calculated as described in the literature²⁰ and presented in Table 3. According to previous study²⁰, there are three levels of risks: Class I or high risk of sublethal effects on aquatic organisms, with $\text{MaxRI} < 10$; Class II or risk of sublethal effects on aquatic organisms, with $10 < \text{MaxRI} < 100$ and Class III or low risk of sublethal effects on aquatic organisms with $\text{MaxRI} > 100$. The results for ibuprofen showed that all sampling sites have low risk (Class III) on aquatic organisms with MaxRIs ranging 156.25–476.19 ($\text{MaxRI} > 100$). MaxRIs for caffeine varied from 23.26–28.57 and belonged to Class II ($10 < \text{MaxRI} < 100$) where risk of sublethal effects on aquatic organisms exists. The results are similar to those obtained for caffeine in the Danube in 2014¹³, which confirms the fact that in wastewater treatment pharmaceuticals are not removed efficiently and end up in natural waters.

4. Conclusion

The analytical method for determining the presence of ibuprofen in surface water developed and optimized in

this work is fast, sensitive, precise and reliable. Traces of ibuprofen and caffeine were detected in most samples of the Danube. Low risk (Class III) on aquatic organisms with MaxRIs ranging 156.25–476.19 ($\text{MaxRI} > 100$) was established for ibuprofen. MaxRIs for caffeine (23.26–28.57) showed that the risk of sublethal effects on aquatic organisms exists (Class II). These findings indicate the need for frequent collection of information for caffeine presence in the Danube in order to determine the real risk for resident organisms. Future researches should also be more focused on determining the origin, chemical stability and persistence of caffeine in aquatic environments.

Acknowledgements

The authors are grateful for the financial support of Provincial Secretariat for Higher Education and Scientific Research, grant number: 142-451-2545/2021-01.

5. References

1. A. Luptakova, J. Derco, *Acta Chim. Slov.* **2015**, *62*, 859–866. DOI:10.17344/acsi.2015.1590
2. S. Grujić, **2009**, “Determination of drug residues in water by liquid chromatography – tandem mass spectrometry.” PhD thesis, Faculty of Technology and Metallurgy, Belgrade. Available at 10.2298/BG20091009GRUJIC.

3. I. B. Gomes, Y. T. Maillard, L. C. Simões et al., *npj Clean Water*, **2020**, 3, 39. DOI:10.1038/s41545-020-00086-y
4. V. Geissen, H. Mol, E. Klumpp et al., *Int. Soil Water Conserv. Res.*, **2015**, 3, 57–65. DOI:10.1016/j.iswcr.2015.03.002
5. Y. Tang, M. Yin, W. Yang et al., *Water Environ. Res.*, **2019**, 91, 984–991. DOI:10.1002/wer.1163
6. P. Paíga, L. H. M. L. M. Santos, S. Ramos et al., *Sci. Total Environ.*, **2016**, 573, 164–177. DOI:10.1016/j.scitotenv.2016.08.089
7. D. M. Wood, J. Monaghal, P. Streete et al., *Crit. Care*, **2006**, 10, 1–5. DOI:10.1186/cc4850
8. J. Castro, T. Pregibon, K. Chumanov, R. K. Marcus, *Talanta*, **2010**, 82, 1687–1695. DOI:10.1016/j.talanta.2010.07.054
9. J. A. Carrillo, J. Benitez, *Clin. Pharmacokinet.* **2000**, 39, 127–153. DOI:10.2165/00003088-200039020-00004
10. J. Sawynok, *Pain*, **2011**, 152, 726–9. DOI:10.1016/j.pain.2010.10.011
11. S. K. Madhusudhan, *J. Orthop. Res.*, **2013**, 10, 144–148. DOI:10.1016/j.jor.2013.07.001
12. S. Chitravathi, N. Munichandraiah, *J. Electroanal. Chem.*, **2016**, 764, 93–103. DOI:10.1016/j.jelechem.2016.01.021
13. N. Grujić-Letić, M. Milanović, N. Milić et al., *Clean (Weinh)*, **2015**, 43, 731–738. DOI:10.1002/clen.201400402
14. Guideline IH, Q2A Text on Validation of Analytical Procedures, *Fed. Regist.* **1994**, 60.
15. Guideline IH, Validation of analytical procedures: text and methodology, Q2 (R1). **2005**.
16. Y. Vander Heyden, S. Kuttatharmmakul, J. Smeyers-Verbeke J. D. L. Massart, *Anal. Chem.*, **2000**, 72, 2869–74. DOI:10.1021/ac991440f
17. P. Höhener, L. Comoretto, F. al Housari et al., *Environ. Model. Softw.*, **2010**, 25, 1837–1844. DOI:10.1016/j.envsoft.2010.05.005
18. P. H. Roberts, K. V. Thomas, *Sci. Total Environ.*, **2006**, 356, 143–153. DOI:10.1016/j.scitotenv.2005.04.031
19. S. Öllers, H. P. Singer, P. Fässler, S. R. Müller, *J. Chromatogr. A*, **2001**, 911, 225–234. DOI:10.1016/S0021-9673(01)00514-3
20. C. Fernández, M. González-Doncel, J. Pro, G. Carbonell, J.V. Tarazona, *Sci. Total Environ.*, **2010**, 408, 543–551. DOI:10.1016/j.scitotenv.2009.10.009
21. L. M. Madikizela, S. Ncube, *Chemosphere*, **2021**, 280, 1–11. DOI:10.1016/j.chemosphere.2021.130688
22. A. Bahlmann, J. J. Carvalho, M. G. Weller et al., *Chemosphere*, **2012**, 89, 1278–1286. DOI:10.1016/j.chemosphere.2012.05.020
23. K. Fu, L. Wang, C. Wei et al., *Ecotoxicol. Environ. Saf.*, **2020**, 189, 1–7.
24. E. S. Gonçalves, S. V. Rodrigues, E. V. da Silva-Filho, *Brazil. Rev. Ambient. Água*, **2016**, 12, 192–202. DOI:10.4136/ambi-agua.1974

Povzetek

Prisotnost različnih snovi v površinski vodi je zelo zaskrbljujoča, saj so površinske vode ponekod glavni vir oskrbe z vodo. Raziskava opisuje razvoj, optimizacijo in uporabo analizne metode za določanje ibuprofena v vzorcih Donave. Določene so bile tudi koncentracije kofeina kot indikatorja človeških izločkov in izračunani maksimalni indeksi tveganja za vodne organizme. Vzorci Donave so bili zbrani na desetih reprezentativnih lokacijah. Za ločevanje ibuprofena in kofeina je bila uporabljena ekstrakcija v trdni fazi, analiza pa je bila izvedena z metodo tekočinske kromatografije visoke ločljivosti (HPLC). Koncentracije ibuprofena so bile (30,62–111,40) ng/L, kofeina pa (305,94–375,97) ng/L. Za ibuprofen je bilo ugotovljeno nizko tveganje za vodne organizme, za kofein pa je bil dosežen potencialni subletalni učinek. Rezultati so pokazali, da je bil ibuprofen učinkovito ločen od drugih snovi v vzorcih pod določenimi kromatografskimi pogoji za kratek čas (4 minute). Uporabljena metoda HPLC je pokazala dobro ponovljivost, natančnost, selektivnost in robustnost. Potrebne so nadaljnje študije, vključno s stalnim spremljanjem kofeina v Donavi, da bi ocenili dejanska tveganja in možno preprečevanje.



Except when otherwise noted, articles in this journal are published under the terms and conditions of the Creative Commons Attribution 4.0 International License

Scientific paper

Biotreatability Improvement of Antibiotic-Contaminated Waters: High Efficiency of Direct Ozonation in Comparison to Hydroxyl Radical Oxidation

Igor Boševski* and Andreja Žgajnar Gotvajn

University of Ljubljana, Faculty of Chemistry and Chemical Technology, Večna pot 113, SI-1000 Ljubljana, Slovenia.

* Corresponding author: E-mail: igor.bosevski@gmail.com

Received: 09-06-2022

Abstract

Efficiencies of direct ozonation and hydroxyl radical oxidation by Fenton process were compared, aiming to improve biotreatability of antibiotics contaminated water (tiamulin, amoxicillin and levofloxacin). Biodegradability, COD (chemical oxygen demand) and TOC (total organic carbon) were measured before and after applying oxidative process. It was confirmed that significantly smaller molar dose of ozone ($1.1 \text{ mg}_{\text{O}_3} / \text{mg}_{\text{atb}}$) against the hydrogen peroxide ($17 \text{ mg}_{\text{H}_2\text{O}_2} / \text{mg}_{\text{atb}}$), deliver comparable improvements of biodegradability; Tiamulin biodegraded up to 60%, levofloxacin close to 100%. Ozonation removed more TOC (10%, 29% and 8% for tiamulin, levofloxacin and amoxicillin, respectively) than Fenton process. This is confirming mineralization of antibiotics, not only biodegradable intermediates formation. In terms of costs, ozonation is more feasible in oxidizing complex antibiotics in water, as it targets functional groups which carry antimicrobial properties. This brings not only improved biodegradability needed for a conventional biological treatment plant, but also reduces long-term impacts of the antibiotics in the environment.

Keywords: Antibiotic, Biodegradability, Fenton process, Ozonation, Water

1. Introduction

Since discovered, antibiotics have brought immense benefits in terms of human and animal health, as well as food production. On the other hand, antibiotics are source of environmental pollution of growing attention, especially in the perspective of bacterial antibiotic resistance phenomena. Studies indicate that surface water concentrations of some most common antibiotics are low, an order of magnitude lower than the toxic concentrations to water organisms.^{1,2,3} A study of Johnson et al.⁴ found, that the average concentration of antibiotic in most European rivers does not exceed 10 ng L^{-1} . Although without any direct toxic effects, such concentrations do promote a development of bacterial antibiotic resistance genes. Resistance was found most frequently against tetracyclines and sulfonamides, as nowadays we see more and more resistance against advanced generation antibiotics such as β -lactams.⁵ In order to control the distribution of antibiotics into the environment, use of proper antibiotic removal or deactivation techniques is mandatory. These should ensure that antimicrobial properties of the substance are removed. This not only enables conventional biological treatment,

but also limits antibiotic resistance development, as the molecules are released into the environment.

Ozone is reacting with organic matter by direct reaction with dissolved ozone or indirectly through hydroxyl radicals. Scope of both mechanisms and degradation rate of the organic matter depends on the properties of the matter itself, ozone dose and pH of the media. Under pH 4, direct reaction is prevailing, while above pH 9, indirect path of oxidation (hydroxyl radicals) is dominant.⁶ Ozonation in general does not lead to full mineralization; therefore, combination with subsequent biological treatment may be appropriate.⁷ In case of antibiotics it has been found that, e.g., erythromycin and ethyl-paraben can be removed by low doses of ozone within two minutes and even erythromycin and ethyl-paraben resistant bacteria (*Escherichia coli*) were eliminated after 15 min of ozonation.⁸ Antibiotics are susceptible to ozonation, as they carry one or more reactive functional groups in their molecular structure, such as amine nitrogen, sulfur, carbon-carbon double bond and the activated aromatic ring. During ozonation the molecule is partially decomposed as well as the structure of the key ozone-susceptible functional groups is changed. This transforms a molecule into pharmacologi-

cally inactive, biodegradable form. Identification and quantification of degradation by products arising from ozonation, as well as their environmental properties are a continuing topic of research.^{9,10}

Fenton oxidation is a technique using free hydroxyl radicals as oxidant reagent. It is a mixture of hydrogen peroxide (oxidizing reagent) and Fe salt (catalyst), which oxidizes organic matter by means of hydroxyl radicals, which are powerful, non-selective oxidants. Reaction rate is determined by the rate of radical generation, which is controlled by a concentration of iron catalyst. Common molar ratio $\text{Fe}^{2+} : \text{H}_2\text{O}_2$ is 1 : (5–10), although concentrations of Fe^{2+} below 25 – 50 mg L^{-1} may lead to disproportionally long reaction time (from 10 to 48 hours). The drawback of oxidation with Fenton process is that it generates waste ferric sludge, which requires further disposal, as well as treated pollutants or by-products of the process at higher concentrations may adsorb to the sludge⁶. A few studies have demonstrated high effectiveness of Fenton process in treating wastewaters from antibiotics formulation (cefuroxime axetil, ceftriaxone, sulfisoxazole), with COD as high as 1,000 mg L^{-1} as well as treatment of wastewater with single antibiotic (norfloxacin), reaching mineralization rate of 55% in 60 min.¹¹

The aim of our study was to evaluate and compare effectiveness of direct ozonation and Fenton process generating non-selective hydroxyl radicals for oxidation of selected antibiotics dissolved in water, leading to increased biodegradability. Selected antibiotics in the study were from three different groups; i) tiamulin (TML), diterpene, veterinary antibiotic, poorly biodegradable; ii) amoxicillin (AMX), β -lactam, biodegradable; and iii) levofloxacin (LFX), fluoroquinolone, non-biodegradable. This study has generated new data regarding behaviour of the antibiotics during different AOPs, evaluated through biodegradability and process kinetics. This should support both development of a treatment process that delivers an optimum effectiveness in terms of cost and long-term environment impact mitigation.

2. Materials and Methods

Lab scale ozonation of water, contaminated with antibiotic was conducted in a continuous mode with water circulation, while Fenton oxidation experiments were conducted in a conventional homogenous batch mode, with hydrogen peroxide and Fe(II)sulfate as a catalyst. The effectiveness of the methods applied was evaluated by measuring a change of Chemical Oxygen Demand (COD), Total Organic Carbon (TOC) and aerobic biodegradability. Antibiotics belonging to three different groups were used in the experiments, all containing several functional groups in their structure (amine nitrogen, sulfur, carbon-carbon double bond, activated aromatic ring), which are susceptible to direct reactions with ozone, as presented in Table 1.

These groups, marked in Table 1, are susceptible to a reaction with hydroxyl radicals as well.¹² Experiments were performed using 400 and 100 mg L^{-1} solutions of antibiotics in demineralized water. pH of the solutions was in the case of TML 6.0 ± 0.1 , and for AMX and LFX 7.0 ± 0.1 , at the ambient temperature of 22 ± 2 °C. In this case, the prevailing reaction route was assumed a direct reaction with ozone. Before or during the ozonation, no pH adjustment was done.

2.1. Ozonation

In the experimental set-up, ozone was purged through a glass column (3,500 mL, diameter 12 cm, height 50 cm), as shown in Figure 1.

Water solution of antibiotic was circulated in a counter-current mode with respect to ozone bubble path, in a closed loop including a reservoir with a flow of 1 mL s^{-1} at ambient temperature (22 ± 2 °C). The operating pressure of the ozone generator (Xylem Water Solutions, Herford GmbH, Germany, 2012) was 0.5 bar, the gas flow of 0.05 $\text{m}^3 \text{h}^{-1}$, and the capacity of the system was 7 g h^{-1} . The

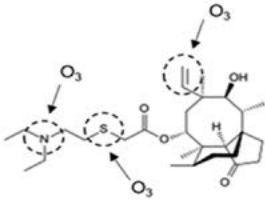
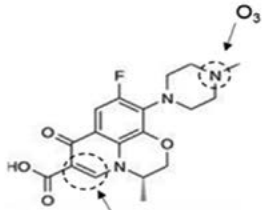
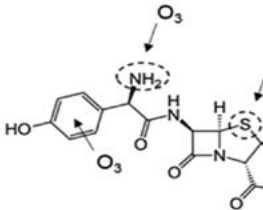
Tiamulin (TML)	Amoxicilin (AMX)	Levofloksacin (LFX)
		
Diterpene antibiotic $\text{C}_{32}\text{H}_{51}\text{NO}_8\text{S}$ 609.8 g mol^{-1}	β -lactam, penicillin $\text{C}_{16}\text{H}_{19}\text{N}_3\text{O}_5\text{S}$ 365.4 g mol^{-1}	Fluoroquinolone $\text{C}_{18}\text{H}_{20}\text{FN}_3\text{O}_4$ 361.4 g mol^{-1}
Ben et al. 2012	Andreozzi et al. 2005	El Najjar et al. 2013

Table 1: Molecular structure of antibiotics and proposed attack points of ozone in direct ozonation reaction.

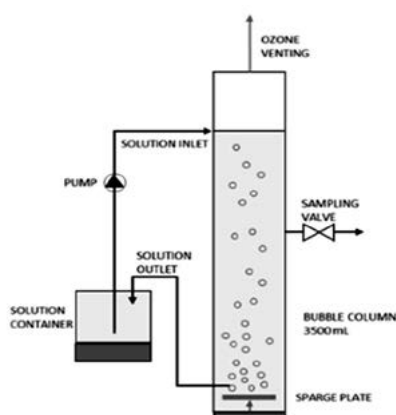


Figure 1: Bench-scale ozonation system

nominal concentration of ozone in the gas phase was 140 g m^{-3} (NTP). The ozone amount delivered into the liquid phase was determined by the calibration line.¹³ Calibration line was derived by ozonating water in the same set-up and conditions as the experiments, while measuring ozone concentration colorimetrically (118755, Merck Ozone Test) every five minutes until saturation. Ozone concentration (y , $\text{mg}_{\text{ozone}} \text{L}^{-1}$) was plotted against time (x , min) and the ozone delivery rate was determined by the constant in the line equation, which was $3 \text{ mg}_{\text{ozone}} \text{L}^{-1} \text{min}^{-1}$. Oxidant dose was then determined by the time of ozonation, which was ranging from 45 to 180 minutes as a maximal ozonation time for selected antibiotic. Doses and other experimental details are outlined in Table 2. In order to achieve significant, measurable changes in COD, TOC and especially in biodegradability, rather large doses of ozone were used.

Table 2: Ozone doses used at experiments.

Ozonation time, min	Ozone dose*			Ozone dose **
	TML	LFX	AMX	$\text{mg}_{\text{ozone}} \text{g}_{\text{antibiotic}}^{-1}$ All antibiotics
0	0.00	0.00	0.00	0
15	0.04	0.03	0.04	104
30	0.07	0.07	0.07	182
45	0.11	0.10	0.15	286
90	0.22	0.21	0.23	572
120	0.29	0.28	0.29	754
135	0.33	0.31	0.35	858
180	0.44	0.42	0.44	1,144

* Calculated according to the initial COD of the solution of the antibiotic. ** Calculated according to the initial mass of the antibiotic in the solution, the same for all antibiotics.

2. 2. Fenton Process

For Fenton process, common laboratory glassware was used. 200 mL of antibiotic solution (400 mg L^{-1}) was put in a beaker and stirred at 200 rpm; pH was adjusted to

2.5–3.0 with concentrated HCl (Merck, Germany). Reagents Ferrrous sulphate heptahydrate ($\text{FeSO}_4 \cdot 7\text{H}_2\text{O}$; Fluka Analytical, Germany) and hydrogen peroxide (H_2O_2 , 30%; Merck, Germany) were used in a molar ratio $\text{FeSO}_4/\text{H}_2\text{O}_2 = 1/10$. This ratio is at the high end among the commonly used ratios in Fenton process, aiming to have most oxidant available for the reaction. Experiments were conducted at ambient temperature ($22 \pm 2 \text{ }^\circ\text{C}$). After 30 minutes, solution was boiled for 3 minutes to remove any possible residual peroxide. Antibiotic molecules were proven to be stable during this period, as separate blank test was carried out, with boiling antibiotic solution for 3 minutes – there was no change observed in TOC before and after the boiling. Samples were cooled, pH raised to 9.0 ± 0.1 to precipitate Fe^{3+} salts, then filtered by using paper filter Whatman No. 41. Filtrate was used for further analysis. Experiments were run in duplicates. Doses of oxidant are outlined in Table 3. Same as for the ozonation, rather large doses of oxidant were used to deliver significant, measurable changes in COD, TOC and especially in biodegradability.

Table 3: Hydrogen peroxide doses used at Fenton process.

Experiment	V H_2O_2 ml	Dose H_2O_2^* $\text{mol}_{\text{H}_2\text{O}_2} \text{mol}_{\text{COD}}^{-1}$			Dose $\text{H}_2\text{O}_2^{**}$ $\text{mg}_{\text{H}_2\text{O}_2} \text{g}_{\text{antibiotic}}^{-1}$
		TML	LFX	AMX	All antibiotics
I.	0.5	0.9	1.1	1.1	2,081
II.	1.0	1.8	2.1	2.2	4,163
III.	2.0	3.6	4.1	4.4	8,325
IV.	4.0	7.1	8.5	8.8	16,650

* Calculated according to the initial COD of the antibiotic solution.

** Calculated according to the initial mass of the antibiotic in the solution, the same for all antibiotics.

2. 3. Analytical Methods

The degradation rate of all selected antibiotics before and after the oxidation was evaluated by measuring COD and TOC, according to standard ISO methods 6060:1989 and 8245:1999.^{14,15} Actual concentrations of the antibiotics were not measured. Biodegradability was assessed according to ISO 9408:1999 method.¹⁶ This method evaluates the ultimate aerobic biodegradability of organic compounds, by determining oxygen demand in a closed respirometer, using aerobic microorganisms. Solution (150 mL) of investigated antibiotic (400 mg L^{-1}) was added to non-adapted activated sludge microorganisms ($30 \text{ mg}_{\text{VSS}} \text{L}^{-1}$), including nutrient mineral solution (6.5 mL) and stirred in a closed flask (total volume 500 mL). The degradation was followed over a period of 22 days by measuring oxygen consumption as a consequence of biodegradation. Activated sludge microorganisms were taken from a municipal wastewater treatment plant of Ljubljana city, Slovenia. Overall measuring accuracy was $\pm 2\%$ for the TOC, $\pm 4\%$ for the COD and $\pm 6\%$ for the biodegradability.

3. Results and Discussion

3.1. Ozonation

COD and TOC removal yields in ozonation experiments for all three investigated antibiotics are shown in Figure 2. pH remained constant during the process.

Figure 2 (A-C) comparison of COD and TOC removal yields in ozonation experiments with antibiotics, shows that the maximum incremental effect is achieved with the smallest dose of $0.1 \text{ mol}_{\text{Ozone}} \text{ mol}_{\text{COD}}^{-1}$. At this dose, a COD reduction of 15% is achieved with TML (Fig 2 A), 49% with LFX (Fig 2 B) and 42% with AMX (Fig 2 C). TOC reduction is 10%, 29% and 8% for TML, LFX and AMX, respectively. A double or even quadruple dose of ozone did not lead to proportionally larger effect; a four-fold dose size resulted in doubled effect of COD removal

As Figure 3 (A-C) biodegradability before and after ozonation (100 mg L^{-1} of antibiotics) shows, analogous to the removal of COD or TOC, a double dose ($0.2 \text{ vs. } 0.4 \text{ mol ozone per mol}_{\text{COD}}^{-1}$) did not significantly affect the change in biodegradability. At both doses, TML biodegradability improves from less than 20 to 60% and for LFX from non-biodegradable to completely biodegradable. According to the studies of El Najjar et al. (2013) and Andreozzi et al. (2005) where oxidative degradation of LFX and AMX was studied, complex organic molecules react with ozone in a direct or indirect way to the point where products are formed, that do not react with ozone anymore. For this reason, further increase in ozone dose delivers no significant improvement in COD or TOC removal, as noticed in our study, too. Furthermore, biodegradability of AMX after ozonation is lower (from 100 to 80%), which could be

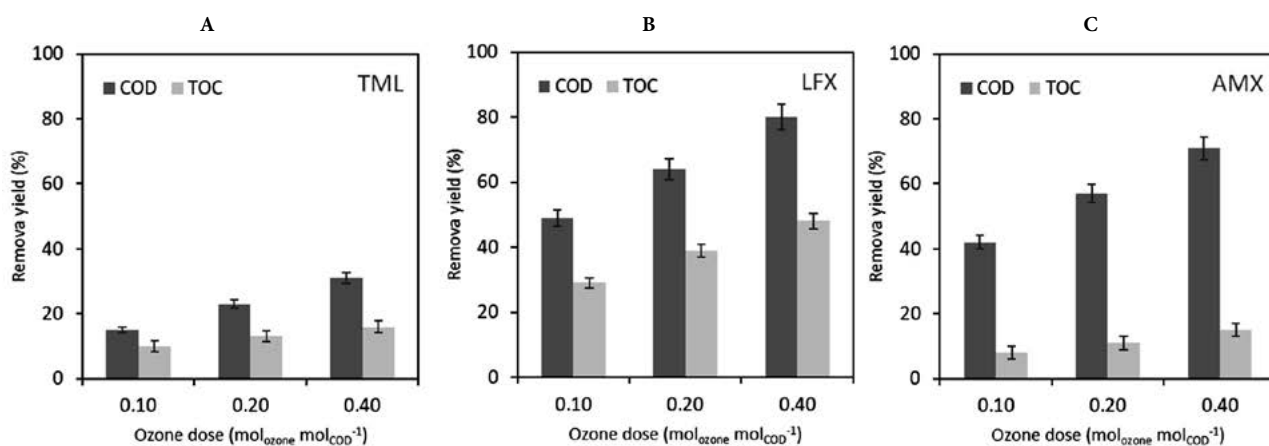


Figure 2 (A-C): Comparison of COD and TOC removal yields in ozonation experiments with antibiotics (100 mg L^{-1} of antibiotics); A – tiamulin; B – levofloxacin; C – amoxicillin.

for TML, and 1.7 times larger removal with LFX and AMX. The increase in TOC reduction effect was 1.6-fold for TML and LFX and 1.9-fold for AMX.

Since ozonation is considered primarily as a pre-treatment method prior to biological treatment, its effect on biodegradation is particularly important, which is shown in Figure 3.

due to a product of ozonation (2-amino-2-(p-hydroxyphenyl)aceto acid) which exhibits lower biodegradability than the parent molecule (Andreozzi et al. 2005). The biodegradation was followed over a period of 22 days although in most cases, maximal level of biodegradation was reached within 14 days. Abiotic degradation of all three antibiotics was checked and found to be $< 2\%$ which confirms that

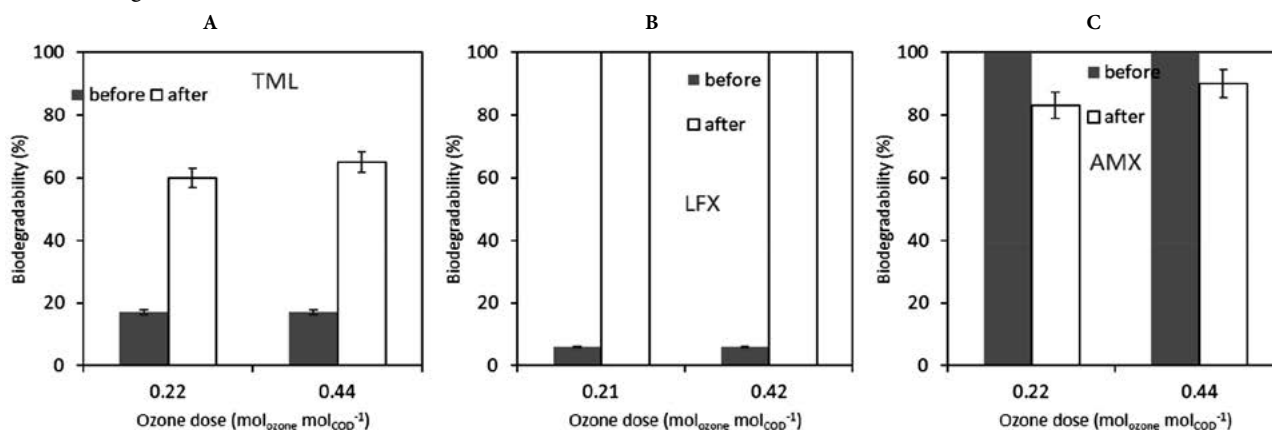


Figure 3: Biodegradability before and after ozonation (100 mg L^{-1} of antibiotics): A – tiamulin; B – levofloxacin; C – amoxicillin.

measured degradation is not related to any non-biological, physicochemical processes.

Combining the data from Figures 2 and 3, it can be assumed that for the pretreatment of the antibiotics TML and LFX, a dose of ozone $0.22 \text{ mol}_{\text{ozone}} \text{ mol}_{\text{COD}}^{-1}$ is sufficient to achieve a significant biodegradability improvement (TML to 60% and LFX to 100%). Furthermore, COD was reduced by 23% in the case of TML (Fig 2 A) and by 64% in the case of LFX (Fig 2 B); TOC was reduced by 13% in the case of TML (Fig 2 A) and by 39% in the case of LFX (Fig 2 B). Considering the reduction of biodegradation of AMX after ozonation (from 100 to 82 % at $0.22 \text{ mol}_{\text{ozone}} \text{ mol}_{\text{COD}}^{-1}$ and from 100 to 91% at $0.44 \text{ mol}_{\text{ozone}} \text{ mol}_{\text{COD}}^{-1}$; Fig 3 C), ozonation is of no value here, although the biodegradation process begins earlier (in two days) comparing to the start of biodegradation of parent molecule (six days).

3. 2. Hydroxyl Radical Oxidation – Fenton Process

COD and TOC removal yields achieved by Fenton process are shown in Figure 4 (A–C) comparison of COD and TOC removal yields in Fenton process experiments

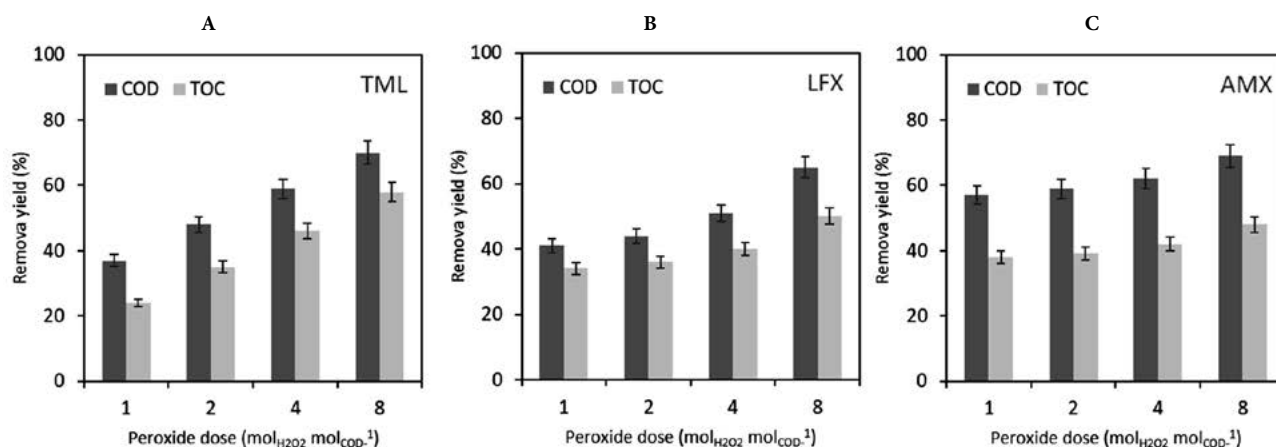


Figure 4: Comparison of COD and TOC removal yields in Fenton process experiments with antibiotics (400 mg L^{-1} of antibiotics): A – tiamulin; B – levofloxacin; C – amoxicillin.

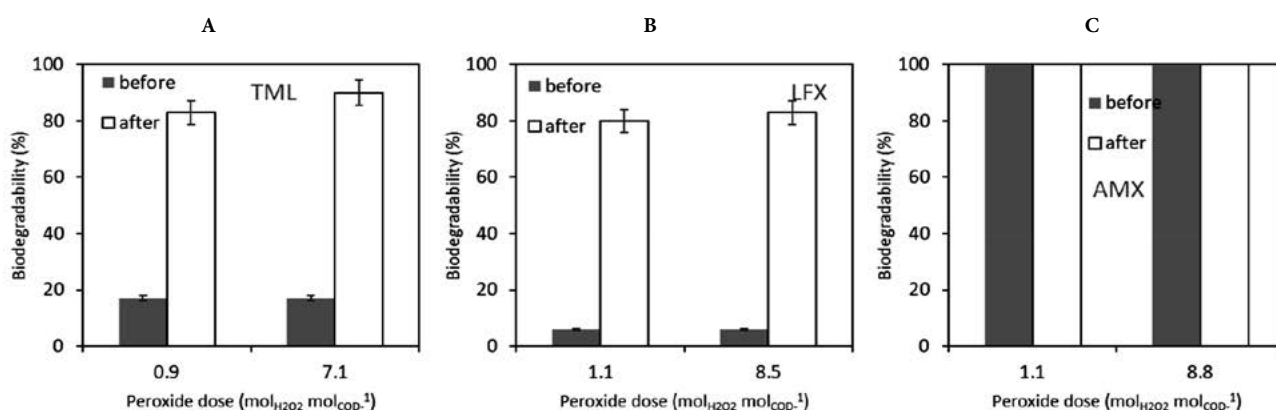


Figure 5: Biodegradability before and after Fenton process (400 mg L^{-1} of antibiotic): A – tiamulin; B – levofloxacin; C – amoxicillin.

with antibiotics. pH remained constant during the experiments (± 0.4). Figure 4 shows that the maximum incremental effect is achieved with the lowest dose, $1 \text{ mol}_{\text{H}_2\text{O}_2} \text{ mol}_{\text{COD}}^{-1}$. At this dose, a COD reduction of 37% for TML (Fig 4 A), 41% for LFX (Fig 4 B) and 57% for AMX (Fig 4 C) is achieved. The TOC reduction is 24%, 34% and 38% for TML, LFX and AMX respectively. Reduction is larger for COD than TOC as the antibiotics are oxidized, but only partially mineralized, so COD decreases faster than TOC.

An increased dose of hydrogen peroxide does not result in a linear increase of removal yield; a fourfold dose resulted in a 60% removal yield increase of COD at TML, a 7% increase at LFX, and 8% increase at AMX. The reduction of TOC was 90% higher for TML, 10% for LFX and 7% for AMX. The oxidation products apparently no longer react with hydroxyl radicals, so oxidation does not progress and the removal effects do not increase proportionally with the H_2O_2 dose increase (Figure 4).

Since Fenton oxidation is considered here as a pre-treatment method before biological treatment, the effect on biodegradation is important, shown in Figure 5 (A–C), biodegradability before and after Fenton process.

As can be seen from Figure 5 (A-C), biodegradability before and after Fenton process, the largest change in biodegradability is achieved with relatively small doses of hydrogen peroxide, $1 \text{ mol}_{\text{H}_2\text{O}_2} \text{ mol}_{\text{COD}}^{-1}$. At this dose of oxidant, biodegradability of both TML and LFX reached 80%. Increasing the dose does not have a proportional effect on increasing biodegradability because the oxidation products no longer react with hydroxyl radicals. It can be assumed that for the purpose of antibiotic pretreatment, resulting in increased biodegradability, a dose of $1 \text{ mol}_{\text{H}_2\text{O}_2} \text{ mol}_{\text{COD}}^{-1}$ is sufficient.

3. 3. Comparison of Direct Reaction with Ozone and Oxidation by Hydroxyl Radicals

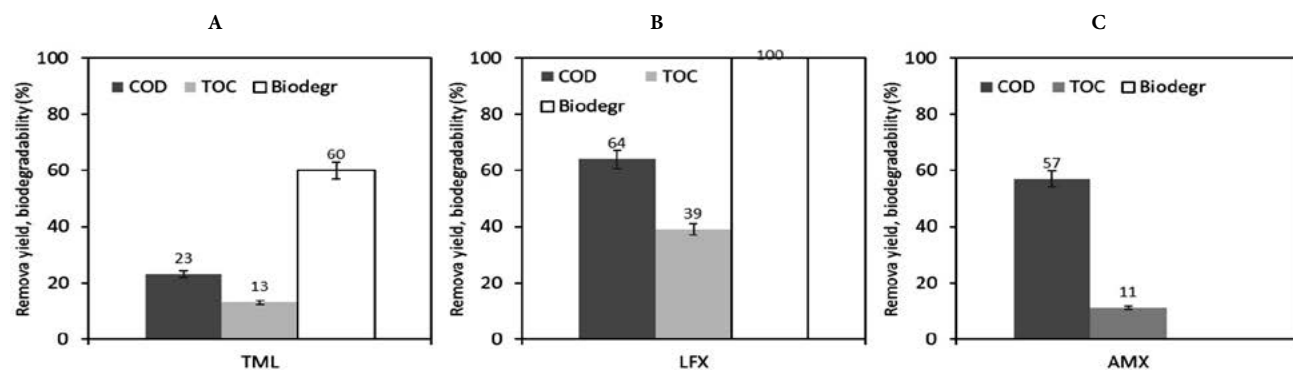
A comparison of the effects of direct reaction with ozone and oxidation with hydroxyl radicals from Fenton process is outlined in Figure 6 (A-F), comparison of effects of ozonation and Fenton process to COD/TOC reduction and change of biodegradability of antibiotics water solution. With Fenton process five times higher molar dose of oxidant per unit of COD was used in comparison to ozonation. Reaction mechanism of Fenton process is based on generation of free radicals, which then react with organic matter, while ozone reacts directly with organic com-

pounds. In spite of higher oxidant dose in the case of Fenton as well as with more aggressive reaction mechanism, the effects on COD or TOC reduction between the two techniques do not

For TML, reduction of COD with Fenton's process is 1.6-fold larger than in the case of ozonation while a reduction of TOC is larger by 1.8 times. The opposite is true with LFX, where reductions of COD and TOC are larger in the case of ozone against the Fenton's process. For AMX, reduction of COD with Fenton's process is the same as with ozone, while the reduction in TOC is 3.5-fold larger with Fenton's process. Oxidation with Fenton improves biodegradability of TML from 17 to 83%, biodegradability of LVX is increased up to 80%, and the biodegradability of AMX is 100%.

Figure 6 shows that for comparable COD and TOC removal efficiencies, significantly higher doses of oxidant need to be used for Fenton process comparing to ozonation. The improvement of LFX biodegradability actually larger at a lower dose of ozone compared to a higher dose of hydrogen peroxide. Higher doses of Fenton otherwise achieve better biodegradability for TML and AMX. The results show that both ozonation and Fenton process are effective techniques for the oxidation of antibiotics in aqueous solution, but the effects are not easily predictable due to formation of variety of different transformation

Ozone, dose: $0.2 \text{ mol}_{\text{ozone}} \text{ mol}_{\text{COD}}^{-1}$



Fenton, dose: $1 \text{ mol}_{\text{H}_2\text{O}_2} \text{ mol}_{\text{COD}}^{-1}$

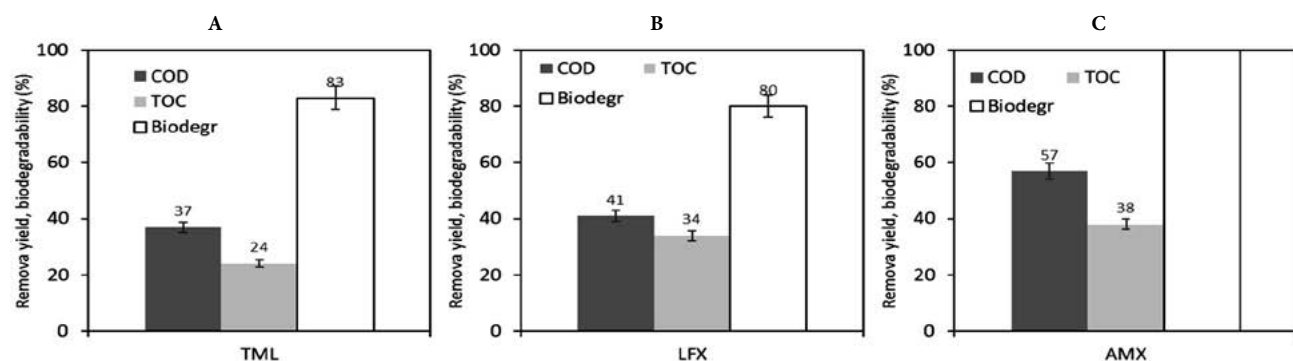


Figure 6: Comparison of effects of ozonation and Fenton process to COD/TOC reduction and change of biodegradability of antibiotics water solution, ozone dose $0.2 \text{ mol}_{\text{ozone}} \text{ mol}_{\text{COD}}^{-1}$ (100 mg L^{-1} of antibiotics), Fenton dose $1.0 \text{ mol}_{\text{H}_2\text{O}_2} \text{ mol}_{\text{COD}}^{-1}$; (400 mg L^{-1} of antibiotics) A, D – tiamulin; B, E – levofloxacin; C, F – amoxicillin.

products, exhibiting lower or higher biodegradability as the parent molecule. Above all, experiments indicated that it may not be assumed that higher doses of oxidant will result in proportionally larger effects in COD/TOC reductions, regardless of the oxidation technique used.

Considering the operational costs of both ozone and Fenton, referencing to the study of Cañizares et al.,¹⁷ cost of ozone treatment according to Figure 6 is 0.5 € mol_{COD}⁻¹, while Fenton treatment cost is in the range of 0.1 € mol_{COD}⁻¹. This is considerable difference, also if sludge treatment costs are added, in the range of 100 € m⁻³ dry sludge. On the other hand, ozone treatment neither generates any waste that needs further disposal nor uses any chemicals that require transport, storage and disposal. In terms of environmental sustainability, this advantage, which economically may not yet be fully recognized.

3. 4. Reaction Kinetics of Ozonation

To determine the kinetics of the direct reaction of ozone, measured through the removal of COD and TOC, a completely mixed two-phase system was assumed. CO₂ and ozonation intermediates are constantly generated in the process. The reaction stops at the stage where oxidation products no longer react with ozone. Due to the purging of the solution with ozone-containing gas, CO₂ formed during the oxidation of antibiotics is continuously removed from the system. For both TML and LFX, reduction of TOC and COD over time follows zero-order kinet-

ics, however in two phases – where the reaction rate is higher in the first than in the second phase. The stepwise nature of the reaction can be justified by the analysis of structural changes of the molecule during ozonation. First, oxidation intermediates appear in the process, which react further and are transformed into molecular entities, which eventually no longer react with ozone.

Ozonation of TML leads in the first 30 minutes to the formation of a carboxylic acid and as well as sulfur atom is oxidized, which produces the molecule (with a mass of 543 g mol⁻¹), predominant in the first phase of ozonation. In the second phase, this is then followed by the oxidation of the nitrogen atom and thus the degradation of TML gradually progresses.¹⁸ The two reaction phases are clearly seen in Figure 7 for TOC and Figure 8 for COD.

The reaction rate constants are; TOC (Figure 7): $k_1 = 0.15 \text{ min}^{-1}$, $k_2 = 0.02 \text{ L mg}^{-1}$ and COD (Figure 8): $k_1 = 0.57 \text{ min}^{-1}$, $k_2 = 0.22 \text{ L mg}^{-1}$; respectively for the first and for the second phase of reaction.

In case of LFX, the first ozonation product is formed as a consequence of a rapid direct attack of ozone on to the double bond of the quinolone moiety, followed by decarboxylation. The second product is formed because of the ozone attack on to the tertiary amine of the piperazine moiety. The ozonation products are in the second phase formed due to the ozone attack on to the tertiary amine of the piperazine moiety with the loss of the methyl group, which is again followed by the quinolone double bond attack and decarboxylation.¹⁹ Reaction kinetics of COD and

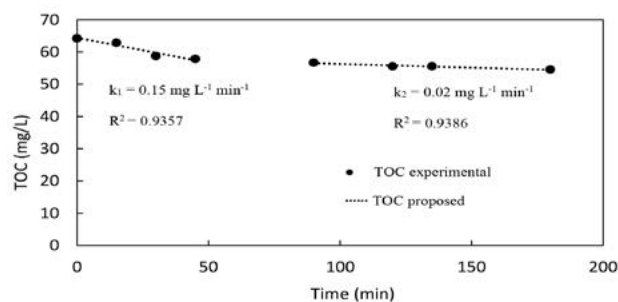


Figure 7. Removal of TOC by ozonation of tiamulin solution (100 mg L⁻¹), measured values and assumed course by zero-order kinetics.

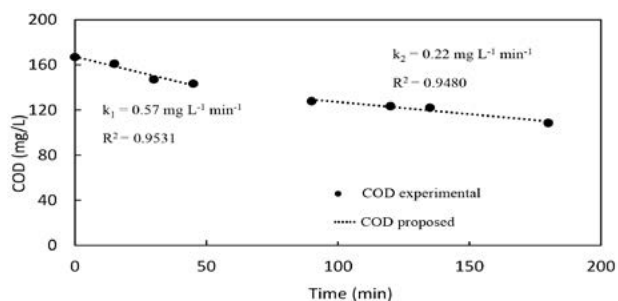


Figure 8. Removal of COD by ozonation of tiamulin solution (100 mg L⁻¹), measured values and assumed course by zero-order kinetics.

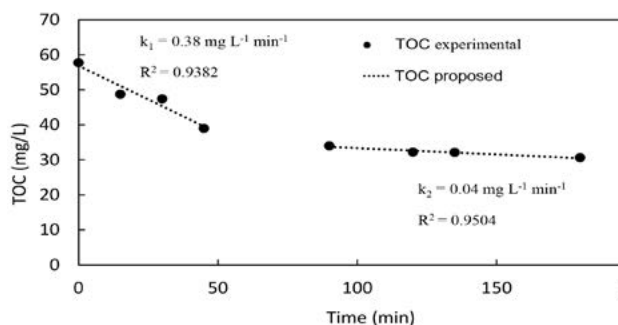


Figure 9. Removal of TOC by ozonation of levofloxacin solution (100 mg L⁻¹), measured values and assumed course by zero-order kinetics.

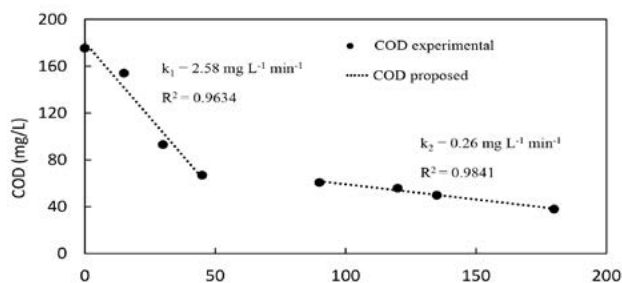


Figure 10. Removal of COD by ozonation of levofloxacin solution (100 mg L⁻¹), measured values and assumed course by zero-order kinetics.

TOC removal follows zero order (Figure 9 for TOC and Figure 10 for COD), with two phases, first being significantly faster than the second is. The reaction rate constants are; TOC (Figure 9): $k_1 = 0.38 \text{ min}^{-1}$, $k_2 = 0.04 \text{ L mg}^{-1}$ and COD (Figure 10): $k_1 = 2.58 \text{ min}^{-1}$, $k_2 = 0.26 \text{ L mg}^{-1}$ respectively for the first and for the second phase of reaction. A rate constant of LFX (parent molecule) ozonation was reported to be $6.0 \times 10^4 \text{ M}^{-1} \text{ s}^{-1}$ at pH 7.2.¹⁹

As can be seen from Figures 9 and 10, the transition from the first and the second stage of the reaction is very pronounced. The TOC decreases 11 times faster in the first stage and the COD 10 times faster than in the second stage.

For AMX data shows that the decrease of TOC and COD over time follows kinetics of variable order (from zero to first). Reaction rate constants are; TOC (Figure 11): $k_{1(s)} = 0.18 \text{ min}^{-1}$, $k_{2(s)} = 1.29 \text{ L mg}^{-1}$ and COD (Figure 12): $k_1 (s) = 0.85 \text{ min}^{-1}$, $k_2 (s) = 0.25 \text{ L mg}^{-1}$, respectively for the first and for the second phase of reaction. AMX is degraded by an attack of ozone on the phenolic ring and the sulfur atom, leading to the formation of two isomers, and the reaction is terminated by a single product.²⁰

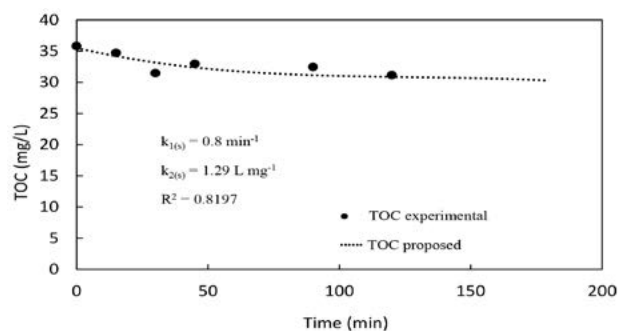


Figure 11. Removal of TOC by ozonation of amoxicillin solution (100 mg L^{-1}), measured values and assumed course of variable order kinetics.

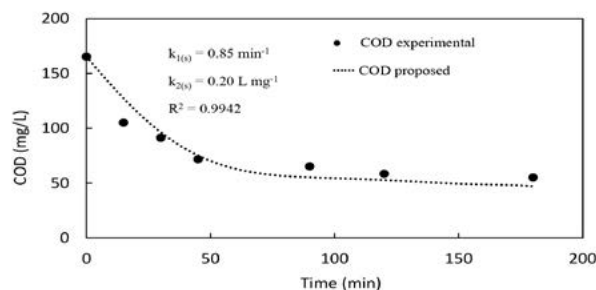


Figure 12. Removal of COD by ozonation of amoxicillin solution (100 mg L^{-1}), measured values and assumed course of variable order kinetics

As it can be seen from Figure 11, TOC reduces for only about 5 %, while the final product of amoxicillin ozonation is formed with 90% yield²⁰ – which is also consistent with a significant COD reduction of 70 % (Figure 12).

4. Conclusions

The aim of the work was to compare oxidation efficiency in case of antibiotics dissolved in water, either by a direct reaction with ozone or by means of indirect oxidation with hydroxyl radicals from Fenton reagent. Overall goal was to increase biodegradability to a degree that enables further biological treatment. Selected antibiotics were TML, LFX and AMX.

In terms of oxidant reagent consumption, direct reaction with ozone has proven to be more efficient, as comparable biodegradability improvement, including TOC reduction was achieved with an ozone dose, tenfold smaller than the equivalent molar dose of oxidant (H_2O_2) from Fenton reagent. On the other hand, comparable COD reductions were achieved with oxidant doses (O_3 and H_2O_2) in the same order of magnitude. This means that antibiotics were oxidized equally either by direct reaction with ozone or hydroxyl radicals from Fenton reagent. In case of direct ozone reaction however, entities of the molecule, which carry antibiotic potential, were targeted. This delivers effective biodegradability improvements already at low doses of oxidant. Overall rate of mineralization is not critical, as this is not primary the objective of the oxidation. Reaction kinetics of ozonation shows that there are two phases of the reaction, with the first being significantly faster than the second. This is also the part, where biodegradability is improved most, while in the second phase, molecule is being degraded further and mineralized.

In terms of operational costs, Fenton costs about five times less than ozone, providing the effectiveness discussed in this study, however ozone has advantages in terms of broader sustainability, given that generates no side waste that requires further treatment and disposal.

Acknowledgements

The authors are grateful to Nastja Smolnikar, Polona Starašinič, Damjan Koder and Matjaž Škedelj for laboratory assistance. This work was financed by the Slovenian Research Agency, research program of Chemical Engineering (P2-0191).

5. References

1. A. B. A. Boxall, D. W. Kolpin, B. Halling-Sørensen, J. Tolls, *Environ. Sci. Technol.* **2003**, 37(15), 286A–294A.
DOI:10.1021/es032519b
2. P. H. Jensen John, *Chemosphere* **2003**, 50(3), 437–443.
DOI:10.1016/S0045-6535(02)00336-3
3. B. Halling-Sørensen, *Chemosphere* **2000**, 40(7), 731–739.
DOI:10.1016/S0045-6535(99)00445-2
4. A. C. Johnson, V. Keller, E. Dumont, J. P. Sumpter, *Sci. Total Environ.* **2015**, 511, 747–755.
DOI:10.1016/j.scitotenv.2014.12.055

5. R. Singh, A. P. Singh, S. Kumar, B. S. Giri, K. H. Kim, *J. Clean. Prod.* **2019**, 234, 1484–1505. DOI:10.1016/j.jclepro.2019.06.243
6. E. M. Cuerda-Correa, M. F. Alexandre-Franco, C. Fernández-González, *Water* **2020**, 12(1), 2–52. DOI:10.3390/w12010102
7. J. Gomes, R. Costa, R. M. Quinta-Ferreira, R. C. Martins, *Sci. Total Environ.* **2017**, 586, 265–283. DOI:10.1016/j.scitotenv.2017.01.216
8. I. Michael-Kordatou, R. Andreou, M. Iacovou, Z. Frontistis, E. Hapeshi, C. Michael, D. Fatta-Kassinos, *J. Hazard. Mater.* **2017**, 323(A), 414–425. DOI:10.1016/j.jhazmat.2016.02.023
9. I. C. Iakovides, I. Michael-Kordatou, N. F. F. Moreira, A. R. Ribeiro, T. Fernandes, M. F. R. Pereira, O. C. Nunes, C. M. Manaia, A. M. T. Silva, D. Fatta-Kassinos, *Water Res.* **2019**, 159, 333–347. DOI:10.1016/j.watres.2019.05.025
10. Y. Zheng, D. Chen, T. Chen, M. Cai, Q. Zhang, Z. Xie, R. Li, Z. Xiao, G. Liu, W. Lv, *Chemosphere* **2019**, 227, 198–206. DOI:10.1016/j.chemosphere.2019.04.039
11. L. V. Santos, A. M. Meireles, L. C. Lange, *J. Environ. Manage.* **2015**, 154, 8–12. DOI:10.1016/j.jenvman.2015.02.021
12. I. Epold, M. Trapido, N. Dulova, *J. Chem. Eng.* **2015**, 279, 452–462. DOI:10.1016/j.cej.2015.05.054
13. M. Muz, M. S. Ak, O. T. Komesli, C. F. Gökçay, *J. Chem. Eng.* **2013**, 217, 273–280. DOI:10.1016/j.cej.2012.11.134
14. International organization for standardization, international standard, ISO 6060:1989, **1989**.
15. International organization for standardization, international standard ISO 8245:1999, **1999**.
16. International organization for standardization, international standard ISO 9408:1999, **1999**.
17. P. Cañizares, R. Paz, C. Sáez, M. A. Rodrigo, *J. Environ. Manage.* **2009**, 90(1), 410–420. DOI:10.1016/j.jenvman.2007.10.010
18. I. Bosevski, G. Kalcikova, J. Cerkovnik J., A. Zgajnar Gotvajn, *Ozone: Sci. Eng.* **2019**, 42(2), 128–135. DOI:10.1080/01919512.2019.1624149
19. N. H. El Najjar, A. Touffet, M. Deborde, R. Journal, N. K. Vel Leitner, *Chemosphere* **2013** 93(4), 604–611. DOI:10.1016/j.chemosphere.2013.05.086
20. R. Andreozzi, M. Canterino, R. Marotta, N. Paxeus, *J. Hazard. Mater* **2005**, 122(3), 243–250. DOI:10.1016/j.jhazmat.2005.03.004

Povzetek

Primerjana je bila učinkovitost neposrednega ozoniranja in oksidacije hidroksilnih radikalov s Fentonovim postopkom z namenom izboljšanja čiščenja vode, onesnažene z antibiotiki (tiamulin, amoksicilin in levofloksacin). Biorazgradljivost, KPK (kemijska potreba po kisiku) in TOC (celotni organski ogljik) so bili izmerjeni pred in po uporabi oksidativnega postopka. Potrjeno je bilo, da znatno manjši molski odmerek ozona ($1,1 \text{ mg}_{\text{O}_3} / \text{mg}_{\text{atb}}$) v primerjavi z vodikovim peroksidom ($17 \text{ mg}_{\text{H}_2\text{O}_2} / \text{mg}_{\text{atb}}$) zagotavlja primerljive izboljšave biorazgradljivosti: tiamulin je biorazgradljiv do 60 % in levofloksacin blizu 100 %. Ozoniranje je odstranilo več TOC (10 % za tiamulin, 29 % za levofloksacin in 8 % za amoksicilin) kot Fentonov postopek. To potrjuje mineralizacijo antibiotikov, ne le tvorbo biorazgradljivih intermediatov. Z vidika stroškov je ozoniranje pri oksidaciji kompleksnih antibiotikov v vodi bolj primerno, saj cilja na funkcionalne skupine, ki imajo protimikrobne lastnosti. To ne vpliva samo na izboljšanje biološke razgradljivosti, potrebne za konvencionalno biološko čistilno napravo, ampak tudi zmanjša dolgoročni vpliv antibiotikov na okolje.



Except when otherwise noted, articles in this journal are published under the terms and conditions of the Creative Commons Attribution 4.0 International License

Scientific paper

Interaction of Copper(II) Complexes of Bidentate Benzaldehyde Nicotinic Acid Hydrazones with BSA: Spectrofluorimetric and Molecular Docking Approach

Adnan Zahirović,¹ Irnesa Osmanković,¹ Amar Osmanović,²
Aleksandar Višnjevac,³ Amina Magoda,⁴ Selma Hadžalić¹ and Emira Kahrović^{*1}

¹ Laboratory for Inorganic and Bioinorganic Chemistry, Department of Chemistry, Faculty of Science, University of Sarajevo, Sarajevo, Bosnia and Herzegovina

² Faculty of Pharmacy, University of Sarajevo, Sarajevo, Bosnia and Herzegovina

³ Laboratory for Chemical and Biological Crystallography, Ruđer Bošković Institute, Zagreb, Croatia

⁴ Faculty of Veterinary Medicine, University of Sarajevo, Sarajevo, Bosnia and Herzegovina

* Corresponding author: E-mail: emira_kahrovic@yahoo.com
Phone: +387 33 279 910

Received: 09-29-2022

Abstract

Two copper(II) complexes of 4-chloro- and 4-dimethylaminobenzaldehyde nicotinic acid hydrazones were prepared and characterized by elemental analysis, mass spectrometry, infrared and electron spectroscopy and conductivity. These rare examples of bis(hydrazonato)copper(II) complexes are neutral complex species with copper(II) center coordinated with two monoanionic bidentate O,N-donor hydrazone ligands coordinated in enol-imine form. The interaction of hydrazone ligands and corresponding copper(II) complexes with CT DNA and BSA was investigated. Copper(II) complexes are slightly effective in binding the DNA than pristine hydrazones. The results indicate groove binding or moderate intercalation which are not significantly affected by the nature of substituent at hydrazone ligands. On contrary, affinities of two copper(II) complexes toward BSA significantly differs and depends on the nature of the substituent, however in absence of thermodynamic data difference in nature of binding forces cannot be excluded. The complex bearing electron-withdrawing 4-chloro substituent has larger affinity toward BSA compared to 4-dimethylamino analogue. These findings were theoretically supported by molecular docking study.

Keywords: Copper, nicotinic acid, hydrazone, bidentate, CT DNA, BSA

1. Introduction

Since the discovery of the cytostatic properties of cis-platin more than half a century ago, research into metal-based chemotherapeutics has increased exponentially. Essentially, today there is no metal whose complexes had not been tested as potential antitumor drugs. Although these researches were not always postulated on clear scientific motivations, these colossal expanses of progress in medicinal inorganic chemistry provided a couple of promising candidates with antitumor properties.¹ In addition to compounds of the platinum group metals, complex compounds of copper attracted a lot of attention. Copper, as a

vital trace element, is cofactor of many metalloenzymes and has important functional and metabolic roles in growth, function and development of living organisms.^{2,3} Compared to platinum group metals, it has a very well-studied physiological role and there are well defined pathways of its intake, transportation and elimination.^{4,5} Moreover, copper compounds possess promising anticancer properties while the low cost and ease of their synthesis make it of huge interest.^{6,7} Furthermore, hydrophobic nature of neutral copper(II) complexes with aromatic ligands improves its peculiar chemotherapeutic role in depositing in tumor tissues due to a selective cell membrane permeability.⁸

Hydrazones are type of Schiff base ligands which are discerned from oximes and imines by having two adjacent nitrogen atoms. Their biological activity is well documented and includes potential antibacterial,⁹ antiviral,¹⁰ antioxidant,¹¹ antifungal¹² and anticancer activity.^{13,14} From the aspect of the coordination chemistry, aroylhydrazones are good candidates for chelation of many metal ions since their versatile coordinating ability allows coordination as bidentate or tridentate neutral, monoanionic or dianionic ligands thus providing complexes with attractive structural, magnetic, electrochemical, catalytic or biological properties.¹⁵ Additionally, coordination of organic ligands to metal ions regularly results with improved biological properties of corresponding complexes making hydrazones as tempting choice for metal ligation. Coordination of hydrazones to copper(II) results in complexes of different nuclearities ranging from mononuclear, binuclear, tetranuclear, cuban-like or polymeric, depending on the number and sterical availability of functional groups on hydrazone core.^{16–19} Hydrazones having phenolic group readily form binuclear complexes with phenolic oxygen acting as bridging ligand. Complexes of higher nuclearities most often have lower solubility compared to their mononuclear analogues and thus weaker potential for application in biological purposes. As a contribution to copper(II) hydrazone complexes chemistry we prepared two novel bis(hydrazonato)copper(II) complexes of 4-substituted benzaldehyde nicotinic acid hydrazones. The hydrazones featuring heterocyclic moieties are known for their strong biological activity,²⁰ while substitution on a hydrazone moiety can affect biological activity of compounds.^{21,22} From biological point of view benzaldehyde derivatives including imines, hydrazones, (thio)semicarbazones and chalcones, along with their metal complexes, are well documented in literature as promising synthetic agents having wide range of biological activities including anticancer, antimicrobial, antifungal etc.^{23–26} From synthetic point of view, benzaldehyde is convenient synthetic precursor for substitution to obtain substituted derivatives which can serve as models to elucidate structure-activity relationship in terms of substituent directed biological activity. These results would provide information how substitution patterns and substituents could be potentially used for manipulation and improvement of the biological activity of more structurally complex ligands.

We aimed to test how electron-accepting or electron-donating properties of substituent on benzaldehyde component of hydrazone ligand can affect the binding of ligands and corresponding copper(II) complexes to nucleic acid or albumins. Clear understanding of factors that govern the reactivity of copper(II) complexes toward biomolecules can lead to rational design of novel compounds with desirable properties, high selectivity and efficiency in disease treatments.

2. Experimental

2.1. Chemicals

All chemicals used for syntheses, spectroscopic characterization and interaction with CT DNA and BSA were of analytical grade unless otherwise stated. Tetra- μ_2 -acetatodiaquadicopper(II) (>98%) was obtained from Fluka. Nicotinic hydrazide (97%) and 4-substituted benzaldehyde (>98%) were purchased from Sigma. Highly polymerized deoxyribonucleic acid sodium salt from calf thymus (CT DNA), Type I, fibers ($A_{260}/A_{280}>1.8$) and lyophilized powder of Bovine serum albumin (BSA, $\geq 98\%$) were acquired from Sigma. Organic solvents were used as received from commercial sources, while dimethylsulfoxide was dried over molecular sieves (3 Å).

2.2. Physical Measurements

Fourier transformed infrared spectra were collected in transmission mode using KBr pellet technique on a Perkin Elmer BX FTIR. Electronic spectra of complexes and ligands were recorded in DMSO (5×10^{-5} M) using Perkin Elmer BioLambda 35 in 260–1100 nm range. Fluorimetric measurements were done on PerkinElmer LS55 Luminescence. Elemental analyses of C, H and N content were performed on a Perkin Elmer 2400 Series II CHNS analyzer. Copper content in complexes was determined by spectrophotometry using neocuproin method.²⁷ Mass spectra were collected from DMSO solution of complexes using Shimadzu LCMS-2020. Conductometry measurements were done in DMSO solution using Phywe conductometer.

2.3. Syntheses of Hydrazone Ligands

Hydrazone ligands were prepared following previously reported procedure.^{28,29} Nicotinic hydrazide (10 mmol, 1.37 g) dissolved in absolute ethanol (15 mL) was added to a stirring solution of equimolar amount of appropriate 4-substituted benzaldehyde (10 mmol, 1.41 g for 4-chlorobenzaldehyde nicotinic acid hydrazone, hereinafter HL¹, 1.49 g for 4-(dimethylamino)benzaldehyde nicotinic acid hydrazone, hereinafter HL²) in ethanol (10 mL). One drop of concentrated sulfuric acid was added and the reaction mixture was kept under reflux for 3 hours. Upon cooling to room temperature corresponding hydrazone ligands separated out and were filtered off, washed with ice-cold ethanol and dried in vacuum. Yields: 1.87 g (72%) for HL¹ and 2.02 g (75%) for HL².

2.4. Syntheses of Copper(II) Complexes

To a vigorously stirred methanol solution (20 mL) of tetra- μ_2 -acetatodiaquadicopper(II) ($[\text{Cu}_2(\text{OAc})_4(\text{OH}_2)_2]$, 100 mg, 0.25 mmol) a methanol solution of appropriate hydrazone ligand was added (1 mmol, 260 mg for $[\text{Cu}(\text{L}^1)_2]$, hereinafter (**1**) and 268 mg for $[\text{Cu}(\text{L}^2)_2]$, here-

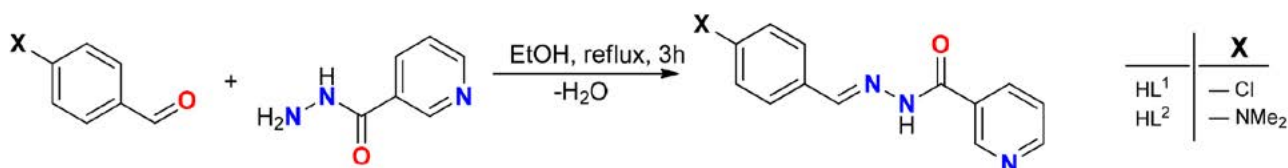
inafter (2)). The reaction mixture was refluxed for 2 hours and left standing overnight. Green-brown powders of copper(II) complexes were collected by suction filtration, washed thoroughly with cold methanol and dried in vacuum overnight.

bis(*N*⁷-4-chlorobenzylidenenicotinohydronato-κ²*N*,*O*)copper(II) dihydrate (1). Green powder. Yield: 222 mg (72%). *Anal. Calc.* (%) for C₂₆H₂₂Cl₂CuN₆O₄ (*M*_r = 616.94): C, 50.62; H, 3.59; N, 13.62; Cu, 10.30; *Found* (%): C, 50.70; H, 3.44; N, 13.64; Cu, 10.11. MS for [C₂₆H₁₉Cl₂CuN₆O₂]⁺ *Found* (*Calc.*): 582.05 (582.03). IR (KBr) ν(cm⁻¹): 3437 ν(O–H), 1608 ν(C=N⁷N), 1526 ν(C=NN⁷), 1340 ν(C–O_{enol}), 1158 ν(N–N). UV/Vis (DMSO) λ_{max} / nm (log ε): 316 (4.58).

bis[*N*⁷-4-(dimethylamino)benzylidenenicotinohydronato-κ²*N*,*O*]copper(II) dihydrate (2). Green-brown powder. Yield: 203 mg (64%). *Anal. Calc.* (%) for C₃₀H₃₄CuN₈O₄ (*M*_r = 634.19): C, 56.82; H, 5.40; N, 17.62; Cu, 10.02; *Found* (%): C, 57.40; H, 4.90; N, 17.40; Cu, 9.94. MS for [C₃₀H₃₁CuN₈O₂]⁺ *Found* (*Calc.*): 598.20 (598.20). IR (KBr) ν (cm⁻¹), intensity: 3435 ν(O–H), 1598 ν(C=N⁷N), 1509 ν(C=NN⁷), 1317 ν(C–O_{enol}), 1163 ν(N–N). UV/Vis (DMSO) λ_{max} / nm (log ε): 403 (4.67).

2. 5. Interaction with CT DNA

Interaction of hydrazone ligands and corresponding copper(II) complexes was carried out in 10 mM Tris-HCl buffer pH 7.42 using method of spectroscopic titration. Stock solution of CT DNA was prepared in 10 mM Tris-HCl buffer pH 7.42 by continuous stirring of CT DNA during 24 hours to assure proper hydration and to obtain millimolar concentration of stock solution. The concentration and purity of CT DNA was determined based on extinction coefficient of 6,600 M⁻¹ cm⁻¹ at 260 nm (7.20 mM, A₂₆₀/A₂₈₀ = 1.83, A₂₃₀/A₂₆₀ = 0.39). Stock solutions of complexes and ligands (1 mM) were prepared in dry DMSO. Working solutions of compounds (5 × 10⁻⁵ M) were always freshly prepared by diluting aliquot (100 μL) of DMSO stock solution of compounds by Tris-HCl buffer up to a volume of 2000 μL. Thus, obtained solutions were used for spectroscopic titration of compound with DNA by successive addition of 10-microliter amounts of CT DNA stock solution and recording the electronic spectra in 250–500 nm range. The equilibration time after each addition of DNA was 2 minutes.



Scheme 1. Synthesis of hydrazone ligands.

2. 6. Interaction with BSA

The interaction of compounds with BSA was investigated in 10 mM Tris-HCl buffer solution by spectrofluorimetric titration of BSA with ligands and complexes. The working solution of BSA was prepared by dissolving BSA in 10 mM Tris-HCl buffer until 1 μM solution was obtained. The concentration of BSA was determined by electron spectroscopy based on extinction coefficient of 43,824 M⁻¹ cm⁻¹ at 280 nm. Stock solution of ligands and complexes were prepared in methanol (1 × 10⁻⁴ M). Spectrofluorimetric titration was carried out by titrating solution of BSA (2000 μL, 1 μM) with 10-μL amounts of ligand or complex and recording emission spectra in 290–420 nm range with 278 nm as excitation wavelength. Synchronous emission spectra were collected similarly as mentioned above only in 250–310 nm range with Δλ = 15 nm and Δλ = 60 nm.

2. 7. Molecular Docking Study

The docking study was set up in YASARA Structure 19.12.14^{30,31} and performed using AutoDock 4.2.³² The crystal structure of BSA (PDB ID: 3V03)³³ from Protein Data Bank was used as the target molecule. The protein structure was prepared by removing water molecules, adding polar hydrogen atoms and optimizing in the AMBER03 force field.³⁴ The 3D structures of the copper(II) complexes and ligand molecules were prepared and geometries optimized by the density functional theory (DFT) (B3LYP/LanL2DZ and B3LYP/6-31G* basis sets) using Gaussian 09.³⁵ A blind docking approach was used, searching the whole protein for potential binding sites, with a grid point spacing of 0.375 Å for all compounds. During the docking process, copper(II) complex molecules were kept rigid, to maintain their square planar molecular geometries. The Lamarckian genetic algorithm was employed with the following parameters: 150 docking runs with a maximum of 17,500,000 energy evaluations and 27,000 generations for each run, providing this way the lowest energy docked structures.

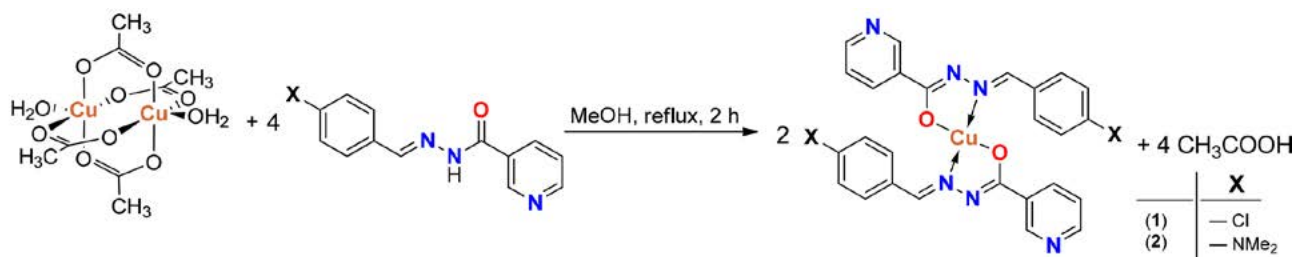
3. Results and Discussion

3. 1. Syntheses

Preparation of hydrazone ligands HL¹ and HL² was carried out using standard condensation procedure of appropriate 4-substituted benzaldehyde with nicotinic acid

hydrazide in ethanol (**Scheme 1**). The products were identified by infrared and electronic spectroscopy.^{28,29}

Copper(II) hydrazone complexes were prepared by refluxing tetra- μ_2 -acetatodiaquadicopper(II) and appropriate hydrazone ligand in methanol in molar ratio 1:4 (**Scheme 2**). Besides the fact that acetic anion is a good leaving group, in preparative chemistry of copper complexes it also behaves as a base deprotonating hydrazone ligand. The copper compounds isolated are neutral complex species having copper(II) coordinated by two mono-anionic bidentate O,N-donor hydrazone ligands in enol-imine form based on elemental and spectroscopic analysis. Complexes are moderately soluble in DMSO and DMF, weakly soluble in lower alcohols, acetonitrile, dichloromethane and insoluble in water and non-polar organic solvents. All of our attempts to prepare single crystals of suitable quality for diffraction were unfortunately unsuccessful, except in case for complex **1** from pyridine. Recrystallization of **1** from pyridine afforded green prismatic single crystals of suitable size for SCXRD. However, our attempts to resolve the structure were unsuccessful due to a dynamic process in a crystal lattice during the measurements even at temperatures of liquid nitrogen.



Scheme 2. Synthesis of copper(II) hydrazone complexes.

3. 2. Characterization

Characterization of bis(hydrazone)copper(II) complexes **1** and **2** was carried out by elemental analysis, infrared and electronic spectroscopy, mass spectrometry and conductometry. The results of elemental analysis of carbon, hydrogen, nitrogen and copper content in copper(II) complexes **1** and **2** confirm formulation, composition and purity of the prepared complexes. Theoretical and experimental mass spectra of copper(II) complexes are shown in ESI (Figures S2–S5). Isotopic distribution pattern arising from two stable copper isotopes (⁶³Cu and ⁶⁵Cu) is clearly seen for [M+H]⁺ ion of both bis(hydrazone)copper(II) complexes thus confirming the [Cu₂] composition.

Infrared spectra of hydrazone ligands and copper(II) complexes **1** and **2** are shown in Figure 1. Hydrazones generally show tautomerism and can be present in keto-amine or enol-imine form. Infrared spectra of hydrazone ligands HL¹ and HL² in solid state showed absence of band corresponding to stretching vibrations of O–H bond and showed vibrations assigned to N–H and C=O vibrations

indicating that both ligands are present in keto-amine form (Table 1). Upon coordination to copper(II) hydrazones are deprotonated and bands corresponding to stretching of N–H (~3190 cm⁻¹) and deformation of N–H (1298–1305 cm⁻¹) disappear in spectra of copper(II) complexes. Moreover, the band located in spectra of hydrazone in 1663–1685 cm⁻¹ range, predominantly attributed to C=O stretching, is absent in spectra of copper(II) complexes, while new band in 1317–1340 cm⁻¹ range, assigned to C–O_{enol} stretching, arises. If we add the fact that a new band appears in the spectra of the complex in 1598–1608 cm⁻¹ region, which is attributed to C=N_{hyd}N bond stretching, then the coordination of the hydrazone through the deprotonated enol oxygen is beyond a doubt. The band in 1524–1544 cm⁻¹ range in spectra of hydrazone ligands arises from C=NN_{hyd} stretching and upon coordination to Cu(II) it is shifted to lower wavenumbers for 15–18 cm⁻¹ appearing in spectra of complexes in 1509–1526 cm⁻¹ region, thus indicating coordination of hydrazone through imine nitrogen. Infrared spectra clearly demonstrate deprotonated enol-imine coordination of Cu(II) with HL¹ and HL² hydrazone ligand. Beside enol oxygen and imine nitrogen both ligands, HL¹ and HL², possess additional

coordination sites – pyridine nitrogen and in case of HL² dimethylamino nitrogen. Considering the fact that copper(II) is coordinated by two bidentate ligands occupying four equatorial positions, two axial positions remain available for cross coordination of copper(II) centers *via* pyridine and dimethylamino nitrogen atoms thus creating polymeric structures, which are immanent to copper(II) complexes of ligands with additional side chain donors.^{36–38} However, solid state infrared spectra of copper(II) complexes **1** and **2** do not indicate this is likely to occur here, since band shifting corresponding to bonds which would be affected by bridging is not observed in spectra of complexes compared to free ligands. The C–N bonds of Me₂N–Ar and ArN–Me are intact upon coordination indicating no interaction of Cu(II) with nitrogen atom of –NMe₂ (Table 1). Vibrations of pyridine ring, as the most sensitive for coordination to metal center, are not affected by ligating Cu(II) with hydrazone ligands HL¹ and HL² demonstrating no coordination of Cu(II) through pyridine nitrogen of hydrazone ligand occurred (Table 1). Although there is no infrared evidence of polymeric na-

ture of copper(II) complexes **1** and **2** in solid state this reasonable possibility cannot be excluded *a priori* in the absence of crystal structure.

Trans configuration of donor atoms in copper coordination sphere of **1** and **2** is indicated by the appearance of only one new band corresponding to Cu–N vibration in low energy region of infrared spectra of complexes. *Cis* isomer, *cis*-[CuN₂O₂] with C_{2v} symmetry, is expected to

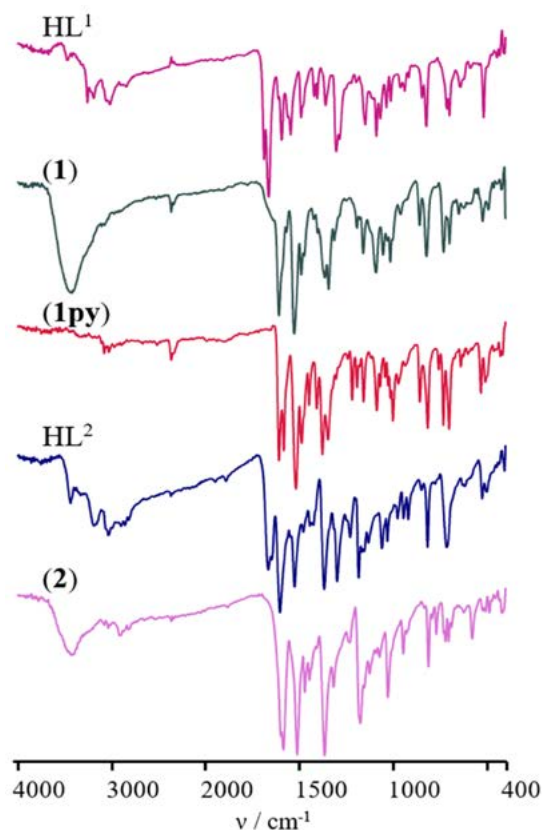


Figure 1. Infrared spectra of hydrazone ligands and corresponding copper(II) complexes.

exhibit two bands for each bond (Cu–N and Cu–O), while *trans* isomer, *trans*-[CuN₂O₂] with C_{2h} symmetry, has only one infrared active vibration for each bond.³⁹ In our case, new bands in infrared spectrum of complexes **1** and **2**, with purely Gaussian shape and without any obvious splitting, were found at 462 and 485 cm⁻¹, respectively indicating *trans* configuration of [CuN₂O₂] entity in **1** and **2**.

Electronic spectra of ligands and bis(hydrazone) copper(II) complexes were recorded in DMSO (Figure S6). As expected for heavily electron populated *d*⁹ system, the electronic spectrum of copper(II) complexes is dominated by ligand-centered transition. The band assigned to *n*→*π** transition, initially positioned in spectra of ligands in 309–359 nm range is red shifted in spectra of complexes thus confirming hydrazone deprotonation and coordination to copper(II) center. Low intensity band arising from Laporte forbidden *d*–*d* transition, related to *d*⁹ copper(II) center in complexes, is seen in low energy red part of the electronic spectrum and is found in 680–750 nm range. The molar conductivity of **1** and **2** in DMSO were measured as 9 and 11 S cm² mol⁻¹, respectively and are in accordance with non-electrolyte nature of bis(hydrazone) copper(II) complexes. Complexes **1** and **2** are stable toward hydrolysis in aqueous solution and thus all their biological reactivity can be attributed to authentically formulated species.

3. 3. Interaction with CT DNA

Evaluation of the biological activity of new complexes that have potential anticancer activity almost always relies on their interaction with biomolecules that are potential targets *in vivo*. Following the concept of anticancer activity of platinum-based chemotherapeutics, such as cisplatin, which exhibits cytotoxicity by preventing DNA replication by forming covalent bonds with neighboring intrastrand guanines, DNA molecule remains target of focus in gaining the insights of complexes biological activi-

Table 1. Assignment of the most important vibrational bands in FTIR spectra of hydrazone ligands and corresponding copper(II) complexes.

Compound	ν(O–H)	ν(N–H)	ν(C–H) _{sat.}	ν(C=O)	ν(CO) + ν(CN)+δ(NH)	ν(C=N _{hyd} N)	ν(C=N _{hyd} N)	δ(py) ring deformation	ν(Ar–NMe ₂)	ν(C–O _{enol})	δ(N–H)	ν(N–N)	ν(ArN–Me)	ν(C–Cl)	δ(C–H)py out of plane	ν(Cu–N)
HL ¹	–	3189	<i>n.a.</i>	1685	1661	–	1544	1421	<i>n.a.</i>	–	1305	1146	<i>n.a.</i>	846	821	<i>n.a.</i>
1	3437	–	<i>n.a.</i>	–	–	1608	1526	1421	<i>n.a.</i>	1340	–	1158	<i>n.a.</i>	857	821	462
HL ²	–	3190	2898	1663	1645	–	1524	1422	1366	–	1298	1163	1029	<i>n.a.</i>	815	<i>n.a.</i>
2	3435	–	2914	–	–	1598	1509	1425	1366	1317	–	1172	1027	<i>n.a.</i>	811	485

n.a. – not applicable

ties. The condition for the formation of covalent interactions with DNA is the existence of a coordination position on the metal that can be activated in physiological conditions to ensure the replacement of the easily removable ligand with the donor atoms of the ligating group of biomolecules. Moreover, unoccupied coordination position on metal center is also opportune. In this context, non-sterically closed copper complexes of square-planar or square-pyramidal geometries are of interest. However, covalent binding of DNA remains the most prominent feature of platinum-based complexes while many other metal complexes bind to DNA by non-covalent interactions such as groove binding, intercalation and hydrophobic or electrostatic interactions. Planar aromatic systems that can achieve a π -interaction by inserting between pairs of adjacent bases are said to intercalate DNA. This type of interaction is typical for planar organic molecules and complex compounds that have condensed aromatic systems such as bipyridine, phenanthroline, terpyridine, etc. as ligands, but it is not limited to them, since the coordination of the ligand to the metal limits the conformational freedom of the ligand, which can result in aromatic systems that are bridged with a non-planar bridge to become planar after coordination, which is often the case with the coordination of bidentate ligands to copper(II) in a square-planar geometry. Furthermore, if hydrophobic interactions of ligands with DNA is possible, groove binding cannot be excluded. Bis(hydrazone)copper(II) complexes **1** and **2** meet all the above mentioned conditions to bind the DNA. The interaction of pristine hydrazone ligands and the corresponding copper(II) complexes with DNA was investigated by the method of spectroscopic titration with DNA. Typical spectroscopic titration is shown in **Figure 2**. Additional data on titration experiments can be found in ESI (Tables S3–S6 and Figures S7–S9). The binding constants were determined graphically using equation (1):

$$\frac{[\text{DNA}]}{(\varepsilon_a - \varepsilon_f)} = \frac{[\text{DNA}]}{(\varepsilon_b - \varepsilon_f)} + \frac{1}{K_b(\varepsilon_b - \varepsilon_f)} \quad (1)$$

by plotting $[\text{DNA}]$ vs $[\text{DNA}]/(\varepsilon_f - \varepsilon_a)$, where $[\text{DNA}]$ is concentration of DNA, and ε_f and ε_a are extinction coefficients of complex in free and bound form at apparent concentration of DNA, respectively. The binding constant (K_b) is obtained as a slope to intercept ratio. The obtained values of binding constants are summarized in Table 2.

The spectroscopic titration showed moderate hypochromism without the obvious shifting of the peak maximum. The obtained values of the binding constants are of 10^3 M^{-1} magnitude for pristine ligands and 10^4 M^{-1} for corresponding bis(hydrazone)copper(II) complexes. The values of K_b for complexes are approximately twice as those for uncoordinated hydrazone ligands indicating that complexes show greater affinity toward DNA (Table 2). The values of binding constants of 10^4 M^{-1} and the fact that redshift was not observed suggests that the groove binding could be a mode of interaction of these complexes with

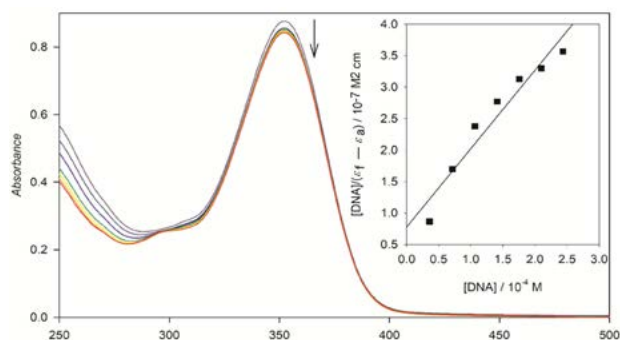


Figure 2. Spectroscopic titration of **1** ($5.00 \times 10^{-5} \text{ M}$) with CT DNA in 10 mM Tris-HCl buffer. *Inset:* Graphical determination of binding constant.

DNA, however due the presence of hydrazone ligands capable of π -binding, intercalation cannot be *a priori* excluded. Literature reveals that many copper(II) hydrazone complexes moderately intercalate or bind DNA through grooves with binding constants of 10^4 M^{-1} . Indeed, copper(II) complexes of bidentate hydrazones are not numerous as those of tridentate hydrazones, and even for those reported the interaction with DNA was not investigated,^{22,40,41} so the rational comparison is hard to make. The rare examples of copper(II) complexes with bidentate hydrazones, whose interaction with DNA was investigated, are those of dimedone-derived hydrazones⁴² with $K_b = (3.67\text{--}6.84) \times 10^5 \text{ M}^{-1}$, which are considered as DNA intercalators and mononuclear copper(II) complexes of 4-aminobenzoylhydrazones bearing quaternary alkyl ammonium salts⁴³ with $K_b = (3\text{--}4) \times 10^4 \text{ M}^{-1}$, which are considered as moderate intercalators and groove binders. On the other hand, interaction of copper(II) complexes of tridentate hydrazones with DNA is extensively documented and data reveal that bis(hydrazone)copper(II) complexes **1** and **2** have binding constant comparable to those of square-planar copper(II) complexes with hydrazones derived from salicylaldehyde and ibuprofen- and naproxen-hydrazides ($K_b = (1.02\text{--}3.50) \times 10^4 \text{ M}^{-1}$)⁴⁴ and 1,1,1-trifluoropentanedione and 4-chlorobenzhydrazide ($K_b = 4.02 \times 10^4 \text{ M}^{-1}$).⁴⁵ Also, complexes **1** and **2** have K_b comparable to mixed square-planar square-pyramidal and octahedral copper(II) complexes of tridentate hydrazone of 2-acetylpyridine and benzhydrazide ($K_b = (1.88\text{--}4.66) \times 10^4 \text{ M}^{-1}$).²⁰ The cited paper also reports that uncoordinated hydrazone ligand shows binding constant ($K_b = 9.50 \times 10^3 \text{ M}^{-1}$), which is comparable to HL¹ and HL², and that corresponding copper(II) complexes have 2–5 fold higher binding constants, which agrees well with our findings. The similar 2-fold increase in binding constant of the complex compared to native hydrazone ligand was reported for copper(II) complexes of 2-acetylpyridine thiophene-2-carboxylic acid hydrazone and 2-acetylpyridine benzoyl hydrazone.⁴⁶ All the above mentioned complexes are considered as moderate DNA intercalators and/or

groove binders. Copper(II) complexes that exclusively intercalate DNA have higher K_b values such acetylhydrazone copper(II) complexes of 2-acetylpyridine and 2-benzoylpyridine ($K_b = (1.42\text{--}8.08) \times 10^5 \text{ M}^{-1}$).⁴⁷

Table 2. Binding constant values of copper(II) complexes and hydrazone ligands with CT DNA.

Compound	K_b / M^{-1}
1	1.19×10^4
2	1.61×10^4
HL ¹	6.36×10^3
HL ²	9.14×10^3

3. 4. Interaction with BSA

Albumins, as the most important proteins in the blood, liable for normal osmotic pressure, transportation of fatty acids and hormones and neutralization of free radicals, are the first biological target of many drugs. Considering that proteins have nucleophile rich side-chains of amino acids, such as imidazole of histidine, thiol of cysteine, sulfide of methionine, carboxylate of aspartic and glutamic acid and amide group of asparagine and glutamine, it is not surprising that metal complexes readily bind to proteins. Indeed, some of the drugs become deactivated after binding to proteins, while for others binding to proteins is an essential aspect of their biological activity and target specific delivery. For laboratory studies bovine serum albumin (BSA) is most convenient as it has high

structural and functional similarity to human serum albumin (HSA). When excited at 278 nm, BSA shows strong emission near 340 nm, owing to fluorescence of endogenous aromatic amino acids tryptophan, tyrosine and phenylalanine. The interaction of copper(II) complexes and hydrazone ligands with BSA was investigated by spectrofluorimetric titration. The linear decrease of fluorescence with increasing concentration of complex 1 and ligands HL¹ and HL² obeys to Stern-Volmer relation (Eq. 2) and K_{SV} values were graphically obtained as a slope of the linear regression of an emission intensities ratio in the absence (I_0) and presence (I) of the compound versus concentration of the compound (Table 3).

$$\frac{I_0}{I} = 1 + K_{SV}[\text{compound}] \quad (2)$$

Typical decrease of fluorescence intensity is shown in **Figure 3a** while additional data can be found in ESI (Tables S7–S9, Figures S10–S12). For bis(hydrazone)copper(II) complex 2, bearing dimethylamino substituent, continual decrease of fluorescence was not observed. Initial decrease of BSA fluorescence is followed with an increase of fluorescence as the concentration of the complex increases (Figure S10). The increase in fluorescence can occur when complex has its own intrinsic fluorescence, which is not case for 2, or when the tryptophan intrinsic fluorescence enhances due to conformational change that leads to better stacking in hydrophobic pockets of BSA as observed for nickel(II) hydrazone complex.⁴⁸ For complex 1 and the corresponding hydrazone ligand decrease of the fluorescence results with significant blueshifting of the peak maximum for 13 and 5 nm, respectively indicating

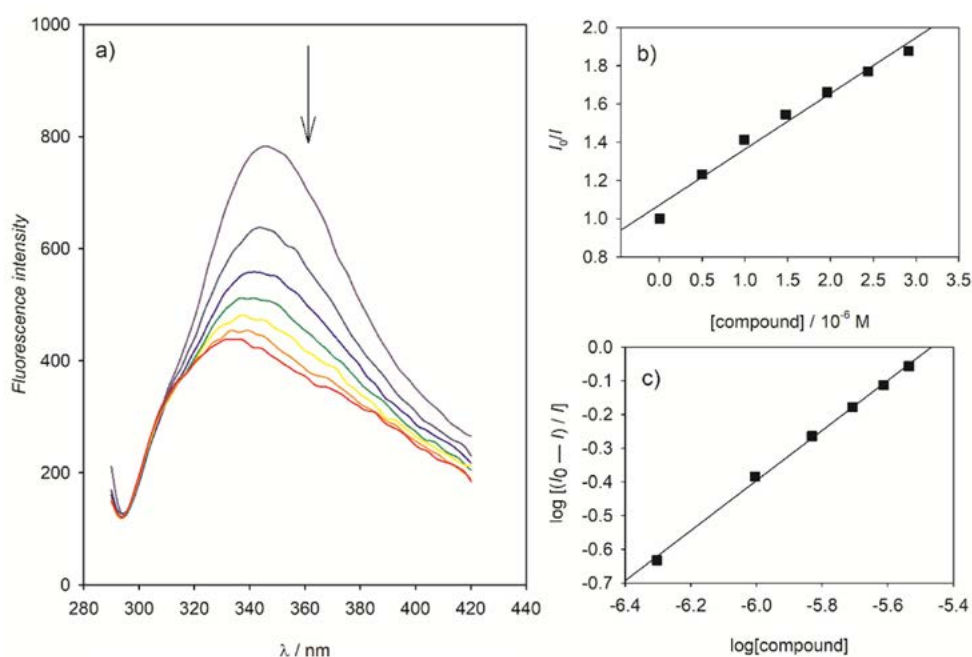


Figure 3. Interaction of 1 with BSA (1 μM) in 10 mM Tris-HCl buffer: a) Decrease of BSA fluorescence with increasing concentration of 1, b) graphical determination of Stern-Volmer constant, c) graphical determination of binding constant and number of binding sites.

significant change in hydrophobicity of tryptophan residues.⁴⁹ For ligand HL² the minor blueshifting ($\Delta\lambda = 2$ nm) of the peak was observed suggesting no significant change in the local dielectric environment of BSA occurs.⁴⁹

Further quantification of the interaction was carried out by determining the values of the binding constant (K_b) and the number of the binding sites (n) by plotting $\log[(I_0 - I)/I]$ vs [compound] (Eq. 3).

$$\log \frac{I_0 - I}{I} = \log K_b + n \log [\text{compound}] \quad (3)$$

Hydrazone ligands HL¹ and HL² showed low affinity to BSA ($K_b \leq 10^3 \text{ M}^{-1}$) with binding constants that differ significantly from each other. The ligand having dimethylamino substituent (HL²) showed ~75-fold lower binding constant to BSA compared to the one having chloro substituent (HL¹). This indicates that the nature of the substituent on hydrazone ligand has reasonable impact on the BSA binding properties of the compounds and can be exploited in designing the compounds of desirable affinity to BSA. Electron-accepting nature of chlorine substituent, compared to electron-donating nature of dimethylamino substituent, decreases π -electron density of hydrazone ligands making it more susceptible for interaction with negatively charged BSA. The coordination of HL¹ to Cu(II) center results with complex **1** having 2-fold larger binding constant ($K_b = 1.15 \times 10^4$) compared to corresponding ligand. The value of the binding constant suggests moderate affinity to BSA which is very favorable in designing new bioactive compounds, since the interaction is strong enough that the compound can be transported by albumin, but weak enough that release of the compound at the

target site can occur.⁵⁰ Bis(hydrazone)copper(II) complex **1** has larger binding constant compared to copper(II) 2-benzoylpyridine benzhydrazone complex ($K_b = 6.68 \times 10^3 \text{ M}^{-1}$)⁴⁸ but is comparable to mononuclear [Cu(hydrazone)Cl₂] complexes of nitrogen-rich hydrazone ligands derived from pyrazine-2-carbaldehyde and isonicotino-based hydrazides ($K_b \sim 5 \times 10^4 \text{ M}^{-1}$).⁵¹ It is also comparable to copper(II) complexes of dehydroacetic acid benzoyl hydrazone featuring DMSO as coligand ($K_b = 7.59 \times 10^4 \text{ M}^{-1}$), while it has significantly lower K_b compared to analogous complexes having water or imidazole as coligands ($K_b = 2.68 \times 10^6 \text{ M}^{-1}$ and $1.50 \times 10^7 \text{ M}^{-1}$, respectively).⁵² Complex **1** has 10-fold lower binding constant compared to monomeric square-pyramidal copper(II) complexes of tridentate NNO neutral acetylhydrazones of 2-acetylpyridine and 2-benzoylpyridine.⁴⁷

The values of quenching rate constant (k_q), obtained as K_{SV}/τ_0 ($\tau_0 = 10^{-8}$ s), are larger than $2 \times 10^{12} \text{ M}^{-1} \text{ s}^{-1}$, thus indicating that hydrazone ligands and copper(II) complex quench BSA fluorescence through static mechanism.⁵³

More detailed insight into the changes of the microenvironment of tryptophan and tyrosine residues of BSA can be gathered using synchronous spectrofluorimetry. The difference between excitation and emission wavelengths ($\Delta\lambda = \lambda_{\text{ex}} - \lambda_{\text{em}}$) results in spectra of different fluorophores. If the difference is large ($\Delta\lambda = 60$ nm) tryptophan synchronous spectra are collected, but if the difference is small ($\Delta\lambda = 15$ nm) emission arises from tyrosine residues. The synchronous spectra are shown in **Figure 4** and Figs. S13–S15. The typical features of the spectra are decrease of tryptophan fluorescence, significantly lower decrease of tyrosine fluorescence and blueshifting of both peak maximums. Only for

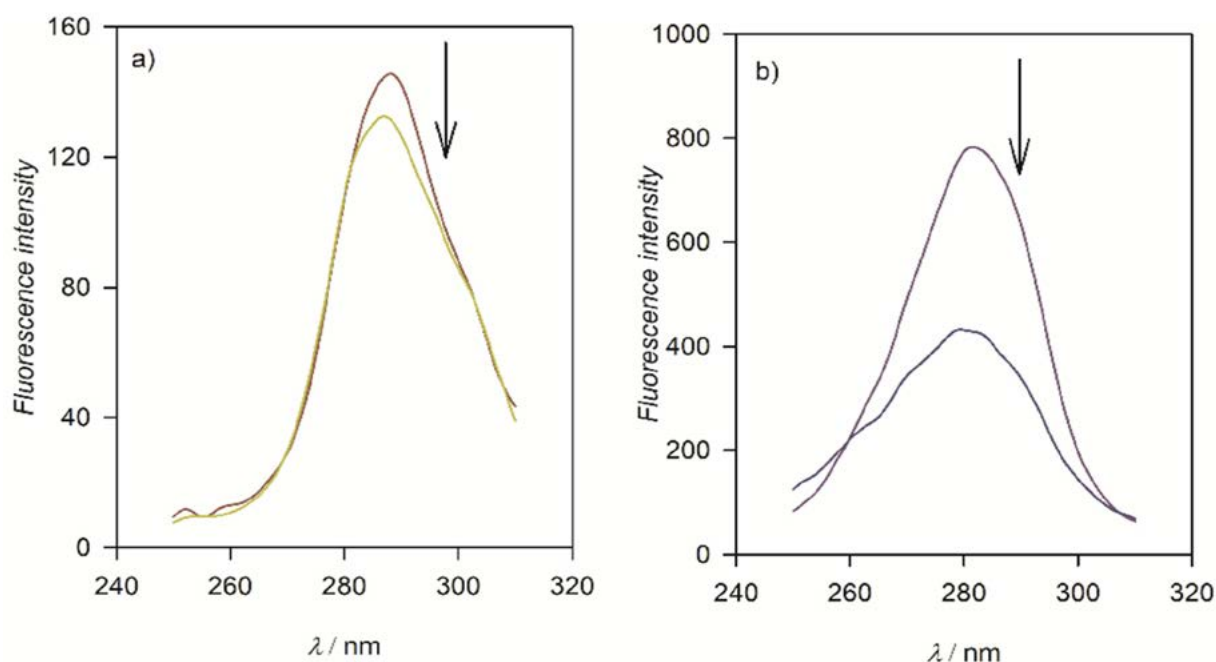


Figure 4. Changes in synchronous emission spectra of BSA (1 μM) in 10 mM Tris-HCl buffer pH 7.42 in absence and presence of **1** at [complex]/[BSA] = 3: a) $\Delta\lambda = 15$ nm; b) $\Delta\lambda = 60$ nm.

complex **2** synchronous spectra showed increase of tryptophan fluorescence and no obvious change in fluorescence of tyrosine followed with blue shift. This is consistent with previously commented data (*vide supra*).

Molecular docking was further used to analyze the interaction and binding modes between bis(hydrazone) copper(II) complexes and BSA, as well as between pristine hydrazone ligands and BSA. The docking results are shown in **Table 4** and Figure 5Figure 6. Calculations indicate that both copper(II) complexes occupied the same domain of BSA (Pro-110, His-145, Ala-193, Glu-424, Arg-458, etc.). This was also observed previously for the copper(II) complexes of similar structures.⁵⁴ However, the binding energies and dissociation constants of two copper(II) complexes were quite different in comparison to each other (**Table 4**). Complex **1** showed much lower/better binding energy and dissociation constant of 3.42 μM indicating better binding affinity toward BSA, while **2** with a higher binding energy value showed a 100-fold higher dissociation constant. No hydrogen bonds were observed in the interactions.

Molecular docking parameters obtained for the ligands alone were in relatively good accordance with the docking parameters of the complexes. Ligand HL¹ showed quite similar values to those of **1** including the same BSA domain, with observed hydrogen bonds between the ligand and amino acid residues. Ligand HL² showed higher binding energy and dissociation constant, same as **2**, although the dissociation constant was about 7.5 times higher compared to ligand HL¹. The biggest difference was actually in the occupied domain of BSA, where ligand HL² alone occupied the outer domain of BSA, and had no overlapping contacting amino acids in comparison to interactions of other compounds (**Table 4**), and showed hydrogen bonding to Phe508 (**Figure 5**). This finding indicates the influence of the ligand's nature on the lower overall binding affinity of the **2** to BSA. Docking parameters also indicate the influence and importance of electron-withdrawing chlorine substituent in **1** for binding to BSA, while electron-donating dimethyl amino substituent greatly decreased binding affinity in both, ligand HL² and complex

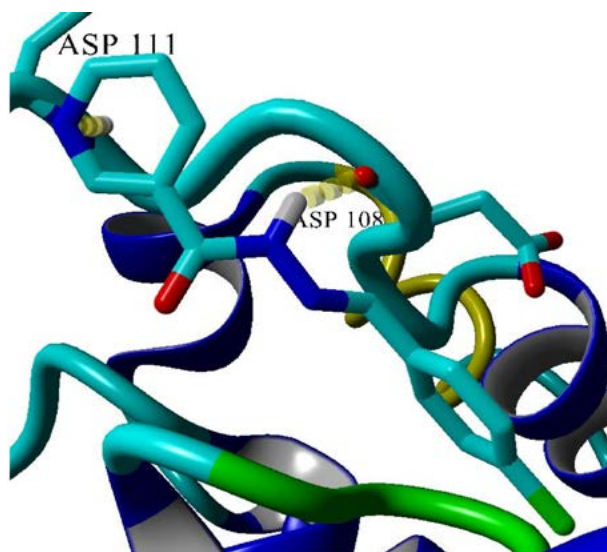


Figure 5. Binding pose of ligand HL¹ to BSA.

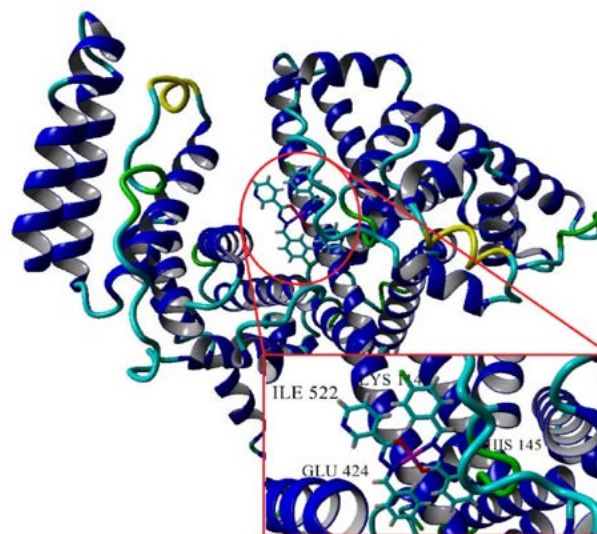


Figure 6. Binding of **1** to BSA. *Inset:* Close-up projection of binding pose.

Table 4. Molecular docking parameters of analyzed interaction between copper(II) complexes and BSA.

Compound (amino acids)	Binding energy (kcal mol ⁻¹)	Contacting receptor residues
1	-7.46	Asp 108, Pro 110, Leu 112, Pro 113, Lys 114, Arg 144, His 145, Pro 146, Tyr 147, Arg 185 , Leu 189 , Ser 192, Ala 193, Arg 196, Leu 197, Glu 424, Ser 428, Leu 454, Ile 455, Asn 457, Arg 458, Ile 522
2	-4.75	Asp 108, Pro 110, Leu 112, Pro 113, Lys 114, Arg 144, His 145, Pro 146, Tyr 147, Ser 192, Ala 193, Arg 194 , Arg 196, Leu 197, Glu 424, Arg 427 , Ser 428, Leu 454, Ile 455, Asn 457, Arg 458, Thr 518 , Glu 519 , Ile 522
HL ¹	-7.77	Asp 107 , Asp 108*, Ser 109 , Pro 110, Asp 111* , Leu 112, Arg 144, His 145, Pro 146, Tyr 147, Phe 148 , Ser 192, Ala 193, Gln 195 , Arg 196, Glu 424, Arg 458
HL ²	-6.56	Phe 506 , Thr 507 , Phe 508* , His 509 , Ala 510, Phe 550 , Phe 553 , Glu 564 , Phe 567 , Ala 568, Gly 571 , Pro 572 , Leu 574 , Val 575

Bolded amino acids are involved in only one compound-BSA interaction. Asterisk indicates a hydrogen bond to specified amino acid.

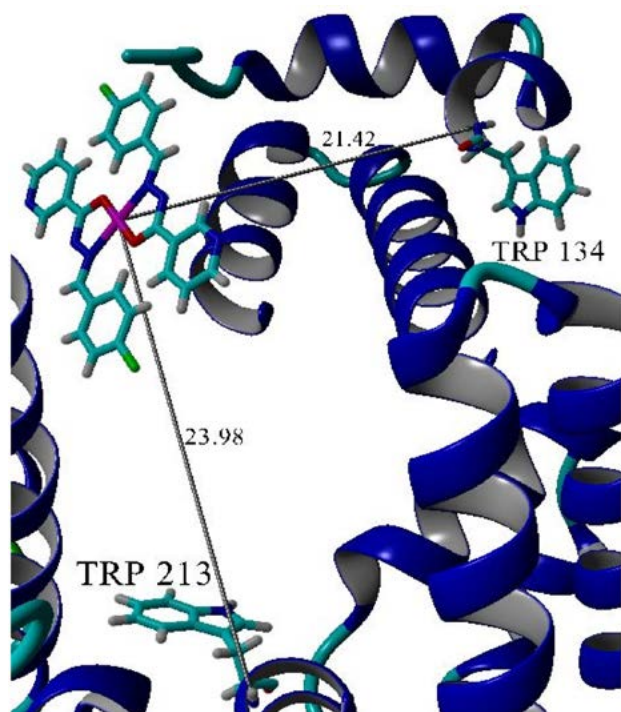


Figure 7. Distance from copper center in complex 1 from two tryptophan residues in complex-BSA adduct.

2. However, the observed change in the binding constant cannot be exclusively addressed to electron-withdrawing or electron-accepting properties of substituents based only on these two examples, especially not in the absence of thermodynamic data that indicate nature of the binding forces responsible for the interaction. A decrease in the binding affinity could also be considered as the effect of the steric hindrance and polar properties of the dimethyl amino group. The molecular docking results suggest that binding of complexes to BSA is weaker compared to pristine hydrazone ligands, however this is not experimentally confirmed. Moreover, coordination of small organic ligands to metal center generally results in larger binding constants to BSA as found in our case.^{8,46,53,55–58}

The distances between copper(II) complexes with tryptophan residues in BSA were also determined from the docking analysis as shown for complex **1** in **Figure 7**. Obtained results showed that distances between two tryptophan residues and complexes were as follows: 23.98 Å (Trp-213) and 21.42 Å (Trp-134) with an average of 22.70 Å for **1**, and 25.18 Å (Trp-213) and 22.48 Å (Trp-134) with an average of 23.83 Å for **2**.

4 Conclusion

Solution synthesis afforded two novel copper(II) hydrazone complexes of general composition $[\text{CuL}_2]$. Hydrazone ligands act as bidentate monoanionic chelators coordinating Cu(II) through oxygen and nitrogen of deprotonated

enol-imine form of hydrazones. The interaction with CT DNA revealed that complexes have nearly 2-fold higher affinity toward DNA. The binding constant of copper(II) complexes to DNA is not significantly affected by the nature of the substituent at hydrazone ligand and groove binding or moderate intercalation are indicative as interaction modes which is in agreement with previously reported data for hydrazone complexes of copper(II) binding to DNA. The interaction of complexes and ligands with BSA revealed that substituent effect on hydrazone ligand has much more impact to binding with BSA compared to DNA. The complex bearing hydrazone ligand with electron-withdrawing chlorine substituent shows stronger quenching of tryptophan fluorescence and causes significant perturbation in microenvironment of tryptophan and increases the hydrophobicity. In all cases static mechanism of fluorescence quenching was observed suggesting that tested compounds interact with BSA in ground state. The substituent effect of hydrazone ligand on BSA binding affinity was confirmed for pristine ligands, experimentally and theoretically through molecular docking study. We found that benzaldehyde nicotinic acid hydrazone ligand having a chloro substituent has ~75-fold larger binding constant to BSA compared to its 4-dimethylamino analogue, which is supported by theoretical calculations that dissociation constant for these two ligands significantly differs with chloro analogue being more tightly bound to BSA. Results of molecular docking suggest that ligands interact with BSA mostly through hydrogen bonding while interaction of copper(II) complexes is more hydrophobic in nature. These results indicate that the nature of the substituent on benzaldehyde component of hydrazone ligand has reasonable impact on the BSA binding properties of the compounds and can be exploited in designing the compounds of desirable affinity toward BSA. However, in the absence of thermodynamic data on the nature of the binding forces between complex and BSA, electron-donating and electron-accepting properties of the substituent cannot be claimed as governing factor in these interactions.

Declaration of Competing Interest

The authors declare that they have no known competing financial interests or personal relationships that could have appeared to influence the work reported in this paper.

Funding

This work was supported by the Federal Ministry of Education and Science of Bosnia and Herzegovina (grant no. 05-35-1965-1/21).

Supplementary materials

Supplementary material associated with this article can be found in the online version.

5. References

- E. Boros, P. J. Dyson, G. Gasser, *Chem.* **2020**, *6*, 41–60.
DOI:10.1016/j.chempr.2019.10.013
- B. G. Malmström, J. Leckner, *Curr. Opin. Chem. Biol.* **1998**, *2*, 286–292. DOI:10.1016/S1367-5931(98)80071-9
- W. Kaim, J. Rall, *Angew. Chem. Int. Ed. Engl.* **1996**, *35*, 43–60.
DOI:10.1002/anie.199600431
- K. D. Karlin, Z. Tyeklár, *Bioinorganic chemistry of copper*, Springer Science & Business Media, **2012**.
- R. A. Festa, D. J. Thiele, *Curr. Biol.* **2011**, *21*, R877–R883.
DOI:10.1016/j.cub.2011.09.040
- F. Tisato, C. Marzano, M. Porchia, M. Pellei and C. Santini, *Med. Res. Rev.* **2010**, *30*, 708–749.
- C. Santini, M. Pellei, V. Gandin, M. Porchia, F. Tisato, C. Marzano, *Chem. Rev.* **2014**, *114*, 815–862.
DOI:10.1021/cr400135x
- M. Alagesan, N. S. Bhuvanesh, N. Dharmaraj, *Dalton Trans.* **2013**, *42*, 7210–7223. DOI:10.1039/c3dt50371b
- T. Govindasami, A. Pandey, N. Palanivelu, A. Pandey, *Org. Chem. Int.* **2011**, *1*, 71–77. DOI:10.4236/ijoc.2011.13012
- Z. Yang, P. Li, X. Gan, *Molecules* **2018**, *23*, 1798.
DOI:10.3390/molecules23071798
- N. O. Anastassova, D. Y. Yancheva, A. T. Mavrova, M. S. Kondeva-Burdina, V. I. Tzankova, N. G. Hristova-Avakumova, V. A. Hadjimitova, *J. Mol. Struct.* **2018**, *1165*, 162–176.
DOI:10.1016/j.molstruc.2018.03.119
- A. E. Dascalu, A. Ghinet, E. Lipka, C. Furman, B. Rigo, A. Fayeulle, M. Billamboz, *Bioorg. Med. Chem. Lett.* **2020**, *30*, 127220. DOI:10.1016/j.bmcl.2020.127220
- T. Nasr, S. Bondock, M. Youns, *Eur. J. Med. Chem.* **2014**, *76*, 539–548. DOI:10.1016/j.ejmech.2014.02.026
- K. D. Katariya, S. R. Shah, D. Reddy, *Bioorg. Chem.* **2020**, *94*, 103406. DOI:10.1016/j.bioorg.2019.103406
- M. M. Shakhdoifa, M. H. Shtaiwi, N. Morsy, T. Abdel-rassel, *Main Group Chem.* **2014**, *13*, 187–218.
DOI:10.3233/MGC-140133
- M. Cindrić, A. Bjelopetrović, G. Pavlović, V. Damjanović, J. Lovrić, D. Matković-Čalogović, V. Vrdoljak, *New J. Chem.* **2017**, *41*, 2425–2435. DOI:10.1039/C6NJ03827A
- V. Vrdoljak, G. Pavlović, N. Maltar-Strmečki, M. Cindrić, *New J. Chem.* **2016**, *40*, 9263–9274.
DOI:10.1039/C6NJ01036A
- S. Shit, S. K. Dey, C. Rizzoli, E. Zangrando, G. Pilet, C. J. Gomez-Garcia, S. Mitra, *Inorg. Chim. Acta* **2011**, *370*, 18–26.
DOI:10.1016/j.ica.2011.01.008
- A. K. Patel, R. N. Jadeja, H. Roy, R. Patel, S. K. Patel, R. J. Butcher, M. Cortijo, S. Herrero, *Polyhedron* **2020**, *186*, 114624. DOI:10.1016/j.poly.2020.114624
- M. Nandy, D. L. Hughes, G. M. Rosair, R. K. B. Singh, S. Mitra, *J. Coord. Chem.* **2014**, *67*, 3335–3353.
DOI:10.1080/00958972.2014.964697
- P. Sathyadevi, P. Krishnamoorthy, M. Alagesan, K. Thanigaimani, P. T. Muthiah, N. Dharmaraj, *Polyhedron* **2012**, *31*, 294–306. DOI:10.1016/j.poly.2011.09.021
- A. A. El-Sherif, *Inorg. Chim. Acta* **2009**, *362*, 4991–5000.
DOI:10.1016/j.ica.2009.08.004
- E. J. Siddiqui, I. Azad, A. R. Khan, T. Khan, *J. Drug Deliv. Ther.* **2019**, *9*, 689–703.
- R. Narang, B. Narasimhan, S. Sharma, *Curr. Med. Chem.* **2012**, *19*, 569–612. DOI:10.2174/092986712798918789
- R. K. Mohapatra, P. K. Das, M. K. Pradhan, A. A. Maihub, M. M. El-ajaily, *J. Iran. Chem. Soc.* **2018**, *15*, 2193–2227.
DOI:10.1007/s13738-018-1411-2
- M. Vyas, R. Jain, N. Bhojak, *Int. J. Biotechnol. Biochem.* **2013**, *9*, 45–48.
- A. Gahler, *Anal. Chem.* **1954**, *26*, 577–579.
DOI:10.1021/ac60087a052
- D. K. Singh, S. Kumar, G. Udayabhanu, R. P. John, *J. Mol. Liq.* **2016**, *216*, 738–746. DOI:10.1016/j.molliq.2016.02.012
- H. Adibi, S. Zaker, H. Monkaresi, *J. Rep. Pharm. Sci.* **2012**, *1*, 60–66. DOI:10.5455/medarh.2012.66.89-91
- E. Krieger, G. Vriend, *Bioinformatics* **2014**, *30*, 2981–2982.
DOI:10.1093/bioinformatics/btu426
- E. Krieger, G. Vriend, *J. Comput. Chem.* **2015**, *36*, 996–1007.
DOI:10.1002/jcc.23899
- G. M. Morris, R. Huey, W. Lindstrom, M. F. Sanner, R. K. Belew, D. S. Goodsell, A. J. Olson, *J. Comput. Chem.* **2009**, *30*, 2785–2791. DOI:10.1002/jcc.21256
- K. A. Majorek, P. J. Porebski, A. Dayal, M. D. Zimmerman, K. Jablonska, A. J. Stewart, M. Chruszcz, W. Minor, *Mol. Immunol.* **2012**, *52*, 174–182. DOI:10.1016/j.molimm.2012.05.011
- Y. Duan, C. Wu, S. Chowdhury, M. C. Lee, G. Xiong, W. Zhang, R. Yang, P. Cieplak, R. Luo, T. Lee, *J. Comput. Chem.* **2003**, *24*, 1999–2012. DOI:10.1002/jcc.10349
- Gaussian 09, Revision D.01. M. J. Frisch, G. W. Trucks, H. B. Schlegel, G. E. Scuseria, M. A. Robb, J. R. Cheeseman, et al. Gaussian, Inc. Wallingford CT, **2016**.
- D. Matoga, J. Szklarzewicz, R. Grybos, K. Kurpiewska, W. Nitek, *Inorg. Chem.* **2011**, *50*, 3501–3510.
DOI:10.1021/ic1024586
- P. H. Santiago, C. M. Aiube, J. L. de Macedo, C. C. Gatto, *Mol. Catal.* **2020**, *496*, 111177. DOI:10.1016/j.mcat.2020.111177
- R. Bikas, P. Aleshkevych, H. Hosseini-Monfared, J. Sanchiz, R. Szymczak, T. Lis, *Dalton Trans.* **2015**, *44*, 1782–1789.
DOI:10.1039/C4DT03060E
- P. O'Brien, *J. Chem. Educ.* **1982**, *59*, 1052–1053.
DOI:10.1021/ed059p1052
- H. B. Küçük, E. Kara, B. Ö. Çelik, *Turk. J. Chem.* **2015**, *39*, 939–954. DOI:10.3906/kim-1502-122
- J. Devi, S. Kumar, D. Kumar, D. K. Jindal, Y. Poornachandra, *Res. Chem. Intermed.* **2022**, *48*, 423–455.
DOI:10.1007/s11164-021-04602-8
- A. Shoir, A. El-Bindary, N. El-Ghamaz, G. Rezk, *J. Mol. Liq.* **2018**, *269*, 619–638. DOI:10.1016/j.molliq.2018.08.075
- E. E. Şengül, T. Göktürk, C. G. Topkaya, R. Gup, *J. Chil. Chem. Soc.* **2020**, *65*, 4754–4758.
- L. M. Wu, H. B. Teng, X. B. Ke, W. J. Xu, J. T. Su, S. C. Liang, X. M. Hu, *Chem. Biodivers.* **2007**, *4*, 2198–2209.
DOI:10.1002/cbdv.200790177
- P. R. Inamdar, R. Chauhan, J. Abraham, A. Sheela, *Inorg. Chem. Commun.* **2016**, *67*, 67–71.

- DOI:10.1016/j.inoche.2016.03.012
46. S. Kanchanadevi, F. R. Fronczek, C. I. David, R. Nandhakumar, V. Mahalingam, *Inorg. Chim. Acta*, **2021**, 526, 120536. DOI:10.1016/j.ica.2021.120536
47. A. A. R. Despaigne, J. G. Da Silva, P. R. Da Costa, R. G. Dos Santos, H. Beraldo, *Molecules*, **2014**, 19, 17202–17220. DOI:10.3390/molecules191117202
48. P. Krishnamoorthy, P. Sathyadevi, A. H. Cowley, R. R. Butorac, N. Dharmaraj, *Eur. J. Med. Chem.* **2011**, 46, 3376–3387. DOI:10.1016/j.ejmech.2011.05.001
49. A. Ray, B. K. Seth, U. Pal, S. Basu, *Spectrochim. Acta A Mol. Biomol. Spectrosc.* **2012**, 92, 164–174. DOI:10.1016/j.saa.2012.02.060
50. T. Topalä, A. Bodoki, L. Oprean, R. Oprean, *Clujul Med.* **2014**, 87, 215–219. DOI:10.15386/cjmed-357
51. J. Qin, S.-S. Zhao, Y.-P. Liu, Z.-W. Man, P. Wang, L.-N. Wang, Y. Xu, H.-L. Zhu, *Bioorg. Med. Chem. Lett.* **2016**, 26, 4925–4929. DOI:10.1016/j.bmcl.2016.09.015
52. S. A. Elsayed, I. M. Elnabky, A. di Biase, A. M. El-Hendawy, *Appl. Organomet. Chem.* **2022**, 36, e6481. DOI:10.1002/aoc.6481
53. A. Zahirović, D. Žilić, S. K. Pavelić, M. Hukić, S. Muratović, A. Harej, E. Kahrović, *New J. Chem.* **2019**, 43, 5791–5804. DOI:10.1039/C9NJ00826H
54. M. Memišević, A. Zahirović, A. Višnjevac, A. Osmanović, D. Žilić, M. Kralj, S. Muratović, I. Martin-Kleiner, D. Završnik, E. Kahrović, *Inorg. Chim. Acta*, **2021**, 525, 120460. DOI:10.1016/j.ica.2021.120460
55. F. Darabi, H. Hadadzadeh, J. Simpson, A. Shahpiri, *New J. Chem.* **2016**, 40, 9081–9097. DOI:10.1039/C6NJ01880G
56. A. Zahirović, S. Roca, E. Kahrović, A. Višnjevac, *J. Mol. Struct.* **2021**, 1236, 130326. DOI:10.1016/j.molstruc.2021.130326
57. A. Zahirović, E. Kahrović, M. Cindrić, S. Kraljević Pavelić, M. Hukić, A. Harej, E. Turkušić, *J. Coord. Chem.* **2017**, 70, 4030–4053. DOI:10.1080/00958972.2017.1409893
58. G. Ayyannan, M. Mohanraj, M. Gopiraman, R. Uthayamalar, G. Raja, N. Bhuvanesh, R. Nandhakumar, C. Jayabalakrishnan, *Inorg. Chim. Acta*, **2020**, 512, 119868.

Povzetek

Pripravili smo dva bakrova(II) kompleksa s 4-kloro- in 4-dimetilaminobenzaldehidnim hidrazonom nikotinske kisline in ju okarakterizirali z elementno analizo, masno spektrometrijo, infrardečo in elektronsko spektroskopijo ter konduktometrijo. Ta dva redka primera bis(hidrazonato)bakrovih(II) kompleksov sta nevtralni kompleksni vrsti z bakrovim(II) centrom, koordiniranim z dvema monoanionskima bidentatnima O,N-donorskima hidrazonskima ligandoma, koordiniranim v enol-iminski obliki. Proučevali smo interakcijo hidrazonskih ligandov in njihovih bakrovih(II) kompleksov s CT DNA in BSA. Bakrova(II) kompleksa sta nekoliko učinkovitejša pri vezavi na DNK kot prosta hidrazona. Rezultati kažejo na vezavo ali interkalacijo, na katero narava substituenta na hidrazonskih ligandih ne vpliva bistveno. Nasprotno pa se afiniteti dveh bakrovih(II) kompleksov do BSA bistveno razlikujeta in sta odvisni od narave substituenta, vendar zaradi pomanjkanja termodinamskih podatkov ni mogoče izključiti razlike v naravi veznih sil. Kompleks z elektronakceptorskim 4-kloro substituentom ima večjo afiniteto do BSA v primerjavi s 4-dimetiaminskim analogom. Te ugotovitve so bile teoretično podprte s študijo molekularnega dockinga.



Except when otherwise noted, articles in this journal are published under the terms and conditions of the Creative Commons Attribution 4.0 International License

Scientific paper

Determination of Copper at Extended Dose Levels of Copper (II)-acetylsalicylate and Pharmacokinetics Applications

Muhammad Sher^{1,*} Muhammad Ajaz Hussain,² Shahzad Hassan Khan,¹ Muhammad Naeem-ul-Hassan,¹ Muhammad Amin³ and Hafeezullah Khan⁴

¹ Institute of Chemistry, University of Sargodha, Sargodha 40100, Pakistan

² School of Chemistry, University of the Punjab, Lahore 54590, Pakistan

³ The University of Lahore, Sargodha Campus, Sargodha 40100, Pakistan

⁴ College of Pharmacy, University of Sargodha, Sargodha 40100, Pakistan

* Corresponding author: E-mail: msherawan@yahoo.com.
Phone: (0092) 300-6022454. Fax: (0092) 48-3768409

Received: 11-18-2022

Abstract

Rheumatoid arthritis has long been treated with acetylsalicylic acid, despite many side effects, including gastric ulcers. These side effects can be curtailed by preparing the metal complexes of acetylsalicylic acid, such as copper (II)-acetylsalicylate (CAS). Present study evaluates the pharmacokinetics parameters of CAS and the level of copper at extended dose levels using rabbit model. The concentrations of CAS and copper in plasma samples were determined by validated HPLC and atomic absorption spectroscopic (AAS) methods, respectively. Three doses, 1–3 mg kg⁻¹ were orally administered to six rabbits with two wash out periods. The blood samples were collected at different time intervals for 24 hours. The peak drug concentration (C_{max}) for these doses at a time to peak drug concentration (t_{max}) 0.5 h was determined to be 0.38, 0.76 and 1.14 µg mL⁻¹. The half-life of drug ($t_{1/2}$) was 8.67, 8.73 and 8.81 h, which are perfect results for once a day dosing. The values of volume of distribution (V_d) and clearance (Cl) for CAS were 829, 833 and 837 L kg⁻¹ and 66.30, 66.74 and 66.95 L h⁻¹, respectively. The AAS results showed that copper levels in rabbit blood plasma were increased with increasing the dosage of CAS, but still remains under the safer limit, which was twofold higher than the reported safe limit.

Keywords: Copper (II)-acetylsalicylate, Copper level, Atomic Absorption Spectroscopic Method, Pharmacokinetics, HPLC-UV

1. Introduction

Acetylsalicylic acid (ASA) is commonly used for the treatment of rheumatoid arthritis since the last century. However, prolonged use of this medication is associated with many side effects. Peptic ulcers are among the major side effects ascribed to ASA.^{1,2} One approach to diminish these serious gastric side effects is the development of polymer based prodrugs of salicylic acid and ASA.^{3,4} However, the synthesis of copper (II)-acetylsalicylate (CAS) by Sorenson (1976) not only subsided these side effects, but it was also found to possess antiulcer potential and with enhanced activity.^{5–8} Many other copper complexes have also been found to possess greater anti-inflammatory (AI) activity than their parent compounds or ligands, therefore copper complexes have attracted a great atten-

tion as anti-arthritis and AI drugs since the last two to four decades.^{9–11} The only possible hindrance left behind for the safer use of CAS as anti-rheumatic drug is the rationalization between concentration of copper metal and its levels in the body. Recently, we have reported that CAS has improved pharmacokinetics compared with ASA after administration of a single oral dose in the human volunteers.¹² However, plasma copper levels, while using moderate to higher dose levels of CAS were not carried out and need to be determined.

In the present study, pharmacokinetics parameters of CAS with enhanced dose along with the monitoring of plasma copper level is presented for the first time by validated HPLC/UV and atomic absorption spectrophotometric (AAS) methods.

2. Materials and Methods

2.1. Participants and Study Design

Six white male albino rabbits, weighing 1.4–1.8 kg were used from the laboratory animal house, University of Sargodha, Sargodha, Pakistan. All the rabbits were healthy and never used previously for any type of studies. The animals were kept in separate cages under a 12 h light/dark cycle and were given free access to pelleted feed concentrate and water. A crossover design was used in three phases ($2 \times 2 \times 2$), with two washout periods of 15 days each. The rabbits were kept on fast for at least 10 h (overnight). Rabbits were prevented from taking water 1 h before the drug administration. A pre-dose blood sample was taken from all the rabbits, which was termed and used as blank. In the first phase, a single dose of 1.0 mg kg^{-1} of CAS with water was administered to six rabbits. After the blood sampling, the rabbits were fed with natural food and given a washout period of 15 days. The given procedure was repeated for second and third blood sampling at dosage of 2.0 mg kg^{-1} and 3.0 mg kg^{-1} of CAS, respectively. The study protocol was approved by the Institutional Animal Ethics Committee (IEC), Faculty of Pharmacy, University of Sargodha (Approval No.31-C12 IEC UOS). All the experiments performed complied with the rulings of National Research Council.¹³

2.2. Specimen Collection

Blood samples (3–5 mL) were taken from jugular vein of each rabbit using heparin (Leo, Denmark) added disposable syringes (*Injekt*) under aseptic conditions. The blood samples were transferred to blood collection tubes (BD Vacutainer®) and labeled consequently with great care. Post-dose blood samples were collected after 0.15, 0.3, 0.5, 0.75, 1, 1.5, 2, 4, 6, 8, 10, 12 and 24 h. The blood samples were centrifuged at $4000 \times g$ for 5 min and supernatant layer (plasma) of each sample was separated carefully and frozen.

2.3. Specimen Analysis

The test plasma sample (1.0 mL) was thawed quickly under cold water and then promptly but briefly vortex mixed and processed further for protein precipitation according to a reported method by M. S. Iqbal *et al.* (2008)¹². The plasma samples were analyzed by an already reported HPLC/UV method¹² and concentrations of CAS were determined. All the chemicals used for HPLC analyses were of analytical reagent grade and obtained from Merck, Germany. Standard samples of CAS were prepared according to reported method¹². The HPLC/UV system consisted of: LC-10 ATVP pump, UV-Vis detector SPD-10A VP, and SCL-10A VP system controller all from Shimadzu, Japan. The column used was Shim-pack ODS ($5 \mu\text{m}$, $4.6 \text{ mm i.d.} \times 250 \text{ mm}$). The methanol and acetic acid were used as mo-

bile phase in a ratio of 20:01. The flow rate, detection wavelength and injection volume used were 1.0 mL min^{-1} , 294 nm and $20 \mu\text{L}$, respectively.

2.4. Pharmacokinetic Analysis

Concentration-time curves were plotted and the pharmacokinetic parameters i.e., area under curve from time zero to time t (AUC_{0-t}) and area under curve from time zero to time infinity ($AUC_{0-\infty}$) were calculated by the following formula;

$$AUC_{0-\infty} = AUC_{last} + C_t/ke$$

Where, $AUC_{0-\infty}$ is the area under curve from time zero to time infinity, C_t concentration at a particular time and ke , absorption constant. Other parameters include, $t_{1/2} = 0.693/ke$, half-life of drug; C_{max} , peak drug concentration; t_{max} , time to peak drug concentration.

Area under the concentration-time curve was determined by the linear trapezoidal method. The terminal rate constant was resolved by regression analysis of at least three data points in the terminal phase. One way analysis of variance (ANOVA) was used to compare variations in the results obtained at extended dose levels.

2.5. Copper Analysis

The copper level in plasma was measured by an AAS method using graphite furnace.¹⁴ The instrument used was an AA 6300 (Shimadzu, Japan) operational with copper hollow cathode lamp and GFA-EX7i graphite furnace. A $20 \mu\text{L}$ pipette was used for sample injection and the instrument operating conditions were as follows: wavelength: 324.7 nm, lamp current: 8mA, spectral band width: 0.7 nm, drying time: 30 s, drying temperature: $120 \text{ }^\circ\text{C}$, ashing time: 30 s, ashing temperature: $800 \text{ }^\circ\text{C}$, atomization time: 10 s, atomization temperature: $2500 \text{ }^\circ\text{C}$ and argon flow rate: 1.5 L min^{-1} at 40 psi.

Stock solution of copper: A $1000 \mu\text{g mL}^{-1}$ of copper stock solution was prepared from copper acetate diluted with double-distilled water. Working standard solution of copper: 1.0 mL of stock solution of copper ($1000 \mu\text{g mL}^{-1}$) was transferred into a 100 mL calibrated flask and made up to the mark with double-distilled water to provide a working standard solution of copper having a concentration of $10 \mu\text{g mL}^{-1}$. 2, 4, 6, ..., 18 and 20 mL of $10 \mu\text{g mL}^{-1}$ copper solutions were added separately to the 100 mL calibrated flasks and made the volume up to the mark with double-distilled water. Resulting solutions were of 0.2, 0.4, 0.6, 0.8, 1.0, 1.2, 1.4, 1.6, 1.8, $2.0 \mu\text{g mL}^{-1}$ concentration, respectively. These solutions were used as working standard solutions of copper.

Preparation of sample solution: 1.0 mL of 10^{-2} M nitric acid was added to 1.0 mL of blank plasma, heated, cooled and then transferred to auto sampler of graphite atomic absorption spectrometer. Other plasma sample

taken at time intervals 0.15, 0.3, 0.5, 0.75, 1, 1.5, 2, 4, 6, 8, 10, 12 and 24 h of three doses (1.0, 2.0 and 3.0 mg kg⁻¹ body weight of rabbit) were prepared by the procedure used for blank plasma.

3. Results and Discussion

3.1. Pharmacokinetic Evaluation

The pharmacokinetic analysis was completed with the help of a model independent method. The C_{max} as well as the t_{max} of CAS were measured by assessment of the individual drug plasma concentration-time profiles. The elimination rate constant (k_e) was attained from least-square fitted terminal log-linear portion of the plasma concentration-time profile. The $t_{1/2}$ was considered equal to $0.693/k_e$. AUC_{0-t} was evaluated by linear trapezoidal rule. $AUC_{0-\infty}$ was considered equal to $AUC_{0-t} + C_t/k_e$ whereas, C_t is the last measurable concentration. In the pharmacokinetics analysis, AUC_{0-t} , $AUC_{0-\infty}$ and C_{max} were regarded as primary variables and converted to logarithmic terms.

The pharmacokinetic parameters for CAS after oral administration of 1.0, 2.0 and 3.0 mg kg⁻¹ are given in Table 1. The C_{max} in case of 1.0 mg kg⁻¹ dose was determined 0.38 $\mu\text{g mL}^{-1}$ at a t_{max} 0.5 h and the $t_{1/2}$ was 8.67 h. However, volume of distribution (V_d) and clearance (Cl) values for CAS were 829 L kg⁻¹ and 66.30 L h⁻¹, respectively. In case of 2 mg kg⁻¹ dose, the C_{max} was determined 0.76 $\mu\text{g mL}^{-1}$ at a t_{max} 0.5 h and the $t_{1/2}$ was found 8.73 h. Nevertheless, V_d and Cl values for CAS were 833 L kg⁻¹ and 66.74 L h⁻¹, respectively. Whereas, in 3 mg kg⁻¹ dose the C_{max} was calculated to be 1.14 $\mu\text{g mL}^{-1}$ and the $t_{1/2}$ was 8.81 h. The V_d and Cl values for CAS were obtained to be 837 L kg⁻¹ and 66.95 L h⁻¹, respectively. In all three studies, the value of $t_{1/2}$ is greater than 8 h, which is ideal for once a day dosing. The massive V_d might be as a result of absorption by a particular tissue or membrane, as very lipophilic compounds are recognized to distribute into lipids in cell membranes and fat stores; these competently form slow discharge depots of the drug and extend the plasma levels.¹⁵ The comparatively large clearance may direct to low exposure and less plasma average concentrations throughout chronic dosing.

In pharmacokinetic evaluation studies, it was observed that with the increase in dose, there is a change in the C_{max} value for each dose, whereas the values for other

parameters do not show any significant difference from one another. It clearly indicates that the absorption and elimination behavior of the drug is same in all cases and it was independent of dose administered except the value of C_{max} . The pharmacokinetic results obtained in this study are quite consistent and determine the safety of CAS at extended dose levels.

3.2. Copper Level Determination

The plasma copper levels were measured by AAS at 0.0, 0.15, 0.3, 0.5, 0.75, 1.0, 1.5, 2.0, 4.0, 8.0, 12 and 24 h after oral administration of three doses of CAS 1.0, 2.0 and 3.0 mg kg⁻¹ body weight of six rabbits (A, B, C, D, E and F) with two wash periods of 15 days. The average concentration of copper in plasma of six rabbits at different time intervals for extended doses (1, 2 and 3 mg kg⁻¹ body weight of rabbits) is recorded and the trend is shown in Figure 1.

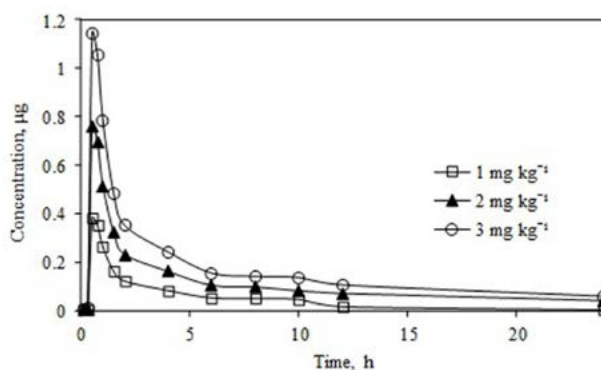


Figure 1. Overlay plot of copper concentrations (μg) vs. time (h) at different dose levels.

The trend in the Figure 1 shows that the concentration of copper in plasma increases with an increase in the concentration of CAS. There is an increase in the level of copper up to 0.5 h and later on the level of copper drops down to acceptable limits. Moreover, two way ANOVA (Tukey's multiple comparison test) revealed that extended dose of 3 mg kg⁻¹ showed some variations in terms of significance as compared to the dose of 1 mg/kg levels up to 1 h. Afterwards, no significant variation in plasma concentration of copper was documented in the three

Table 1. Pharmacokinetic data after oral dose of 1.0, 2.0 and 3.0 mg of CAS per kg body weight.

Dose (mg kg ⁻¹)	Pharmacokinetic parameters						
	t_{max} (h)	C_{max} ($\mu\text{g mL}^{-1}$)	$t_{1/2}$ (h)	AUC_{0-t} (h $\mu\text{g L}^{-1}$)	$AUC_{0-\infty}$ (h $\mu\text{g L}^{-1}$)	V_d (L kg ⁻¹)	Cl (L h ⁻¹)
1.0	0.5	0.38	8.67	0.71	0.91	829	66.30
2.0	0.5	0.76	8.73	0.74	0.95	833	66.74
3.0	0.5	1.14	8.81	0.75	0.97	827	66.45

Table 2. Two way ANOVA chart; mean plasma concentration vs. time at extended dose levels.

Dosage	0.15 h			0.3 h			0.5 h		
	Mean	±	Standard error (S.E)	Mean	±	S.E	Mean	±	S.E
1 mg kg ⁻¹	0.003	±	0.0006	0.003	±	0.001	0.38	±	0.02
2 mg kg ⁻¹	0.004	±	0.0006	0.005	±	0.0008	0.76	±	0.05
3 mg kg ⁻¹	0.005	±	0.0008	0.093	±	0.026	1.14	±	0.06***
Dosage	0.75 h			1 h			1.5 h		
	Mean	±	S.E	Mean	±	S.E	Mean	±	S.E
1 mg kg ⁻¹	0.35	±	0.03	0.263	±	0.017	0.16	±	0.02
2 mg kg ⁻¹	0.69	±	0.079	0.513	±	0.076	0.32	±	0.07
3 mg kg ⁻¹	1.05	±	0.03***	0.78	±	0.048*	0.48	±	0.03
Dosage	2 h			4 h			6 h		
	Mean	±	S.E	Mean	±	S.E	Mean	±	S.E
1 mg kg ⁻¹	0.12	±	0.02	0.08	±	0.012	0.051	±	0.008
2 mg kg ⁻¹	0.23	±	0.07	0.16	±	0.031	0.103	±	0.005
3 mg kg ⁻¹	0.35	±	0.035	0.24	±	0.012	0.153	±	0.007
Dosage	8 h			10 h			12 h		
	Mean	±	S.E	Mean	±	S.E	Mean	±	S.E
1 mg kg ⁻¹	0.05	±	0.004	0.045	±	0.003	0.016	±	0.004
2 mg kg ⁻¹	0.10	±	0.008	0.083	±	0.02	0.07	±	0.014
3 mg kg ⁻¹	0.14	±	0.016	0.135	±	0.006	0.105	±	0.006
Dosage	24 h								
	Mean	±	S.E						
1 mg kg ⁻¹	0.002	±	0.0004						
2 mg kg ⁻¹	0.042	±	0.012						
3 mg kg ⁻¹	0.058	±	0.007						

* show statistically significant variation in plasma concentration of copper at different time intervals when comparing between group 1&3 at significance level of $\alpha = 0.05$

groups. Nevertheless, the plasma concentration of copper achieved from this dose of 3 mg kg⁻¹ remains within safe therapeutic limits.

4. Conclusion

The animal model (rabbits) were used to evaluate the pharmacokinetics parameters of CAS and copper level at extended doses of CAS. Validated HPLC and AAS methods were employed to determine the plasma concentrations of CAS and copper, respectively. Results of pharmacokinetic studies have revealed that copper level in plasma increases under safer limits up to 2 mg kg⁻¹ dose level that is equivalent to 120 mg human dose. It is two-fold higher safe limit than the reported of dose 60 mg, i.e., useful for rheumatoid arthritis and therefore a higher dose of 2 mg kg⁻¹ can be used safely. It is also worth mentioning here that the dose 3 mg kg⁻¹, which is equivalent to 180 mg can also be used. Although at time interval 0.5 h, copper levels increase (1.9 mg kg⁻¹) little up to the acceptable level of copper in plasma (0.5–1.7 mg kg⁻¹), however within about 15 min the plasma maintains the copper levels under the acceptable limits. Therefore, present work indicates that CAS is a safe prodrug of ASA even at three fold extend-

ed dose levels than a normal dose i.e. 60 mg suggested for humans.¹² However, the toxicity due to high dose may be determined by analyzing the accumulation of copper metal in different tissues of the body.

Conflict of Interest Statement

The authors confirm that this article content has no conflict of interest.

5. References

1. B. Cryer, M. Feldman, *Gastroenterology* **1999**, *117*, 17–25. DOI:10.1016/S0016-5085(99)70545-7
2. P. Roderick, H. Wilkes, T. Meade, *Br J Clin Pharmacol* **1993**, *35*, 219–226. DOI:10.1111/j.1365-2125.1993.tb05689.x
3. M. A. Hussain, K. Abbas, M. Sher, M. N. Tahir, W. Tremel, M. S. Iqbal, M. Amin, M. Badshah, *Macromol Res* **2011**, *19*, 1296–1302. DOI:10.1007/s13233-011-1212-2
4. M. A. Hussain, M. Badshah, M. S. Iqbal, M. N. Tahir, W. Tremel, S. V. Bhosale, M. Sher, M. T. Haseeb, *J Polym Sci A1* **2009**, *47*, 4202–4208. DOI:10.1002/pola.23463
5. J. R. Sorenson, *J Med Chem* **1976**, *19*, 135–148. DOI:10.1021/jm00223a024

6. I. Mazzetti, B. Grigolo, R. Borzi, R. Meliconi, A. Facchini, *Int J Clin Lab Res* **1996**, *26*, 245–249. DOI:10.1007/BF02602957
7. L. Tyrer, *J Reprod Med* **1984**, *29*, 547–550. DOI:10.1177/070674378402900701
8. A. Sukul, S. Kumar Poddar, S. Haque, S. Kumar Saha, S. Chandra Das, Z. Al Mahmud, S. Abdur Rahman, *Antiinflamm Antiallergy Agents Med Chem* **2016**, *15*, 221–233. DOI:10.2174/1871523016666170217103402
9. J. R. Sorenson, in *Inflammatory Diseases and Copper*, Springer, **1982**, pp. 289–301. DOI:10.1007/978-1-4612-5829-2_28
10. R. Puranik, S. Bao, A. M. Bonin, R. Kaur, J. E. Weder, L. Casbolt, T. W. Hambley, P. A. Lay, P. J. Barter, K.-A. Rye, *Cell Bio-sci* **2016**, *6*, 9. DOI:10.1186/s13578-016-0076-8
11. X. Tang, X. Liang, *Chem Biol Drug Des* **2013**, *81*, 311–322. DOI:10.1111/cbdd.12090
12. M. S. Iqbal, M. Sher, H. Pervez, M. Saeed, *Biol Trace Elem Res* **2008**, *124*, 283–288. DOI:10.1007/s12011-008-8146-3
13. N. R. Council, *Guide for the care and use of laboratory animals*. Editor, National Academies Press, **2010**.
14. H. Kamel, J. Teape, D. Brown, J. Ottaway, W. Smith, *Analyst* **1978**, *103*, 921–927. DOI:10.1039/an9780300921
15. G. Levy, *Pediatrics* **1978**, *62*, 867–872. DOI:10.1542/peds.62.5S.867

Povzetek

Revmatoidni artritis so dolgo zdravili z acetilsalicilno kislino, kljub njenim številnim neželenim učinkom, ki vključujejo želodčne razjede. Te neželene učinke je mogoče zmanjšati s pripravo kovinskih kompleksov acetilsalicilne kisline, kot je bakrov (II)-acetilsalicilat (CAS). Pričujoča študija ocenjuje farmakokinetične parametre CAS in raven bakra pri povečanih odmerkih na modelu kunca. Koncentracije CAS in bakra v plazemskih vzorcih so določili z validirano HPLC metodo in atomsko absorpcijsko spektroskopijo (AAS). Šestim kuncem so peroralno aplicirali tri odmerke, 1–3 mg kg⁻¹, z dvema obdobjema izpiranja. Vzorce krvi so zbirali v različnih časovnih intervalih znotraj 24 ur. Največja koncentracija učinkovine (C_{max}) za te odmerke pri času do največje koncentracije učinkovine (t_{max}) 0,5 h je znašala 0,38; 0,76 in 1,14 µg mL⁻¹. Razpolovna doba učinkovine (t_{1/2}) je znašala 8,67; 8,73 in 8,81 h, kar so ustrezni rezultati za odmerjanje enkrat na dan. Vrednosti volumna porazdelitve in očistka za CAS so po vrsti znašale 829, 833 in 837 L kg⁻¹ ter 66,30, 66,74 in 66,95 L h⁻¹. Rezultati AAS so pokazali, da so se vrednosti bakra v krvni plazmi kunccev povečale z večanjem odmerka CAS, vendar so še vedno ostale pod varnejšo mejo, ki je bila dvakrat višja od priporočene varne meje.



Except when otherwise noted, articles in this journal are published under the terms and conditions of the Creative Commons Attribution 4.0 International License

Scientific paper

The Effect of Different Numerical Approaches on the Accuracy of Calculating Relaxation Spectra for Polysaccharides

Anatolij Nikonov¹ and Urška Florjančič^{2*}¹ Faculty of Mechanical Engineering, University of Ljubljana, Slovenia² Center for Technology Transfer and Innovation, Jožef Stefan Institute, Slovenia* Corresponding author: E-mail: urska.florjancic@ijs.si
Tel. +386 31 261 813

Received: 01-12-2023

Abstract

For polymeric materials, the relaxation spectrum contains complete information about the time-dependent part of the material response. The contribution of different numerical schemes, *i.e.*, different methods of reconstructing the dynamic relaxation modulus, to the accuracy of the approximation by calculating the corresponding relaxation spectra is investigated by analysing experimental data for four types of polysaccharides. It was found that there is no unique mathematical approach for the calculation of relaxation spectra that ensures a satisfactory approximation of the experimentally determined dynamic moduli for the selected types of polymeric materials. It is recommended to combine different numerical methods in parallel to achieve a reasonable approximation of the material functions.

Keywords: Polysaccharide, rheology, viscoelastic properties, relaxation spectrum, mathematical modelling

1. Introduction

When polymeric materials are exposed to mechanical loading during rheological testing, the changes in material structure manifest in their viscoelastic responses. Therefore, the rheological investigation of their material properties has become a widely used tool for obtaining information on the structural characteristics and behaviour under mechanical loading of very broad range of materials, *e.g.*, polymer melts, polymer solutions, blood, biological tissues, food gels, colloidal gels, emulsions, alumina suspensions, magnesium alloys, dispersions, asphalt, etc.

In line with the theory of viscoelasticity, the relaxation spectrum of polymers reflects molecular movements of macromolecules and thus can be interrelated with the molecular structure, *i.e.*, molecular mass and molecular weight distribution, branching and other aspects of molecular architecture. For example, Stadler¹ used relaxation spectra to understand molecular processes, such as entanglement and reptation, in ring polymers. Many authors, *e.g.*, Thimm *et al.*² and Friedrich *et al.*³ showed analytical relation between the relaxation time spectrum and the molecular weight distribution which greatly reduces the

computational efforts to determine the molecular weight distribution from the relaxation time spectrum. Nobile and Cocchini⁴ introduced a generalized relationship between the molecular weight distribution and the relaxation time spectrum for sharp molecular weight distributions.

Polysaccharides are natural (bio)polymers, widely used in numerous applications due to their ability to form specific structures which manifest in diverse macroscopic behaviour and properties. They are polycarbohydrates composed of monosaccharide units bound together by glycosidic linkages to form long chain polymeric carbohydrate structures. Their functional properties depend not only on their chemical structure, but also on the microstructure which develops during processing.

Microbial polysaccharides xanthan, gellan, welan, and structural polysaccharide sodium carboxymethylcellulose have been extensively studied for several decades, *see, e.g.*, Lapasin *et al.*⁵ and Carmona *et al.*⁶ The rheological examination of these water-soluble polysaccharide systems have been used as a practical and efficient tool to investigate correlation between structural and mechanical characteristics of the systems, *see, e.g.*, Lim *et al.*⁷ and Song

*et al.*⁸ By using empirical approach researchers analyse different rheological responses to study the influence of different parameters, *i.e.*, pH, temperature, polymers concentration, additive content, mechanical loading, on the structure evolution in polysaccharide systems such as gelation, crosslinking, formation of entangled polymer networks, crystalline aggregates, etc.^{9,10}

Many papers discuss a linear viscoelastic behaviour of polysaccharides xanthan, gellan, welan, and Na CMC in terms of frequency dependence of elastic (storage) and viscous (loss) dynamic moduli, but only few of them report on the relaxation spectra of these materials.

2. Relaxation Spectra of Polysaccharides

The relaxation spectra of polymeric materials can only be calculated from the experimental data, for example frequency dependence of dynamic functions, creep or relaxation functions. In last decades, many different mathematical approaches have been developed to model mechanical behaviour of numerous polymeric materials, and to determine either their discrete or continuous spectra. In fact, the spectra calculated by using different mathematical models and corresponding numerical approaches for the same polymeric material may differ significantly which naturally leads to the question about uniqueness of the spectra calculations.

In the last decades, numerous publications have been devoted to development of the methodologies for spectra calculation, *see, e.g.*, Honerkamp and Weese,¹¹ Baumgaertel and Winter,¹² Emri and Tschoegl,¹³ Malkin,¹⁴ Shtrauss and Kalpinsh,¹⁵ Bae and Cho,¹⁶ and references therein. For calculation of the relaxation spectra of polysaccharides xanthan, gellan, welan, and Na CMC different models and mathematical approaches have been applied, that has been presented by numerous authors, for example Zupančič and Žumer,¹⁷ Florjančič *et al.*,¹⁸ Quintana *et al.*,¹⁹ Moraes *et al.*,²⁰ Lorenzo *et al.*,²¹ Lapasin *et al.*,²² and many others. Some authors used commercial software for spectra analysis, *e.g.*, Berta *et al.*²³ compared continuous relaxation time spectra of a xanthan aqueous solution, calculated by applying the IRIS® software and the TRIOS® software. Jaishankar and McKinley²⁴ used a fractional K-BKZ constitutive mathematical model for describing the nonlinear rheology of multiscale complex fluids such as water-soluble polysaccharide xanthan.

In the theory of linear viscoelasticity, the relaxation spectrum contains complete information on the time-dependent part of the material response.²⁵ The spectrum itself is not accessible by direct experiment, rather it can be calculated exactly from experimental data as an approximation to the unknown 'true' continuous spectrum by numerical differentiation or by the use of finite difference calculus. Another approach is based on the representation

of the experimental response by discrete models leading to distributions of line spectra.

There are two main reasons for the interest in the continuous spectra. They generally present the details of the time-dependent behaviour of a given material more clearly than the discrete line spectra do. In addition, a continuous spectrum is unique, while the appearance of a line spectrum depends on the somewhat arbitrary choice of the density and the location of the lines along the relaxation time coordinate. Therefore, a discrete relaxation spectrum is not unique. Poudel and Shanbhag²⁶ investigated strategies to improve the quality and interpretability of the extracted discrete spectrum for viscoelastic liquids and solids and found out that the number of modes has a significant effect on the height and location of the discrete relaxation spectrum lines.

Therefore, it is important to investigate the contribution of different numerical schemes, *i.e.*, different methodologies for approximating dynamic material functions such as relaxation modulus, to accuracy of the approximation by means of calculating the appropriate relaxation spectra. In the paper, three different approaches for the calculation of the relaxation spectra from frequency dependencies of dynamic functions, experimentally determined in oscillatory shear conditions, are explored. The experimental data on dynamic moduli for four water-based polysaccharide systems of xanthan, gellan, welan, and sodium carboxymethylcellulose were analysed.

2. Experimental

2.1. Materials

The materials, used in our research, are listed in Table 1. Gellan, welan and xanthan are microbial extracellular polysaccharides produced by different species of bacteria in aerobic fermentation process, while sodium carboxymethylcellulose (Na CMC) is water-soluble cellulose derivative.

Table 1. List of tested materials.

Material	Type	Producer
gellan	KELCOGEL	CP Kelco
welan	K1C376	CP Kelco
xanthan	KELTROL	CP Kelco
Na CMC	BLANOSE 7HF Cellulose gum	Aqualon

For all four materials, no stability problems occurred during the storage period and the measurements.

2.2. Sample Preparation

The samples were prepared by dissolving powdered polymers in distilled water by mechanical stirring. Welan,

xanthan and Na CMC are soluble in water at ambient temperature, while gellan requires temperature above 90 °C. The aqueous gellan solutions undergo thermally induced sol – gel transition; at higher temperatures exhibit sol behaviour, and after cooling the gelation appears.

Water-based systems of welan, xanthan and Na CMC were prepared at ambient temperature, having the same overall polymer concentration of 1 wt. %. Gellan powder at the same polymer concentration of 1 wt. % was dissolved in distilled water at 96 °C by mechanical stirring. When gellan solution was cooled the gelation appeared at temperature about 29 °C.

All samples were stored for two days in a refrigerator at 4 °C in covered glass beakers to prevent the evaporation of water and to ensure a complete wetting of the polymers, before the rheological tests were carried out.

2. 3. Testing Methodology

The viscoelastic properties of water-based polysaccharide systems were measured by using a controlled stress rheometer HAAKE RS 150,¹⁸ equipped with a cone and plate sensor (measuring) system, having diameter of 60 mm and the cone angle of 4 °. The rheological tests were performed under oscillatory shear conditions at 20 ± 0.3 °C. Each measurement was repeated several times in order to achieve proper repeatability of experimental results.

Welan, xanthan, and Na CMC samples, tempered for 10 min at room temperature and manually stirred to assure homogeneous substance before testing, were poured onto sensor system from glass beaker. After applying the sample to the measuring system, the sample was left to rest for few minutes before testing to be evenly tempered to 20 °C throughout the measuring system.

Gellan sample had to be heated in water bath to 50 °C and manually stirred to become homogenous, because it was still not fluid-like to be applied to the sensor system. Still warm it was poured onto sensor system and then left to cool down to 20 °C, which was testing temperature for all examined samples.

2. 3. 1. Determination of the Linear Viscoelastic Response of Tested Materials

It is required for frequency tests to be performed in a linear viscoelastic range, where shear storage (elastic) modulus G' and shear loss (viscous) modulus G'' are independent on maximum amplitude of shear strain.¹⁷ Above the limit of a linear viscoelastic response, both dynamic shear moduli G' and G'' characteristically change with increasing shear strain amplitude. In a non-linear viscoelastic range, a response of periodic oscillation is no longer sinusoidal and values of measured rheological quantities change with shear strain amplitude. The transition from a linear to a non-linear viscoelastic range is determined by the critical amplitude of shear strain and the critical shear

stress, which depend on the mechanical properties of the sample under investigation.

Therefore, the amplitude tests were performed first to determine the limit of the linear viscoelastic response. In the amplitude test, the shear storage modulus G' and the shear loss modulus G'' were monitored as a function of the shear strain amplitude at constant oscillation frequency. For all samples under investigation the amplitude tests were performed at constant oscillation frequency ω of 1 Hz.

2. 3. 2. Frequency Test

In the frequency test, the dependence of shear storage modulus G' and shear loss modulus G'' is measured as a function of oscillation frequency ω . It is a non-destructive method which is performed in the range of linear viscoelastic response to keep the internal structure of the sample non destructed.¹⁸ Therefore, it is important to choose appropriate sensor system, to run experiment at shear strain which is required for linear viscoelastic response and to select appropriate frequency range for the experiments. For all investigated samples a constant shear strain amplitude of 0.03 was chosen to measure dynamic shear storage modulus G' and dynamic shear loss modulus G'' as functions of oscillation frequency ω in a range from 0.01 to 100 rad/s.

3. Mathematical Treatment for Calculating Relaxation Spectra

Below, three conceptually different mathematical approaches for calculating relaxation spectra from experimental data on storage and loss moduli are presented in short, *i.e.*, (i) generalized Maxwell model, (ii) interconversion between material functions and (iii) Honerkamp & Weese method using the commercial software. To the best of our knowledge, there is no mathematically consistent comparative analysis of the existing mathematical models for spectra calculations, commonly used in practical applications, until now.

3. 1. Generalized Maxwell Model

Discrete relaxation spectra for the examined polysaccharide systems were calculated using generalized Maxwell model with five Maxwell elements, based on experimentally determined discrete data of dynamic moduli, G' and G'' , as functions of oscillation frequency, ω :

$$\begin{aligned} G'(\omega) &= \sum_{i=1}^n g_i \frac{(\omega\lambda_i)^2}{1+(\omega\lambda_i)^2} \\ G''(\omega) &= \sum_{i=1}^n g_i \frac{\omega\lambda_i}{1+(\omega\lambda_i)^2} \end{aligned} \quad (1)$$

where λ_i are characteristic relaxation times and g_i corresponding relaxation strengths. First, it is required to select

a set of relaxation times, λ_i evenly spaced on a log scale, *i.e.*, one per decade, and then the fitting procedure to determine the relaxation strengths, g_i , using the least-squares regularization method that minimizes the sum of squared relative deviations between the calculated values and the experimental data, has to be run. The resulted complete set of (λ_i, g_i) is called the spectrum of the relaxation times, *i.e.*, a discrete relaxation spectrum.

3. 2. Interconversion between material functions

The material functions in frequency- and time-domain are interrelated in a close form via the corresponding relaxation (or retardation) spectrum. The time-dependent relaxation modulus can be obtained from the relaxation spectrum, *i.e.*, from the set of (λ_i, g_i) , using the relation

$$G(t) = \sum_{i=1}^n g_i \exp\left(-\frac{t}{\lambda_i}\right). \quad (2)$$

Calculation of the relaxation and retardation spectra, and correspondingly determination of the material functions, requires an inverse solution of the Fredholm integral equation of the first or second kind, which is an ill-posed problem. Therefore, numerous approximate methods for the interconversion between frequency- and time-dependent material functions have been developed in the past. Then time-domain response, *i.e.*, the relaxation modulus $G(t)$ can be predicted from the experimental data of dynamic moduli $G'(\omega)$ and $G''(\omega)$.

Ninomiya and Ferry²⁷ developed an algorithm for calculating $G(t)$ that comprises contributions from the real and the imaginary parts of the dynamic modulus, *i.e.*,

$$G(t) \cong [G'(\omega) - 0.4G''(0.4\omega) + 0.014G''(10\omega)]_{\omega=1/t}. \quad (3)$$

It should be noted that the relaxation spectrum (λ_i, g_i) used in Eq. (2) is identical to that used in Eq. (1). Thus, for the purpose of comparative analysis of all three methods for spectra calculations, we first reconstructed the relaxation modulus $G(t)$ from experimentally determined dynamic moduli $G'(\omega)$ and $G''(\omega)$ using the approximate formula, *i.e.*, Eq. (3). In the next step we calculated the spectrum using the least-squares minimization method that incorporates Levenberg–Marquardt algorithm.

3. 3. Honerkamp & Weese Method using the Commercial Software

The third approach, used for calculating relaxation spectra for all four selected polysaccharides with the aim of comparative analysis of three mathematical models or methodologies, is based on the earlier developed Honerkamp & Weese method²⁸ exploiting an efficient, open-

source, multi-platform computer program ReSpect to infer the continuous and discrete relaxation spectra from dynamic moduli measurements.^{29,30}

This approach employs the numerical calculations that include nonlinear Tikhonov regularization and the Levenberg-Marquardt method to extract the continuous relaxation spectrum $h(\tau)$ that is an essential part of the mathematical representation of the dynamic moduli $G'(\omega)$ and $G''(\omega)$ in the form

$$\begin{aligned} G'(\omega) &= \int_{-\infty}^{\infty} \frac{(\omega\tau)^2}{1+(\omega\tau)^2} h(\tau) d \ln \tau, \\ G''(\omega) &= \int_{-\infty}^{\infty} \frac{\omega\tau}{1+(\omega\tau)^2} h(\tau) d \ln \tau. \end{aligned} \quad (4)$$

To obtain the discrete relaxation spectrum presented in the Eq. (1), a novel algorithm that exploits the continuous spectrum to position the modes was introduced. It uses a simple criterion which balances accuracy and conditioning of the resulting least-squares problem to determine a parsimonious number of modes.

In this commercial software, an intermediate approach was used, *e.g.*, a potentially parsimonious choice for the number and location of the relaxation time was enabled. However, the user was allowed to incrementally overlay the simple strategy of equally spaced discrete values of relaxation times on the parsimonious choice. According to the developed methodology, first the continuous spectrum has to be computed using the Levenberg-Marquardt algorithm, and then the resulting linear least squares problem is solved to obtain the discrete spectrum.

4. Results and Discussion

The frequency dependent shear storage modulus $G'(\omega)$ and shear loss modulus $G''(\omega)$ for all four investigated materials, *i.e.*, three microbial extracellular polysaccharides welan, gellan and xanthan, and water-soluble cellulose derivative sodium carboxymethylcellulose, are experimentally determined accordingly to the procedure reported in Section 2, and presented in Fig. 1.

From the diagrams of dynamic moduli for polysaccharides welan, gellan and xanthan, it is clearly seen that both dynamic moduli show relatively slight variation, *e.g.*, monotonic change (increase) of the moduli is within one decade or less over three decades of oscillation frequency range. Moreover, storage moduli predominate over the loss moduli for all those three polysaccharides. Such rheological behaviour is typical for weak gel structures, having elastic properties more pronounced than viscous. On the other hand, rheological behaviour of the material Na CMC is different. Namely, it exhibits significantly bigger change of the dynamic moduli over the same oscillation frequency range as for the rest three materials, and in a contrast to welan, gellan and xanthan, its loss modulus predominates over the storage modulus. More pronounced viscous char-

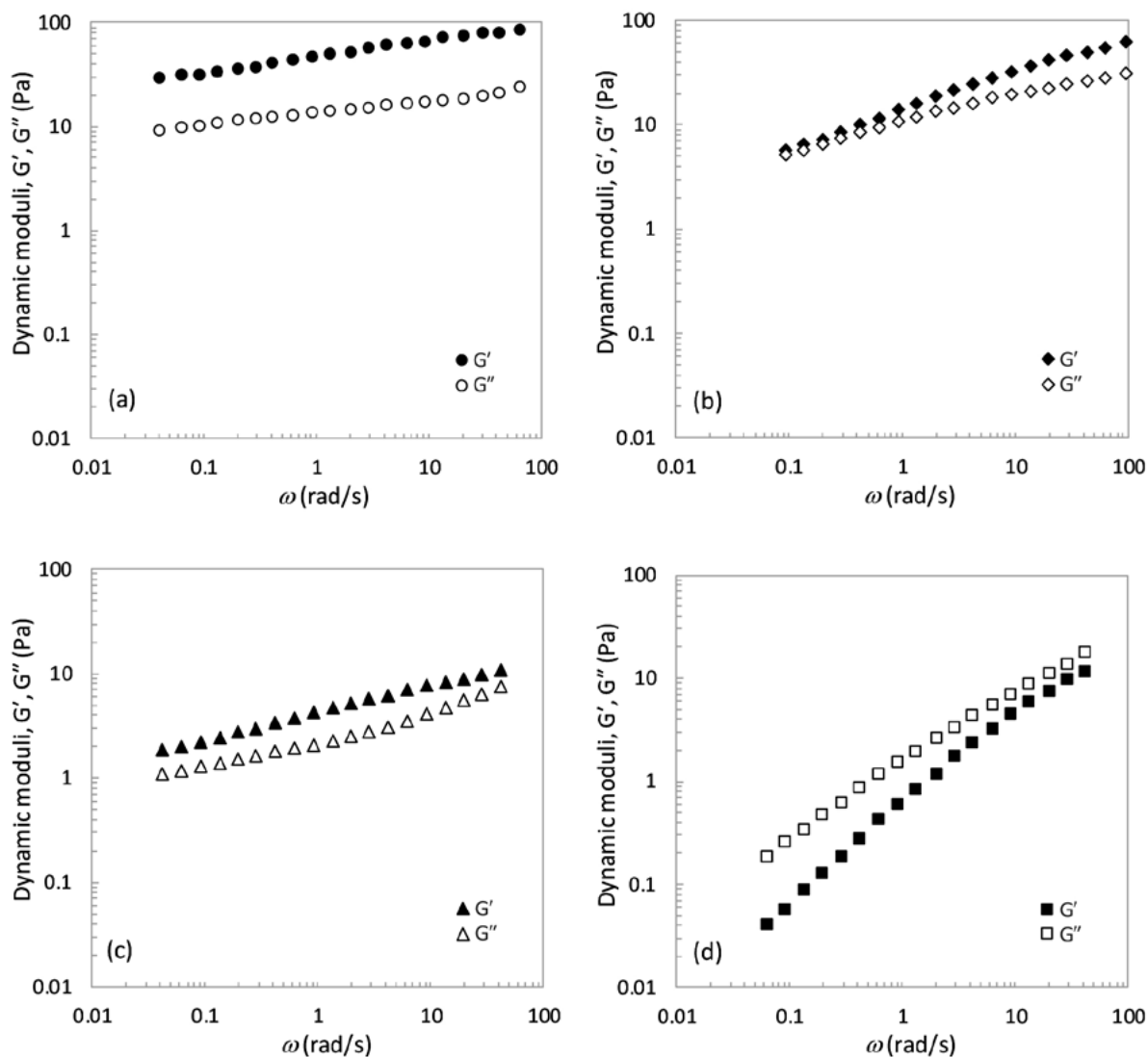


Fig. 1. The frequency dependence of the storage modulus $G'(\omega)$ and the loss modulus $G''(\omega)$ for 1 wt. % water-based systems of (a) welan, (b) gellan, (c) xanthan and (d) Na CMC.

acter in the whole frequency range examined is typical viscoelastic response for solutions.

The corresponding relaxation moduli $G'(t)$ for all four investigated materials are reconstructed from the dynamic moduli $G'(\omega)$ and $G''(\omega)$ using the methodology developed for interconversion between material functions in frequency- and time-domain, and presented in Fig. 2 (see the graph on the left). The accuracy of prediction of the relaxation moduli, obtained as a difference between the approximated values of the relaxation moduli calculated accordingly to Eq. (3) and the values calculated accordingly to Eq. (2), *i.e.*, reconstructed from spectrum, may be estimated from the graph on the right in Fig. 2.

From the diagram of relative errors of relaxation moduli reconstruction, one may conclude that the interconversion methodology works successfully for all examined materials except sodium carboxymethylcellulose, for which deviations are bigger than 10 % at longer times, *e.g.*,

at the range above 1 s. We can assume, that the apparent discrepancy between the experimental data and the corresponding approximation for Na CMC is due to a significant change in the dynamic moduli (about 3 decades within frequency range, see Fig. 1d) which much stronger increase than for the other three materials.

The corresponding relaxation spectra for all four materials, calculated using three methodologies described in Section 3, are shown in Fig. 3.

Similar difference, as for dynamic moduli itself, is observed in spectra change for the group of microbial extracellular polysaccharides (welan, gellan and xanthan) and for water-soluble cellulose derivative, *i.e.*, sodium carboxymethylcellulose (Na CMC) as well. Namely, the decrease of relaxation strength within the same range of relaxation times is much deeper for Na CMC rather than for the rest of three materials. In addition, we observe the difference in spectra for all four examined materials resulting

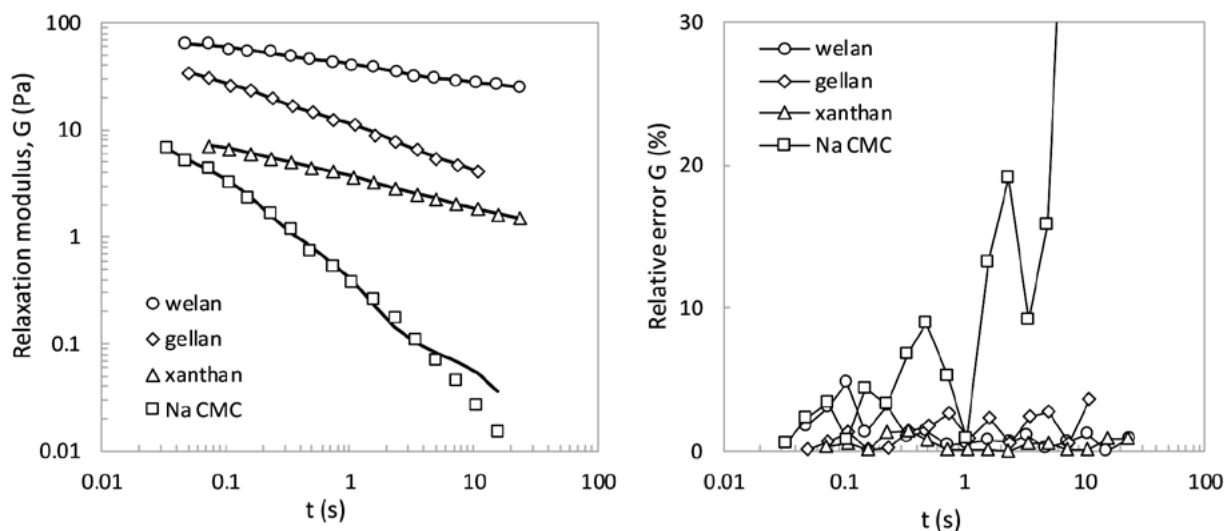


Fig. 2. The relaxation moduli (left) and the relative errors of moduli reconstruction (right) for all four investigated materials.

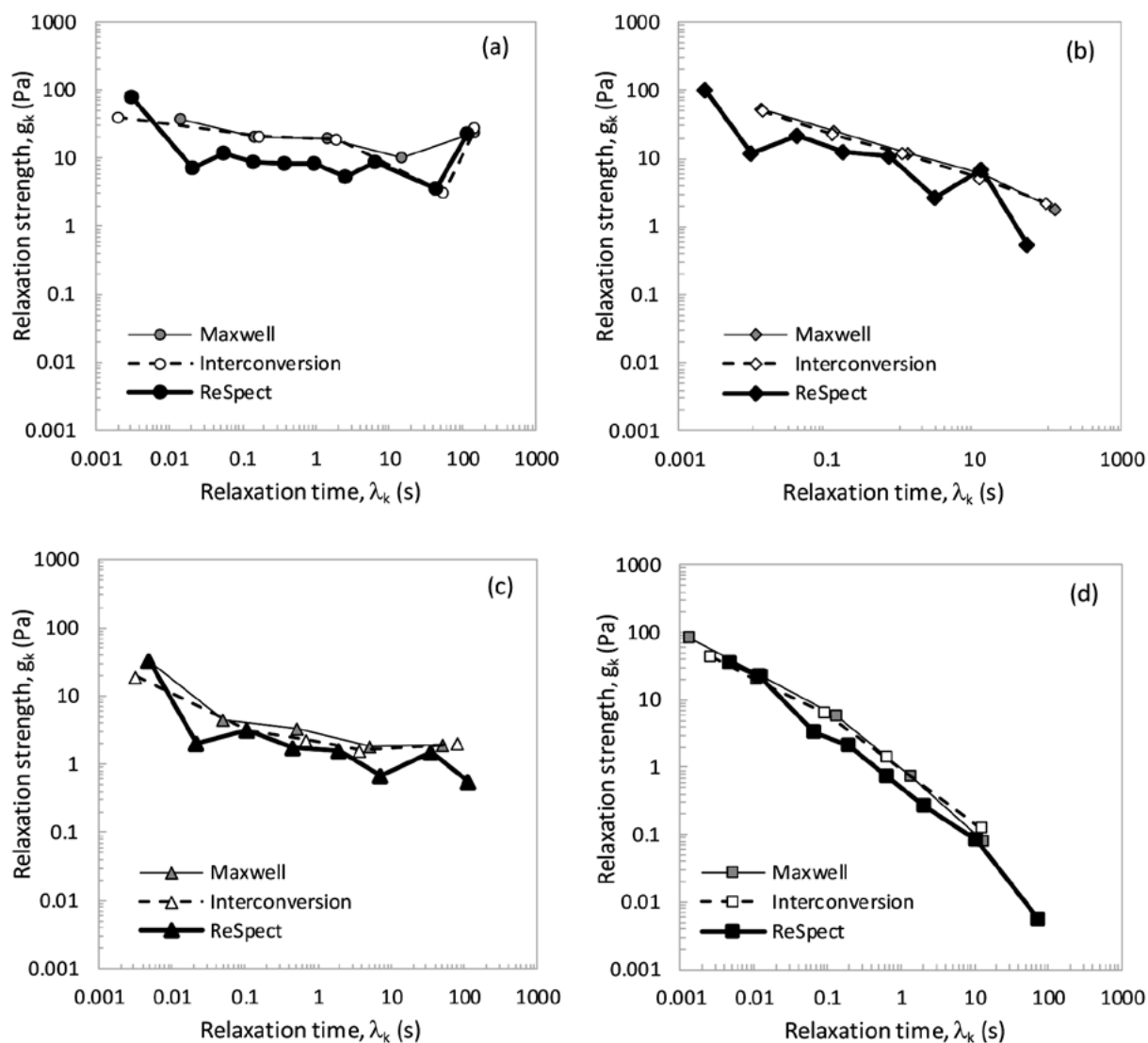


Fig. 3. The relaxation spectra for 1 wt. % water-based systems of (a) welan, (b) gellan, (c) xanthan and (d) Na CMC.

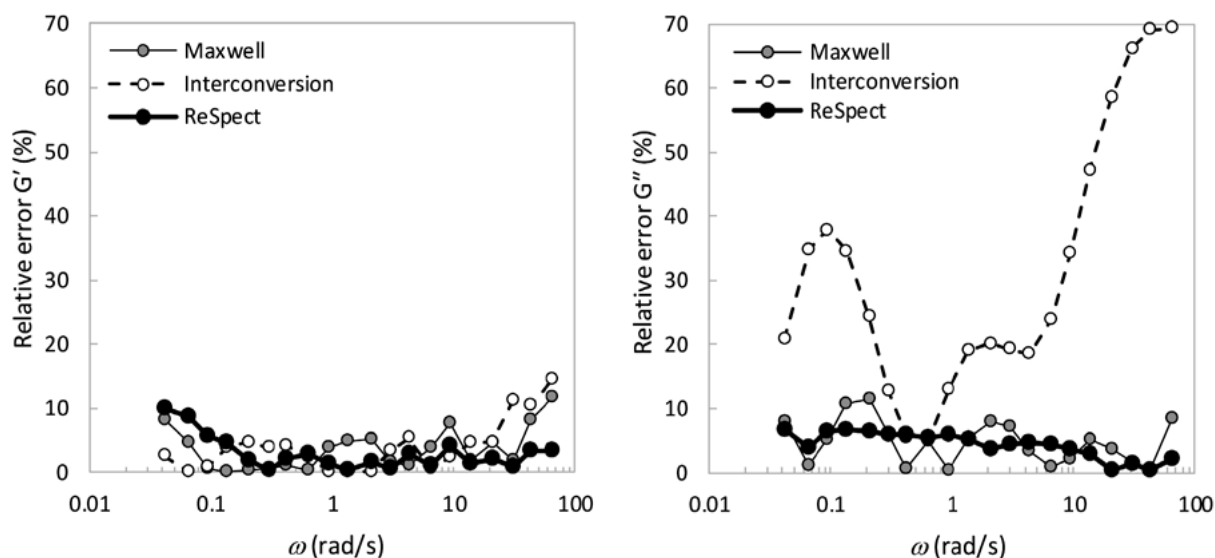


Fig. 4. The relative errors for reconstructed storage moduli (left) and loss moduli (right) as functions of frequency for welan.

from the application of three used methodologies for their calculating.

We also considered the findings of the work of Davies and Anderssen³¹ related to the sampling of the storage and loss moduli over the frequency range and its influence on the determining the relaxation spectrum. The authors emphasised that the relaxation spectrum is determined on a shorter interval of relaxation times than the reciprocal frequency range. In order to assess the reliability of the calculated relaxation spectra, we performed error analysis using experimental data on moduli and their reconstructed values based on the calculated relaxation spectra.

To demonstrate the deviations of the approximated functions for shear storage moduli, $G'(\omega)$, and shear loss moduli, $G''(\omega)$, obtained by their reconstruction with the help of Eq. (1) on one hand, and using the relaxation spectra presented in Fig. 3 on the other hand, from the corresponding experimentally determined moduli, the relative

errors calculated as differences between both material properties, *i.e.*, experimentally obtained and mathematically reconstructed, as functions of frequency, have been calculated and are shown in Figs. 4–7. Each diagram involves three curves for the relative errors of the approximations obtained by applying three different methodologies described in details in Section 3.

The diagrams vividly show that the accuracy of prediction of the dynamic moduli for all four materials depends on the methodology of calculating relaxation spectra applied.

Two of three approaches, *i.e.*, the computation of the relaxation spectra using generalized Maxwell model and the commercial software ReSpect based on Honerkamp & Weese method, demonstrated more or less similar results on the accuracy of prediction of experimentally obtained material functions. In most cases, the errors of approximation did not exceed 10%. However, it is clearly seen in

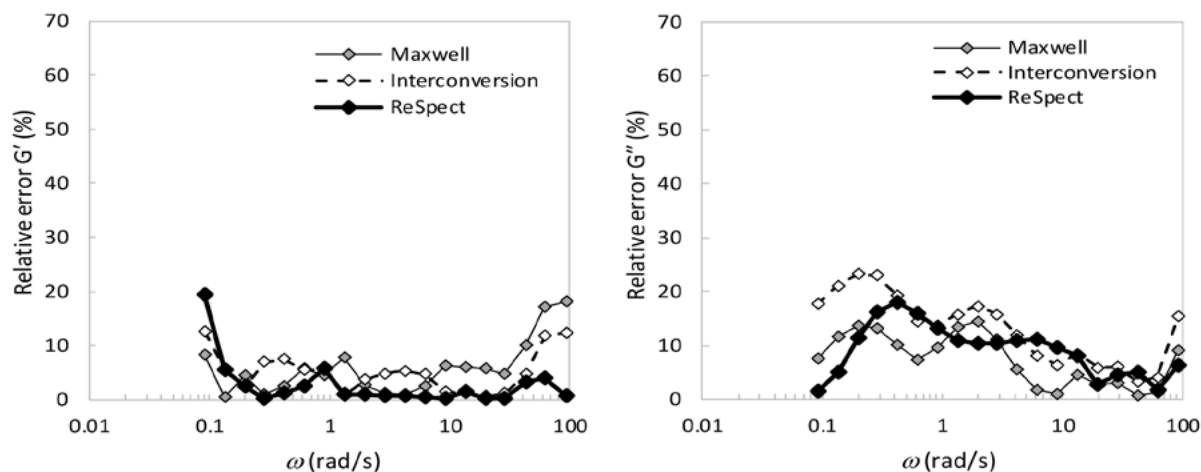


Fig. 5. The relative errors for reconstructed storage moduli (left) and loss moduli (right) as functions of frequency for gellan.

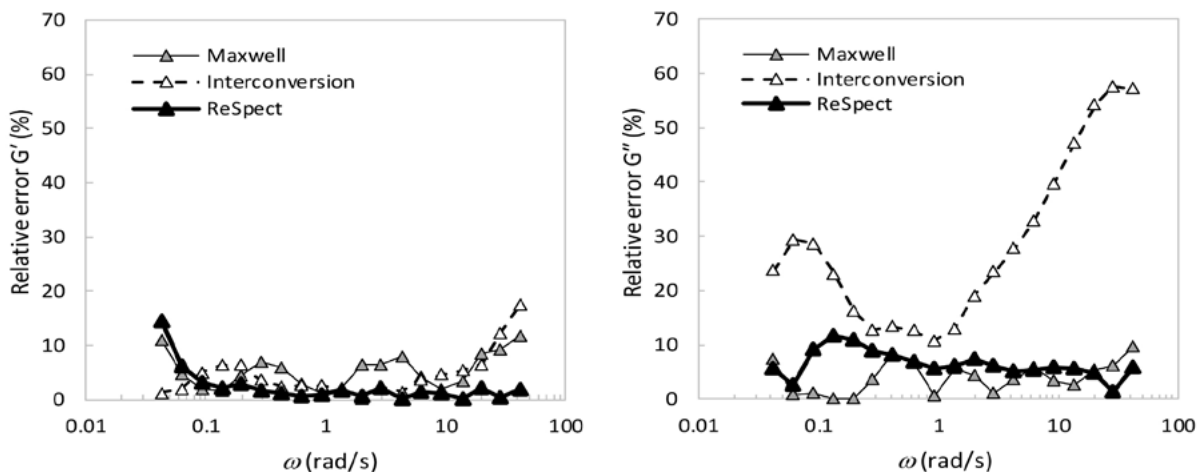


Fig. 6. The relative errors for reconstructed storage moduli (left) and loss moduli (right) as functions of frequency for xanthan.

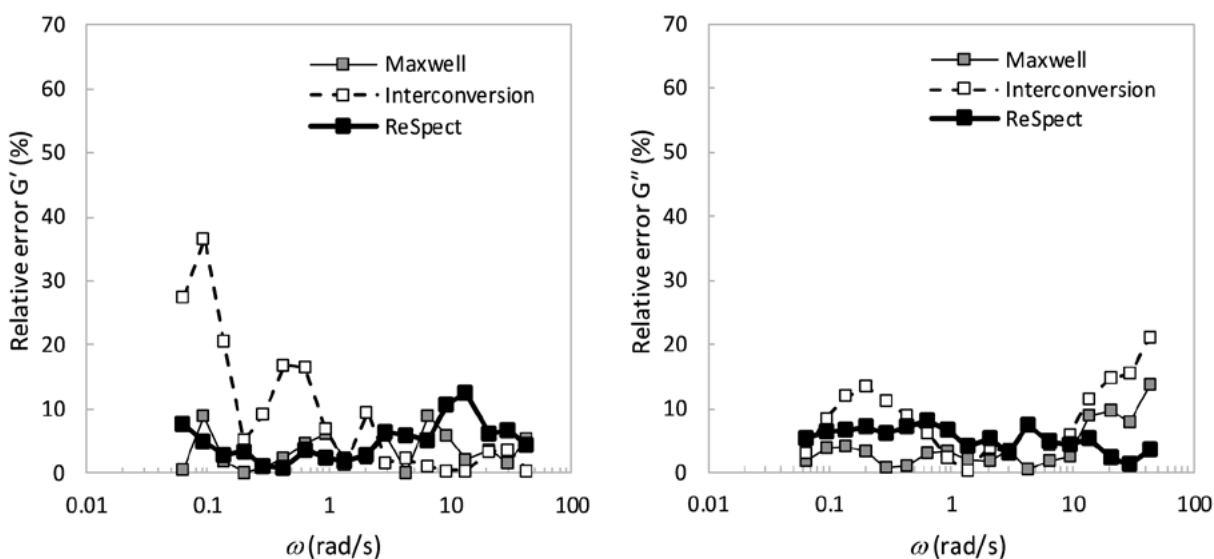


Fig. 7. The relative errors for reconstructed storage moduli (left) and loss moduli (right) as functions of frequency for Na CMC.

Fig. 5 that for gellan the error increased to 15 %, and even up to 20 % for certain frequencies.

At the same time, the numerical analysis showed that the computation of the relaxation spectra using interconversion between material functions demonstrated much lower capabilities in case of three materials, *i.e.*, welan, xanthan and Na CMC, *see, e.g.*, diagrams in Fig. 4, on the right, Fig. 6, on the right, and Fig. 7, on the left. Relative errors for reconstructing loss moduli of welan and xanthan, and the storage modulus of Na CMC are extremely high.

The effect of the calculus scheme on the accuracy of calculating relaxation spectra for polysaccharides, and consequently on the quality of approximation of the dynamic moduli is even more vividly demonstrated via diagrams containing the experimental data of storage and loss moduli of welan and their appropriate approximations with the help of all three approaches described in Section 3, as shown in Fig. 8.

It is necessary to point out that the value of relative errors for approximation of the dynamic relaxation moduli is not the only criteria for a goodness of the selected mathematical approach. Regardless the fact that applying generalized Maxwell model and the commercial software ReSpect for calculating relaxation spectra we obtain relatively small errors of approximation, in some cases the reconstructed dynamic moduli from the calculated spectra do not satisfy general necessary conditions required by the theory of viscoelasticity.

Indeed, in the case of welan the reconstructed curves of storage and loss moduli using the relaxation spectrum calculated with the help of generalized Maxwell model and presented in Fig. 3a, are non-monotonic, see Fig. 8, whereas accordingly to the theory of viscoelasticity the material functions for all polymeric materials must be smooth and monotonic. Similar is valid for the reconstructed curves of storage and loss moduli using relaxation spectrum calcu-

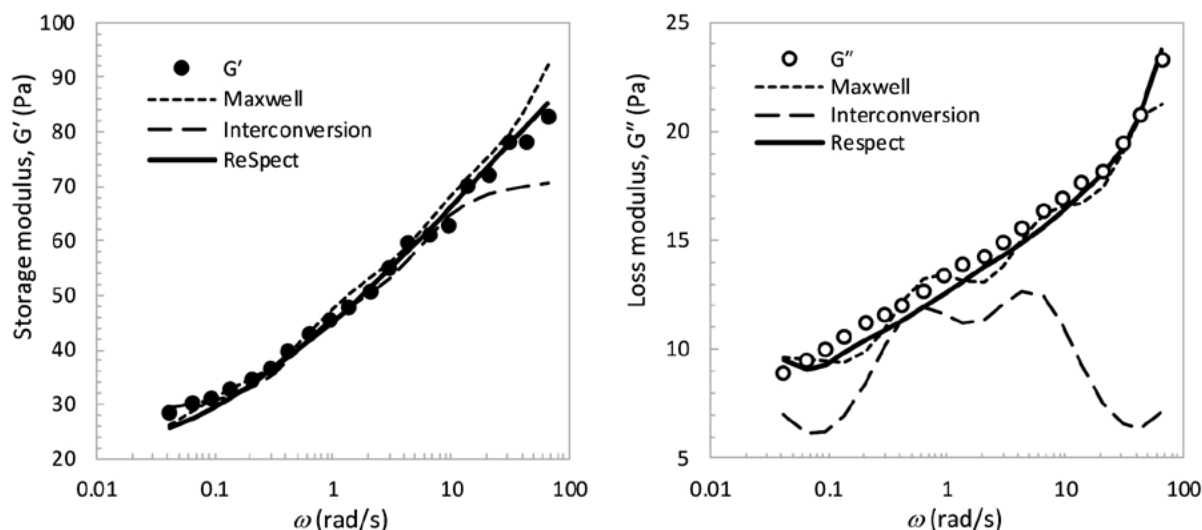


Fig. 8. The experimental data on the storage moduli (left) and the loss moduli (right) for wellan and their corresponding approximations.

lated with the help of interconversion between material functions.

Note as well that the error curves presented in Figs. 4–7 are non-monotonic within the whole frequency range under investigation. The reason for that could be experimental errors in discrete values of storage and loss moduli determined in the oscillatory shear conditions. It is known that the determination of the discrete relaxation spectra from the point of view of a mathematical problem statement is an ill-posed problem, and consequently may cause significant errors in the predicted data of the dynamic moduli even if the experimental data errors are relatively small.

One may observe that the best methodology for reconstructing material functions curves is Honerkamp & Weese method with combination of calculating continuous and discrete spectra. It is known from practical application of the theory of viscoelasticity that for accurate spectra calculation in order to provide more exact approximation of relaxation curves, it is required to obtain experimental data for the “complete” curve, *i.e.*, including the whole frequency range from the glassy state to the rubbery state. In this regard, truncation errors, *i.e.*, the absence of information outside of the experimentally obtained dynamic moduli, play an important role. The truncation errors always occur because we never have experimental information extending from $\omega = 0$ to $\omega = \infty$.

5. Conclusions

Three different numerical methodologies for calculating relaxation spectra of water-based polysaccharide systems were compared. The experimental data of frequency dependent shear storage modulus and shear loss modulus for three different microbial extracellular poly-

saccharides, *i.e.*, gellan, welan and xanthan, and one water-soluble cellulose derivative, *i.e.*, sodium carboxymethylcellulose (Na CMC), were used for the numerical analysis.

All three numerical approaches demonstrated significant differences in the resulted calculated spectra for each of the materials. Moreover, error analysis for reconstructing storage and loss moduli as functions of frequency showed that the contribution from all three applied numerical approaches to approximation accuracy differ for the studied materials. Therefore, we may conclude that there is no any unique mathematical approach for calculating relaxation spectra for polysaccharides that ensure satisfactory approximation of the experimentally determined dynamic moduli for any polymeric material.

The results showed that the application of Honerkamp & Weese method with combination of calculating continuous and discrete spectra demonstrated significantly better prediction of polymer dynamic response in the sense of better accuracy in approximation of the dynamic moduli.

Based on the systematically performed numerical analysis, for practical purposes, one may recommend applying combination of different numerical schemes in parallel, *i.e.*, different methodologies, for calculating relaxation spectra with the aim of proper approximation of dynamic material functions such as relaxation modulus.

6. References

1. F. J. Stadler, *Korea Aust. Rheol. J.* **2012**, 24(3), 199–203. DOI:10.1007/s13367-012-0024-z
2. W. Thimm, C. Friedrich, M. Marth, J. Honerkamps, *J. Rheol.* **1999**, 43, 1663. DOI:10.1122/1.551066
3. C. Friedrich, R. J. Loy, R. S. Anderssen, *Rheol. Acta* **2009**, 48,

- 151–162. DOI:10.1007/s00397-008-0314-z
4. M. R. Nobile, F. Cocchini, *Rheol. Acta* **2008**, 47, 509–519. DOI:10.1007/s00397-007-0228-1
 5. R. Lapasin, S. Pricl, *Rheology of Industrial Polysaccharides: Theory and Applications*, Blackie Academic & Professional, Glasgow, **1995**. DOI:10.1007/978-1-4615-2185-3
 6. L. Xu, G. Xu, T. Liu, Y. Chen, H. Gong, *Carbohydr. Polym.* **2013**, 92(1), 516–522. DOI:10.1016/j.carbpol.2012.09.082
 7. T. Lim, J. T. Uhl, R. K. Prud'homme, *J. Rheol.* **1984**, 28, 367–379. DOI:10.1122/1.549757
 8. K.-W. Song, H.-Y. Kuk, G.-S. Chang, *Korea Aust. Rheol. J.* **2006**, 18(2), 67–81.
 9. E. Choppe, F. Puaud, T. Nicolai, L. Benyahia, *Carbohydr. Polym.* **2010**, 82, 1228–1235. DOI:10.1016/j.carbpol.2010.06.056
 10. L. Fagioli, L. Pavoni, S. Logrippo, C. Pelucchini, L. Rampoldi, M. Cespi, G. Bonacucina, L. Casettari, *J. Food Sci.* **2019**, 84(1), 65–72.
 11. J. Honerkamp, J. Weese, *Macromolecules* **1989**, 22, 4372–4377. DOI:10.1021/ma00201a036
 12. M. Baumgaertel, H. H. Winter, *J. Non-Newtonian Fluid Mech.* **1992**, 44, 15–36. DOI:10.1016/0377-0257(92)80043-W
 13. I. Emri, N.W. Tschoegl, *Int. J. Solids Struct.* **1995**, 32(6/7), 817–826. DOI:10.1016/0020-7683(94)00162-P
 14. A. Ya. Malkin, *Int. J. Appl. Mech. Eng.* **2006**, 11(2), 235–243.
 15. V. Shtrauss, A. Kalpinsh, *WSEAS Trans. Appl. Theor. Mech.* **2012**, 7(1), 29–38.
 16. J.-E. Bae, K. S. Cho, *J. Rheol.* **2015**, 59, 1081. DOI:10.1122/1.4922851
 17. A. Zupančič, M. Žumer, *Acta Chim. Slov.* **2001**, 48, 469–486. DOI:10.36576/summa.7701
 18. U. Florjancic, A. Zupancic, M. Zumer, *Chem. Biochem. Eng. Q.* **2002**, 16(3), 105–118.
 19. J. M. Quintana, A. N. Califano, N. E. Zaritzky, P. Partal, J. M. Franco, *J. Texture Stud.* **2002**, 33, 215–236. DOI:10.1111/j.1745-4603.2002.tb01346.x
 20. I. C. F. Moraes, L. H. Fasolin, R. L. Cunha, F. C. Menegalli, *Brazilian J. Chem. Eng.* **2011**, 28(3), 483–494. DOI:10.1590/S0104-66322011000300014
 21. G. Lorenzo, N. Zaritzky, A. Califano, *Food Hydrocoll.* **2013**, 30, 672–680. DOI:10.1016/j.foodhyd.2012.08.014
 22. R. Lapasin, D. Mercuri, F. Segatti, G. De Conti, M. Grassi, M. Abrami, *Chem. Biochem. Eng. Q.* **2018**, 32(4), 439–449.
 23. M. Berta, J. Moser, P. Lopez-Sanchez, M. Stading, *Annual Transactions of the Nordic Rheology Society* **2018**, 26, 183–186.
 24. A. Jaishankar, G. H. McKinley, *J. Rheol.* **2014**, 58(6), 1751–1788. DOI:10.1122/1.4892114
 25. I. Emri, N. W. Tschoegl, *Rheol. Acta* **1993**, 32, 311–321. DOI:10.1007/BF00434195
 26. S. Poudel, S. Shanbhag, *Korea Aust. Rheol. J.* **2022**, 34, 369–379. DOI:10.1007/s13367-022-00041-y
 27. K. Ninomiya, J. D. Ferry, *Colloid Sci.* **1959**, 14(1), 36–48. DOI:10.1016/0095-8522(59)90067-4
 28. J. Honerkamp, J. Weese, *Rheol. Acta* **1993**, 32, 65–73. DOI:10.1007/BF00396678
 29. S. Shanbhag, ReSpect v2.0, MATLAB Central File Exchange, **2020**, <https://www.mathworks.com/matlabcentral/fileexchange/54322-respect-v2-0>, (assessed: May 30, 2022).
 30. A. Takeh, S. Shanbhag, *Appl. Rheol.* **2013**, 23(2), 24628.
 31. A. R. Davies, R. S. Anderssen, *J. Non-Newtonian Fluid Mech.* **1997**, 73(1), 163–179. DOI:10.1016/S0377-0257(97)00056-6

Povzetek

Pri polimernih materialih relaksacijski spekter vsebuje popolne informacije o časovno odvisnem delu odziva materiala. Z analizo eksperimentalnih podatkov za štiri vrste polisaharidov raziskujemo prispevek različnih numeričnih shem, tj. različnih metod rekonstrukcije dinamičnega relaksacijskega modula, k natančnosti aproksimacije z izračunom pripadajočih relaksacijskih spektrov. Ugotovljeno je bilo, da ne obstaja edinstven matematični pristop za izračun relaksacijskih spektrov, ki bi zagotavljal zadovoljivo aproksimacijo eksperimentalno določenih dinamičnih modulov za izbrane vrste polimernih materialov. Priporočljivo je vzporedno kombinirati različne numerične metode, da dosežemo razumno aproksimacijo funkcij materiala.



Except when otherwise noted, articles in this journal are published under the terms and conditions of the Creative Commons Attribution 4.0 International License

Scientific paper

Copper and Magnetic Activated Carbon Nanocomposites: Application as Recoverable Catalyst for C–S Coupling Reaction

Vajihe Nejadshafiee,^{1,2,*} Ehsan Ghonchepour,¹ Hojatollah Khabazzadeh,¹ Shahrzad Mahdavi Aliabad,¹ Fatemeh Hassani Bagheri¹ and Mohammad Reza Islami¹

¹ Chemistry Department, Shahid Bahonar University of Kerman, Kerman 76169, Iran.

² Central Lab, Vali-e-Asr University, 77176, Rafsanjan, Iran.

* Corresponding author: E-mail: nejadshafiee@sci.uk.ac.ir
Tel: +98 034 31312200

Received: 08-13-2022

Abstract

In this study, activated carbon (AC) was prepared from pistachio nut shell precursor as agricultural by-product. The prepared AC was used to synthesize an efficient nanocomposite via loading of the copper metal and magnetic nanoparticles (Cu-MAC@C₄H₈SO₃H NCs) onto its structure. The structure of the nanocatalyst was characterized by different methods such as FT-IR, TEM, EDS, XRD, VSM, and TGA analysis. The catalytic activity of the prepared composite was tested in a special C–S coupling, namely with the reaction of 2-mercapto-3-phenylquinazolin-4(3H)-one with iodobenzene or bromobenzene. The products of the aryl thioquinazoline derivatives were obtained in good yields and in short reaction times and the products were characterized with ¹H, ¹³C NMR and CHNS analysis. On the other hand, with easy and high recovery of Cu-MAC@C₄H₈SO₃H NCs through magnetic separation, a simple and green method to enhance the efficiency of the nanocatalyst has been provided. The nanocatalyst was reused in the next reaction in up to five cycles without obvious activity decrease.

Keywords: Magnetic nanoparticles, C–S coupling, green catalyst, quinazoline, activated carbon.

1. Introduction

According to the environmental movement of the 1960s, green chemistry prevents pollution by avoiding toxic and hazardous substances and minimizing waste in the production and application of chemical products.¹ In recent years, chemists and engineers have been involved in the development of chemical products and processes that do not interfere with the environment or human health. The results of these research show that one of the fundamental pillars of green chemistry is the application of catalysts that can improve the chemical products and processes and reduce or eliminate the use and generation of hazardous substances.^{2–4} The fundamental properties of green catalysts are high stability, high activity, low preparation cost, great selectivity, easy and efficient recoverability and good recyclability. According to mentioned proper-

ties, heterogeneous catalysts can be good choice because they can be prepared via straightforward experimental procedures, they can be used under mild reaction conditions, their reusability is good and minimal waste disposal is needed.^{5–13} Two general strategies have been identified to facilitate catalyst recovery and reuse: the use of biphasic solvent systems and the use of heterogeneous or solid catalysts.¹⁴ One of the most important factors in the preparation of solid catalysts is the supporting of catalyst by magnetic nanoparticles, which can be easily separated from the reaction mixture by an external magnet. Activated carbon has been included in various chemical processes such as adsorbent for adsorption processes and as a suitable solid bed for the preparation of heterogeneous catalysts in organic reactions due to its remarkable physical and chemical characteristics.^{15–18} To improve the catalytic activity, recent studies have focused on supporting magnetic nano-

particles onto AC structure. By impregnating magnetic nanoparticles into AC, the characteristics of the resulting surface are modified so that there are a large number of active sites that can increase the catalytic capacity.¹⁹ In particular, magnetic nanoparticles-loaded AC can be easily and quickly separated by using an external magnet.

Quinazoline is an aromatic heterocycle with a bicyclic structure consisting of two fused six-membered aromatic rings, a benzene ring and a pyrimidine ring. The synthesis of quinazoline compounds has received special attention from researchers because some quinazoline systems are biologically active and pharmaceutically useful, possessing antifungal,^{20,21} anti-HIV,²² antiviral,²³ antimalarial,²⁴ anti-inflammatory,²⁵ and antibacterial²⁶ activities. For example, Gefitinib can bind to the ATP-binding site of EGFR, thus inactivating the anti-apoptotic Ras signal transduction cascade preventing further growth of cancer cells, and Lapatinib eliminates the growth of breast cancer stem cells that cause tumor growth, and Erlotinib binding to the ATP-binding sites of the EGFR receptors prevents EGFR from producing phosphotyrosine residues.^{27–29}

Herein, we report the preparation of modified magnetic activated carbon (MAC) with 1,4-butane sultone and copper (Cu-MAC@C₄H₈SO₃H NCs). Then the nanocomposites were studied for their catalytic activity in C–S coupling reaction for the synthesis of aryl thioquinazoline derivatives and the results exhibited an excellent catalytic activity in the reaction. The nanocomposite structure was characterized systematically by different techniques such as FT-IR, TEM, EDX, XRD, VSM and TGA.

2. Experimental Section

2.1. Materials

All solvents and reagents were directly used in analytical grade purity without further purification. All experiments were performed using deionized water (DI).

2.2. Synthesis of MAC@C₄H₈SO₃H NCs

The dried pistachio nut shells were firstly crushed into dimensions 1–2 mm and carbonized at 700 °C for 1.5 h. Then, the carbon was activated under steam at 900 °C for 10 h duration. To increase the active sites on the AC, firstly, the AC (1.5 g) was stirred in HCl solution (0.05 M, 15 mL) for 48 h and then immersed into HNO₃ solutions (50%, then 69%) at 50 °C for 10 h, finally, the obtained AC was washed with the DI water three times and dried at 40 °C for 12 h.

Preparation of MAC: FeCl₃·6H₂O (50 mL, 0.3 M) was added to a dilute solution of HCl (0.5 mL, 0.2 M) and the reaction flask was placed in the ultrasonic probe and irradiated at 80 kHz for 5 min. Then Na₂SO₃ (20 mL, 0.3 M) was added into 40 mL of the above solution, after 5 min under ultrasound irradiation, the AC (1 g) was added to the reaction mixture. In the following, the resulting mix-

ture was poured to the solution containing water and ammonia (400 mL, 60 mL) and was sonicated for 30 min. Finally, the obtained magnetic dispersion was subjected to magnetic separation with a magnet, washed with water three times, and dried under vacuum at 60 °C for 12 h.

Preparation of MAC@C₄H₈SO₃H NCs: compound 1,4-butane sultone (5.75 mmol) was added to a KCl solution (0.575 M) and was sonicated for 20 min. Then the dispersed MAC (0.2 g in EtOH (10 mL)) was added to the above mixture and the reaction was stirred for 4 h at 60 °C. After this time the reaction was continued for 10 h at room temperature. The magnetic product (MAC@C₄H₈SO₃H NCs) was separated by an external magnet and washed with DI water and dried under vacuum in an oven.

2.3. Synthesis of Cu-MAC@C₄H₈SO₃H NCs

The MAC@C₄H₈SO₃H nanocomposite (0.5 g) was added to a mixture of 134 mg of copper(II) chloride and 50 mL solvent (H₂O/MeOH 1:1). The mixture was continuously stirred for 24 h at room temperature. The final product (Cu-MAC@C₄H₈SO₃H NCs) was separated by an external magnet and washed with DI water and dried under vacuum oven.

General Procedure for the Synthesis of Aryl Thioquinazoline Derivatives in the Presence of Cu-MAC@C₄H₈SO₃H NCs

To a solution of arylhalide compound (0.5 mmol), 2-mercapto-3-phenylquinazolin-4(3*H*)-one (0.5 mmol) and 0.75 mmol K₂CO₃ in 1.5 mL DMF was added, followed by 20 mg of the catalyst Cu-MAC@C₄H₈SO₃H. The mixture was heated and stirred at 110 °C for 4 h. The progress of the reaction was monitored by TLC. After 4 h, the nanoparticles were separated with an external magnet from the reaction mixture and washed with DI water and diethyl ether. Water (50 mL) was added to the reaction mixture and extracted with CH₂Cl₂ (2×25 mL) and dried over Na₂SO₄. The solvent was removed under reduced pressure to give the crude product. The residue was subjected to column chromatography using mixture of *n*-hexane and ethyl acetate as the eluent to afford pure product.

3-Phenyl-2-(phenylthio)quinazoline-4-(3*H*)-one (3a).

White solid, m.p. 149–152 °C. IR (KBr): 3057, 2921, 1691, 1626, 1541, 1465, 1295, 1257, 1202, 767 cm⁻¹, ¹H NMR (400 MHz, CDCl₃): δ 8.24 (s, 1H, ArH), 7.58–7.56 (m, 4H, ArH), 7.42–7.33 (m, 4H, ArH); ¹³C NMR (100 MHz, CDCl₃): δ 161.9, 157.1, 147.7, 136.0, 135.7, 134.4, 130.0, 129.7, 129.6, 129.3, 129.0, 128.6, 127.1, 126.7, 125.9, 119.9. Anal. calcd for C₂₀H₁₄N₂OS (330.40): C, 72.70; H, 4.27; N, 8.48; S, 9.70; found: C, 72.77; H, 4.55; N, 8.15; S, 9.88.

2-((4-Methoxyphenyl)thio)-3-phenylquinazoline-4-(3*H*)-one (3b).

White solid, m.p. 150–152 °C. IR (KBr):

3065, 1728, 1626, 1573, 1468, 1250, 1173, 690 cm^{-1} . ^1H NMR (400 MHz, CDCl_3): δ 8.22 (s, 1H, ArH), 7.63–7.61 (m, 3H, ArH), 7.60–7.58 (m, 2H, ArH), 7.45–7.42 (m, 4H, ArH), 7.37–7.352 (m, 2H, ArH), 7.45–7.42 (m, 4H, ArH), 6.95 (d, 1H, ArH), 3.85 (s, 1H, OCH_3); ^{13}C NMR (100 MHz, CDCl_3): δ 161.9, 160.7, 157.7, 147.7, 137.3, 135.9, 134.3, 129.9, 129.6, 129.2, 126.9, 125.8, 119.8, 119.1, 114.6, 55.3. Anal. calcd for $\text{C}_{21}\text{H}_{16}\text{N}_2\text{O}_2\text{S}$ (360.43): C, 69.98; H, 4.47; N, 7.77; S, 8.90; found: C, 69.84; H, 4.54; N, 7.97; S, 8.50.

3-Phenyl-2-(*p*-tolylthio)quinazoline-4-(3*H*)-one (3c). White solid, m.p. 151–153 °C. IR (KBr): 3066, 1682, 1573, 1464, 1256, 1197, 766 cm^{-1} . ^1H NMR (400 MHz, CDCl_3): δ 8.23 (s, 1H, ArH), 7.65–7.57 (m, 3H, ArH), 7.45–7.42 (m, 4H, ArH), 7.37–7.36 (m, 3H, ArH), 7.26–7.23 (m, 2H, ArH), 2.42 (s, 1H, CH_3); ^{13}C NMR (100 MHz, CDCl_3): δ 162.1, 157.6, 147.9, 139.9, 136.2, 135.3, 130.1, 129.9, 129.4, 127.2, 126.8, 126.0, 120.1, 21.5. Anal. calcd for $\text{C}_{21}\text{H}_{16}\text{N}_2\text{OS}$ (344.43): C, 73.23; H, 4.68; N, 8.13; S, 9.31; found: C, 72.99; H, 4.67; N, 8.23; S, 9.10.

2-((4-Nitrophenyl)thio)-3-phenylquinazoline-4-(3*H*)-one (3d). Orange solid, m.p. 153–155 °C. IR (KBr): 3104, 2974, 2925, 1690, 1548, 1511, 1466, 1343, 1258, 1050, 769 cm^{-1} . ^1H NMR (400 MHz, CDCl_3): δ 8.27–8.25 (m, 2H, ArH), 8.23 (m, 1H, ArH), 7.76–7.74 (m, 2H, ArH), 7.68 (m, 1H, ArH), 7.62–7.61 (m, 2H, ArH), 7.44–7.42 (m, 4H, ArH), 7.37–7.35 (m, 1H, ArH); ^{13}C NMR (100 MHz, CDCl_3): δ 161.0, 154.5,

147.7, 146.7, 136.5, 134.3, 135.0, 134.2, 129.8, 129.3, 128.6, 125.9, 123.2, 119.5. Anal. calcd for $\text{C}_{20}\text{H}_{13}\text{N}_3\text{O}_3\text{S}$ (344.43): C, 63.99; H, 3.49; N, 11.19; S, 8.54; found: C, 63.77; H, 3.44; N, 11.31; S, 8.84.

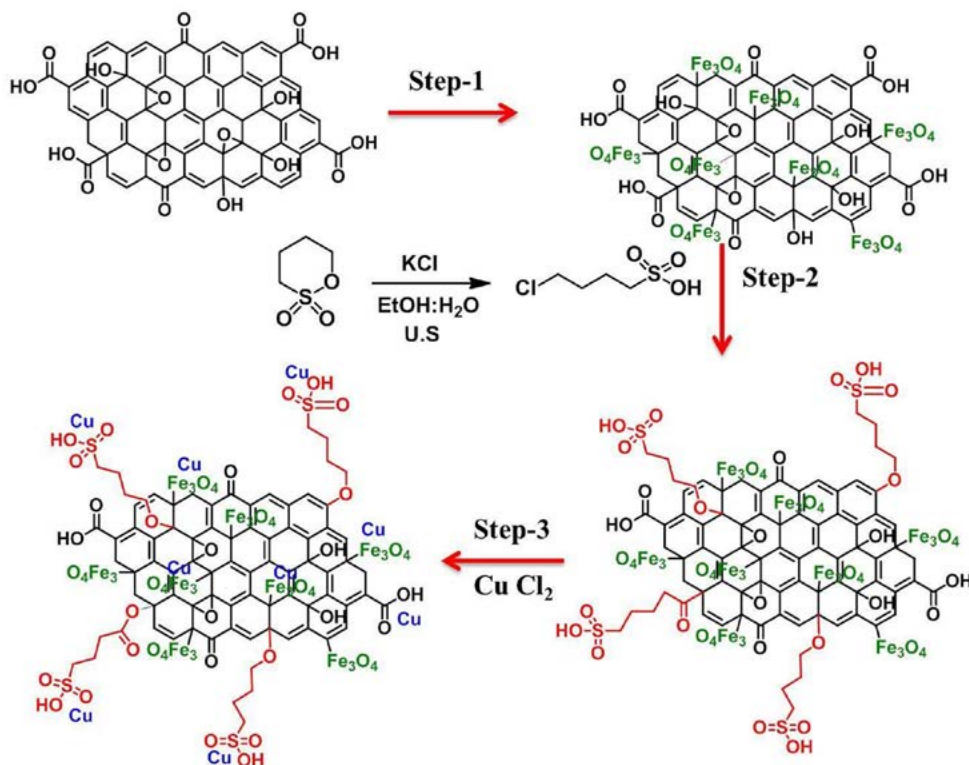
2-((4-Bromophenyl)thio)-3-phenylquinazoline-4-(3*H*)-one (3e). White solid, m.p. 154–156 °C. IR (KBr): 3067, 1695, 1549, 1466, 1260, 1110, 765 cm^{-1} . ^1H NMR (400 MHz, CDCl_3): δ 8.23 (m, 1H, ArH), 7.66–7.64 (m, 1H, ArH), 7.61–7.58 (m, 2H, ArH), 7.57–7.55 (m, 2H, ArH), 7.43–7.36 (m, 7H, ArH); ^{13}C NMR (100 MHz, CDCl_3): δ 161.6, 156.2, 147.4, 137.0, 135.6, 132.0, 129.6, 129.0, 127.5, 126.9, 126.5, 125.9, 124.1, 119.8. Anal. calcd for $\text{C}_{20}\text{H}_{13}\text{BrN}_2\text{O}_3\text{S}$ (409.30): C, 58.69; H, 3.20; N, 6.84; S, 7.83; found: C, 58.92; H, 3.24; N, 6.91; S, 7.55.

3. Results and Discussion

The synthesis of Cu-MAC@ $\text{C}_4\text{H}_8\text{SO}_3\text{H}$ NCs catalyst, along with the growth of Fe_3O_4 NPs and the loading of $\text{C}_4\text{H}_8\text{SO}_3\text{H}$ and copper onto AC is shown in Scheme 1.

3. 1. Characterization

FT-IR spectra were recorded on a commercial spectrophotometer (Bruker Tensor 27 FT -IR). ^1H and ^{13}C NMR spectra were recorded on a Bruker 400 Ultrashield NMR Magnet (400 MHz for ^1H NMR) with TMS as the internal standard. Powder X-ray diffraction (XRD) spectra



Scheme 1. Synthesis steps of Cu-MAC@ $\text{C}_4\text{H}_8\text{SO}_3\text{H}$ NCs.

were recorded at room temperature with a Philips X-Pert 1710 diffractometer using Co K α ($\lambda = 1.78897 \text{ \AA}$) at a voltage of 40 kV and a current of 40 mA and data were collected from 10° to 90° (2θ) with a scan speed of 0.02° s . The morphology of the catalyst was studied using scanning electron microscopy (SEM; Philips XL 30 and S-4160) with coated gold equipped with dispersive X-ray spectroscopy capability. Thermogravimetric analysis (TGA) and differential thermal analysis (DTA) were performed using a thermal analyzer with a heating rate of $20 \text{ }^\circ\text{C/min}$ in a temperature range of $25\text{--}1100 \text{ }^\circ\text{C}$ under flowing compressed nitrogen. The magnetic properties of the catalyst were measured with a vibrating sample magnetometer (VSM).

The FT-IR spectrum of the AC exhibits the bands corresponding to the functionalities containing hydroxyl OH group ($\sim 3442 \text{ cm}^{-1}$), carboxyl C=O group ($\sim 1719 \text{ cm}^{-1}$), C=C ($\sim 1577 \text{ cm}^{-1}$), C–O group ($\sim 1384 \text{ cm}^{-1}$) (Figure 1a). The presence of Fe–O band ($\sim 673 \text{ cm}^{-1}$) in the FT-IR spectrum of Fe $_3$ O $_4$ NPs@AC confirms that the Fe $_3$ O $_4$ NPs are located on the AC structure (Figure 1b). In the Figure 1c, the new bands observed at 2919 cm^{-1} and 1036 cm^{-1} due to the stretching vibrations of sp^3 C–H and C–S bands respectively prove that 1,4-butane sultone was loaded on the MAC@C $_4$ H $_8$ SO $_3$ H. Furthermore, the FT-IR spectrum of Cu-MAC@C $_4$ H $_8$ SO $_3$ H NCs exhibits a new absorption band at 583 cm^{-1} due to the presence of copper in the structure (Figure 1d).

Figure 2 illustrates the XRD patterns of AC, MAC and MAC@C $_4$ H $_8$ SO $_3$ H. A broad diffraction peak was obtained at $2\theta = 25.31^\circ$ for AC due to the plane of amorphous activated carbon. In XRD patterns of MAC, some peaks appeared at 30.51° , 35.81° , 43.51° , 54.15° , 57.46° , 63.06° and 74.60° related to the cubic spinel structure of magnetic

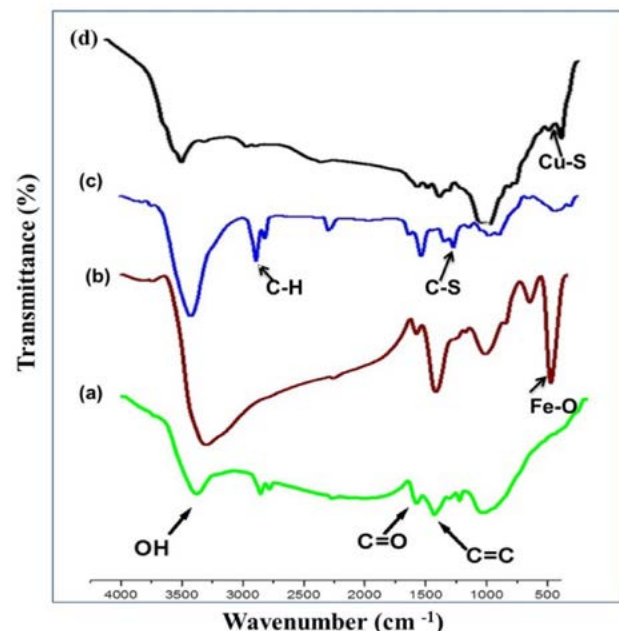


Figure 1. FTIR spectra of (a) AC, (b) MAC (c) MAC@C $_4$ H $_8$ SO $_3$ H and (d) Cu-MAC@C $_4$ H $_8$ SO $_3$ H NCs.

nanoparticles. The XRD pattern of MAC@C $_4$ H $_8$ SO $_3$ H was almost similar to the MAC but the intensity of peaks decreased which could be related to immobilizing of C $_4$ H $_8$ SO $_3$ H onto MAC.

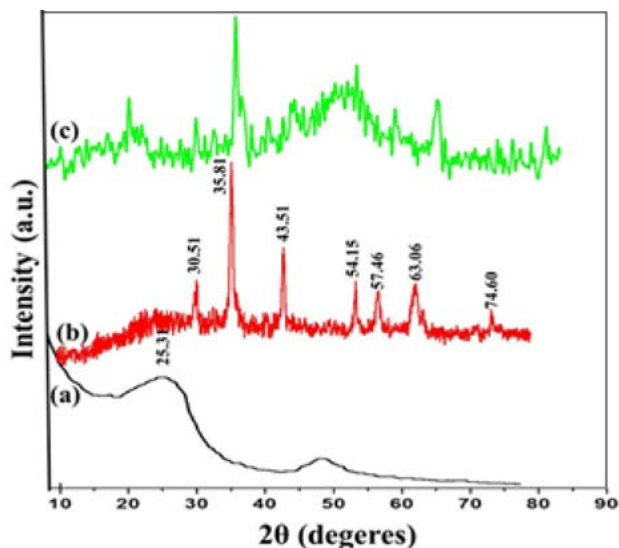


Figure 2. XRD patterns of (a) AC, (b) MAC and MAC@C $_4$ H $_8$ SO $_3$ H.

The morphology of AC, MAC and MAC@C $_4$ H $_8$ SO $_3$ H were deduced by TEM analysis and the TEM images are shown in Figure 3. The mesoporous structure of AC was observed by TEM (Figure 3a). The TEM images of MAC and MAC@C $_4$ H $_8$ SO $_3$ H show that the Fe $_3$ O $_4$ nanoparticles are coated onto AC (Figures 3b–c). Figures 3b and c show that the particle size of MAC@C $_4$ H $_8$ SO $_3$ H is larger than MAC (from 30 to 50 nm, respectively), which could be due to the immobilization of 1,4-butane sultone onto the surface of the MAC.

Thermal stability was studied by thermal gravimetric analysis of AC, MAC, MAC@C $_4$ H $_8$ SO $_3$ H and Cu-MAC@C $_4$ H $_8$ SO $_3$ H NCs (Figure 4). The thermal gravimetric analysis of AC displayed a weight loss below at temperatures of $175 \text{ }^\circ\text{C}$, at $200\text{--}400 \text{ }^\circ\text{C}$, and $500\text{--}750 \text{ }^\circ\text{C}$, which could be ascribed to the loss of adsorbed water (15.43%), exclusion of oxygenated functional groups (8.85%), and ultimately to the decomposition of AC (72.48%), respectively (Figure 4a). The TGA curve of MAC showed a weight loss of about 51.14% (Figure 4b). For MAC@C $_4$ H $_8$ SO $_3$ H a weight loss occurred at $160\text{--}350 \text{ }^\circ\text{C}$ about 4.45%, resulting from the pyrolysis of C $_4$ H $_8$ SO $_3$ H functional groups (Figure 4c). Also, about 40.0% of MAC and H $_3$ NSO $_3$ -MAC NCs retained at $750 \text{ }^\circ\text{C}$, due to the remaining iron oxide. The TGA curve of Cu-MAC@C $_4$ H $_8$ SO $_3$ H showed an increase in temperature to $950 \text{ }^\circ\text{C}$ which is related to the coordination of Cu(II) ions with the active sites of MAC@C $_4$ H $_8$ SO $_3$ H surface. Also, Cu-MAC@C $_4$ H $_8$ SO $_3$ H retained about 64.0% of its weight at

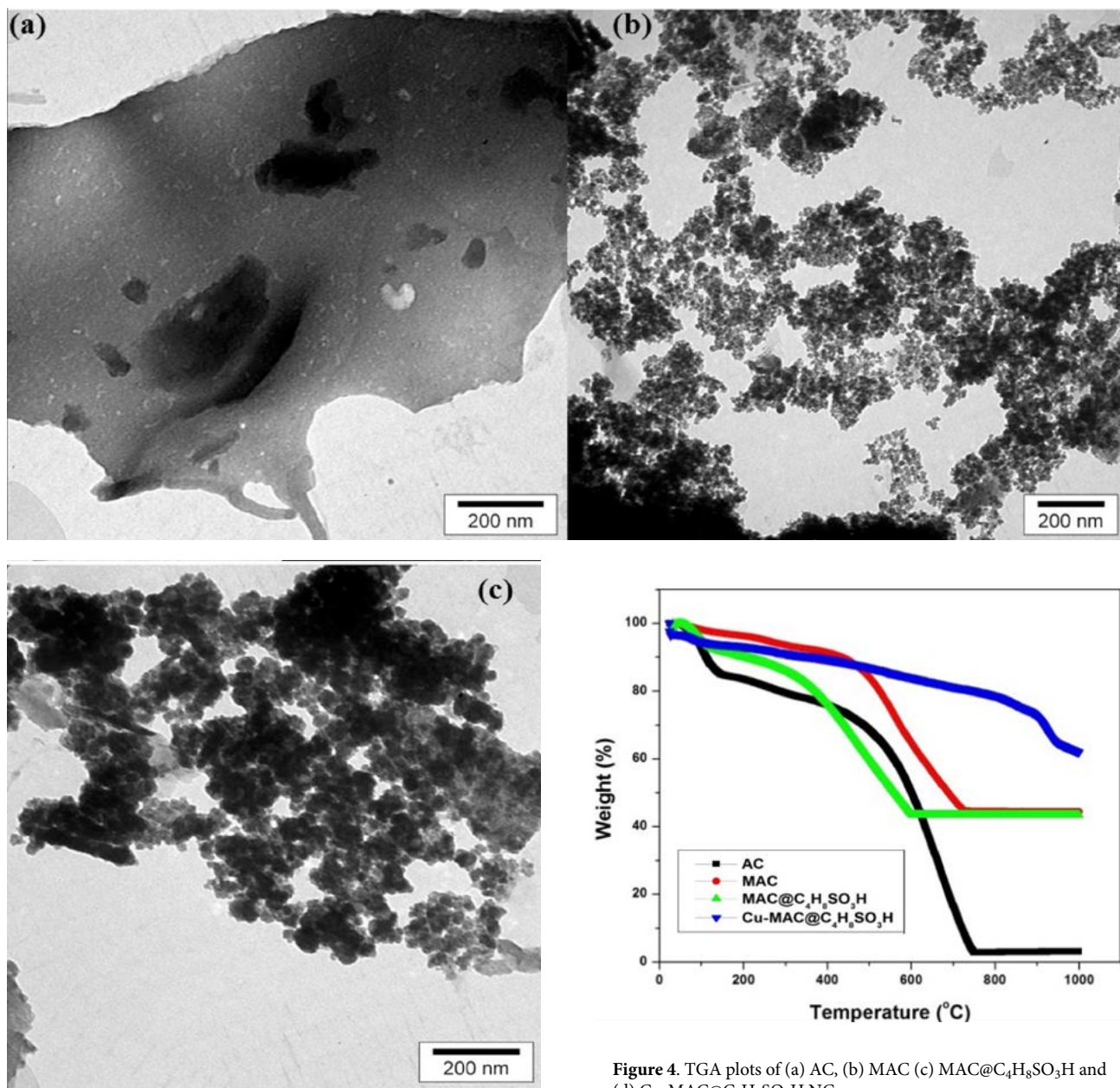


Figure 3. TEM images of, (a) AC (b) MAC (c) MAC@C₄H₈SO₃H NCs.

950 °C, due to the residual of copper oxide and iron oxide (Figure 4d).

The magnetization curves of the MAC, MAC@C₄H₈SO₃H and Cu-MAC@C₄H₈SO₃H NCs are exhibited in Figure 5. The saturation magnetization of the MAC and MAC@C₄H₈SO₃H NCs was 21.73 and 16.33 emu g⁻¹ respectively; showing that this decrease in saturation magnetization can be attributed to the loading of C₄H₈SO₃H on the MAC. Also, the saturation magnetization of the Cu-MAC@C₄H₈SO₃H NCs was 14.23 emu g⁻¹. This observed decrease in magnetic property was due to the loading of copper onto the surface of MAC@C₄H₈SO₃H NCs.

Figure 4. TGA plots of (a) AC, (b) MAC (c) MAC@C₄H₈SO₃H and (d) Cu-MAC@C₄H₈SO₃H NCs.

The presence of Fe₃O₄, sulfamic acid and copper groups on the AC surface was further confirmed by the EDS analysis of the MAC@C₄H₈SO₃H and Cu-MAC@C₄H₈SO₃H NCs (Figure 6).

3. 2. Catalytic Activity

The catalytic activity of Cu-MAC@C₄H₈SO₃H NCs was evaluated by the C–S coupling reaction for the synthesis of aryl thioquinazoline derivatives. The reaction of 2-mercapto-3-phenylquinazolin-4(3H)-one and iodobenzene was chosen to optimize the conditions of reaction and the results are reported in Table 1. Our observations

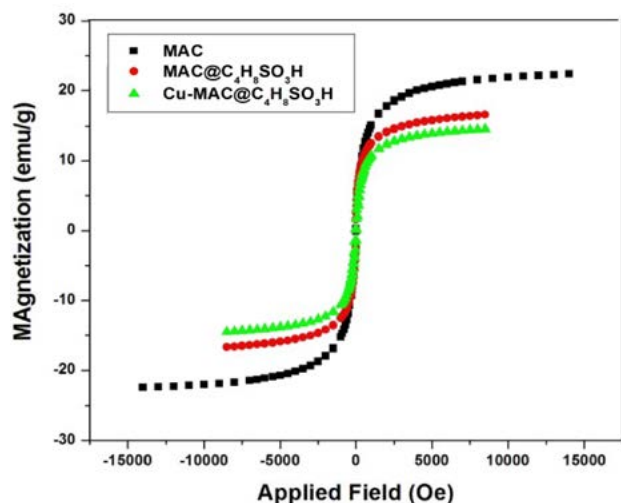


Figure 5. Magnetization curves of MAC, MAC@C₄H₈SO₃H NCs and Cu-MAC@C₄H₈SO₃H NCs.

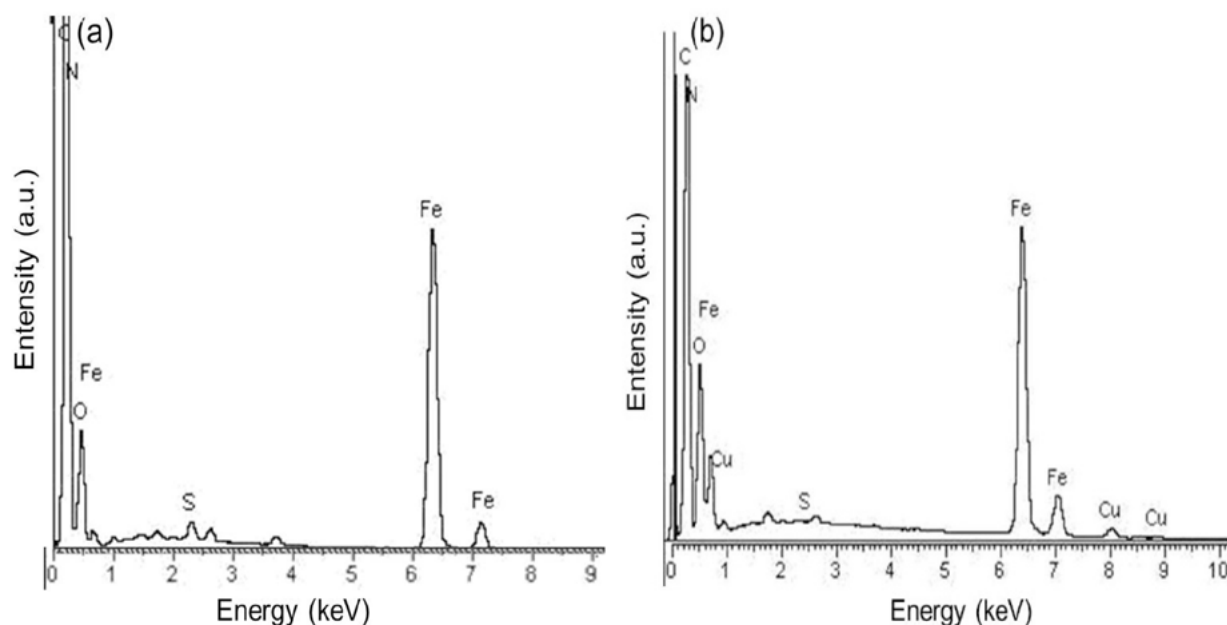


Figure 6. EDS pattern of (a) MAC@C₄H₈SO₃H NCs and (b) Cu-MAC@C₄H₈SO₃H NCs.

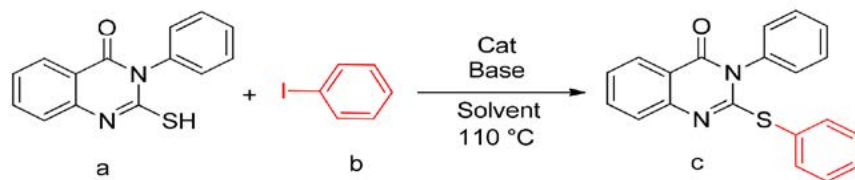
showed that the reaction carried out without catalyst was not successful under the following conditions: 2-mercapto-3-phenylquinazolin-4(3*H*)-one (a) (0.5 mmol, 0.127 g), iodobenzene (b) (0.5 mmol, 0.102 g) and 0.75 mmol (0.104 g) potassium carbonate as a base in 1.5 mL dimethylformamide (DMF) at 110 °C in closed vial for 2 h (Table 1, entry 1). This result confirmed that the catalyst has a vital role in this reaction. In next reaction, the MAC@C₄H₈SO₃H nanocomposites as a catalyst was added to the reaction mixture and only trace yield was observed, but by using Cu-MAC@C₄H₈SO₃H NCs the yield of reaction increased to 55% (Table 1, entries 2 and 3).

To investigate the effect of time on the reaction yield, the reaction was performed for 4 and 6 h, and the results

showed that at this time the reaction had the same yield of 80% and therefore 4 hours was chosen as the optimal time for this reaction (Table 1, entries 4 and 5). Several solvent systems such as DMF, CH₃CN, dioxane, EtOH and H₂O were also tested and the high yield (80% yield) was obtained in DMF (Table 1, entries 6–9). In the next step, the reaction was performed in the presence of various bases such as K₂CO₃, Na₂CO₃, Et₃N, and NaOH among which K₂CO₃ had the best performance (Table 1, entries 4 and 10–12). Also, the reaction was tested in the presence of MAC and MAC@C₄H₈SO₃H NCs as the catalyst for 4 h and no product was detected, so the copper has the important catalytic role in this reaction (Table 1, entries 13 and 14).

According to the optimal conditions, capability and efficiency of Cu-MAC@C₄H₈SO₃H NCs were investigated in this reaction by screening different types of aryl halides and the results are presented in Table 2. In optimal condi-

tion, iodobenzene and bromobenzene were converted into the corresponding aryl thioquinazoline (3a) with 80 and 20% yields, respectively. In this reaction, aryl thioquinazoline was not formed when chlorobenzene was used instead of iodobenzene (Table 2, entries 1–3). The results showed that the methoxy (MeO) group in the *para* position of aryl halide could be effective and increase the yield of the product. For example, the isolated yields of aryl thioquinazoline from the reaction of 4-iodoanisole and 4-bromoanisole were 90 and 40%, respectively (Table 2, entries 4 and 5), while the yield of the corresponding product from 2-methoxyiodobenzene dropped to trace amounts (Table 2, entry 6). 3-Phenyl-2-(*para*-tolylthio)quinazolin-4(3*H*)-one (3d) was obtained from the reaction of 2-mercapto-3-phen-

Table 1. Results of the C–S coupling reaction of 2-mercapto-3-phenylquinazolin-4(3H)-one and iodo-benzene^a

Entry	Catalyst	Solvent	Base	Time (h)	Yield ^b %
1	-	DMF	K ₂ CO ₃	2	0
2	MAC@C ₄ H ₈ SO ₃ H	DMF	K ₂ CO ₃	2	trace
3	Cu-MAC@C ₄ H ₈ SO ₃ H	DMF	K ₂ CO ₃	2	55
4	Cu-MAC@C₄H₈SO₃H	DMF	K₂CO₃	4	80
5	Cu-MAC@C ₄ H ₈ SO ₃ H	DMF	K ₂ CO ₃	6	80
6	Cu-MAC@C ₄ H ₈ SO ₃ H	CH ₃ CN	K ₂ CO ₃	4	50
7	Cu-MAC@C ₄ H ₈ SO ₃ H	Dioxane	K ₂ CO ₃	4	15
8	Cu-MAC@C ₄ H ₈ SO ₃ H	EtOH	K ₂ CO ₃	4	52
9	Cu-MAC@C ₄ H ₈ SO ₃ H	H ₂ O	K ₂ CO ₃	4	0
10	Cu-MAC@C ₄ H ₈ SO ₃ H	DMF	Na ₂ CO ₃	4	trace
11	Cu-MAC@C ₄ H ₈ SO ₃ H	DMF	Et ₃ N	4	5
12	CuMAC@C ₄ H ₈ SO ₃ H	DMF	NaOH	4	5
13	MAC	DMF	K ₂ CO ₃	4	0
14	MAC@C ₄ H ₈ SO ₃ H	DMF	K ₂ CO ₃	4	0

^a Reaction conditions: a (0.5 mmol), b (0.5 mmol), base (0.75 mmol), solvent (1.5 mL), catalyst (20 mg), 110 °C. ^b Isolated yield.

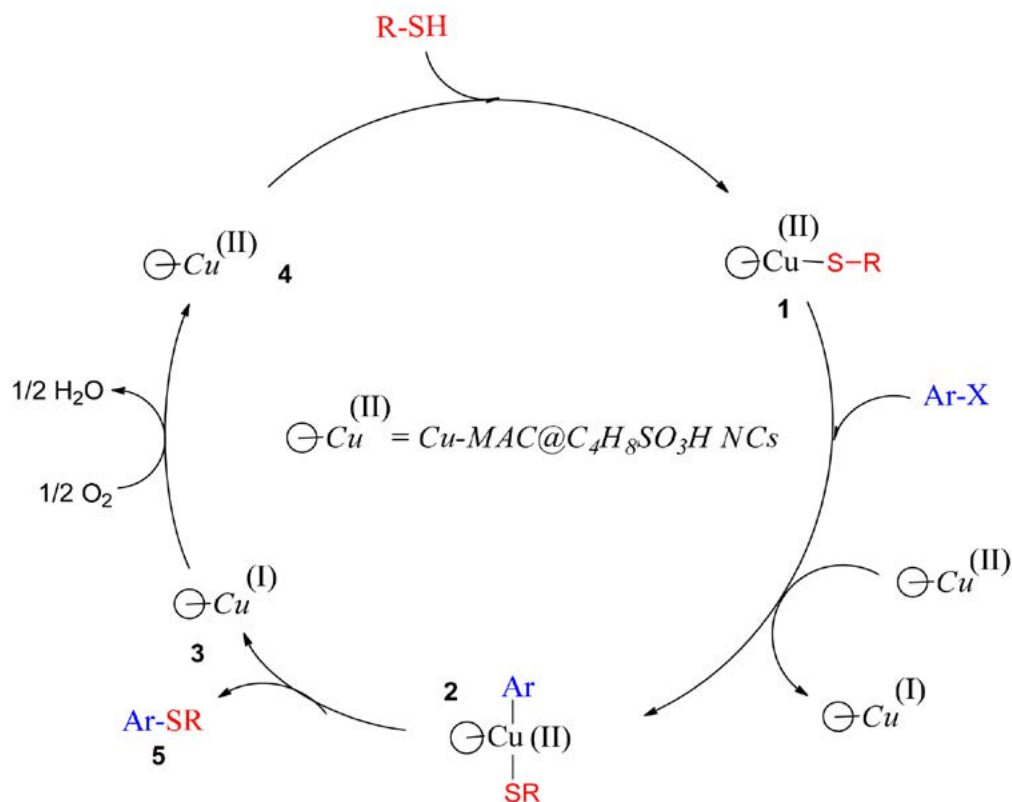
**Scheme 2.** A reasonable mechanism for the formation of product by Cu-MAC@C₄H₈SO₃H NCs.

Table 2. Synthesis of aryl thioquinazoline derivatives.^a

entry	Ar-X	product	yield ^b (g) ^c
1			80% (0.132 g)
2			20% (0.033 g)
3			0
4			90% (0.162 g)
5			40% (0.072 g)
6			Trace
7			83% (0.143 g)
8			20% (0.034 g)
9			94% (0.176 g)
10			74% (0.151 g)

^a Reaction conditions: arylhalide (0.5 mmol), 2-mercapto-3-phenylquinazolin-4(3H)-one (0.5 mmol), K₂CO₃ (0.75 mmol), DMF (1.5 mL), catalyst (20 mg), 110 °C for 4 h. ^b Isolated yield. ^c Yield as mass.

nylquinazolin-4(3H)-one with 4-iodotoluene and 4-bromotoluene in 83 and 20% yields, respectively (Table 2, entries 7 and 8). Also, 2-((4-nitrophenyl)thio)-3-phenylquinazolin-4(3H)-one (**3e**) was formed in 94% yield from the reaction of 4-iodonitrobenzene under the optimal conditions (Table 2, entry 9). This result shows that the electron withdrawing (NO_2) group in the *para* position of iodobenzene can increase the yield of the mentioned product. In the final reaction, 4-iodobromobenzene was tested as the reactant and the corresponding product was isolated as 2-((4-bromophenyl)thio)-3-phenylquinazolin-4(3H)-one (**3f**) with 74% yield (Table 2, entry 10). All products were characterized by FT-IR, ^1H and ^{13}C NMR spectroscopy and CHN analysis data (see supplementary material for details). According to the previous literature, the following reasonable mechanism can be suggested for this reaction (Scheme 2).^{30–32} In the first step of the mechanism transmetalation occurred to produce intermediate I. In the next step, Ar-X is attached to the catalyst and an intermediate (II) is formed. This process continues by the oxidation and reduction of the copper cation and finally conversion to the coupled product **5** and copper(I) completes the catalytic cycle. In the cycle, oxidation of Cu(I) to Cu(II) is done by molecular oxygen from the atmosphere.

3. 3. Reusability of the Catalyst

The reusability of the catalyst was checked in the model reaction. After completion of the reaction and separation of the catalyst by using an external magnet, the composite was washed with DI water and ethyl acetate, dried under vacuum and reused in a subsequent reaction. As shown in Figure 7, there is only a slight decrease in the catalytic capacity after five cycles.

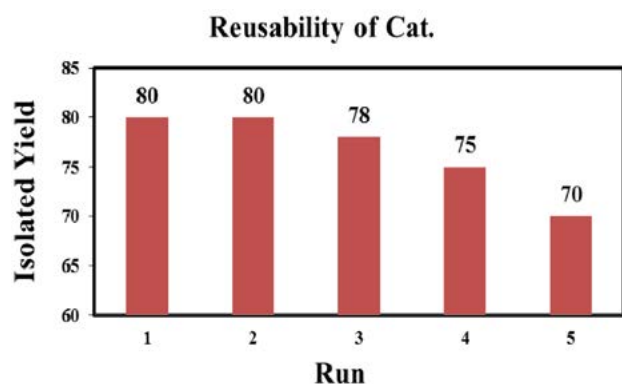


Figure 7. Reusability of Cu-MAC@C₄H₈SO₃H NCs in model reaction.

4. Conclusions

In conclusion, we developed a nanocomposite as an efficient and reusable catalyst, which was prepared from activated carbon as solid phase with loading of copper and

magnetic nanoparticles (Cu-MAC@C₄H₈SO₃H NCs). The catalytic activity of the prepared nanocomposite was tested in a special C–S coupling reaction for the synthesis of aryl thioquinazoline derivatives in short times and high yields. In addition to the efficient and easy recycling, the catalyst can be used on a larger scale, making it a valuable candidate for practical applications.

Acknowledgments

We thank the Shahid Bahonar University of Kerman for financial support.

5. References

- R. A. Sheldon, *Green Chem.* **2016**, *18*, 3180–3183. DOI:10.1039/C6GC90040B
- P. J. Walsh, H. Li, C. A. Parrodi, *Chem. Rev.* **2007**, *107*, 2503–2545. DOI:10.1021/cr0509556
- S. Yenice, C. Maden, N. Cakir, *Clinical Biochem.* **2009**, *4*, 333–342. DOI:10.1016/j.clinbiochem.2008.09.063
- P. T. Anastas, J. C. Warner, *Green Chemistry*, “Green Chemistry” *Frontiers* **1998**, *640*, 1998–2002.
- K. Azizi, E. Ghonchepour, M. Karimi, A. Heydari, *Appl. Organometal. Chem.* **2015**, *29*, 187–194. DOI:10.1002/aoc.3258
- E. Ghonchepour, E. Yazdani, D. Saberi, M. Arefi, A. Heydari, *Appl. Organometal. Chem.* **2017**, *54*, 3822–3830. DOI:10.1002/aoc.3822
- E. Ghonchepour, M. R. Islami, T. A. Momeni, *J. Org. Chem.* **2019**, *883*, 1–10. DOI:10.1016/j.jorgchem.2019.01.008
- F. Nikbakht, E. Ghonchepour, H. Ziyadi, A. Heydari, *RSC Adv.* **2014**, *4*, 34428–34435. DOI:10.1039/C4RA04911J
- E. Ghonchepour, D. Saberi, A. Heydari, *Org. Chem. Res.* **2017**, *3*, 44–49.
- H. Naeimi, V. Nejadshafiee, S. Masoum, *RSC Adv.* **2015**, *5*, 15006–15016. DOI:10.1039/C4RA17229A
- H. Naeimi, V. Nejadshafiee, M. R. Islami, *B C S J.* **2016**, *89*, 212–219. DOI:10.1246/bcsj.20150291
- H. Naeimi, V. Nejadshafiee, M. R. Islami, *Micropor. Mesopor. Mater.* **2016**, *227*, 23–30. DOI:10.1016/j.micromeso.2016.02.036
- H. Naeimi, V. Nejadshafiee, *New J. Chem.* **2014**, *38*, 5429–5435. DOI:10.1039/C4NJ00909F
- P. G. Jessop, *Syn. Org. Chem. Jpn.* **2003**, *61*, 484–495. DOI:10.5059/yukigoseikyokaishi.61.484
- V. Nejadshafiee, M. R. Islami, *Mater. Sci. Eng. C.* **2019**, *101*, 42–52. DOI:10.1016/j.msec.2019.03.081
- M. M. Titirici, *Sustainable carbon materials from hydrothermal processes*, John Wiley & Sons **2013**. DOI:10.1002/9781118622179
- V. Nejadshafiee, M. R. Islami, *Environ. Sci. Pollut. Res.* **2020**, *27*, 1625–1639. DOI:10.1007/s11356-019-06732-4
- V. Nejadshafiee, M. R. Islami, *ChemistrySelect.* **2020**, *5*, 8814–8822. DOI:10.1002/slct.202001801
- F. Maghsoodi Goushki, M. R. Islami, V. Nejadshafiee, *Mater.*

- Sci. Eng. B.* **2022**, *277*, 115591–115601.
DOI:10.1016/j.mseb.2021.115591
20. E. Jafari, M. R. Khajouei, F. Hassanzadeh, G. H. Hakimelahi, G. A. Khodarahmi, *Res. Pharm. Sci.* **2016**, *11*, 1–14.
21. M. M. Ghorab, M. S. Alsaied, *Acta Pharma.* **2015**, *65*, 271–279.
DOI:10.1515/acph-2015-0030
22. A. A. Radwan, F. K. Alanazi, M. H. Al-Agamy, *Braz. J. Pharm. Sci.* **2017**, *53*, 53–60.
23. S. Sangkharomaya, S. Nitayaphan, Research and Operational Support for the Study of Military Relevant Infectious Diseases of Interest to United States and Royal Thai Government; Armed forces research, Royal Thai Army Medical **2002**.
DOI:10.21236/ADA412783
24. T. A. Ignatowski, R. N. Spengler, K. M. Dhandapani, R. F. H. Folkersma, Butterworth, E. Tobinick, *CNS Drugs.* **2014**, *28*, 679–697. DOI:10.1007/s40263-014-0174-2
25. C. B. Ahn, W. K. Jung, S. J. Park, Y. T. Kim, W. S. Kim, J. Y. Je, Gallic Acid-g-Chitosan Modulates Inflammatory Responses in LPS-Stimulated RAW264.7 Cells Via NF- κ B, AP-1, and MAPK Pathways **2016**, *39*, 366–374.
DOI:10.1007/s10753-015-0258-2
26. A. R. Khosropour, H. G. I. Mohammadpoor-Baltork, *Tetrahedron Lett.* **2006**, *47*, 3561–3564.
DOI:10.1016/j.tetlet.2006.03.079
27. E. R. Wood, A. T. Truesdale, O. B. McDonald, D. Yuan, A. Hassell, S. H. Dickerson, B. Ellis, C. Pennisi, E. Horne, K. Lackey, *Cancer Res.* **2004**, *64*, 6652–6659.
DOI:10.1158/0008-5472.CAN-04-1168
28. E. Raymond, S. Faivre, J. P. Armand, *Drugs.* **2000**, *60*, 15–23.
DOI:10.2165/00003495-200060001-00002
29. T. J. Lynch, D. W. Bell, R. Sordella, S. Gurubhagavatula, R. A. Okimoto, B. W. Brannigan, P. L. Harris, S. M. Haserlat, J. G. Supko, F. G. Haluska, *NEJM.* **2004**, *350*, 2129–2139.
DOI:10.1056/NEJMoa040938
30. N. A. Dangroo, T. Ara, B. A. Dar, M. Khuroo, *Catal Commun.* **2019**, *118*, 76–80. DOI:10.1016/j.catcom.2018.10.006
31. C. Sambiagio, S. P. Marsden, A. J. Blacker, P. C. McGowan, *Chem. Soc. Rev.* **2014**, *43*, 3525–3550.
DOI:10.1039/C3CS60289C
32. A. Casitas, X. Ribas, *Chem. Sci.* **2013**, *4*, 2301–2318.
DOI:10.1039/c3sc21818j

Povzetek

V tej študiji smo aktivno oglje (AC) pripravili iz lupin pistacij kot kmetijskega odpadka. Pripravljeno aktivno oglje smo uporabili kot nosilec za vezavo bakrovih in magnetnih nanodelcev in tako sintetizirali učinkovite nanokompozite (Cu-MAC@C₄H₈SO₃H NC). Strukturo nanokatalizatorja smo določili z različnimi metodami, vključno z FT-IR, TEM, EDS, XRD, VSM in TGA analizami. Katalitsko aktivnost pripravljenih kompozitov smo preverili na primeru posebnega C–S spajanja med 2-merkaptto-3-fenilkinazolin-4(3H)-onom in jodo- oz. bromobenzenom. Po kratkih reakcijskih časih smo z dobrimi izkoristki kot produkte izolirali derivate aril tiokinazolinov. Produkte smo karakterizirali s pomočjo ¹H, ¹³C NMR in CHNS elementnih analiz. Ker je recikliranje katalizatorja Cu-MAC@C₄H₈SO₃H na osnovi njegovih magnetnih lastnosti enostavno in učinkovito, smo torej prikazali zeleni pristop k povečanju aktivnosti nanokatalizatorjev. Nanokatalizatorje smo uporabili v petih ciklih in ob tem ni prišlo do opaznega zmanjšanja aktivnosti.

Scientific paper

Corrosion Inhibition Behavior and Adsorption Mechanism of Ethyl Acetate Extract from *Scorzonera Undulata* for Carbon Steel in 1 M HCl Solution

Asma Soudani,^{1,2} Brahim Harkati,² Abdelkader Nadjem³
and Abdelkrim Gouasmia¹

¹ Laboratory of Organic Materials and Heterochemistry, Larbi Tebessi University, 12002, Tebessa – Algeria.

² Laboratory of Bioactive Molecules and Applications, Larbi Tebessi University, 12002, Tebessa – Algeria.

³ Laboratory of Electrical Engineering, Larbi Tebessi University, 12002, Tebessa – Algeria.

* Corresponding author: E-mail: asma.soudani@univ-tebessa.dz

Received: 09-09-2022

Abstract

For carbon steel X70 in a 1 M hydrochloric acid solution, *Scorzonera undulata* acetate extract (SUAc) was investigated as an ecological corrosion inhibitor. The anti-corrosion effect of *Scorzonera undulata* extract is studied using potentiodynamic polarization analysis and electrochemical impedance spectroscopy (EIS). The polarization curves clearly show that the extract is an excellent mixed inhibitor. Our findings show that the maximum inhibition efficiency of 83% has been found with inhibitor concentration up to 400 mg/L at 298 Kelvin. The Langmuir isotherm is followed by the inhibitor's adsorption on the steel surface and physical adsorption was discovered to be the mechanism. To understand the inhibitory mechanism, thermodynamic parameters ($\Delta G_{\text{ads}}^{\circ}$) and activation parameters (E_{a} , ΔH_{a} , and ΔS_{a}) were determined. Scanning electron microscopy (SEM) and X-ray photoelectron spectrometry studies of the surface chemistry and morphology are included to this investigation. The results obtained from chemical and electrochemical measurements, confirm that a protective film is formed on the carbon steel surface.

Keywords: *Scorzonera undulata*; corrosion inhibitor; scanning electron microscopy; X-ray photoelectron spectrometry.

1. Introduction

Metal corrosion is a natural phenomenon that affects, causes damage and change the chemical and physical properties of these metals. Many investigations and scientific research have been conducted on this phenomenon, which is considered as one of the major industrial issues. Metal contact with hydrochloric acid can be harmful and lead to strong corrosion during certain processes such as cleaning, descaling, pickling or even transportation.¹ Due to their p-electron system and heteroatoms such S, P, N, and O, the organic molecules utilized as inhibitors are adsorbed on the metal surface.^{2–4} This adsorption is either chemical (chemisorption) or physical (physisorption). After a lot of research and investigation looking into the best and the most effective methods of protecting metals from corrosion, it has been found that the use of inhibitors is one of the most practical methods and one of the best op-

tions available.^{5–6} Although synthetic chemicals have good inhibitory efficiency, their application is restricted due to their higher cost, non-biodegradability, and adverse effects on both humans and environment. Recent studies are increasingly focusing on corrosion inhibition properties and working to create stable, non-toxic organic compounds in an attempt to overcome these drawbacks. The use of affordable, biodegradable, natural products is crucial for protection. Plant extracts are typically produced using straightforward extraction techniques and exhibit good acidic medium inhibitory characteristics.⁷ *Scorzonera undulata* is a genus belonging to the sunflower family (Asteraceae). With the use of LCMS-MS analysis, we started a preliminary study on the acetate extract of *Scorzonera undulata*, and we noted the presence of three major molecules: 3',4',5-trihydroxy-6, 7-dimethoxy-flavone (Cirsiliol), 4',5-Dihydroxy-6, 7-dimethoxyflavone (Skrofulein), 2S,3S, 4aS,5aS,9aS,10aS)-3,5a,10a- Tris(methoxymethyl)-2-me-

thyldecahydro-2H-dipyrano[3,2-b:2',3'-e] pyran-3-ol). Using potentiodynamic polarization and electrochemical impedance methods, the effect of the ethyl acetate extract of *Scorzonera undulata* on adsorption and corrosion inhibition was investigated in this work. This investigation is complemented morphological and surface chemistry studies using scanning electron microscopy and X-ray photoelectron spectrometry.

2. Experimental

2.1. Preparation of Solutions

The corrosive solution used in this study is an acidic solution (1 M HCl), obtained by diluting concentrated hydrochloric acid (37%) with distilled water and adding different concentrations of ethyl acetate extract from the *Scorzonera undulata*.

2.2. Specimen Preparation

X70 steel is the substance utilized to make the working electrode. Table 1 lists the chemical composition and mechanical characteristics.

Table 1. Chemical composition and mechanical properties of X70 raw rolled steel

Element	C	Si	Mn	P	S	Cr	Ni	Mo	Al	Sn	Cu	Nb	Ti	V	(Nb+Ti+V)
Composition	70	350	1580	0	3	41	32	9	46	1	22	57	4	80	141

2.3. Extraction

Markham's approach (1982) is followed for the extraction procedure, with a change made in response to Bruneton's method (1993). It is based on how well flavonoids dissolve in organic solvents. The two primary steps in this process are the first extraction phase, which uses methanol to solubilize the flavonoids, and the second extraction phase, which uses diethyl ether to extract free genins, ethyl acetate to extract monoglycosides, and n-butanol to extract free genins (to solubilize di and triglycosides). Flavonoid extraction is carried out from the finely ground dry matter with methanol. The macerate is filtered on a Büchner under reduced pressure and then subjected to low-pressure evaporation at 38°C (Rota Vapor, Büchi 461, Germany). Three successive washings with petroleum ether (v/v) liberate the filtrate of waxes, lipids, and chlorophyll to produce an aqueous phase. The aqueous phase is combined with diethyl ether (v/v) to create an organic phase that contains the flavonoids aglycones and the methoxylated aglycones, which are used to separate the flavonoids into aglycones, monoglycosides, di-, and triglycosides. Three ethyl acetate extractions are then applied to the remaining aqueous phase in order to recover some fla-

vonoid aglycones, primarily monoglycosides, for the organic phase. In order to extract the flavonoids di and triglycosides in particular, the residual aqueous phase is combined with n-butanol. The majority of the most polar glycosylated flavonoids are present in the final aqueous phase. Low-pressure evaporation is employed to concentrate the four collected phases.⁸⁻⁹

3. Methods

3.1. Electrochemical Tests

In a Pyrex cell with a typical three-electrode configuration steel as the working electrode (ET), platinum as the auxiliary electrode and a saturated Hg/Hg₂Cl₂/KCl calomel electrode (ECS) as the reference electrode, the electrochemical experiments are carried out. The latter is equipped with a Luggin capillary, the end of which is placed opposite the working electrode. The measurements are carried out with a set comprising a PGZ301 potentiostat-galvanostat, type Radiometer, associated with the "voltmaster 4" software. Before plotting the curves, the working electrode is held at its drop potential for 60 minutes. Electrochemical impedance spectroscopies (EIS)

were performed in the frequency range of 10 kHz to 10 mHz with a sinusoidal voltage amplitude of 10 mV at open circuit potential (OCP). The potentiodynamic polarization test was performed in the potential range and at a slew rate of -250 to +250 mV relative to the OCP and at 1 mV/s, respectively. We first plotted the electrochemical impedance spectroscopy and potentiodynamic polarization spectroscopy curves.

3.2. Scanning Electron Microscopy (SEM)

After being submerged in a corrosive solution (1M HCl) for two hours at 293 K with and without the addition of the ideal concentration of ethyl acetate extract, the surface morphology of carbon steel was examined using SEM analysis (JEOLJSM-6360LV).

3.3. X-ray Photoelectron Spectrometry

The X-ray photoelectron spectroscopy (XPS) spectra were recorded using the ESCALAB 220XL instrument. The X70 steel disks were submerged in a 100 mg/L XCAE solution in a 1M HCl. All the parameters of XPS analysis have been described by earlier research.¹⁰⁻¹²

4. Results and Discussion

The phytochemical study reveals that tannins, flavonoids, and phenols are present in the acetate extract of *Scorzonera undulata*. Table 2 displays the findings of the phytochemical examination of *Scorzonera undulata* acetate extract.¹³

Table 2. Phytochemical analysis results of *Scorzonera undulata* plant extract.

TPC ($\mu\text{g GAE/mg}$)	435.72549 \pm 14.741134
TFC ($\mu\text{g QE/mg}$)	74.130719 \pm 3.5312268
Tanin	0.6288 \pm 0.0098

TPC: Total Phenols, TFC: Total flavonoids. GAE: gallic acid, QE: quercetin

The Folin-Ciocalteu reagent was used to determine the total phenolic content (TPC) and flavonoid content (TFC) in the SUAc fraction, which were then expressed as gallic acid (GAE) and quercetin (QE) equivalents, respectively. The results of the assays show that the acetate extract of *Scorzonera undulata* (SUAc) is rich in polyphenols 435.72549 \pm 14.741134 mg eq.gallic ac/g (sample) and with regard to flavonoids and tannins values of 74.130719 \pm 3.5312268 mg eq. Quercetin /g and 0.6288 \pm 0.0098 were recorded.

4. 1. LC–MS/MS Analysis

Three compounds were detected in the LC-MS/MS analysis of the ethyl acetate extract of *scorzonera undulata* (Table 3).

Table 3. Three major molecules of acetate extract of scorzonera undulata using LC-MS/MS analysis.

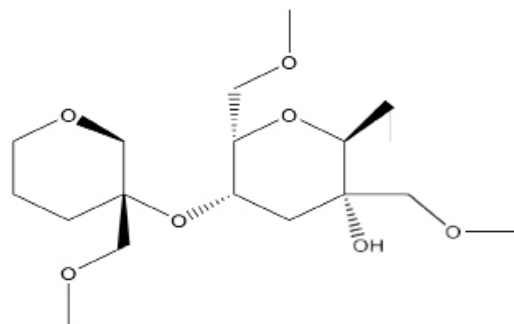
Name	Formula	MW	RT
3',4',5'-trihydroxy-6,7-dimethoxy-flavone (Cirsiliol)	C ₁₇ H ₁₄ O ₇	330.0737	5.65
4',5'-Dihydroxy-6,7-dimethoxyflavone (Skrofulein)	C ₁₇ H ₁₄ O ₆	314.0082	7.13
2S,3S,4aS,5aS,9aS,10aS)-3,5a, 10a-Tris(methoxymethyl)-2-methyldecahydro-2H-dipyrano[3,2-b:2',3'-e] pyran-3-ol	C ₁₈ H ₃₂ O ₇	360.2145	10.21

MW: molecular weight; RT: retention time

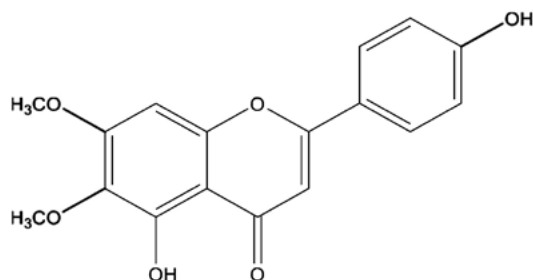
4. 2. Electrochemical Measurement

4. 2. 1. Potentiodynamic Polarization

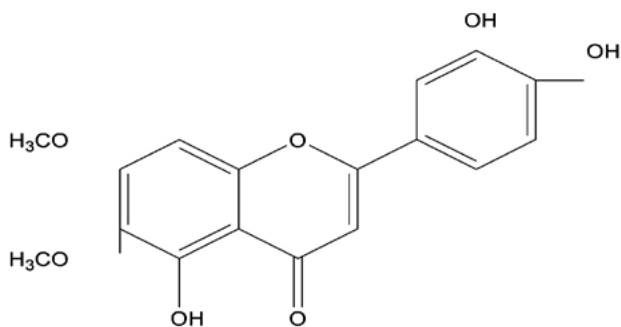
Fig. 1 displays the cathodic and anodic polarization curves of X70 steel in 1M HCl medium in both the absence and the presence of various concentrations of the extract of *Scorzonera undulata* at 298 K. For Table 4, it lists the



(2S, 3S, 4aS, 5aS, 9aS, 10aS)-3, 5a, 10a-Tris (methoxymethyl)-2-methyldecahydro-2H- dipyrano [3, 2-b: 2', 3'-e] pyran-3-ol



4', 5'-Dihydroxy-6, 7-dimethoxyflavone (Skrofulein)



3', 4', 5'-trihydroxy-6, 7-dimethoxy-flavone (Cirsiliol)

Fig 1. Different compounds present in *Scorzonera undulata*.

electrochemical characteristics derived from the polarization curves, including recovery rate, corrosion inhibition efficiency EI (%), corrosion current density (I_{corr}), corrosion potential (E_{corr}), cathodic and anodic Tafel constants (β_c and β_a), and others.

Inhibitory efficacy is defined as follows:

$$EI \% = \frac{(i_0 - i_{inh})}{i_0} \times 100 \quad (1)$$

where i_0 and i_{inh} are the values of the steel's corrosion current density after immersion in an acidic medium, respectively without and with the addition of an inhibitor, as extrapolated from the cathodic or anodic lines of Tafel. A first analysis of these curves shows that there is a reduction of the corrosion potential as the inhibitor concentration

increases. The addition of the inhibitor in solution induces a significant decrease of both anodic and cathodic partial currents.

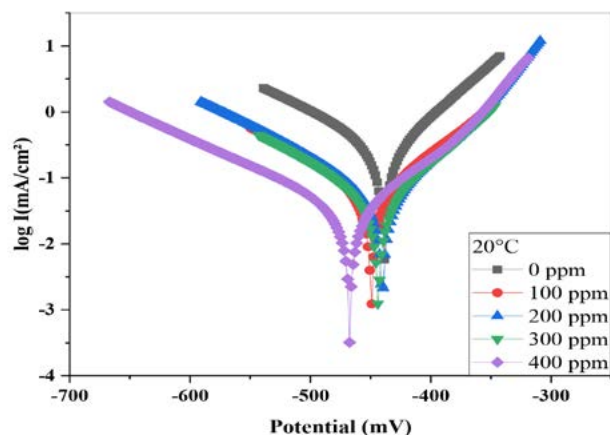


Fig 2. Polarization curves of X70 steel in solution at 1 M HCl and different SUAc concentrations.

Table 4. Electrochemical parameters of X70 steel in 1M HCl without and with the addition of different concentrations at 298K temperature of the *Scorzonera undulata* extract.

C (mg L ⁻¹)	E (mV)	i _{corr} (mA.cm ⁻²)	R _p Ωcm ²	β _a (mV.dec ⁻¹)	-β _c (mV.dec ⁻¹)	EI (%)
0	-438.9	0.2019	62.37	62.7	90.9	-
100	-449.4	0.0754	284.57	89.1	114.3	62.65
200	-440.3	0.0661	321.59	65.6	112.5	67.26
300	-443.6	0.053	370.42	73	107.1	73.75
400	-467.3	0.0332	579.57	77.7	124.3	83.56
500	-463.8	0.0462	205.58	53.7	97.6	77.12

The active area of the electrode decreases as the inhibitor concentration and the inhibitory efficiency rise, and the adsorbed film can exhibit ohmic behavior. When the inhibitor is present, the reaction of hydrochloric acid reduction and dihydrogen release might proceed according to the same mechanism.

In relation to the polarization of the steel in 1M HCl, the slope of the anodic Tafel line (β_a) is 62.7 mV. The β_a value represents a reduction in oxidation current density when an inhibitor is present.¹⁴ this outcome demonstrates unequivocally the anodic and cathodic effects of our inhibitor. The results show that the active sites on the metal surface are being blocked by the adsorbed molecules of the extract, decreasing the corrosion current density,^{15–16} with a maximum efficiency of 83.56 % at 400 mg L⁻¹. The addition of this inhibitor results in a decrease in the cathodic and anodic current densities without modifying the corrosion potential value, according to the cathodic and anodic the polarization curves.

4. 3. Electrochemical Impedance Spectroscopy

Fig.3 shows Nyquist diagrams of steel immersed in acid solution with and without the addition of different inhibitor doses.

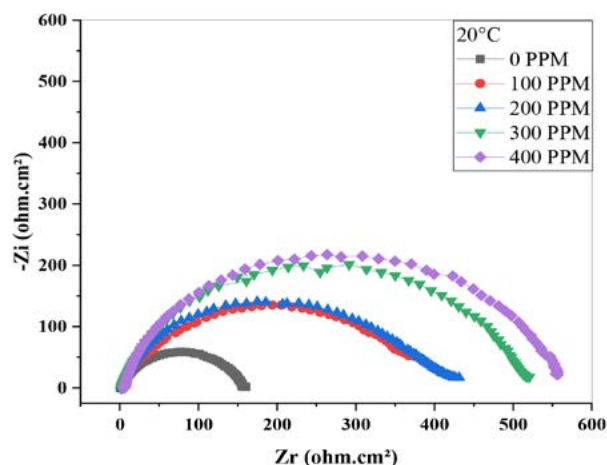


Fig 3. Electrochemical impedance of steel X70 in solution with 1 M HCl and different concentrations of SUAc (Representation in the Nyquist plane).

According to the following relationship, the load transfer resistance is used to calculate how well steel resists corrosion:

$$EI \% = \frac{(R_{tinh} - R_t)}{R_{tinh}} \times 100 \quad (2)$$

where R_t and R_{tinh} represent the steel's load transfer resistances after immersion, without and with the inhibitor added, respectively. Table 5 summarizes the electrochemical impedance spectroscopy (EIS) results for the inhibitory efficiency and electrochemical parameters for various concentrations of steel corrosion inhibitor in 1M HCl medium¹⁷.

Table 5. At various concentrations of SUAc extract, electrochemical impedance characteristics were measured in both the absence and the presence of the inhibitor.

C (mg L ⁻¹)	R _t (Ωcm ²)	C _{dl} (μF cm ⁻²)	EI %
0	156.5	56.91	-
100	395.6	254.2	60.44
200	413.6	86.19	62.16
300	514.7	77.29	69.59
400	557.9	31.94	71.95
500	257.4	69.22	39.20

The evaluation of these findings prompts us to make the following conclusions:

A single capacitive loop being present. This kind of graph often shows that a charge transfer process regulates the breakdown of carbon steel.^{18–19} It is obvious that add-

ing SUAc extract causes the loops to grow in size, which increases their resistance to the medium's corrosiveness. This behavior might be brought on by the development of a shield once the inhibitors have been absorbed onto the steel surface.

The area of active sites on the metal surface appears to decrease when inhibitor concentration is increased. This decrease may be due to the blocking of the active surface by adsorption of the inhibitor on the metal surface and consequently the increase of the transfer resistance R_t which gives a maximum inhibitory efficiency of 71.95% at 400 mg L⁻¹.

As the concentration of SUAc rises, the charge transfer resistance also increases (Table 5). This can be explained by a strengthening of the most inhibitive oxide layer's protective qualities, which causes a rise in R_t values. The impedance study and polarization measurement's results are therefore in good accord²⁰.

4. 4. Effect of Temperature

One of the factors that can alter a material's response to a corrosive environment is temperature. At different temperature, the identical electrochemical tests on X70 steel in 1 M HCl solution were carried out in both the absence and the presence of the inhibitor (298 K, 308 K and

318 K). Table 6 lists the values for the corrosion potential (E_{corr}), corrosion current density (i_{corr}), anode β_a and cathode β_c slopes, and inhibitor efficiency (EI). It appears that as the temperature increases, the corrosion current density increases while the inhibition efficiency decreases.

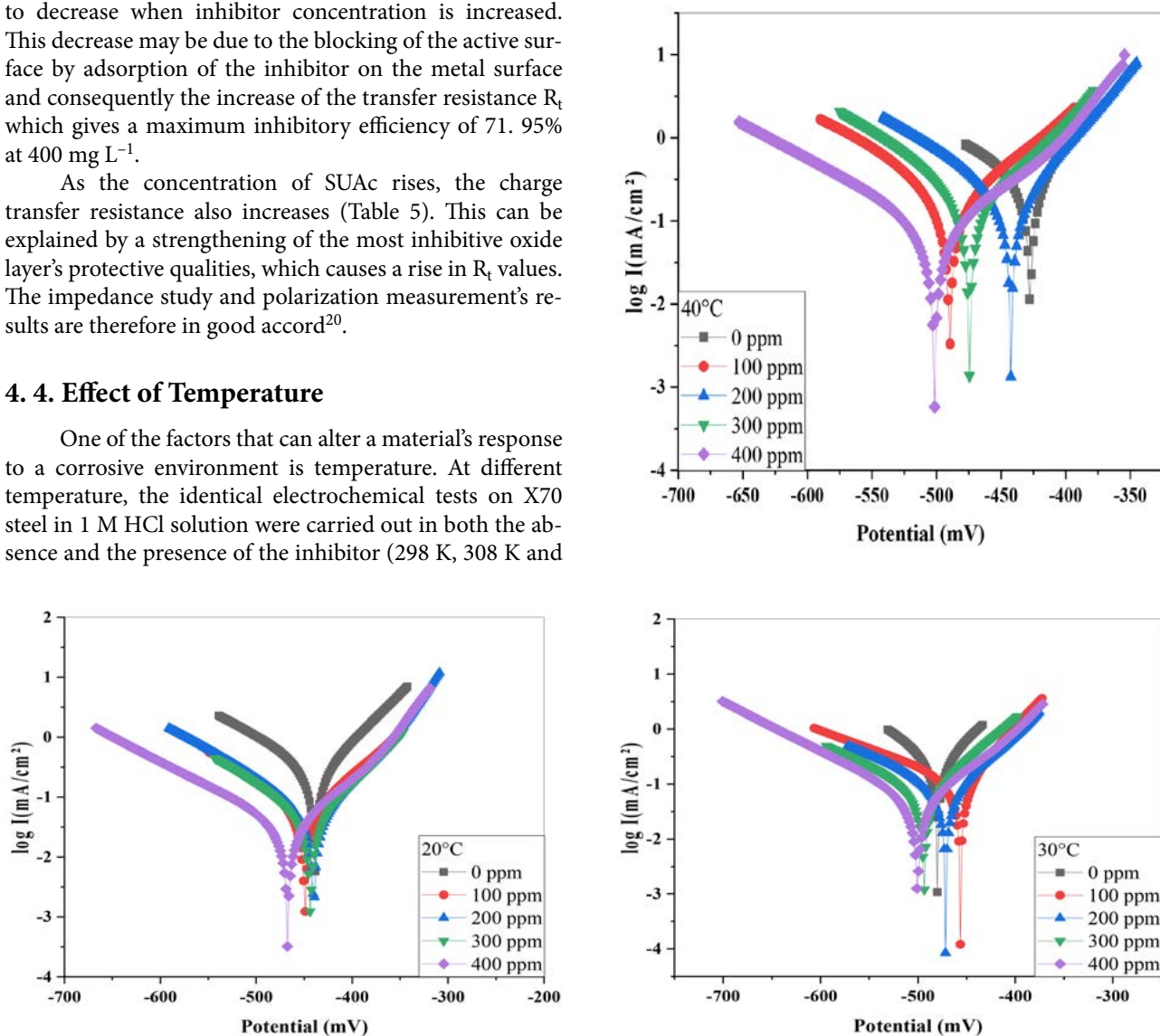


Fig 4. Curves of polarization in 1 M HCl at various temperatures in the presence and the absence of an inhibitor.

Table 6. Electrochemical parameters of 1 M HCl and inhibitor at different temperatures

Electrolyte	Temperatures	E_{corr} (mV)	i_{corr} (mA.cm ⁻²)	R_p Ωcm^2	β_a (mV.dec ⁻¹)	$-\beta_c$ (mV.dec ⁻¹)	θ (%)	EI
HCl 1M	298	-438.9	0.2019	62.37	62.7	90.9	-	-
	308	-480.1	0.2392	56.81	67.1	82.8	-	-
	318	-427.5	0.2764	46.32	56.1	103.4	-	-
Extract	298	-467.3	0.0332	579.57	77.7	124.3	0.8356	83.56
	308	-500.5	0.0492	377.74	71.6	110.7	0.7943	79.43
	318	-501.7	0.0799	239.96	71.8	116.6	0.7109	71.09

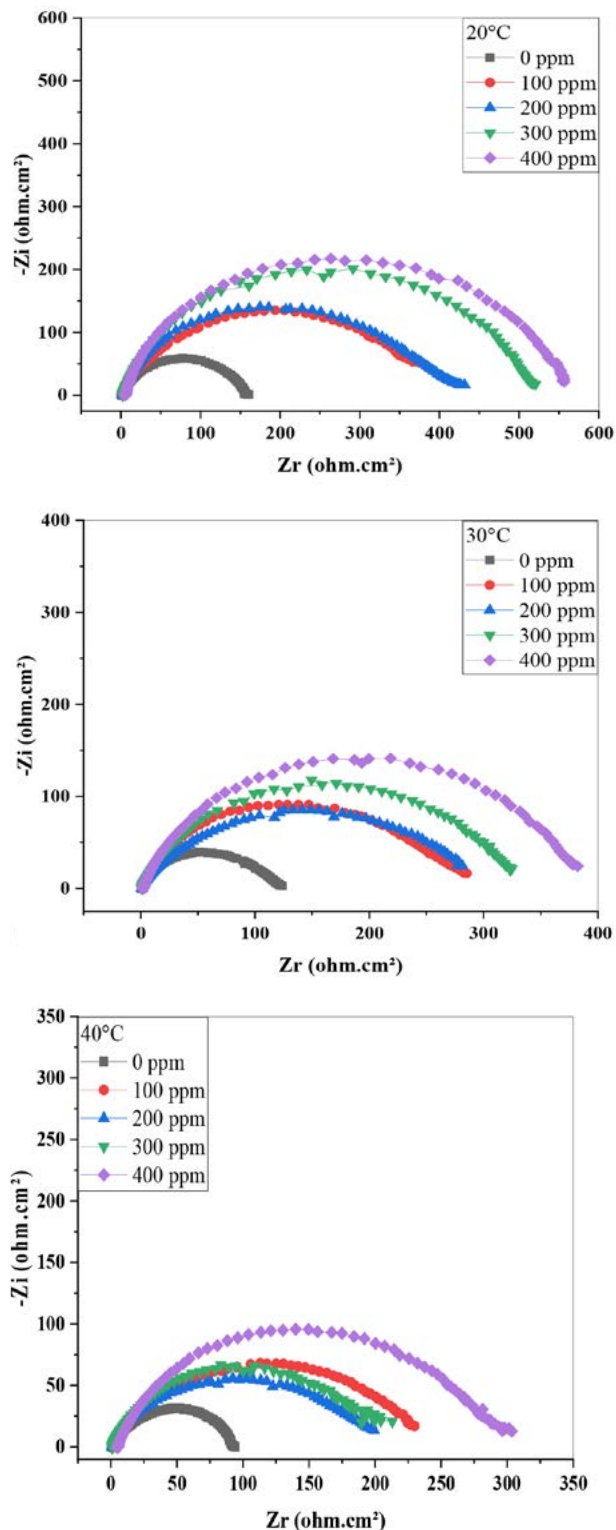


Fig 5. SIE curves obtained at different temperatures (20, 30 and 40 °C).

Fig. 5 shows the impedance diagrams obtained at different temperatures (20, 30 and 40 °C), showing a pattern of the diagrams that is not modified by temperature; however, the size of

the capacitive loop decreases with increasing temperature. These results are in a good agreement with the results obtained from the polarization curves.

Table 7. Results of electrochemical impedance tests in 1M HCl at different temperatures without and with the addition of 400 mg L⁻¹ of SUAc.

Electrolyte	Temperatures (K)	R (Ωcm ²)	C _{dl} (μF cm ⁻²)	EI %
HCl 1M	298	37.28	213.4	–
	308	119.7	106.2	–
	318	94.84	106	–
Extract	298	557.9	31.94	76.14
	308	384.8	92.63	72.10
	318	306.1	116.4	69.02

4. 5. Thermodynamic Study

The variation laws of the adsorbed quantity, as a function of inhibitor concentration, can often be represented by different types of 4, 4' isotherms.

Table 8. Correlation coefficient.

Isotherm	R ²		
	20 °C	30 °C	40 °C
Langmuir	0.996	0.999	0.990
Temkin	0.963	0.94	0.927
Fremkin	0.622	0.574	0.526
Freundlich	0.984	0.92	0.91

$$\text{Langmuir: } \frac{c}{\theta} = \frac{1}{K} + C \tag{3}$$

$$\text{Temkin: } \theta = \frac{1}{\alpha} \times \text{Ln} (K \times C) \tag{4}$$

$$\text{Freundlich: } \text{Ln}\theta = \text{Ln} K + \alpha \text{Ln} C \tag{5}$$

According to the variation in the recovery, rate (C/θ) as a function of the concentration of SUAc at various temperatures, the plot of the Langmuir isotherm is shown in Fig. 6.

The values of the adsorption constants (K_{ads}), adsorption energies (ΔG^o_{ads}), enthalpy (ΔH^o_{ads}) and entropies (ΔS^o_{ads}) are grouped in Table 9.

Table 9. Thermodynamic parameters related to the adsorption of SUAc on the surface of X70 steel.

Temperatures	K _{ads} (Lmg ⁻¹)	ΔG ^o _{ads} (kJ mol ⁻¹)	ΔH ^o _{ads} (kJ mol ⁻¹)	ΔS ^o _{ads} (J mol ⁻¹ K ⁻¹)
20°C	0.016975	-18.42		-18.4006
30°C	0.014428	-18.32	-23.9	-18.4282
40°C	0.010681	-18.14		-18.4065

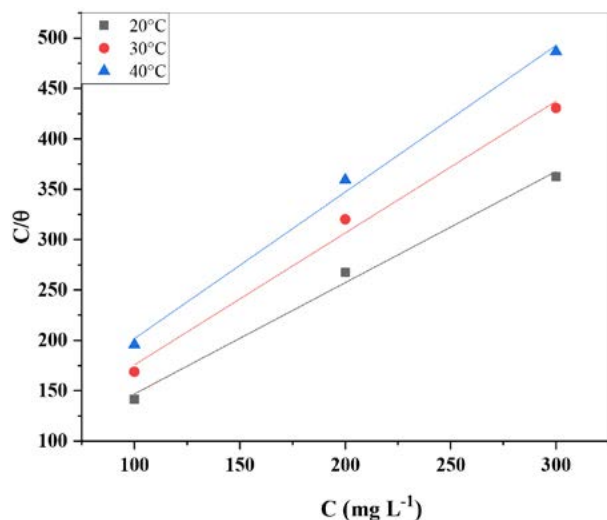


Fig 6. Langmuir adsorption isotherm of SUAc on the surface of steel X70 in the 1M HCl solutions at different temperatures.

The spontaneity of the adsorption process and the durability of the double layer adsorbed on the metal surface are shown by the negative values of the free energy of adsorption ($\Delta G_{\text{ads}}^{\circ}$).²¹ Typically, the electrostatic interactions between the charged molecules and the charged metal are what cause the values of $\Delta G_{\text{ads}}^{\circ}$ to be close to or less than -20 kJ/mol (physical adsorption). SUAc is physisorbed on the metal surface, as shown by the predicted values of $\Delta G_{\text{ads}}^{\circ}$ near to -20 kJ mol⁻¹ (Table 9).

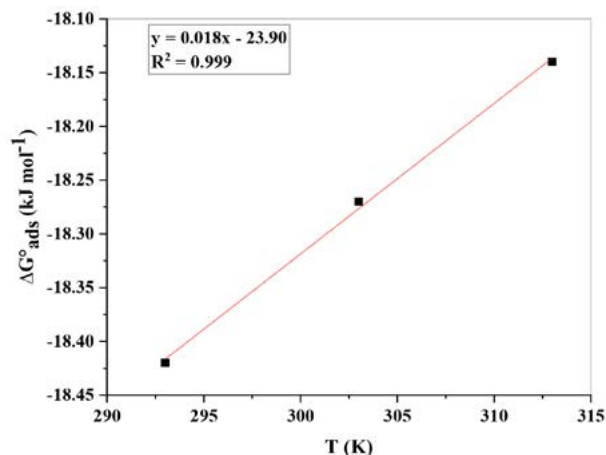


Fig 7. Variation of the adsorption free energy ($\Delta G_{\text{ads}}^{\circ}$) as a function of the temperature.

The apparent activation energy (thermodynamic parameters relating to the dissolution of steel X70 in solution)

The activation energy for the various concentrations of SUAc is higher according to the data shown in Table 10

than the activation energy without the addition of SUAc. This higher activation energy is due to the extract's physisorption on the surface of X70 steel.^{22–25}

Table 10. Parameters of carbon steel's activation energy in an acidic solution, both with and without SUAc present in varied concentrations

C (mg L ⁻¹)	E _a (kJ mol ⁻¹)
0	13.05
100	24.11
200	24.67
300	26.95
400	36.49

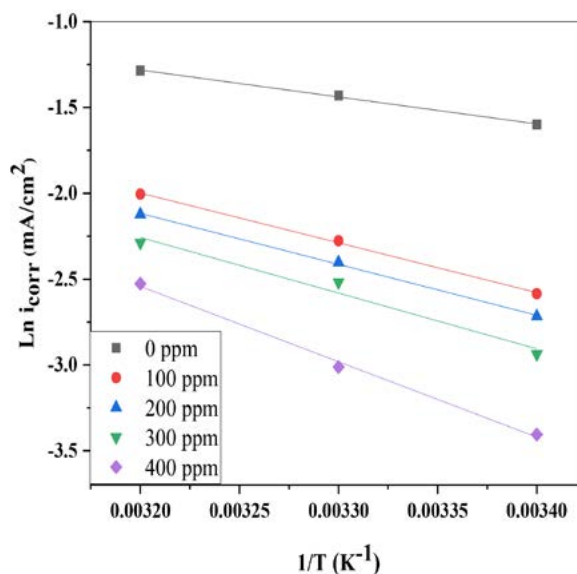


Fig 8. Graph of $\ln(i_{\text{corr}})$ in the presence and absence of SUAc as a function of the temperature's inverse.

4. 6. Morphological Investigation

In both the absence and the presence of a plant extract, top view SEM micrographs of carbon steel submerged in 1 M HCl are shown in Fig. 9. Without plant extract, the carbon steel specimen's SEM picture reveals an uneven, acid-damaged surface. It is very clear from Fig. 8 that the addition of the inhibitor under study (SUAc) to the corrosive medium stops the dissolution and consequently the corrosion of the metal. The creation of a protective layer by the SUAc extract on the surface of the steel is thought to be the cause of this visual variation.^{26–27}

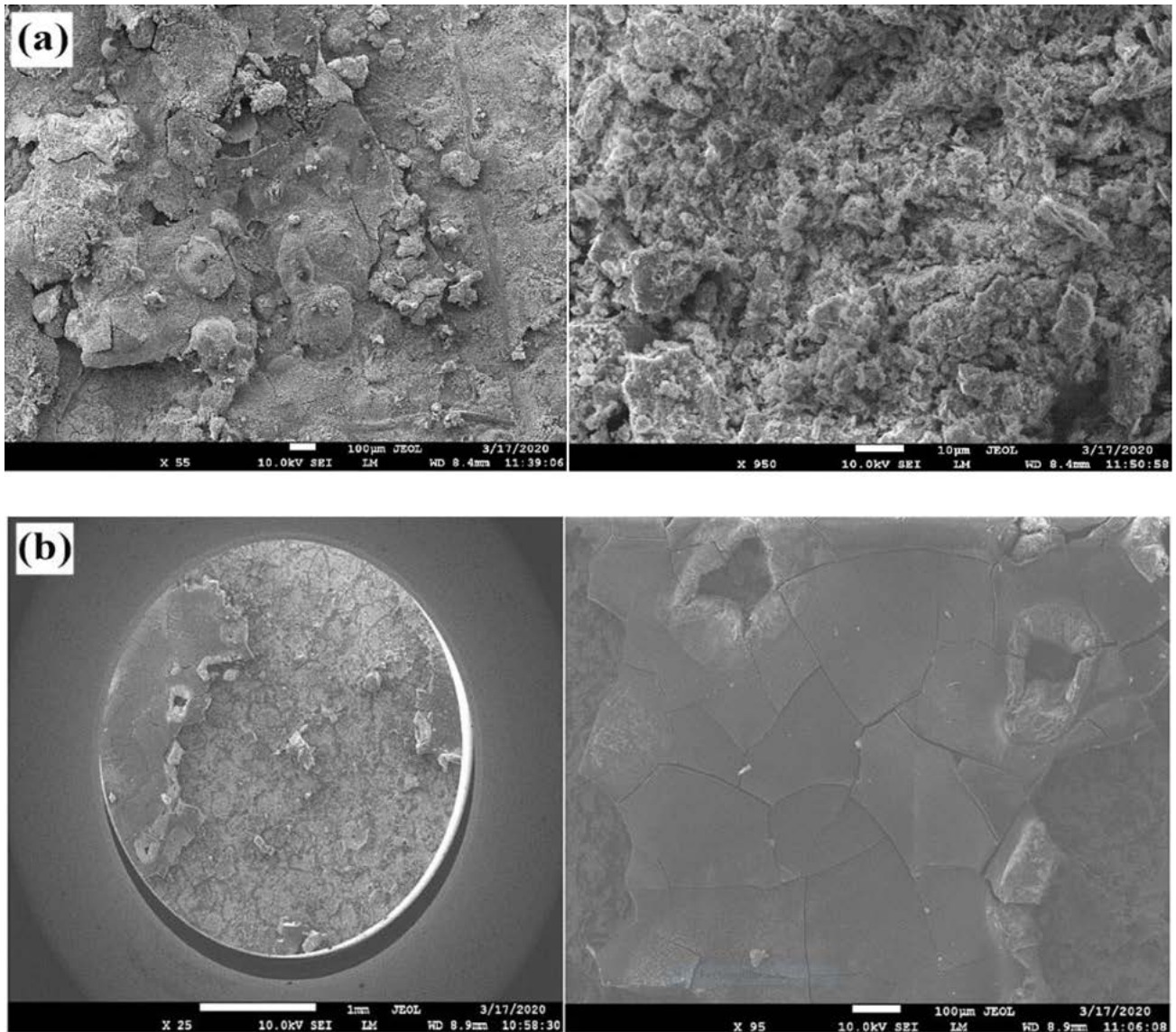


Fig 9. SEM top view images of carbon steel in acidic solution: (a) in absence of SUAc and (b) in presence of SUAc.

4. 7. XPS (X-ray Photoelectron Spectrometry)

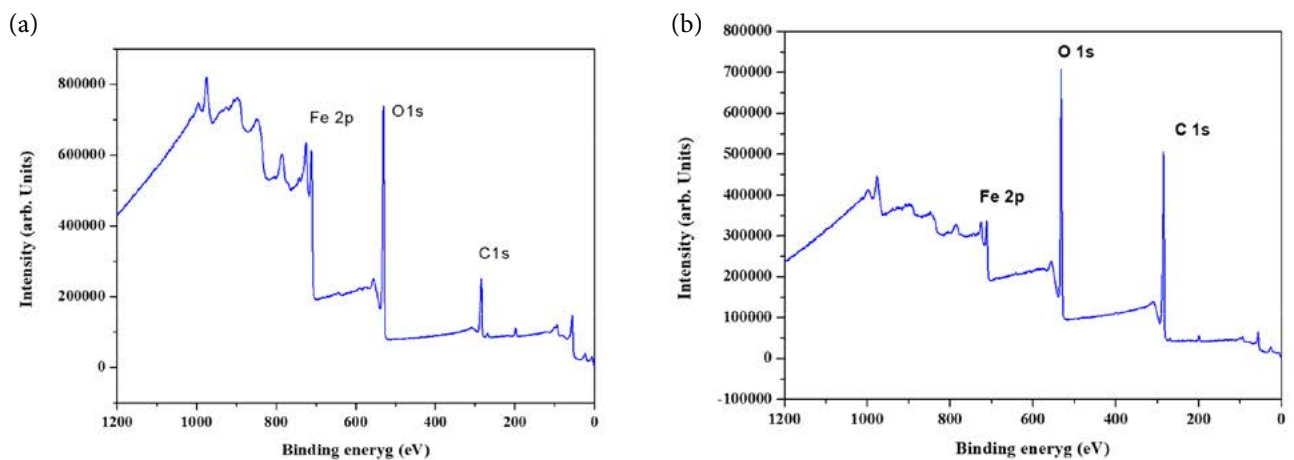


Fig 10. XPS survey spectra (a) without and (b) with SUAc.

Fig. 10 displays the XPS survey spectra of the films before and after SUAc treatment. All samples' surfaces include carbon (C), iron (Fe), and oxygen as would be expected (O). Though no nitrogen impurities were found in either sample, it is significant to note that the CNW films that have not been treated have a higher concentration of O impurities. Therefore, it is believed that the increase of the O amount before the use of SUAc is due to the higher surface oxidation.

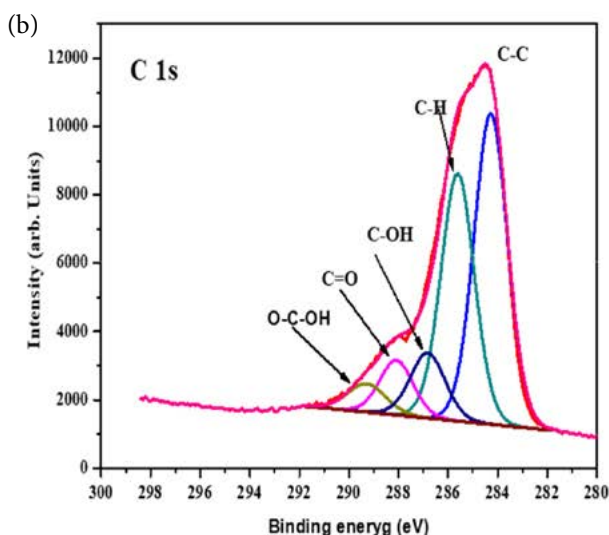
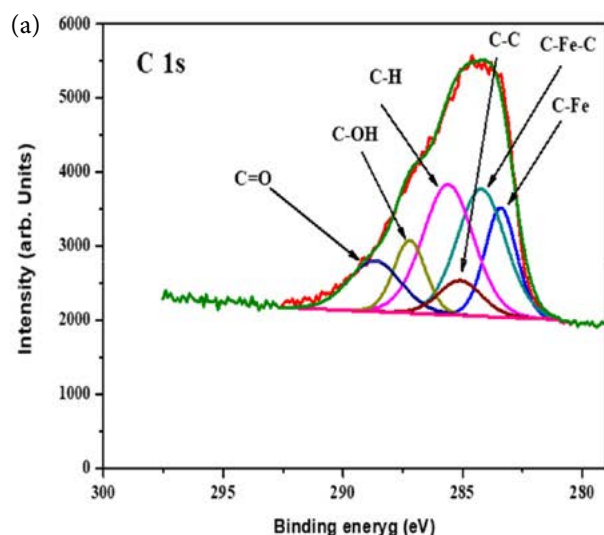


Fig 11. XPS C1s higher resolution spectra of sample (a) without and (b) with SUAc.

The sample's C 1s higher resolution de-convoluted XPS spectra with and without SUAc are shown in Fig. 11. The (Fe-C), C-Fe-FeC C, C-C, C-H, C OH, and (C O) C OH) bonds on the surface of the carbide phase are responsible for the peaks at 283.2, 284.4, 286.1, 288.1, and eV, respectively, in Fig. 10(a). The task outlined in the literature,^{28–30} can be compared to these binding energies. After the use of SUAc, it can be observed the disappearance of the carbide

bonds (Fe-C....), which indicates a surface passivation by an amorphous carbon layer especially with the increase of C-H amount. The appearance of new bond O-C-OH after the use of SUAc indicates the presence of hydroxyl groups probably originates from the SUAc inhibitor.

The O1s core level envelope in the XPS spectra of the sample without SUAc (Fig.12 (a)) may be deconvoluted into three component peaks known as O1, O2, and O3. The Fe-O bonds in the FeOx lattice are typically credited with

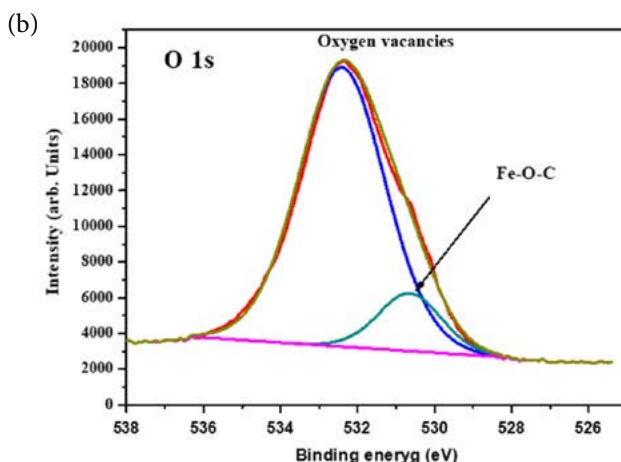
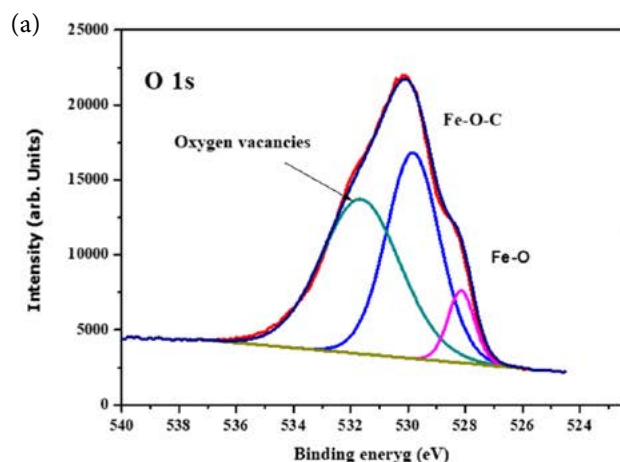


Fig 12. XPS O1s higher resolution spectra of sample (a) without and (b) with SUAc.

producing the O1 component, which is located at about 528.0 eV on the low binding energy (BE) side of the O 1s spectrum. The O2 component can be assigned to the Fe-O-C bond, whereas the O3 component can be attributed to oxygen vacancies. Its intensity is a measurement of the number of oxygen atoms around the oxidized iron. With the addition of SUAc, the Fe-O-C peak disappear (Fig.12 (b)) in accordance with the XPS analysis of C1s spectra.

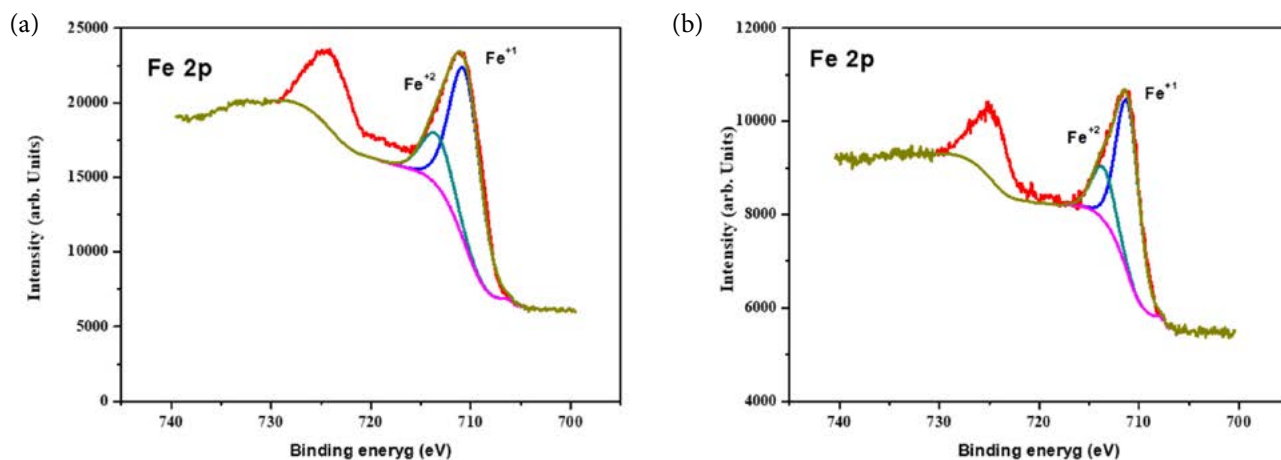


Fig 13. XPS Fe2P high resolution spectra of sample (a) without and (b) with SUAc.

The XPS study spectra before and after the SUAc treatment are shown in Fig. 13, the surfaces of all samples contain iron (Fe^{2+}), and (Fe^{3+})³¹.

5. Conclusion

This study presents the inhibitory impact and adsorption behavior of a *Scorzonera undulata* ethyl acetate extract on X70 steel in a 1M HCl media. Tafel plots have shown that the extract is an excellent mixed inhibitor. Additionally, the data show that the effectiveness of the inhibition rises with extract concentration, reaching a maximum of 83% at 400 ppm *Scorzonera undulata*. The extract remained active at the studied temperatures range. Finally, the obtained thermodynamic parameters revealed a physical adsorption between the extract and the metal surface. The inhibitor molecules interact with the mild steel surface strongly, as evidenced by the Gibbs free energy of adsorption's ($\Delta G_{\text{ads}}^{\circ}$) negative value.

Conflict of Interest

The authors declare that they are responsible for the content and writing of the article.

The authors also declare that they have no conflict of interest with suggested reviewers.

6. References

1. M. Goyal, S. Kumar, I. Bahadur, C. Verma, E. E. Ebenso. *J. Mol. Liq.* **2018**, 256, 565–573. DOI:10.1016/j.molliq.2018.02.045
2. T. Gu, Z. Chen, X. Jiang, L. Zhou, Y. Liao, M. Duan, H. Wang, Q. Pu. *Corros. Sci.* **2015**, 90, 118–132. DOI:10.1016/j.corsci.2014.10.004 640.
3. R. Yıldız. *Corros. Sci.* **2015**, 90, 544–553. DOI:10.1016/j.corsci.2014.10.047
4. A. Zarrouk, B. Hammouti, T. Lakhlifi, M. Traisnel, H. Vezin, F. Bentiss. *Corros. Sci.* **2015**, 90, 572–584. DOI:10.1016/j.corsci.2014.10.052
5. N. I. Kairi & J. Kassim. *Int J Electrochem Sci.* **2013**, 8, 7138–7155.
6. V. G. Vasudha, & P. K. Shanmuga. *Res. J. Chem. Sci.* **2013**, 3, 21–26
7. J. Halambek, I. Cindrić, & A. N. Grassino. *Carbohydr. Polym.* **2020**, 234. DOI:10.1016/j.carbpol.2020.115940
8. K.R. Markham. *Techniques of flavonoids identification*. Ed Academic Press., 1982, 6100.
9. J. Bruneton, *Pharmacognosie, phytochimie des plantes medicinales*. 2 édition, Tec et Doc (Ed.), Paris, 1993,914.
10. M. Outirite, M. Lagrenée, M. Lebrini, M. Traisnel, C. Jama, H. Vezin, F. Bentiss. *ac. Electrochim. Acta.* **2010**, 55, 1670–1681. DOI:10.1016/j.electacta.2009.10.048
11. M. Lebrini, M. Lagrenée, H. Vezin, M. Traisnel, F. Bentiss. *Corros. Sci.* **2007**, 49, 2254–2269. DOI:10.1016/j.corsci.2006.10.029
12. E. Ituen, O. Akaranta, A. James, S. Sun. *Sustainable Mater. Technol.* **2017**, 11, 12–18. DOI:10.1016/j.susmat.2016.12.001
13. V. L. Singleton, J. A. Rossi. *Am. J. Enol. Vitic.* **1965**, 16, 144–158.
14. A. Dehghani, G. Bahlakeh, B. Ramezanzadeh, M. Ramezanzadeh. *J. Mol. Liq.* **2019**, 277, 895–911. DOI:10.1016/j.molliq.2019.01.008
15. B. R. Linter & G. T. *Corros. Sci.* **1999**, 41, 117–139. DOI:10.1016/S0010-938X(98)00104-8
16. Da Silva, M.V.L.; de BrittoPolicarpi, E.; Spinelli, A. *J. Taiwan Inst. Chem. Eng.* **2021**, 129, 342–349. DOI:10.1016/j.jtice.2021.09.026
17. Kaur, J.; Daksh, N.; Saxena, A. *Arab. J. Sci. Eng.* **2022**, 47, 57–74. DOI:10.1007/s13369-021-05699-0
18. M. Lebrini, F. Robert, A. Lecante, C. Roos, *Corros. Sci.* **2011**, 53, 687–695. DOI:10.1016/j.corsci.2010.10.006
19. About, S.; Chebabe, D.; Zouahri, M.; Rehioui, M.; Lakbaibi, Z.; Hajjaji, N. *J. Mol. Struct.* **2021**, 1240, 130611. DOI:10.1016/j.molstruc.2021.130611

20. Khadom, A. A.; Kadhim, M. M.; Anae, A. R.; Mahood, H. B.; Mahdi, M. S.; Salman, A. W. *J. Mol. Liq.* **2021**, *343*, 116978 DOI:10.1016/j.molliq.2021.116978
21. M. M. Solomon, S. A. Umoren, I. I. Udosoro, A. P. Udoh. *Corros. Sci.* **2010**, *52*, 1317–1325. DOI:10.1016/j.corsci.2009.11.041. DOI:10.1016/j.corsci.2009.11.041
22. K. Tebbji, N. Faska, A. Tounsi, H. Oudda, M. Benkaddour, B. Hammouti, *Mater. Chem. Phys.* **2007**, *106*, 260–267. DOI:10.1016/j.matchemphys.2007.05.046
23. X. Li, S. Deng, H. Fu. *Corros. Sci.* **2012**, *62*, 163–175. DOI:10.1016/j.corsci.2012.05.008
24. K. Ramya, R. Mohan, K. K. Anupama, & A. Joseph. *Mater. Chem. Phys.* **2015**, *149*, 632–647. DOI:10.1016/j.matchemphys.2014.11.020
25. Hamdy, A.; El-Gendy, N. S. *Egypt. J. Pet.* **2013**, *22*, 17–25. DOI:10.1016/j.ejpe.2012.06.002
26. R. Laamari, J. Benzakour, F. Berrekis, A. Villemin. *Les Technologies de Laboratoire.* **2010**, *5*, 18–25.
27. J. Zhang, X. L. Gong, H. H. Yu, M. Du. *Corros. Sci.* **2011**, *53*, 3324–3330. DOI:10.1016/j.corsci.2011.06.008
28. Alibakhshi, E.; Ramezanzadeh, M.; Bahlakeh, G.; Ramezanzadeh, B.; Mahdavian, M.; Motamedi, M. *J. Mol. Liq.* **2018**, *255*, 185–198. DOI:10.1016/j.molliq.2018.01.144
29. C. T. Wirth, S. Hofmann, J. Robertson. *Diam. Relat. Mater.* **2009**, *18*, 940–945. DOI:10.1016/j.diamond.2009.01.030
30. G. J. Kovacs, I. Bertóti, G. Radnóczy. *Thin Solid Films.* **2008**, *516*, 7942–7946. DOI:10.1016/j.tsf.2008.06.005
31. D. Yang, A. Velamakanni, G. Bozoklu, S. Park, M. Stoller, R. D. Piner, R. S. Ruoff. *Carbon.* **2009**, *47*, 145–152. DOI:10.1016/j.carbon.2008.09.045

Povzetek

Za ogljikovo jeklo X70 v 1 M raztopini klorovodikove kisline je bil raziskan acetatni ekstrakt *Scorzonera undulata* (SU-Ac) kot ekološki inhibitor korozije. Protikorozijski učinek izvlečka *Scorzonera undulata* je bil preučevan s potenciometrično polarizacijsko analizo in elektrokemijsko impedančno spektroskopijo (EIS). Polarizacijske krivulje jasno kažejo, da je ekstrakt odličen mešani inhibitor. Ugotovitve dodatno kažejo, da je največja učinkovitost inhibicije v vrednosti 83 % dosežena s koncentracijo inhibitorja do 400 mg/L pri 298 K. Langmuirjevi izotermi sledi adsorpcija inhibitorja na jekleni površini po mehanizmu fizične adsorpcije. Za razumevanje inhibitornega mehanizma so bili določeni termodinamični ($\Delta G_{\text{ads}}^{\circ}$) in aktivacijski parametri (E_a , ΔH_a in ΔS_a). Dodatno so bile opravljene študije površinske kemije in morfologije z vrstično elektronsko mikroskopijo (SEM) in rentgensko fotoelektronsko spektrometrijo. Rezultati kemijskih in elektrokemijskih meritev potrjujejo, da se na površini ogljikovega jekla tvori zaščitni film.



Except when otherwise noted, articles in this journal are published under the terms and conditions of the Creative Commons Attribution 4.0 International License

Scientific paper

Novel Antioxidants Based on Selected 3d Metal Coordination Compounds with 2-Hydroxybenzaldehyde 4,S-Diallylthiosemicarbazone

Vasiliu Graur,^{1,*} Anastasia Mardari,¹ Pavlina Bourosh,² Victor Kravtsov,² Irina Usataia,¹ Ianina Ulchina,¹ Olga Garbuz^{1,3} and Aurelian Gulea¹

¹ Laboratory of Advanced Materials in Biofarmaceutics and Technics, Moldova State University, Chişinău, MD-2009, Republic of Moldova

² Laboratory of Physical Methods of Solid State Investigation “Tadeusz Malinowski”, Institute of Applied Physics, Chişinău, MD-2028, Republic of Moldova

³ Institute of Zoology, MD-2028, Republic of Moldova

* Corresponding author: E-mail: vgraur@gmail.com

Received: 11-16-2022

Abstract

2-Hydroxybenzaldehyde 4,S-diallylthiosemicarbazone (**HL**) was synthesized and characterized by ¹H, ¹³C NMR and FTIR spectroscopies. It exists in solution in two isomeric forms: *cis* (~25%) and *trans* (~75%). Six stable complexes were obtained by interaction of **HL** with copper(II), nickel(II), cobalt(III) and iron(III) salts: [Cu(L)Cl] (**1**), [Cu(L)NO₃] (**2**), [Cu(3,4-Lut)(L)NO₃] (**3**), [Ni(L)OAc] (**4**), [Co(L)₂]Cl (**5**), [Fe(L)₂]NO₃ (**6**). The synthesized complexes have been studied by elemental analysis, FTIR, molar electrical conductivity and single crystal X-ray diffraction (**6**). For all compounds the antioxidant activity against cation radicals ABTS^{•+} was studied. All complexes and free ligand are more active than trolox that is used in medicine practice. Complex **4** (IC₅₀ = 7.20 µM) is the most active one. The introduction of heterocyclic amine did not improve the antioxidant activity. The introduction of S-allyl group into isothiosemicarbazone affected the activity of the synthesized substances, and in some cases the resulting complexes exhibit greater activity than complexes with isothiosemicarbazones with other S-radicals.

Keywords: Isothiosemicarbazone, complexes, crystal structure, antioxidant activity.

1. Introduction

Free radical can be defined as an atom or molecule containing one or more unpaired electrons in valency shell or outer orbit and is capable of independent existence. They are formed in the body as by-products of natural processes of electron transfer between metabolites, and as intermediates in reactions catalyzed by enzymes.¹ Free radicals play a key role in the development of many diseases: cancer, brain diseases, immune system disorders, heart diseases, diabetes et al.^{2–5} There are also discussions about the participation of free radicals in the aging of the body, due to the derivatization of proteins by free radicals, which leads to the loss of biological function and subsequent degradation of proteins. Thus, the body's natural antioxidants no longer function normally as they did in a young body.⁶

Antioxidant substances could be natural or synthetic. Natural antioxidants are obtained entirely from natural sources and are used in food, cosmetics, and pharmaceutical industries.⁷ On the other hand, synthetic antioxidants are more active than natural ones and possess constant antioxidant activity.⁸ The content of natural antioxidants in plants is extremely low, therefore, after going through all the stages of extraction, a very small amount of the antioxidant is obtained as a result. While the amount of synthetic antioxidant can be controlled during the synthesis. So, the synthesis of new biologically active compounds is one of the important directions of the modern chemistry.

Thiosemicarbazones are an important class of biologically active substances. They often have promising anticancer, antimicrobial, and antifungal properties, while their antioxidant properties are less studied.^{9–13} Much less

attention is paid to the biological properties, especially antioxidant properties, of such thiosemicarbazone derivatives as *S*-substituted isothiosemicarbazones.^{14–16} The biological properties of thiosemicarbazones and isothiosemicarbazones often changes upon coordination of metal ions.¹⁷ The isothiosemicarbazones differ from the thiosemicarbazones in the way of coordination to the metal ion, because the alkylation of the sulfur atom in the composition of thiosemicarbazones, leads to the fact that the sulfur atom is not involved in the coordination.¹⁸ The lipophilicity, which controls the rate of penetration into the cell, is modified in the process of coordination. That may lead to the enhance of biological activity of metal complex comparing to free ligand.¹⁹ The complexes of copper, zinc, nickel and cobalt with 2-formylpyridine and 2-acetylpyridine 4-allyl-*S*-methylisothiosemicarbazones show promising anticancer activity but their antioxidant activity is rather moderate.^{10,20} Replacement of 2-formylpyridine moiety with 2-hydroxybenzaldehyde moiety in 4-allyl-*S*-methylisothiosemicarbazone led to a significant increase of the antioxidant activity of not only the coordination compounds but also the initial ligands.²¹ The complexes of 3*d* metals with 2-hydroxy-3-methoxybenzaldehyde 4-allyl-*S*-methylisothiosemicarbazone still posses a strong antioxidant activity that is superior to such substance as trolox that is used in medical practice, but it does not exceed the corresponding compounds with 2-hydroxybenzaldehyde 4-allyl-*S*-methylisothiosemicarbazone. So, the introduction of the methoxy group 2-hydroxybenzaldehyde fragment did not cause the strengthening of their antioxidant activity.²²

That is why in this work we replaced the *S*-methyl group in the structure of 2-hydroxybenzaldehyde 4-allyl-*S*-methylisothiosemicarbazone with an *S*-allyl group and synthesized new antioxidants with thus obtained 2-hydroxybenzaldehyde 4,*S*-diallylisothiosemicarbazone (HL) (Fig. 1).

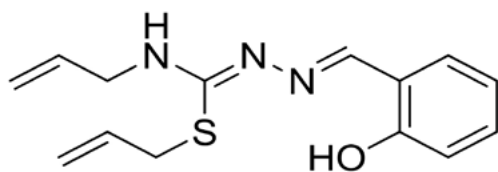
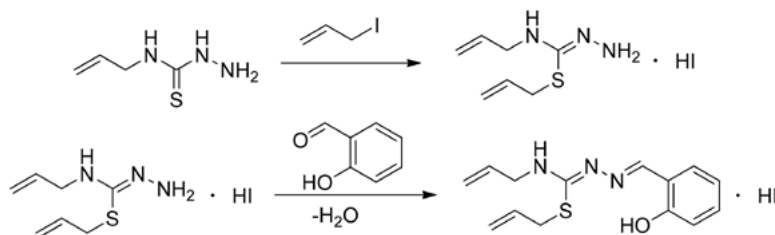


Figure 1. 2-Hydroxybenzaldehyde 4,*S*-diallylisothiosemicarbazone (HL).



Scheme 1. Synthesis of 2-hydroxybenzaldehyde 4,*S*-diallylisothiosemicarbazone hydroiodide

2. Experimental

2. 1. Materials and Methods

*N*⁴-Allylthiosemicarbazide was synthesized by the reaction between allyl isothiocyanate and hydrazine hydrate.²³ Allyl isothiocyanate, hydrazine hydrate, 2-hydroxybenzaldehyde, copper(II) chloride dihydrate, copper(II) nitrate trihydrate, nickel(II) acetate tetrahydrate, cobalt(II) chloride hexahydrate, iron(III) nitrate hexahydrate, sodium carbonate anhydrous, 3,4-lutidine were obtained from Sigma-Aldrich.

The ¹H and ¹³C NMR spectra were recorded on a Bruker DRX-400 using CDCl₃ as a solvent. The ¹H and ¹³C NMR chemical shifts are reported in ppm relative to the residual solvent peak (7.26 ppm for ¹H NMR; 77.16 ppm for ¹³C NMR). FT-IR spectra were obtained on a Bruker ALPHA FTIR spectrophotometer at room temperature in the range of 4000–400 cm⁻¹. The elemental analysis was performed similarly to the literature procedures²⁴ and on the automatic Perkin Elmer 2400 elemental analyzer. The resistance of solutions of complexes in methanol (20 °C, c 0.001 M) was measured using an R-38 rheochord bridge.

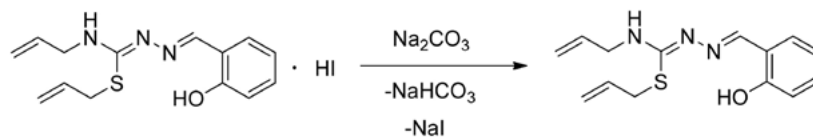
2. 2. Synthesis of 2-hydroxybenzaldehyde 4,*S*-diallylisothiosemicarbazone (HL)

The isothiosemicarbazone HL was obtained as a result of a three-step process.

At the first step, the allyl iodide (1.68 g, 10.0 mmol) has been added to the solution of *N*⁴-allylthiosemicarbazide (1.31 g, 10.0 mmol) in ethanol.

After 2 hours of stirring at room temperature 2-hydroxybenzaldehyde (1.22 g, 10.0 mmol) was added. The solution was stirred at 80 °C for 30 min. After cooling to room temperature, a yellow precipitate formed from the solution, which was filtered off, washed with ethanol and dried in air (Scheme 1).

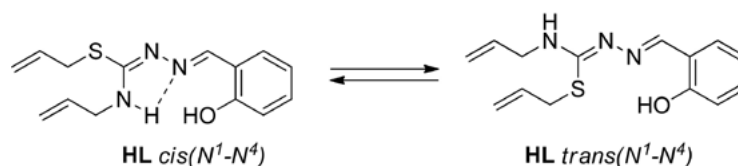
At the third step, the aqua solution of sodium carbonate had been added to the solution of 2-hydroxybenzaldehyde 4,*S*-diallylisothiosemicarbazone hydroiodide (4.03 g, 10.0 mmol) until the pH reached value 7–8. After that, the 2-hydroxybenzaldehyde 4,*S*-diallylisothiosemicarbazone was extracted by chloroform and dried in *vacuo* (Scheme 2).



Scheme 2. Neutralization of 2-hydroxybenzaldehyde 4,S-diallylisothiosemicarbazone hydroiodide

Pale yellow solid. Yield: 90%; mp 120–121 °C. FW: 275.369 g/mol; Anal. Calc. for $C_{14}H_{17}N_3OS$: C, 61.06; H, 6.22; N, 15.26; S, 11.64; found: C, 60.91; H, 6.00; N, 15.08; S, 11.49%. IR data (cm^{-1}): ν (O–H) 3427; ν (N^4 –H) 3150; ν (C=C allyl) 1642; ν (C=N) 1606, 1571; ν (C–O) 1265; ν (CH_2 –S) 1152; ν (C–S) 743.

was added. The mixture was stirred for 1 hour at 60 °C. The green precipitate was formed during stirring. The resulting precipitate was filtered off, washed with a small amount of ethanol and dried. Yield: 87%. Anal. calc. for $C_{14}H_{16}ClCuN_3OS$: Cu, 17.02; C, 45.04; H, 4.32; N, 11.25; S, 8.59; found: Cu, 16.55; C, 44.89; H, 4.01; N, 11.05; S, 8.30%.



Scheme 3. The isomeric forms of the isothiosemicarbazone HL.

HL trans(N^1 – N^4) form (Scheme 3, ~75%): 1H NMR (400 MHz; $CDCl_3$; δ , ppm): 11.73 (br, 1H, OH); 8.40 (s, 1H, CH=N); 7.24 (m, 2H, CH aromatic); 6.98 (d, 8.0 Hz, 1H, CH aromatic); 6.88 (t, 7.5 Hz, 1H, CH aromatic); 5.95 (m, 1H, CH from allyl moiety); 5.37 (d, 16.6 Hz, 1H, $CH_2=C$ (trans)); 5.27 (d, 10.0 Hz, 1H, $CH_2=C$ (cis)); 5.26 (d, 16.6 Hz, 1H, $CH_2=C$ (trans)); 5.20 (d, 10.0 Hz, 1H, $CH_2=C$ (cis)); 4.80 (br, 1H, NH); 4.05 (t, 4.8 Hz, 2H, CH_2 –N); 3.57 (d, 6.5 Hz, 2H, CH_2 –S). ^{13}C NMR (100 MHz; $CDCl_3$; δ , ppm): 160.60 (C–S); 158.83 (C–O aromatic); 155.57 (C=N); 134.02, 133.70, 119.05, 116.62 (CH aromatic); 130.85, 130.83 (CH from allyl moieties); 118.86 (C aromatic); 118.82, 117.18 (CH_2 =); 45.95 (CH_2 –N); 33.80 (CH_2 –S).

HL cis(N^1 – N^4) form (Scheme 3, ~25%): 1H NMR (400 MHz; $CDCl_3$; δ , ppm): 11.28 (br, 1H, OH); 8.47 (s, 1H, CH=N); 7.25 (m, 2H, CH aromatic); 6.97 (d, 7.7 Hz, 1H, CH aromatic); 6.91 (t, 7.4 Hz, 1H, CH aromatic); 5.86 (m, 1H, CH from allyl moiety); 5.77 (br, 1H, NH); 5.31 (d, 1H, 16.6 Hz, $CH_2=C$ (trans)); 5.21 (d, 1H, 10.0 Hz, $CH_2=C$ (cis)); 5.20 (d, 1H, 16.6 Hz, $CH_2=C$ (trans)); 5.16 (d, 10.0 Hz, 1H, $CH_2=C$ (cis)); 3.94 (t, 4.8 Hz, 2H, CH_2 –N); 3.80 (d, 6.5 Hz, 2H, CH_2 –S). ^{13}C NMR (100 MHz; $CDCl_3$; δ , ppm): 160.70 (C–S); 158.56 (C–O aromatic); 157.12 (C=N); 133.87, 133.16, 119.50, 116.38 (CH aromatic); 131.31, 131.26 (CH from allyl moieties); 118.63 (C aromatic); 118.33, 116.98 (CH_2 =); 45.91 (CH_2 –N); 33.32 (CH_2 –S).

2. 3. Synthesis of Coordination Compounds

2. 3. 1. Synthesis of [Cu(L)Cl] (1)

The 2-hydroxybenzaldehyde 4,S-diallylisothiosemicarbazone **HL** (0.275 g, 1.00 mmol) was dissolved in 20 mL of ethanol. After that, $CuCl_2 \cdot 2H_2O$ (0.171 g, 1.00 mmol)

IR data (cm^{-1}): 3125, 1601, 1550, 1202, 757. λ (MeOH, $\Omega^{-1} \cdot cm^2 \cdot mol^{-1}$): 74.

2. 3. 2. Synthesis of [Cu(L)NO₃] (2)

The reaction was carried out as described above, but $Cu(NO_3)_2 \cdot 3H_2O$ was used (0.242 g, 1.00 mmol) instead of copper(II) chloride dihydrate. The green precipitate was formed during stirring. The resulting precipitate was filtered off, washed with a small amount of ethanol and dried. Yield: 90%. Anal. calc. for $C_{14}H_{16}CuN_4O_4S$: Cu, 15.89; C, 42.05; H, 4.03; N, 14.01; S, 8.02; found: Cu, 16.18; C, 41.67; H, 4.38; N, 14.05; S, 8.04%. IR data (cm^{-1}): 3187, 1604, 1548, 1214, 759. λ (MeOH, $\Omega^{-1} \cdot cm^2 \cdot mol^{-1}$): 82.

2. 3. 3. Synthesis of [Cu(3,4-Lut)(L)NO₃] (3)

Complex **2** (0.400 g, 1.00 mmol) was dissolved in 20 mL of ethanol by stirring at 60 °C. After that, 3,4-dimethylpyridine (3,4-Lut) (0.179 g, 1.00 mmol) was added to the solution. The mixture was stirred for 1 hour at 60 °C. The green precipitate was formed after stirring. The resulting precipitate was filtered off, washed with a small amount of ethanol and dried.

Yield: 82%. Anal. calc. for $C_{17}H_{20}CuN_6O_4S$: Cu, 13.58; C, 43.63; H, 4.31; N, 17.96; S, 6.85; found: Cu, 13.74; C, 43.32; H, 4.69; N, 17.75; S, 6.56%. IR data (cm^{-1}): 3111, 1601, 1557, 1198, 755. λ (MeOH, $\Omega^{-1} \cdot cm^2 \cdot mol^{-1}$): 70.

2. 3. 4. Synthesis of [Ni(L)OAc] (4)

The reaction was carried out analogically to the synthesis of complex **1**, but $Ni(CH_3COO)_2 \cdot 4H_2O$ (0.249 g, 1.00 mmol) was used instead of copper(II) chloride dihydrate.

Yield: 81%. Anal. calc. for $C_{16}H_{19}N_3NiO_3S$: Ni, 14.97; C, 49.01; H, 4.88; N, 10.72; S, 8.18; found: Ni, 14.79; C, 49.02; H, 4.93; N, 10.96; S, 8.23%. IR data (cm^{-1}): 3121, 1601, 1565, 1210, 753. λ (MeOH, $\Omega^{-1}\cdot cm^2\cdot mol^{-1}$): 12.

2. 3. 5. Synthesis of [Co(L)₂]Cl (5)

The 2-hydroxybenzaldehyde 4,S-diallylisothiosemicarbazone **HL** (0.275 g, 1.00 mmol) was dissolved in 20 mL of ethanol. After that, $CoCl_2\cdot 6H_2O$ (0.119 g, 0.50 mmol) was added. The mixture was stirred for 1 hour at 60 °C. The dark brown precipitate was formed during stirring. The resulting precipitate was filtered off, washed with a small amount of ethanol and dried. Yield: 85%. Anal. calc. for $C_{28}H_{33}ClCoN_6O_2S_2$: Co, 9.15; C, 52.21; H, 5.16; Cl, 5.50; N, 13.05; S, 9.96; found: Co, 8.99; C, 52.35; H, 5.21; N, 13.02; S, 9.89%. IR data (cm^{-1}): 3111, 1599, 1552, 1218, 748. λ (MeOH, $\Omega^{-1}\cdot cm^2\cdot mol^{-1}$): 74.

2. 3. 6. Synthesis of [Fe(L)₂]NO₃ (6)

The reaction was carried out analogically to the synthesis of complex **6**, but $Fe(NO_3)_3\cdot 6H_2O$ (0.175 g, 0.50 mmol) was used instead of cobalt(II) chloride hexahydrate. As a result the dark brown single crystals were formed. Yield: 86%. Anal. calc. for $C_{28}H_{33}FeN_7O_5S_2$: Fe, 8.15; C, 49.05; H, 5.15; N, 14.30; S, 9.35; found: Fe, 8.28; C, 48.96; H, 5.20; N, 14.02; S, 9.21%. IR data (cm^{-1}): 3144, 1599, 1532, 1215, 751. λ (MeOH, $\Omega^{-1}\cdot cm^2\cdot mol^{-1}$): 72.

2. 4. X-ray Crystallography

Single crystal X-ray diffraction analysis was performed on an Xcalibur E diffractometer (room temperature, Eos CCD detector, graphite monochromator, MoK α radiation, CrysAlis PRO software²⁵). Structure solution and refinement were performed using the SHELX2014²⁶. The crystallographic data with refinement details of compound **6** are summarized in Table 1. All non-hydrogen atoms were refined using an anisotropic model and hydrogen atoms isotropically. The structure of **6** revealed the disorder of the C_3H_5 groups at N3 over two positions with equal probability. Selected bond lengths, angles and hydrogen bonds are presented in Table 2 and Table 3, respectively. Mercury software²⁷ was used for visualization of the studied structures.

2. 5. Antioxidant Activity

The antioxidant activity was studied using the ABTS free radical-scavenging assay according to Re et al.²⁸ The ABTS (7 mM) was mixed (1:1, v/v) with potassium persulfate (4.95 mM) and was incubated at 25 °C overnight in the dark place to prepare the stock solution. The prepared ABTS^{•+} solution was diluted with acetate-buffered saline (0.02 M, pH 6.5) to obtain an absorbance of 0.7 ± 0.01 at

Table 1: Crystal and Structure Refinement Data for **6**

Empirical formula	$C_{28}H_{32}Fe_1N_7O_5S_2$
M	666.57
Crystal system, sp. gr., Z	Monoclinic, $P2_1/n$, 4
<i>a</i> , Å	12.0411(10)
<i>b</i> , Å	18.005(2)
<i>c</i> , Å	14.6997(14)
β , deg	102.922(10)
<i>V</i> , Å ³	3106.2(5)
ρ_{calc} , g cm ⁻³	1.425
μ , mm ⁻¹	0.669
<i>F</i> (000)	1388
Crystal size, mm	0.36 × 0.12 × 0.10
θ Range, °	3.008 to 25.049
Reflections collected / unique	10768/5460 [R(int) = 0.0493]
Reflections with <i>I</i> > 2 σ (<i>I</i>)	2343
Number of refined parameters	383
Completeness, %	99.3
GOOF	1.002
<i>R</i> (for <i>I</i> > 2 σ (<i>I</i>))	<i>R</i> 1 = 0.0740,
<i>wR</i> 2 = 0.1424	
<i>R</i> (for all reflections)	<i>R</i> 1 = 0.1793,
<i>wR</i> 2 = 0.1831	
$\Delta\rho_{max}/\Delta\rho_{min}$, e · Å ⁻³	0.537, -0.438

Table 2: Selected Bond Lengths (Å) and Angles (deg) in Coordination Metal Environment in **6**

Bonds	(Å)
Fe(1)–O(1)	1.909(4)
Fe(1)–O(2)	1.894(5)
Fe(1)–N(1)	2.126(4)
Fe(1)–N(3)	2.125(5)
Fe(1)–N(4)	2.122(4)
Fe(1)–N(6)	2.132(6)
Angles (°)	
O(1)Fe(1)O(2)	100.3(2)
O(1)Fe(1)N(1)	83.7(2)
O(1)Fe(1)N(3)	156.3(2)
O(1)Fe(1)N(4)	95.7(1)
O(1)Fe(1)N(6)	93.9(2)
O(2)Fe(1)N(1)	98.6(2)
O(2)Fe(1)N(3)	89.8(2)
O(2)Fe(1)N(4)	82.9(2)
O(2)Fe(1)N(6)	153.5(2)
N(1)Fe(1)N(3)	73.5(2)
N(1)Fe(1)N(4)	178.5(2)
N(1)Fe(1)N(6)	105.1(2)
N(3)Fe(1)N(4)	106.9(2)
N(3)Fe(1)N(6)	85.8(2)
N(4)Fe(1)N(6)	73.6(2)

734 nm that is suitable for measurements. The solutions of trolox, **HL** and complexes **1–6** in DMSO were prepared. Then, 20 μ L of each dilution was added to a 96-well microtiter plate and 180 μ L of prepared solution of ABTS^{•+} was dispensed with the dispense module of hybrid reader

Table 3: Hydrogen Bond Distances (Å) and Angles (deg) for **6**

D–H...A	Å			∠(DHA)	Symmetry transformation for A
	D–H	H...A	D...A		
N(2)–H(1N)...O(5)	0.86	2.11	2.946(7)	165	<i>x, y, z</i>
N(5)–H(2N)...O(3)	0.86	2.46	3.201(9)	146	<i>x-1, y, z</i>
C(2)–H(2)...O(3)	0.93	2.45	3.379(9)	175	<i>x, y, z</i>
C(12)–H(12B)...O(5)	0.97	2.36	3.29(1)	160	<i>x, y, z</i>
C(26)–H(26B)...O(3)	0.97	2.19	3.09(1)	154	<i>x-1, y, z</i>

(BioTek) and was shaken for 15 s. The decrease in absorbance was measured at 734 nm after 30 min of incubation. Blank samples do not contain ABTS⁺.

3. Results and Discussion

3.1. Synthesis and Characterization

The ligand was synthesized in a good yield and characterized by ¹H NMR, ¹³C NMR and FTIR spectroscopy.

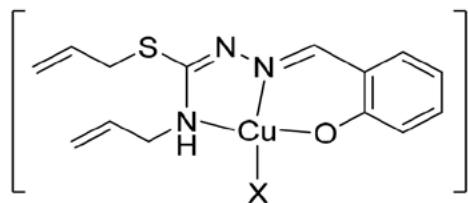
The main feature of the NMR spectra is the fact that all the peaks are doubled, that indicates the presence of two tautomeric (*cis-trans* isomers relative to the C=N² bond) forms of isothiosemicarbazone in solution. In the *cis* form, there is a hydrogen bond of the hydrogen atom at N⁴, that leads to a shift of the N⁴H peak towards a higher chemical shift (to a weaker field). The ratio of the integral

intensity of the peaks of the two forms of isothiosemicarbazone HL shows that the *trans* form prevails in the solution (~75%).

Complexes **1**, **2**, **5-6** were prepared by the reaction between isothiosemicarbazone HL and corresponding metal salts. Coordination compounds of copper(II) (**1**, **2**) and nickel(II) (**4**) were synthesized in 1:1 molar ratio, but cobalt(III) (**5**) and iron(III) (**6**) complexes were synthesized in 2:1 (HL : metal salt) molar ratio. Complex **3** was obtained by reaction between complex **2** and 3,4-dimethylpyridine in 1:1 molar ratio.

The elemental analysis confirms the composition of isothiosemicarbazone HL and complexes **1-6**. The molar conductivity values of all synthesized complexes, except complex **4**, are in the range 70–75 Ω⁻¹·cm²·mol⁻¹ that indicates that they are 1:1 electrolytes and dissociate on complex cation and acid residue anion in the process of disso-

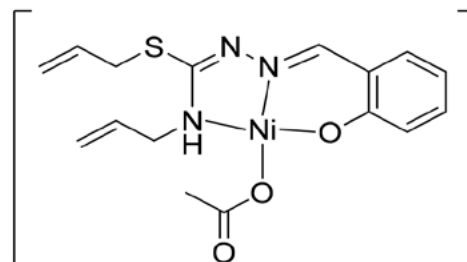
1, 2:



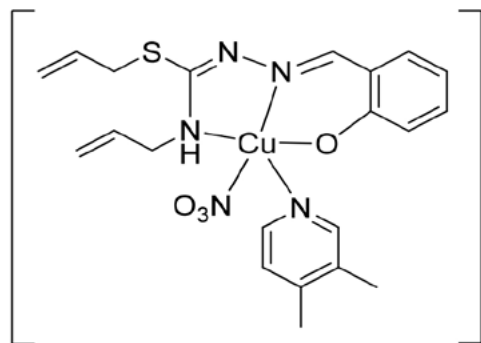
1: X = Cl⁻

2: X = NO₃⁻

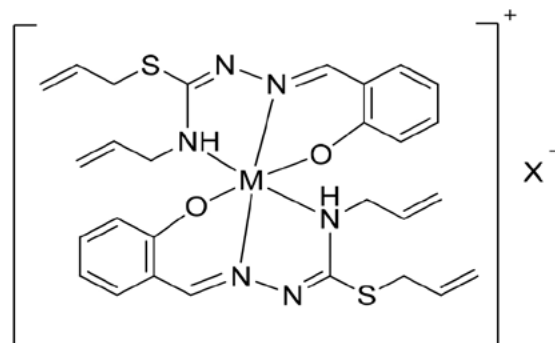
4:



3:



5, 6:



5: M = Co³⁺; X = Cl⁻

6: M = Fe³⁺; X = NO₃⁻

Figure 2. Proposed chemical structures of complexes **1-6**.

lution in methanol. The molar conductivity value of nickel complex **4** is $12 \Omega^{-1}\cdot\text{cm}^2\cdot\text{mol}^{-1}$, which means that acetate-ion is not washed out from the inner sphere by methanol molecules.

The comparative analysis of the FTIR spectra of the synthesized compounds and the free ligand (**HL**) was made in order to determine the coordination mode of **HL** with metal ions. It was established that the 2-hydroxybenzaldehyde 4,*S*-diallylthiosemicarbazone behaves as a monodeprotonated tridentate O,N,N-ligand, connected to the central ion by a deprotonated phenolic oxygen atom, azomethine nitrogen and thiocarbamide nitrogen, forming five- and six- members metallacycles. This is confirmed by the disappearance of the $\nu(\text{O-H})$ absorption band that was in the region 3427 cm^{-1} . The absorption bands $\nu(\text{N-H})$, $\nu(\text{C=N})$ and $\nu(\text{C-O})$ have shifted to the low-frequency region with corresponding values $3187\text{--}3111 \text{ cm}^{-1}$, $1565\text{--}1532 \text{ cm}^{-1}$, and $1218\text{--}1198 \text{ cm}^{-1}$. The absorption band $\nu(\text{C-S})$ has not changed, that confirms that sulfur does not take part in the coordination of isothiosemicarbazone **HL**.

For the complexes **1-6** the proposed formula are presented in figure 2.

3. 2. Structure Description of the Complex 6

The X-ray diffraction analysis showed that compound **6** is an ionic compound with formula $[\text{Fe}(\text{L})_2]\text{NO}_3$

and comprises mononuclear complex cation and an outer-sphere nitrate anion (Fig. 3).

Two tridentate monodeprotonated ligands L^- are coordinated by O,N,N-sets of donor atoms to the central metal atom in the complex cation. The coordination polyhedron of the Fe(1) atom is a distorted octahedron with the average Fe–O and Fe–N distances $1.902(5)$ and $2.126(5) \text{ \AA}$, respectively, and the angles from $73.5(2)$ to $106.9(2)^\circ$ for atoms in *cis*- and $153.5(2)$ to $178.5(2)^\circ$ in *trans*-positions (Table 2). These distances are similar to those found in 2-hydroxybenzaldehyde 4-allyl-*S*-methylthiosemicarbazone (*S*-MeTsch)²¹ and 4-allyl-*S*-ethylthiosemicarbazone (*S*-EtTsch)²⁹. A similar way of coordination of L^- , *S*-MeTsc⁻, and *S*-EtTsc⁻ is observed in the Fe(III) complexes despite the difference in substituents at the sulfur atom of these isothiosemicarbazones. At the same time, another method of coordination of similar isothiosemicarbazone ligands, that involves the sulfur atom, was reported^{14,30,31} for the complexes of Zn(II), Cu(II), Pd(II) transition metals.

The conformation of isothiosemicarbazones ligands with substituents at the terminal nitrogen atom or at both the nitrogen and sulfur atom^{32,33} is predisposed for their coordination with O,N,S-set of donor atoms, but their coordination to the transitional metal atoms takes place through O,N,N-set of donor atoms with rearrangement of the isothiosemicarbazone ligand³⁴. In the crystal, complex cations and anions alternate and form chains along crys-

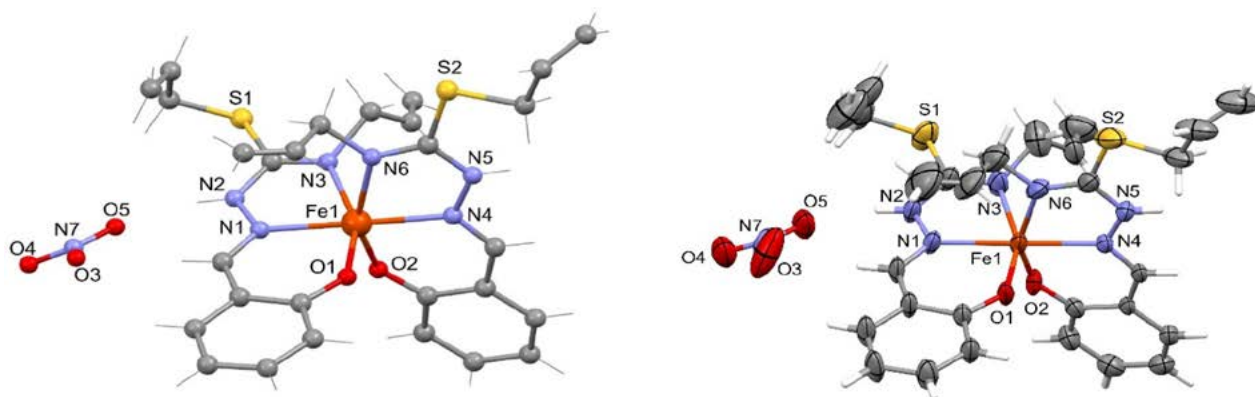


Figure 3. Molecular structure of the compound **6**, ellipsoids are shown at 30% probability level.

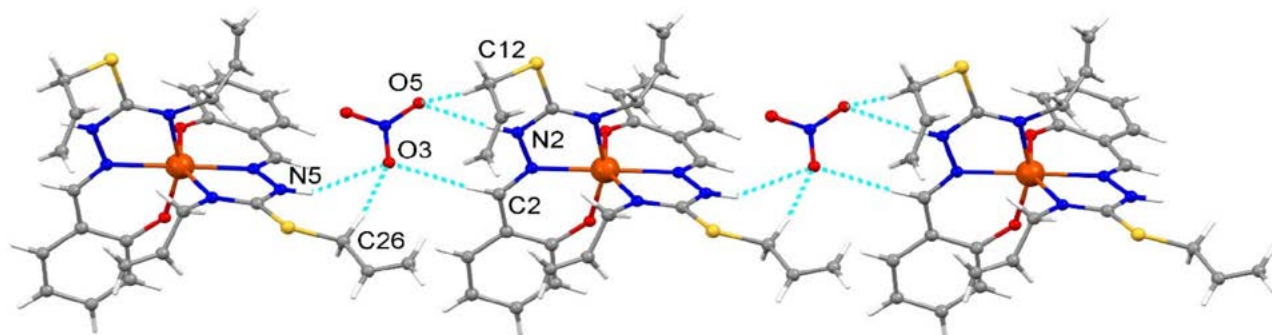


Figure 4. H-bonded chain in the crystal of complex **6**

tallographic *a* axis due to N–H...O and C–H...O hydrogen bonds (Fig. 4, Table 3).

3. 3. Antioxidant Activity

The antioxidant activity of the compounds was studied and determined using the ABTS^{•+} method. All studied substances (Table 4) are more active than trolox that is used in medicine to reduce oxidative stress or damage.

The isothiosemicarbazone **HL** exhibits antioxidant activity that is comparable with trolox. Coordination of **HL** to the copper(II) ions (complexes **1** and **2**) leads to a 2.1–2.6 times increase of antioxidant activity. The acid residue anion in the composition of complex does not have a major influence on the concentration of semi-maximal inhibition (IC₅₀) of ABTS^{•+}.

The introduction of heterocyclic amine (3,4-dimethylpyridine) into the inner sphere of copper(II) nitrate complex has a negative effect on the antioxidant activity of the obtained mixed-ligand complex and leads to a 1.4 times decrease of antioxidant activity comparing to copper(II) nitrate complex **2**, but it still remains 1.9 times more active than **HL** and 2.3 times more active than trolox.

Nickel(II), cobalt(III) and iron(III) complexes manifest better antioxidant properties than copper(II) complexes. Their IC₅₀ values are in the range of 7.20–9.37 μM, so they are 2.9–3.7 times more active than initial isothiosemicarbazone **HL**, 1.1–1.4 times more active than the most active copper(II) complex **2** of this series of substances and 3.6–4.6 times more active than trolox, a water soluble analog of vitamin E that is used as standard antioxidant in medical practice.

For the studied series of coordination compounds the activity of complexes substantially depends on the nature of central atom in the following way: Ni≈Fe>Co>Cu.

Table 4. Antioxidant activity of ligand and compounds **1–6** against cation radicals ABTS^{•+}.

Compound	IC ₅₀ , μM
HL	26.8 ± 0.2
[Cu(L)Cl] (1)	12.5 ± 0.1
[Cu(L)NO ₃] (2)	10.3 ± 0.1
[Cu(3,4-Lut)(L)NO ₃] (3)	14.4 ± 0.1
[Ni(L)OAc] (4)	7.20 ± 0.03
[Co(L) ₂]Cl (5)	9.37 ± 0.05
[Fe(L) ₂]NO ₃ (6)	7.33 ± 0.11
Trolox	33.3 ± 0.2

Previously, coordination compounds of some *3d* metals with 2-hydroxybenzaldehyde 4-allylthiosemicarbazone (TscH)³⁵, 2-hydroxybenzaldehyde 4-allyl-S-methylisothiosemicarbazone (S-MeTscH)²¹, 2-hydroxybenzaldehyde 4-allyl-S-ethylisothiosemicarbazone (S-EtTscH)²⁹ have been described.

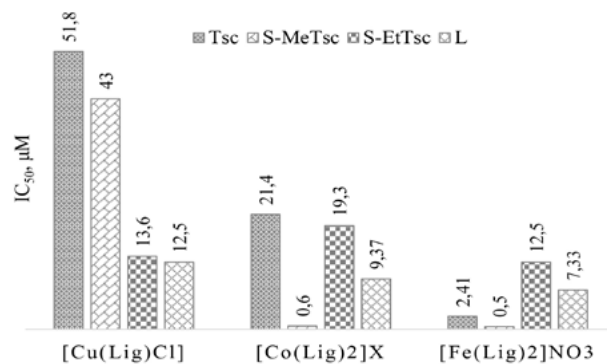


Figure 5. Comparison of the IC₅₀ values of analogous copper(II), cobalt(III) and iron(III) complexes with 2-hydroxybenzaldehyde 4-allylthiosemicarbazone and its *S*-substituted derivatives. (TscH – 2-hydroxybenzaldehyde 4-allylthiosemicarbazone; S-MeTscH – 2-hydroxybenzaldehyde 4-allyl-S-methylisothiosemicarbazone; S-EtTscH – 2-hydroxybenzaldehyde 4-allyl-S-ethylisothiosemicarbazone; Lig = Tsc[−], S-MeTsc[−], S-EtTsc[−], L; X = Cl[−], NO₃[−])

As it can be seen from the diagram (Fig. 5), the alkylation of 4-allylthiosemicarbazone in most cases leads to the increase of antioxidant properties as the corresponding IC₅₀ become smaller. In case of copper(II) chloride complexes the antioxidant activity grows in the following order: [Cu(Tsc)Cl] < [Cu(S-MeTsc)Cl] < [Cu(S-EtTsc)Cl] < [Cu(L)Cl].

In case of cobalt(III) and iron(III) complexes the sequence changes. The complexes with S-MeTscH become the most active ones. The complexes with 4,*S*-diallylthiosemicarbazone **HL** manifest higher activity than corresponding complexes with S-EtTscH, but have lower activity than corresponding complexes with S-MeTscH. The activity grows in following orders: [Co(S-MeTsc)₂]NO₃ < [Co(L)₂]Cl < [Co(S-EtTsc)₂]NO₃ < [Co(Tsc)₂]Cl and [Fe(S-MeTsc)₂]NO₃ < [Fe(Tsc)₂]NO₃ < [Fe(L)₂]NO₃ < [Fe(S-EtTsc)₂]NO₃.

4. Conclusion

2-Hydroxybenzaldehyde 4,*S*-diallylthiosemicarbazone (**HL**) was synthesized and characterized using spectroscopic methods: FTIR, ¹H and ¹³C NMR. There is an equilibrium between *trans*(*N*¹-*N*⁴) and *cis*(*N*¹-*N*⁴) isomeric forms in the solution. The *trans*-form is predominant in the CDCl₃ solution. Six new copper(II), nickel(II), cobalt(III) and iron(III) complexes with **HL** were prepared and characterized using elemental analysis, molar conductivity and FTIR spectroscopy. The structure of the iron(III) complex **6** was confirmed by single crystal X-ray diffraction. Isothiosemicarbazone **HL** coordinates to the *3d* metal central atoms in monodeprotonated form (L[−]) using O,N,N-set of donor atoms in the *cis*(*N*¹-*N*⁴) isomeric form.

The obtained substances manifest high antioxidant activity against ABTS^{•+} that exceeds the activity of trolox that is used in medical practice. Nickel(II), cobalt(III) and iron(III) complexes manifest higher activity than copper(II) complexes. Modification of the inner sphere of the copper(II) complexes by introduction of heteroaromatic amine did not lead to the amplification of the antioxidant properties. The nickel(II) coordination compound **4** manifests the highest antioxidant activity in this series of synthesized substances.

Introduction of the S-allyl group affects the antioxidant properties of the corresponding coordination compounds. Therefore, alkylation is one of the ways to enhance the antioxidant activity of complexes with thiosemicarbazones. The nature of the radical at the sulfur atom affects the antioxidant activity, however, its effect also depends on the nature of the metal, so it is necessary to continue the search for new antioxidants by changing the nature of the substituent at the sulfur atom in S-alkylisothiosemicarbazones.

Supporting Information

Crystallographic data for **6** has been deposited with the Cambridge Crystallographic Data Center, CCDC 2218005. Copies of this information may be obtained from The Director, CCDC, 12 Union Road, Cambridge, CB2 1EZ, UK (fax: +44-1233-336033; e-mail: deposit@ccdc.cam.ac.uk or www: <http://www.ccdc.cam.ac.uk>).

Acknowledgments

This work was fulfilled with the financial support of the ANCD projects 20.80009.5007.10 and 20.80009.5007.15.

5. References

- J. Moskovitz, M. B. Yim, P. B. Chock, *Arch. Biochem. Biophys.* **2002**, *397*, 354–359. DOI:10.1006/abbi.2001.2692
- D. Dreher, A. F. Junod, *EJC.* **1996**, *32*, 30–38. DOI:10.1016/0959-8049(95)00531-5
- P. H. Evans, *Br. Med. Bull.* **1993**, *49*, 577–587. DOI:10.1093/oxfordjournals.bmb.a072632
- M. M. Elahi, B. M. Matata, *Arch. Biochem. Biophys.* **2006**, *450*, 78–88. DOI:10.1016/j.abb.2006.03.011
- L. W. Oberley, *Free Radic. Biol. Med.*, **1988**, *5*, 113–124. DOI:10.1016/0891-5849(88)90036-6
- D. Harman, *Age.* **1983**, *6*, 86–94. DOI:10.1007/BF02432509
- A. M. Mahmoud, F. L. Wilkinson, A. P. Lightfoot, J. M. Dos Santos, M. A. Sandhu, *Oxid. Med. Cell. Longev.* **2021**, *2021*, Article ID 9892021, 3 pages. DOI:10.1155/2021/9892021
- M. Stoia, S. Oancea, *Antioxidants.* **2022**, *11*, 638. DOI:10.3390/antiox11040638
- P. Heffeter, V. F. Pape, É. A. Enyedy, B. K. Keppler, G. Szakacs, C. R. Kowol, *ARS.* **2019**, *30*, 1062–1082. DOI:10.1089/ars.2017.7487
- V. Graur, Y. Chumakov, O. Garbuz, C. Hureau, V. Tsapkov, A. Gulea, *Bioinorg. Chem. Appl.* **2022**, *2022*, Article ID 2705332, 18 pages. DOI:10.1155/2022/2705332
- O. E. Offiong, S. Martelli, *Farmaco.* **1994**, *49*, 513–518. DOI:10.1017/S0004972700016610
- E. Pahontu, V. Fala, A. Gulea, D. Poirier, V. Tapcov, T. Rosu, *Molecules.* **2013**, *18*, 8812–8836. DOI:10.3390/molecules18088812
- M. Galanski, V. B. Arion, M. A. Jakupec, B. K. Keppler, *Curr. Pharm. Des.* **2003**, *9*, 2078–2089. DOI:10.2174/1381612033454180
- V. Graur, I. Usataia, P. Bouroush, V. Kravtsov, O. Garbuz, C. Hureau, A. Gulea, *Appl. Organomet. Chem.* **2021**, *35*, e6172. DOI:10.1002/aoc.6172
- B. Holló, M. V. Rodić, L. S. Vojinović-Ješić, V. Živković-Radovanović, G. Vučković, V. M. Leovac, K. M. Szécsényi, *J. Therm. Anal. Calorim.* **2014**, *116*, 655–662. DOI:10.1007/s10973-013-3489-1
- V. M. Leovac, V. S. Jevtović, L. S. Jovanovic, G. A. Bogdanović, *J. Serb. Chem. Soc.* **2005**, *70*, 393–422. DOI:10.2298/JSC0503393L
- V. B. Arion, *Coord. Chem. Rev.* **2019**, *387*, 348–397. DOI:10.1016/j.ccr.2019.02.013
- V. I. Gerasimov, M. D. Revenko, V. N. Biyushkin, V. M. Golyshev, N. V. Gerbeleu, N. V. Belov, *Kristallografiya.* **1976**, *21*, 399–402.
- H. Beraldo, D. Gambino, *Med Chem.* **2004**, *9*, 31–37.
- G. Balan, O. Burduniuc, I. Usataia, V. Graur, Y. Chumakov, P. Petrenko, A. Gulea, E. Pahontu, *Appl. Organomet. Chem.* **2020**, *34*, e5423. DOI:10.1002/aoc.5423
- E. Pahontu, I. Usataia, V. Graur, Y. Chumakov, P. Petrenko, V. Gudumac, A. Gulea, *Appl. Organomet. Chem.* **2018**, *32*, e4544. DOI:10.1002/aoc.4544
- I. Usataia, V. Graur, V. Tsapkov, A. Gulea, *Studia Universitatis Moldaviae.* **2018**, *116*, 89–96.
- Z. Xian, Z. Gen, *Chin. J. Org. Chem.* **2001**, *21*, 681–684.
- J. Fries, H. Getrost, *Organic Reagents for Trace Analysis*, Vol. 291, E. Merck, Darmstadt **1977**.
- CrysAlisPro, *Oxford Diffraction Ltd.*, Version 1.171.34.49 (release 20-01-2011 CrysAlis171 .NET).
- G.M. Sheldrick, *Acta Crystallogr.* **2015**, *C71*, 3.
- C. F. Macrae, P. R. Edgington, P. McCabe, E. Pidcock, G. P. Shields, R. Taylor, M. Towler, J. van De Streek, *J. Appl. Crystallogr.* **2006**, *39*, 453. DOI:10.1107/S002188980600731X
- R. Re, N. Pellegrini, A. Proteggente, A. Pannala, M. Yang, C. Rice-Evans, *Free Radic. Biol. Med.*, **1999**, *26*, 1231. DOI:10.1016/S0891-5849(98)00315-3
- A. P. Gulea, I. S. Usataia, V. O. Graur, Y. M. Chumakov, P. A. Petrenko, G. G. Balan, O. S. Burduniuc, V. I. Tsapkov, V. F. Rudic, *Russ. J. Gen. Chem.* **2020**, *90*, 630–639. DOI:10.1134/S107036322004012X
- S. Eglence-Bakir, M. Sahin, B. Z. Salt, E. Tuzun, E. M. Kara, G. Atun, S. Cavus, I. Kizilcikli, *Spectrochim. Acta, Part A* **2020**, *237*, 118358. DOI:10.1016/j.saa.2020.118358
- M. Revenco, P. Bulmaga, E. Jora, O. Palamarciuc, V. Kravtsov, P. Bouroush *Polyhedron.* **2014**, *80*, 250. DOI:10.1016/j.poly.2014.05.006

32. P. N. Bourosh, M. A. Yampol'skaya, Yu. A. Simonov, N. V. Gerbeleu, S. G. Shova *Zh.Strukt.Khim.(Russ.)(J.Struct.Chem.)* **1986**, 27, 95–5.
33. I. N. Bourosh, N. V. Gerbeleu, M. D. Revenko, Yu. A. Simonov, V. K. Bel'skii, N. I. Vyrtosu *Zh.Neorg.Khim.(Russ.)(Russ. J.Inorg.Chem.)* **1987**, 32, 2482.
34. C. R. Groom, I. J. Bruno, M. P. Lightfoot, S. C. Ward, *Acta Cryst.* **2016**, B72, 171–179. DOI:10.1107/S2052520616003954
35. S. I. Orysyk, G. G. Repich, V. V. Bon, V. V. Dyakonenko, V. V. Orysyk, Y. L. Zborovskii, O. V. Shishkin, V. I. Pekhnyo, M. V. Vovk, *Inorg. Chim. Acta.* **2014**, 423, 496–503. DOI:10.1016/j.ica.2014.08.056

Povzetek

Sintetizirali smo 2-hidroksibenzaldehid 4,S-dialilizotiosemikarbazon (**HL**) in ga karakterizirali z metodami ^1H , ^{13}C NMR in FTIR spektroskopijo. Spojina v raztopini obstaja v dveh izomernih oblikah: *cis* (~25%) in *trans* (~75%). Z reakcijami med **HL** in bakrovimi(II), nikljevimi(II), kobaltovimi(III) in železovimi(III) solmi smo dobili šest stabilnih kompleksov: $[\text{Cu}(\text{L})\text{Cl}]$ (**1**), $[\text{Cu}(\text{L})\text{NO}_3]$ (**2**), $[\text{Cu}(3,4\text{-Lut})(\text{L})\text{NO}_3]$ (**3**), $[\text{Ni}(\text{L})\text{OAc}]$ (**4**), $[\text{Co}(\text{L})_2]\text{Cl}$ (**5**) in $[\text{Fe}(\text{L})_2]\text{NO}_3$ (**6**). Komplekse smo karakterizirali z elementno analizo, FTIR, meritvami molske prevodnosti in v primeru spojine (**6**) z monokristalno rentgensko difrakcijo. Za vse spojine smo preučevali antioksidativno aktivnost proti kationskemu radikalu ABTS $^{+\cdot}$. Vsi kompleksi in prosti ligand izkazujejo višjo aktivnost kot Trolox, ki je v uporabi v medicini. Najaktivnejši je kompleks **4** ($\text{IC}_{50}=7.20\mu\text{M}$). Dodatek heterocikličnega amina ni izboljšal antioksidativne aktivnosti. Uvedba S-alilne skupine v izotiosemikarbazon je vplivala na aktivnost sintetiziranih spojin, zato v nekaterih primerih takšni kompleksi kažejo večjo aktivnost kot kompleksi, ki vsebujejo izotiosemikarbazone z drugimi S-radikali.



Scientific paper

Oxidative Brain Injury Induced by Amiodarone in Rats: Protective Effect of S-Methyl Methionine Sulfonium Chloride

Ismet Burcu Turkyilmaz*

Istanbul University-Cerrahpaşa, Faculty of Engineering, Department of Chemistry, 34320, Avcilar-Istanbul, Turkey

* Corresponding author: E-mail: burcut@iuc.edu.tr

Phone: +90 212 473 70 70 / 17672; Fax: +90 212 473 71 80

Received: 11-25-2022

Abstract

Amiodarone (AMD) is a powerful antiarrhythmic drug preferred for treatments of tachycardias. Brain can be affected negatively when some drugs are used, including antiarrhythmics. S-methyl methionine sulfonium chloride (MMSC) is a well-known sulfur containing substance and a novel powerful antioxidant. It was intended to investigate the protective effects of MMSC on amiodarone induced brain damage. Rats were divided to four groups as follows, control (given corn oil), MMSC (50 mg/kg per day), AMD (100 mg/kg per day), AMD (100 mg/kg per day) + MMSC (50 mg/kg per day). The brain glutathione and total antioxidant levels, catalase, superoxide dismutase, glutathione peroxidase, paraoxonase, and Na⁺/K⁺-ATPase activities were decreased, lipid peroxidation and protein carbonyl, total oxidant status, oxidative stress index and reactive oxygen species levels, myeloperoxidase, acetylcholine esterase and lactate dehydrogenase activities were increased after AMD treatment. Administration of MMSC reversed these results. We can conclude that MMSC ameliorated AMD induced brain injury probably due to its antioxidant and cell protective effect.

Keywords: amiodarone, brain, oxidative stress, S-methyl methionine sulfonium chloride, free radical

1. Introduction

Amiodarone (AMD), 2-n-Butyl-3-(3,5'-diiodo-4', N-diethylaminoethoxy-3-benzoylfuran, is an effective antiarrhythmic drug used all around the world for decades. According to the four Vaughan-Williams classification, AMD strongly belongs to class III antiarrhythmic drug (AAD),¹ although it shows all the effects of all electrophysiological characteristics of this classification. This drug inhibits myocardial potassium channels and alters the activity of fast sodium channels in heart.² Albeit its positive effect on arrhythmia treatment, AMD has been declared as having many toxic effects, due to its highly lipophilic nature, and in turn accumulation tendency on many organs like liver, lung, lens, skin, gingiva.³⁻⁶ Likewise, AMD can easily cross blood brain barrier (BBB).⁷ In addition to this, the cardiac and nerve systems (conductive cells and neurons) share the same histologically specialized cells, sodium-potassium channels, excitability, and conductivity.⁸ This phenomenon can facilitate AADs penetrating through brain. AMD also triggers free radical formation by trans-

forming into a radical itself via interaction with electron transport chain (ETC).⁹ If the high oxygen demand of brain is considered, brain damage will be inevitable owing to its metabolic interactions.

S-methyl methionine sulfonium chloride (MMSC) is also known as Vitamin U, is a sulfur-containing derivative of the essential amino acid L-methionine. Nevertheless, it is not actually in the vitamin classification, but this substance is called as vitamin due to its vitamin-like effects.¹⁰ It is mainly found in raw cabbage, tomatoes, spinach, and garlic.¹¹ Their consumption has been growing day by day following knowledge of their protective effects. MMSC has been reported to have many protective activities including antiulcer, lipid lowering, wound healing, hepatoprotective, renoprotective, and anti-thrombotic.^{6,12-16} In addition, the most amazing and breath-taking attention of this sulfur containing compound is its antioxidant property, which has been proven by many researchers.¹⁷⁻¹⁹

In the current study, the protective effects of MMSC on amiodarone induced brain damage was investigated.

2. Materials and Methods

2.1. Animals

In this study, 3.5–4.0 months old male Sprague Dawley rats were obtained from Istanbul University Experimental Medical Research and Application Institute, DE-TAE. The experimental procedures were approved by the local Animal Care and Use Committee of Istanbul University (with the certification number 2012/127). All the animals were fed with standard animal pellet food and tap water ad libitum.

2.2. Experimental Design

AMD dose was chosen by considering the method of Reasor *et al.*²⁰ and MMSC dose was applied according to the method of Sokmen *et al.*²¹

Rats were divided randomly into 4 groups as follows: Group I; control group, which received corn oil (for 7 days and n=6). Group II; MMSC group, received MMSC at a dose of 50 mg/kg by gavage technique (for 7 days and n=7). Group III; AMD group; received AMD at a dose of 100 mg/kg by gavage technique (for 7 days and n = 8). Group IV; AMD+MMSC group; animals receiving MMSC (50 mg/kg) for 7 days 1 h prior to the administration of AMD (100 mg/kg) (n = 8). Due to reason of the increasing weight lose effect of high doses of AMD, which was indicated in the study of Reasor *et al.*²⁰ 100 mg/kg per day AMD dose was preferred in this study.

On the 8th day, all the animals, which were fasted overnight, then sacrificed. Brain tissues were taken from animals under anesthesia. All the tissues were homogenized with 0.9% NaCl, and all the homogenates were centrifuged. For MPO activity, the brain tissues were separately homogenized in hexadecyl trimethyl ammonium bromide (HETAB) solution (prepared in 50 mM phosphate buffer at a pH level 6.0) and then centrifuged. The supernatants were collected for the biochemical analysis and kept frozen until the experiments were done.

2.3. Biochemical Experiments

From the supernatants, reduced glutathione (GSH) levels were determined according to the reduction reaction of Ellman's reagent via free thiol groups for producing a yellow substance with 5,5'-dithiobis (2- nitrobenzoic acid).²² Lipid peroxidation (LPO) levels were determined with tiobarbutiric acid reaction²³. Protein carbonyl (PC) levels were determined as measuring carbonyl levels with the reaction of 2,4-dinitrophenylhydrazine.²⁴

Total antioxidant capacity (TAC) levels were determined with a reaction based on decolorization reaction of 2,2'-azinobis-(3-ethylbenzothiazoline-6-sulfonic acid radical cation (ABTS^{•+}) by antioxidants²⁵. The alteration of color is measured at 660 nm. Total oxidant status (TOS)

levels were determined by the presence of o-dianisidine, ferric ammonium sulfate, and xylenol orange indicator for detecting the hydrogen peroxide levels at 660 nm.²⁶ Oxidative stress index (OSI) levels were calculated by the ration of TAC/TOS levels and the results were multiplied with 100 for expressing % ratio.^{25,26} Reactive oxygen species (ROS) levels were determined with a fluorescent substance (2,7-dichloro fluorescein) and extinction/emission values were recorded.²⁷

Catalase (CAT) activity was measured as considering the transformation of hydrogen peroxide to water and the alteration of absorbance was recorded at 240 nm.²⁸ Superoxide dismutase (SOD) activity was determined as regarding riboflavin related o-dianisidine reaction to increase the rate of photooxidation at 460 nm.²⁹ Glutathione peroxidase (GPx) activity was measured the transformation of GSH to GSSG by the presence of GR and NADPH at 366 nm.³⁰

Paraoxonase (PON) activity was determined with the paraoxon ethyl substrate, and the absorbance alteration was recorded at 405 nm.³¹ Myeloperoxidase (MPO) activity was determined by the presence of 4-aminoantipyrine, phenol and hydrogen peroxide, and the absorbance alteration was detected at 510 nm.³² Acetylcholine esterase (AChE) reaction was determined at 405 nm using the acetylthiocholine iodide as substrate.³³ Lactate dehydrogenase (LDH) activity was measured at 340 nm using sodium pyruvate as substrate via NADH cofactor.³⁴ Sodium potassium ATPase (Na⁺/K⁺-ATPase) activity was determined according to the formation of phosphate and blue colored substance was recorded at 680 nm.³⁵ The protein levels were determined using the Lowry *et al.*³⁶ method.

2.4. Statistical Analyses

Statistical analysis of biochemical results was performed via GraphPad Prism 6.0 (GraphPad Software, San Diego, California, USA). The values were expressed as means ± standard deviation (SD). The results were evaluated using an unpaired t-test and analysis of variance (ANOVA) followed by Tukey's multiple comparison tests. The value of P < 0.05 was considered statistically significant. The biochemical results were also evaluated by using Origin for performing principal component analysis (PCA).

3. Results

Brain GSH, LPO and PC levels are presented in Figure 1. AMD caused a significant decrease in GSH levels (P < 0.05) and significant increase in LPO and PC levels when comparison were made with control group (P < 0.05; P < 0.01, respectively). MMSC increased GSH and decreased LPO levels significantly in AMD group (P < 0.05; P < 0.001) (Figure 1).

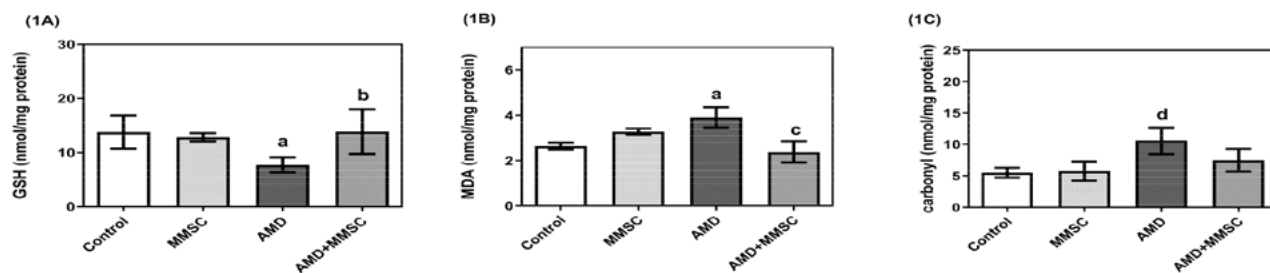


Figure 1. The brain (A) reduced glutathione (GSH), (B) lipid peroxidation (LPO) and (C) protein carbonyl (PC) levels of all groups. Each column represents mean \pm SD. ^a $P < 0.05$ versus control group, ^b $P < 0.05$ versus AMD group, ^c $P < 0.001$ versus AMD group, ^d $P < 0.01$ versus control group. AMD: Amiodarone, MMSC: S-methyl methionine sulfonium chloride.

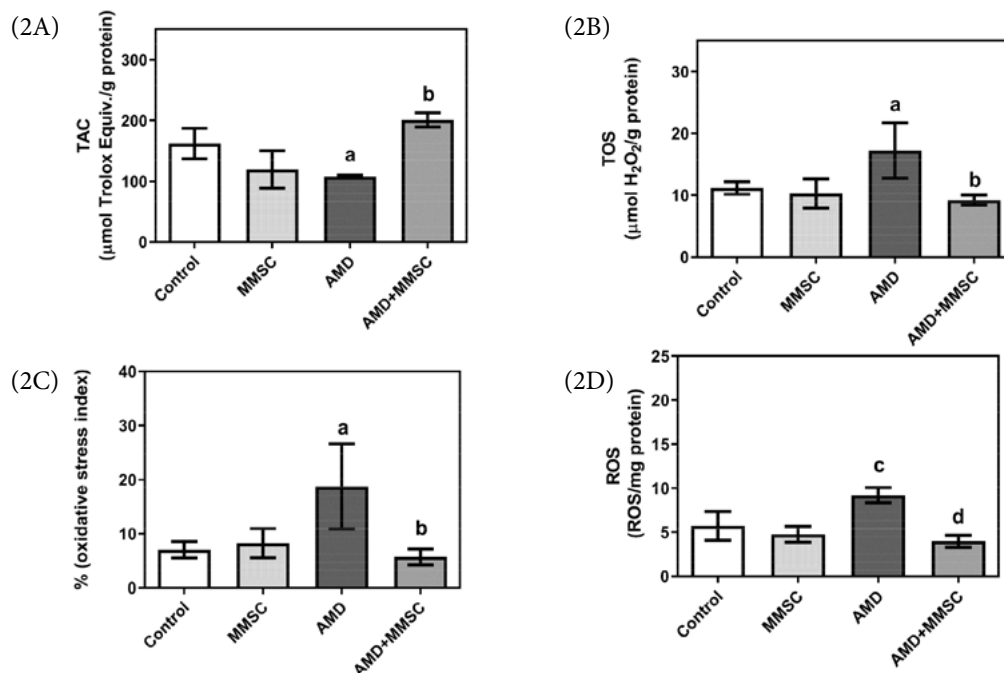


Figure 2. The brain (A) total antioxidant capacity (TAC), (B) total antioxidant status (TOS), (C) oxidative stress index (OSI) and (D) reactive oxygen species (ROS) levels of all groups. Each column represents mean \pm SD. ^a $P < 0.05$ versus control group, ^b $P < 0.01$ versus AMD group, ^c $P < 0.0001$ versus control group, ^d $P < 0.0001$ versus AMD group. AMD: Amiodarone, MMSC: S-methyl methionine sulfonium chloride.

In Figure 2, brain TAC, TOS, OSI and ROS levels are shown. AMD administration decreased TAC levels significantly ($P < 0.05$), increased TOS and OSI ($P < 0.05$) signifi-

cantly compared to control group. The alteration of ROS levels in AMD group was very significant as compared to control group ($P < 0.0001$). Administration of MMSC increased TAC

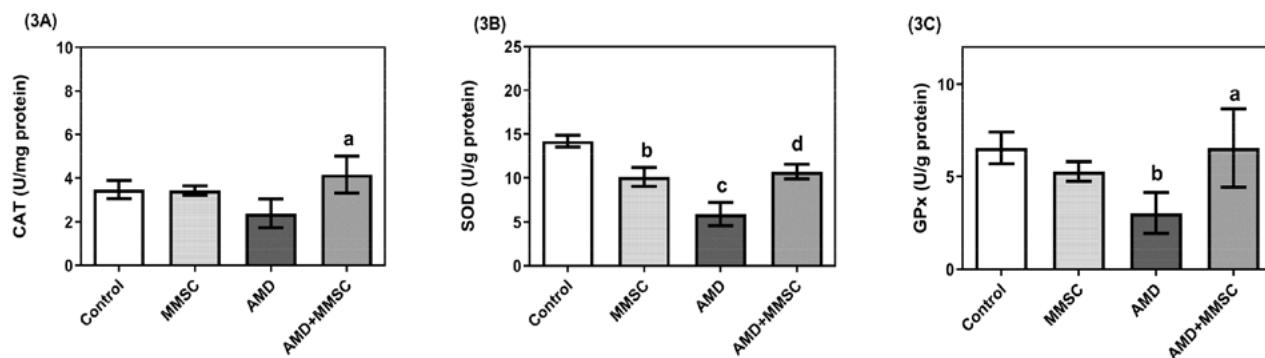


Figure 3. The brain (A) catalase (CAT), (B) superoxide dismutase (SOD) and (C) glutathione peroxidase (GPx) activities of all groups. Each column represents mean \pm SD. ^a $P < 0.01$ versus AMD group, ^b $P < 0.01$ versus control group, ^c $P < 0.0001$ versus control group, ^d $P < 0.001$ versus AMD group. AMD: Amiodarone, MMSC: S-methyl methionine sulfonium chloride.

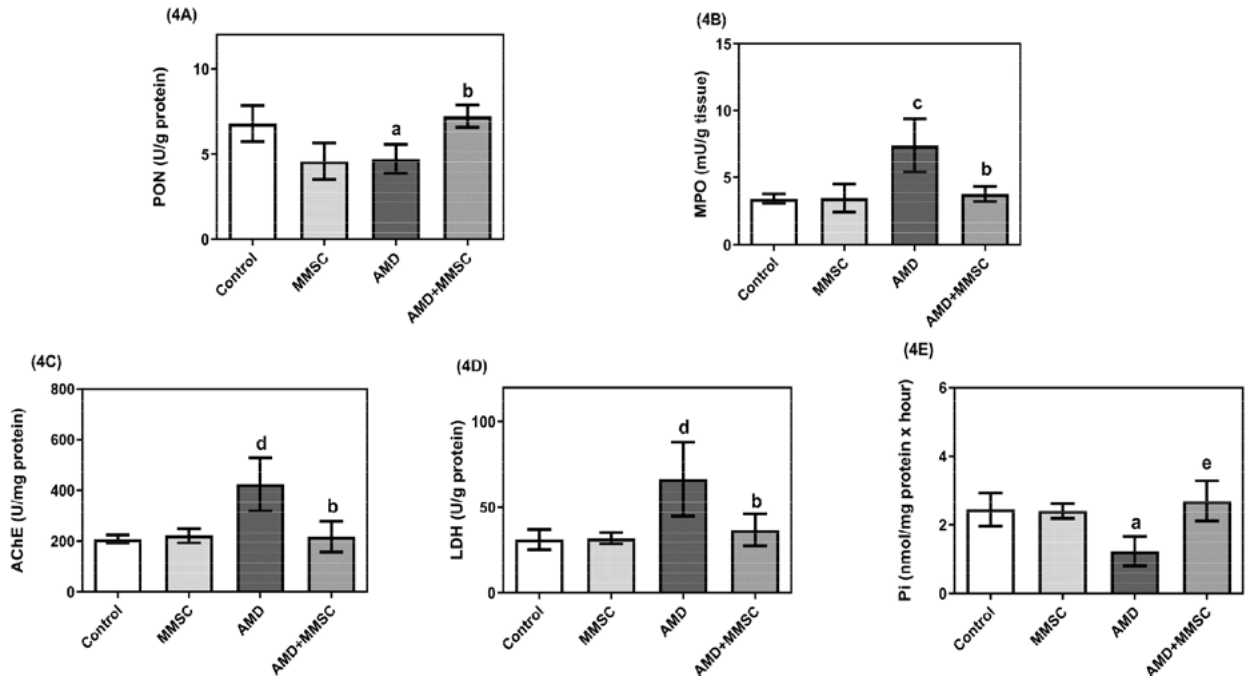


Figure 4. The brain (A) paraoxonase (PON), (B) myeloperoxidase (MPO), (C) acetylcholine esterase (AChE), (D) lactate dehydrogenase (LDH) and (E) Na^+/K^+ -ATPase activities of all groups. Each column represents mean \pm SD. ^a $P < 0.05$ versus control group, ^b $P < 0.01$ versus AMD group, ^c $P < 0.01$ versus control group, ^d $P < 0.001$ versus control group, ^e $P < 0.001$ versus AMD group. AMD: Amiodarone, MMSC: S-methyl methionine sulfonium chloride.

levels and decreased oxidative stress parameters TOS, OSI and ROS in a significant manner ($P < 0.01$; $P < 0.0001$).

The brain CAT, SOD and GPx activities are given in Figure 3. MMSC significantly ($P < 0.01$) decreased SOD activity in comparison to control group. AMD decreased SOD and GPx activities in a significant manner when compared to control group ($P < 0.0001$; $P < 0.01$). In AMD+MMSC group, all enzyme activities showed a tendency of significant elevation as compared to AMD group ($P < 0.01$, $P < 0.001$) (Figure 3).

Brain PON, MPO, AChE, LDH and Na^+/K^+ -ATPase activities of all groups are seen in Figure 4. The PON and

Na^+/K^+ -ATPase activities of AMD group were found to decrease ($p < 0.05$), while MPO, AChE and LDH activities were found to increase significantly as compared to control group ($p < 0.01$, $p < 0.001$, respectively). Administration of MMSC reversed these activities significantly in comparison to AMD group ($p < 0.01$, $p < 0.001$, respectively) (Figure 4).

Principal component analysis (PCA) was used to determine the correlation between all biochemical parameters (Figure 5). According to the PCA, the first two components were determined around 70.51% (as total result). PC1 and PC2 values were calculated as 61.11% and 9.40%,

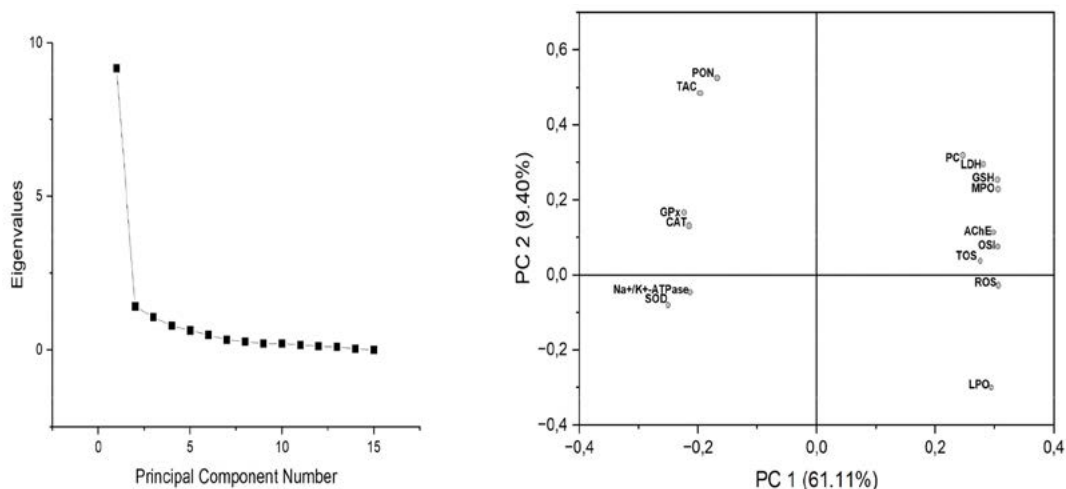


Figure 5. Principal component analysis (PCA) results for all biochemical parameters. (A) Scree plot and (B) PCA score plot of the first two PCs.

respectively. At the first component part, PC, LDH, GSH, MPO, AChE, OSI, TOS, ROS and LPO data were observed to be clustered together. These parameters were negatively correlated with PON, TAC, GPx, CAT, Na^+/K^+ -ATPase and SOD (Figure 5B).

4. Discussion

The cardiac and neuronal systems share some common features due to sodium inward and potassium outward currents. Likewise, it has been reported that the cardiorespiratory system was tightly regulated with autonomic nervous system.⁸ AMD is a trigger for inducing oxidative stress, and in turn ROS formation by either itself or its radical form.⁹ The oxidative stress, which will occur for many reasons, may harm lipid membranes, interfere with DNA structure, and interrupt cellular respiration system.³⁷ By the way, oxidative stress is responsible for many brain diseases like Alzheimer's disease (AD) and Parkinson's disease, via increased protein modification and LPO levels.³⁸

GSH is a vital tripeptide and shows unique antioxidant property via its sulfhydryl group which helps GSH to scavenge free radicals.³⁹ GSH is transformed to oxidized glutathione, GSSG. In particular, the brain ratio of these molecules must be balanced for regulating redox homeostasis and NADPH levels, as well as activities of GSH dependent enzymes like GPx.⁴⁰ When a dramatic diminishment of GSH occurs in cell media, elevated ROS is experienced. Likewise, LPO metabolisms is affected due to the existence of ROS. Elevated LPO means that there is an alteration in structure of membrane integrity and permeability.⁴¹ In different brain disorders like Alzheimer's disease, LPO is directly associated with amyloid beta plaque formation.⁴² As a free radical initiator, both AMD and other pharmacological agents like AADs directly target membrane structure by changing ion transport flux.⁴³ In another angle, PC products that likely occur as LPO are also unwanted threats for brain and many tissues due to oxidation of side chains of amino acids via LPO products.⁴⁴ Increased PC products change cell viability. According to the research of Zheng *et al.*,⁴⁵ most of the PC product have tendency to accumulate in mitochondria. In the present study, AMD decreased GSH levels and increased LPO and PC levels dramatically. Administration of MMSC reversed these levels in brain tissue. This ameliorating effect can be associated with membrane structure protection and antioxidant effect of MMSC, which has been published by different researchers indicating various toxicity models.^{46,47}

This high oxygen demand of brain is mainly used for ATP production via oxidative phosphorylation.⁴⁸ At the end of AMD metabolism, excess iodine is released while the rest of the molecule becomes trigger for ROS formation.⁴⁹ Secondly, AMD like other cationic amphiphilic drugs, enters the cell as neutral. Thereafter, tertiary amine group is protonated because of the pH difference between

inner and outer mitochondrial membrane. When protonated, AMD enters matrix, and a proton is released due to the more alkaline matrix media versus matrix intermedia. Hence, AMD accumulation begins in this way.⁵⁰ Due to these reasons, excess formation of superoxide anion will be needed to transform hydrogen peroxide (H_2O_2) by SOD, H_2O_2 will be scavenged by CAT via transforming the molecule to water and molecular oxygen.⁴⁸ Their activities were found to be decreased in AMD induced brain tissues. GPx activity was also decreased in this group, probably due to elevated levels of H_2O_2 and decreased GSH levels. An in turn, TAC levels of brain tissue dramatically decreased, and in turn TOS, OSI and ROS levels were increased. The present results are in accordance with antioxidant enzyme activities study of Hazineci *et al.*⁴⁶ on AMD induced heart damage. Sulfur containing food and other compounds like garlic, white cabbage, taurine, and N-acetyl cysteine have been reported to protect brain and other organ against damages induced by oxidative stress.^{46, 51–53} MMSC reversed these activities and levels in brain tissue. Its protective effect can be explained by its unique antioxidant capacity due to its sulfur content.

PON enzymes are very sensitive during the existence of oxidative stress. In brain tissue, PON2 exist at various region, it is highly active and enhances coenzyme Q function in ETC. This helps to decrease excessive ROS production.⁵⁴ MPO catalyzes the conversion of H_2O_2 in the presence of chloride ions to hypochlorous acid (HOCl). The acid formed is capable of attacking different amino acid residues of various proteins, e.g. tyrosine residues.⁵⁵ In addition to that, HOCl may inhibit mitochondrial respiration system, thereby leading to decreased of NAD levels and distorted cellular ATP metabolism.⁵⁶ Altered PON and MPO activities have been reported in different brain disorders related to ROS elevation.^{57,58} In this study, the outcomes suggest that AMD administration caused a significant diminishment of PON, and elevation of MPO activities probably due to its ability to increase ROS levels. MMSC administration reversed these activities compared to AMD group probably by successfully decreasing ROS levels.

Acetyl choline (ACh), an important neurotransmitter, is degraded by AChE. The activity of this enzyme is related to various neurologic problems like Alzheimer's disease⁵⁹, as well as age related oxidative stress and in turn, memory and learning problems. These problems may also occur by increasing AChE activity, and the excess degradation of ACh.⁶⁰ In the present study, AMD increased AChE activity as compared to control group. MMSC decreased AChE activity of AMD group as compared to AMD group. This effect of MMSC on this enzyme can be related to its sulfur group. The anti-AChE activity of sulfur groups has been published by Osmaniye *et al.*⁶¹

LDH is a key enzyme for glycolysis. Its activity is important for brain NADH/NAD⁺ transformation, a vital marker for brain redox balance.⁶² AMD has been reported

to increase LDH activity in various pulmonary and hepatic toxicity models, by promoting cell death.^{63,64} This elevation has been associated with altered mitochondrial capacity and NADH/NAD⁺ ratio. In this study, increased activity of LDH in brain tissues of AMD group was observed. The situation caused by AMD was reversed by MMSC probably due to its antioxidant activity.

Na⁺/K⁺-ATPase is an essential membrane bound enzyme. It stimulates Na⁺/K⁺ inward/outward movements through ATP hydrolysis. Harris *et al.*⁶⁵ indicates that this enzyme accounts for half of the total consumption of ATP in healthy brains. Its activity is also vital for protecting the membrane potential.⁶⁶ In many neurological diseases, there is a well-known connection between ROS and oxidized products, LDH activity, affected antioxidant enzyme metabolism and diminished Na⁺/K⁺-ATPase activity.⁶⁷ In the present study, diminished activities of this enzyme in AMD treated group was observed. This diminishment may be either due to ROS-triggering effect and metabolic alterations caused by AMD. Gray *et al.*⁶⁸ and Pitt *et al.*⁶⁹ revealed that AMD inhibited this enzyme in cardiac tissue. The present findings are coherent with the functional relationship between cardiovascular system and nervous system as Borowicz and Banach⁸ mentioned. MMSC administration increased this activity in AMD+MMSC group as compared to AMD group. This effect may be due to membrane repairing and antioxidant effects of MMSC, as earlier indicated by Rącz *et al.*,⁴⁷ Turkyilmaz and Yanardag,⁷⁰ and Topaloglu *et al.*,¹⁸ respectively.

Our biochemical results for antioxidant and other toxicity parameters were proven to be in accordance with performing correlation analysis with PCA. These results showed that the elevations of toxicity parameters and, diminishments of antioxidant levels and enzyme activities were evidence for existence of conditions formed by AMD.

5. Conclusion

To summarize, the present finding proves that the antioxidant property of MMSC (an important sulfur containing substance) had excellent scavenging effect on ROS and protected redox balance by reversing the deleterious effects of AMD in brain tissue.

Data Availability Statement

The author declares that [the/all other] data supporting the findings of this study are available within the article.

6. References

1. S. A. Papiris, C. Triantafyllidou, L. Kolilekas, D. Markoulaki, E. D. Manali, *Drug Saf.* **2010**, *33*, 539–558. DOI:10.2165/11532320-000000000-00000
2. R. M. Colunga Biancatelli, V. Congedo, L. Calvosa, M. Ciacciarelli, A. Polidoro, L. Iuliano, *J. Geriatr. Cardiol.* **2019**, *16*, 552–566. DOI:10.1155/2019/3418950
3. K. Jaworski, I. Walecka, L. Rudnicka, M. Gnatowski, D. A. Kosior, *Med. Sci. Monit.* **2014**, *20*, 2369–2372. DOI:10.12659/MSM.890881
4. L. T. Keng, M. T. Liao, *Postgrad. Med. J.* **2018**, *94*, 603. DOI:10.1136/postgradmedj-2018-135779
5. U. Turk, B. G. Turk, S. G. Yilmaz, E. Tuncer, E. Alioğlu, T. Dereli, *Middle East Afr. J. Ophthalmol.* **2015**, *22*, 258–260. DOI:10.4103/0974-9233.154411
6. I. B. Turkyilmaz, R. Yanardag, *Bulg. Chem. Commun.* **2019**, *51*, 20–24.
7. M. Banach, M. Popławska, K. K. Borowicz-Reutt, *Epilepsy Res.* **2018**, *140*, 105–110. DOI:10.1016/j.eplesyres.2018.01.003
8. K. K. Borowicz, M. Banach, *Pharmacol. Rep.* **2014**, *66*, 545–551. DOI:10.1016/j.pharep.2014.03.009
9. A. C. Nicolescu, J. L. Comeau, B. C. Hill, L. L. Bedard, T. Takahashi, J. F. Brien, W. J. Racz, T. E. Massey, *Toxicol. Appl. Pharmacol.* **2007**, *220*, 60–71. DOI:10.1016/j.taap.2006.12.031
10. E. H. Choi, S. B. Lee, D. Y. Lee, G. T. Kim, S. M. Shim, T. S. Park, *Nutrients.* **2019**, *11*, 1334. DOI:10.3390/nu11061334
11. N. R. Augspurger, C. S. Scherer, T. A. Garrow, D. H. Baker, *J. Nutr.* **2005**, *135*, 1712–1717. DOI:10.1093/jn/135.7.1712
12. S. Gezginici-Oktayoglu, I. B. Turkyilmaz, M. Ercin, R. Yanardag, S. Bolkent, *Protoplasma.* **2016**, *253*, 127–135. DOI:10.1007/s00709-015-0796-3
13. W. S. Kim, Y. J. Yang, H. G. Min, M. G. Song, J. S. Lee, K. Y. Park, J. J. Kim, J. H. Sung, J. S. Choi, H. J. Cha, *Pharmacology.* **2010**, *85*, 68–76. DOI:10.1159/000276495
14. A. S. Salim, *J. Pharm. Sci.* **1992**, *81*, 70–73. DOI:10.1002/jps.2600810114
15. S. Sancar Bas, I. B. Turkyilmaz, S. Bolkent, R. Yanardag, *Eur. J. Biol.* **2016**, *75*, 1–10.
16. K. Seri, T. Matsuo, T. Taniguchi, K. Amemiya, M. Kudo, G. Saito, T. Kato, *Arzneimittelforschung.* **1980**, *30*, 1694–1703.
17. S. Tunali, S. Kahraman, R. Yanardag, *Hum. Exp. Tox.* **2015**, *34*, 904–910. DOI:10.1177/0960327114561665
18. D. Topaloglu, I. B. Turkyilmaz, R. Yanardag, *J. Biochem. Mol. Toxicol.* **2022**, *36*, e23124. DOI:10.1002/jbt.23124
19. D. Mahmarzayeva, B. B. Bayrak, I. B. Turkyilmaz, O. Sacan, R. Yanardag, *J. Biochem. Mol. Toxicol.* **2022**, *36*, e23126. DOI:10.1002/jbt.23126
20. M. J. Reasor, C. M. McCloud, T. L. Beard, D. C. Ebert, S. Kacew, M. F. Gardner, K. A. Aldern, K. Y. Hostetler, *Toxicology.* **1996**, *106*, 139–147. DOI:10.1016/0300-483X(95)03175-F
21. B. B. Sokmen, S. Tunali, R. Yanardag, *Food Chem. Toxicol.* **2012**, *50*, 3562–3566. DOI:10.1016/j.fct.2012.07.056
22. E. Beutler, Glutathione in red cell metabolism, A Manual of Biochemical Methods, Grune and Stratton, Eds. New York, **1975**, 112–114.
23. A. Ledwozyw, J. Michalak, A. Stepień, A. Kadziolka, *Clin. Chim. Acta.* **1986**, *155*, 275–283. DOI:10.1016/0009-8981(86)90247-0
24. R. L. Levine, D. Garland, C. N. Oliver, A. Amici, I. Climent, A. G. Lenz, B. W. Ahn, S. Shaltiel, E. R. Stadtman, *Methods*

- Enzymol.* **1990**, *186*, 464–478.
DOI:10.1016/0076-6879(90)86141-H
25. O. Erel, *Clin. Biochem.* **2004**, *37*, 277–285.
DOI:10.1016/j.clinbiochem.2003.11.015
26. O. Erel, *Clin. Biochem.* **2005**, *38*, 1103–1111.
DOI:10.1016/j.clinbiochem.2005.08.008
27. Y. Zhang, J. Chen, H. Ji, Z. G. Xiao, P. Shen, L. H. Xu, *BMC Complement. Altern. Med.* **2018**, *18*, 343.
DOI:10.1186/s12906-018-2414-3
28. H. Aebi, *Methods Enzymol.* **1984**, *105*, 121–126.
DOI:10.1016/S0076-6879(84)05016-3
29. A. A. Mylroie, H. Collins, C. Umbles, J. Kyle, *Toxicol. Appl. Pharmacol.* **1986**, *82*, 512–520.
DOI:10.1016/0041-008X(86)90286-3
30. A. Wendel, *Methods Enzymol.* **1981**, *77*, 325–333.
DOI:10.1016/S0076-6879(81)77046-0
31. C. E. Furlong, R. J. Richter, S. L. Seidel, A. G. Motulsky, *Am. J. Hum. Genet.* **1988**, *43*, 230–238.
32. H. Wei, K. Frenkel, *Cancer Res.* **1991**, *51*, 4443–4449.
33. G. L. Ellman, K. D. Courtney, V. Andres, R. M. Feather-Stone, *Biochem. Pharmacol.* **1961**, *7*, 88–95.
DOI:10.1016/0006-2952(61)90145-9
34. R. Bais, M. Philcox, *Eur. J. Clin. Chem. Clin. Biochem.* **1994**, *32*, 639–655.
35. A. Ridderstap, S. Bonting, *Am. J. Physiol.* **1969**, *217*, 1721–1727. DOI:10.1152/ajplegacy.1969.217.6.1721
36. O. H. Lowry, N. J. Rosebrough, A. L. Farr, R. J. Randall, *J. Biol. Chem.* **1951**, *193*, 265–275.
DOI:10.1016/S0021-9258(19)52451-6
37. M. Smeyne, R. J. Smeyne, *Free Radic. Biol. Med.* **2013**, *62*, 13–25. DOI:10.1016/j.freeradbiomed.2013.05.001
38. P. Poprac, K. Jomova, M. Simunkova, V. Kollar, C. J. Rhodes, M. Valko, *Trends Pharmacol. Sci.* **2017**, *38*, 592–607.
DOI:10.1016/j.tips.2017.04.005
39. D. Shen, T. P. Dalton, D. W. Nebert, H. G. Shertzer, *J. Biol. Chem.* **2005**, *280*, 25305–25312. DOI:10.1074/jbc.M500095200
40. D. Dwivedi, K. Megha, R. Mishra, P. K. Mandal, *Neurochem. Res.* **2020**, *45*, 1461–1480. DOI:10.1007/s11064-020-03030-1
41. R. M. Lasagni Vitar, C. G. Reides, S. M. Ferreira, S. F. Llesuy, *Food Funct.* **2014**, *5*, 557–563. DOI:10.1039/c3fo60392j
42. D. A. Butterfield, *Ageing Res. Rev.* **2020**, *64*, 101049.
DOI:10.1016/j.arr.2020.101049
43. C. L. H. Huang, L. Wu, K. Jeevaratnam, M. Lei, *J. Cardiovasc. Electrophysiol.* **2020**, *31*, 579–592. DOI:10.1111/jce.14347
44. R. Fan, L. M. Schrott, S. Snelling, J. Felty, D. Graham, P. L. McGauly, T. Arnold, N. L. Korneeva, *BMC Neurosci.* **2020**, *21*, 4. DOI:10.1186/s12868-020-0552-2
45. J. Zheng, C. L. Hu, K. L. Shanley, O. A. Bizzozero, *Neurochem. Res.* **2018**, *43*, 609–618. DOI:10.1007/s11064-017-2456-9
46. H. Hazineci, İ. B. Türkyılmaz, Ü. V. Üstündağ, E. Emekli-Alturfan, B. Alev Tüzüner, H. İpekçi, T. Tunali-Akbay, R. Yanardağ, A. Yarat, *Experimed.* **2020**, *10*, 1–6.
DOI:10.26650/experimed.2020.0004
47. I. Rácz, E. Páldi, G. Szalai, T. Janda, M. Pál, D. Lásztity, *J. Plant Physiol.* **2008**, *165*, 1483–1490.
DOI:10.1016/j.jplph.2006.03.020
48. L. E. Salminen, R. H. Paul, *Rev. Neurosci.* **2014**, *25*, 805–819.
49. R. A. Eid, M. S. A. Zaki, M. Al-Shraim, M. A. Eldeen, M. A. Haidara, *Ultrastruct. Pathol.* **2021**, *45*, 49–58.
DOI:10.1080/01913123.2020.1864076
50. A. C. Nicolescu, Y. Ji, J. L. Comeau, B. C. Hill, T. Takahashi, J. F. Brien, W. J. Racz, T. E. Massey, *Toxicol. Appl. Pharmacol.* **2008**, *227*, 370–379. DOI:10.1016/j.taap.2007.12.009
51. E. Akbay, B. Erdem, A. Ünlü, A. B. Durukan, M. A. Onur, *Kardiochir. Torakochirurgia Pol.* **2019**, *16*, 88–92.
DOI:10.5114/kitp.2019.86361
52. X. Niu, S. Zheng, H. Liu, S. Li, *Mol. Med. Rep.* **2018**, *18*, 4516–4522.
53. H. Song, J. Cui, V. V. Mossine, C. M. Greenlief, K. Fritsche, G. Y. Sun, Z. Gu, *Exp. Ther. Med.* **2020**, *19*, 1554–1559.
54. J. K. Blackburn, D. W. Curry, A. N. Thomsen, R. H. Roth, J. D. Elsworth, *Exp. Neurol.* **2020**, *327*, 113234.
DOI:10.1016/j.expneurol.2020.113234
55. S. Gellhaar, D. Sunnemark, H. Eriksson, L. Olson, D. Galter, *Cell Tissue Res.* **2017**, *369*, 445–454.
DOI:10.1007/s00441-017-2626-8
56. R. S. Ray, A. Katyal, *Neurosci. Biobehav. Rev.* **2016**, *68*, 611–620. DOI:10.1016/j.neubiorev.2016.06.031
57. I. Bednarz-Misa, I. Berdowska, M. Zboch, B. Misiak, B. Zieliński, S. Płaczowska, M. Fleszar, J. Wiśniewski, A. Gamian, M. Krzystek-Korpacka, *Adv. Clin. Exp. Med.* **2020**, *29*, 71–78.
DOI:10.17219/acem/111377
58. C. Shao, J. Yuan, Y. Liu, Y. Qin, X. Wang, J. Gu, G. Chen, B. Zhang, H. K. Liu, J. Zhao, H. L. Zhu, Y. Qian, *Proc. Natl. Acad. Sci. USA.* **2020**, *117*, 10155–10164.
DOI:10.1073/pnas.1917946117
59. M. Simunkova, S. H. Alwasel, I. M. Alhazza, K. Jomova, V. Kollar, M. Rusko, M. Valko, *Arch. Toxicol.* **2019**, *93*, 2491–2513. DOI:10.1007/s00204-019-02538-y
60. S. Asha Devi, *Sci. World J.* **2009**, *9*, 366–372.
DOI:10.1100/tsw.2009.46
61. D. Osmaniye, B. N. Sağlık, U. Acar Çevik, S. Levent, B. Kaya Çavuşoğlu, Y. Özkay, Z. A. Kaplancıklı, G. Turan, *Molecules.* **2019**, *24*, 2392. DOI:10.3390/molecules24132392
62. S. Cerdán, T. B. Rodrigues, A. Sierra, M. Benito, L. L. Fonseca, C. P. Fonseca, M. L. García-Martín, *Neurochem. Int.* **2006**, *48*, 523–530. DOI:10.1016/j.neuint.2005.12.036
63. J. W. Card, W. J. Racz, J. F. Brien, S. B. Margolin, T. E. Massey, *Toxicol. Sci.* **2003**, *75*, 169–180.
64. K. M. Waldhauser, M. Török, H. R. Ha, U. Thomet, D. Konrad, K. Brecht, F. Follath, S. Krähenbühl, *J. Pharmacol. Exp. Ther.* **2006**, *319*, 1413–1423. DOI:10.1124/jpet.106.108993
65. J. J. Harris, R. Jolivet, D. Attwell, *Neuron.* **2012**, *75*, 762–777.
DOI:10.1016/j.neuron.2012.08.019
66. A. N. Shrivastava, A. Triller, R. Melki, *Neuropharmacology.* **2020**, *169*, 107461. DOI:10.1016/j.neuropharm.2018.12.008
67. L. N. Zhang, Y. J. Sun, S. Pan, J. X. Li, Y. E. Qu, Y. Li, Y. L. Wang, Z. B. Gao, *Fundam. Clin. Pharmacol.* **2013**, *27*, 96–103.
DOI:10.1111/fcp.12000
68. D. F. Gray, A. S. Mihailidou, P. S. Hansen, K. A. Buhagiar, N. L. Bewick, H. H. Rasmussen, D. W. Whalley, *J. Pharmacol. Exp. Ther.* **1998**, *284*, 75–82.

69. A. D. Pitt, C. Fernandes, N. L. Bewick, P. D. Hemsworth, K. A. Buhagiar, P. S. Hansen, H. H. Rasmussen, L. Delbridge, D. W. Whalley, *Cardiovasc. Res.* **2003**, *57*, 101–108.
70. I. B. Turkyilmaz, R. Yanardag, *Marmara Pharm. J.* **2016**, *20*, 131–136. DOI:10.12991/mpj.20162062716

Povzetek

Amiodaron (AMD) je močna antiaritmična učinkovina, ki je primerna za zdravljenje tahikardij. Pri uporabi nekaterih učinkovin, vključno z antiaritmiki, lahko pride do negativnega vpliva na možgane. S-metil metionin sulfonijev klorid (MMSC) je znana spojina, ki vsebuje žveplo, in predstavlja nov močan antioksidant. Namen raziskave je bil raziskati zaščitne učinke MMSC na poškodbe možganov, ki jih povzročata amiodaron. Podgane so bile razdeljene v naslednje štiri skupine: kontrolna skupina (s koruznim oljem), MMSC (50 mg/kg na dan), AMD (100 mg/kg na dan), AMD (100 mg/kg na dan) + MMSC (50 mg/kg na dan). Po zdravljenju z AMD so se v možganih zmanjšale ravni glutationa, in celokupnih antioksidantov, katalaze, superoksidne dismutaze, glutation peroksidaze, paraoksonaze in Na⁺/K⁺-ATPaze, povečale pa so se lipidna peroksidacija in proteinski karbonil, skupni oksidativni status, indeks oksidativnega stresa in reaktivne kisikove zvrsti, ter aktivnosti mieloperoksidaze, acetilholin esteraze in laktat dehidrogenaze. Aplikacija MMSC je te rezultate spremenila. Zaključimo lahko, da je MMSC ublažila možganske poškodbe, ki jih je povzročil AMD, verjetno zaradi antioksidativnega in zaščitnega učinka na celice.



Except when otherwise noted, articles in this journal are published under the terms and conditions of the Creative Commons Attribution 4.0 International License

Scientific paper

Synthesis, Crystal Structures and Urease Inhibition of Zinc Complexes Derived from 4-Chloro-2-(((2-(pyrrolidin-1-yl)ethyl)imino)methyl)phenol

Jian Jiang,^{1,*} Yao Liu,¹ Bo Liu,¹ Yijin Wang¹ and Zhonglu You²

¹ College of Chemical Engineering and Machinery, Eastern Liaoning University, Dandong 118003, P.R. China

² Department of Chemistry and Chemical Engineering, Liaoning Normal University, Dalian 116029, P.R. China

* Corresponding author: E-mail: jiangjiandd2012@126.com

Received: 12-20-2022

Abstract

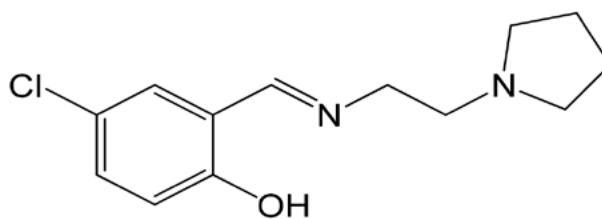
Three new zinc(II) complexes, $[Zn_3(\mu_2-\eta^1:\eta^1-OAc)_2(\mu_2-\eta^2:\eta^0-OAc)_2L_2]$ (**1**), $[Zn_3(\mu_2-\eta^1:\eta^1-OAc)_2(\mu_{1,1}-N_3)(N_3)L_2]$ (**2**), $[Zn_2(\mu_{1,3}-N_3)(N_3)(H_2O)L_2]$ (**3**), with the Schiff base ligand 4-chloro-2-(((2-(pyrrolidin-1-yl)ethyl)imino)methyl)phenol (HL) have been synthesized and characterized by elemental analysis, IR and UV-Vis spectroscopic studies. Crystal structures of the complexes were confirmed by single crystal X-ray diffraction. Complex **1** is a bidentate acetato, monooctatomic bridging acetato, and phenolato co-bridged trinuclear zinc compound. The Zn atoms are in octahedral and square pyramidal coordination. Complex **2** is a bidentate acetato, end-on azido, and phenolato co-bridged trinuclear zinc compound. The Zn atoms are in trigonal bipyramidal and square pyramidal coordination. Complex **3** is an end-to-end azido bridged dinuclear zinc compound. The Zn atoms are in square pyramidal and trigonal bipyramidal coordination. The Schiff base ligands in the complexes coordinate to the Zn atoms through the phenolate oxygen, imino nitrogen and pyrrolidine nitrogen. The complexes have interesting inhibitory activity on *Jack bean* urease, with IC_{50} values of 7.1–15.3 $\mu\text{mol}\cdot\text{L}^{-1}$.

Keywords: Schiff base; zinc complex; crystal structure; urease inhibition

1. Introduction

Urease catalyzes the rapid hydrolysis of urea to form ammonia, which is harmful for environment, agriculture and human health.¹ In the last few years, urease inhibitors have attracted much attention and numerous urease inhibitors have been reported.² Among the known urease inhibitors, hydroxamic acids, phosphoramides and thiols are the best recognized species. Because the low efficiency and negative side effects of the present urease inhibitors, the discovery of new and more efficient urease inhibitors is of high urgency. Schiff bases constitute a class of important ligands that have attracted much attention for their versatile coordination behavior toward various metal ions,³ and wide applications especially in biological fields such as antibacterial,⁴ antitumor,⁵ anti-inflammatory⁶ and cytotoxic,⁷ etc. Interestingly, Schiff base compounds have been reported to have urease inhibitory activities.⁸ Metal complexes with Schiff base ligands are reported to show effective biological activities, like antibacterial and urease in-

hibitory aspects.⁹ Zinc is an important biological element, its complexes play important roles in various enzymatic processes.¹⁰ In addition, acetate and azide anions are interesting bridging blocks in the construction of polynuclear complexes.¹¹ In this work, three new zinc complexes, $[Zn_3(\mu_2-\eta^1:\eta^1-OAc)_2(\mu_2-\eta^2:\eta^0-OAc)_2L_2]$ (**1**), $[Zn_3(\mu_2-\eta^1:\eta^1-OAc)_2(\mu_{1,1}-N_3)(N_3)L_2]$ (**2**), $[Zn_2(\mu_{1,3}-N_3)(N_3)(H_2O)L_2]$ (**3**), with the Schiff base ligand 4-chloro-2-(((2-(pyrrolidin-1-yl)ethyl)imino)methyl)phenol (HL, Scheme 1), are presented.



Scheme 1. The Schiff base HL

2. Experimental

2. 1. Materials and Methods

5-Chlorosalicylaldehyde and 1-(2-aminoethyl)pyrrolidine with analytical grade were purchased from TCI. All other chemicals were obtained from Xiya Chemical Co. Ltd. All the starting materials were used as received. Elemental analyses (CHN) were performed on a Perkin-Elmer 240C elemental analyzer. Infrared spectra were recorded on a Jasco FT/IR-4000 spectrophotometer in the region 4000–400 cm^{-1} using KBr pellets. Electronic absorption spectra were recorded with a Lambda 35 spectrophotometer. Single crystal X-ray diffraction was carried out with a Bruker SMART 1000 CCD diffractometer.

2. 2. Synthesis of $[\text{Zn}_3(\mu_2\text{-}\eta^1\text{:}\eta^1\text{-OAc})_2(\mu_2\text{-}\eta^2\text{:}\eta^0\text{-OAc})_2\text{L}_2]$ (1)

5-Chlorosalicylaldehyde (0.16 g, 1.0 mmol) was dissolved in 10 mL methanol, to which was added 10 mL methanol solution of 1-(2-aminoethyl)pyrrolidine (0.11 g, 1.0 mmol). The mixture was stirred for 10 min at room temperature. Then, zinc acetate dihydrate (0.44 g, 2.0 mmol) was added to the mixture. The final mixture was stirred at room temperature for 30 min to give a colorless solution. The solution was kept in air for several days to give colorless block-shaped single crystals of the complex. Yield: 0.18 g (38%). Anal. Calcd for $\text{C}_{34}\text{H}_{44}\text{Cl}_2\text{N}_4\text{O}_{10}\text{Zn}_3$: C, 43.64; H, 4.74; N, 5.99. Found: C, 43.47; H, 4.83; N, 6.12%. FT-IR data (KBr, cm^{-1}): $\nu(\text{C}=\text{N})$ 1646; 1585, 1526, 1463, 1436, 1387, 1310, 1293, 1185, 1126, 1071, 1023, 902, 868, 797, 673, 613, 545, 469. UV-Vis data [10^{-3} mol L^{-1} in methanol, λ/nm ($\epsilon/\text{L mol}^{-1} \text{cm}^{-1}$): 235 (16,370), 265 (5,725), 360 (3,130). Λ_{M} (10^{-3} M in methanol): $26 \Omega^{-1} \text{cm}^2 \text{mol}^{-1}$.

2. 3. Synthesis of $[\text{Zn}_3(\mu_2\text{-}\eta^1\text{:}\eta^1\text{-OAc})_2(\mu_{1,1}\text{-N}_3)(\text{N}_3)\text{L}_2]$ (2)

5-Chlorosalicylaldehyde (0.16 g, 1.0 mmol) was dissolved in 10 mL methanol, to which was added 10 mL methanol solution of 1-(2-aminoethyl)pyrrolidine (0.11 g, 1.0 mmol). The mixture was stirred for 10 min at room temperature. Then, zinc acetate dihydrate (0.44 g, 2.0 mmol) and sodium azide (0.13 g, 2.0 mmol) were added to the mixture. The final mixture was stirred at room temperature for 30 min to give a colorless solution. The solution was kept in air for several days to give colorless block-shaped single crystals of the complex. Yield: 0.23 g (51%). Anal. Calcd for $\text{C}_{30}\text{H}_{38}\text{Cl}_2\text{N}_{10}\text{O}_6\text{Zn}_3$: C, 39.96; H, 4.25; N, 15.53. Found: C, 40.12; H, 4.33; N, 15.41%. FT-IR data (KBr, cm^{-1}): $\nu(\text{N}_3)$ 2093, 2063; $\nu(\text{C}=\text{N})$ 1646; 1595, 1466, 1439, 1385, 1296, 1180, 1123, 1074, 1054, 897, 827, 798, 709, 667, 645, 615, 573, 538, 465, 440. UV-Vis data [10^{-3} mol L^{-1} in methanol, λ/nm ($\epsilon/\text{L mol}^{-1} \text{cm}^{-1}$): 238 (15,230), 265 (6,850), 360 (3,345). Λ_{M} (10^{-3} M in methanol): $31 \Omega^{-1} \text{cm}^2 \text{mol}^{-1}$.

2. 4. Synthesis of $[\text{Zn}_2(\mu_{1,3}\text{-N}_3)(\text{N}_3)(\text{H}_2\text{O})\text{L}_2]$ (3)

5-Chlorosalicylaldehyde (0.16 g, 1.0 mmol) was dissolved in 10 mL methanol, to which was added 10 mL methanol solution of 1-(2-aminoethyl)pyrrolidine (0.11 g, 1.0 mmol). The mixture was stirred for 10 min at room temperature. Then, zinc nitrate hexahydrate (0.60 g, 2.0 mmol) and sodium azide (0.13 g, 2.0 mmol) were added to the mixture. The final mixture was stirred at room temperature for 30 min to give a colorless solution. The solution was kept in air for several days to give colorless block-shaped single crystals of the complex. Yield: 0.23 g (51%). Anal. Calcd for $\text{C}_{26}\text{H}_{34}\text{Cl}_2\text{N}_{10}\text{O}_3\text{Zn}_2$: C, 42.41; H, 4.65; N, 19.02. Found: C, 42.26; H, 4.58; N, 18.89%. FT-IR data (KBr, cm^{-1}): $\nu(\text{N}_3)$ 2140, 2069; $\nu(\text{C}=\text{N})$ 1643; 1595, 1528, 1467, 1390, 1308, 1245, 1173, 1131, 1047, 901, 826, 795, 706, 647, 605, 521, 472, 435. UV-Vis data [10^{-3} mol L^{-1} in methanol, λ/nm ($\epsilon/\text{L mol}^{-1} \text{cm}^{-1}$): 233 (16,110), 265 (5,473), 370 (4,125). Λ_{M} (10^{-3} M in methanol): $36 \Omega^{-1} \text{cm}^2 \text{mol}^{-1}$.

2. 5. X-Ray Crystallography

The X-ray data of the three complexes were collected at 298(2) K on a Bruker SMART 1000 CCD diffractometer with graphite-monochromated Mo K α radiation (0.71073 Å) from a classical sealed tube. The intensity data were reduced with SAINT.¹² The multi-scan absorption correction was performed with SADABS.¹³ Structures of the complexes were solved with SHELXTL by direct methods and refined against F^2 by full-matrix least-squares method.¹⁴ All non-hydrogen atoms of the compounds were refined anisotropically. The water H atoms in complex 3 were located from a difference Fourier map and refined with O–H and H...H distances restrained to 0.85(1) and 1.37(2) Å, respectively. All other hydrogen atoms were placed in calculated positions and constrained to ride on their parent atoms. The group C21–C22–N4–C23–C24–C25–C26 in complex 2 is disordered over two sites, with occupancies of 0.47(2) and 0.53(2), respectively. The low bond precision on C–C bonds of complex 1 may be due to the poor diffraction quality of the crystal. In complexes 2 and 3, the large differences of atoms N2, C8–C13 (for 2) and N7, N8, C22 (for 3) are due to the slight disorder of the groups. Crystallographic data for the complexes are summarized in Table 1.

3. Results and Discussion

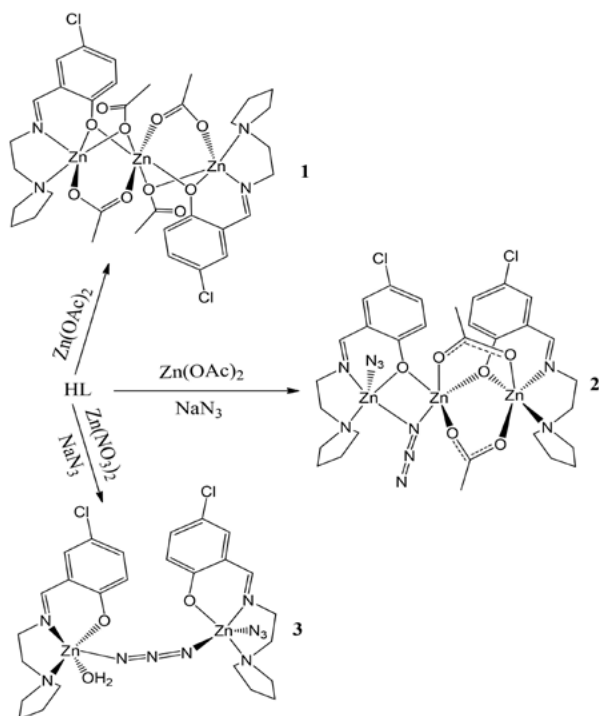
3. 1. Synthesis

The complexes 1–3 were facile prepared by reaction of the newly formed Schiff base with zinc acetate (1), zinc acetate and sodium azide (2), zinc nitrate and sodium azide (3), respectively in methanol. Single crystals of the

Table 1. Crystal data for the complexes

	1	2	3
Formula	C ₃₄ H ₄₄ Cl ₂ N ₄ O ₁₀ Zn ₃	C ₃₀ H ₃₈ Cl ₂ N ₁₀ O ₆ Zn ₃	C ₂₆ H ₃₄ Cl ₂ N ₁₀ O ₃ Zn ₂
FW	935.74	901.71	736.27
Crystal shape/color	block/colorless	block/colorless	block/colorless
Crystal size /mm	0.15'0.13'0.13	0.19'0.18'0.15	0.26'0.23'0.21
Crystal system	Monoclinic	Monoclinic	Triclinic
Space group	<i>P</i> 2 ₁ / <i>c</i>	<i>P</i> 2 ₁ / <i>n</i>	<i>P</i> 1
<i>a</i> (Å)	24.5043(12)	12.9152(11)	8.9470(7)
<i>b</i> (Å)	8.4919(6)	17.0982(14)	12.9416(11)
<i>c</i> (Å)	21.1838(13)	17.0597(15)	14.5580(12)
α (°)	90	90	79.583(1)
β (°)	115.138(1)	93.113(2)	89.490(1)
γ (°)	90	90	74.624(1)
<i>V</i> (Å ³)	3990.6(4)	3761.7(6)	1597.2(2)
<i>Z</i>	4	4	2
λ (MoK α) (Å)	0.71073	0.71073	0.71073
<i>T</i> (K)	298(2)	298(2)	298(2)
μ (MoK α) (cm ⁻¹)	1.980	2.094	1.714
<i>T</i> _{min}	0.7555	0.6917	0.6642
<i>T</i> _{max}	0.7828	0.7441	0.7148
<i>R</i> _{int}	0.0406	0.0344	0.0415
Reflections	20735	19896	17089
Parameters	481	508	394
Unique reflections	7410	7011	5892
Observed reflections [<i>I</i> ≥ 2σ(<i>I</i>)]	5263	4926	4542
Restraints	0	106	43
Goodness of fit on <i>F</i> ²	1.147	1.020	1.096
<i>R</i> ₁ , <i>wR</i> ₂ [<i>I</i> ≥ 2σ(<i>I</i>)] ^a	0.0724, 0.1990	0.0439, 0.1074	0.0818, 0.2496
<i>R</i> ₁ , <i>wR</i> ₂ (all data) ^a	0.1008, 0.2118	0.0720, 0.1240	0.1006, 0.2637

$$^a R_1 = \sum ||F_o| - |F_c|| / \sum |F_o|, wR_2 = [\sum w(F_o^2 - F_c^2)^2 / \sum w(F_o^2)]^{1/2}$$

**Scheme 2.** The synthetic procedure for the complexes

complexes were formed by slow evaporation method. Molar conductivity of the zinc complexes in methanol with concentrations of about 10⁻³ mol·L⁻¹ is 26–36 Ω⁻¹·cm²·mol⁻¹, indicating the non-electrolytic nature of the complexes.¹⁵

3. 2. Structure Description of Complex 1

Molecular structure of the trinuclear zinc complex **1** is shown in Figure 1. Selected bond lengths and angles are given in Table 2. There are two independent molecules in the compound. Both molecules possess crystallographic inversion center symmetry, with the centers located at the Zn2 and Zn4 atoms. The Zn1...Zn2 and Zn3...Zn4 distances are 3.091(2) and 3.070(2) Å, respectively. The Schiff base ligand coordinates to the Zn atoms through the phenolate O, imino N, and pyrrolidine N atoms, generating a five- and a six-membered chelate rings with bite angles of 80.5(3)° and 88.0(3)°, respectively for Zn1, and 81.8(3)° and 87.1(2)°, respectively for Zn3. The Zn1 and Zn3 atoms are in coordination geometry between square pyramidal and trigonal bipyramidal, as evidenced by the index factor τ (0.50 for Zn1 and 0.47 for Zn3).¹⁶ Three donor atoms come from a Schiff base ligand, and the other two come

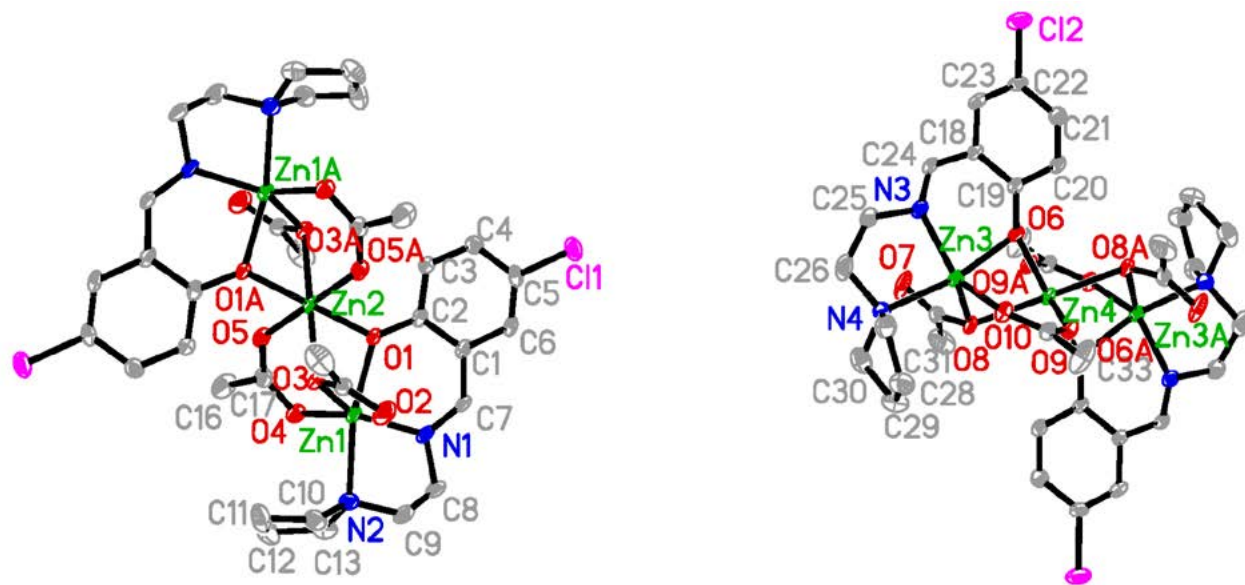


Figure 1. Molecular structure of complex **1**, showing the atom-numbering scheme. Displacement ellipsoids are drawn at the 30% probability level. Unlabeled atoms are related to the symmetry operations $1 - x, 1 - y, - z$ (left) and $- x, 1 - y, 1 - z$ (right). Hydrogen atoms are omitted for clarity.

respectively from a bidentate acetate and a monoatomic acetate ligands. The Zn2 and Zn4 atoms are in octahedral coordination, with the two phenolate O atoms from two Schiff base ligands and two O atoms from two bidentate acetate ligands defining the equatorial plane, and with the two O atoms from two monoanionic acetate ligands occupying the axial positions. The bond lengths around the Zn atoms are within normal values with the reported zinc(II) complexes derived from Schiff base ligands.¹⁷

The neighboring molecules of the complex are connected by intermolecular C7–H7...O2 and C24–H24...O7

hydrogen bonds (Table 3), to form one-dimensional chains running along the *c* axis (Figure 2).

3. 3. Structure Description of Complex 2

Molecular structure of the trinuclear zinc complex **2** is shown in Figure 3. Selected bond lengths and angles are given in Table 2. The Zn1...Zn2 and Zn2...Zn3 distances are 3.310(2) and 3.195(2) Å, respectively. The Schiff base ligand coordinates to the Zn atoms through the phenolate O, imino N, and pyrrolidine N atoms, generating a five- and a six-membered chelate rings with bite angles of 80.57(16)° and 83.67(14)°, respectively for Zn1, and 82.17(16)° and 86.42(14)°, respectively for Zn3. The Zn1 atom is in distorted square pyramidal coordination, as evidenced by the index factor τ (0.29). The basal plane is defined by the three donor atoms (O1, N1, N2) of the Schiff base ligand, and the N8 atom of the end-on azide ligand, and the apical position is occupied by the N5 atom of the terminal azide ligand. The distortion of the square pyramidal coordination is also indicated by the bond angles. The *cis* and *trans* angles in the basal plane are 76.77(14)-102.38(16)° and 137.59(17)-154.98(14)°, respectively. The bond angles among the apical and basal donor atoms are 101.51(18)-111.32(18)°. The Zn2 atom is in trigonal bipyramidal coordination, as evidenced by the index factor τ (0.72). The equatorial plane is defined by two phenolate O atoms (O1, O2) from two Schiff base ligands, and one O atom (O3) of an acetate ligand, and the two axial positions are occupied by one O atom (O5) of the other acetate ligand and one N atom (N8) of the end-on azide ligand. The three bond angles in the equatorial plane are 110.86(13)-125.86(13)°, and the angles among the axial and equatorial donor atoms are

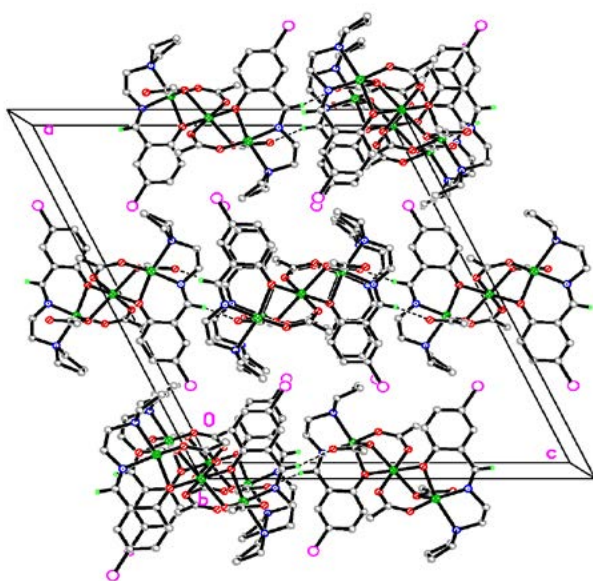


Figure 2. Molecular packing structure of complex **1**, viewed down the *b* axis. Hydrogen bonds are drawn as dotted lines.

76.51(14)–96.74(15)°. The Zn3 atom is in trigonal bipyramidal coordination, as evidenced by the index factor τ (0.70). The equatorial plane is defined by the imino N atom (N3) of the Schiff base ligand, and two O atoms (O4, O6) from two acetate ligands, and the two axial positions are occupied by one phenolate O atom (O2) and one pyrrolidine N atom (N4) of the Schiff base ligand. The three bond angles in the equatorial plane are 115.96(15)–126.26(16)°, and the angles among the axial and equatorial donor atoms are 82.17(16)–94.31(13)°. The bond lengths around the three Zn atoms are within normal values with the reported zinc(II) complexes derived from Schiff base ligands.¹⁷

The neighboring molecules of the complex are connected by intermolecular C7–H7...O3, C8–H8A...O5 and C20–H20...N10 hydrogen bonds (Table 3), to form one-dimensional chains running along the *b* axis (Figure 4). In addition, there are C–H... π interactions in the crystal packing [C9–H9B...Cg1^{#1}, 2.76 Å; C18–H18...Cg2^{#2}, 2.67 Å; C22–H22A...Cg3^{#3}, 2.56 Å; C25–H25A...Cg1^{#4}, 2.68 Å; Cg1 = C1–C6; Cg2 = Zn1–O1–Zn2–N8; Cg3 = C14–C19; symmetry codes: #1, 1 – *x*, 1 – *y*, 1 – *z*; #2, *x*, *y*, *z*; #3, 1 – *x*, – *y*, 1 – *z*; #4, 1/2 + *x*, 1/2 – *y*, –1/2 + *z*].

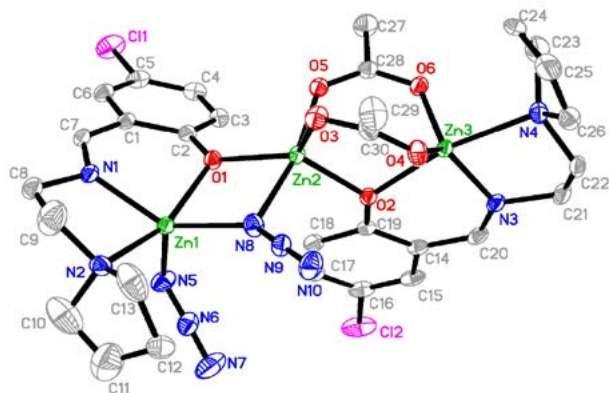


Figure 3. Molecular structure of complex 2, showing the atom-numbering scheme. Displacement ellipsoids are drawn at the 30% probability level.

3. 4. Structure Description of Complex 3

Molecular structure of the dinuclear zinc complex 3 is shown in Figure 5. Selected bond lengths and angles are given in Table 2. The Zn1...Zn2 distance is 5.797(2) Å. The Schiff base ligand coordinates to the Zn atoms through the phenolate O, imino N, and pyrrolidine N atoms, generating a five- and a six-membered chelate rings with bite angles of 79.1(3)° and 88.9(2)° for Zn1, and 79.3(3)° and 87.0(3)° for Zn2, respectively. The Zn1 atom is in a distorted square pyramidal coordination, as evidenced by the index factor τ (0.37). The basal plane is defined by the three donor atoms of one Schiff base ligand, and one water O atom. The apical position is occupied by one N atom of the bridging azide ligand. The Zn1 atom deviates from the least-squares plane defined by the four basal donor atoms by 0.367(2) Å. The Zn2 atom is in a distorted trigonal-bipyramidal coordination, as evidenced by the index factor τ (0.63). The equatorial plane is defined by the imino N atom of one Schiff base ligand, two N atoms respectively from one bridging and one terminal azide ligands. The two

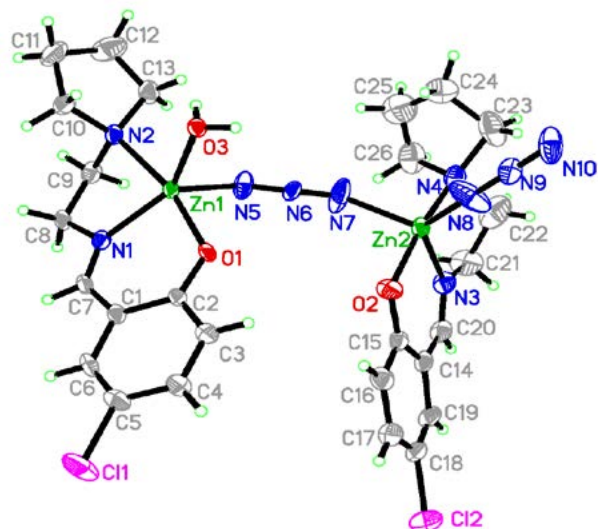


Figure 5. Molecular structure of complex 3, showing the atom-numbering scheme. Displacement ellipsoids are drawn at the 30% probability level.

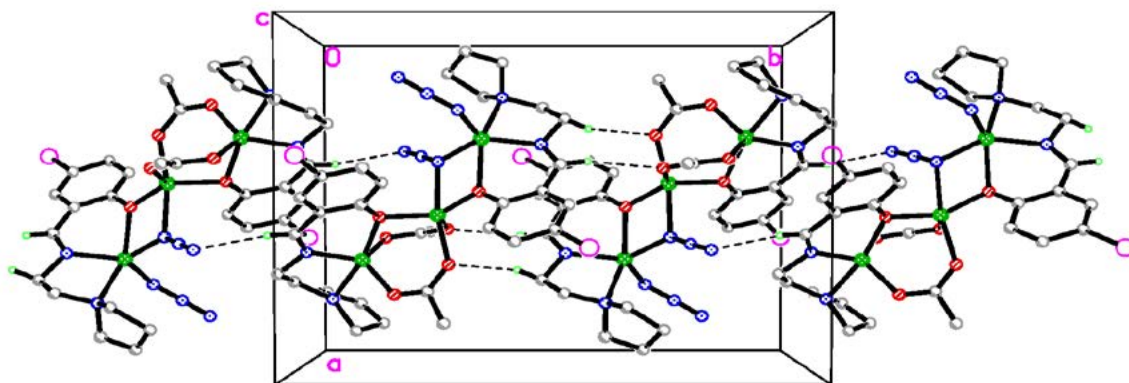


Figure 4. Molecular packing structure of complex 2, viewed down the *c* axis. Hydrogen bonds are drawn as dotted lines.

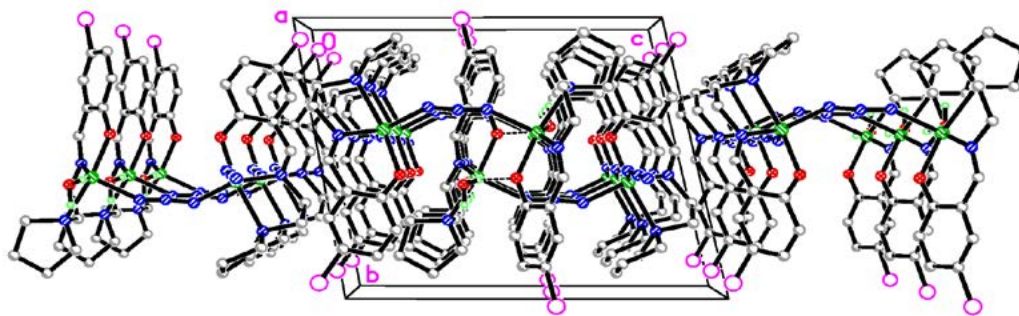


Figure 6. Molecular packing structure of complex 3, viewed down the *a* axis. Hydrogen bonds are drawn as dotted lines.

axial positions are occupied by one phenolate O and one pyrrolidine N atoms of the Schiff base ligand. The Zn2 atom deviates from the least-squares plane defined by the three equatorial donor atoms by 0.023(2) Å. The bond lengths around the Zn1 and Zn2 atoms are within normal values with the reported zinc(II) complexes derived from Schiff base ligands.¹⁷

The neighboring molecules of the complex are connected by intermolecular O3–H3B...O1^v hydrogen bonds (Table 3), to form dimeric structure (Figure 6). In addition, there are C–H... π interactions in the crystal packing [C9–H9A...Cg4^{#5}, 2.77 Å; C24–H24A...Cg4^{#1}, 2.97 Å; Cg4 = C1–C6; symmetry codes: #5, 2 – *x*, 1 – *y*, 1 – *z*].

3. 5. Pharmacology Study

The assay of the urease inhibitory activity was in accordance with the literature method.¹⁸ The free Schiff base and zinc acetate have weak activity, with inhibition rates of 15.1% and 22.8% at concentration of 100 $\mu\text{mol}\cdot\text{L}^{-1}$. However, the three zinc complexes have stronger activity than the Schiff base, with IC₅₀ values of 15.3 $\mu\text{mol}\cdot\text{L}^{-1}$ (1), 13.9 $\mu\text{mol}\cdot\text{L}^{-1}$ (2), and 7.1 $\mu\text{mol}\cdot\text{L}^{-1}$ (3). It is obvious that the azide coordinated complexes have better activity than those with acetate ligands. However, the sodium azide itself has no activity on urease. Thus, the zinc complexes have better activities than their starting materials. In addi-

Table 2. Selected bond lengths (Å) and angles (°) for the complexes

1			
Zn1–O1	2.120(5)	Zn1–O3	2.020(5)
Zn1–O4	1.979(6)	Zn1–N1	2.021(7)
Zn1–N2	2.259(7)	Zn2–O1	2.097(5)
Zn2–O3	2.177(5)	Zn2–O5	2.038(6)
Zn3–O10	1.992(6)	Zn3–N3	2.051(7)
Zn3–O8	2.058(6)	Zn3–O6	2.105(5)
Zn3–N4	2.248(7)	Zn4–O9	2.045(6)
Zn4–O6	2.086(5)	Zn4–O8	2.196(5)
O4–Zn1–O3	99.0(2)	O4–Zn1–N1	121.8(3)
O3–Zn1–N1	138.5(3)	O4–Zn1–O1	93.7(2)
O3–Zn1–O1	81.8(2)	N1–Zn1–O1	88.0(3)
O4–Zn1–N2	95.3(3)	O3–Zn1–N2	104.6(3)
N1–Zn1–N2	80.5(3)	O1–Zn1–N2	168.0(2)
O5–Zn2–O5A	180	O5–Zn2–O1A	89.9(2)
O5–Zn2–O1	90.1(2)	O1–Zn2–O1A	180
O5–Zn2–O3A	91.1(2)	O5–Zn2–O3	88.9(2)
O1–Zn2–O3A	101.3(2)	O1–Zn2–O3	78.7(2)
O5–Zn2–O3A	91.1(2)	O1–Zn2–O3A	101.3(2)
O3–Zn2–O3A	180		
O10–Zn3–N3	119.2(3)	O10–Zn3–O8	99.7(2)
N3–Zn3–O8	140.3(3)	O10–Zn3–O6	93.1(2)
N3–Zn3–O6	87.1(2)	O8–Zn3–O6	83.2(2)
O10–Zn3–N4	94.2(3)	N3–Zn3–N4	81.8(3)
O8–Zn3–N4	104.0(3)	O6–Zn3–N4	168.7(2)
O9–Zn4–O9B	180	O9–Zn4–O6B	90.1(2)
O9–Zn4–O6	89.9(2)	O6–Zn4–O6B	180
O9–Zn4–O8B	90.8(2)	O6–Zn4–O8B	99.7(2)

O9–Zn4–O8	89.2(2)	O9–Zn4–O8B	90.8(2)
O6–Zn4–O8	80.3(2)	O8–Zn4–O8B	180
Symmetry codes: A: 1 - x, 1 - y, - z; B: - x, 1 - y, 1 - z.			
2			
Zn1–O1	2.183(3)	Zn1–N1	2.048(4)
Zn1–N2	2.263(4)	Zn1–N5	1.965(4)
Zn1–N8	2.032(4)	Zn2–O1	1.995(3)
Zn2–O2	1.997(3)	Zn2–O3	2.007(4)
Zn2–O5	2.046(3)	Zn2–N8	2.226(4)
Zn3–O2	2.134(3)	Zn3–O4	1.980(3)
Zn3–O6	1.966(3)	Zn3–N3	2.029(4)
Zn3–N4	2.213(4)		
N5–Zn1–N8	109.28(19)	N5–Zn1–N1	111.32(18)
N8–Zn1–N1	137.59(17)	N5–Zn1–O1	101.51(18)
N8–Zn1–O1	76.77(14)	N1–Zn1–O1	83.67(14)
N5–Zn1–N2	102.28(19)	N8–Zn1–N2	102.38(16)
N1–Zn1–N2	80.57(16)	O1–Zn1–N2	154.98(14)
O1–Zn2–O2	125.86(13)	O1–Zn2–O3	121.73(14)
O2–Zn2–O3	110.86(13)	O1–Zn2–O5	95.54(13)
O2–Zn2–O5	93.99(14)	O3–Zn2–O5	92.62(16)
O1–Zn2–N8	76.51(14)	O2–Zn2–N8	96.74(15)
O3–Zn2–N8	85.46(16)	O5–Zn2–N8	169.09(15)
O6–Zn3–O4	117.78(15)	O6–Zn3–N3	115.96(15)
O4–Zn3–N3	126.26(16)	O6–Zn3–O2	94.31(13)
O4–Zn3–O2	90.56(13)	N3–Zn3–O2	86.42(14)
O6–Zn3–N4	94.11(15)	O4–Zn3–N4	93.10(14)
N3–Zn3–N4	82.17(16)	O2–Zn3–N4	167.97(13)
3			
Zn1–O1	2.020(6)	Zn1–O3	1.982(5)
Zn1–N1	2.042(7)	Zn1–N2	2.246(7)
Zn1–N5	2.063(8)	Zn2–O2	2.052(7)
Zn2–N3	2.049(8)	Zn2–N4	2.310(9)
Zn2–N7	2.025(12)	Zn2–N8	1.975(13)
O3–Zn1–O1	95.8(2)	O3–Zn1–N1	145.3(2)
O1–Zn1–N1	88.9(2)	O3–Zn1–N5	96.8(3)
O1–Zn1–N5	95.4(3)	N1–Zn1–N5	117.0(3)
O3–Zn1–N2	91.9(2)	O1–Zn1–N2	167.3(2)
N1–Zn1–N2	79.1(3)	N5–Zn1–N2	93.7(3)
N8–Zn2–N7	114.6(7)	N8–Zn2–N3	128.9(5)
N7–Zn2–N3	116.5(5)	N8–Zn2–O2	91.6(4)
N7–Zn2–O2	93.7(4)	N3–Zn2–O2	87.0(3)
N8–Zn2–N4	99.2(5)	N7–Zn2–N4	89.8(4)
N3–Zn2–N4	79.3(3)	O2–Zn2–N4	166.0(3)

Table 3. Hydrogen bond distances (Å) and bond angles (°) for the complexes

D–H...A	d(D–H)	d(H...A)	d(D...A)	Angle (D–H...A)
1				
C7–H7...O2 ⁱ	0.93	2.25	3.1709(2)	169(3)
C24–H24...O7 ⁱⁱ	0.93	2.27	3.1649(2)	162(3)
2				
C7–H7...O3 ⁱⁱⁱ	0.93	2.56	3.4745(3)	167(4)
C8–H8A...O5 ⁱⁱⁱ	0.97	2.37	3.3022(3)	160(4)
C20–H20...N10 ^{iv}	0.93	2.56	3.4785(3)	170(4)
3				
O3–H3A...O1 ^v	0.85(1)	1.76(2)	2.615(7)	176(11)
O3–H3B...O2 ^v	0.85(1)	1.82(2)	2.593(7)	149(11)

Symmetry codes: (i): 1 - x, 1/2 + y, 1/2 - z; (ii): - x, -1/2 + y, 1/2 - z; (iii): 1 - x, 1 - y, 1 - z; (iv): 1 - x, - y, 1 - z; (v): 1 - x, 1 - y, 1 - z.

tion, the present zinc complexes have stronger activities than the reference drug acetohydroxamic acid ($IC_{50} = 28.1 \mu\text{mol}\cdot\text{L}^{-1}$).

4. Conclusion

In summary, three new acetate and azide coordinated polynuclear zinc complexes have been synthesized. Structures of the complexes have been confirmed with single crystal X-ray diffraction. The Schiff base compound coordinates to the zinc atoms through the phenolate oxygen, imino nitrogen and pyrrolidine nitrogen. The Zn atoms in the complexes are in square pyramidal or trigonal-bipyramidal coordination, or that between them. The complexes have interesting urease inhibitory activity, which may be used as new urease inhibitors.

Supplementary Data

CCDC 2231647 (1), 2231648 (2) and 2231649 (3) contain the supplementary crystallographic data for this paper. These data can be obtained free of charge via <http://www.ccdc.cam.ac.uk/conts/retrieving.html>, or from the Cambridge Crystallographic Data Centre, 12 Union Road, Cambridge CB2 1EZ, UK; fax: (+44) 1223-336-033; or e-mail: deposit@ccdc.cam.ac.uk.

5. References

- (a) A. T. Fiori-Duarte, R. P. Rodrigues, R. R. Kitagawa, D. F. Kawano, *Curr. Med. Chem.* **2020**, *27*, 3967–3982; DOI:10.2174/0929867326666190301143549
(b) M. Taha, N. H. Ismail, S. Imran, A. Wadood, F. Rahim, M. Riaz, *J. Bioorg. Med. Chem.* **2015**, *23*, 7211–7218. DOI:10.1515/reveh-2020-0088
(c) A. Ray, C. Nkwonta, P. Forrestal, M. Danaher, K. Richards, T. O'Callaghan, S. Hogan, E. Cummins, *Rev. Environ. Health* **2021**, *36*, 477–491;
(d) T. Lan, Y. X. Huang, X. Song, O. P. Deng, W. Zhou, L. Luo, X. Y. Tang, J. Zeng, G. D. Chen, X. S. Gao, *Environ. Pollut.* **2021**, *293*, 118499; DOI:10.1016/j.envpol.2021.118499
(e) M. P. Byrne, J. T. Tobin, P. J. Forrestal, M. Danaher, C. G. Nkwonta, K. Richards, E. Cummins, S. A. Hogan, T. F. O'Callaghan, *Sustainability* **2020**, *12*, 6018. DOI:10.3390/su12156018
- (a) G. I. Perez-Perez, C. B. Gower, M. J. Blaser, *Infect. Immun.* **1994**, *62*, 299–302. DOI:10.1128/iai.62.1.299-302.1994
(b) R. Mamidala, S. R. S. Bhimathati, A. Vemn, *Bioorg. Chem.* **2021**, *114*, 105010;
(c) S. Iqbal, A. Khan, R. Nazir, S. Kiran, S. Perveen, K. M. Khan, M. I. Choudhary, *Med. Chem.* **2020**, *16*, 244–255; DOI:10.2174/1573406415666190415163309
(d) S. Daud, O. U. R. Abid, A. Sardar, B. A. Shah, M. Rafiq, A. Wadood, M. Ghufuran, W. Rehman, Zain-ul-Wahab, F. Iftikhar, R. Sultana, H. Daud, B. Niaz, *Med. Chem. Res.* **2022**, *31*, 316–336; DOI:10.1007/s00044-021-02814-6
(e) M. Talebi, E. Hamidian, F. Niasari-Naslaji, S. Rahmani, F. S. Hosseini, S. Boumi, M. N. Montazer, M. Asadi, M. Amanlou, *Med. Chem. Res.* **2021**, *30*, 1220–1229; DOI:10.1007/s00044-021-02727-4
(f) M. A. S. Aslam, S. Mahmood, M. Shahid, A. Saeed, J. Iqbal, *Eur. J. Med. Chem.* **2011**, *46*, 5473–5479; DOI:10.1016/j.ejmech.2011.09.009
(g) E. Menteşe, M. Emirik, B. B. Sökmen, *Bioorg. Chem.* **2019**, *86*, 151–158. DOI:10.1016/j.bioorg.2019.01.061
- (a) L.-W. Xue, X. Fu, G.-Q. Zhao, Q.-B. Li, *Acta Chim. Slov.* **2021**, *68*, 17–24; DOI:10.17344/acsi.2020.5817
(b) N. Biswas, S. Saha, E. Zangrando, A. Frontera, C. R. Choudhury, *Acta Chim. Slov.* **2021**, *68*, 212–221; DOI:10.17344/acsi.2020.6379
(c) S. A. Majid, J. M. Mir, G. Jan, A. H. Shalla, *J. Coord. Chem.* **2022**, *75*, 2018–2038; DOI:10.1080/00958972.2022.2131402
(d) A. Soroceanu, A. Bargan, *Crystals* **2022**, *12*, 1436; DOI:10.3390/cryst12101436
(e) A. S. Hossain, J. M. Mendez-Arriaga, C. K. Xia, J. M. Xie, S. Gomez-Ruiz, *Polyhedron* **2022**, *217*, 115692. DOI:10.1016/j.poly.2022.115692
- (a) E. Keshavarzian, Z. Asadi, M. Kucerakova, M. Dusek, B. Rastegari, *Polyhedron* **2022**, *223*, 115987; DOI:10.1016/j.poly.2022.115987
(b) S. H. Sumrra, W. Zafar, S. A. Malik, K. Mahmood, S. S. Shafqat, S. Arif, *Acta Chim. Slov.* **2022**, *69*, 200–216; <http://dx.doi.org/10.17344/acsi.2021.7182>
(c) H. E. Hashem, A. Nath, A. Kumer, *J. Mol. Struct.* **2022**, *1250*, 131915; DOI:10.1016/j.molstruc.2021.131915
(d) Y. Yuan, X.-K. Lu, G.-Q. Zhou, X.-Y. Qiu, *Acta Chim. Slov.* **2021**, *68*, 1008–1015; DOI:10.17344/acsi.2021.7070
(e) X.-Q. Luo, Q.-R. Liu, Y.-J. Han, L.-W. Xue, *Acta Chim. Slov.* **2020**, *67*, 159–166. DOI:10.17344/acsi.2019.5303
- (a) M. Diz, M. L. Duran-Carril, J. Castro, S. Alvo, L. Bada, D. Vina, J. A. Garcia-Vazquez, *J. Inorg. Biochem.* **2022**, *236*, 111975; DOI:10.1016/j.jinorgbio.2022.111975
(b) Y. Sun, Y. L. Lu, M. L. Bian, Z. B. Yang, X. Y. Ma, W. K. Liu, *Eur. J. Med. Chem.* **2021**, *211*, 113098; DOI:10.1016/j.ejmech.2020.113098
(c) K. Venkateswarlu, N. Ganji, S. Daravath, K. Kanneboina, K. Rangan, Shivaraj, *Polyhedron* **2019**, *171*, 86–97. DOI:10.1016/j.poly.2019.06.048
- (a) M. Azam, S. I. Al-Resayes, A. Trzesowska-Kruszynska, R. Kruszynski, F. Shakeel, S. M. Soliman, M. Alam, M. R. Khan, S. M. Wabaidur, *J. Mol. Struct.* **2020**, *1201*, 127177; DOI:10.1016/j.molstruc.2019.127177
(b) A. M. Shawky, M. A. S. Abourehab, A. N. Abdalla, A. M. Gouda, *Eur. J. Med. Chem.* **2020**, *185*, 111780; DOI:10.1016/j.ejmech.2019.111780
(c) J. Ki, A. Mukherjee, S. Rangasamy, B. Purushothaman, J. M. Song, *RSC Advances* **2016**, *6*, S7530–S7539;
(d) M. S. Iqbal, S. J. Khurshid, B. Muhammad, *Med. Chem. Res.* **2013**, *22*, 861–868. DOI:10.1007/s00044-012-0068-0
- (a) A. Savci, N. Turan, K. Buldurun, M. E. Alkis, Y. Alan, *In-*

- org. Chem. Commun. **2022**, 143, 109780; DOI:10.1016/j.inoche.2022.109780
- (b) D. Dinev, K. B. Popova, T. Zhivkova, L. Dyakova, A. Abdalleh, R. Alexandrova, D. C. Culita, T. Mocanu, C. Maxim, G. Marinescu, *Appl. Organomet. Chem.* **2022**, 36, e6862; DOI:10.1002/aoc.6862
- (c) S.-Y. Chen, X.-H. Jiang, R.-X. Liu, Y. Huang, W.-Y. Shen, Y.-H. Jiang, K.-B. Huang, Y.-C. Liu, *Inorg. Chim. Acta* **2021**, 516, 120171. DOI:10.1016/j.ica.2020.120171
8. (a) S. A. S. Tirmazi, M. A. Qadir, M. Ahmed, M. Imran, R. Hussain, M. Sharif, M. Yousaf, M. Muddassar, *J. Mol. Struct.* **2021**, 1235, 130226; DOI:10.1016/j.molstruc.2021.130226
- (b) F. Naz, Kanwal, M. Latif, U. Salar, K. M. Khan, M. Al-Rashida, I. Ali, B. Ali, M. Taha, S. Perveen, *Bioorg. Chem.* **2020**, 105, 104365; DOI:10.1016/j.bioorg.2020.104365
- (c) A. De Fatima, C. D. Pereira, C. R. S. D. G. Olimpio, B. G. D. Oliveira, L. L. Franco, P. H. C. da Silva, *J. Adv. Res.* **2018**, 13, 113–126. DOI:10.1016/j.jare.2018.03.007
9. (a) Y. M. Li, L. Y. Xu, M. M. Duan, B. T. Zhang, Y. H. Wang, Y. X. Guan, J. H. Wu, C. L. Jing, Z. L. You, *Polyhedron* **2019**, 166, 146–152; DOI:10.1016/j.poly.2019.03.051
- (b) A. Barakat, S. M. Soliman, M. Ali, A. Elmarghany, A. M. Al-Majid, S. Yousuf, Z. Ul-Haq, M. I. Choudhary, A. El-Faham, *Inorg. Chim. Acta* **2020**, 503, 119405; DOI:10.1016/j.ica.2019.119405
- (c) J. Q. Wang, Y. Y. Luo, Y. X. Zhang, Y. Chen, F. Gao, Y. Ma, D. M. Xian, Z. L. You, *J. Coord. Chem.* **2020**, 74, 1028–1038; DOI:10.1080/00958972.2020.1861603
- (d) S. Han, Y. Wang, *Acta Chim. Slov.* **2021**, 68, 961–969. DOI:10.17344/acsi.2021.6965
10. (a) N. M. Plugis, N. D. Rudd, J. Krzystek, D. C. Swenson, J. Telser, J. A. Larrabee, *J. Inorg. Biochem.* **2020**, 203, 110876; DOI:10.1016/j.jinorgbio.2019.110876
- (b) J. C. Dewar, A. S. Thakur, W. W. Brennessel, M. Cafiero, L. W. Peterson, W. T. Eckenhoff, *Inorg. Chim. Acta* **2018**, 473, 15–19. DOI:10.1016/j.ica.2017.12.023
11. (a) J.-L. Hou, H.-Y. Wu, C.-B. Sun, Y. Bi, W. Chen, *Acta Chim. Slov.* **2020**, 67, 860–865; DOI:10.17344/acsi.2020.5824
- (b) G. Liu, B. Chen, D. X. Chen, *Russ. J. Coord. Chem.* **2012**, 37, 738–742; DOI:10.1134/S1070328411090053
- (c) A. Donmez, G. Oylumluoglu, M. B. Coban, C. Kocak, M. Aygun, H. Kara, *J. Mol. Struct.* **2017**, 1149, 569–575; DOI:10.1016/j.molstruc.2017.08.027
- (d) M. H. Sadhu, C. Mathoniere, Y. P. Patil, S. B. Kumar, *Polyhedron* **2017**, 122, 210–218; DOI:10.1016/j.poly.2016.11.036
- (e) S. Ray, S. Konar, A. Jana, K. Das, R. J. Butcher, T. K. Mondal, S. K. Kar, *Polyhedron* **2013**, 50, 51–58. DOI:10.1016/j.poly.2012.09.061
12. Bruker, SMART (Version 5.628) and SAINT (Version 6.02); Bruker AXS: Madison, Wisconsin, USA, 1998.
13. G. M. Sheldrick, SADABS Program for Empirical Absorption Correction of Area Detector, University of Göttingen, Germany, 1996.
14. G. M. Sheldrick, *Acta Crystallogr.* **2008**, A64, 112–122. DOI:10.1107/S0108767307043930
15. W. J. Geary, *Coord. Chem. Rev.* **1971**, 7, 81–120. DOI:10.1016/S0010-8545(00)80009-0
16. A. W. Addison, T. N. Rao, J. Reedijk, J. van Rijn, G. C. Verschoor, *J. Chem. Soc., Dalton Trans.* **1984**, 7, 1349–1356. DOI:10.1039/DT9840001349
17. (a) D.-L. Peng, N. Sun, *Acta Chim. Slov.* **2018**, 65, 895–901; DOI:10.17344/acsi.2018.4543
- (b) H.-Y. Qian, *Acta Chim. Slov.* **2021**, 68, 638–644; DOI:10.17344/acsi.2021.6656
- (c) I. Mondal, S. Chatterjee, S. Chattopadhyay, *Polyhedron* **2020**, 190, 114735; DOI:10.1016/j.poly.2020.114735
- (d) Z.-L. You, P. Hou, L.-L. Ni, S. Chen, *Inorg. Chem. Commun.* **2009**, 12, 444–446. DOI:10.1016/j.inoche.2009.03.009
18. T. Tanaka, M. Kawase, S. Tani, *Life Sci.* **2003**, 73, 2985–2990. DOI:10.1016/S0024-3205(03)00708-2

Povzetek

Sintetizirali smo tri nove komplekse cinka(II), $[Zn_3(\mu_2-\eta^1-\text{OAc})_2(\mu_2-\eta^2:\eta^0-\text{OAc})_2L_2]$ (**1**), $[Zn_3(\mu_2-\eta^1-\text{OAc})_2(\mu_{1,1}-N_3)(N_3)L_2]$ (**2**) in $[Zn_2(\mu_{1,3}-N_3)(N_3)(H_2O)L_2]$ (**3**), z ligandom 4-kloro-2-(((2-(pirolidin-1-il)etil)imino)metil)fenol (HL). Spojine smo karakterizirali z elementno analizo, IR in UV-Vis spektroskopskimi metodami. Kristalne strukture kompleksov smo potrdili z monokristalno rentgensko difrakcijo. Spojina **1** je trijedrna in vsebuje bidentatne acetatne ligande, mostovne acetate in mostovne fenolatne ligande. Tudi kompleks **2** je trijedrn z bidentatnimi acetatnimi, azidnimi in mostovnimi fenolatnimi ligandi. Kompleks **3** je dvojedrn z mostovnimi azidnimi ligandi. Koordinacija okoli cinkovih atomov je kvadratno piramidalna in trigonalno bipiramidalna. Ligandi, ki so Schiffove baze, se na cinkov atom koordinirajo preko kisika iz fenolatne skupine, dušika iz imino skupine in dušika iz pirolidina. Kompleksi delujejo kot inhibitorji na ureazo *Jack bean* z vrednostmi IC_{50} med 7.1 in 15.3 $\mu\text{mol}\cdot\text{L}^{-1}$.



Except when otherwise noted, articles in this journal are published under the terms and conditions of the Creative Commons Attribution 4.0 International License

Scientific paper

Trinuclear Zinc(II) Complexes Derived from *N,N'*-Bis-(5-bromosalicylidene)-1,2-cyclohexanediamine: Syntheses, Crystal Structures and Antimicrobial Activity

Guo-Xu He,¹ Xue-Yao Guo² and Ling-Wei Xue^{1,*}¹ School of Chemical and Environmental Engineering, Pingdingshan University, Pingdingshan Henan 467000, P.R. China² Pingdingshan Ecological Environment Monitoring Center, Pingdingshan Henan 467000, P.R. China

* Corresponding author: E-mail: pdsuchemistry@163.com

Received: 09-18-2022

Abstract

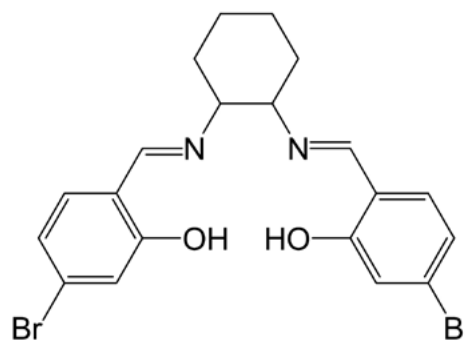
Two new trinuclear zinc(II) complexes, $[Zn_3I_2L_2(H_2O)_2]$ (**1**) and $[Zn_3(CH_3OH)(DMF)_2(NCS)_2]$ (**2**), where L is the dianionic form of *N,N'*-bis(5-bromosalicylidene)-1,2-cyclohexanediamine (H_2L), have been synthesized and characterized by elemental analyses, IR and UV spectra. Structures of the complexes were further confirmed by single crystal X-ray diffraction. Both complexes are trinuclear zinc compounds. Both compounds are solvated, with water ligand for **1** and methanol ligand for **2**. The outer two Zn atoms are in square pyramidal coordination, while the inner one is in octahedral coordination. The effect of the complexes on the antimicrobial activity against *Staphylococcus aureus*, *Escherichia coli* and *Candida albicans* were evaluated, and gave interesting results.

Keywords: Zinc complex, Trinuclear complex, Schiff base, Crystal structure, Antimicrobial activity

1. Introduction

Schiff bases have received increasing interest in the synthesis and structural studies because of their bioactivity and coordination properties.¹ Schiff bases have been reported to be active on fungal, cancer, convulsant, oxidant and diuretic activities.² The complexes of Schiff bases with various metal atoms have attracted remarkable interest due to their extensive biological activity like antibacterial, antifungal and antitumor.³ Moreover, the metal complexes have usually better biological activities than the free Schiff bases. It has been reported that the Salen type Schiff base complexes have excellent antimicrobial activities.⁴ Among the metal atoms, zinc is an important biological element, and its complexes with Schiff base ligands have interesting antimicrobial potential.⁵ Recent research indicated that the halide and pseudohalide groups can severely increase the antimicrobial activities.⁶ Our research group has reported some metal complexes with effective antimicrobial activities.⁷ In pursuit of new and efficient antimicrobial agents, in the present work, two new trinuclear zinc(II) complexes, $[Zn_3I_2L_2(H_2O)_2]$ (**1**) and $[Zn_3(CH_3OH)(DMF)_2(NCS)_2]$ (**2**), where L is the dianionic form of *N,N'*-bis(5-bromosalicylidene)-1,2-cyclohexanediamine

(H_2L) (Scheme 1), are reported. To our knowledge, no complexes with L have been reported so far.



Scheme 1. The Schiff base H_2L

2. Experimental

2.1. Material and Methods

4-Bromosalicylaldehyde and 1,2-diaminocyclohexane were purchased from Fluka. Other reagents and solvents were analytical grade and used without further puri-

fication. The Schiff base was prepared according to the literature method.⁸ Elemental (C, H, and N) analyses were made on a PerkinElmer Model 240B automatic analyser. Zinc analysis was carried out by EDTA titration. Infrared (IR) spectra were recorded on an IR-408 Shimadzu 568 spectrophotometer. UV-Vis spectra were recorded on a Lambda 900 spectrometer. X-ray diffraction was carried out on a Bruker SMART 1000 CCD area diffractometer.

2. 2. Synthesis of $[\text{Zn}_3\text{I}_2\text{L}_2(\text{H}_2\text{O})_2]$ (1)

H_2L (0.48 g, 1.0 mmol) was dissolved in 50 mL hot methanol, then, a methanolic solution (20 mL) of ZnI_2 (0.64 g, 2.0 mmol) was added dropwise at reflux. The mixture was stirred for 1 h to give a colorless solution. Colorless block-shaped single crystals suitable for X-ray diffraction were formed by slow evaporation of the solution in air for several days. Yield: 0.26 g (36%). Analysis Calcd. (%) for $\text{C}_{40}\text{H}_{40}\text{Br}_4\text{I}_2\text{N}_4\text{O}_6\text{Zn}_3$: C 33.31, H 2.80, N 3.88, Zn 13.60. Found (%): C 33.12, H 2.93, N 3.75, Zn 13.87. IR data (KBr, cm^{-1}): 1636 (CH=N). UV in methanol (λ , ϵ): 227 nm, $2.32 \times 10^3 \text{ L mol}^{-1} \text{ cm}^{-1}$; 245 nm, $2.41 \times 10^3 \text{ L mol}^{-1} \text{ cm}^{-1}$; 265 nm, $1.38 \times 10^3 \text{ L mol}^{-1} \text{ cm}^{-1}$; 350 nm, $5.25 \times 10^2 \text{ L mol}^{-1} \text{ cm}^{-1}$.

2. 3. Synthesis of $[\text{Zn}_3(\text{CH}_3\text{OH})(\text{DMF})\text{L}_2(\text{NCS})_2]$ (2)

H_2L (0.48 g, 1.0 mmol) was dissolved in 50 mL hot methanol, then, a methanolic solution (20 mL) of $\text{Zn}(\text{NO}_3)_2 \cdot 6\text{H}_2\text{O}$ (0.60 g, 2.0 mmol) and ammonium thiocyanate (0.15 g, 2.0 mmol) was added dropwise at reflux. DMF (10 mL) was added to the mixture to dissolve the precipitate. The mixture was stirred for 1 h to give a colorless solution. Colorless block-shaped single crystals suitable for X-ray diffraction were formed by slow evaporation of the solution in air for several days. Yield: 0.31 g (45%). Analysis Calcd. (%) for $\text{C}_{46}\text{H}_{47}\text{Br}_4\text{N}_7\text{O}_6\text{S}_2\text{Zn}_3$: C 40.22, H 3.45, N 7.14, Zn 14.28. Found (%): C 40.51, H 3.35, N 7.23, Zn 14.50. IR data (KBr, cm^{-1}): 2080 (NCS), 1638 (CH=N). UV in methanol (λ , ϵ): 230 nm, $2.46 \times 10^3 \text{ L mol}^{-1} \text{ cm}^{-1}$; 245 nm, $2.53 \times 10^3 \text{ L mol}^{-1} \text{ cm}^{-1}$; 262 nm, $1.16 \times 10^3 \text{ L mol}^{-1} \text{ cm}^{-1}$; 353 nm, $4.61 \times 10^2 \text{ L mol}^{-1} \text{ cm}^{-1}$.

2. 4. X-Ray Diffraction

Data were collected from selected crystals mounted on glass fibers. The data were collected with MoK_α radi-

Table 1. Crystallographic data and experimental details for the complexes

	1	2
Molecular formula	$\text{C}_{40}\text{H}_{40}\text{Br}_4\text{I}_2\text{N}_4\text{O}_6\text{Zn}_3$	$\text{C}_{46}\text{H}_{47}\text{Br}_4\text{N}_7\text{O}_6\text{S}_2\text{Zn}_3$
Formula weight	1442.31	1373.77
Crystal size, mm	0.19×0.15×0.15	0.25×0.23×0.22
Radiation (λ , Å)	MoK_α (0.71073)	MoK_α (0.71073)
Crystal system	Monoclinic	Monoclinic
Space group	$C2/c$	$P2_1/c$
Unit cell dimensions:		
a , Å	25.7336(13)	16.7986(14)
b , Å	14.6897(12)	15.1552(13)
c , Å	15.8224(12)	20.5748(15)
α , °	90	90
β , °	112.643(1)	99.539(1)
γ , °	90	90
V , Å ³	5520.1(7)	5165.6(7)
Z	4	4
ρ_{calcd} , g cm^{-3}	1.735	1.766
$F(000)$	2768	2728
T_{min} , T_{max}	0.430, 0.501	0.392, 0.430
Absorption coefficient, mm^{-1}	5.348	4.610
θ Range for data collection, °	1.63–25.50	1.23–25.50
Reflections collected	13966	27194
Independent reflections (R_{int})	5023 (0.0656)	9620 (0.0636)
Reflections with $I > 2\sigma(I)$	2362	5155
Data/parameters	5023/273	9620/619
Restraints	3	43
Goodness-of-fit on F^2	0.943	1.020
Final R indices ($I > 2\sigma(I)$)	$R_1 = 0.0696$ $wR_2 = 0.1674$	$R_1 = 0.0626$ $wR_2 = 0.1506$
R indices (all data)	$R_1 = 0.1542$ $wR_2 = 0.2153$	$R_1 = 0.1335$ $wR_2 = 0.1892$
Largest diff. peak and hole, $e/\text{Å}^3$	1.578, -1.043	1.107, -0.882

tion (0.71073 Å) at 298(2) K with a Bruker SMART 1000 CCD area diffractometer. The data for the complexes were processed with SAINT⁹ and corrected for absorption using SADABS.¹⁰ Multi-scan absorption corrections were applied with ψ -scans.¹¹ Structures of the two complexes were solved by direct method using SHELXS-97 and refined by full-matrix least-squares techniques on F^2 using anisotropic displacement parameters.¹² The water H atoms in complex **1** and the methanol H atom in complex **2** were located from difference Fourier maps and refined with O–H distances of 0.85(1) Å. All other hydrogen atoms were placed at the calculated positions. Idealized H atoms were refined with isotropic displacement parameters set to 1.2 (1.5 for methyl groups) times the equivalent isotropic U values of the parent carbon atoms. The crystallographic data for the complexes are listed Table 1.

Supplementary material has been deposited with the Cambridge Crystallographic Data Centre (nos. 2207640 (1), 2207645 (2)); deposit@ccdc.cam.ac.uk or <http://www.ccdc.cam.ac.uk>).

2. 5. Antimicrobial Assay

Qualitative determination of antimicrobial activity was done using the disk diffusion method.¹³ The antibacterial activity was tested against *B. subtilis*, *E. coli*, *P. fluorescence* and *S. aureus* using MH medium (Mueller–Hinton medium). The MICs (minimum inhibitory concentrations) of the test compounds were determined by a colorimetric method using the dye MTT [3-(4,5-dimethylthiazol-2-yl)-2,5-diphenyltetrazolium bromide]. A stock solution of the synthesized compound (50 $\mu\text{g}\cdot\text{mL}^{-1}$) in DMSO was prepared and quantities of the test compounds were incorporated in specified quantity of sterilized liquid MH medium. A specified quantity of the medium containing the compound was poured into micro-titration plates. A suspension of the microorganism was prepared to contain approximately 10^5 cfu $\cdot\text{mL}^{-1}$ and applied to micro-titration plates with serially diluted compounds in DMSO to be tested and incubated at 37 °C for 24 h. After the MICs were visually determined on each of the micro-titration plates, 50 μL of PBS containing 2 mg of MTT per millilitre was added to each well. Incubation was continued at room temperature for 4–5 h. The content of each well was removed and 100 μL of isopropanol containing hydrochloric acid was added to extract the dye. After 12 h of incubation at room temperature, the optical density (OD) was measured with a micro-plate reader at 550 nm.

3. Results and Discussion

3. 1. Chemistry

The Schiff base was facile prepared by the reaction of equimolar quantities of 4-bromosalicylaldehyde and 1,2-diaminocyclohexane in methanol. The two zinc com-

plexes are stable at room temperature in the solid state and soluble in common organic solvents, such as methanol, ethanol, chloroform, and acetonitrile. The results of the elemental analyses are in accord with the composition suggested for the complexes.

3.2. IR and Electronic Spectra

The IR spectra of the complexes were analyzed and compared with those of their free Schiff base. The intense absorption band at 1645 cm^{-1} in the spectrum of the Schiff base can be assigned to the C=N stretching. In the zinc complexes, these bands are shifted to 1636 cm^{-1} for **1** and 1638 cm^{-1} for **2** upon complexation, which can be attributed to the coordination of the imine nitrogen to the metal centre.¹⁴ The typical intense absorption at 2080 cm^{-1} in the spectrum of complex **2** is assigned to the vibration of the NCS ligand.¹⁵

UV–Vis spectra of the zinc complexes were recorded in methanol solution. The charge transfer bands at 220–270 nm can be assigned to $\pi\rightarrow\pi^*$ and $n\rightarrow\pi^*$ transitions of the Schiff base ligands. The bands at 350–355 nm can be assigned to the metal to ligand charge transfer (MLCT) transition.¹⁶

3. 4. Crystal Structure Description of Complex 1

Selected bond lengths and angles are listed in Table 2. The complex is a phenolato-bridged trinuclear zinc(II) compound (Figure 1), with Zn...Zn distance of 3.179(2) Å. The crystal of the complex possesses crystallographic two-fold rotation axis symmetry. The Zn1 atom is five-coordinated in a square pyramidal coordination, as evidenced by the structural index τ of 0.22.¹⁷ The basal plane of the square pyramidal coordination is defined by two phenolate O (O1, O2) and two imine N (N1, N2) atoms of the Schiff base ligand, and the apical position is occupied by I1 atom. The Zn1 atom deviates from the least-squares plane defined by the four basal donor atoms by 0.671(2) Å. The Schiff base acts as a tetradentate ligand, and forms one five- and two six-membered chelate rings with the Zn1 atom. The Zn2 atom is six-coordinated in an octahedral coordination. The equatorial plane of the octahedral coordination is defined by three phenolate O (O1, O2, O1A) atoms from two Schiff base ligands, and one O (O3) atom of a water ligand, and the axial positions are occupied by one phenolate O (O2A) atom of a Schiff base ligand, and one O (O3A) atom of the other water ligand. The dihedral angle between the two benzene rings C1–C6 and C15–C20 is 10.3(5)°. The bond distances subtended at the Zn atoms are comparable to those observed in similar zinc(II) complexes with Schiff bases.¹⁸ There present C–H...I hydrogen bonds (C6–H6 = 0.93 Å, H6...I1 = 3.129(3) Å, C6–H6...I1 = 165.0(3)°) in the crystal structure (Figure 2).

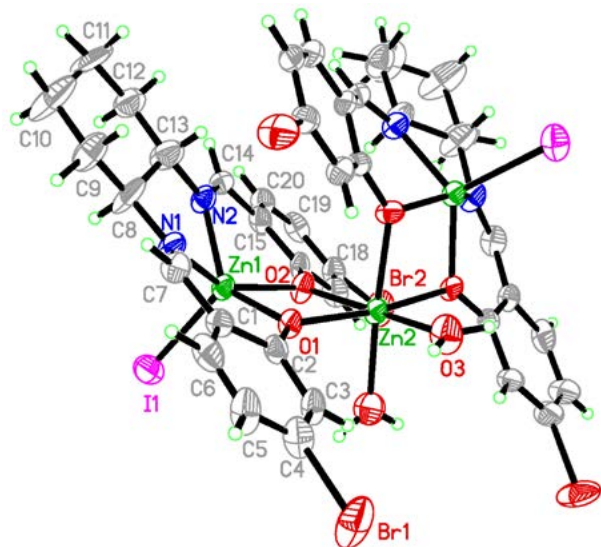


Figure 1. Molecular structure of complex 1. Unlabeled atoms are at the symmetry position $1 - x, - y, - z$.

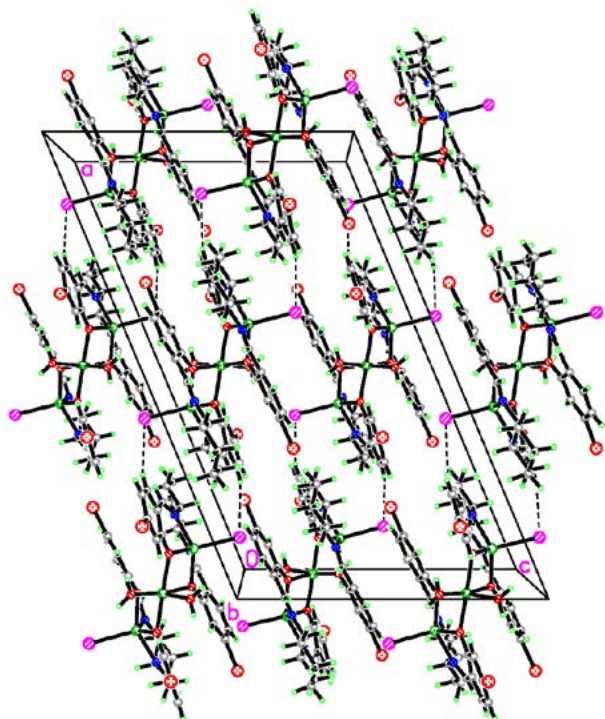


Figure 2. Molecular packing structure of complex 1, viewed along the b axis. Hydrogen bonds are shown as dashed lines.

3. 5. Crystal Structure Description of Complex 2

Selected bond lengths and angles are listed in Table 2. The complex is a phenolato-bridged trinuclear zinc(II) compound (Figure 3), with Zn...Zn distances of 3.170(2) and 3.202(2) Å. The Zn1 and Zn3 atoms are five-coordinated in square pyramidal coordination, as evidenced by

the structural index τ of 0.27 for Zn1 and 0.19 for Zn3.¹⁷ The basal planes of the square pyramidal coordination are defined by two phenolate O (O1 and O2 for Zn1, O3 and O4 for Zn3) and two imine N (N1 and N2 for Zn1, N3 and N4 for Zn3) atoms of the Schiff base ligands, and the apical positions are occupied by N5 atom for Zn1 and N6 atom for Zn3. The Zn1 and Zn3 atoms deviate from the least-squares planes defined by the four basal donor atoms by 0.640(2) and 0.646(2) Å, respectively. The Schiff base acts as a tetradentate ligand, and forms one five- and two six-membered chelate rings with the Zn atoms. The

Table 2. Selected bond distances (Å) and angles (°) for the complexes

1			
Zn1–O1	2.005(7)	Zn1–O2	2.017(6)
Zn1–N1	2.066(9)	Zn1–N2	2.027(9)
Zn1–I1	2.5854(15)	Zn2–O2	2.073(7)
Zn2–O1	2.086(5)	Zn2–O3	2.099(9)
O1–Zn1–O2	79.0(2)	O1–Zn1–N2	133.9(3)
O2–Zn1–N2	88.4(3)	O1–Zn1–N1	87.7(3)
O2–Zn1–N1	148.2(4)	N2–Zn1–N1	80.2(4)
O1–Zn1–I1	115.9(2)	O2–Zn1–I1	104.6(2)
N2–Zn1–I1	110.2(3)	N1–Zn1–I1	107.2(3)
O2–Zn2–O2A	88.0(4)	O2–Zn2–O1	75.9(2)
O2–Zn2–O1A	98.2(2)	O1–Zn2–O1A	172.0(4)
O2–Zn2–O3	172.5(3)	O2–Zn2–O3A	91.6(4)
O1–Zn2–O3	96.7(3)	O1–Zn2–O3A	89.0(3)
O3–Zn2–O3A	89.9(7)		
2			
Zn1–O1	2.021(5)	Zn1–O2	2.018(5)
Zn1–N1	2.080(8)	Zn1–N2	2.035(9)
Zn1–N5	2.000(10)	Zn2–O1	2.092(5)
Zn2–O2	2.140(5)	Zn2–O4	2.080(5)
Zn2–O5	2.057(6)	Zn2–O6	2.133(6)
Zn2–O3	2.156(5)	Zn3–O3	2.010(5)
Zn3–O4	2.028(5)	Zn3–N6	1.992(9)
Zn3–N3	2.054(7)	Zn3–N4	2.043(7)
N5–Zn1–O2	110.9(3)	N5–Zn1–O1	105.7(3)
O2–Zn1–O1	81.7(2)	N5–Zn1–N2	102.9(4)
O2–Zn1–N2	89.9(3)	O1–Zn1–N2	151.3(3)
N5–Zn1–N1	113.8(3)	O2–Zn1–N1	135.3(3)
O1–Zn1–N1	87.6(3)	N2–Zn1–N1	79.2(3)
O5–Zn2–O4	96.6(2)	O5–Zn2–O1	171.9(2)
O4–Zn2–O1	90.0(2)	O5–Zn2–O6	86.0(2)
O4–Zn2–O6	167.2(2)	O1–Zn2–O6	88.6(2)
O5–Zn2–O2	97.1(2)	O4–Zn2–O2	99.1(2)
O1–Zn2–O2	77.2(2)	O6–Zn2–O2	93.0(2)
O5–Zn2–O3	87.3(2)	O4–Zn2–O3	75.6(2)
O1–Zn2–O3	98.9(2)	O6–Zn2–O3	92.0(2)
O2–Zn2–O3	173.6(2)	N6–Zn3–O3	110.0(3)
N6–Zn3–O4	104.8(3)	O3–Zn3–O4	80.1(2)
N6–Zn3–N4	113.0(3)	O3–Zn3–N4	137.1(3)
O4–Zn3–N4	89.0(2)	N6–Zn3–N3	106.4(3)
O3–Zn3–N3	88.4(3)	O4–Zn3–N3	148.8(3)
N4–Zn3–N3	79.9(3)		

Symmetry code for A: $1 - x, - y, - z$.

Zn2 atom is six-coordinated in an octahedral coordination. The equatorial plane of the octahedral coordination is defined by three phenolate O (O1, O2, O3) from two Schiff base ligands, and one O (O5) atom of DMF ligand. The axial positions of the octahedral coordination are occupied by one phenolate O (O4) of a Schiff base ligand, and one O (O6) atom of the methanol ligand. There forms a four-membered chelate ring Zn1-O1-Zn2-O2 with the phenolate bridging groups. The dihedral angle between the two benzene rings C1-C6 and C15-C20 is $11.5(4)^\circ$, and that between the benzene rings C21-C26 and C35-C40 is $7.5(4)^\circ$. The bond distances subtended at the Zn atoms are comparable to those observed in similar zinc(II) complexes with Schiff bases.¹⁸ There present weak Br...S ($3.649(3)$ Å) interactions in the crystal structure (Figure 4).

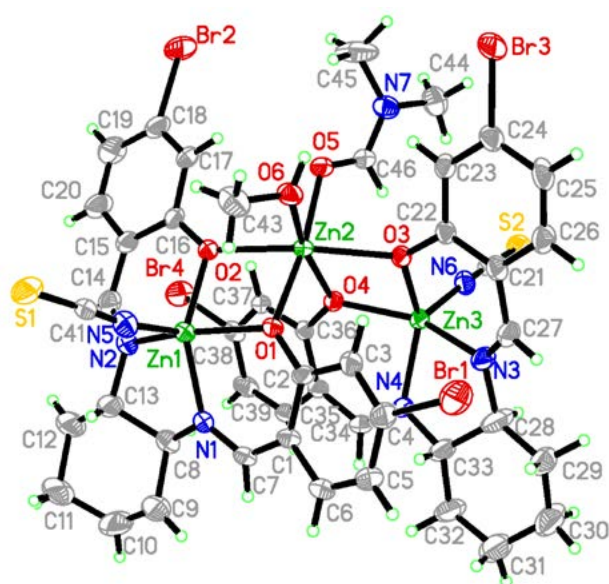


Figure 3. Molecular structure of complex 2.

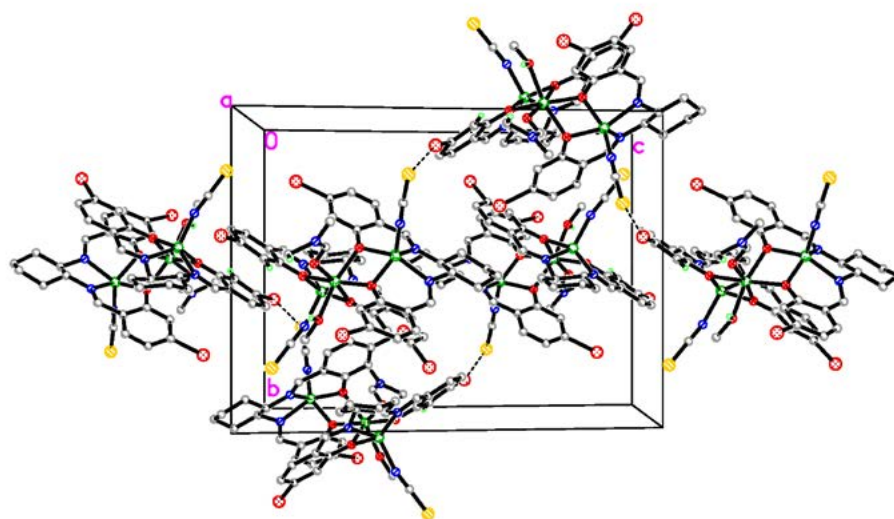


Figure 4. Molecular packing structure of complex 2, viewed along the *a* axis. The weak Br...S interactions are shown as dashed lines.

3. 5. Thermal Analysis

Thermal analysis of complex 1 is shown in Figure 5, which revealed that the complex is stable up to 286°C . The complex decomposed from 286 to 618°C , and converted into ZnO. The agreement between calculated (83.07%) and experimental (83.55%) mass losses is within experimental errors.

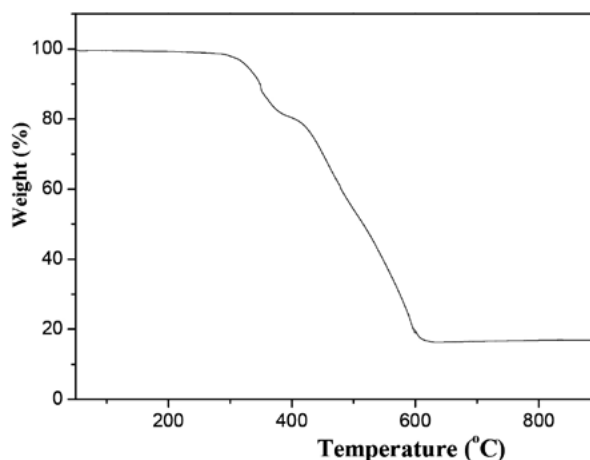


Figure 5. Thermal analysis of complex 1.

3. 6. Antimicrobial Activity

The results of the antimicrobial activity are summarized in Table 4. A comparative study of minimum inhibitory concentration (MIC) values of the Schiff base and the zinc complexes indicated that the complexes have more effective activity against *Staphylococcus aureus*, *Escherichia coli* and *Candida albicans* than the free Schiff base H_2L . Generally, this is caused by the greater lipophilic nature of the complex than the ligand. Such increased activity of

the metal chelates can be explained on the basis of chelating theory.²¹ On chelating, the polarity of the metal atoms will be reduced to a greater extent due to the overlap of the ligand orbital and partial sharing of positive charge of the metal atoms with donor atoms. Further, it increases the delocalization of π -electrons over the whole chelate ring and enhances the lipophilicity of the complex. This increased lipophilicity enhances the penetration of the complexes into lipid membrane and blocks the metal binding sites on enzymes of micro-organisms.

The two zinc complexes have strong activities against *Staphylococcus aureus*, medium activity against *Escherichia coli*, and weak activity against *Candida albicans*. For *Staphylococcus aureus* and *Escherichia coli*, the activities of both complexes are less than the control drug Tetracycline. While for *Candida albicans*, the complexes have stronger activities than Tetracycline. Complex **1** has the most activity against *Staphylococcus aureus* with MIC value of 1.0 $\mu\text{g}\cdot\text{mL}^{-1}$. Both complexes have higher activities against *Staphylococcus aureus* and lower activities against *Escherichia coli* and *Candida albicans* than the zinc(II) and manganese(II) complexes with the ligand N^2 -(1-(pyridin-2-yl)ethylidene)isonicotinohydrazide.²² Further work needs to be carried out to investigate the structure-activity relationship.

Table 4. MIC values ($\mu\text{g}\cdot\text{mL}^{-1}$) for the antimicrobial activities of the tested compounds

Compound	<i>Staphylococcus aureus</i>	<i>Escherichia coli</i>	<i>Candida albicans</i>
H ₂ L	64	128	> 1024
1	1.0	8.0	64
2	2.0	8.0	64
Tetracycline	0.25	2.0	> 1024

4. Conclusion

In summary, two new trinuclear zinc(II) complexes with the tetradentate Schiff base ligand N,N' -bis(5-bromo-salicylidene)-1,2-cyclohexanediamine have been prepared and characterized. The structures of both complexes are confirmed by single crystal X-ray crystallographic determination. The Zn atoms in the complexes are in square pyramidal and octahedral coordination. The complexes have effective activities on the bacteria *Staphylococcus aureus* and *Escherichia coli*. Moreover, both complexes have stronger activities against *Candida albicans* than Tetracycline. The iodide coordinated complex **1** has the most activity against *Staphylococcus aureus* with MIC value of 1.0 $\mu\text{g}\cdot\text{mL}^{-1}$.

Acknowledgments

This research was supported by the National Science Foundation of China (nos. 20676057 and 20877036)

and Top-class foundation of Pingdingshan University (no. 2008010).

5. References

- L. N. Obasi, J. C. Ezeorah, V. Ossai, A. Jude, U. S. Oruma, A. Ibezim, M. Lutter, L. Rhyman, K. Jurkschat, N. Dege, P. Ramasami, *J. Mol. Struct.* **2019**, *1188*, 69–75. DOI:10.1016/j.molstruc.2019.03.081
- (a) S. K. Bharti, G. Nath, R. Tilak, S. K. Singh, *Eur. J. Med. Chem.* **2010**, *45*, 651–660; DOI:10.1016/j.ejmech.2009.11.008
(b) M. Ceruso, F. Carta, S. M. Osman, Z. Allothman, S. M. Monti, C. T. Supuran, *Bioorg. Med. Chem.* **2015**, *23*, 4181–4187; DOI:10.1016/j.bmc.2015.06.050
(c) W. L. Wang, D. Agustin, R. Poll, *Mol. Catal.* **2017**, *443*, 52–59; DOI:10.1016/j.mcat.2017.09.033
(d) M. Hanif, M. Hassan, M. Rafiq, Q. Abbas, A. Ishaq, S. Shahzadi, S.-Y. Seo, M. Saleem, *Pharm. Chem. J.* **2018**, *52*, 424–437; DOI:10.1007/s11094-018-1835-0
(e) P. Mishra, P. N. Gupta, K. Ashok, R. Shukla, R. C. Srimal, *Indian J. Physiol. Pharm.* **1995**, *39*, 169–172.
- (a) K. Venkateswarlu, N. Ganji, S. Daravath, K. Kanneboina, K. Rangan, Shivaraj, *Polyhedron* **2019**, *171*, 86–97; DOI:10.1016/j.poly.2019.06.048
(b) R. A. Ammar, A. N. M. A. Alaghaz, M. E. Zayed, L. A. Al-Bedair, *J. Mol. Struct.* **2017**, *1141*, 368–381; DOI:10.1016/j.molstruc.2017.03.080
(c) N. R. Palepu, S. L. Nongbri, J. R. Premkumar, A. K. Verma, K. Bhattacharjee, S. R. Joshi, S. Forbes, Y. Mozharivskyj, R. Thounaojam, K. Aguan, M. R. Kollipara, *J. Biol. Inorg. Chem.* **2015**, *20*, 619–638; DOI:10.1007/s00775-015-1249-3
(d) M. Aidi, H. Keypour, A. Shooshtari, M. Mahmoudabadi, M. Bayat, Z. Ahmadvand, R. Karamian, M. Asadbegy, S. Tavatli, R. W. Gable, *Polyhedron* **2019**, *167*, 93–102. DOI:10.1016/j.poly.2019.02.030
- (a) C. X. Yuan, L. P. Lu, X. L. Gao, Y. B. Wu, M. L. Guo, Y. Li, X. Q. Fu, M. L. Zhu, *J. Bio. Inorg. Chem.* **2009**, *14*, 841–851; DOI:10.1007/s00775-009-0496-6
(b) P. A. Khalf-Alla, S. S. Hassan, M. M. Shoukry, *Inorg. Chim. Acta* **2019**, *492*, 192–197; DOI:10.1016/j.ica.2019.04.035
(c) S. Daravath, A. Rambabu, N. Vamsikrishna, N. Ganji, S. Raj, *J. Coord. Chem.* **2019**, *72*, 1973–1993; DOI:10.1080/00958972.2019.1634263
(d) M. S. S. Adam, L. H. Abdel-Rahman, A. M. Abu-Dief, N. A. Hashem, *Inorg. Nano-Met. Chem.* **2019**, *50*, 136–150; DOI:10.1080/24701556.2019.1672735
(e) M. Sonmez, M. Celebi, I. Berber, *Eur. J. Med. Chem.* **2010**, *45*, 1935–1940; DOI:10.1016/j.ejmech.2010.01.035
(f) L. W. Xue, G. Q. Zhao, Y. J. Han, Y. X. Feng, *Russ. J. Coord. Chem.* **2011**, *37*, 262–269; DOI:10.1134/S1070328411030110
(g) L. W. Xue, Y. J. Han, G. Q. Zhao, Y. X. Feng, *Russ. J. Coord. Chem.* **2012**, *38*, 24–28. DOI:10.1134/S1070328411120104
- (a) Q.-M. Hasi, Y. Fan, X.-X. Feng, X.-Q. Yao, J.-C. Liu, *Transition Met. Chem.* **2016**, *41*, 685–692; DOI:10.1007/s11243-016-0069-9

- (b) P. A. Khalf-Alla, S. S. Hassan, M. M. Shoukry, *Inorg. Chim. Acta* **2019**, 492, 192–197; DOI:10.1016/j.ica.2019.04.035
- (c) S. Daravath, A. Rambabu, N. Vamsikrishna, N. Ganji, S. Raj, *J. Coord. Chem.* **2019**, 72, 1973–1993; DOI:10.1080/00958972.2019.1634263
- (d) M. S. S. Adam, L. H. Abdel-Rahman, A. M. Abu-Dief, N. A. Hashem, *Inorg. Nano-Met. Chem.* **2019**, 50, 136–150. DOI:10.1080/24701556.2019.1672735
6. M. Zhang, D.-M. Xian, H.-H. Li, J.-C. Zhang, Z.-L. You, *Aust. J. Chem.* **2012**, 65, 343–350. DOI:10.1071/CH11424
7. (a) L.-W. Xue, H.-J. Zhang, P.-P. Wang, *Acta Chim. Slov.* **2019**, 66, 190–195;
 (b) G.-X. He, L.-W. Xue, Q.-L. Peng, P.-P. Wang, H.-J. Zhang, *Acta Chim. Slov.* **2019**, 66, 570–575; DOI:10.17344/acsi.2018.4868
 (c) L.-W. Xue, Y.-J. Han, X.-Q. Luo, *Acta Chim. Slov.* **2019**, 66, 622–628. DOI:10.17344/acsi.2019.5039
8. Y. Luo, J. Wang, X. Ding, R. Ni, M. Li, T. Yang, J. Wang, C. Jing, Z. You, *Inorg. Chim. Acta* **2021**, 516, 120146. DOI:10.1016/j.ica.2020.120146
9. Bruker, SMART and SAINT, *Area Detector Control and Integration Software*, Madison (WI, USA): Bruker Analytical X-ray Instruments Inc., 1997.
10. G. M. Sheldrick, SADABS, *Program for Empirical Absorption Correction of Area Detector Data*, Göttingen (Germany): Univ. of Göttingen, 1997.
11. A. C. T. North, D. C. Phillips, F. S. Mathews, *Acta Crystallogr. A* **1968**, 24, 351–359. DOI:10.1107/S0567739468000707
12. G. M. Sheldrick, SHELXL-97, *Program for the Refinement of Crystal Structures*, Göttingen (Germany): Univ. of Göttingen, 1997.
13. (a) A. Barry, *Procedures and Theoretical Considerations for Testing Antimicrobial Agents in Agar Media*, In: *Antibiotics in Laboratory Medicine*, Lorian, V., Ed., Baltimore: Williams and Wilkins, 1991;
 (b) T. Rosu, M. Negoiu, S. Pasculescu, E. Pahontu, D. Poirier, A. Gulea, *Eur. J. Med. Chem.* **2010**, 45, 774–781. DOI:10.1016/j.ejmech.2009.10.034
14. A. Ray, D. Sadhukhan, G. M. Rosair, C. J. Gomez-Garcia, S. Mitra, *Polyhedron* **2009**, 28, 3542–3550. DOI:10.1016/j.poly.2009.07.017
15. S. B. Asak, S. Sen, S. Banerjee, S. Mitra, G. Rosair, M. T. G. Rodriguez, *Polyhedron* **2007**, 26, 5104–5112. DOI:10.1016/j.poly.2007.07.025
16. M. Enamullah, M. A. Quddus, M. A. Halim, M. K. Islam, V. Vasylyeva, C. Janiak, *Inorg. Chim. Acta* **2015**, 103–111. DOI:10.1016/j.ica.2014.11.020
17. A. W. Addison, T. N. Tao, J. Reedijk, J. van Rijn, G. C. Verschoor, *J. Chem. Soc. Dalton Trans.* **1984**, 1349–1355.
18. (a) F.-W. Wang, Y.-J. Wei, Q.-Y. Zhu, *Chin. J. Struct. Chem.* **2007**, 26, 1327–1331;
 (b) Z.-L. You, X. Han, J. Wang, J.-Y. Chi, *Chin. J. Struct. Chem.* **2006**, 25, 1043–1046;
 (c) T. Chattopadhyay, M. Mukherjee, K. S. Banu, A. Banerjee, E. Suresh, E. Zangrando, D. Das, *J. Coord. Chem.* **2009**, 62, 967–979; DOI:10.1080/00958970802385837
 (d) A. Guha, T. Chattopadhyay, N. D. Paul, M. Mukherjee, S. Goswami, T. K. Mondal, E. Zangrando, D. Das, *Inorg. Chem.* **2012**, 51, 8750–8759; DOI:10.1021/ic300400v
 (e) J. Qin, Y. Sun, Z. N. Xia, Y. Zhang X. L. Zhao, Z. L. You, H. L. Zhu, *Russ. J. Coord. Chem.* **2016**, 42, 330–337. DOI:10.1134/S1070328416050055
19. (a) N. Wang, L. Chen, L. Yang, Y. Wan, *Synth. React. Inorg. Met.-Org. Nano-Met. Chem.* **2014**, 44, 315–319; DOI:10.1080/15533174.2013.770763
 (b) D.-H. Shi, Z.-L. Cao, W.-W. Liu, R.-B. Xu, L.-L. Gao, Q. Zhang, *Synth. React. Inorg. Met.-Org. Nano-Met. Chem.* **2012**, 42, 864–867. DOI:10.1080/15533174.2011.618483
20. (a) J.-N. Li, *Synth. React. Inorg. Met.-Org. Nano-Met. Chem.* **2013**, 43, 832–837;
 (b) S. S. Qian, X. S. Cheng, J. Q. Ren, Z. L. You, H. L. Zhu, *Russ. J. Coord. Chem.* **2013**, 39, 836–843. DOI:10.1134/S1070328413110080
21. J. W. Searl, R. C. Smith, S. Wyard, *J. Proc. Phys. Soc.* **1961**, 78, 1174–1178. DOI:10.1088/0370-1328/78/6/311
22. L.-W. Xue, H.-J. Zhang, P.-P. Wang, *Acta Chim. Slov.* **2019**, 66, 190–195. DOI:10.17344/acsi.2018.4773

Povzetek

Sintetizirali smo dva nova trijedrna kompleksa cinka(II), $[\text{Zn}_3\text{I}_2\text{L}_2(\text{H}_2\text{O})_2]$ (**1**) in $[\text{Zn}_3(\text{CH}_3\text{OH})(\text{DMF})\text{L}_2(\text{NCS})_2]$ (**2**), pri čemer je L dianionska oblika *N,N'*-bis(5-bromosaliciliden)-1,2-cikloheksandiamina (H_2L). Spojini smo karakterizirali z elementno analizo, IR in UV spektroskopijo, strukturi obeh spojin pa smo določili z monokristalno rentgensko difrakcijo. Obe spojini sta trijedrni in solvatirani, z vodnimi ligandi v primeru spojine **1** in metanolom v primeru spojine **2**. Zunanja atoma Zn sta v kvadratno piramidalni koordinaciji, notranji pa v oktaedrični koordinaciji. Ocenili smo protimikrobno učinkovitost obeh kompleksov na bakterije *Staphylococcus aureus*, *Escherichia coli* in *Candida albicans*, pri čemer smo dobili zanimive rezultate.



Except when otherwise noted, articles in this journal are published under the terms and conditions of the Creative Commons Attribution 4.0 International License

Scientific paper

Methyl Maltolate and Ethyl Maltolate Coordinated Oxidovanadium(V) Complexes with *N*'-(2-Hydroxy-5-methylbenzylidene)-4-trifluoromethylbenzohydrazide: Synthesis, Crystal Structures and Catalytic Epoxidation Property

Zhongduo Xiong^{1,2} and Ping Zhang^{1,2,*}¹ Analysis and Testing Center, Wuhan Textile University, Wuhan 430073, P. R. China² National Local Joint Laboratory for Advanced Textile Processing and Clean Production, Wuhan Textile University, Wuhan 430073, P. R. China

* Corresponding author: E-mail: sobear521@sohu.com

Received: 11-29-2022

Abstract

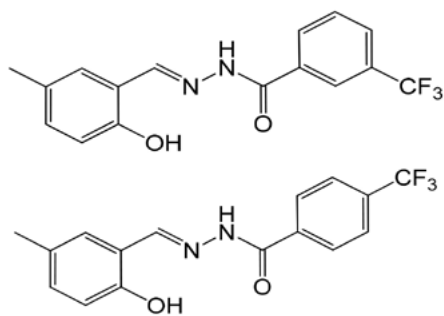
A mononuclear methyl maltolate (Hm) coordinated oxidovanadium(V) complex [VOL¹(mm)] (1), and a mononuclear ethyl maltolate (Hem) coordinated oxidovanadium(V) complex [VOL²(em)] (2), where L¹ and L² are the dianionic form of *N*'-(2-hydroxy-5-methylbenzylidene)-3-trifluoromethylbenzohydrazide (H₂L¹) and *N*'-(2-hydroxy-5-methylbenzylidene)-4-trifluoromethylbenzohydrazide (H₂L²), respectively, have been prepared. The hydrazones and the complexes were characterized by elemental analysis, FT-IR and UV-Vis spectra. Structures of H₂L¹ and the two complexes were further characterized by single crystal X-ray diffraction. The two complexes have similar structures, with the V atoms in octahedral coordination. The hydrazones behave as ONO tridentate ligands with the V atoms. Both complexes have interesting properties on the catalytic epoxidation of cyclooctene.

Keywords: Hydrazone; oxidovanadium complex; mononuclear complex; crystal structure; catalytic epoxidation property

1. Introduction

Vanadium is an interesting element in various biological systems. Vanadium haloperoxidases are enzymes catalyzing the oxidation of halides to hypohalous acids, which then form oxygen.¹ The enzymes can catalyze cyclization of terpene substrates, and the oxidation of sulfides to sulfoxides.² Oxidation reaction is one of the most important reaction types in organic chemistry and chemical industry. However, without catalysts most oxidation processes are difficult. A deeper understanding of the catalytic functions of vanadium haloperoxidases prompted the synthesis and investigation of small molecule models for the active sites of these enzymes. In recent years, transition metal complexes with different ligands have been used as heterogeneous or homogenous or catalysts in the catalytic oxidation of organic substrates and in bioinorganic modeling of oxygen transfer metalloenzymes.³ Among the metal complexes, those with Schiff bases as ligands have

received particular attention because of their facile synthesis and wide application in the fields of biological, catalytic and magnetic.⁴ Vanadium complexes have been proved to show effective catalytic capability in the oxidation reactions of olefins and sulfides.⁵ Methyl maltol and ethyl maltol are food additive. In recent years, limited work has been reported that maltolate coordinated vanadium and molybdenum complexes have catalytic properties.⁶ The colleague of our research group has reported some vanadium complexes with catalytic properties.⁷ Aiming at obtaining new and efficient catalysts for the epoxidation of olefins, in this work, two new oxidovanadium(V) complexes, [VOL¹(mm)] (1) and [VOL²(em)] (2), where L¹ and L² are the dianionic form of *N*'-(2-hydroxy-5-methylbenzylidene)-3-trifluoromethylbenzohydrazide (H₂L¹) and *N*'-(2-hydroxy-5-methylbenzylidene)-4-trifluoromethylbenzohydrazide (H₂L²), respectively (Scheme 1), and mm is methyl maltolate, em is ethyl maltolate, are presented.



Scheme 1. The hydrazones H_2L^1 and H_2L^2 .

2. Experimental

2. 1. Materials and Methods

5-Methylsalicylaldehyde, 3-trifluoromethylbenzohydrazide, 4-trifluoromethylbenzohydrazide and $VO(acac)_2$ were purchased from Alfa Aesar and used as received. Methyl maltol and ethyl maltol were obtained from Aladin Chemical Co. Ltd. Reagent grade solvents were used as received. Microanalyses of the complexes were performed with a Vario EL III CHNOS elemental analyzer. Infrared spectra were recorded as KBr pellets with an FTS-40 spectrophotometer. Electronic spectra were recorded on a Lambda 900 spectrometer. 1H NMR and ^{13}C NMR spectra were recorded on a 500 MHz Bruker Advance instrument. The catalytic reactions were followed by gas chromatography on an Agilent 6890A chromatograph equipped with an FID detector and a DB5-MS capillary column (30 m \times 0.32 mm, 0.25 μ m). The X-ray powder diffraction patterns of the complexes were recorded on a Bruker AXS D8 Advance diffractometer.

Synthesis of N' -(2-hydroxy-5-methylbenzylidene)-3-trifluoromethylbenzohydrazide (H_2L^1)

5-Methylsalicylaldehyde (10 mmol, 1.36 g) and 3-trifluoromethylbenzohydrazide (10 mmol, 2.04 g) were refluxed in methanol (50 mL). The reaction was continued for 1 h in oil bath during which a solid compound separated. It was filtered and washed with cold methanol. The crude product was recrystallized from methanol and dried over anhydrous $CaCl_2$. Yield: 2.7 g (84%). IR data (KBr pellet, cm^{-1}): 3197 $\nu(N-H)$, 1649 $\nu(C=O)$, 1612 $\nu(C=N)$. UV-Vis data in methanol (nm): 218, 290, 300, 337, 433. Analysis: Found: C 59.45, H 4.14, N 8.76%. Calculated for $C_{16}H_{13}F_3N_2O_2$: C 59.63, H 4.07, N 8.69%. 1H NMR (d_6 -DMSO, 500 MHz) δ (ppm): 12.22 (s, 1H, NH), 10.87 (s, 1H, OH), 8.63 (s, 1H, CH=N), 8.28 (s, 1H, ArH), 8.25 (d, 1H, ArH), 7.98 (d, 1H, ArH), 7.80 (t, 1H, ArH), 7.39 (s, 1H, ArH), 7.12 (d, 1H, ArH), 6.85 (d, 1H, ArH), 2.26 (s, 3H, CH_3). ^{13}C NMR (d_6 -DMSO, 126 MHz) δ (ppm): 161.32, 155.30, 150.49, 148.54, 133.84, 132.27, 131.83, 129.87, 129.03, 128.42, 127.94, 124.10, 122.82, 118.37, 116.27, 19.91. Single crystals suitable for X-ray diffraction

were obtained by slow evaporation of the methanol solution containing the compound.

Synthesis of N' -(2-hydroxy-5-methylbenzylidene)-4-trifluoromethylbenzohydrazide (H_2L^2)

This compound was prepared by similar method as described for H_2L^1 , with 3-trifluoromethylbenzohydrazide replaced by 4-trifluoromethylbenzohydrazide (10 mmol, 2.04 g). Yield: 2.8 g (87%). IR data (KBr pellet, cm^{-1}): 3201 $\nu(N-H)$, 1657 $\nu(C=O)$, 1614 $\nu(C=N)$. UV-Vis data in methanol (nm): 220, 290, 301, 339, 435. Analysis: Found: C 59.52, H 4.16, N 8.62%. Calculated for $C_{16}H_{13}F_3N_2O_2$: C 59.63, H 4.07, N 8.69%. 1H NMR (d_6 -DMSO, 500 MHz) δ (ppm): 12.24 (s, 1H, NH), 10.91 (s, 1H, OH), 8.63 (s, 1H, CH=N), 8.15 (d, 2H, ArH), 7.93 (d, 2H, ArH), 7.38 (s, 1H, ArH), 7.11 (d, 1H, ArH), 6.85 (d, 1H, ArH), 2.25 (s, 3H, CH_3). ^{13}C NMR (d_6 -DMSO, 126 MHz) δ (ppm): 161.62, 155.34, 148.78, 136.69, 132.26, 131.79, 131.53, 129.17, 128.54, 127.93, 125.49, 118.30, 116.27, 19.87.

Synthesis of the Complex [VOL 1 (mm)] (1)

The hydrazone H_2L^1 (1.0 mmol, 0.32 g), methyl maltol (1.0 mmol, 0.13 g) and $VO(acac)_2$ (1.0 mmol, 0.26 g) were refluxed in methanol (30 mL). The reaction was continued for 1 h in oil bath to give a deep brown solution. Single crystals of the complex were formed during slow evaporation of the reaction mixture in air. The crystals were isolated by filtration, washed with cold methanol and dried over anhydrous $CaCl_2$. Yield: 0.27 g (53%). IR data (KBr pellet, cm^{-1}): 1607 $\nu(-C=N-N=C-)$, 1264 $\nu(C-O_{phenolate})$, 1133 $\nu(N-N)$, 972 $\nu(V=O)$. UV-Vis data in methanol (nm): 247, 272, 325, 408. Analysis: Found: C 51.41, H 3.26, N 5.54%. Calculated for $C_{22}H_{16}F_3N_2O_6V$: C 51.58, H 3.15, N 5.47%. 1H NMR (d_6 -DMSO, 500 MHz) δ (ppm): 9.20 (s, 1H, MMH), 8.43 (s, 1H, CH=N), 8.14 (s, 1H, ArH), 8.12 (d, 1H, ArH), 7.93 (d, 1H, ArH), 7.73 (t, 1H, ArH), 7.62 (s, 1H, ArH), 7.42 (d, 1H, ArH), 6.80 (d, 1H, ArH), 6.68 (d, 1H, MMH), 2.33 (s, 3H, CH_3), 2.24 (s, 3H, CH_3). ^{13}C NMR (d_6 -DMSO, 126 MHz) δ (ppm): 175.54, 167.77, 161.71, 158.37, 157.96, 155.59, 145.81, 136.63, 134.24, 132.65, 131.95, 130.86, 130.19, 129.92, 129.53, 128.15, 124.90, 122.73, 118.90, 118.14, 19.87, 15.08.

Synthesis of the Complex [VOL 2 (em)] (2)

This complex was prepared by similar method as described for **1**, with H_2L^1 replaced by H_2L^2 (1.0 mmol, 0.32 g), and with methyl maltol replaced by ethyl maltol (1.0 mmol, 0.14 g). Yield: 0.25 g (48%). IR data (KBr pellet, cm^{-1}): 1607 $\nu(-C=N-N=C-)$, 1268 $\nu(C-O_{phenolate})$, 1124 $\nu(N-N)$, 969 $\nu(V=O)$. UV-Vis data in methanol (nm): 255, 270, 325, 412. Analysis: Found: C 52.61, H 3.38, N 5.40%. Calculated for $C_{23}H_{18}F_3N_2O_6V$: C 52.48, H 3.45, N 5.32%. 1H NMR (d_6 -DMSO, 500 MHz) δ (ppm): 9.18 (s, 1H, EMH), 8.45 (s, 1H, CH=N), 8.06 (d, 2H, ArH), 7.83 (d, 2H, ArH), 7.65 (s, 1H, ArH), 7.43 (d, 1H,

ArH), 6.82 (d, 1H, ArH), 6.68 (d, 1H, MMH), 2.33 (s, 3H, CH₃), 2.13 (q, 2H, CH₂), 1.13 (t, 3H, CH₃). ¹³C NMR (*d*₆-DMSO, 126 MHz) δ (ppm): 175.78, 167.56, 161.83, 158.47, 155.69, 154.70, 153.20, 136.68, 134.58, 133.67, 133.19, 130.08, 129.91, 128.80, 125.65, 124.35, 118.92, 115.58, 21.30, 20.78, 10.81.

2. 2. Crystal Structure Determination

Data were collected on a Bruker SMART 1000 CCD area diffractometer using a graphite monochromator Mo K α radiation ($\lambda = 0.71073$ Å) at 298(2) K. The data were corrected with SADABS programs and refined on F^2 with SHELXL software.⁷ Structures of H₂L¹ and the complexes were solved by direct methods and difference Fourier syntheses. All non-hydrogen atoms were refined anisotropically. The N and O attached H atoms were located from a difference Fourier map and refined with N–H and O–H distances restrained to 0.90(1) and 0.85(1) Å, respectively. The remaining hydrogen atoms were placed in calculated positions and included in the last cycles of refinement. The trifluoromethyl groups in H₂L¹ and complex **1** are disordered over two sites, with occupancies of 0.55(1) and 0.45(1), and 0.71(1) and 0.29(1), respectively. Crystal data and details of the data collection and refinement are listed in Table 1.

2. 3. Catalytic Epoxidation Process

A mixture of cyclooctene (2.76 mL, 20 mmol), acetophenone (internal reference) and the complex as the catalyst (0.05 mmol) was stirred and heated up to 80 °C before addition of aqueous *tert*-butyl hydroperoxide (TBHP; 70% w/w, 5.48 mL, 40 mmol). The mixture is initially an emulsion, but two phases become clearly visible as the reaction progresses, a colorless aqueous one and a colorful organic one. The reaction was monitored for 5 h with withdrawal and analysis of organic phase aliquots (0.1 mL) at required times. Each withdrawn sample was mixed with 2 mL of diethylether, treated with a small quantity of MnO₂ and then filtered through silica and analyzed by GC.

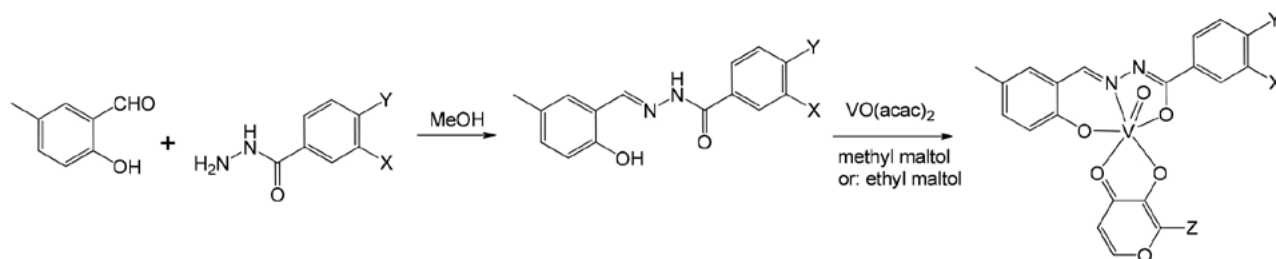
3. Results and Discussion

3. 1. Synthesis

The hydrazones H₂L¹ and H₂L² were prepared from 5-methylsalicylaldehyde with 3-trifluoromethylbenzohydrazide and 4-trifluoromethylbenzohydrazide, respectively, in methanol. The two complexes were facile prepared by the hydrazones with VO(acac)₂ in the presence of methyl maltol and ethyl maltol, respectively (Scheme 2).

Table 1. Crystallographic Data for H₂L¹ and the Complexes

Parameters	H ₂ L ¹	1	2
Empirical formula	C ₁₆ H ₁₃ F ₃ N ₂ O ₂	C ₂₂ H ₁₆ F ₃ N ₂ O ₆ V	C ₂₃ H ₁₈ F ₃ N ₂ O ₆ V
Formula weight	322.28	512.31	526.33
Crystal system	Monoclinic	Monoclinic	Triclinic
Space group	<i>P</i> 2 ₁ / <i>c</i>	<i>P</i> 2 ₁ / <i>c</i>	<i>P</i> -1
<i>a</i> [Å]	11.7599(7)	12.163(1)	7.503(1)
<i>b</i> [Å]	15.0697(8)	7.652(1)	11.877(1)
<i>c</i> [Å]	8.7575(4)	24.871(2)	13.302(1)
α [°]	90	90	107.289(1)
β [°]	95.259(1)	100.430(1)	93.212(1)
γ [°]	90	90	90.773(1)
<i>V</i> [Å ³]	1545.45(14)	2276.5(4)	1129.5(2)
<i>Z</i>	4	4	2
ρ_{calcd} [g cm ⁻³]	1.385	1.495	1.548
μ [mm ⁻¹]	0.117	0.501	0.507
<i>F</i> (000)	664	1040	536
Index ranges	-14 ≤ <i>h</i> ≤ 14 -18 ≤ <i>k</i> ≤ 18 -10 ≤ <i>l</i> ≤ 10	-14 ≤ <i>h</i> ≤ 14 -7 ≤ <i>k</i> ≤ 9 -30 ≤ <i>l</i> ≤ 28	-6 ≤ <i>h</i> ≤ 9 -10 ≤ <i>k</i> ≤ 14 -16 ≤ <i>l</i> ≤ 16
Measured reflections	16591	12860	6007
Independent reflections	2876	4244	4154
Observed reflections (<i>I</i> > 2 σ (<i>I</i>))	2192	2423	2751
Parameters	243	341	316
Restraints	50	54	18
Final R indices [<i>I</i> > 2 σ (<i>I</i>)]	0.0437, 0.1110	0.0788, 0.2237	0.0507, 0.1144
R indices (all data)	0.0596, 0.1234	0.1359, 0.2663	0.0905, 0.1355
Goodness-of-fit on F^2	1.012	1.041	1.029



Scheme 2. The synthesis procedure of the hydrazones and the complexes. H_2L^1 : X = CF_3 , Y = H; H_2L^2 : X = H, Y = CF_3 ; **1**: X = CF_3 , Y = H, Z = Me; **2**: X = H, Y = CF_3 , Z = Et.

The hydrazones behave as tridentate dianionic ONO donor ligands toward the VO^{3+} core. The two complexes were synthesized by the reaction of the hydrazones with $VO(acac)_2$ in the presence of methyl maltol or ethyl maltol, in 1:1:1 molar proportion in methanol under reflux. Both H_2L^1 and the vanadium complexes were isolated as single crystals from the reaction mixtures by slow evaporation method at room temperature. Crystals of H_2L^1 and the complexes are fairly soluble in most organic solvents like ethanol, methanol, acetonitrile, DMF and DMSO.

The experimental powder X-ray diffraction (XRD) patterns of the bulk samples of both complexes agree well

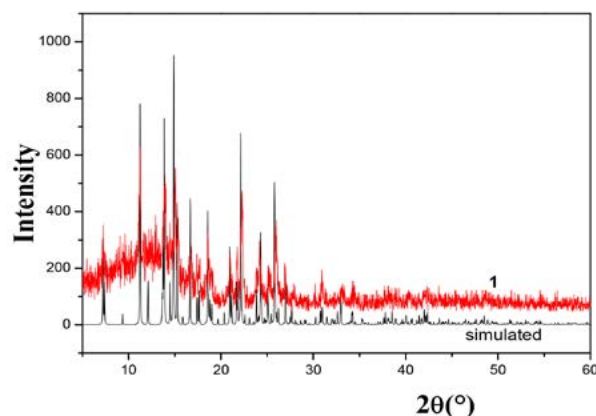


Figure 1. Experimental and simulated powder XRD patterns of complex 1.

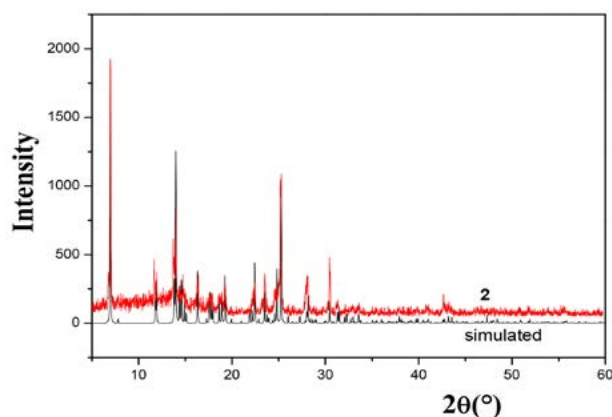


Figure 2. Experimental and simulated powder XRD patterns of complex 2.

with the simulated patterns calculated from single crystal X-ray diffraction (Figures 1 and 2).

3. 2. IR and Electronic Spectra

The infrared spectra of the hydrazones show weak bands centered at about 3200 cm^{-1} for $\nu(N-H)$ and $1649\text{--}1657\text{ cm}^{-1}$ for $\nu(C=O)$.⁸ On complexation the absence of N-H and C=O bands and red shifts in azomethine ($-C=N=N=C-$) bands of the ligands show coordination of the hydrazones in the enol form.⁹ The infrared spectra of the complexes display IR absorption bands at 1607 cm^{-1} which can be assigned to the C=N stretching frequency of the coordinated hydrazone ligands whereas for the free hydrazones the same bands are observed at $1612\text{--}1614\text{ cm}^{-1}$.¹⁰ The vanadium complexes exhibit characteristic bands at about 970 cm^{-1} for the stretching vibrations of the V=O bonds.¹¹ Based on the infrared absorption, it is clear that the hydrazones exist in *keto*-amino tautomer form in free, and in imino-enol tautomeric form in the vanadium complexes.¹²

Electronic spectra of both vanadium complexes recorded in methanol show weak absorption bands centered at about 410 nm, which can be assigned to charge transfer transitions of $N(p\pi)-M(d\pi)$ LMCT. The medium absorption bands centered at 320 nm for the vanadium complexes are assigned as charge transfer transitions of $O(p\pi)-M(d\pi)$ LMCT, which is similar to that reported in literature.¹³

3. 3. Description of the Structure of H_2L^1

The perspective view of the hydrazone H_2L^1 is shown in Figure 3. Selected bond lengths and angles are listed in Table 1. The hydrazone molecule presents in *E* conformation with respect to the C=N double bond. The dihedral angles between the mean planes of the central N-N=C spacer unit and the C1-C6 and C9-C14 benzene rings are $20.3(3)$ and $9.3(3)^\circ$, respectively, while the dihedral angle between the two aromatic rings is $12.2(4)^\circ$. An intra-molecular N-H...O hydrogen bond makes an *S(6)* ring motif. In the crystal of the compound, the molecules are linked by N-H...O and C-H...O hydrogen bonds (Table 2), to form one-dimensional chain along the *c* axis (Figure 4). The molecules are further linked by three $\pi\cdots\pi$ stacking

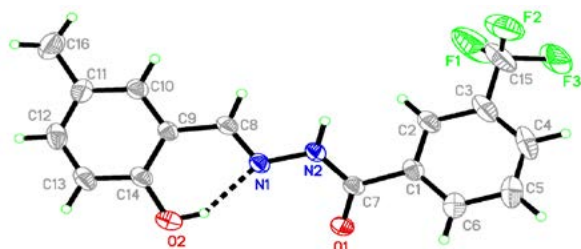


Figure 3. ORTEP plots (30% probability level) and numbering scheme for H_2L^1 .

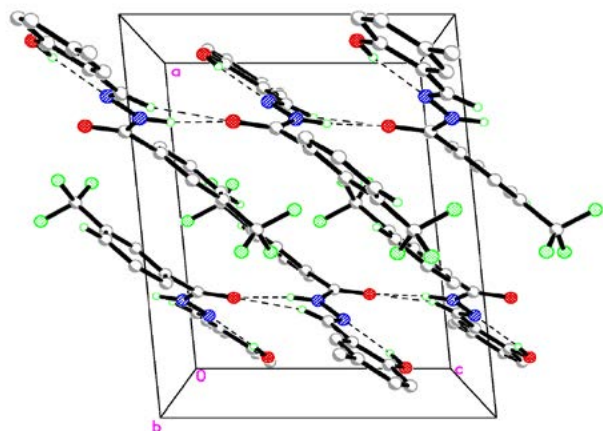


Figure 4. The molecular packing diagram of H_2L^1 , viewed down the b axis. Hydrogen bonds are shown as dashed lines.

interactions involving pairs of benzene rings with the ring-centroid separations of 3.806–4.147 Å.

3. 4. Description of the Structures of the Complexes

The perspective views of the vanadium complexes **1** and **2** are shown in Figures 5 and 6, respectively. In each complex, the V atom is in distorted octahedral coordination with NO_5 chromophore. The hydrazone compound behaves as dianionic tridentate ligand binding through the phenolate oxygen (O2), the enolate oxygen (O1) and the imine nitrogen (N1), and occupies three positions in the equatorial plane of the octahedral coordination. The fourth position of the equatorial plane is occupied by the deprotonated hydroxyl oxygen (O5) of the MM or EM ligand. The carbonyl oxygen (O4) of the MM or EM ligand occupies one axial position of the octahedral coordination, and the other axial position is defined by the oxido group (O3). The V atoms are found to be deviated from the mean equatorial planes defined by the four donor atoms by 0.308(1) Å for **1** and 0.293(1) Å for **2**. The V–O4 bonds are longer than the typical single bonds (2.267(4) Å and 2.253(2) Å against 1.9–2.0 Å). This indicates that the carbonyl oxygen atom is loosely binds with the V atom. The V–O bonds (1.57–1.94 Å) and the V–N bonds (2.09–2.10

Å) are similar to those observed in other vanadium(V) complexes.^{4e,14} The C7–O1 bonds in both complexes are 1.299(6) Å and 1.322(4) Å, respectively, which are longer than that in the free hydrazone H_2L^1 , and are closer to single bonds rather than double bonds. The shorter bond lengths compared to C–O single bond may be due to extended electron delocalization in the hydrazone ligands.¹⁵ Moreover, the shortening of C7–N2 bonds (1.28–1.29 Å, instead of 1.34 Å in H_2L^1) and the elongation of N1–N2 bonds (1.39–1.41 Å) also prove the electron cloud delocalization in the hydrazone ligand systems. The hydrazones bind with the V atoms through five- and six-membered chelate rings. The five-membered rings are rather planar, while the six-membered rings are obviously distorted. The two benzene rings form dihedral angles of 5.1(4)° for **1** and 2.8(5)° for **2**. The *trans* angles in both complexes are in the range 153.1(2)–174.5(2)°, indicating the distortion of the octahedral coordination.

In the crystal structure of complex **1**, the complex molecules are linked by C–H...O hydrogen bonds (Table 2), to form 1D chain running along the b -axis (Figure 7). The molecules are further linked by five π ... π stacking interactions involving pairs of V–O1–C7–N2–N1, V–O4–C19–C18–O5, O6–C17–C18–C19–C20–C21 and C1–C2–C3–C4–C5–C6 rings with the ring-centroid separations of 2.826–4.850 Å. In the crystal packing diagram of complex

Table 2. Selected Bond Lengths (Å) and Angles (°) for H_2L^1 and the Complexes

	H_2L^1	1	2
V–O1		1.929(4)	1.937(2)
V–O2		1.831(4)	1.837(3)
V–O3		1.582(5)	1.582(3)
V–O4		2.264(4)	2.253(2)
V–O5		1.857(4)	1.867(2)
V–N1		2.088(5)	2.100(3)
C8–N1	1.279(3)	1.285(8)	1.281(4)
N2–C7	1.340(3)	1.300(8)	1.289(4)
N1–N2	1.388(2)	1.391(6)	1.392(4)
C7–O1	1.227(2)	1.294(7)	1.322(4)
O3–V–O2		101.3(2)	100.8(2)
O3–V–O5		99.2(2)	98.2(1)
O2–V–O5		99.9(2)	98.9(1)
O3–V–O1		97.2(2)	95.0(1)
O2–V–O1		153.1(2)	155.5(1)
O5–V–O1		96.2(2)	97.3(1)
O3–V–N1		99.2(2)	101.2(1)
O2–V–N1		83.3(2)	83.6(1)
O5–V–N1		160.3(2)	159.7(1)
O1–V–N1		74.6(2)	75.0(1)
O3–V–O4		174.7(2)	173.5(1)
O2–V–O4		83.4(2)	84.7(1)
O5–V–O4		77.4(2)	77.5(1)
O1–V–O4		79.3(2)	80.9(1)
N1–V–O4		83.6(2)	82.7(1)

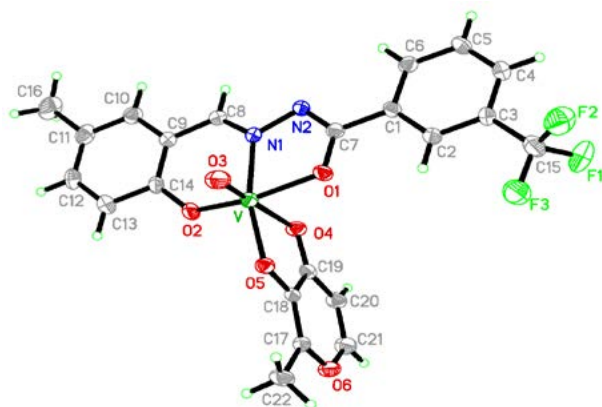


Figure 5. ORTEP plots (30% probability level) and numbering scheme for complex 1.

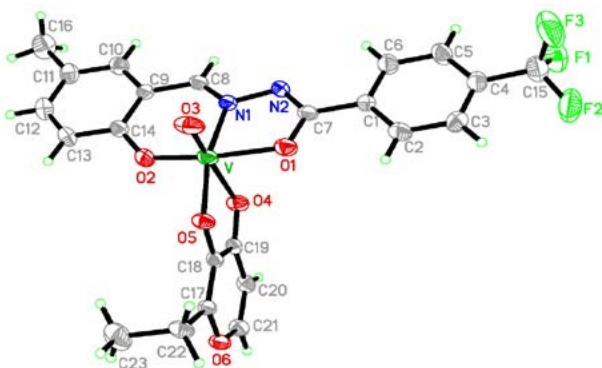


Figure 6. ORTEP plots (30% probability level) and numbering scheme for complex 2.

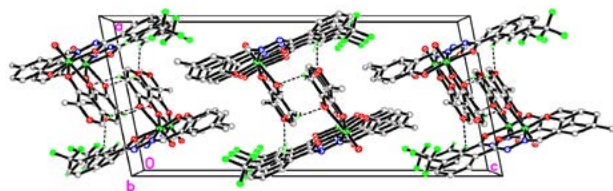


Figure 7. The molecular packing diagram of complex 1, viewed down the *b* axis. Hydrogen bonds are shown as dashed lines.

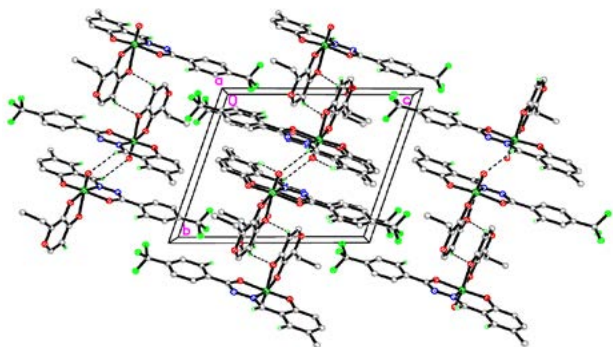


Figure 8. The molecular packing diagram of complex 2, viewed down the *b* axis. Hydrogen bonds are shown as dashed lines.

2, the molecules are linked by C–H...O hydrogen bonds (Table 2), to form 1D chain running along the *b*-axis (Figure 8). The molecules are further linked by nine π ... π stacking interactions involving pairs of V–O1–C7–N2–N1, V–O4–C19–C18–O5, V–O2–C14–C9–C8–N1, O6–C17–C18–C19–C20–C21 and C9–C10–C11–C12–C13–C14 rings with the ring-centroid separations of 2.856–4.951 Å.

Table 3. Hydrogen Bond Distances (Å) and Bond Angles (°) for H_2L^1 and the Complexes

<i>D</i> –H... <i>A</i>	<i>d</i> (D–H)	<i>d</i> (H... <i>A</i>)	<i>d</i> (D... <i>A</i>)	Angle (D–H... <i>A</i>)
H_2L^1				
O2–H2A...N1	0.86(1)	1.90(2)	2.665(2)	148(4)
N2–H2B...O1 ⁱ	0.90(1)	1.99(2)	2.879(2)	165(4)
C8–H8...O1 ⁱ	0.93	2.52(2)	3.263(3)	138(5)
1				
C2–H2...O6 ⁱⁱ	0.93	2.50(2)	3.315(3)	147(5)
C20–H20...O4 ⁱⁱⁱ	0.93	2.52(2)	3.316(3)	143(5)
2				
C2–H2...O6 ^{iv}	0.93	2.60(3)	3.429(4)	149(6)
C8–H8...O3 ^v	0.93	2.54(3)	3.133(4)	122(5)
C10–H10...O3 ^{vi}	0.93	2.52(3)	3.390(5)	156(6)
C20–H20...O4 ^{vii}	0.93	2.46(3)	3.287(4)	149(65)

Symmetry codes: i): $x, 1/2 - y, -1/2 + z$; ii): $1 - x, 1 - y, -z$; iii): $1 - x, 2 - y, -z$; iv): $1 - x, -y, 1 - z$; v): $2 - x, 1 - y, 1 - z$; vi): $1 + x, y, z$; vii): $2 - x, -y, 1 - z$.

3. 5. Catalytic Epoxidation Results

Before addition of aqueous TBHP at 80 °C, the two vanadium complexes were dissolved in the organic phase. Since the organic phase was colorful and the aqueous phase was colorless, both complexes are mainly confined in the organic phase. Moreover, TBHP was mainly transferred into the organic phase under this condition. Cyclooctene oxide and cyclooctene are poorly soluble in water, so the determination of the epoxide selectivity (epox-

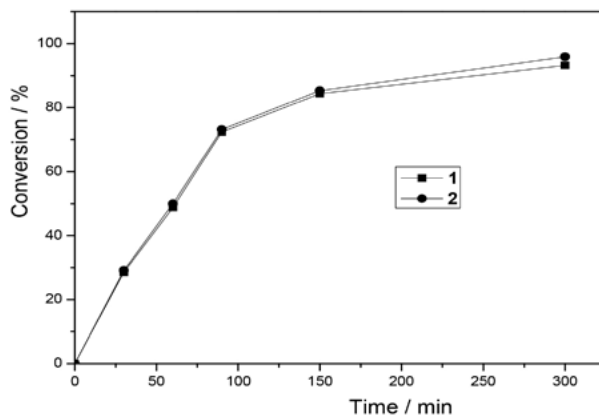


Figure 9. Kinetic monitoring of *cis*-cyclooctene epoxidation with TBHP– H_2O in the presence of the complexes.

ide formation/cyclooctene conversion) is expected to be accurate. The present study indicates effective property for the cyclooctene epoxidation by using aqueous TBHP. Kinetic profiles of both complexes are shown in Figure 9. The cyclooctene conversions of the two complexes are similar before 90 min of the reaction. After 90 min, complex **2** is a little better than complex **1**. The cyclooctene conversion is 93% for **1** and 96% for **2** at 5 h, and the selectivity toward cyclooctene oxide is 75% for **1** and 77% for **2**. The catalytic properties of the present two complexes are similar to the vanadium and molybdenum complexes reported in literature.¹⁶

4. Conclusion

Two new methyl maltolate and ethyl maltolate coordinated oxidovanadium(V) complexes derived from similar tridentate hydrazone ligands *N'*-(2-hydroxy-5-methylbenzylidene)-3-trifluoromethylbenzohydrazide and *N'*-(2-hydroxy-5-methylbenzylidene)-4-trifluoromethylbenzohydrazide were prepared. The hydrazone ligands coordinate to the V atoms through the ONO donor set. The maltolate ligands coordinate to the V atoms through the carbonyl and phenolate O atoms. The V atoms in both complexes are in octahedral coordination. Both complexes have effective catalytic epoxidation properties on cyclooctene.

Supplementary Data

CCDC numbers 2222502 (H₂L¹), 2222504 (**1**) and 2222505 for (**2**) contain the supplementary crystallographic data. These data can be obtained free of charge via <http://www.ccdc.cam.ac.uk/conts/retrieving.html>, or from the Cambridge Crystallographic Data Center, 12, Union Road, Cambridge CB2 1EZ, UK; fax: +44 1223 336 033; or e-mail: deposit@ccdc.cam.ac.uk.

Acknowledgments

This work was supported by the Collaborative Innovation Plan of Hubei Province for Key Technology of Eco-Ramie Industry.

5. References

- (a) J. B. Fournier, E. Rebuffet, L. Delage, R. Grijol, L. Meslet-Cladiere, J. Rzonca, P. Potin, G. Michel, M. Czjzek, C. Leblanc, *Appl. Environ. Microbiol.* **2014**, *80*, 7561–7573; DOI:10.1128/AEM.02430-14
(b) G. J. Colpas, B. J. Hamstra, J. W. Kampf, V. L. Pecoraro, *J. Am. Chem. Soc.* **1996**, *118*, 3469–3478. DOI:10.1021/ja953791r
- (a) T. S. Smith, V. L. Pecoraro, *Inorg. Chem.* **2002**, *41*, 6574–6760; DOI:10.1021/ja029271v
(b) J. N. Carter-Franklin, J. D. Parrish, R. A. Tschirret-Guth, R. D. Little, A. Butler, *J. Am. Chem. Soc.* **2003**, *125*, 3688–3689.
- (a) T. Q. Liu, G. Li, N. N. Shen, L. Q. Wang, B. J. J. Timmer, A. Kravchenko, S. Y. Zhou, Y. Gao, Y. Yang, H. Yang, B. Xu, B. B. Zhang, M. S. G. Ahlquist, L. C. Sun, *Chem. Eur. J.* **2022**, *28*, e202104562;
(b) K. Moghe, A. K. Sutar, I. K. Kang, K. C. Gupta, *RSC Advances* **2019**, *9*, 30823–30834; DOI:10.1039/C9RA05811G
(c) Y. Lei, *Acta Chim. Slov.* **2022**, *69*, 235–242;
(d) Q. B. Li, Y. J. Han, G. Q. Zhao, L. W. Xue, *Acta Chim. Slov.* **2017**, *64*, 500–505; DOI:10.17344/acsi.2017.3416
(e) M. R. Maurya, N. Kumar, F. Avecilla, *ACS Omega* **2022**, DOI:10.1021/acsomega.2c06732
(f) P. Devi, M. Kannan, Kiran, Virender, A. Kumar, S. Muthaiah, *J. Organomet. Chem.* **2022**, 980–981, 122515; DOI:10.1016/j.jorgchem.2022.122515
(g) K. S. Yu, Y. Sun, D. W. Zhu, Z. Y. Xu, J. Y. Wang, J. Y. Shen, Q. J. Zhang, W. Zhao, *Chem. Commun.* **2022**, *58*, 12835–12838; DOI:10.1039/D2CC04846A
(h) R. K. Sahoo, S. Rajput, A. G. Patro, S. Nembenna, *Dalton Trans.* **2022**, *51*, 16009–16016. DOI:10.1039/D2DT02846H
- (a) T. A. Bazhenova, V. S. Mironov, I. A. Yakushev, R. D. Svetogorov, O. V. Maximova, Y. V. Manakin, A. B. Kornev, A. N. Vasiliev, E. B. Yagubskii, *Inorg. Chem.* **2020**, *59*, 563–578; DOI:10.1021/acs.inorgchem.9b02825
(b) S. K. Patel, K. Kolte, C. J. Savani, P. Raghavaiah, D. Dave, A. A. Isab, D. Mistry, D. Suthar, V. K. Singh, *Inorg. Chim. Acta* **2022**, *543*, 121139; DOI:10.1016/j.ica.2022.121139
(c) K. Kim, S. Nayab, Y. Cho, H. Jung, H. Yeo, H. Lee, S. H. Lee, *RSC Advances* **2023**, *12*, 35896–35904; DOI:10.1039/D2RA07241F
(d) K. Dankhoff, M. Gold, L. Kober, F. Schmitt, L. Pfeifer, A. Durrmann, H. Kostrhunova, M. Rothemund, V. Brabec, R. Schobert, B. Weber, *Dalton Trans.* **2019**, *48*, 15220–15230; DOI:10.1039/C9DT02571E
(e) N. Ranjitha, G. Krishnamurthy, H. S. B. Naik, M. Pari, L. Afroz, K. R. Sumadevi, M. N. Manjunatha, *Inorg. Chim. Acta* **2022**, *543*, 121191; DOI:10.1016/j.ica.2022.121191
(g) E. Zarenezhad, S. Esmailzadeh, *Acta Chim. Slov.* **2018**, *65*, 416–428. DOI:10.17344/acsi.2018.4159
- (a) A. Mahdian, M. H. Ardakani, E. Heydari-Bafrooei, S. Saeednia, *Appl. Organomet. Chem.* **2021**, *35*, e6170; DOI:10.1002/aoc.6170
(b) P. Mokhtari, G. Mohammadnezhad, *Polyhedron* **2022**, *215*, 115655; DOI:10.1016/j.poly.2022.115655
(c) H. Hayashibara, X. H. Hou, K. Nomura, *Chem. Commun.* **2018**, *54*, 13559–13562; DOI:10.1039/C8CC07974A
(d) M. Q. E. Mubarak, S. P. de Visser, *Dalton Trans.* **2019**, *48*, 16899–16910; DOI:10.1039/C9DT03048D
(e) M. Liang, N. Sun, D.-H. Zou, *Acta Chim. Slov.* **2018**, *65*, 964–969; DOI:10.17344/acsi.2018.4625
(f) A. M. F. Phillips, H. Y. Suo, M. D. C. G. da Silva, A. J. L. Pombeiro, W. H. Sun, *Coord. Chem. Rev.* **2020**, *416*, 213332. DOI:10.1016/j.ccr.2020.213332

6. (a) D.-H. Zou, M. Liang, W. Chen, *Acta Chim. Slov.* **2021**, *68*, 441–446; DOI:10.17344/acsi.2020.6553
 (b) Y.-M. Cui, Y.-Q. Wang, X.-X. Su, H. Huan, P. Zhang, *J. Struct. Chem.* **2019**, *60*, 1299–1305; DOI:10.1134/S0022476619080092
 (c) R. C. Maurya, P. Bohre, S. Sahu, M. H. Martin, A. K. Sharma, P. Vishwakarma, *Arab. J. Chem.* **2016**, *9*, S150–S160. DOI:10.1016/j.arabjc.2011.02.027
7. (a) Y.M. Cui, Y.Q. Wang, X.X. Su, H. Huan, P. Zhang, *J. Struct. Chem.* **2019**, *60*, 1299–1305; DOI:10.1134/S0022476619080092
 (b) Q.A. Peng, X.P. Tan, Y.D. Wang, S.H. Wang, Y.X. Jiang, Y.M. Cui, *Acta Chim. Slov.* **2020**, *67*, 644–650; DOI:10.17344/acsi.2019.5650
 (c) Y.J. Cai, Y.Y. Wu, F. Pan, Q.A. Peng, Y.M. Cui, *Acta Chim. Slov.* **2020**, *67*, 896–903. DOI:10.17344/acsi.2020.5895
8. G. M. Sheldrick, SHELXS97 Program for solution of crystal structures, University of Göttingen, Germany, **1997**.
9. (a) Y.-T. Ye, F. Niu, Y. Sun, D. Qu, X.-L. Zhao, J. Wang, D.-M. Xian, H. Jurg, Z.-L. You, *Chinese J. Inorg. Chem.* **2015**, *31*, 1019–1026;
 (b) H.-Y. Qian, *Inorg. Nano-Met. Chem.* **2018**, *48*, 615–619. DOI:10.1080/24701556.2019.1567542
10. R. Bikas, V. Lippolis, N. Noshiranzadeh, H. Farzaneh-Bonab, A. J. Blake, M. Siczek, H. Hosseini-Monfared, T. Lis, *Eur. J. Inorg. Chem.* **2017**, *6*, 999–1006. DOI:10.1002/ejic.201601359
11. (a) R. A. Lal, M. Chakrabarty, S. Choudhury, A. Ahmed, R. Borthakur, A. Kumar, *J. Coord. Chem.* **2010**, *63*, 163–175; DOI:10.1080/00958970903259451
 (b) T. Glowiak, L. Jerzykiewicz, J. A. Sobczak, J. J. Ziolkowski, *Inorg. Chim. Acta* **2003**, *356*, 387–392. DOI:10.1016/S0020-1693(03)00301-3
12. C. A. Koellner, N. A. Piro, W. S. Kassel, C. R. Goldsmith, C. R. Graves, *Inorg. Chem.* **2015**, *54*, 7139–7141. DOI:10.1021/acs.inorgchem.5b01136
13. (a) A. Kumar, S. D. Kurbah, I. Syiemlieh, S. A. Dhanpat, R. Borthakur, R. A. Lal, *Inorg. Chim. Acta* **2021**, *515*, 120068; DOI:10.1016/j.ica.2020.120068
 (b) P. R. Patil, R. Javarappa, A. C. Kumar, N. Naik, *ChemistrySelect* **2022**, *7*, e202200752; DOI:10.1002/slct.202200752
 (c) J. Szklarzewicz, A. Jurowska, D. Matoga, K. Kruczala, G. Kazek, B. Mordyl, J. Sapa, M. Papiez, *Polyhedron* **2020**, *185*, 114589. DOI:10.1016/j.poly.2020.114589
14. (a) R. Hahn, U. Kusthardt, W. Scherer, *Inorg. Chim. Acta* **1993**, *210*, 177–182; DOI:10.1016/S0020-1693(00)83325-3
 (b) S. Gupta, A. K. Barik, S. Pal, A. Hazra, S. Roy, R. J. Butcher, S. K. Kar, *Polyhedron* **2007**, *26*, 133–141; DOI:10.1016/j.poly.2006.08.001
 (c) M. Bagherzadeh, M. Zare, V. Amani, A. Allern, L. K. Woo, *Polyhedron* **2013**, *53*, 223–229. DOI:10.1016/j.poly.2013.01.054
15. (a) L. Y. He, X. Y. Qiu, J. Y. Cheng, S. J. Liu, S. M. Wu, *Polyhedron* **2018**, *156*, 105–110; DOI:10.1016/j.poly.2018.09.017
 (b) T. M. Asha, M. R. P. Kurup, *Polyhedron* **2019**, *169*, 151–161; DOI:10.1016/j.poly.2019.04.045
 (c) Z. Q. Sun, S. F. Yu, X. L. Xu, X. Y. Qiu, S. J. Liu, *Acta Chim. Slov.* **2020**, *67*, 1281–1289. DOI:10.17344/acsi.2020.6236
16. Y. M. Cui, W. T. Liu, W. X. Yan, *Russ. J. Coord. Chem.* **2019**, *45*, 222–229. DOI:10.1134/S1070328419030023
17. (a) L. Liu, J. Lin, J. Liu, W. Chen, Y. Cui, *Synth. React. Inorg. Met.-Org. Nano-Met. Chem.* **2016**, *46*, 1871–1878; DOI:10.1080/15533174.2015.1137075
 (b) Y. M. Cui, Y. Q. Wang, X. X. Su, H. Huang, P. Zhang, *J. Struct. Chem.* **2019**, *60*, 1299–1305. DOI:10.1134/S0022476619080092

Povzetek

Sintetizirali smo enojedrni oksidovanadijev(V) kompleks [VOL¹(mm)] (1) z ligandom metil maltolat (Hm) in enojedrni oksidovanadijev(V) kompleks z etil maltolatom (Hem) [VOL²(em)] (2), pri čemer sta L¹ in L² dianionski obliki N²-(2-hidroksi-5-metilbenziliden)-3-trifluorometilbenzohidrazida (H₂L¹) in N²-(2-hidroksi-5-metilbenziliden)-4-trifluorometilbenzohidrazida (H₂L²). Hidrazoni in komplekse smo karakterizirali z elementno analizo, FT-IR in UV-Vis spektroskopijo. Strukture H₂L¹ in obeh kompleksov smo določili z monokristalno rentgensko difrakcijo. Oba kompleksa imata podobne strukture z oktaedrično koordiniranimi vanadijevimi atomi. Hidrazoni se na vanadij vežejo kot tridentatni ONO ligandi. Oba kompleksa kažeta zanimive katalitske lastnosti pri epoksidaciji ciklooktena.



Except when otherwise noted, articles in this journal are published under the terms and conditions of the Creative Commons Attribution 4.0 International License

Scientific paper

Carbon-Paste Electrode Modified by β -Cyclodextrin as Sensor for Determination of Sunset Yellow FCF and Ponceau 4R in Soft Drinks

Konstantin Pliuta and Denys Snigur*

Department of Analytical and Toxicological Chemistry, Faculty of Chemistry and Pharmacy,
Odesa I.I. Mechnikov National University, Odesa, 65082, Ukraine

* Corresponding author: E-mail: 270892denis@gmail.com

Received: 07-18-2022

Abstract

One of the disadvantages of voltammetric analysis is the significant amount of sample required for electrolysis in the cell. In this paper a methodology close to adsorption stripping voltammetry was proposed to solve this problem at an analysis of two azo dyes – Sunset Yellow FCF and Ponceau 4R. As a working electrode, a carbon-paste electrode modified with β -cyclodextrin, a cyclic oligosaccharide that can form supramolecular complexes with azo dyes was proposed. The redox behavior of Sunset Yellow FCF and Ponceau 4R, the number of electrons, protons, and charge transfer coefficients onto the proposed sensor have been studied. Using square-wave voltammetry, the conditions for the determination of two dyes were optimized. Under the optimal conditions the calibration plots are linear in the ranges 71–565 $\mu\text{g/L}$ and 189–3024 $\mu\text{g/L}$ for Sunset Yellow FCF and Ponceau 4R, respectively. Finally, the new sensor has been tested for square-wave voltammetric determination of Sunset Yellow FCF and Ponceau 4R in soft drinks, and RSD values (max. 7.8 and 8.1%) indicated satisfactory precision for both analyzed samples.

Keywords: Voltammetry, carbon-paste electrode, food azo dyes, β -cyclodextrin, azo dyes.

1. Introduction

Sunset Yellow FCF (SY, E110) and Ponceau 4P (P4R, E124) belong to the class of sulfonated azo dyes that are widely used today in the food and pharmaceutical industries.¹ WHO allows the use of these dyes in various food and pharmaceutical products with an acceptable daily intake of 4 mg/kg of body weight.² As with other similar food azo dyes, EFSA conducted studies on the possible toxicity of SY and P4R³ and concluded that these dyes do not have a mutagenic and carcinogenic effect, and do not harm human health when consumed within the established limits by WHO. However, there is a different opinion in the scientific community involved in research on the effects of food azo dyes. Thus, several researchers argue that prolonged use of such dyes as SY and P4R can lead to damage to liver and kidney cells,^{4,5} as well as an increase in oxidative stress of lipids in various tissues.⁴ A similar effect is exerted by other food azo dyes similar in structure, such as tartrazine, carmoisine, and Allura Red.^{6,7}

Over the past 20 years, many electrochemical sensors have been proposed for the determination of food azo

dyes.^{8–10} To increase the sensitivity and selectivity of sensors, various modifiers were used, such as carbon nanomaterials,¹¹ metal nanoparticles and their oxides,¹² polymeric materials,¹³ and others.¹⁴ Most often, both carbon paste^{15–17} and glassy carbon electrodes¹⁸ were used for sensor bases, like other types of electrodes.¹⁹ However, in most cases the voltammetric determination was accompanied by some disadvantages – a significant amount of supporting electrolyte solution to fill the electrolytic cell for electrolysis. Standard electrochemical cell is designed for 15–25 mL of sample for electrolysis.²⁰ To solve this problem, either low-capacity cells with small electrodes or an alternative method of electrolysis are required. In this work, a methodology close to adsorptive stripping voltammetry was proposed. The single drop methodology can be represented as follows: a small amount of sample (10 μL) is pipetted onto the modified electrode surface and is kept a certain time for the sorption stage, after which the electrode is rinsed and electrolysis is carried out in a pure buffer solution.

β -Cyclodextrin (β -CD) is a cyclic oligosaccharide in which 7 molecules of glucopyranose are linked by α -(1,4) bond.²¹ The production of β -CD is based on the enzymatic

breakdown of starch, and today it is produced on an industrial scale.²¹ Cyclodextrins are widely used in the food and pharmaceutical industries and are also often used to create sensors for various purposes.²² β -CD is also used to create sorbents for the various azo dyes removal.^{23,24} The ability of β -CD to form supramolecular inclusion complexes with azo dyes,^{25,26} and its inexpensiveness make it a promising sorption modifier for working electrodes.

The current study is aimed to investigate the possibility of voltammetric determination of SY and P4R using carbon-paste electrode modified by β -CD (CPE/ β -CD) from one drop. The usage of β -CD as modifier that improves the sorption affinity of the carbon-paste electrode surface opens up the possibility of implementing the “single-drop method”. Thus, it is possible to accumulate analytes on the sensor surface from a small volume of liquid (10 μ L) – one drop.

2. Experimental

2.1. Reagents and Apparatus

SY, P4R, silicone oil and β -CD were obtained from Merck (Germany). Carbon C1 grade with a particle size of $\leq 15 \mu\text{m}$ (UkrSpecMasla, Ukraine) was used for the preparation of carbon-paste electrode. Double distilled water was used to prepare standard and buffer solutions, as well as to rinse the electrode.

Voltammograms were recorded using an Ecotest VA potentiostat (Econiks Expert, Russia) equipped with an auxiliary platinum electrode, a silver chloride reference

electrode, and a working CPE/ β -CD electrode. The pH was monitored using an I-500 pH-meter (LLC Akvilon, Russia), coupled with a glass electrode.

The Shimadzu Prominence liquid chromatograph, which consists of a pump (LC-20), autosampler (SIL-20), column oven (CTO-20) and spectrophotometric detector (SPD-20), was used to determine food azo dyes in various samples by HPLC. Nucleodur C18ec (length 250 mm, i.d. 4.6 mm and particle size 5 μm) was used as an analytical column for the separation of azo dyes.

2.2. Preparation of CPE/ β -CD

For the preparation of carbon-paste, the carbon powder, β -CD, and silicone oil were thoroughly mixed in a mortar until a homogeneous paste was formed. The constant ratio of dry matter to the binder was maintained as 2.3:1 (by weight) in all prepared electrodes. An unmodified electrode was prepared in the same way but without β -CD. As the electrode body, a Teflon tube with an inner diameter of 3 mm was used. For the contact of the carbon-paste electrode with the output of the potentiostat the copper wire was used. The electrode surface was refreshed before each measurement by squeezing out a small portion of the paste, cutting off, and polishing on a piece of weighing paper.

2.3. Determination of Azo Dyes in Soft Drinks

For the soft drinks degassing, a small portion (~ 10 mL) was heated to 45 $^{\circ}\text{C}$ and sonicated for 15 min. If nec-

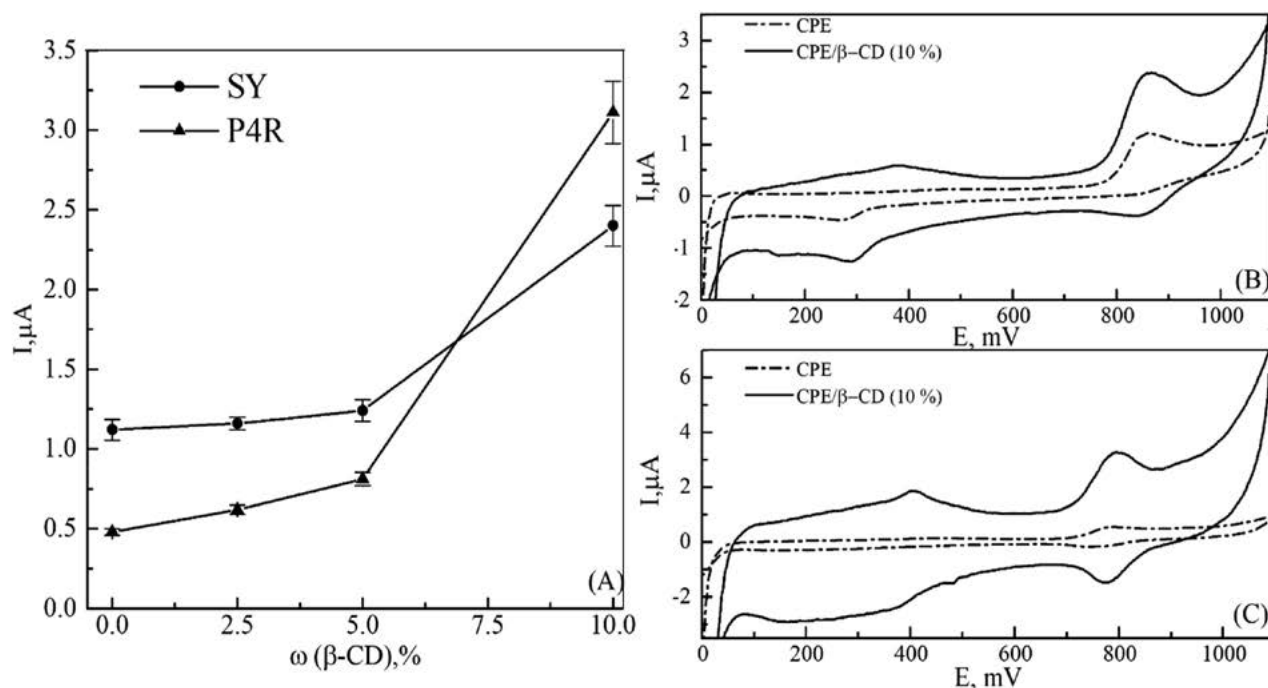


Fig. 1. (A) The plot of oxidation current of dyes as a function of β -CD content in CPE. Cyclic voltammogram of a bare CPE and CPE/ β -CD in a supporting electrolyte (pH = 2) after accumulation of (B) SY (100 μM) and (C) P4R (100 μM) onto electrode surface from one drop of dyes solution.

essary, the sample was filtered through a hydrophilic PTFE filter. The sample aliquot was transferred in a 5 ml flask and diluted to the mark with a Britton-Robinson buffer solution with pH 2. For single drop methodology procedure, 10 μL of the analyzed sample was pipetted onto the sensor surface and held for 5 min, after which the electrode was gently rinsed with double distilled water. A square wave voltammetry ($\Delta E = 50$ mV, $f = 15$ Hz, $t_{\text{ads}} = 5$ min) was used for signal registration at a scan rate of 25 mV/s from 300 mV to 1100 mV. Quantitative analysis was carried out according to the standard addition method.

3. Results and Discussion

3.1. Optimization of Sensor Composition

For the first time the optimal content of the modifier in the working electrode was established. A series of sensors with different contents of β -CD (from 2.5 to 10 wt. %) was fabricated. One drop (10 μL) of the working solution of dyes was pipetted onto the sensor surface and kept for 3 min for sorption. After that, the electrode was rinsed and electrolysis was carried out in a pure buffer solution (pH 2). Oxidation current of dyes was used as a signal for optimal sensor composition (Fig. 1).

As can be seen, with an increase in the content of the modifier, the oxidation currents for both dyes increase and reach maxima at 10 wt % β -CD in the electrode. This behavior confirms that β -CD promotes the sorption of dyes on the sensor surface. With a further increase of the β -CD content, a carbon paste that was difficult to work with was obtained. Therefore, 10 wt.% of β -CD was chosen as optimal modifier content.

To evaluate the effect of β -CD on the CPE conductive properties, cyclic voltammograms (CV) of a solution of potassium ferrocyanide (1 mM) in 0.1 M potassium chloride on both CPE/ β -CD and bare CPE (Fig. S1) were recorded. As can be seen from Fig. S1, the ferrocyanide oxidation and reduction currents on CPE/ β -CD were increased compared to bare CPE. The difference between the ferrocyanide oxidation and reduction peak potential (ΔE_p) for bare CPE is 85 mV, while for CPE/ β -CD it is 70 mV, which indicates a higher electrocatalytic activity of the modified sensor. The Randles–Sevcik equation was used to determine the CPE/ β -CD active area (Equation 1).²⁰

$$I_p = (2.69 \cdot 10^5) n^{3/2} A D_{\text{red}}^{1/2} \nu^{1/2} C_{\text{red}}^0 \quad (1)$$

where I_p – current in amperes, n – number of electrons in the redox reaction, A – the electrode surface area in cm^2 , D_{red} – diffusion coefficient in cm^2/s ($D([\text{Fe}(\text{CN})_6]^{4-}) = 7.6 \cdot 10^{-6} \text{ cm}^2/\text{s}$), ν – scan rate in V/s, C_{red}^0 – concentration in mol/cm^3 .

Using the equation above, the active surface area for CPE/ β -CD can be calculated as 0.105 cm^2 , which is ~ 1.2 -times that of bare CPE (0.090 cm^2). Thus, an increase in the active surface area, as well as a lower value of ΔE_p in the case of CPE/ β -CD, indicates an increase in the electron transfer rate from the electrode surface.

3.2. Electrochemical Behavior of Sunset Yellow FCF and Ponceau 4R on the CPE/ β -CD Sensor

The suggested methodology was applied to study the redox behavior of SY and P4R on the proposed sensor. To carry out these experiments, after the stage of dye sorption from the solution by the electrode surface, a series of CVs in pure buffer solutions were recorded under different conditions.

pH effect

It is known that the pH of a buffer solution strongly affects the protolytic state of dyes in the solution²⁸ and, consequently, their sorption equilibrium.²⁹ Using the suggesting methodology, it is possible to carry out sorption and electrolysis at different pH values of the buffer solution, which gives a much greater possibility of the analysis conditions optimization. The influence of buffer solution pH on dyes sorption ability onto the electrode surface and the electrolysis current were investigated (Fig. 2).

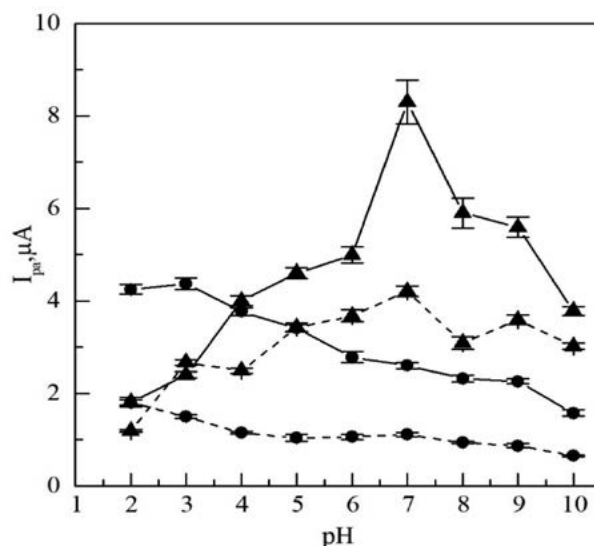


Fig. 2. The plot of the oxidation peak current as a function of pH-dependent adsorption for SY (circles, solid line) and P4R (circles, dashed line) and as a function of pH-dependent electrolysis for SY (triangle, solid line) and P4R (triangle, dashed line) onto CPE/ β -CD.

In the case of sorption ability increase, buffer solution pH decreases the oxidation current, which indicates the decrease of sorption of dyes onto the sensor surface. This can be explained by the specificity of the formation of

inclusion complexes between dyes and β -CD. The mechanism of formation of complexes between azo dyes and β -CD can include both supramolecular and electrostatic interactions.³⁰ It should be also noted that azo dyes can interact with the electrode surface both due to π - π interactions and via electrostatic forces between carboxyl/carbonyl groups, which are always present on the surface of the carbon-paste electrode.³¹ According to the data of protolytic equilibria of SY and P4R, the lowest degree of ionization of dye molecules is observed in an acidic medium. Given what follows, it can be assumed that, along with supramolecular and electrostatic forces on the modified electrode play an important role in the ability to form inclusion complexes between dyes and β -CD. The pH shift to the alkaline zone increases the ionization of dyes, which may increase their electrostatic repulsions from the electrode surface. As a result, there may be less inclusion complex formation, which will result in lower dye oxidation currents.

The oxidation current of SY and P4R increased at pH 6–7 in the case of the effect of buffer solution pH on electrolysis. At pH > 7, a decrease in the oxidation current was observed for both SY and P4R. In our further studies, pH 2 for the adsorption of dyes and pH 7 for carrying out of electrolysis were chosen.

With an increase in the pH of the supporting electrolyte, the potentials of the oxidation and reduction peaks of dyes shift to the cathodic region (Fig. S2A and S3A), which indicates the participation of the proton in the electrochemical processes.³² To determine the ratio of protons to electrons (m/n), the dependences of the potentials of the oxidation/reduction peaks (E_{pa}/E_{pc}) on the pH (Fig. S2B and S3B) were studied. The following linear equations were obtained for SY: $E_{pa}(I_{ox}) = -34.2\text{pH} + 944.4$ and $E_{pc}(I_{red}) = -32.0\text{pH} + 922.0$, and for P4R: $E_{pa}(I_{ox}) = -31.5\text{pH} + 860.1$ and $E_{pc}(I_{red}) = -33.8\text{pH} + 854.6$. Thus, based on the values of slopes of the obtained equations in the oxidation/reduction processes, the ratio m/n is 1:2 for both SY and P4R.^{20,32}

Scan rate effect

For investigation of the nature of the oxidation/reduction current and to establish the number of electrons involved in the redox processes, the CVs of dyes solutions on CPE/ β -CD at different scan rates were recorded (Fig. S4).

Based on the obtained data, the dependences of the dyes oxidation current on the scan rate were plotted (Fig. S4C) and can be expressed by the following equations: $I_{pa}(\text{SY}) = 0.076v + 2.34$ ($R^2 = 0.997$), $I_{pa}(\text{P4R}) = 0.032v + 2.39$ ($R^2 = 0.995$). The linear dependences of the oxidation current on the scan rate indicates the adsorption nature of the dyes oxidation current on CPE/ β -CD.^{20,32}

Laviron model was used for the determination the number of electrons (n) and the charge transfer coefficient (α) involved in the redox processes (Equation 2 and 3).³³

For this, the dependences between the dyes oxidation/reduction peak potential (E_{pa}/E_{pc}) and the decimal logarithm of the scan rate were constructed (Fig. S5). Using the slope of obtained lines and equations 2 and 3 the n and α were calculated as: for SY: $n = 2.16 \approx 2$ and $\alpha = 0.62$, and for P4R: $n = 2.05 \approx 2$ and $\alpha = 0.56$. Taking into account the obtained experimental data it can be concluded that two electrons and one proton are involved in the process of oxidation and reduction of SY and P4R onto the CPE/ β -CD.

$$E_{pa} = \frac{2.3RT}{(1-\alpha)nF} \cdot \lg v + \text{const} \quad (2)$$

$$E_{pc} = \frac{-2.3RT}{\alpha nF} \cdot \lg v + \text{const} \quad (3)$$

Thus, SY and P4R can be reversibly oxidized on the surface of the proposed sensor. However, it should be noted that the dye oxidation peak current (I_{ox}) is much higher than the corresponding reduction current (I_{red}). According to Wopschall and Shain,³⁴ this behavior may indicate the presence of an irreversible chemical reaction with an oxidation intermediate. To confirm this assumption, the ratio of the reduction current (I_{red}) to the oxidation current (I_{ox}) was plotted for both dyes as a function of the scan rate ($I_{red}/I_{ox} = f(v)$) (Fig. S6). As can be seen, as the sweep rate increases, the ratio between the reduction and oxidation currents for both dyes decrease. This confirms that the process of oxidation of SY and P4R proceeds with the participation of an irreversible chemical reaction (EC_{ir} mechanism).

Cyclic voltammetry profile

CVs at different numbers of cycles were recorded and thoroughly examined to gain a better knowledge of the mechanism of dyes oxidation.

For two dyes in the first scan cycle, one oxidation peak I_{ox} (SY: $E_p(I_{ox}) = 880$ mV; pH = 2, P4R: $E_p(I_{ox}) = 764$ mV; pH = 3) and the corresponding reduction peak I_{red} (SY: $E_p(I_{ox}) = 862$ mV; pH = 2, P4R: $E_p(I_{ox}) = 751$ mV; pH = 3) were observed (Fig. 3). The presence of the corresponding oxidation/reduction peaks is confirmed by many authors,^{35,36} which can be attributed to both the oxidation of the azo group and the hydroxyl group located in the naphthalene ring.³⁷ Also, on the CV of dyes, there is an irreversible reduction peak I_{red} (SY: $E_p(I_{red}) = 58$ mV; pH = 2, P4R: $E_p(I_{red}) = -131$ mV; pH = 3), which refers to the destructive reduction of the azo group to corresponding amines.³⁸ As can be seen from Fig. 3, in an acidic medium, there is no I_{ox} oxidation peak for both dyes upon potential reverse scan cycle. This can be explained by the specificity of the measurement according to the suggested methodology. During the first scan cycle, dyes are almost completely irreversibly oxidized at the electrode surface. However, as can be seen in the neutral medium (Fig. 3 inset), there are insignificant dye oxidation peaks in the second scan cycle, which most likely indicate much greater stability of

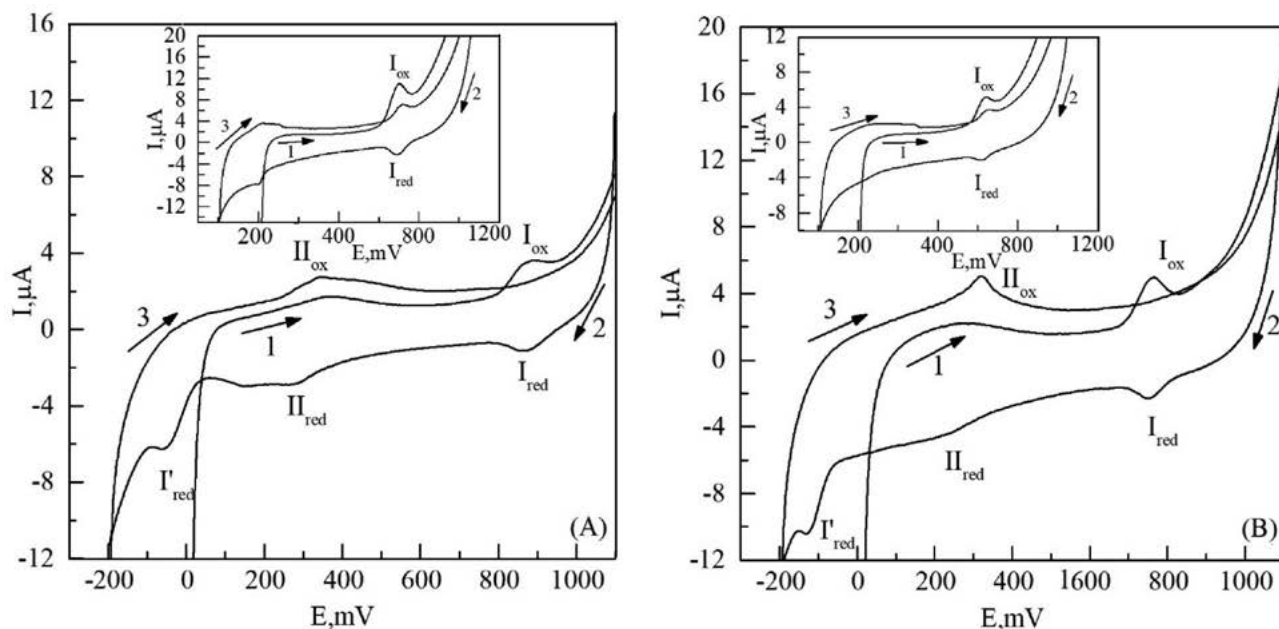


Fig. 3. (A) CV of a buffer solution with pH 2 and pH 7 (insert (A)) onto CPE/ β -CD after adsorption on the surface of a solution (10 μ l) of SY with a concentration of 100 μ M for 3 min. (B) CV of a buffer solution with pH 3 and pH 7 (insert (B)) onto CPE/ β -CD after adsorption on its surface of a solution (10 μ l) of P4R with a concentration of 100 μ M for 3 min. Arrows and numbers indicate the direction and order of potential sweep.

the intermediate oxidation products of these dyes in the neutral medium. This, in turn, makes it possible to partially restore the oxidized form of the dye, which is expressed in insignificant oxidation peaks during the subsequent potential sweep (direction № 3 in Fig. 3).

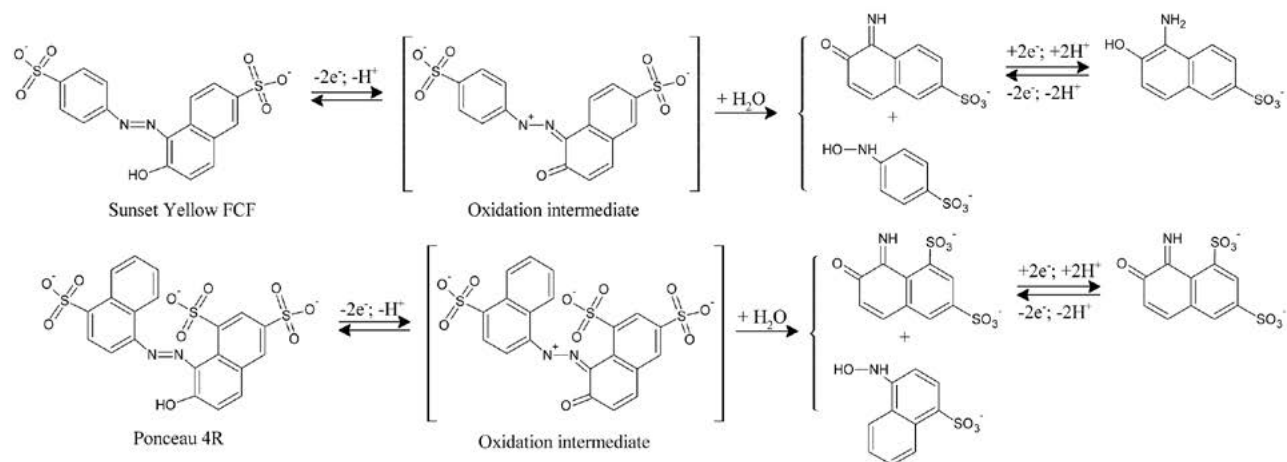
It should be noted that in both cases of SY and P4R, the appearance of a new redox pair II_{red} (SY: $E_p(II_{red}) = 284$ mV; pH = 2, P4R: $E_p(II_{red}) = 241$ mV; pH = 3) and II_{ox} (SY: $E_p(II_{ox}) = 343$ mV; pH = 2, P4R: $E_p(II_{ox}) = 321$ mV; pH = 3) after dyes oxidation process in next sweep cycles, which may be related to the oxidative destruction of dye molecules. The appearance of a new redox pair after the oxidation process was also noted by researchers studying the mechanisms of oxidation in partially sulfonated³⁹ and fully nonsulfonated azo dyes.⁴⁰ In both cases, the authors^{39,40} noted that the new redox peaks belong to the fragments formed after the oxidative degradation of the molecule.

In this regard, the question was raised about the similarity of the behavior during the reduction of dyes at the azo group. To do this, a series of CVs were recorded with a separate process of oxidation and reduction of dyes to prove the presence of a common redox pair in both oxidative and reductive destruction products (Fig. S7). After the oxidation process and the accumulation of oxidation products, the first and second cycles of the II_{ox} - II_{red} redox-pair potential range coincide (Fig. S7). In the case of preliminary reduction of azo dyes, the first and second scan cycles in the potential range of the II_{ox} - II_{red} pair do not coincide. Thus, in the first cycle, the oxidation potential of III_{ox} is shifted relative to II_{ox} by 62 mV for SY and by 26 mV for P4R to the anode region. The second cycle

after the pre-reduction process completely coincides with the first and second cycles after the pre-oxidation of the dye. This behavior can be explained by the presence of the azo dyes' reduction products intermediates and the requirement of higher energy for the oxidation of this form, which causes a small shift in the potential of the oxidation peak of III_{ox} relative to II_{ox} .

Thus, during the reduction of dyes, new redox pairs also appear, coinciding with the redox pair formed during its oxidation. Consequently, the products of oxidative and reductive destruction of azo dyes have a common redox pair.

In conclusion, it was assumed that a significant disproportion between the currents of oxidation and reduction of azo dyes in the first cycle (I_{ox} - I_{red}) indicates the predominant oxidative degradation of the dyes' molecules under the conditions of signal recording. The destruction of the molecule can be associated with the oxidation process by the EC_{ir} mechanism, in which the subsequent chemical reaction can lead to a rearrangement of bonds in the molecule and, as a consequence, to the cleavage of the azo group.³² Also based on the obtained CV of dye solutions at various scan rates (Fig. S4), it can be concluded that P4R has a more stable oxidation intermediate than SY. This may be evidenced by the presence of a reversible reduction peak in P4R at a minimum scan rate (25 mV/s) in comparison with SY. Thus, at low scan rates for SY, the rate of the subsequent irreversible chemical reaction begins to strongly dominate, which is expressed in the absence of the reduction peak according to I_{ox} . It was supposed that the match stability of the intermediate oxidation product of P4R is realized due to the compen-



Scheme 1. Suggested mechanism of SY and P4R oxidation onto CPE/ β -CD

sation of the excess positive charge in the molecule after the oxidation process. For example, it can be implemented due to the negative charge of the sulfo group located in the peri-position to the azo group. The formation of new redox pairs after the first potential sweep cycle can also confirm our assumption about the oxidative degradation of the molecule due to an irreversible chemical reaction with intermediate oxidation products that produce new electroactive fragments:

3. 3. Optimization of Dyes Determination Parameters on CPE/ β -CD Sensor

Square wave voltammetry coupled with suggested single drop methodology on the developed CPE/ β -CD sensor for the determination of dyes was used. Such typical parameters as potential amplitude (ΔE), frequency (f),

accumulation time (t_{ads}) and potential sweep rate (v) were chosen for optimization (Fig. S8, S9).

At increasing potential amplitude and frequency, the resulting current also increased, respectively. The 50 mV and 15 Hz were chosen as the optimal values for the determination of dyes. This is due to the fact that with a subsequent increase in amplitude and frequency, the shape of the peak was strongly distorted (Fig. S8, S9A,B). When investigating the effect of accumulation time, the resulting current plateaus after 5 min for both dyes (Fig. S8, S9B). At increasing scan rate from 25 mV/s to 200 mV/s, a decrease in peak current was observed and less and less clearly identified peak. Probably, this effect arises due to the combination of the registration signal by the suggested methodology with the peculiarity of the potential change in square-wave voltammetry. The optimal scan rate of 25 mV/s was chosen for both dyes.

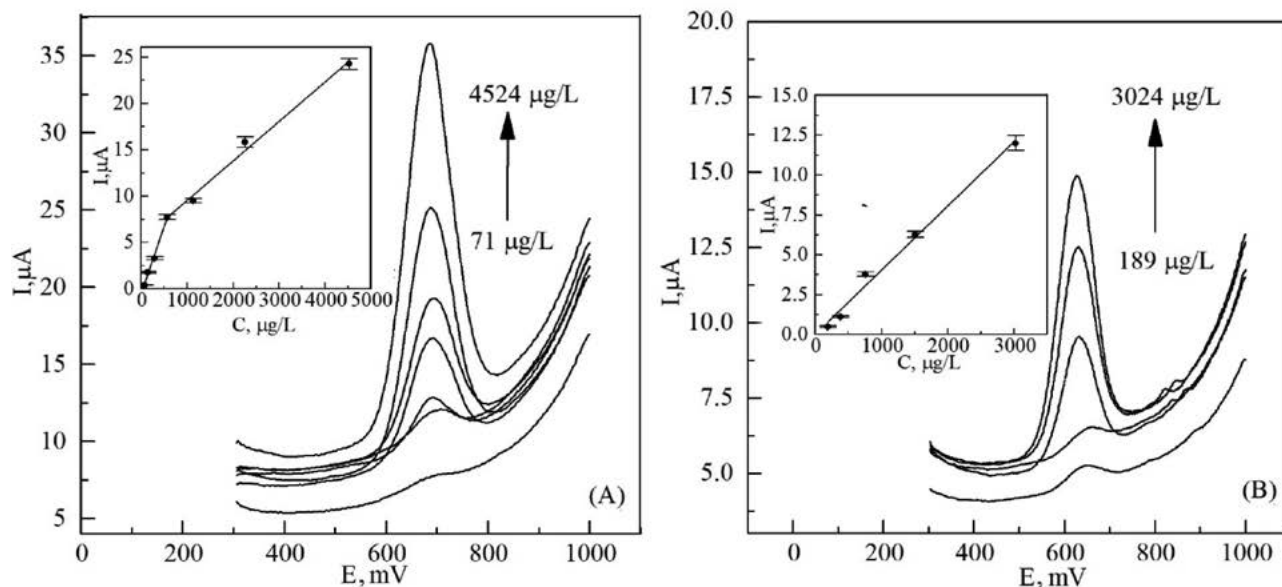


Fig. 4. Square-wave voltammograms of (A) SY and (B) P4R solution for various concentrations. Inserts: plots of the peak currents as a function of concentration.

3. 4. Determination of Sunset Yellow FCF and Ponceau 4R on CPE/ β -CD in Real Samples

Under the optimal conditions, calibration curves for dyes' determination via proposed method were plotted (Fig. 4).

The obtained calibration curve for SY has two linear sections: 71–565 $\mu\text{g/L}$ and 565–4524 $\mu\text{g/L}$, which are described by the equations $I_{pa}(\text{SY}) = 14.4C(\text{SY}) + 0.59 \pm 0.14$ ($R^2 = 0.993$) and $I_p(\text{SY}) = 4.3C(\text{SY}) + 5.09 \pm 0.81$ ($R^2 = 0.995$), respectively. For P4R, the calibration curve is linear in the concentration range 189–3024 $\mu\text{g/L}$ and is described by the equation $I_p(\text{P4R}) = 13.2C(\text{P4R}) + 0.59 \pm 0.148$ ($R^2 = 0.990$). According to the 3σ and 6σ approach,⁴¹ LOD and LOQ for dyes were calculated using data from 6 parallel measurements of SY and P4R solutions at concentrations of 71 and 189 $\mu\text{g/L}$, respectively. The calculated values were for SY: LOD = 42 $\mu\text{g/L}$, LOQ = 85 $\mu\text{g/L}$; and for P4R: LOD = 102 $\mu\text{g/L}$, LOQ = 204 $\mu\text{g/L}$. The proposed sensor was tested on model solutions and soft drinks samples that do not contain dyes. The results of analyses are presented in Table 1.

To test the developed sensor, soft drinks samples were analyzed according to proposed method and via HPLC as a reference method. A description of the HPLC determination method is provided in the Supplementary Materials. Fisher's F-test and Student's and Welch's t-test were used to compare the determination results obtained via the two methods (Table S1).⁴² As can be seen from Table S1, the obtained t-statistic values are less than the critical value, which indicates that there is no statistical difference between the results obtained by HPLC and the proposed voltammetric method. According to the obtained results, it can be concluded that the proposed sensor and suggested methodology proved to be satisfactory in the analysis of SY and P4R in soft drinks samples with RSD no more than 8%.

4. Conclusions

In this work, CPE/ β -CD for the SY and P4R determination was proposed. Using CV, the influence of supporting electrolyte's pH, as well as the potential sweep rate was studied. It has been established that SY and P4R are oxidized quasi-reversibly with the participation of one proton and two electrons. For both dyes, the formation of a new redox pair was noted in subsequent potential sweep cycles. Based on the obtained data, it was concluded that the oxidation of SY and P4R onto CPE/ β -CD occurs with the participation of an irreversible chemical reaction that leads to cleavage of dyes' molecules at the azo group, creating new electroactive piece (the corresponding dyes oxidation scheme was proposed). Using a single drop methodology, a lowering in the minimum amount of sample required for analysis to 10 μL was achieved. Suggested methodology and developed CPE/ β -CD sensor was successfully tested at dyes determination in real soft drinks samples with a recovery ratio of 95% and RSD no more than 8%.

Conflicts of interest

There are no conflicts to declare

5. References

- 1 D. Villaño, C. García-Viguera and P. Mena, *Encycl. Food Heal.*, **2015**, 265–272. DOI:10.1016/B978-0-12-384947-2.00190-2
- 2 World Health Organization, *WHO Technical Report Series: Evaluation of certain food additives and contaminants*, **2011**.
- 3 E. Food and S. Authority, *EFSA J.*, **2015**, 13, 1–35.
- 4 L. I. Khayyat, A. E. Essawy, J. M. Sorour and A. Soffar, *PeerJ*, **2018**, 2018, 1–17.
- 5 K. Elbanna, O. M. Sarhan, M. Khider, M. Elmogy, H. H. Abulreesh and M. R. Shaaban, *J. Food Drug Anal.*, **2017**, 25, 667–680. DOI:10.1016/j.jfda.2017.01.005

Table 1. Results of SY and P4R determination in model solutions and soft drink ($n = 3$, $P = 0.95$)

Analyte	Sample	Spiked, $\mu\text{g/mL}$	Found, $\mu\text{g/mL}$	Recovery, %	RSD, %
Sunset Yellow FCF	Model solution	5	4.75 ± 0.45	95	3.8
		2.5	2.45 ± 0.31	98	5.1
		0.5	0.48 ± 0.08	96	6.9
	Soft drink	5	4.78 ± 0.75	96	6.3
		2.5	2.41 ± 0.43	96	7.1
		0.5	0.461 ± 0.09	92	7.8
Ponceau 4R	Model solution	5	4.82 ± 0.47	96	3.9
		2.5	2.51 ± 0.3	100	4.75
		0.5	0.55 ± 0.08	110	5.9
	Soft drink	5	4.68 ± 0.63	94	5.4
		2.5	2.35 ± 0.43	94	7.3
		0.5	0.53 ± 0.11	106	8.1

- 6 D. Bhatt, K. Vyas, S. Singh, P. J. John and I. Soni, *Food Chem. Toxicol.*, **2018**, *113*, 322–327. DOI:10.1016/j.fct.2018.02.011
- 7 H. Imane, S. Bellahcen and F. Souana, *Int. J. Pharm. Pharm. Sci.*, **2011**, *3*, 159–169.
- 8 H. Karimi-Maleh, H. Beitollahi, P. Senthil Kumar, S. Tajik, P. Mohammadzadeh Jahani, F. Karimi, C. Karaman, Y. Vasseghian, M. Baghayeri, J. Rouhi, P. L. Show, S. Rajendran, L. Fu and N. Zare, *Food Chem. Toxicol.*, **2022**, *164*, 112961. DOI:10.1016/j.fct.2022.112961
- 9 N. Vladislavić, M. Buzuk, I. Š. Rončević and S. Brinić, *Int. J. Electrochem. Sci.*, **2018**, *13*, 7008–7019.
- 10 K. Rovina, L. A. Acung, S. Siddiquee, J. H. Akanda and S. M. Shaarani, *Food Anal. Methods*, **2017**, *10*, 773–787. DOI:10.1007/s12161-016-0645-9
- 11 W. Zhang, T. Liu, X. Zheng, W. Huang and C. Wan, *Colloids Surfaces B Biointerfaces*, **2009**, *74*, 28–31. DOI:10.1016/j.colsurfb.2009.06.016
- 12 P. S. Dorraji and F. Jalali, *Food Chem.*, **2017**, *227*, 73–77. DOI:10.1016/j.foodchem.2017.01.071
- 13 L. Zhao, F. Zhao and B. Zeng, *Electrochim. Acta*, **2014**, *115*, 247–254. DOI:10.1016/j.electacta.2013.10.181
- 14 Y. Songyang, X. Yang, S. Xie, H. Hao and J. Song, *Food Chem.*, **2015**, *173*, 640–644. DOI:10.1016/j.foodchem.2014.10.075
- 15 A. Chebotarev, K. Pliuta and D. Snigur, *Turkish J. Chem.*, **2018**, *42*, 1534–1543. DOI:10.3906/kim-1805-37
- 16 A. N. Chebotarev, K. V. Pliuta and D. V. Snigur, *ChemistrySelect*, **2020**, *5*, 3688–3693. DOI:10.1002/slct.202000518
- 17 K. Pliuta and D. Snigur, *Anal. Sci.*, **2022**, *38*, 1377–1384. DOI:10.1007/s44211-022-00170-y
- 18 Y. Zhang, X. Zhang, X. Lu, J. Yang and K. Wu, *Food Chem.*, **2010**, *122*, 909–913. DOI:10.1016/j.foodchem.2010.03.035
- 19 R. A. Medeiros, B. C. Lourencao, R. C. Rocha-Filho and O. Fatibello-Filho, *Talanta*, **2012**, *99*, 883–889. DOI:10.1016/j.talanta.2012.07.051
- 20 B. Allen J. and F. Larry R., *Electrochemical methods: Fundamental and applications*, **2004**, vol. 677.
- 21 S. V. Kurkov and T. Loftsson, *Int. J. Pharm.*, **2013**, *453*, 167–180. DOI:10.1016/j.ijpharm.2012.06.055
- 22 T. Ogoshi and A. Harada, *Sensors*, **2008**, *8*, 4961–4982. DOI:10.3390/s8084961
- 23 A. Yilmaz, E. Yilmaz, M. Yilmaz and R. A. Bartsch, *Dye. Pigment.*, **2007**, *74*, 54–59. DOI:10.1016/j.dyepig.2006.01.011
- 24 E. Y. Ozmen, M. Sezgin, A. Yilmaz and M. Yilmaz, *Bioresour. Technol.*, **2008**, *99*, 526–531. DOI:10.1016/j.biortech.2007.01.023
- 25 B. Hosangadi and S. Palekar, *J. Incl. Phenom. Mol. Recognit. Chem.*, **1989**, *7*, 321–325. DOI:10.1007/BF01076985
- 26 M. Suzuki, Y. Sasaki and M. Sugiura, *Chem. Pharm. Bull.*, **1970**, *8*, 1797–1805.
- 27 Y. Li, Y. Li, L. Jia, Y. Li, Y. Wang, P. Zhang and X. Liu, *J. Iran. Chem. Soc.*, **2021**, *19*, 1251–1260. DOI:10.1007/s13738-021-02375-w
- 28 D. V. Snigur, A. N. Chebotarev and K. V. Bevziuk, *J. Appl. Spectrosc.*, **2018**, *85*, 21–26. DOI:10.1007/s10812-018-0605-9
- 29 K. Bevziuk, A. Chebotarev, A. Koicheva and D. Snigur, *Monatshfte fur Chemie*, **2018**, *149*, 2153–2160. DOI:10.1007/s00706-018-2301-0
- 30 X. Qin and X. Zhu, *Anal. Lett.*, **2016**, *49*, 189–199. DOI:10.1080/00032719.2015.1065880
- 31 G. M. D. Ferreira, G. M. D. Ferreira, M. C. Hespanhol, J. de Paula Rezende, A. C. dos Santos Pires, L. V. A. Gurgel and L. H. M. da Silva, *Colloids Surfaces A Physicochem. Eng. Asp.*, **2017**, *529*, 531–540. DOI:10.1016/j.colsurfa.2017.06.021
- 32 D. K. Gosser, *Cyclic Voltammetry: Simulation and Analysis of Reaction Mechanisms*, New York, **1994**.
- 33 E. Laviron, *J. Electroanal. Chem.*, **1979**, *101*, 19–28. DOI:10.1016/S0022-0728(79)80075-3
- 34 R. H. Wopschall and I. Shain, *Anal. Chem.*, **1967**, *39*, 1535–1542. DOI:10.1021/ac50156a020
- 35 Y. Zhang, L. Hu, X. Liu, B. Liu and K. Wu, *Food Chem.*, **2015**, *166*, 352–357. DOI:10.1016/j.foodchem.2014.06.048
- 36 A. Chebotarev, A. Koicheva, K. Bevziuk, K. Pliuta and D. Snigur, *J. Food Meas. Charact.*, **2019**, *13*, 1964–1972. DOI:10.1007/s11694-019-00115-6
- 37 P. Sierra-Rosales, C. Berríos, S. Miranda-Rojas and J. A. Squella, *Electrochim. Acta*, **2018**, *290*, 556–567. DOI:10.1016/j.electacta.2018.09.090
- 38 S. Combeau, M. Chatelut and O. Vittori, *Talanta*, **2002**, *56*, 115–122. DOI:10.1016/S0039-9140(01)00540-9
- 39 S. Momeni and D. Nematollahi, *Sci. Rep.*, **2017**, *7*, 1–10. DOI:10.1038/s41598-017-04581-0
- 40 D. Yang, L. Zhu and X. Jiang, *J. Electroanal. Chem.*, **2010**, *640*, 17–22. DOI:10.1016/j.jelechem.2009.12.022
- 41 Eurachem, *The Fitness for Purpose of Analytical Methods: A Laboratory Guide to Method Validation and Related Topics*, **2014**.
- 42 S. Ellison, V. Barwick and T. Duguid Farrant, *Practical Statistics for the Analytical Scientist*, RSC Publishing, London, 2nd edn., **2009**.

Povzetek

Ena od slabih strani voltametrijske analize je znatna količina vzorca, potrebnega za elektrolizo v celici. V članku za rešitev tega problema predstavljamo metodologijo, podobno adsorpcijski inverzni (*stripping*) voltametriji, za analizo dveh azo barvil – Sunset Yellow FCF in Ponceau 4R. Za delovno elektrodo predlagamo elektrodo iz ogljikove paste, modificirano z β -ciklodekstrinom, cikličnim oligosaharidom, ki lahko tvori supramolekularne komplekse z azo barvili. Preučili smo redoks obnašanje barvil Sunset Yellow FCF in Ponceau 4R: število elektronov in protonov ter koeficiente prenosa naboja na predlagani senzor. Pogoje za določevanje obeh barvil smo optimizirali z uporabo voltametrije pravokotnih pulzov (*square-wave*). Pri optimalnih pogojih so bile umeritvene krivulje linearne v območju 71–565 $\mu\text{g/L}$ za Sunset Yellow FCF in 189–3024 $\mu\text{g/L}$ za Ponceau 4R. Na koncu smo novi senzor preizkusili za določitev Sunset Yellow FCF in Ponceau 4R v brezalkoholnih pijačah z voltametrijo pravokotnih pulzov. Vrednosti RSD so bile največ 7,8 in 8,1 %, kar je zadovoljiva ponovljivost za oba analizirana vzorca.



Except when otherwise noted, articles in this journal are published under the terms and conditions of the Creative Commons Attribution 4.0 International License

DRUŠTVENE VESTI IN DRUGE AKTIVNOSTI SOCIETY NEWS, ANNOUNCEMENTS, ACTIVITIES

Vsebina

Doktorska in magistrska dela, diplome v letu 2022	S3
Koledar važnejših znanstvenih srečanj s področja kemije in kemijske tehnologije	S32
Navodila za avtorje	S34

Contents

Doctoral theses, master degree theses, and diplomas in 2022	S3
Scientific meetings – Chemistry and chemical engineering.....	S32
Instructions for authors	S34

UNIVERZA V LJUBLJANI
FAKULTETA ZA KEMIJO IN KEMIJSKO TEHNOLOGIJO

1. januar – 31. december 2022

DOKTORATI

DOKTORSKI ŠTUDIJSKI PROGRAM KEMIJSKE ZNANOSTI

KEMIJA

Tanja BANČIČ

Mentor: prof. dr. Robert Dominko
Somentor: prof. dr. Jurij Svete
POLIIMIDI KOT ORGANSKI KATODNI MATERIALI ZA
MAGNEZIJEVE AKUMULATORJE
Datum zagovora: 30. 3. 2022

Valentina METLIČAR

Mentor: znan. sod. dr. Alen Albreht
STABILIZACIJA KAROTENOIDOV, IZOLIRANIH IZ
INVAZIVNIH TUJERODNIH RASTLINSKIH VRST IN
KARAKTERIZACIJA NJIHOVIH PRIPRAVKOV
Datum zagovora: 31. 3. 2022

Monika HORVAT

Mentor: prof. dr. Jernej Iskra
UPORABNE SPOJINE IN MATERIALI NA OSNOVI
LIGNINA IN BARVIL INVAZIVNIH TUJERODNIH
RASTLIN
Datum zagovora: 27. 6. 2022

Marko BUNC

Mentor: prof. dr. Jurij Lah
Somentor: doc. dr. Matjaž Bončina
MEHANIZEM, TERMODINAMIKA IN KINETIKA
AGREGACIJE TERAPEVTSKIH MONOKLONSKIH
PROTITELES
Datum zagovora: 28. 9. 2022

Anže ZUPANC

Mentor: prof. dr. Marjan Jereb
PRETVORBE HALOGENIRANIH IN HALKOGENIRANIH
ORGANSKIH SPOJIN PO NAČELIH ZELENE KEMIJE
Datum zagovora: 29. 9. 2022

Nina PODJED

Mentorica: izr. prof. dr. Barbara Modec
PREUČEVANJE REAKCIJ CINKOVEGA(LL) IN
BAKROVEGA(LL) KINALDINATA S CIKLIČNIMI AMINI
TER AMINO ALKOHOLI
Datum zagovora: 30. 9. 2022

KEMIJSKO INŽENIRSTVO

Filip STRNIŠA

Mentor: prof. dr. Igor Plazl
Somentor: prof. dr. Tomaž Urbič
VEČNIVOJSKO MODELIRANJE KEMIJSKIH IN
BIOKEMIJSKIH PROCESOV V MIKROFLUIDNIH
NAPRAVAH
Datum zagovora: 18. 5. 2022

Tilen KOPAČ

Mentor: izr. prof. dr. Aleš Ručigaj
NAČRTOVANJE IN MATEMATIČNO MODELIRANJE
PH ODZIVNIH BIOPOLIMERNIH HIDROGELOV ZA
CILJNO DOSTAVO UČINKOVIN S KONTROLIRANIM
SPROŠČANJEM
Datum zagovora: 4. 10. 2022

BIOKEMIJA

Daša PAVC

Mentor: znan. sod. dr. Primož Šket
VPLIV TERMINALNIH KONCEV IN NARAVE KATIONOV
NA TVORBO G-KVADRUPLEKSOV
Datum zagovora: 14. 6. 2022

Tjaša GORIČAN

Mentor: izr. prof. dr. Marko Novinec
RACIONALNO NAČRTOVANJE OPTIMIZIRANIH
ALOSTERIČNIH EFEKTORJEV ČLOVEŠKIH KATEPSINOV
K IN S
Datum zagovora: 1. 7. 2022

MAGISTRSKI ŠTUDIJI**MAGISTRSKI ŠTUDIJSKI PROGRAM 2. STOPNJE – KEMIJA****Rebeka KAMIN**

Mentor: doc. dr. Krištof Kranjc
SELEKTIVNOST DIELS–ALDERJEVE REAKCIJE NA
PRIMERU SUBSTITUIRANIH 2H-PIRAN-2-ONOV:
MIKROVALOVNI ALI KLASIČNI POGOJI KOT NAČIN ZA
POSPEŠITEV AROMATIZACIJE ALI CIKLOADICIJE
Datum zagovora: 25. 1. 2022

Denis MATOH

Mentor: prof. dr. Matevž Pompe
RAZVOJ IN VALIDACIJA HPLC METOD ZA DOLOČANJE
VSEBNOSTI IN SORODNIH SUBSTANC NIKOTINAMID
MONONUKLEOTIDA V AKTIVNI UČINKOVINI
Datum zagovora: 26. 1. 2022

Primož BANFI

Mentor: doc. dr. Črtomir Podlipnik
RAZVOJ IN UPORABA KNJIŽNICE SPOJIN
Datum zagovora: 2. 2. 2022

Špela MAROLT

Mentorica: doc. dr. Nataša Gros
USTVARJANJE KONCENTRACIJSKEGA GRADIENTA V
PRETOČNEM SISTEMU IN ANALIZNA UPORABA
Datum zagovora: 10. 2. 2022

Domen OBREZ

Mentor: prof. dr. Mitja Kolar
Somentor: znan. svet. dr. Samo Hočevnar
ŠTUDIJE IN UPORABA BAKROVIH ELEKTROD V
SODOBNI ELEKTROANALIZI
Datum zagovora: 15. 2. 2022

Aleš MARSEL

Mentor: prof. dr. Miran Gaberšček
ELEKTROKEMIJSKA KARAKTERIZACIJA
KATALIZATORJEV PRI POVEČANEM MASNEM
TRANSPORTU
Datum zagovora: 28. 2. 2022

Nika ŽNIDARŠIČ

Mentor: doc. dr. Martin Gazvoda
POSPEŠEVANJE SONOGASHIROVE REAKCIJE
BREZ BAKRA S POMOČJO ORGANOKOVINSKIH
KATALIZATORJEV
Datum zagovora: 9. 3. 2022

Maja ŠUBIC

Mentor: prof. dr. Matija Strlič
MIGRACIJA IN IZGUBA MEHČAL V POLIVINIL KLORIDU
Datum zagovora: 16. 5. 2022

Petra LAPAJNE

Mentorica: prof. dr. Barbara Hribar Lee
VPLIV POLIELEKTROLITA NA SREDNJI AKTIVNOSTNI
KOEFCIENT NABR V VODNI RAZTOPINI
Datum zagovora: 26. 5. 2022

Tamara ILIOSKA

Mentor: prof. dr. Jernej Iskra
Somentorica: doc. dr. Jasna Dolenc Koce
SINTEZA 1,2,4,5-TETRAOKSANOV IN NJIHOVA
HERBICIDNA UČINKOVITOST
Datum zagovora: 15. 6. 2022

Mina NIKOLIČ

Mentor: izr. prof. dr. Drago Kočar
Somentor: dr. Martin Šala
RAZVOJ LC-MS METODE ZA DOLOČITEV ASKORBINSKE
IN ERITORBINSKE KISLINE
Datum zagovora: 15. 6. 2022

Sergeja LEBAR

Mentor: prof. dr. Matevž Pompe
KARAKTERIZACIJA PROTAMIN SULFATA V FORMULACIJI
Datum zagovora: 1. 7. 2022

Martina ANDREJAŠIČ

Mentor: izr. prof. dr. Janez Cerkovnik
ŠTUDIJ STABILNOSTI RAZLIČNIH FORMULACIJ
VODIKOVEGA PEROKSIDA
Datum zagovora: 5. 7. 2022

Klemen KOZLOVIČ

Mentor: doc. dr. Krištof Kranjc
SINTEZE NOVIH 5,6-DISUBSTITUIRANIH
3-BENZOILAMINO-2H-PIRAN-2-ONOV TER NADALJNJE
CIKLOADICIJE DO IZOBENZOFURANSKIH ALI
BICIKLO[2.2.2]OKTENSKIH DERIVATOV
Datum zagovora: 6. 7. 2022

Ida BRCAR

Mentor: prof. dr. Janez Košmrlj
UPORABA SONOGASHIROVE REAKCIJE BREZ BAKRA V
SINTEZI ZDRAVILNIH UČINKOVIN
Datum zagovora: 6. 7. 2022

Uroš VEZONIK

Mentor: prof. dr. Janez Košmrlj
SINTEZA NOVIH FLUORESCENTNIH MOLEKUL NA
OSNOVI NAFTALENA
Datum zagovora: 6. 7. 2022

Mihaela REBERNIK

Mentor: doc. dr. Jakob Kljun
SINTEZA IN KARAKTERIZACIJA RUTENIJEVIH
KOORDINACIJSKIH SPOJIN Z IZBRANIMI
ŠKORPIONATNIMI LIGANDI
Datum zagovora: 7. 7. 2022

David SIMONIČ

Mentor: znan. sod. dr. Aljaž Iveković
Somentor: prof. dr. Anton Meden
IZBOLJŠANJE OKSIDACIJSKE ODPORNOSTI
VOLFRAMOVEGA KOMPOZITA S KARBIDNIMI
VKLUČKI Z DODATKOM KROMA IN ITRIJA
Datum zagovora: 7. 7. 2022

Izabela STOJANOSKA

Mentor: izr. prof. dr. Drago Kočar
DOLOČANJE BIORAZPOLOŽLJIVEGA ŽELEZA V
PREHRANSKIH DOPOLNILIH
Datum zagovora: 8. 7. 2022

Katja VODLAN

Mentorica: izr. prof. dr. Amalija Golobič
Somentorica: prof. dr. Nataša Zabukovec Logar
NAPREDNI PRISTOPI SINTEZE ZEOLITOM PODOBNIH
IMIDAZOLATOV TER NJIHOVA KARAKTERIZACIJA
Datum zagovora: 26. 8. 2022

Neža DROFENIK

Mentor: doc. dr. Krištof Kranjc
DIELS-ALDERJEVE CIKLOADICIJE CIKLIČNIH
ALKENSKIH DIENOFILOV NA SUBSTITUIRANE 2H-PIRAN-
2-ONE V OKOLJU IN ČLOVEKU PRIJAZNEJŠIH TOPILIH
Datum zagovora: 31. 8. 2022

Jan HOČEVAR

Mentor: prof. dr. Jernej Iskra
SINTEZA IN KARAKTERIZACIJA HIDROGELOV,
SINTEZIRANIH IZ CELULOZE
Datum zagovora: 31. 8. 2022

Aleksandra ZAMLJEN

Mentor: prof. dr. Anton Meden
Somentor: izr. prof. dr. Blaž Likozar
DOLOČEVANJE KINETIKE ADSORPCIJE IN DESORPCIJE
VODIKA NA PLATINSKEM KATALIZATORJU
Datum zagovora: 1. 9. 2022

Luka JEDLOVČNIK

Mentor: prof. dr. Janez Košmrlj
POSKUS SINTEZE 5-DEVTEROPIRIMIDIN-4-
KARBOKSILNE KISLINE
Datum zagovora: 2. 9. 2022

Maksimiljan DEKLEVA

Mentorica: prof. dr. Helena Prosen
Somentorica: viš. znan. sod. dr. Danjela Kuščer Hrovatin
OPTIMIZACIJA MATERIALOV IN PREIZKUŠANJE
DELOVNE ELEKTRODE ELEKTROKEMIJSKEGA
SENZORSKEGA SISTEMA ZA DOLOČANJE
NEONIKOTINOIDOV
Datum zagovora: 8. 9. 2022

Ines KULAŠIČ

Mentor: prof. dr. Janez Košmrlj
SINTEZA BIFENILNIH DERIVATOV Z ZANIMIVIMI
SOLVATOKROMNIMI LASTNOSTMI
Datum zagovora: 9. 9. 2022

Guerrero MEJÍA, Luis MIGUEL

Mentor: prof. dr. Marjan Marinšek
DEVELOPMENT OF POLYMER ELECTROLYTES FOR
SOLID STATE BATTERIES
Datum zagovora: 14. 9. 2022

Marko GABROVŠEK

Mentor: prof. dr. Janez Košmrlj
SINTEZA CINOLINSKIH DERIVATOV IZ
O-VINILANILINOV
Datum zagovora: 15. 9. 2022

Jan JELEN

Mentor: prof. dr. Jernej Iskra
Somentor: viš. znan. sod. dr. Gašper Tavčar
PRAKTIČEN PRISTOP K DEOKSIFLUORIRANJU
ELEKTRON-DEFICITNIH FENOLOV
Datum zagovora: 19. 9. 2022

Peter ROBIČ

Mentor: doc. dr. Andrej Pevec
KOORDINACIJSKE SPOJINE Z 1-(PIRIDIN-2-IL)
TIOSEČNINO KOT LIGANDOM
Datum zagovora: 21. 9. 2022

Agata LIPOVŠEK

Mentor: doc. dr. Krištof Kranjc
UPORABA RAZLIČNIH MONOKARBONILNIH SPOJIN Z
AKTIVIRANO METILNO SKUPINO ZA SINTEZO NOVIH
3-BENZOILAMINO-2H-PIRAN-2-ONOV
Datum zagovora: 28. 9. 2022

Eva JNCIGAJ

Mentor: izr. prof. dr. Drago Kočar
ŠTUDIJ VEZAVE IZBRANIH KOVINSKIH IONOV Z
VINSKO KISLINO
Datum zagovora: 28. 9. 2022

Kristjan MEŽA

Mentor: prof. dr. Matevž Pompe
DOLOČEVANJE L- IN D-AMINOKISLINSKE SESTAVE V
BIOLOŠKIH VZORCIH
Datum zagovora: 28. 9. 2022

Pia KRŽAN

Mentor: prof. dr. Matevž Pompe
RAZVOJ METODE ZA DOLOČEVANJE UROLITINA A V
REALNIH VZORCIH
Datum zagovora: 28. 9. 2022

Tibor MLAKAR

Mentorica: prof. dr. Barbara Hribar Lee
SENČENJE MEDIONSКИH INTERAKCIJ V NABITEM
ADSORBENTU – UPORABA REPLIKA ORNSTEIN-
ZERNIKOVИH ENAČB
Datum zagovora: 29. 9. 2022

Rabail Badar ABBASI

Mentor: prof. dr. Robert Dominko
Somentor: znan. sod. dr. Primož Jovanovič
CORE/SHELL STRUCTURES FOR LI-ION CAPACITORS
Datum zagovora: 29. 9. 2022

Katerina RADEVSKA

Mentor: prof. dr. Jurij Reščič
MERITVE ZETA POTENCIALA NEKATERIH PROTEINOV
PRI RAZLIČNIH PH-VREDNOSTIH TER V PRISOTNOSTI
POLIETILENGLIKOLA
Datum zagovora: 30. 9. 2022

Zala DREŠAR

Mentor: prof. dr. Franc Perdih
PRISOTNOST HALOGENSKIH VEZI V KOKRISTALIH IN
SOLEH DIATRIZOIČNE KISLINE
Datum zagovora: 12. 10. 2022

Jure JAKOŠ

Mentor: doc. dr. Martin Gazvoda
SINTEZA CEFALANDOLA C IN RAZVOJ
AVTOMATIZIRANE METODE ZA DOLOČEVANJE
STRUKTUR ORGANSKIH MOLEKUL NA PODLAGI
EKSPERIMENTALNIH SPEKTROSKOPSKIH PODATKOV
Datum zagovora: 14. 10. 2022

Luka JAMŠEK

Mentor: doc. dr. Krištof Kranjc
PRETVORBE DIANHIDRIDOV BIKIKLO[2.2.2]OKTENSKIH
SISTEMOV V N-SUBSTITUIRANE DERIVATE S POMOČJO
NUKLEOFILNIH SUBSTITUCIJ SUKCIANHIDRIDNIH
FRAGMENTOV
Datum zagovora: 26. 10. 2022

Maša LOGAR

Mentor: prof. dr. Matevž Pompe
Somentorica: doc. dr. Tina Trdan Lušin
RAZVOJ IN OPTIMIZACIJA ANALITSKE METODE
ZA DOLOČITEV NITRITOV V POMOŽNIH SNOVEH
ZA NAMEN OCENE TVEGANJA ZA TVORBO
NITROZAMINOV
Datum zagovora: 28. 10. 2022

May KORDEŽ

Mentorica: prof. dr. Helena Prosen
RAZVOJ ANALIZNE METODE ZA DOLOČANJE
FITOESTROGENIH SPOJIN V PIVU IN HMELJU
Datum zagovora: 28. 10. 2022

Lara BARTOL

Mentor: doc. dr. Martin Gazvoda
PRIPRAVA IN MODIFIKACIJE IZBRANIH PEPTIDOV
IN MANJŠIH PROTEINOV NA TRDNEM NOSILCU Z
UPORABO FMOC STRATEGIJE
Datum zagovora: 17. 11. 2022

Lara ŽIBERNA

Mentor: prof. dr. Alain Chaumont

Somentor: doc. dr. Črtomir Podlipnik
NAPROTI RAZVOJU PRILAGODLJIVIH TOPIL:
RAZISKAVA SOLVATACIJSKIH LASTNOSTI TOPIL NA
OSNOVI MENTOLA, TIMOLA IN KAFRE Z POMOČJO
SIMULACIJ MOLEKULSKE DINAMIKE
Datum zagovora: 14. 11. 2022

Tjaša KOŽELJ

Mentor: izr. prof. dr. Uroš Grošelj
SINTEZA DERIVATOV (+)-IZOKAMFOLENSKE KISLINE
KOT POTENCIALNIH DIŠAV
Datum zagovora: 24. 11. 2022

Sara KONČEK

Mentor: prof. dr. Marjan Jereb
FUNKCIONALIZACIJA TILOV S HALOGENIRANIMI
SPOJINAMI
Datum zagovora: 28. 11. 2022

Martin Rafael GULIN

Mentor: prof. dr. Emmanuel Fromager
Somentor: doc. dr. Črtomir Podlipnik
TEORIJA VLOŽITVE FUNKCIONALA LOKALNEGA
POTENCIALA: KVANTNI KEMIJI NAPROTI
Datum zagovora: 28. 11. 2022

Ariana ŠUŠTARIČ

Mentorica: znan. svet. dr. Ester Heath
Somentorica: prof. dr. Helena Prosen
DOLOČANJE OSTANKOV DOVOLJENIH IN
NEDOVOLJENIH DROG V POVRŠINSKIH IN PODZEMNIH
VODAH TER NJIHOV VPLIV NA ZELENE ALGE
CHLAMYDOMONAS REINHARDTII
Datum zagovora: 30. 11. 2022

Patrik HORŽEN

Mentor: izr. prof. dr. Barbara Modec
KOORDINACIJSKA KEMIJA [MOVOC₄(H₂O)]- S
PIKOLINATOM ALI PIRAZINKARBOKSILATOM

MAGISTRSKI ŠTUDIJSKI PROGRAM 2. STOPNJE – KEMIJSKO INŽENIRSTVO**Anja ERZIN**

Mentor: prof. dr. Igor Plazl
Somentor: viš. znan. sod. dr. Aleš Lapanje
IZBOR IN KARAKTERIZACIJA BAKTERIJ ZA UPORABO
V BIOLOŠKEM ČIŠČENJU TEHNOLOŠKIH VOD TOVARN
BREZLESNEGA PAPIRJA
Datum zagovora: 21. 1. 2022

Monika NEDVEŠ

Mentor: prof. dr. Aleš Podgornik
KARAKTERIZACIJA RAZMNOŽEVANJA BAKTERIOFAGOV
V KONTINUIRNEM MEŠALNEM SISTEMU
Datum zagovora: 28. 1. 2022

Luicija BELINGAR

Mentorica: prof. dr. Andreja Žgajnar Gotvajn
KARAKTERIZACIJA BIOGLJA IZ LIGNOCELULOZNE
BIOMASE
Datum zagovora: 31. 1. 2022

Janja ŠUSTER

Mentor: prof. dr. Robert Dominko
VPLIV UPORABE RAZLIČNIH MG ELEKTROLITOV NA
DELOVANJE MG KOVINSKE ANODE
Datum zagovora: 3. 2. 2022

Enej VRHUNEC

Mentor: prof. dr. Aleš Podgornik
PRIPRAVA MIKROKAPSUL Z RAZLIČNIMI POVRŠINSKIMI
NABOJI
Datum zagovora: 17. 2. 2022

Erik HARTMAN

Mentorica: prof. dr. Polona Žnidaršič Plazl
OPIS PRENOSA KISIKA V MIKROREKTORJU Z
MEMBRANO
Datum zagovora: 17. 2. 2022

Urban SAJEVC

Mentor: izr. prof. dr. Boštjan Genorio
Somentor: prof. dr. Violeta Bokan Bosiljkov
UPORABA BOROGENA V SPEKTRALNO SELEKTIVNIH
PREMAZIH
Datum zagovora: 2. 3. 2022

Žan LAVRIČ

Mentorica: prof. dr. Polona Žnidaršič Plazl
PRIPRAVA IN UPORABA ZAMREŽENIH ENCIMSKIH
AGREGATOV V MIKROPRETOČNIH SISTEMIH
Datum zagovora: 17. 3. 2022

Andrej GREBENC

Mentor: prof. dr. Igor Plazl
Somentor: prof. dr. Tomaž Urbič
MODELIRANJE ENCIMSKO KATALIZIRANE
BIOTRANSFORMACIJE Z IMOBILIZIRANIMI ENCIMI NA
MAGNETNIH NANO DELCIH V MIKROREAKTORSKEM
SISTEMU
Datum zagovora: 23. 3. 2022

Tanja SEME

Mentorica: prof. dr. Andreja Žgajnar Gotvajn
Somentor: prof. dr. Matevž Dular
VPLIV KAVITACIJE V KOMBINACIJI Z OZONACIJO
NA MOŽNOST BIOLOŠKEGA ODSTRANJEVANJA
ANTIBIOTIKOV IZ ODPADNIH VOD
Datum zagovora: 30. 3. 2022

Sofija NIKOLIČ

Mentor: doc. dr. Matjaž Spreitzer
Somentor: prof. dr. Marjan Marinšek
OBDELAVA PIEZOELEKTRIČNIH POLIMEROV IN
KOMPOZITOV NA OSNOVI POLI(L-MLEČNE KISLINE)
(PLLA) ZA BIOMEDICINSKO UPORABO
Datum zagovora: 11. 4. 2022

Teja URBANC

Mentorica: prof. dr. Andreja Žgajnar Gotvajn
PRIMERJAVA KATALITSKE IN NEKATALITSKE
OZONACIJE ZA ODSTRANJEVANJE ANTIBIOTIKOV IZ
ODPADNIH VODA
Datum zagovora: 20. 4. 2022

Benjamin BOŽIČ

Mentor: prof. dr. Aleš Podgornik
PRIPRAVA IN KARAKTERIZACIJA POLIHIPE NOSILCEV S
KRISTALI SREBRA
Datum zagovora: 13. 5. 2022

Žiga SKOČIR

Mentor: izr. prof. dr. Boštjan Genorio
SINTEZA IN KARAKTERIZACIJA Z DUŠIKOM
DOPIRANEGA TERMIČNO OBDELANEGA GRAFEN
OKSIDA
Datum zagovora: 13. 5. 2022

Urban KOŠIR

Mentor: prof. dr. Robert Dominko
ŠTUDIJA ELEKTROKEMIJSKEGA MEHANIZMA V
ALUMINIJ-ORGANSKEM AKUMULATORJU
Datum zagovora: 14. 6. 2022

Ana ČERNE

Mentor: prof. dr. Igor Plazl
Somentor: izr. prof. dr. Blaž Likozar
KINETIKA KATALITSKE HIDRODEOKSIGENACIJE
MODELNIH GRADNIKOV LIGNINA
Datum zagovora: 1. 7. 2022

Gašper KRAJEC

Mentorica: prof. dr. Urška Šebenik
VPLIV DODATKA PLASTOVITIH NANODELCEV
NA REOLOŠKE LASTNOSTI HIDROGELA IZ
SKLEROGLUKANA
Datum zagovora: 1. 7. 2022

Patrik LIKAR

Mentorica: prof. dr. Urška Šebenik
ZAMREŽENJE TEMPO-MODIFICIRANE NANOCELULOZE
S CIRKONIJEVIMI IONI
Datum zagovora: 6. 7. 2022

Katja LUKANČIČ

Mentorica: izr. prof. dr. Gabriela Kalčikova
ADSORPCIJA MIKROPLASTIKE NA VODNE RASTLINE
Datum zagovora: 24. 8. 2022

Matej KRNC

Mentor: prof. dr. Aleš Podgornik
DOLOČANJE VELIKOSTI KAPLJIC TROKANALNE ŠOBE Z
LASERSKO DIFRAKCIJO
Datum zagovora: 24. 8. 2022

Mojca SIMONČIČ

Mentorica: izr. prof. dr. Gabriela Kalčikova
ADSORPCIJA KOVIN IZ ODPADNIH VOD NA
MIKROPLASTIKO
Datum zagovora: 24. 8. 2022

Ožbej VODEB

Mentor: prof. dr. Miran Gaberšček
OSNOVE VOLTAMETRIJE Z IZMENIČNO NAPETOSTJO ZA
UPORABO V ELEKTROKATALIZI
Datum zagovora: 2. 9. 2022

Žan BOČEK

Mentor: izr. prof. dr. Aleš Ručigaj
ALGINATNI HIDROGELI S KOLAGENOM IN CELICAMI
ZELENE ALGE CHLAMYDOMONAS REINHARDTII ZA
POSPEŠENO CELJENJE RAN
Datum zagovora: 5. 9. 2022

Klara OGOREVC

Mentor: prof. dr. Marjan Marinšek
UPORABA TEKOČINSKE EKSTRAKCIJE ZA
PRIDOBIVANJE SKANDIJA IZ RDEČEGA BLATA
Datum zagovora: 6. 9. 2022

Maja CAF

Mentor: prof. dr. Aleš Podgornik
ULTRA VISOKOTLAČNA IONSKO IZMENJEVALNA
KROMATOGRAFIJA PROTEINOV
Datum zagovora: 6. 9. 2022

Mitja KOSTELEČ

Mentor: prof. dr. Miran Gaberšček
OPTIMIZACIJA PROIZVODNJE
ELEKTROKATALIZATORJEV NA OSNOVI PLATINSKIH
ZLITIN IN PRENOS NA REAKTORSKE SISTEME
Datum zagovora: 6. 9. 2022

Jan GALE

Mentor: prof. dr. Miran Gaberšček
MODELIRANJE IMPEDANČNEGA ODZIVA POROZNIH
ELEKTROD
Datum zagovora: 7. 9. 2022

Ana MARKOVIČ

Mentorica: prof. dr. Urška Šebenik
PRIPRAVA SFERIČNIH HIDROGELNIH DELCEV NA
OSNOVI POLISAHARIDOV
Datum zagovora: 9. 9. 2022

Stefan SERAFIMOSKI

Mentorica: prof. dr. Urška Šebenik
REOLOŠKE LASTNOSTI VODNIH SUSPENZIJ
NANOFIBRILIRANE CELULOZE
Datum zagovora: 12. 9. 2022

Katja DROBEŽ

Mentorica: doc. dr. Tina Skalar
MEHANIZMI, REAKCIJE IN KINETIKA KATALITSKEGA
RAZKLOPA BORANOV DO VODIKA
Datum zagovora: 14. 9. 2022

Žiga LIPOVŠEK

Mentor: prof. dr. Aleš Podgornik
VPLIV HITROSTI SEGREVANJA RAZTOPINE NA
KRISTALIZACIJO TIO₂
Datum zagovora: 15. 9. 2022

Marjeta SPASOVIČ

Mentorica:izr. prof. dr. Gabriela Kalčikova
STARANJE MIKROPLASTIKE V POVRŠINSKIH VODAH IN
SPREMEMBE NJENIH LASTNOSTI
Datum zagovora: 16. 9. 2022

Katja POMBERG

Mentor: prof. dr. Matevž Dular
OCENA RAZGRADNJE ODPADNEGA BLATA S
KAVITACIJO
Datum zagovora: 29. 9. 2022

Samo SOTLART

Mentorica: prof. dr. Polona Žnidaršič Plazl
RAZVOJ MIKROPRETOČNE NAPRAVE Z
IMOBILIZIRANIMI SPORAMI BACILLUS SUBTILIS NA
OSNOVI MAGNETNEGA POLJA
Datum zagovora: 14. 10. 2022

Nima SHADANI

Mentorica: prof. dr. Andreja Žgajnar Gotvajn
ODSTRANJEVANJE ANTIBIOTIKA AMOKSICILINA IZ
ODPADNE VODE IN ODPADNEGA BLATA Z OZONACIJO
Datum zagovora: 14. 10. 2022

Petra JAGODIČ

Mentor: prof. dr. Aleš Podgornik
DOLOČANJE DEBELINE ADSORBIRANEGA SLOJA NA
POLYHIPE NOSILCIH Z MERJENJEM PADCA TLAKA
Datum zagovora: 14. 10. 2022

Živa NOVAK

Mentor: prof. dr. Miran Gaberšček
Somentorica: znan. svet. dr. Tadeja Kosec
KARAKTERIZACIJA IN ZAŠČITA PATINIRANIH BRONOV
V ATMOSFERSKIH POGOJIH
Datum zagovora: 14. 10. 2022

Ana SIMČIČ ZULJAN

Mentorica: doc. dr. Tina Skalar
SINTEZA IN KARAKTERIZACIJA MEŠANIH ORGANO-
KOVINSKIH PEROVSKITNIH MATERIALOV
Datum zagovora: 18. 10. 2022

VITO PRŠA

Mentorica: doc. dr. Lidija Slemenik Perše
REOLOŠKE IN TERMIČNE LASTNOSTI RAZLIČNIH VRST
MASLA IZ OREŠČKOV
Datum zagovora: 25. 10. 2022

Žan SPOLENAK

Mentor: prof. dr. Marjan Marinšek
OPTIMIZACIJA MLETJA EMAJLIRSKE FRITE V
BOBNASTEM KROGLIČNEM MLINU
Datum zagovora: 28. 10. 2022

Katarina VUKOSAV

Mentor: prof. dr. Robert Dominko
Somentor: prof. dr. Marjan Marinšek
SOL-GEL PREVLEKE NA LINIO₂ KATODNEM MATERIALU

MAGISTRSKI ŠTUDIJSKI PROGRAM 2. STOPNJE – BIOKEMIJA**Tanja PERIC**

Mentorica: doc. dr. Marina Klemenčič
DOLOČANJE FUNKCIJE PROTEAZE CRMC1 IZ
ORGANIZMA CHLAMYDOMONAS REINHARDTII
Datum zagovora: 4. 1. 2022

Vid MODIC

Mentor: znan. svet. dr. Anže Županič
UPORABA KAVZALNIH OMREŽIJ PRI NAČRTOVANJU
POTI Z NEUGODNIM IZIDOM
Datum zagovora: 4. 1. 2022

Nives RAŽNJEVIČ

Mentor: izr. prof. dr. Marko Novinec
PROTIMIKROBNO DELOVANJE NEKATERIH ORGANSKIH
SPOJIN IZ KNJIŽNICE SPOJIN FKKT
Datum zagovora: 17. 1. 2022

Tina ŠILC

Mentorica: izr. prof. dr. Alja Videtič Paska
OPTIMIZACIJA IZOLACIJE ZUNAJCELIČNIH VEZIKLOV
IZ PLAZME IN CEREBROSPINALNE TEKOČINE
Datum zagovora: 21. 1. 2022

Peter ŠKRINJAR

Mentorica: prof. dr. Brigita Lenarčič
OPTIMIZACIJA BIOSINTEZE BETA KAROTENA V
BAKTERIJSKIH CELICAH Z UPORABO ROBOTA ZA
RAVNANJE S TEKOČINAMI
Datum zagovora: 28. 1. 2022

Aleksandta UZAR

Mentor: prof. dr. Gregor Anderlüh
Somentor: doc. dr. Miha Pavšič
PRIPRAVA IN BIOKEMIJSKA KARAKTERIZACIJA
REKOMBINANTNIH EGEROLIZINOV S PODALJŠANIM
N-KONCEM
Datum zagovora: 9. 2. 2022

Samo PURIČ

Mentor: doc. dr. San Hadži
PREPOZNAVANJE PROTEINOV S POMOČJO
STRUKTURNE PRILAGODLJIVOSTI: PRIMERJAVA
VEZANJA INTRINZIČNO NESTRUKTURIRANIH
PROTEINOV IN KAMELOIDNIH PROTITELES
Datum zagovora: 9. 2. 2022

Uroš PREŠERN

Mentor: doc. dr. Aljaž Gaber
PRIPRAVA IN ANALIZA REKOMBINANTEGA
SIGNALNEGA KOMPLEKSA ZNOTRAJCELIČNE DOMENE
EPCAM S PROTEINI FHL2, B-KATENINOM IN LEF-1
Datum zagovora: 20. 4. 2022

Ines MEDVED

Mentorica: dr. Mateja Manček Keber
Somentorica: doc. dr. Vera Župunski
INHIBICIJA SIGNALIZIRANJA MYD88 S KRATKIMA
RAZLIČICAMA MYD88SWT IN MYD88SL265P
Datum zagovora: 21. 4. 2022

Primož BEMBIČ

Mentor: izr. prof. dr. Marko Novinec
Somentor: prof. dr. Iztok Turel
ŠTUDIJA VPLIVA IZBRANIH IONOV TEŽKIH KOVIN NA
AKTIVNOST KATEPSINOV B, L IN S
Datum zagovora: 6. 6. 2022

Ana HALUŽAN VASLE

Mentor: prof. dr. Marko Dolinar
DELOVANJE ORTOKASPAZE MAOC1 NA PAR TOKSIN-
ANTITOKSIN IPF_1067-IPF_1065 CIANOBAKTERIJE
MICROCYSTIS AERUGINOSA PCC 7806
Datum zagovora: 17. 6. 2022

Luka LAVRIČ

Mentor: prof. dr. Aljoša Bavac
IZOLACIJA IN KARAKTERIZACIJA REKOMBINANTNEGA
ENCIMA PARAOKSONAZE 1
Datum zagovora: 22. 6. 2022

Aljoša MARINKO

Mentor: prof. dr. Igor Križaj
Somentor: doc. dr. Gregor Gunčar
PRIPRAVA PROTEINA CRISP IZ MODRASOVEGA STRUPA
V BAKTERIJSKEM EKSPRESIJSKEM SISTEMU
Datum zagovora: 8. 7. 2022

Barbara SLAPNIK

Mentorica: doc. dr. Maruša Debeljak
Somentorica: doc. dr. Vera Župunski
SEKVENCIANJE MITOHONDRIJSKEGA GENOMA
Z UPORABO CRISPR/CAS9 IN TEHNOLOGIJE
SEKVENCIANJA DNA Z NANOPORO
Datum zagovora: 18. 8. 2022

Jernej IMPERL

Mentor: prof. dr. Marko Dolinar
SISTEMI VAPBC CIANOBAKTERIJE MICROCYSTIS
AERUGINOSA PCC 7806
Datum zagovora: 24. 8. 2022

Nuša KELHAR

Mentorica: izr. prof. dr. Katarina Černe
Somentor: izr. prof. dr. Borut Kobal
POMEN DOLOČANJA EKSTRACELULARNIH VEZIKLOV
PRI SEROZNEM TIPU RAKA JAJČNIKOV
Datum zagovora: 26. 8. 2022

Lana VOGRINEC

Mentorica: doc. dr. Marina Klemenčič
POVEZAVE MED STRUKTURO IN FUNKCIJO
METAKASPAZ CRMCA-I IN CRMCA-II IZ ALGE
CHLAMYDOMONAS REINHARDTII
Datum zagovora: 26. 8. 2022

Žiga VIČIČ

Mentorica: prof. dr. Damjana Rozman
PRIMERJAVA TEHNOLOGIJE DNA-MIKROMREŽ IN
SEKVENCIANJA CDNA Z NANOPORAMI PRI ANALIZI
TRANSKRIPTOMA CELIČNE LINIJE HEPG2 DIVJEGA TIPA
IN Z IZBITIM GENOM SC5D
Datum zagovora: 31. 8. 2022

Sara KOROŠEC

Mentorica: izr. prof. dr. Marjetka Podobnik
Somentor: doc. dr. Miha Pavšič
PRIPRAVA TER KARAKTERIZACIJA METALOPROTEAZE
MPL IZ PATOGENE BAKTERIJE LISTERA
MONOCYTOGENES
Datum zagovora: 7. 9. 2022

Ernestina LAVRIH

Mentor: prof. ddr. Boris Turk
PRIMERJAVA LASTNOSTI RAZLIČNIH VRST LUCIFERAZ
IZ KRESNIČK V CELIČNIH, IN VITRO IN IN VIVO
ŠTUDIJA
Datum zagovora: 8. 9. 2022

Martina LOKAR

Mentor: doc. dr. Gregor Gunčar
IZRAŽANJE IN KARAKTERIZACIJA SINTETIČNE
SAMOSESTAVLJAJOČE SE PROTEINSKE KLETKE,
ZGRAJENE IZ SVEŽNJEV A-VIJAČNIC IN
B-PROPELERSKEGA ZVITJA
Datum zagovora: 9. 9. 2022

Martin ŠPENDL

Mentor: doc. dr. Gregor Gunčar
NOV NACIN OPTIMIZACIJE RABE KODONOV Z
UPORABO STROJNEGA UCENJA NA OSNOVI STRUKTUR
PROTEINOV
Datum zagovora: 9. 9. 2022

Tjaša MLAKAR

Mentor: doc. dr. Jernej Murn (Univ. California, Riverside)
Somentorica: doc. dr. Tadeja Režen
RAZVOJ NOVE METODE ZA SLEDENJE KROŽNIH RNK V
ŽIVIH CELICAH
Datum zagovora: 12. 9. 2022

Urša ŠTRANCAR

Mentor: izr. prof. dr. Uroš Kovačič
DOLOČANJE RAVNI MRNA BIOLOŠKIH OZNAČEVALCEV
HOLINERGIČNEGA PROTIVNETNEGA SISTEMA V
LEVKOCITIH PERIFERNE KRVI PRI ČLOVEKU
Datum zagovora: 12. 9. 2022

Katja DOBERŠEK

Mentor: prof. dr. Uroš Petrovič
UPORABA METODE CRISPR-CAS9 ZA ZAMENJAVO
POSAMIČNEGA NUKLEOTIDA IN NJEN VPLIV NA
GENOM KVASOVKE SACCHAROMYCES CEREVISIAE
Datum zagovora: 20. 9. 2022

Tadej MEDVED

Mentorica: doc. dr. Marina Klemenčič
KARAKTERIZACIJA IZBRANIH BICIKLIČNIH
PIRAZOLIDINONOV IN HIDROKSIPIRAZOLOV KOT
INHIBITORJEV DIHIDROOROTAT DEHIDROGENAZE IZ
ORGANIZMA PLASMIDIUM FALCIPARUM
Datum zagovora: 20. 9. 2022

Maruša MIŠMAŠ ZRIMŠEK

Mentorica: izr. prof. dr. Daša Zupančič
SIGNALNA POT RETINOJSKE KISLINE PRI RAKU
SEČNEGA MEHURJA
Datum zagovora: 22. 9. 2022

Jelena ŠTRBAC

Mentor: prof. dr. Janez Plavec
NMR STUDY OF RNA G-QUADRUPLEX REGULATORY
MOTIF INVOLVED IN INFLAMMATION PROCESSES
Datum zagovora: 23. 9. 2022

Emma KUREŠEPI

Mentorica: prof. dr. Kristina Sepčič
VREDNOTENJE POTENCIALA ORGANSKIH
EKSTRAKTOV LESNIH IN MIKORIZNIH GOB KOT
ZAVIRALCEV ENCIMOV IZ SKUPINE HOLINESTERAZ IN
GLUTATION S-TRANSFERAZ
Datum zagovora: 26. 9. 2022

Ana MAKLIN

Mentorica: doc. dr. Vera Župunski
VPLIV SIGMARI NA AGREGACIJO TDP-43 PRI
NEURODEGENERATIVNIH BOLEZNIH
Datum zagovora: 27. 9. 2022

Milica JANKOVIČ

Mentor: izr. prof. dr. Marko Novinec
VPLIV KAVNE KISLINE IN ŽELEZOVII(III) IONOV TER
NJUNIH KOMPLEKSOV NA AKTIVNOST KATEPSINA B
Datum zagovora: 29. 9. 2022

Andrej RACE

Mentorica: prof. dr. Kristina Gruden
UPORABNOST PROMOTORJA PTI5 ZA PRIPRAVO
SENZORSKIH SISTEMOV PRI UGOTAVLJANJU
IMUNSKEGA ODZIVA KROMPIRJA
Datum zagovora: 30. 9. 2022

Anže JENKO

Mentorica: doc. dr. Marina Klemenčič
BIOKEMIJSKA KARAKTERIZACIJA METAKASPAZE TIP A
II IZ VRSTE BOMBAŽEVCA GOSSYPIUM RAIMONDII
(GRMCA-IID)
Datum zagovora: 30. 9. 2022

Liza ULČAKAR

Mentor: izr. prof. dr. Marko Novinec
RAZVOJ PRESEJALNEGA SISTEMA ZA DETEKCIJO
HOMODIMERIZACIJE PROTEINOV V BAKTERIJI
ESCHERICHIA COLI
Datum zagovora: 6. 10. 2022

Nika ZAVERŠEK

Mentor: doc. dr. Gregor Gunčar
UPORABA HALOALKAN DEHALOGENAZE ZA
OZNAČEVANJE VARIANT MLKL V CELIČNIH LINIJAH HEK
Datum zagovora: 11. 10. 2022

Urban HRIBAR

Mentor: prof. ddr. Boris Turk
PRIPRAVA SINTETIČNIH ENODOMENSKIH PROTITELES
IN NJIHOVO OZNAČEVANJE Z ENCIMOM SORTAZA A
Datum zagovora: 1. 12. 2022

Špela SUPEJ

Mentorica: izr. prof. dr. Alja Videtič Paska
POLIMORFIZMI POSAMEZNIH NUKLEOTIDOV V GENIH
ADARB1 IN TPH2 IN SAMOMOR V SLOVENIJI
Datum zagovora: 6. 12. 2022

Veronika RAZPOTNIK

Mentorica: znan. sod. dr. Tinkara Tinta
Somentor: prof. dr. Marko Dolinar
BIOKEMIJSKI PROCESI IN MEHANIZMI MIKROBNE
RAZGRADNJE MEDUZNEGA DETRITA V MORJU
Datum zagovora: 12. 12. 2022

Andrej IVANOVSKI

Mentor: doc. dr. Miha Pavšič
KARAKTERIZACIJA VEZAVE KALCIJEVIH IONOV V
KALMODULINU PODOBNO DOMENO α -AKTININA-4 IN
PRIPRAVA KRISTALOV ZA STRUKTURNE RAZISKAVE
Datum zagovora: 12. 12. 2022

MAGISTRSKI ŠTUDIJSKI PROGRAM 2. STOPNJE – TEHNIŠKA VARNOST

Nika BERČIČ

Mentorica: doc. dr. Klementina Zupan
VARNOST IN ZDRAVJE PRI DELU V PODJETJU: PRIJAVA
IN PREISKOVANJE DELOVNIH NEZGOD
Datum zagovora: 30. 3. 2022

Matej LIPOVŠEK

Mentorica: doc. dr. Klementina Zupan
PAMETNA OMARICA ZA PRVO POMOČ IN MOBILNA
APLIKACIJA TEHELP
Datum zagovora: 32. 6. 2022

Marko KOŠUTA

Mentor: doc. dr. Mitja Robert Kožuh
Somentorica: doc. dr. Klementina Zupan
METODE ZA OCENO TVEGANJ
Datum zagovora: 20. 6. 2022

Iztok KUŠAR

Mentor:izr. prof. dr. Simon Schnabl
MATEMATIČNO MODELIRANJE POŽAROV V NARAVI
Datum zagovora: 28. 9. 2022

Klara KOŠIR

Mentor: prof. dr. Matija Tomšič
SPREMLJANJE UPORABE OSEBNE VAROVALNE OPREME
Z INFORMACIJSKO TEHNOLOGIJO S POMOČJO
MOBILNE APLIKACIJE
Datum zagovora: 28. 9. 2022

Alja LESAR

Mentorica: doc. dr. Klementina Zupan
OZAVEŠČENOST SLOVENCEV O VARNOSTI V PRIMERU
NARAVNIH NEZGOD
Datum zagovora: 5. 10. 2022

MAGISTRSKI ŠTUDIJSKI PROGRAM 2. STOPNJE – KEMIJSKO IZOBRAŽEVANJE

Tomaž ŽIGON

Mentorica: prof. dr. Vesna Ferk Savec
OVREDNOTENJE UPORABE PODDAJ PRI POUKU KEMIJE
Datum zagovora: 13. 1. 2022

Veronika KORADIN

Mentorica: doc. dr. Nataša Čelan Korošin
PREUČEVANJE OLJČNIH OLJ SLOVENSKEGA PRIMORJA
Z METODAMI TERMIČNE ANALIZE IN UPORABA OLJ V
ŠOLSKIH KEMIJSKIH POSKUSIH
Datum zagovora: 12. 12. 2022

DIPLOME - UNIVERZITETNI ŠTUDIJI**KEMIJA – 1. STOPNJA****Neža LANIŠEK**

Mentorica: prof. dr. Irena Kralj Cigić
OPTIMIZACIJA HPLC METODE ZA DOLOČANJE
ANTIOKSIDANTOV V POLIMERIH
Datum zagovora: 14. 1. 2022

Filip DŽEROSKI

Mentor: prof. dr. Marjan Jereb
SELEKTIVNE MICHAELOVE ADICIJE BREZ TOPILO
Datum zagovora: 26. 1. 2022

Veronika ŠKRJANC

Mentor: prof. dr. Matevž Pompe
PROFILIRANJE O-GLIKANOV PRI PROUČEVANJU
BIOLOŠKO PODOBNIH ZDRAVIL
Datum zagovora: 4. 2. 2022

Mihael TURKOVIC

Mentorica: prof. dr. Romana Cerc Korošec
IZBOLJŠAVA INTUMESCENTNIH PREMAZOV Z
DODATKOM PLASTOVITIH DVOJNIH HIDROKSIDOV
Datum zagovora: 11. 3. 2022

Lara REMS

Mentor: izr. prof. dr. Uroš Grošelj
SINTEZA TETRAMSKE KISLINE IZ BOC-GLY-GLY-OH IN
NJENA UPORABA V ORGANOKATALIZIRANI ADICIJI NA
DERIVATE TRANS-B-NITROSTIRENA
Datum zagovora: 7. 6. 2022

Zala STOPAR

Mentor: doc. dr. Jakob Kljun
SINTEZA KELATNIH S-METILIRANIH TIOPIRIMIDINOV
Datum zagovora: 16. 6. 2022

Chris ČERNE

Mentor: prof. dr. Urška Lavrenčič Štangar
HIDROGENIRANJE OGLJIKOVEGA DIOKSIDA V
METANOL S KATALIZATORJI NA OSNOVI ŽLAHTNIH
KOVIN
Datum zagovora: 20. 6. 2022

Gregor MEDOŠ

Mentor: prof. dr. Tomaž Urbič
RAČUNALNIŠKE SIMULACIJE ANOMALNIH TEKOČIN
Z INTERAKCIJAMI Z MEHKO SREDICO V DVEH
DIMENZIJAH
Datum zagovora: 24. 6. 2022

Maja OSOLNIK

Mentor: prof. dr. Jernej Iskra
NAČINI SINTEZE LIGNINSKIH MODELOV
Datum zagovora: 28. 6. 2022

Tadej HUMAR

Mentor: prof. dr. Jurij Svete
SINTEZA IN PRETVORBE 1-FENIL-5-HIDROKSI-1H-
PIRAZOL-4-KARBOKSILNE KISLINE
Datum zagovora: 28. 6. 2022

Priya KUMAR

Mentor: prof. dr. Jurij Svete
SINTEZA NEKATERIH ETIL 1-ARIL-5-HIDROKSI-1H-
PIRAZOL-4-KARBOKSILATOV KOT INHIBITORJEV
DIHIDROOROTAT DEHIDROGENAZE
Datum zagovora: 1. 7. 2022

Žan TOMŠIČ

Mentor: prof. dr. Bogdan Štefane
SINTEZA BENZILIDEN SUBSTITUIRANIH
PIRAZOLO[1,2-A]PIRAZOLOV
Datum zagovora: 6. 7. 2022

Mitja KODERMAN

Mentor: izr. prof. dr. Mitja Kolar
SENZORJI ZA DOLOČANJE PESTICIDOV IZ SKUPINE
NEONIKOTINOIDOV
Datum zagovora: 6. 7. 2022

Katarina ČUBEJ

Mentor: prof. dr. Matevž Pompe
DOLOČEVANJE MESTA VEZAVE O-GLIKANA NA
PROTEINU
Datum zagovora: 8. 7. 2022

Nik NIKOLIČ

Mentor: prof. dr. Matija Strlič
PRESOJA VISKOZIMETRIČNE METODE ZA DOLOČANJE
MOLSKE MASE RAZGRAJENE CELULOZE
Datum zagovora: 11. 7. 2022

Nika KAVČIČ

Mentor: prof. dr. Mitja Kolar
DOLOČANJE ELEMENTNE SESTAVE KAPNIKOV IZ
PODZEMNIH ROVOV CONE TEZNO
Datum zagovora: 22. 8. 2022

Nika KUNAVAR

Mentor: prof. dr. Marjan Jereb
SINTEZA IN NEKATERE PRETVORBE DIAZO SPOJIN
Datum zagovora: 25. 8. 2022

Jan VAN ELTEREN

Mentor: izr. prof. dr. Drago Kočar
DOLOČEVANJE HLAJNIH KOMPONENT V MEDU
Datum zagovora: 25. 8. 2022

Anita ZUPANC

Mentor: prof. dr. Bogdan Štefane
MULTIKOMPONENTNA SINTEZA INDAZOLSKIH
DERIVATOV
Datum zagovora: 29. 8. 2022

Filip KÓŠA

Mentorica: izr. prof. dr. Amalija Golobič
RENTGENSKA PRAŠKOVNA ANALIZA KERAMIKE IZ
BINARNEGA SISTEMA LA₂O₃-TA₂O₅
Datum zagovora: 29. 8. 2022

Nina MARTINC

Mentor: prof. dr. Anton Meden
RENTGENSKA PRAŠKOVNA DIFRAKCIJA LIVARSKIH
PESKOV
Datum zagovora: 29. 8. 2022

Pia PODOBNIK

Mentor: prof. dr. Franc Požgan
KATALITSKA C-H AKTIVACIJA S 3D PREHODNIMI
KOVINAMI
Datum zagovora: 30. 8. 2022

Žak Ruben ŠINKOVEC

Mentor: doc. dr. Krištof Kranjc
SINTEZA KANABINOLA (CBN) IZ KANABIDIOLA (CBD)
Datum zagovora: 30. 8. 2022

Jure KOVAČ

Mentor: prof. dr. Matija Tomšič
VPLIV RAZLIČNIH POLJ SIL NA LASTNOSTI MODELNIH
ORGANSKIH TEKOČIN
Datum zagovora: 30. 8. 2022

Katarina KOKALJ

Mentor: prof. dr. Andrej Jamnik
RAČUNALNIŠKE SIMULACIJE MODELNIH TEKOČIN
Datum zagovora: 30. 8. 2022

Manca JURAJEVČIČ

Mentor: prof. dr. Jurij Svete
SINTEZA NEKATERIH METIL 1-ARIL-3-HIDROKSI-1H-
PIRAZOL-4-KARBOKSILATOV
Datum zagovora: 30. 8. 2022

Martin ŠKRINJAR

Mentor: prof. dr. Bogdan Štefane
SINTEZA VINIL SUBSTITUIRANIH AZOMETIN IMINSKIH
DERIVATOV IN NJIHOVE FOTOKEMIČNE PRETVORBE
Datum zagovora: 30. 8. 2022

Urban BARBIČ

Mentor: doc. dr. Martin Gazvoda
POSKUS PRIPRAVE MODIFICIRANIH LANTIBIOTIKOV
NA TRDNEM NOSILCU Z UPORABO FMOC METODE
Datum zagovora: 31. 8. 2022

Metka ZALOŽNIK

Mentorica: prof. dr. Urška Lavrenčič Štangar
PRETVORBA CO₂ V METANOJSKO KISLINO
S POSREDNIM VIROM VODIKA IN ZRO₂
KATALIZATORJEM
Datum zagovora: 31. 8. 2022

Nadja SUHOREPEC

Mentor: prof. dr. Jurij Svete
SINTEZA DERIVATOV L-ARGININA IZ
N-BENZILOKSIKARBONIL-L-ORNITINA
Datum zagovora: 31. 8. 2022

Alja HODNIK

Mentorica: doc. dr. Nives Kitanovski
KARAKTERIZACIJA DVEH KOORDINACIJSKIH SPOJIN
MOLIBDENA Z ENAKO KOORDINACIJSKO ZVRSTJO
Datum zagovora: 2. 9. 2022

Anja EČIMOVIČ

Mentorica: doc. dr. Nives Kitanovski
SINTEZA IN KARAKTERIZACIJA VZORCA NASTALEGA
PRI REAKCIJI KCR(SO₄)₂ X12H₂O S KALIJEVIM
TIOCIANATOM
Datum zagovora: 2. 9. 2022

Martin PODLIPEC

Mentor: prof. dr. Marjan Jereb
PRETVORBE AROMATSKIH SPOJIN S KARBOKSILNIMI
ANHIDRIDNI
Datum zagovora: 2. 9. 2022

Jan OCEPEK

Mentor: prof. dr. Matija Strlič
OPTIMIZACIJA METODE ZA TESTIRANJE
KOROZIVNOSTI HLAJNIH ORGANSKIH SPOJIN
Datum zagovora: 2. 9. 2022

Dominik FENDRE

Mentor: doc. dr. Krištof Kranjc
DVOSTOPENJSKA SINTEZNA POT DO
POLISUBSTITUIRANIH 3-ACILAMINO-2H-PIRAN-2-
ONOV TER POIZKUSI NADALJNIH PRETVORB DO
BICIKLO[2.2.2]OKTENSKIH SISTEMOV
Datum zagovora: 2. 9. 2022

Žiga ORAŽEM

Mentor: prof. dr. Janez Košmrlj
PRETVORBE IZBRANIH DERIVATOV
2-BROMONAFTALENA
Datum zagovora: 2. 9. 2022

Matevž TURK

Mentor: prof. dr. Janez Košmrlj
OPTIMIZACIJA SONOGASHIROVE REAKCIJE MED
4-BROMOACETOFENONOM IN 4-ETINIL-N,N-
DIMETILANILINOM
Datum zagovora: 2. 9. 2022

Tomaž MAROH

Mentor: izr. prof. dr. Drago Kočar
ŠTUDIJ VPLIVA LIGANDOV NA DOLOČEVANJE PB, ZN IN
CD V SEDIMENTIH Z AAS
Datum zagovora: 5. 9. 2022

Nika TRNOVEC

Mentor: doc. dr. Bojan Šarac
KOLEKTIVNI EFEKTI V AKTIVNI NEMATSKI EMULZIJ
Datum zagovora: 5. 9. 2022

Zoja VUČIČ

Mentorica: izr. prof. dr. Barbara Modec
INFRARDEČI SPEKTRI IZBRANIH ORGANSKIH SPOJIN
Datum zagovora: 5. 9. 2022

Ana Marija KODRA

Mentor: prof. ddr. Boris Turk
VPLIV GLUT1 NA VIABILNOST TUMORSKIH CELIC 4T1
OB PRISOTNOSTI RAZLIČNIH KEMOTERAPEVTIKOV
Datum zagovora: 5. 9. 2022

Rok BREZNIKAR

Mentor: prof. dr. Tomaž Urbič
HIERARHIJA ANOMALIJ V MODELU Z MEHKO SREDICO
Datum zagovora: 5. 9. 2022

Urh BERTONCELJ

Mentor: prof. dr. Iztok Turel
POSKUSI POVEČANJA TOPNOSTI IZBRANIH
FENANTROLINSKIH LIGANDOV
Datum zagovora: 6. 9. 2022

Pia PAJK

Mentor:izr. prof. dr. Janez Cerkovnik
NOVE STABILNE FORMULACIJE 12 % VODIKOVEGA
PEROKSIDA IN SURFAKTANTOV
Datum zagovora: 6. 9. 2022

Špela ZALOŽNIK

Mentor: doc. dr. Krištof Kranjc
PRIPRAVA 5,6-DISUBSTITUIRANIH 2H-PIRAN-
2-ONOV Z AMINSKO ROČICO KOT MOŽNIH
DIENOV ZA SINTEZE BICIKLO[2.2.2]OKTENOV TER
POLIFUNKCIONALIZIRANIH ANILINOV
Datum zagovora: 6. 9. 2022

Aljaž RENKO

Mentor: doc. dr. Martin Gazvoda
POSKUS SINTEZE MANJŠEGA PROTEINA Z UPORABO
METODE NA TRDNEM NOSILCU
Datum zagovora: 6. 9. 2022

Vuk MARTINOVIČ

Mentor: prof. dr. Jurij Svete
DERIVATIZACIJA 6-AMINOKAPROJSKE KISLINE
Datum zagovora: 6. 9. 2022

Benjamin POLJANC

Mentor: prof. dr. Iztok Turel
OPTIMIZACIJA SINTEZE IZBRANIH DERIVATOV
PIRITIONA IN PRIPRAVA NJIHOVIH CINKOVIH
KOORDINACIJSKIH SPOJIN
Datum zagovora: 6. 9. 2022

Robert KOBE

Mentor: doc. dr. Jakob Kljun
SINTEZA RENIJEVIH(I) TRIKARBONIL KOMPLEKSOV S
KELATNIMI TIOPIRIMIDINI
Datum zagovora: 7. 9. 2022

Tim VONČINA

Mentor:izr. prof. dr. Miha Lukšič
VPLIV PLAZEMSKA OBDELAVE POVRŠINE
ELEKTRONSKEGA VEZJA NA IZBOLJŠANJE
OPRIJEMLJIVOSTI KONFORMNIH PREMAZOV
Datum zagovora: 7. 9. 2022

Blaž TOMC

Mentor: doc. dr. Jakob Kljun
SINTEZA LANTANOIDNIH LUMINESCENČNIH
KOMPLEKSOV
Datum zagovora: 7. 9. 2022

Jure VALENČIČ

Mentor: prof. dr. Jernej Iskra
SINTEZA IZBRANEGA BETA-O-4 LIGNINSKEGA MODELA
Datum zagovora: 7. 9. 2022

Jaša HROVAT

Mentorica: prof. dr. Helena Prosen
OPTIMIZACIJA EKSTRAKCIJE DDT IZ TAL
Datum zagovora: 8. 9. 2022

Ivan MITEVSKI

Mentorica: prof. dr. Helena Prosen
DOLOČANJE KLOROFENOLOV V POVRŠINSKIH VODAH
Datum zagovora: 8. 9. 2022

Peter ŠKARABOT

Mentor: prof. dr. Marjan Jereb
NEKATERE PRETVORBE NA OKOLJU PRIJAZEN NAČIN
Datum zagovora: 8. 9. 2022

Rubina VIRIANT

Mentor: prof. dr. Matija Tomšič
VPLIV PORAZDELITVE VELIKOSTI KALCIJEVO
KARBONATNIH DELCEV NA REOLOŠKE LASTNOSTI
NJIHOVIH SUSPENZIJ
Datum zagovora: 9. 9. 2022

Ana ŠIJANEC

Mentor: prof. dr. Matevž Pompe
DOLOČEVANJE ARTEMIZININA V MICELIZIRANIH
FORMULACIJAH
Datum zagovora: 9. 9. 2022

Doroteja LIPOVEC

Mentor: prof. dr. Jurij Svete
SINTEZA IN PRETVORBE NA-BENZILOKSIKARBONIL-
NB-TERC-BUTOKSIKARBONIL-3,7-DIAMINO-1-DIAZO-2-
OKSOHEPTANA
Datum zagovora: 9. 9. 2022

Veronika DEBEVEC

Mentor:izr. prof. dr. Janez Cerkovnik
SINTEZA KLEŠČASTIH KOMPLEKSOV S PALADIJEM IN
ŠTUDIJ NJIHOVE REAKTIVNOSTI
Datum zagovora: 26. 9. 2022

Živana MARC

Mentor:izr. prof. dr. Barbara Modec
REAKCIJE BAKROVEGA(II) KINALDINATA Z IZBRANIMI
PIPERAZINI
Datum zagovora: 6. 10. 2022

Marcel TIŠLER

Mentorica: doc. dr. Nataša Gros
MERILNA NEGOTOVOST PRI REDČENJU RAZTOPINE NA
VOLUMEN ALI Z VOLUMNOM
Datum zagovora: 29. 11. 2022

Klemen TROBEC

Mentorica: prof. dr. Romana Cerc Korošec
ABSORPCIJSKE IN FOTOKATALITSKE LASTNOSTI
TANKIH PLASTI CINK-ALUMINIJEVIH PLASTOVITIH
DVOJNIH HIDROKSIDOV
Datum zagovora: 22. 12. 2022

KEMIJSKO INŽENIRSTVO – 1. STOPNJA**Kris GUŠTIN**

Mentor: prof. dr. Marjan Marinšek
INDUSTRIJSKA MEMBRANSKA FILTRACIJA SUROVEGA
VODIKOVEGA PEROKSIDA
Datum zagovora: 10. 1. 2022

Ines ORAČ

Mentorica: doc. dr. Lidija Slemenik Perše
VPLIV RECIKLIRANJA NA MEHANSKE LASTNOSTI
POLIPROPILENA
Datum zagovora: 1. 2. 2022

Luka CARIČ

Mentorica: doc. dr. Lidija Slemenik Perše
PILOTNO TESTIRANJE UČINKOVITOSTI ČIŠČENJA
VODIKOVEGA PEROKSIDA Z 1,1,3,3-TETRABUTIL UREO
V EKSTRAKCIJSKI KOLONI
Datum zagovora: 6. 5. 2022

Bor ŠTULAR

Mentorica: prof. dr. Andreja Žgajnar Gotvajn
DEŽEVNICA KOT POMEMBEN VIR PITNE VODE
Datum zagovora: 9. 6. 2022

Martin CIRINGER

Mentor: prof. dr. Miran Gaberšček
FOTOKATALITSKA REDUKCIJA CO₂ PRI REVERZNI
REAKCIJI VODNEGA PLINA
Datum zagovora: 24. 6. 2022

Matej PAVLI

Mentor: prof. dr. Igor Plazl
KINETIČNI MODEL KATALITSKE SINTEZE VODIKOVEGA
PEROKSIDA
Datum zagovora: 1. 7. 2022

Lara PLANINC

Mentor: izr. prof. dr. Blaž Likozar
VPLIV ČASA POSTOPKA NA UTEKOČINJANJE BIOMASE
ALG Z DEOKSIGENACIJO
Datum zagovora: 29. 8. 2022

Amadeja SAJOVIC ŽULOVEC

Mentorica: izr. prof. dr. Gabriela Kalčíkova
KOMBINIRAN VPLIV MIKROPLASTIKE IN NANODELCEV
NA VODNE ORGANIZME
Datum zagovora: 30. 8. 2022

Sara ROVAN

Mentorica: doc. dr. Lidija Slemenik Perše
VPLIV VRSTE MEDU NA TOKOVNO VEDENJE
Datum zagovora: 31. 8. 2022

Kaja ZUPANČIČ

Mentor: izr. prof. dr. Boštjan Genorio
SINTEZA IN KARAKTERIZACIJA ELEKTROKEMIJSKEGA
KATALIZATORJA NA OSNOVI REDUCIRANEGA GRAFEN
OKSIDA DEKORIRANEGA S CO
Datum zagovora: 1. 9. 2022

Maks LEVIČAR

Mentor: izr. prof. dr. Aleš Ručigaj
SAMO-OPTIMIZACIJA KEMIJSKIH REAKCIJ V
PRETOČNIH SISTEMIH
Datum zagovora: 1. 9. 2022

Filip BOROVSŠAK

Mentor: prof. dr. Matjaž Krajnc
PULZNO POLNJENJE LITIJ-IONSКИH BATERIJ
Datum zagovora: 1. 9. 2022

Vid BAČAR

Mentorica: doc. dr. Iztok Prislan
MODELIRANJE IN SIMULACIJA PROCESOV V
KEMIJSKEM REAKTORJU S PROGRAMOM MS EXCEL
Datum zagovora: 2. 9. 2022

Robert BAŠ

Mentorica: prof. dr. Andreja Žgajnar Gotvajn
NAPREDNI OKSIDACIJSKI PROCESI ZA ZMANJŠEVANJE
EMISIJ ANTIBIOTIKOV V OKOLJE
Datum zagovora: 2. 9. 2022

Jan JEROVŠEK

Mentor: prof. dr. Robert Dominko
VPLIV SESTAVE ELEKTROLITA NA ELEKTROKEMIJSKO
DELOVANJE NEGRAFITIZIRANEGA OGLJIKA V NA-ION
AKUMULATORJU
Datum zagovora: 2. 9. 2022

Lucija PINTERIČ

Mentorica: prof. dr. Polona Žnidaršič Plazl
UPORABA EVTEKTIČNIH TOPIL PRI SINTEZI
HIDROGELOV
Datum zagovora: 2. 9. 2022

Živa COKLIN

Mentor: prof. dr. Aleš Podgornik
BARVANJE BAKTERIOFAGOV S FLUORESCIN
IZOTIOCIANATOM
Datum zagovora: 2. 9. 2022

Matej MEDVED

Mentor: prof. dr. Robert Dominko
VPLIV RAZLIČNIH PARAMETROV NA KINETIKO
MAGNEZIJ ORGANSKEGA AKUMULATORJA
Datum zagovora: 2. 9. 2022

Nejc URBANIJA

Mentor: prof. dr. Robert Dominko
UPORABA ELEKTROKEMIJSKE IMPEDANČNE
SPEKTROKOPIJE ZA RAZLOČITEV IMPEDANČNIH
PRISPEVKOV REAKCIJE PRENOSA NABOJA IN
DESOLVATACIJE ZA LI KOVINSKO ANODO
Datum zagovora: 2. 9. 2022

Žiga GERDINA

Mentorica: prof. dr. Polona Žnidaršič Plazl
UPORABA MIKROREAKTORJEV Z MAGNETNIM POLJEM
V BIODKATALITSКИH PROCESIH
Datum zagovora: 5. 9. 2022

Anja HRVATIČ

Mentor: izr. prof. dr. Aleš Ručigaj
PRIPRAVA HIDROGELOV ZA UPORABO V BIOSENZORIKI
atum zagovora: 5. 9. 2022

Izak KREUH

Mentor: prof. dr. Igor Plazl
VEČNIVOJSKO MODELIRANJE V KEMIJSKEM
INŽENIRSTVU
Datum zagovora: 5. 9. 2022

Tadej PIRC

Mentor: doc. dr. Rok Ambrožič
OPTIMIZACIJA PROCESNIH SPREMENLJIVK NA OSNOVI
REOLOŠKE ANALIZE
Datum zagovora: 5. 9. 2022

Blaž MUJDRICA

Mentor: izr. prof. dr. Boštjan Genorio
SINTEZA ELEKTROKATALIZATORJEV NA OSNOVI
GRAFENA DOPIRANEGA S KOVINSKIMI ATOMI ZA
REAKCIJO REDUKCIJE CO₂
Datum zagovora: 6. 9. 2022

Julija SOVDAT

Mentor: prof. dr. Igor Plazl
PROIZVODNJA LETALSKEGA GORIVA IZ BIOMASE
Datum zagovora: 6. 9. 2022

Arijana RAMŠAK

Mentor: doc. dr. Rok Ambrožič
INTEGRACIJA HIDROGELOV V PRETOČNE MIKROFLUIDNE
NAPRAVE: TRENUTNI RAZVOJ TER APLIKACIJE
Datum zagovora: 6. 9. 2022

Kasper BOŠNIK

Mentor: prof. dr. Matevž Dular
OCENA RAZGRADNJE ODPADNEGA BLATA Z
LABORATORIJSKIM GENERATORJEM HIDRODINAMSKO
KAVITACIJE
Datum zagovora: 7. 9. 2022

Maruša ATELŠEK

Mentor: izr. prof. dr. Blaž Likozar
KATALITSKA PRETVORBA GLICEROLA V PLINSKI FAZI
atum zagovora: 7. 9. 2022

Tina LAZAR

Mentor: prof. dr. Matevž Dular
VPLIV ULTRAZVOKA NA PRENOS TOPLOTE PRI VRENJU
Datum zagovora: 7. 9. 2022

Tara TRATNJEK

Mentorica: prof. dr. Andreja Žgajnar Gotvajn
ODSTRANJEVANJE STABILNEGA ANTIBIOTIKA
GENTAMICIN SULFATA IZ ODPADNE VODE Z
OZONACIJO
Datum zagovora: 7. 9. 2022

Nives KOKOL

Mentor: izr. prof. dr. Blaž Likozar
DVO-KOVINSKA RENIJEVA KATALIZA ZA
DEHIDROKSILACIJO
Datum zagovora: 7. 9. 2022

Matej HOZJAN

Mentor: izr. prof. dr. Blaž Likozar
STABILNOST HIDROKSIMETILFURFURALA V VODI
IN RAZLIČNIH ORGANSKIH TOPILIH TER NJEGOVA
PRETVORBA DO LEVULINSKE KISLINE
Datum zagovora: 7. 9. 2022

Jan ŠKRUBA

Mentor: prof. dr. Marjan Marinšek
UPORABA OGLJIKOVH NANOCEVK V FILTRI IN
MEMBRANAH ZA TRETIRANJE ODPADNIH VOD
Datum zagovora: 7. 9. 2022

Maja DEVETAK

Mentorica: izr. prof. dr. Gabriela Kalčikova
UPORABA DIMETOATA V OLJKARSTVU IN NJEGOV
VPLIV NA OKOLJE
Datum zagovora: 8. 9. 2022

Tim ŠLOSAR

Mentor: izr. prof. dr. Boštjan Genorio
PROIZVODNJA POSEBNIH TIPOV PIGMENTA TIO₂
– VPLIV SINTEZNIH POGOJEV NA PROCESNE IN
KAKOVOSTNE PARAMETRE
Datum zagovora: 8. 9. 2022

Tjaša LIKEB

Mentorica: izr. prof. dr. Gabriela Kalčikova
VPLIV PH NA DESORPCIJO NANODELCEV
ADSORBIRANIH NA MIKROPLASTIKI
Datum zagovora: 8. 9. 2022

Larisa FABJAN

Mentorica: prof. dr. Polona Žnidaršič Plazl
PRIPRAVA ZAMREŽENIH ENCIMSKIH AGREGATOV NA
OSNOVI LAKAZE V MIKROPRETOČNEM SISTEMU
Datum zagovora: 8. 9. 2022

Benjamin HASANAGIĆ

Mentor: prof. dr. Igor Plazl
PROCESNA INTENZIFIKACIJA PROIZVODNJE
KALCIJEVEGA KARBONATA Z DIMNIMI PLINI
Datum zagovora: 9. 9. 2022

Nejc SUBAN

Mentor: izr. prof. dr. Aleš Ručigaj
ELEKTRO-ODZIVNI HIDROGELI IN NJIHOVE
APLIKACIJE
Datum zagovora: 9. 9. 2022

Dona ZLOBKO

Mentor: prof. dr. Marjan Marinšek
MODERNI ANORGANSKO-ORGANSKI PEROVSKITNI
MATERIALI
Datum zagovora: 9. 9. 2022

Patrik HLEBANJA

Mentorica: prof. dr. Polona Žnidaršič Plazl
VPLIV DODATKA KOFAKTORJA NA AKTIVNOST
AMIN TRANSAMINAZE IMOBILIZIRANE V OBLIKI
ZAMREŽENIH ENCIMSKIH AGREGATOV
Datum zagovora: 9. 9. 2022

Valentin PAVŠEK

Mentor: prof. dr. Marjan Marinšek
NOVI IZZIVI ZA MATERIALE SOLARNIH CELIC TRETJE
GENERACIJE
Datum zagovora: 9. 9. 2022

Tea ŠANDOR

Mentorica: prof. dr. Urška Šebenik
UPORABA GRAFEN OKSIDNIH KOMPOZITOV V
BIOSENZORIKI
Datum zagovora: 12. 9. 2022

Petra JELER

Mentorica: izr. prof. dr. Gabriela Kalčíkova
ABRAZIJA AVTOMOBILSKIH GUM IN NASTAJANJE
MIKROPLASTIKE
atum zagovora: 23. 9. 2022

Tjaša ŽAGAR

Mentorica: doc. dr. Tina Skalar
UPORABA MATERIALOV Z VISOKO ENTROPIJO V
BATERIJAH
Datum zagovora: 30. 9. 2022

Blaž KOVAČIČ

Mentorica: prof. dr. Urška Šebenik
POLIMERNI GELSKI ELEKTROLITI
Datum zagovora: 6. 10. 2022

Dean UŠTAR

Mentorica: doc. dr. Tina Skalar
UPORABA MATERIALOV Z VISOKO ENTROPIJO ZA
SHRANJEVANJE VODIKA
Datum zagovora: 18. 10. 2022

Tilen SKOBIR

Mentor: prof. dr. Marjan Marinšek
IZBIRA MATERIALA ZA ZAVORNE PLOŠČICE V
PROTOTIPNIH DIRKALNIH AVTOMOBILIH
Datum zagovora: 29. 11. 2022

Emina KAPIČ

Mentorica: prof. dr. Urška Šebenik
SHRANJEVANJE ENERGIJE S PRETVORBO V VODIK
Datum zagovora: 20. 12. 2022

BIOKEMIJA – 1. STOPNJA**Oskar NEMEC**

Mentor: doc. dr. Tadeja Režen
FUNKCIJSKA ANOTACIJA DIFERENČNO IZRAŽENIH
KROŽNIH RNA V RAKU JETER
Datum zagovora: 1. 2. 2022

Tadej URŠIČ

Mentorica: prof. dr. Ksenija Kogej
STEARINSKA KISLINA: TITRACIJSKE KRIVULJE,
POVRŠINSKA NAPETOST IN TVORBA DVOPLASTI
Datum zagovora: 19. 4. 2022

Jure POVŠIN

Mentor: doc. dr. Aljaž Gaber
IZRAŽANJE IN IZOLACIJA INHIBITORNEGA PEPTIDA
ZA TACE, KI JE ZASNOVAN NA OSNOVI ZAPOREDJA
PROPEPTIDNE REGIJE
Datum zagovora: 20. 4. 2022

Maša GABRIČ

Mentor: doc. dr. Miha Pavšič
OPTIMIZACIJA POGOJEV ZA IZVEDBO "PULL DOWN"
BIOTINILIRANIH PROTEINOV V CELIČNI LINIJI
HEK293T
Datum zagovora: 22. 4. 2022

Maša ANDOLJŠEK

Mentor: prof. dr. Marko Dolinar
POSKUS IZOLACIJE CIANOFAGA IZ BLEJSKEGA JEZERA
V ČASU MNOŽIČNEGA POJAVLJANJA CIANOBAKTERIJE
PLANKTOTHRIX RUBESCENS
Datum zagovora: 2. 6. 2022

Ana BABNIK

Mentor: doc. dr. Gregor Gunčar
PRIPRAVA PLAZMIDA ZA IZRAŽANJE FUZIJSKEGA
PROTEINA SESTAVLJENEGA IZ GFP IN PROTEAZE IZ
VIBRIO CHOLERAЕ
Datum zagovora: 5. 7. 2022

Greta JUNGER

Mentor: doc. dr. Gregor Gunčar
IZRAŽANJE PROTEINA M33-MCHERRY V CELIČNI LINIJI
HEK293 FLP-IN Z VSTAVLJENIM GENOM ZA MLKL
Datum zagovora: 7. 7. 2022

Tinkara BOŽIČ

Mentorica: doc. dr. Marina Klemenčič
IZRAŽANJE IN AKTIVACIJA PROTEAZE CEP2 IZ
ZELENE ALGE CHLAMYDOMONAS REINHARDTII V
BAKTERIJSKIH CELICAH ESCHERICHIA COLI
Datum zagovora: 8. 7. 2022

Žan FORTUNA

Mentorica: izr. prof. dr. Katarina Černe
NAPOVED REZISTENCE NA KEMOTERAPIJO NA OSNOVI
PLATINE PRI RAKU JAJČNIKOV
Datum zagovora: 25. 8. 2022

Sašo JAKOB

Mentor: prof. dr. Marko Dolinar
PROTEINSKA BARVILA PRI CIANOBKTERIJAH:
LASTNOSTI, POSTOPKI IZOLACIJE IN UPORABA
Datum zagovora: 25. 8. 2022

Vivian NEMANIČ

Mentorica: doc. dr. Marina Klemenčič
KLONIRANJE MUTIRANIH RAZLIČIC ANTTOKSINA 1067 IZ
CIANOBAKTERIJE MICROCYSTIS AERUGINOSA PCC 7806.
Datum zagovora: 25. 8. 2022

Nika BEDRAČ

Mentorica: izr. prof. dr. Katarina Černe
ATP7A KOT POTENCIALNI OZNAČEVALEC ZA NAPOVED
REZISTENCE NA KARBOPLATIN PRI SEROZNEM TIPU
RAKA JAJČNIKOV
Datum zagovora: 5. 9. 2022

Iva MATIČ

Mentorica: doc. dr. Tadeja Režen
PRIPRAVA LENTIVIRUSNIH VEKTORJEV ZA REGULACIJO
IZRAŽANJA CIRC RNA V CELIČNIH LINIJAH
Datum zagovora: 6. 9. 2022

Nika BANOVSĚEK

Mentorica: doc. dr. Barbara Breznik
METALOPROTEAZI MMP2 IN MMP9 V MIKROOKOLJU
GLIOBLASTOMA
Datum zagovora: 6. 9. 2022

Ajda BELTRAM

Mentorica: doc. dr. Vera Župunski
KLONIRANJE IN IZRAŽANJE PROTEINA NONO
Datum zagovora: 6. 9. 2022

Maja KOLAR

Mentor: prof. dr. Janez Plavec
Z GVANINI BOGATA ZAPOREDJA V GENOMU SARS-
COV-2
Datum zagovora: 7. 9. 2022

Anja KONJC

Mentor: doc. dr. Sergej Pirkmajer
FARMAKOLOŠKO URAVNAVANJE FOSFORILACIJE
Z AMP AKTIVIRANE PROTEIN KINAZE V KULTURI
SKELETNOMIŠIČNIH CELIC
Datum zagovora: 7. 9. 2022

Lena TRNOVEC

Mentorica: prof. dr. Ksenija Kogej
OLEINSKA KISLINA: TITRACIJSKE KRIVULJE IN TVORBA
DVOPLASTI
Datum zagovora: 7. 9. 2022

Stefanija IVANOVA

Mentorica: prof. dr. Ksenija Kogej
STABILNOST VEZIKULARNIH STRUKTUR
Datum zagovora: 7. 9. 2021

Luka ŠEGOTA

Mentor: doc. dr. Aljaž Gaber
IZRAŽANJE IN IZOLACIJA SKRAJŠANIH OBLIK
ČLOVEŠKEGA PROTEINA FHL2
Datum zagovora: 7. 9. 2022

Vid DOBROVOLJC

Mentorica: prof. dr. Barbara Hribar Lee
AGREGACIJA BF-KRISTALINOV
Datum zagovora: 7. 9. 2022

Nika TOMSIČ

Mentor: doc. dr. Miha Pavšič
KARAKTERIZACIJA POTENCIALA HIDROFOBNEGA ŽEPA
EPCAM ZA VEZAVO LIPIDOM PODOBNIH MOLEKUL
Datum zagovora: 7. 9. 2022

Marjeta MILOSTNIK

Mentor: doc. dr. Sergej Pirkmajer
POMEN KINAZE FAM20C ZA IZLOČANJE IN DELOVANJE
INTERLEVKINA-6 MIŠIČNEGA IZVORA
Datum zagovora: 7. 9. 2022

Srna ANASTASOVSKA

Mentor: prof. dr. Boris Rogelj
STRUKTURNE ZNAČILNOSTI HEKSANUKLEOTIDNIH
PONOVI TEV POVEZANIH Z MUTACIJO C9ORF72
Datum zagovora: 8. 9. 2022

Nika PERKO

Mentorica: izr. prof. dr. Helena Haque Chowdhury
VPLIV TEMPERATURE GOJENJA PODGANJIH
ASTROCITOV V PRIMARNI KULTURI NA
IZRAŽANJE ADRENERGIČNIH RECEPTORJEV IN
MONOKARBOKSILATNIH PRENAŠALCEV
Datum zagovora: 8. 9. 2022

Gregor STRNIŠA

Mentor: prof. dr. Rok Romih
ŠTUDIJA LOKALIZACIJE PIEZO1 IN PIEZO2 V UROTELIJU
SEČNEGA MEHURJA
Datum zagovora: 8. 9. 2022

Timotej SOTOŠEK

Mentor: izr. prof. dr. Marko Novinec
RACIONALNO NAČRTOVANJE IN PRIPRAVA DIMERNIH
VARIANT ČLOVEŠKEGA KATEPSINA S
Datum zagovora: 9. 9. 2022

Maruša SERNC

Mentorica: doc. dr. Vera Župunski
KLONIRANJE IN IZRAŽANJE PROTEINA TDP-43 IN
NJEGOVIH MUTANTOV V BAKTERIJSKIH CELICAH
Datum zagovora: 9. 9. 2022

Maja TRIFKOVIČ

Mentorica: doc. dr. Vera Župunski
MOLEKULSKO KLONIRANJE IN FILOGENETSKE ANALIZE
NEKODIRAJOČIH RNA Y
Datum zagovora: 15. 9. 2022

Ana VIČIČ

Mentorica: izr. prof. dr. Nataša Debeljak
ANALIZA NOVIH MOLEKULARNIH POTI IN GENOV
POVEZANIH Z ERITROCITOZO
Datum zagovora: 15. 9. 2022

Ela BIZJAK

Mentor: doc. dr. Gregor Gunčar
UČINKOVITOST SAMOIZREZUJOČEGA SE
OZNAČEVALCA CPD IZ BAKTERIJE VIBRIO CHOLERAЕ
Datum zagovora: 6. 10. 2022

Erik PUTAR

Mentor: izr. prof. dr. Marko Novinec
RACIONALNO NAČRTOVANJE IN PRIPRAVA DIMERNIH
VARIANT ČLOVEŠKEGA KATEPSINA B
Datum zagovora: 30. 11. 2022

Nikola JANAKIJEVSKI

Mentor: doc. dr. Aljaž Gaber
Somentorica: Maria dos Anjos López de Macedo
PRIPRAVA IN STRUKTURNA KARAKTERIZACIJA
INHIBITORJA ŽILNE KALCINACIJE, ČLOVEŠKEGA
S KARBOKSIGLUTAMINSKO KISLINO BOGATEGA
PROTEINA (GRP)
Datum zagovora: 9. 12. 2022

TEHNIŠKA VARNOST – 1- STOPNJA**Gašper ZALAZNIK**

Mentor: izr. prof. dr. Simon Schnabl
PRODUKTI GORENJA IZ ODPRTIH KURIŠČ
Datum zagovora: 8. 3. 2022

Luka NORČIČ

Mentor: prof. dr. Tomaž Urbič
SKLADIŠČENJE KEMIKALIJ
Datum zagovora: 6. 9. 2022

Maša NARED

Mentorica: doc. dr. Klementina Zupan
ERGONOMIJA DELOVNIH MEST V PODJETJU ZA PREVOZ
BLAGA V CESTNEM PROMETU
Datum zagovora: 15. 6. 2022

Mara KOZLOVIČ

Mentorica: doc. dr. Sabina Huč
OBRAVNAVA NEŽELENIH DOGODKOV S PODROČJA
VARNOSTI IN ZDRAVJA PRI DELU V MEDNARODNEM
PREHRAMBENEMU PODJETJU
Datum zagovora: 7. 9. 2022

Gašper VESEL

Mentorica: doc. dr. Klementina Zupan
OCENA TVEGANJA PRI PROIZVODNJI POSLOVNEGA
POHIŠTVA
Datum zagovora: 20. 6. 2022

Ana PETEK

Mentorica: doc. dr. Barbara Novosel
VARNA UPORABA ČISTIL V PREHRAMBENI INDUSTRIJI
Datum zagovora: 8. 9. 2022

Pia PIVK

Mentorica: doc. dr. Klementina Zupan
VPLIV PISARNIŠKEGA DELA NA ZGORNJE OKONČINE
Datum zagovora: 8. 7. 2022

Iris HOČEVAR

Mentorica: doc. dr. Barbara Novosel
MERITVE KONCENTRACIJE RADONA V DELOVNEM
OKOLJU IN UKREPI ZA ZMANJŠANJE ŠKODLJIVIH
UČINKOV RADONA NA ZDRAVJE LJUDI
Datum zagovora: 8. 9. 2022

Nejc ZAVRL

Mentorica: doc. dr. Barbara Novosel
DOLOČITEV KONCENTRACIJE TEŽKIH KOVIN V REKI
MEŽI Z OCENO NJIHOVIH NEGATIVNIH VPLIVOV NA
ZDRAVJE PREBIVALCEV
Datum zagovora: 29. 8. 2022

Jaka CIPOT

Mentor: prof. dr. Jurij Reščič
STATISTIČNA PRIMERJAVA VARNOSTI LETALSKEGA
PROMETA V SEVERNLI AMERIKI IN IZBRANIH
EVROPSKIH DRŽAVAH
Datum zagovora: 9. 9. 2022

Peter MEGLIČ

Mentorica: doc. dr. Barbara Novosel
DOLOČITEV KONCENTRACIJ TEŽKIH KOVIN V
KAMNIŠKI BISTRICI
Datum zagovora: 29. 8. 2022

Lara GRIŽON

Mentorica: prof. dr. Marija Bešter Rogač
VPLIV ČRNEGA OGLJIKA NA OKOLJE IN ZDRAVJE LJUDI
Datum zagovora: 9. 9. 2022

Nik PONEBŠEK

Mentorica: doc. dr. Klementina Zupan
ERGONOMIJA DELOVNEGA MESTA ŠIVILJE
Datum zagovora: 2. 9. 2022

Tamara JANKOVIČ

Mentorica: prof. dr. Marija Bešter Rogač
KAKOVOST ZRAKA V ŠOLAH
Datum zagovora: 13. 9. 2022

Nuša TOME

Mentorica: doc. dr. Klementina Zupan
ERGONOMSKA ANALIZA DELOVNEGA MESTA V
PODJETJU FILC D. O. O. ŠKOFJA LOKA
Datum zagovora: 2. 9. 2022

Janja KRESAL

Mentorica: doc. dr. Klementina Zupan
ERGONOMSKI VIDIK DELA OD DOMA ZARADI
PANDEMIJE COVID-19
Datum zagovora: 19. 9. 2022

Tjaša KOŠIR

Mentorica: doc. dr. Sabina Huč
KIBERNETSKO TVEGANJE IN METODE PREPREČEVANJA
Datum zagovora: 2. 9. 2022

Tim KAVČIČ

Mentorica: izr. prof. dr. Simon Schnabl
VARNOST PRI UPORABI EKSPLOZIVNIH SREDSTEV V
KAMNOLOMU
Datum zagovora: 29. 9. 2022

Klemen ERŽEN

Mentor: prof. dr. Grega Bizjak
ELEKTRIČNA VARNOST POLNILNIH POSTAJ ZA
ELEKTRIČNA VOZILA
Datum zagovora: 7. 10. 2022

Miha LAVRIČ

Mentor: doc. dr. Sabina Huč
OCENA TVEGANJA V PROIZVODNJI MEDICINSKIH
LASERSKIH NAPRAV
Datum zagovora: 19. 10. 2022

DIPLOME – VISOKOŠOLSKI STROKOVNI ŠTUDIJ**KEMIJSKA TEHNOLOGIJA – 1. STOPNJA****Denis MAVRIČ**

Mentor: viš. pred. dr. Branko Alič
VPLIV SUPERABSORPCIJSKIH POLIMEROV NA
MIKROSTRUKTURO IN LASTNOSTI SAMOCELJENJA
CEMENTNIH KOMPOZITNIH MATERIALOV
Datum zagovora: 21. 1. 2022

Petra MEGLEN

Mentorica: doc. dr. Saša Petriček
NIKLJEVI IN CINKOVI KOMPLEKSI S
3-HIDROKSIPIRIDINOM
Datum zagovora: 4. 3. 2022

Nika ŠINKOVEC

Mentor: doc. dr. Andrej Pevec
KRISTALNE STRUKTURE BIPIRIDINIJEVIH
HEKSAFLUORIDOMETALATOV
Datum zagovora: 9. 3. 2022

Maša KUŽNIK

Mentor: doc. dr. Andrej Pevec
KRISTALNE STRUKTURE FENANTROLINIJEVIH
HEKSAFLUORIDOMETALATOV
Datum zagovora: 9. 3. 2022

Luka TRAMPUŠ

Mentor: doc. dr. Bojan Kozlevčar
MANGANOVE IN NIKLJEVE SPOJINE Z VINSKO KISLINO
Datum zagovora: 24. 3. 2022

Igor GRUDEN

Mentor: izr. prof. dr. Janez Cerar
VPLIV OKOLJA NA POVRŠINSKO NAPETOST NARAVNIH
VODA
Datum zagovora: 12. 4. 2022

Klara TURK

Mentor: viš. pred. dr. Andrej Godec
ČIŠČENJE PODZEMNIH VODA
Datum zagovora: 24. 5. 2022

Nika STRAJNAR

Mentor: prof. dr. Anton Meden
RENTGENSKA PRAŠKOVNA DIFRAKCIJA ŠUMEČIH
TABLET
Datum zagovora: 23. 6. 2022

Luka GORENČIČ

Mentor: prof. dr. Jernej Iskra
PRETVORBA LIGNINA V UPORABNE KEMIKALIJE
Datum zagovora: 28. 6. 2022

Andreja CUGELJ

Mentorica: doc. dr. Nataša Čelan Korošin
DOLOČITEV POLIMORFIZMA FARMACEVTSKIH
UČINKOVIN Z METODAMI TERMIČNE ANALIZE
Datum zagovora: 4. 7. 2022

Boštjan SLAK

Mentorica: doc. dr. Barbara Novosel
OPTIMIZACIJA POSTOPKA RAVNANJA S PROIZVODNIMI
OSTANKI
Datum zagovora: 5. 7. 2022

Tina LESJAK

Mentor: prof. dr. Franc Perdih
UPORABA KELATNE TERAPIJE
Datum zagovora: 6. 7. 2022

Lana KUŽNIK

Mentor: doc. dr. Jakob Kljun
OPTIMIZACIJA SINTEZE TIADIAZOLOV IZ
4,4-DIMETILTIOSEMIKARBAZIDA
Datum zagovora: 7. 7. 2022

Lara REBOLJ

Mentorica: izr. prof. dr. Barbara Modec
KOORDINACIJSKE SPOJINE CINKA(II) S PIKOLINATOM
IN PIPERIDINOM
Datum zagovora: 25. 8. 2022

Luka RACMAN KNEZ

Mentorica: prof. dr. Helena Prosen
DOLOČANJE VITAMINOV B V PREHRANSKIH DOPOLNILIH
Datum zagovora: 25. 8. 2022

Monika MALOVRH

Mentorica: prof. dr. Helena Prosen
DOLOČITEV NEONIKOTINOIDNIH PESTICIDOV V PIVU
Datum zagovora: 26. 8. 2022

Žan RAJK

Mentor: doc. dr. Bojan Kozlevčar
SINTEZA IN KARAKTERIZACIJA KOORDINACIJSKIH
SPOJIN S FENILOCETNO KISLINO
Datum zagovora: 29. 8. 2022

Gašper PAVLIN

Mentor: izr. prof. dr. Uroš Grošelj
SINTEZA AMIDOV KETOPINSKE KISLINE
Datum zagovora: 1. 9. 2022

Gašper MOŽINA

Mentor: doc. dr. Krištof Kranjc
VPLIV REAKCIJSKIH POGOJEV NA SINTEZE RAZLIČNIH
5,6-DISUBSTITUIRANIH 3-BENZOILAMINO-2H-
PIRAN-2-ONOV KOT VSESTRANSKIH GRADNIKOV V
PERICIKLIČNIH REAKCIJAH
Datum zagovora: 1. 9. 2022

Monika ČAČULOVČIČ

Mentor: prof. dr. Franc Perdih
OPTIMIZACIJA SINTEZE DIPIKOLINATNIH LIGANDOV
ZA VEZAVO NA KOVINSKE IONE
Datum zagovora: 1. 9. 2022

Urška ŽUNIČ

Mentorica: doc. dr. Nives Kitanovski
KARAKTERIZACIJA NEZNANE KROMOVE SPOJINE
Datum zagovora: 2. 9. 2022

Nejc ŠTIFTAR

Mentorica: prof. dr. Romana Cerc Korošec
VPLIV INSTRUMENTALNIH IN VZORČNIH
PARAMETROV NA POTEK UMERITVENIH KRIVULJ
ZA DOLOČITEV STOPNJE TOPLOTNE MODIFIKACIJE
HRASTOVEGA LESA
Datum zagovora: 2. 9. 2022

Kaja RUČIGAJ

Mentorica: prof. dr. Irena Kralj Cigić
DOLOČANJE ANTIOKSIDANTOV V PVC
Datum zagovora: 2. 9. 2022

Maša KUCHAR

Mentorica: prof. dr. Irena Kralj Cigić
RAZVOJ IN VALIDACIJA METODE ZA DOLOČANJE
UROLITINA A
Datum zagovora: 5. 9. 2022

Ana Mari ŠUKLJE

Mentorica: doc. dr. Marija Zupančič
UPORABA IR SPEKTROSKOPIJE PRI PROUČEVANJU
APATITOV ŽIVALSKEGA IZVORA
Datum zagovora: 7. 9. 2022

Nejc ŠULIGOJ

Mentor: doc. dr. Martin Gazvoda
IZVEDBA IZBRANIH Z NIKLJEM (NI) KATALIZIRANIH
REAKCIJ POD INERTNO ATMOSFERO IN V
BREZVODNEM MEDIJU
Datum zagovora: 7. 9. 2022

Petra SINTIČ

Mentor: prof. dr. Franc Požgan
Z BAKROM KATALIZIRANE REAKCIJE SPAJANJA ZA
TVORBO C-C IN C-HETEROATOM VEZI
Datum zagovora: 8. 9. 2022

Nejc ŠMIC

Mentor: prof. dr. Mitja Kolar
ANALITIKA PLEMENITIH KOVIN V ELEKTRONSKIH
ODPADKIH Z METODO ICP-OES IN PRIMERJAVA DVEH
METOD RAZKLOPA
Datum zagovora: 8. 9. 2022

Tajda KRAJNC

Mentor: doc. dr. Jakob Kljun
SINTEZA KELATNIH ANALOGOV HALICINA
Datum zagovora: 9. 9. 2022

Nika ŠKOF

Mentorica: izr. prof. dr. Gabriela Kalčikova
OVREDNOTENJE EKOTOKSIČNOSTI VODOTOPNEGA
AKRILATNEGA KOPOLIMERA UPORABLJENEGA V
KOZMETIKI
Datum zagovora: 9. 9. 2022

Urška OREŠNIK

Mentorica: doc. dr. Marija Zupančič
PROBLEMATIKA POTENCIALNO STRUPENIH
ELEMENTOV V ODPADNIH BLATIH KOMUNALNIH
ČISTILNIH NAPRAV
Datum zagovora: 14. 9. 2022

Petra VARDIJAN

Mentorica: izr. prof. dr. Amalija Golobič
RENTGENSKA PRAŠKOVNA DIFRAKCIJA VITAMINSKIH
IN MINERALNIH PREPARATOV
Datum zagovora: 19. 9. 2022

Miha BLAŽIČ

Mentor: doc. dr. Andrej Pevec
HEKSAFLUORIDOSILIKATI NEKATERIH PURINSKIH BAZ
Datum zagovora: 27. 9. 2022

Barbara ŽIKIČ

Mentor: doc. dr. Črtomir Podlipnik
PREGLED PROTIVIRUSNIH UČINKOVIN ZOPER
KORONAVIRUSE
Datum zagovora: 28. 9. 2022

Mateja DAVIDOVIČ

Mentor: doc. dr. Jakob Kljun
SINTEZA KOVINSKIH KOMPLEKSOV DIHIDROKINIDINA
Datum zagovora: 30. 9. 2022

Jernej PAVLIČ

Mentor: prof. dr. Bogdan Štefane
SINTEZA OKSAZOLONOV, UPORABA IN BIOLOŠKA
AKTIVNOST
Datum zagovora: 6. 10. 2022

Ana PETROVIĆ

Mentorica: doc. dr. Nataša Gros
IZVAJANJE NEKATERIH STATISTIČNIH OBRAVNAV V
EXCELU
Datum zagovora: 13. 10. 2022

Žan MARINKOVIĆ

Mentor: prof. dr. Matevž Pompe
RAZVOJ METODE ZA DOLOČEVANJE VITAMINA D3 V
PREHRANSKIH DOPOLNILIH
Datum zagovora: 18. 10. 2022

Ines SAJE

Mentorica: izr. prof. dr. Amalija Golobič
ANALIZA TEMPERA IN VODENIH BARV Z RENTGENSKO
PRAŠKOVNO DIFRAKCIJO
Datum zagovora: 28. 10. 2022

David ZALOKAR

Mentorica: izr. prof. dr. Gabriela Kalčikova
MINIATURIZACIJA TESTA EKOTOKSIČNOSTI Z MALO
VODNO LEČO LEMNA MINOR
Datum zagovora: 13. 12. 2022

Anja RUPNIK

Mentorica: prof. dr. Urška Lavrenčič Štangar
FOTOKATALITSKA RAZGRADNJA PETIH MODELNIH
FARMACEVTSKIH UČINKOVIN Z NI-OPLAŠČENIM ZNO
Datum zagovora: 20. 12. 2022

UNIVERZA V MARIBORU
FAKULTETA ZA KEMIJO IN KEMIJSKO TEHNOLOGIJO
1. januar – 31. december 2022

DOKTORATI

DOKTORSKI ŠTUDIJ – 3. STOPNJA

David BAJEC

Mentor: Dr. Andrej Pohar
KATALITSKA AKTIVACIJA METANA ZA PRETVORBO V
VIŠJE OGLJIKOVODIKE Z MIKROKINETIČNIM OPISOM
Datum zagovora: 23. 2. 2022

Dragana BORNİK

Mentorica: Izr. Prof. Dr. Maša Knez Marevci
Somentorica: Red. Prof. Dr. Žižovič Irena
TRAJNOSTNO PROCESIRANJE MATERIALOV Z UPORABO
SUPERKRITIČNIH FLUIDOV
Datum zagovora: 27. 9. 2022

Veronika FURLAN

Mentor: Red. Prof. Dr. Urban Bren
PREUČEVANJE MEHANIZMOV ANTIKARCINOGENEGA
IN NEVROPROTEKTIVNEGA DELOVANJA NARAVNIH
POLIFENOLNIH SPOJIN
Datum zagovora: 22. 6. 2022

Viola HOBIGER

Mentor: Red. Prof. Dr. Peter Krajnc
Somentorica: Prof. Dr. Liska Robert
RAZGRADLJIVI POLIHIPE MATERIALI ZA
BIOMEDICINSKE APLIKACIJE Z UPORABO EMULZIJ IN
TIOL-EN KLIK KEMIJE
Datum zagovora: 7. 10. 2022

Tina KEGL

Mentorica: Doc. Dr. Anita Kovač Kralj
MODELIRANJE IN VEČNAMENSKA OPTIMIZACIJA
PRIDOBIVANJA ENERGIJE IN KORISTNIH PRODUKTOV
IZ ORGANSKIH ODPADKOV NA OSNOVI ANAEROBNE
RAZGRADNJE
Datum zagovora: 26. 9. 2022

Anja PETEK

Mentorica: Doc. Dr. Majda Krajnc
Somentor: Red. Prof. Dr. Urban Bren
VPLIV β -CIKLODEKSTRINA NA KINETIKO IN
MEHANIZEM REAKCIJE UMILJENJA ETILACETATAD
DATUM ZAGOVORA: 14. 7. 2022

Anže PRAŠNIKAR

Mentor: Dr. Blaž Likozar
MIKROKINETIČNO MODELIRANJE REAKCIJ KATALITSKE
PRETVORBE OGLJIKOVEGA DIOKSIDA D V METANOL
Datum zagovora: 27. 6. 2022

Eva ŠPANINGER

Mentor: Red. Prof. Dr. Urban Bren
KVANTNO MEHANSKO PROUČEVANJE MOLEKULARNIH
MEHANIZMOV KARCINOGENEZE IN NJENO
PREPREČEVANJE Z NARAVNIMI SPOJINAMI
Datum zagovora: 28. 11. 2022

Taja ŽITEK

Mentorica: Izr. Prof. Dr. Maša Knez Marevci
Somentorica: Doc. Dr. Petra Kotnik
OPTIMIZACIJA PROCESA IZOLACIJE UČINKOVIN IZ
INDUSTRIJSKE KONOPLJE V KOMBINACIJI Z INGVERJEM
TER BIOLOŠKI UČINKI MEŠANIC
Datum zagovora: 13. 12. 2022

MAGISTERIJI

MAGISTRSKI ŠTUDIJ – 2. STOPNJA

Irena ABRAMOVIČ

Mentor: Doc. Dr. Sebastijan Kovačič
Somentor: Dr. David Pahovnik
SINTEZA MAKROPOROZNIH KROGLIC NA OSNOVI
IONSKO-NABITIH MONOMEROV Z UPORABO
MULTIPLIH-EMULZIJ IN NJIHOVA UPORABA KOT
ADSORBENTOV ZA ODSTRANJEVANJE TEŽKIH KOVIN
Datum zagovora: 21. 12. 2022

Damjan ARBEITER

Mentor: Izr. Prof. Dr. Matjaž Finšgar
Spmentor: Asist. David Majer
UPORABA EKSPERIMENTALNEGA NAČRTA ZA
DOLOČITEV VPLIVNIH PARAMETROV NA ANALITSKE
LASTNOSTI ANTIMONOVE ELEKTRODE
Datum zagovora: 23. 3. 2022

Davor BABIČ

Mentor: Red. Prof. Dr. Uroš Potočnik
Somentor: Asist. Dr. Tomaž Büdefeld
VPLIV RETINOJSKE KISLINE ATRA NA IZRAŽANJE GENA
HER3 PRI CELIČNI LINIJI RAKA GLAVE IN VRATU FADU
Datum zagovora: 8. 9. 2022

Rahil BAJRA

Mentorica: Red. Prof. Dr. Andreja Goršek
Somentorica: Izr. Prof. Dr. Darja Pečar
MEZOPOROZNI MATERIALI: UPORABA V HETEROGENI
KATALIZI
Datum zagovora: 22. 6. 2022

Nicole BLAŽEVIČ

Mentorica: Red. Prof. Dr. Marjana Simonič
Somentorica: Dr. Oihana Gordobil
VREDNOTENJE NANODELCEV LIGNINA KOT
STABILIZATORJA V PICKERING EMULZIJAH ZA
APLIKACIJE V KOZMETIKI
Datum zagovora: 1. 9. 2022

Mitja ČUŠ

Mentor: Red. Prof. Dr. Peter Krajnc
VPLIV ADITIVOV NA BARVNO STABILNOST POLIETILENA
Datum zagovora: 8. 9. 2022

Martin ČERANIČ

Mentorica: Izr. Prof. Dr. Darja Pečar
Somentorica: Red. Prof. Dr. Andreja Goršek
KATALITSKA UČINKOVITOST KOVINSKIH
KATALIZATORJEV NA KONVENCIONALNIH TIO2
NOSILCIH
Datum zagovora: 6. 7. 2022

Franjo FREŠER

Mentor: Red. Prof. Dr. Urban Bren
Somentor: Doc. Dr. Gregor Hostnik
KOORDINACIJSKE SPOJINE ELAGITANINOV Z
ŽELEZOVIMI(II) IONI: VPLIV STRUKTURE IN PH
Datum zagovora: 8. 9. 2022

Jernej GABERC

Mentor: Doc. Dr. Gregor Kravanja
Somentorica: Red. Prof. Dr. Zorka Novak Pintarič
EKONOMSKA IN GRADBENA ANALIZA TER ANALIZA
ŽIVLJENJSKEGA CIKLA UPORABE KONOPLJINEGA
BETONA V SLOVENIJI
Datum zagovora: 23. 11. 2022

Ivana GORIČAN

Mentor: Izr. Prof. Dr. Matjaž Kristl
Somentorica: Doc. Dr. Irena Ban
SINTEZA IN KARAKTERIZACIJA KOBALTOVIH
KOORDINACIJSKIH SPOJIN S PIRIDINSKIMI
N-DONORSKIMI LIGANDI
Datum zagovora: 20. 4. 2022

Robert HREN

Mentorica: Izr. Prof. Dr. Lidija Čuček
Somentorja: Dr. Annamaria Vujanović, Dr. Damjan Krajnc
PREGLED TEHNOLOGIJ PROIZVODNJE VODIKA IN
OCENA NJIHOVIH VPLIVOV NA OKOLJE
Datum zagovora: 20. 4. 2022

David HVALEC

Mentorica: Izr. Prof. Dr. Maša Knez Marevci
Somentorici: Asist. Dr. Darija Cör Andrejč,
Doc. Dr. Petra Kotnik
KARAKTERIZACIJA AKTIVNIH BETALAINOV V
EKSTRAKTIH RDEČE PESE
Datum zagovora: 22. 9. 2022

Mihael IRGOLIČ

Mentorica: Red. Prof. Dr. Mojca Škerget
Somentorica: Asist. Dr. Maja Čolnik
HIDROTERMIČNA RAZGRADNJA VEČSLOJNE ODPADNE
EMBALAŽE
Datum zagovora: 6. 7. 2022

Ana JURGEC

Mentorica: Red. Prof. Dr. Zorka Novak Pintarič
Somentorja: Doc. Dr. Miloš Bogataj, Vlasta Marčinko
MOŽNOSTI ZA TOPLOTNO INTEGRACIJO IN
IZKORIŠČANJE ODPADNE TOPLOTE PRI PROCESIH
MEŠANJA
Datum zagovora: 22. 6. 2022

Petra KNAUS

Mentorica: Red. Prof. Dr. Marjana Simonič
Somentorici: Red. Prof. Dr. Lidija Fras Zemljič,
Red. Prof. Dr. Simona Strnad
VPLIV STRUKTURE PERJA IN DODATKOV NA
ODSTRANITEV TEŽKOHLAPNIH LIPOFILNIH SUBSTANC
Datum zagovora: 20. 4. 2022

Anja KONAJZLER

Mentor: Red. Prof. Dr. Uroš Potočnik
Somentorici: Doc. Dr. Helena Sabina Čelešnik,
Red. Prof. Dr. Darja Arko
VALIDACIJA KLINIČNO POMEMBNIH
TRANSKRIPCijskiKIH BIOOZNAČEVALCEV V KRVNIH
VZORCIH PRED IN PO ZDRAVLJENJU TROJNO
NEGATIVNEGA RAKA DOJKE
Datum zagovora: 22. 9. 2022

Klara Laura KONDA

Mentorica: Doc. Dr. Tina Maver
Somentorja: Izr. Prof. Dr. Matjaž Finšgar, Asist. Laura Činč Čurič
DOLOČITEV TERAPEVTSKE KONCENTRACIJE EKSTRAKTA
TRPOTCA V 3D TISKANEM NOSILNEM SISTEMU ZA
OPTIMALNI UČINEK NA RAST KOŽNIH CELIC
Datum zagovora: 19. 10. 2022

Sandra KOPŠE

Mentorica: Izr. Prof. Dr. Maša Knez Marevci
Somentorica: Asist. Katja Andrina Kravanja
FORMULACIJA EKSTRAKTOV GRANATNEGA JABOLKA
(PUNICA GRANATUM, L.) V BIORAZGRADLJIVE
POLIMERNE NOSILCE
Datum zagovora: 19. 10. 2022

Žan KOŠTOMAJ

Mentorica: Doc. Dr. Maša Islamčević Razboršek
Somentorica: Dr. Milena Ivanović
OKOLJU PRIJAZNO PRIDOBIVANJE EKSTRAKTOV
IZ ROŽMARINA (ROSMARINUS OFFICINALIS L.) Z
GLOBOKO EVTEKTIČNIMI TOPILI IN OCENA NJIHOVE
ANTIOKSIDATIVNE UČINKOVITOSTI
Datum zagovora: 18. 5. 2022

Nuša KOTNIK

Mentorica: Izr. Prof. Dr. Maša Knez Marevci
Somentorici: Doc. Dr. Petra Kotnik, Asist. Dr. Darija Čor Andrejč
FORMULACIJA KOMPOZITOV Z RESVERATROLOM S
SUPERKRITIČNIMI FLUIDI
Datum zagovora: 6. 7. 2022

Danijel LAVRIČ

Mentorica: Doc. Dr. Petra Kotnik
Somentorica: Izr. Prof. Dr. Maša Knez Marevci
STABILNOST IN KONTROLIRANO SPROŠČANJE
VITAMINA D V SIMULACIJSKIH RAZTOPINAH
Datum zagovora: 16. 2. 2022

Katja LEČNIK

Mentor: Red. Prof. Dr. Urban Bren
Somentorica: Doc. Dr. Bojana Žegura
ANTIGENOTOKSIČNI POTENCIAL ROŽMARINSKIH
EKSTRAKTOV
Datum zagovora: 20. 4. 2022

Mateja MARINIČ

Mentorica: Red. Prof. Dr. Mojca Škerget
Somentorica: Asist. Dr. Maja Čolnik
NAČRTOVANJE IN OPTIMIZACIJA POSTOPKA IZOLACIJE
VREDNIH SPOJIN IZ DIVJEGA KOSTANJA (AESCULUS
HIPPOCASTANUM L.)
Datum zagovora: 19. 1. 2022

Jan MARKO

Mentor: Doc. Dr. Thomas Luxbacher
Somentor: Asist. Dr. Matej Bračič
PROTEIN ODBOJNI POVRŠINSKI SLOJI NAREJENI IZ
POLIKAPROLAKTON-POLISAHARID ZMESI
Datum zagovora: 6. 7. 2022

Tina MIHELČIČ

Mentorica: Red. Prof. Dr. Maja Leitgeb
Somentorica: Dr. Gordana Hojnik Podrepšek
AKTIVACIJA KSILANAZE V MOKI
Datum zagovora: 8. 9. 2022

Erik MIHELIČ

Mentor: Dr. Dušan Klinar
Somentorica: Red. Prof. Dr. Andreja Goršek
OBRAVNAVA KINETIKE IN MEHANIZMA REAKCIJE
PIROLIZE SMREKOVEGA LESA
Datum zagovora: 28. 9. 2022

Amadej MUROVEC

Mentor: Doc. Dr. Sašo Gyergyek
Somentor: Dr. Miha Grilc
MAGNETNO SEGREVANJE MAGNETNIH
NANOKOMPOZITOV ZA PRIPRAVO VEČELEMENTNIH
KATALIZATORJEV
Datum zagovora: 19. 1. 2022

Jan OPARA

Mentor: Doc. Dr. Sašo Gyergyek
Somentor: Dr. Slavko Kralj
VPLIV POVRŠINSKE FUNKCIONALIZACIJE
ANIZOTROPNIH MAGNETNIH STRUKTUR Z AMINI NA
NJIHOVO AKTIVNOST ZA ALDOLNO KONDENZACIJO
Datum zagovora: 22. 9. 2022

Matic OREL

Mentor: Dr. Marko Bračko
Somentor: Red. Prof. Dr. Urban Bren
VIBRACIJSKI IN ROTACIJSKI PREHODI ENOSTAVNIH
MOLEKUL
Datum zagovora: 20. 4. 2022

Manca PODRIČNIK

Mentorica: Izr. Prof. Dr. Lidija Čuček
Somentorici: Dr. Aleksandra Petrovič,
Asist. Dr. Klavdija Zirngast
SINTEZA DOBAVNEGA OMREŽJA PROIZVODNJE
BIOPLINA IZ ODPADNEGA MULJA ČISTILNIH NAPRAV
IN DRUGIH SUROVIN
Datum zagovora: 20. 4. 2022

Jan POLAK

Mentor: Red. Prof. Dr. Uroš Potočnik
Somentor: Asist. Dr. Tomaž Büdefeld
OPTIMIZACIJA PROTOKOLA ZA PRIPRAVO BELJAKOVIN
IZ CELIČNIH FRAKCIJ CELIČNE LINIJE FADU ZA
PROTEOMSKO ANALIZO NA MASNEM SPEKTROMETRU
Datum zagovora: 22. 9. 2022

Miha PRELOG

Mentor: Red. Prof. Dr. Darko Goričanec
Somentorica: Doc. Dr. Danijela Urbanč
PRIMERJAVA TERMODINAMSKIH LASTNOSTI IN
OKOLJSKIH VPLIVOV HLADILNIH SNOVI ČETRTE
GENERACIJE
Datum zagovora: 26. 5. 2022

Nika PROJE

Mentor: Izr. Prof. Dr. Matjaž Finšgar
Somentor: Asist. David Maje
DOLOČANJE TEŽKIH KOVIN V MESU, MESNIH IZDELKIH
IN MORSKI HRANI Z ICP-OES
Datum zagovora: 19. 10. 2022

Jan PUHAR

Mentorica: Izr. Prof. Dr. Lidija Čuček
Somentorici: Dr. Annamaria Vujanović,
Red. Prof. Dr. Zorka Novak Pintarič
ANALIZA PROIZVODNEGA PROCESA ZA TRAJNOSTNO
PROIZVODNJO FORMALINA
Datum zagovora: 26. 5. 2022

Matjaž RANTAŠA

Mentorica: Red. Prof. Dr. Marjana Simonič
Somentorici: Red. Prof. Dr. Lidija Fras Zemljič,
Asist. Dr. Olivija Plohl
SINTEZA IN UPORABA MAGHEMITNIH NANODELCEV
FUNKCIONALIZIRANIH S POLISAHARIDOM ZA
ADSORPCIJO ELEMENTOV REDKIH ZEMELJ
Datum zagovora: 8. 9. 2022

Neža RAŠL

Mentorica: Doc. Dr. Danijela Urbanč
Somentorica: Dr. Aleksandra Petrovič
TERMIČNA OBDELAVA ODPADKOV IN MULJA IZ
INDUSTRIJE RASTLINSKIH OLJ
Datum zagovora: 1. 9. 2022

Simona SEDONJA

Mentorica: Izr. Prof. Dr. Maša Knez Marevci
Somentorici: Doc. Dr. Petra Kotnik, Asist. Taja Žitek
IZOLACIJA UČINKOVIN INDUSTRIJSKE KONOPLJE
TER SINERGISTIČNI UČINEK MEŠANIC MATERIALOV
DRUŽINE ZINGIBERACEAE
Datum zagovora: 6. 7. 2022

Gal SLAČEK

Mentorica: Izr. Prof. Dr. Maša Knez Marevci
Somentorja: Doc. Dr. Aleš Fajmut, Asist. Taja Žitek
OPTIMIZACIJA EKSTRAKCIJE BIOAKTIVNIH
KOMPONENT KURKUME IN FORMULACIJA V
ORGANOGELE
Datum zagovora: 8. 9. 2022

Saša STANKOVIČ

Mentorica: Doc. Dr. Maša Islamčević Razboršek
GLOBOKO EVTEKTIČNA TOPILA ZA ZELENO IN
TRAJNOSTNO EKSTRAKCIJO BIOAKTIVNIH SPOJIN IZ
ČEBULNIH (ALLIUM CEPA L.) OLUPKOV
Datum zagovora: 1. 9. 2022

Nastja ŠADL

Mentor: Red. Prof. Dr. Uroš Potočnik
Somentorja: Asist. Dr. Tomaž Büdefeld, Red. Prof. Dr. Darja
Arko
IZRAŽANJA SKUPINE GENOV DNA-METILTRANSFERAZ
(DNMT1, DNMT3A IN DNMT3B), DNA-DEMETILAZ
(TET1, TET2, TET3 IN TDG) TER GENA RNA-
METILTRANSFERAZA TRDMT1 V TUMORJIH BOLNIC Z
RAKOM DOJKE
Datum zagovora: 8. 9. 2022

Rok ŠPENDL

Mentor: Red. Prof. Dr. Darko Goričanec
Somentorica: Doc. Dr. Danijela Urbanč
TEHNOEKONOMSKA PRIMERJAVA EJEKTORSKE IN
ABSORPCIJSKE TOPLOTNE ČRPALKE
Datum zagovora: 19. 1. 2022

Mihaela ŠVEC

Mentorica: Red. Prof. Dr. Mojca Škerget
Somentorica: Asist. Dr. Maja Čolnik
VALORIZACIJA STORŽEV IGLAVCEV ZA PRIDOBIVANJE
VREDNIH KOMPONENT
Datum zagovora: 23. 11. 2022

Timotej VIDOVIČ

Mentorica: Izr. Prof. Dr. Lidija Čuček
Somentorici: Red. Prof. Dr. Mojca Škerget,
Dr. Annamaria Vujanović
IDENTIFIKACIJA NEVARNOSTI TER ANALIZA VPLIVOV
NA OKOLJE PRI HIDROTERMIČNI RAZGRADNJI VLAKEN
IZ MELAMINSKIH ETERIFICIRANIH SMOL
Datum zagovora: 26. 5. 2022

Eva VODA

Mentorica: Red. Prof. Dr. Maja Leitgeb
Somentorica: Asist. Dr. Katja Vasić
KOIMOBILIZACIJA ALKOHOL DEHIDROGENAZE IN
KOFAKTORJA β -NAD NA MODIFICIRANE MAGNETNE
NANODELCE
Datum zagovora: 28. 6. 2022

Kaja ZADRAVEC

Mentorica: Red. Prof. Dr. Mojca Škerget
Somentorici: ed. Prof. Dr. Lidija Fras Zemljič, Red. Prof. Dr.
Simona Strnad
UPORABA KERATINSKO-BOGATEGA ODPADNEGA
PERUTNINSKEGA PERJA ZA PRIDOBITEV KERATINA IN
NADALJNI RAZVOJ NANOVLAKEN
Datum zagovora: 16. 2. 2022

DIPLOME – UNIVERZITETNI ŠTUDIJI

UNIVERZITETNI ŠTUDIJI – 1. STOPNJA

Lara BERLOŽNIK

Mentor: Red. Prof. Dr. Peter Krajnc
Somentorica: Doc. Dr. Muzafera Paljevac
POLIAKRILATNE MEMBRANE ZA NADZOROVANO
SPROŠČANJE
Datum zagovora: 8. 9. 2022

Nika BOBINSKI

Mentor: Izr. Prof. Dr. Matjaž Kristl
Somentorica: Doc. Dr. Irena Ban
SINTEZA MAGNETNIH NANODELCEV S PLANETARNIM
MIKROMLINOM
Datum zagovora: 12. 9. 2022

Nika CAF

Mentorica: Doc. Dr. Mateja Primožič
Somentorici: Red. Prof. Dr. Maja Leitgeb, Asist. Dr. Katja Vasić
ŠTUDIJA UČINKOVITOSTI ADSORPCIJE TEŽKIH
KOVIN NA FUNKCIONALIZIRANE MAGNETNE
NANOSTRUKTURE
Datum zagovora: 8. 9. 2022

Melani DOLGOV

Mentorica: Red. Prof. Dr. Maja Leitgeb
Somentorica: Doc. Dr. Mateja Primožič
BIOAKTIVNE SNOVI IZ OLUPKOV MANGA ZA
KOZMETIČNO INDUSTRIJO
Datum zagovora: 8. 9. 2022

Lana EMBREUŠ

Mentorica: Doc. Dr. Irena Ban
Somentorica: Doc. Dr. Janja Stergar
SINTEZA FUNKCIONALIZIRANIH MAGNETNIH
NANODELCEV Z VISOKOENERGETSKIM MLINOM ZA
UPORABO V BIOMEDICINI
Datum zagovora: 1. 9. 2022

Aleksandra FERENC

Mentorica: Red. Prof. Dr. Marjana Simonič
Somentorica: Bošnjak Ksenija
VOLUMETRIČNA METODA DOLOČEVANJA PROSTEGA
IN VEZANEGA OGLJIKOVEGA DIOKSIDA V VODAH
Datum zagovora: 18. 5. 2022

Laura FURMAN

Mentorica: Red. Prof. Dr. Marjana Simonič
Somentorici: Dr. Zdenka Peršin Fratnik, Asist. Dr. Petra Lorbeg
Mohar
ZELENE TEHNOLOGIJE ZA DOSTAVNE SISTEME
FUNKCIONALNIH AGENSOV - LAKTOBACILOV
Datum zagovora: 19. 10. 2022

Tomaž GABROVEC

Mentorica: Dr. Irena Petrič
Somentorica: Red. Prof. Dr. Marjana Simonič
UPORABA PROCESA OSOZE ZA KONCENTRIRANJE
KISLE SIROTKE
Datum zagovora: 23. 9. 2022

Jan GOLE

Mentorica: Doc. Dr. Mateja Primožič
Somentorici: Red. Prof. Dr. Maja Leitgeb, Asist. Dr. Katja Vasić
VLOGA POLISAHARIDNE PREVLEKE ADSORBENTA PRI
ODSTRANJEVANJU TEŽKIH KOVIN IZ VODE
Datum zagovora: 19. 10. 2022

Doroteja GOLOB

Mentor: Red. Prof. Dr. Uroš Potočnik
Somentor: Asist. Dr. Tomaž Büdefeld
CELIČNI ODZIV NA OKSIDATIVNI STRES, POVZROČEN
Z VODIKOVIM PEROKSIDOM, PRI CELIČNIH
LINIJAH AKUTNE LIMFOBLASTNE LEVKEMIJE IN
LIMFOBLASTNEGA LIMFOMA CELIC T
Datum zagovora: 8. 9. 2022

Maja HELBEL

Mentorica: Red. Prof. Dr. Andreja Goršek
Somentorica: Izr. Prof. Dr. Darja Pečar
SINTEZA IN UPORABA KOVINSKEGA KATALIZATORJA
NA TIO₂ NOSILCU
Datum zagovora: 1. 9. 2022

Jernej JURKO

Mentorica: Izr. Prof. Dr. Maša Knez Marevci
Somentorica: Asist. Taja Žitek
VPLIV EKSTRAKCIJSKIH METOD NA BIOLŠKO
AKTIVNOST EKSTRAKTOV BALDRIJANA (VALERIANA
OFFICINALIS)
Datum zagovora: 8. 9. 2022

Urša KEŠE

Mentorica: Red. Prof. Dr. Zorka Novak Pintarič
Somentor: Doc. Dr. Miloš Bogataj
PROGRAMSKI JEZIK PYTHON V KEMIJSKEM
INŽENIRSTVU IN KEMIJI
Datum zagovora: 6. 7. 2022

Vesna KOCIJAN

Mentor: Red. Prof. Dr. Peter Krajnc
Somentorica: Asist. Dr. Amadeja Koler
UPORABA TIOL-EN KLIK REAKCIJE ZA POLIMERIZACIJO
TERPENOV S TIOLI
Datum zagovora: 8. 9. 2022

Meta KOČEVAR

Mentorica: Doc. Dr. Janja Stergar
Somentorica: Doc. Dr. Irena Ban
SINTEZA FUNKCIONALIZIRANIH MAGNETNIH
NANODELCEV Z MIKROVALOVNO PEČICO ZA
UPORABO V PROCESU NAPREDNE OSOZE
Datum zagovora: 1. 9. 2022

Anja KOMAN

Mentorica: Doc. Dr. Mateja Primožič
Somentorica: Red. Prof. Dr. Maja Leitgeb
VGRAJEVANJE UČINKOVIN V LIPOSOME
Datum zagovora: 8. 9. 2022

Helena KOVAČ

Mentorica: Red. Prof. Dr. Maja Leitgeb
Somentorica: Doc. Dr. Mateja Primožič
ŠTUDIJA ENCIMSKE AKTIVNOSTI V BOROVNICAH
Datum zagovora: 8. 9. 2022

Tino KOVAČIČ

Mentorica: Red. Prof. Dr. Maja Leitgeb
Somentorici: Doc. Dr. Mateja Primožič, Asist. Nika Kučuk
ANTIMIKROBNO DELOVANJE UČINKOVIN IZ GOBE
GANODERMA LUCIDUM
Datum zagovora: 8. 9. 2022

Antonija MALEC

Mentorica: Red. Prof. Dr. Mojca Škerget
Somentorica: Asist. Dr. Maja Čolnik
ZDRAVILNI UČINKI NARAVNIH EKSTRAKTOV IZ ZELIŠČ
Datum zagovora: 19. 1. 2022

Jure MEZEK

Mentorica: Doc. Ddr. Andreja Nemet
Somentor: Doc. Dr. Miloš Bogataj
DOLOČANJE UČINKOVITOSTI REGULACIJE PRETOKA
TEKOČIN IN OPTIMIRANJE NASTAVITEV KONSTANT
PID REGULATORJA
Datum zagovora: 18. 5. 2022

Nika Marija MURENC

Mentor: Red. Prof. Dr. Peter Krajnc
Somentor: Asist. Stanko Kramer
POLIMERNE STRUKTURE S SPREMENLJIVO
PORAZDELITVIJO POR
Datum zagovora: 8. 9. 2022

Luna PETROVIČ

Mentorica: Red. Prof. Dr. Maja Leitgeb
Somentorici: Doc. Dr. Mateja Primožič, Dr. Gordana Hojnik
Podrepšek
ENCIMSKA RAZGRADNJA ANTIBIOTIKA Z UPORABO
IMOBILIZIRANE LAKAZE
Datum zagovora: 9. 9. 2021

Kaja PLEŠA

Mentor: Red. Prof. Dr. Peter Krajnc
Somentorica: Asist. Dr. Amadeja Koler
URAVNAVANJE HIDROFILNOSTI POVRŠINE
POLI(AKRILATOV)
Datum zagovora: 25. 8. 2022

Amadeja PRŠA

Mentorica: Izr. Prof. Dr. Lidija Čuček
Somentorici: Dr. Aleksandra Petrovič, Asist. Dr. Maja Čolnik
TERMOGRAVIMETRIČNA, ULTIMATIVNA IN
PROKSIMATIVNA ANALIZA PLASTIČNIH MATERIALOV
Datum zagovora: 8. 9. 2022

Žiga SAMSA

Mentorica: Izr. Prof. Dr. Darja Pečar
Somentorica: Red. Prof. Dr. Andreja Goršek
KATALIZIRANA HIDROLIZA POLIMEROV
Datum zagovora: 26. 8. 2022

Nika SKUŠEK

Mentor: Red. Prof. Dr. Peter Krajnc
Somentor: Asist. Stanko Kramer
POLIMERIZACIJA TERPENOV V KOLOIDNIH
PREKURZORJIH
Datum zagovora: 25. 8. 2022

Nastja SLAVIČ

Mentor: Red. Prof. Dr. Peter Krajnc
Somentor: Asist. Stanko Kramer
PRIPRAVA FUNKCIONALNIH MONOMEROV IZ
ACIKLIČNIH TERPENOV
Datum zagovora: 25. 8. 2022

Melissa STERNIŠA

Mentorica: Izr. Prof. Dr. Maša Knez Marevci
Somentorica: Asist. Dr. Darija Čör Andrejč
DOLOČANJE KOMPONENT V BUČNEM OLJU S
POMOČJO KROMATOGRFSKIH TEHNIK
Datum zagovora: 22. 9. 2022

Urška SUŠEC

Mentor: Red. Prof. Dr. Urban Bren
Somentor: Dr. Marko Jukić
IDENTIFIKACIJA PREVLAJUJOČIH SKELETOV V
PROTIBAKTERIJSKIH UČINKOVINAH
Datum zagovora: 20. 4. 2022

Neža ŠANTL

Mentorica: Doc. Dr. Danijela Urbancl
Somentorici: Doc. Dr. Janja Stergar, Dr. Aleksandra Petrovič
TERMIČNA OBDELAVA ODPADKOV NASTALIH PRI
VZREJI ŽIVALI
Datum zagovora: 1. 9. 2022

Vita TRKULJA

Mentor: Red. Prof. Dr. Peter Krajnc
Somentorica: Doc. Dr. Muzafera Paljevac
ODSTRANJEVANJE ORGANSKIH POLUTANTOV IZ VODE
S POROZNIMI POLIELEKTROLITI
Datum zagovora: 8. 9. 2022

Simona VELJANOVSKA

Mentor: Red. Prof. Dr. Peter Krajnc
Somentorica: Doc. Dr. Muzafera Paljevac
FUNKCIONALIZACIJATIOLNIH SKUPIN V POROZNIH
POLITIOLENIH
Datum zagovora: 8. 9. 2022

Tine VIDMAR

Mentor: Red. Prof. Dr. Urban Bren
Somentorica: Asist. Sara Štumpf
PROTIBAKTERIJSKE UČINKOVINE HMELJA
Datum zagovora: 8. 9. 2022

Anjka VRBEK

Mentor: Red. Prof. Dr. Uroš Potočnik
Somentorja: Doc. Dr. Bogdan Čizmarevič, Dr. Tomaž Büdefeld
IZRAŽANJE IZOBLIK MRNA ZA RECEPTOR ERBB3 IN
SEKRETORNO BELJAKOVINO P22-SERBB3 PRI BOLNIKI
Z RAKOM GLAVE IN VRATU
Datum zagovora: 23. 3. 2022

Simon ZADRAVEC

Mentor: Red. Prof. Dr. Urban Bren
Somentor: Dr. Tomaž Mohorič
VPLIV VELIKOSTI DELCEV KALCIJEVEGA KARBONATA
NA LASTNOSTI PAPIRJA ZA INKJET
Datum zagovora: 8. 9. 2022

Miša ŽNIDARIČ

Mentorica: Doc. Dr. Petra Kotnik
Somentorica: Izr. Prof. Dr. Maša Knez Marevci
DOLOČANJE POLIFENOLNIH KOMPONENT IN
NJIHOVIH ANTIOKSIDATIVNIH LASTNOSTI V
RAZLIČNIH VRSTAH MEDU
Datum zagovora: 8. 9. 2022

DIPLOME – VISOKOŠOLSKI STROKOVNI ŠTUDIJ**VISOKOŠOLSKI STROKOVNI ŠTUDIJ – 1. STOPNJA****Irena AČKO**

Mentor: Red. Prof. Dr. Peter Krajnc
Somentor: Asist. Stanko Kramer
TERPENI IZ BIOLOŠKIH VIROV ZA PRIPRAVO
MAKROMOLEKUL
Datum zagovora: 8. 9. 2022

Deniz AGAČEVIĆ

Mentor: Red. Prof. Dr. Urban Bren
Somentor: Doc. Dr. Marko Jukić
ŠTUDIJ DESKRIPTORJEV MOLEKULSKE OBLIKE
PROTIBAKTERIJSKIH UČINKOVIN
Datum zagovora: 8. 9. 2022

Lovro ANDERLIČ

Mentorica: Izr. Prof. Dr. Lidija Čuček
Somentorja: Doc. Dr. Miloš Bogataj, Asist. Monika Dokl
OPTIMIRANJE NELINEARNIH NEPOGOJENIH
PROBLEMOV Z DETERMINISTIČNIMI IN
STOHAISTIČNIMI METODAMI
Datum zagovora: 12. 9. 2022

Jaka BANIČ

Mentorica: Red. Prof. Dr. Zorka Novak Pintarič
Somentorja: Doc. Dr. Gregor Kravanja, Mirko Šprinzer
TEHNIČNE IN OKOLJSKE ZAHTEVE ZA PRENEHANJE
STATUSA ODPADKA NA PODROČJU GRADBENIH
ODPADKOV
Datum zagovora: 27. 10. 2022

Tjaša CMAGER

Mentorica: Red. Prof. Dr. Maja Leitgeb
Somentorici: Doc. Dr. Mateja Primožič,
Dr. Gordana Hojnik Podrepšek
ENCIMSKA RAZGRADNJA CIPROFLOKSACINA Z
UPORABO ZAMREŽENIH ENCIMSKIH SKUPKOV
Datum zagovora: 8. 9. 2022

David Tian HREN

Mentor: Red. Prof. Dr. Urban Bren
Somentor: Dr. Tomaž Mohorič
EKSPERIMENTALNA RAZISKAVA RUMENENJA PVC
Datum zagovora: 8. 9. 2022

Matej KEBER

Mentor: Red. Prof. Dr. Urban Bren
Somentor: Doc. Dr. Gregor Hostnik
IZOLACIJA NARAVNE SPOJINE IZ HMELJA IN
DOLOČITEV VREDNOSTI PKA
Datum zagovora: 8. 9. 2022

Tija MRAK

Mentor: Izr. Prof. Dr. Matjaž Finšgar
Somentor: Dr. Gregor Žerjav
UPORABA MEHANSKO-KEMIJSKEGA SINTEZNEGA
POSTOPKA ZA PRIPRAVO TIO₂/G-C₃N₄
FOTOKATALIZATORJEV, UPORABLJENIH V NAPREDNIH
OKSIDACIJSKIH POSTOPKIH ZA ČIŠČENJE ODPADNIH
VODA
Datum zagovora: 20. 9. 2022

Amalija OZMEC

Mentorica: Izr. Prof. Dr. Maša Knez Marevci
Somentorica: Asist. Dr. Darija Čör Andrejč
UPORABA RAZLIČNIH IZOLACIJSKIH POSTOPKOV
IN ANTIOKSIDATIVNA UČINKOVITOST TIMIJANA
(THYMUS VULGARIS L.)
Datum zagovora: 8. 9. 2022

Polona POTOČNIK

Mentorica: Red. Prof. Dr. Maja Leitgeb
Somentorica: Doc. Dr. Mateja Primožič
OPTIMIZACIJA SINTEZE NANOCELULOZE IZ BAKTERIJE
KOMAGATAEIBACTER HANSENI
Datum zagovora: 23. 3. 2022

Ajda RAJ MILOŠEVIČ

Mentor: Red. Prof. Dr. Urban Bren
Somentor: Doc. Dr. Gregor Hostnik
TVORBA KOORDINACIJSKIH SPOJIN GALNE KISLINE Z
BAKROVIMI IN ALUMINIJEVIMI IONI
Datum zagovora: 8. 9. 2022

Monika ROČNIK

Mentorica: Izr. Prof. Dr. Maša Knez Marevci
Somentorica: Asist. Dr. Darija Čör Andrejč
OPTIMIZACIJA EKSTRAKCIJE IN DOLOČANJE
KAPSAICINOIDOV V EKSTRAKTIH IZ RDEČE PAPIRIKE
(CAPSICUM ANNUUM L.)
Datum zagovora: 6. 7. 2022

Gaja STRAJNAR

Mentorica: Izr. Prof. Dr. Lidija Čuček
Somentorici: Dr. Annamaria Vujanović, Asist. Monika Dokl
IZOLACIJA ANTIOKSIDANTOV IZ JAGOD ČRNEGA
BEZGA (SAMBUCUS NIGRA)
Datum zagovora: 1. 9. 2022

Andraž ŠPILER

Mentorica: Doc. Ddr. Andreja Nemet
Somentorica: Doc. Dr. Danijela Urbanč
MODELIRANJE VODORAVNEGA GRAVITACIJSKEGA
LOČEVALNIKA TEKOČE-TEKOČE
Datum zagovora: 16. 2. 2022

Neža ŠVAJGER

Mentorica: Red. Prof. Dr. Mojca Škerget
Somentorica: Valerija Lazič
VPLIV MATRIKSA NA VSEBNOST 1,2-BENZIZOTIAZOL-
3(2H)-ONA V ZIDNIH BARVAH
Datum zagovora: 1. 9. 2022

Tim TETITKOVIČ

Mentorica: Doc. Dr. Danijela Urbanč
Somentorja: Red. Prof. Dr. Darko Goričanec, Maja Ivanovski
ANALIZA ONESNAŽENOSTI ZRAKA NA OBMOČJU
SLOVENIJE
Datum zagovora: 6. 7. 2022

Nina TRAVNIKAR

Mentorica: Red. Prof. Dr. Mojca Škerget

Somentorica: Asist. Dr. Maja Čolnik

SEPARACIJA VREDNIH SPOJIN IZ LUPIN PISTACIJE S
PODKRITIČNO VODO

Datum zagovora: 8. 9. 2022

Monika UREMOVIĆ

Mentorica: Doc. Dr. Anita Kovač Kralj

Somentorica: Asist. Dr. Tina Kegl

DOLOČITEV VSEBNOSTI LEGIRNIH ELEMENTOV V
ŽELEZOVIH ZLITINAH

Datum zagovora: 1. 9. 2022

Eva VALANT

Mentorica: Doc. Ddr. Andreja Nemet

Somentor: Doc. Dr. Miloš Bogataj

RAZVOJ SIMULATORJA ZA REGULACIJO PRETOKA S
POVRATNO-ZANČNO IN VNAPREJŠNJO REGULACIJO

Datum zagovora: 19. 1. 2022

Maša VRAČEVIČ

Mentorica: Red. Prof. Dr. Marjana Simonič

Somentorici: Red. Prof. Dr. Lidija Fras Zemljič,

Asist. Dr. Olivija Plohl

FUNKCIONALIZACIJA ZAŠČITNIH MASK Z UPORABO
NARAVNIH SNOVI

Datum zagovora: 1. 9. 2022

Vesna VRANKAR

Mentorica: Doc. Dr. Muzafera Paljevac

Somentor: Red. Prof. Dr. Peter Krajnc

IMOBILIZACIJA ENCIMOV NA POROZNI POLI(GLICIDIL
METAKRILAT)

Datum zagovora: 8. 9. 2022

Karmen ZORIČ

Mentor: Red. Prof. Dr. Uroš Potočnik

Somentorja: Doc. Dr. Boštjan Lanišnik,

Asist. Dr. Larisa Goričan

IZRAŽANJE GENOV ZA DNA IN RNA METILAZE IN
DEMETILAZE PRI BOLNIKIHZ RAKOM GLAVE IN VRATU

Datum zagovora: 1. 9. 2022

UNIVERZA V NOVI GORICI
FAKULTETA ZA PODIPLOMSKI ŠTUDIJ
1. januar – 31. december 2022

DOKTORATI

DOKTORSKI ŠTUDIJSKI PROGRAM ZNANOSTI O OKOLJU

Jelena TOPIĆ BOŽIČ

Mentorici: izr. prof. dr. Branka Mozetič Vodopivec, izr. prof. dr. Dorota Korte

NOVEL ANALYTICAL APPROACHES IN QUALITY AND SAFETY CONTROL IN PRODUCTION OF FERMENTED BEVERAGES

Datum zagovora: 16. 2. 2022

Takwa CHOUKI

Mentor: izr. prof. dr. Saim Mustafa Emin

SYNTHESIS AND APPLICATION OF TRANSITION METAL PHOSPHIDE NANOMATERIALS AS ELECTROCATALYSTS FOR WATER SPLITTING AND CHEMICAL TRANSFORMATIONS

Datum zagovora: 26. 8. 2022

Rowland Adetayo ADESIDA

Mentorici: doc. dr. Melita Sternad Lemut, doc. dr. Lorena Butinar
EXPLORATION OF YEAST BIODIVERSITY POTENTIAL FOR DEVELOPMENT OF ALTERNATIVE BIOFUNGICIDES IN VITICULTURE

Datum zagovora: 6. 7. 2022

Manel MACHREKI

Mentor: izr. prof. dr. Saim Mustafa Emin

OXYGEN VACANCIES ENGINEERING IN METAL OXIDE NANOMATERIALS FOR EFFICIENT PHOTO-ELECTROCATALYTIC DEGRADATION OF ORGANIC POLLUTANTS AND CHEMICAL TRANSFORMATIONS

Datum zagovora: 22. 11. 2022

Hanna BUDASHEVA

Mentorica: izr. prof. dr. Dorota Korte

NONDESTRUCTIVE THERMAL, OPTICAL, CHEMICAL AND STRUCTURAL CHARACTERIZATION OF ADVANCED MATERIALS BY OPTOTHERMAL TECHNIQUES

Datum zagovora: 23. 8. 2022

MAGISTRSKI ŠTUDIJ

MAGISTRSKI ŠTUDIJSKI PROGRAM OKOLJE – 2. STOPNJA

anja BUH

Mentorici: prof. dr. Janja Vaupotič, doc. dr. Mateja Dovjak
OPTIMIZACIJA NARAVNEGA PREZRAČEVANJA V ENODRUŽINSKI HIŠI S POVIŠANO KONCENTRACIJO

RADONA

Datum zagovora: 12. 7. 2022

DIPLOME

UNIVERZITETNI ŠTUDIJSKI PROGRAM OKOLJE – 1. STOPNJA

DIPLOMSKI SEMINARJI:

Tajda HUBER

Datum diplomiranja: 6. 4. 2022

Tjaša ŠTAJNRAJH

Datum diplomiranja: 29. 6. 2022

Katja BELEC

Datum diplomiranja: 6. 4. 2022

Darian RAMPIH

Datum diplomiranja: 29. 6. 2022

Ula URBAS

Datum diplomiranja: 6. 4. 2022

Merima VRŠKIČ

Datum diplomiranja: 8. 9. 2022

Aleksandar TERZIČ

Datum diplomiranja: 29. 6. 2022

Matjaž ŽVOKELJ

Datum diplomiranja: 15. 9. 2022

KOLENDAR VAŽNEJŠIH ZNANSTVENIH SREČANJ S PODROČJA KEMIJE IN KEMIJSKE TEHNOLOGIJE

SCIENTIFIC MEETINGS – CHEMISTRY AND CHEMICAL ENGINEERING

2023

March 2023

- 22 – 24 INTERNATIONAL CONFERENCE ON PHOSPHORUS, BORON AND SILICON
(PBSI 2023)
Berlin, Germany
Information: <https://premc.org/conferences/pbsi-phosphorus-boron-silicon/>

April 2023

- 14 – 15 2023 ECTN ANNUAL MEETING AND GENERAL ASSEMBLY
Amsterdam, Netherlands
Information: <https://ectn.eu/2023-general-assembly-amsterdam/>
- 16 – 21 HTCC 5
Dubrovnik, Croatia
Information: <https://htcc5.org/>
- 23 – 27 14TH ADVANCED POLYMERS VIA MACROMOLECULAR ENGINEERING CONFERENCE
(APME23)
Paris, France
Information: <https://premc.org/apme2023/>

May 2023

- 15 – 17 MEMBRANE COURSE FOR WATER TECHNOLOGIES
Aachen, Germany
Information: https://conferences.avt.rwth-aachen.de/mcw/mcw_en/Home.html
- 16 – 17 EUROPEAN CONFERENCE ON CO₂ CAPTURE, STORAGE & REUSE 2023
Copenhagen, Denmark
- 21 – 25 PPEPPD 2023
Tarragona, Spain
Information: <https://ppeppd.org/ppeppd2023/>
- 29 – June 2 15TH MEDITERRANEAN CONGRESS OF CHEMICAL ENGINEERING – MECCE
Barcelona, Spain
Information: <https://www.mecce.org/>
- 31 – June 2 8TH EUROPEAN PROCESS INTENSIFICATION CONFERENCE
Warsaw, Poland
Information: <https://www.epic2023.pw.edu.pl/index/>

June 2023

- 14 – 16 XXII EUROFOODCHEM CONGRESS
Belgrade, Serbia
Information: <https://xxiieurofoodchem.com/>
- 18 – 21 33RD EUROPEAN SYMPOSIUM ON COMPUTER-AIDED PROCESS ENGINEERING
(ESCAPE-33)
Athens, Greece
Information: <https://escape33-ath.gr/>

July 2023

- 2 – 6 FEZA 2023 – 9TH CONFERENCE OF THE FEDERATION OF THE EUROPEAN ZEOLITE
ASSOCIATIONS
Portorož-Portorose, Slovenia
Information: <https://feza2023.org/en/>
- 2 – 7 XV POSTGRADUATE SUMMER SCHOOL ON GREEN CHEMISTRY
Venice, Italy
Information: <https://www.greenchemistry.school/>
- 7 – 11 9TH EUCHEMS CHEMISTRY CONGRESS (ECC9)
Dublin, Ireland
- 9 – 14 38TH INTERNATIONAL CONFERENCE ON SOLUTION CHEMISTRY
Belgrade, Serbia
Information: <https://icsc2023.pmf.uns.ac.rs/>

August 2023

- 18 – 25 52ND IUPAC GENERAL ASSEMBLY
The Hague, Netherlands
Information: <https://iupac.org/event/ga2023/>
- 20 – 27 IUPAC WORLD CHEMISTRY CONGRESS 2023
The Hague, Netherlands
Information: <https://iupac2023.org/>
- 27 – 31 EUROANALYSIS 2023
Geneva, Switzerland
Information: <https://www.euroanalysis2023.ch/>

September 2023

- 17 – 21 14TH EUROPEAN CONGRESS OF CHEMICAL ENGINEERING AND
7TH EUROPEAN CONGRESS OF APPLIED BIOTECHNOLOGY
Berlin, Germany
Information: <https://ecce-ecab2023.eu/>

October 2023

- 15 – 19 31ST INTERNATIONAL SYMPOSIUM ON THE CHEMISTRY OF NATURAL PRODUCTS
AND 11TH INTERNATIONAL CONGRESS ON BIODIVERSITY
Naples, Italy
Information: <https://www.iscnp31-icob11.org/>

Acta Chimica Slovenica

Author Guidelines

Submissions

Submission to ACSi is made with the implicit understanding that neither the manuscript nor the essence of its content has been published in whole or in part and that it is not being considered for publication elsewhere. All the listed authors should have agreed on the content and the corresponding (submitting) author is responsible for having ensured that this agreement has been reached. The acceptance of an article is based entirely on its scientific merit, as judged by peer review. There are no page charges for publishing articles in ACSi. The authors are asked to read the Author Guidelines carefully to gain an overview and assess if their manuscript is suitable for ACSi.

Additional information

- Citing spectral and analytical data
- Depositing X-ray data

Submission material

Typical submission consists of:

- full manuscript (PDF file, with title, authors, abstract, keywords, figures and tables embedded, and references)
- supplementary files
 - **Full manuscript** (original Word file)
 - **Statement of novelty** (Word file)
 - **List of suggested reviewers** (Word file)
 - **ZIP file containing graphics** (figures, illustrations, images, photographs)
 - **Graphical abstract** (single graphics file)
 - **Proposed cover picture** (optional, single graphics file)
 - **Appendices** (optional, Word files, graphics files)

Incomplete or not properly prepared submissions will be rejected.

Submission process

Before submission, authors should go through the checklist at the bottom of the page and prepare for submission.

Submission process consists of 5 steps.

Step 1: Starting the submission

- Choose one of the journal sections.
- Confirm all the requirements of the **checklist**.
- Additional plain text comments for the editor can be provided in the relevant text field.

Step 2: Upload submission

- Upload full manuscript in the form of a Word file (with title, authors, abstract, keywords, figures and tables embedded, and references).

Step 3: Enter metadata

- First name, last name, contact email and affiliation for all authors, in relevant order, must be provided. Corresponding author has to be selected. Full postal address and phone number of the corresponding author has to be provided.

- **Title and abstract** must be provided in plain text.
- Keywords must be provided (max. 6, separated by semicolons).
- Data about contributors and supporting agencies may be entered.
- **References** in plain text must be provided in the relevant text filed.

Step 4: Upload supplementary files

- Original Word file (original of the PDF uploaded in the step 2)
- **List of suggested reviewers** with at least five reviewers with two recent references from the field of submitted manuscript must be uploaded as a Word file. At the same time, authors should declare (i) that they have no conflict of interest with suggested reviewers and (ii) that suggested reviewers are experts in the field of the submitted manuscript.
- All **graphics** have to be uploaded in a single ZIP file. Graphics should be named Figure 1.jpg, Figure 2.eps, etc.
- **Graphical abstract image** must be uploaded separately
- **Proposed cover picture** (optional) should be uploaded separately.
- Any additional **appendices** (optional) to the paper may be uploaded. Appendices may be published as a supplementary material to the paper, if accepted.
- For each uploaded file the author is asked for additional metadata which may be provided. Depending of the type of the file please provide the relevant title (Statement of novelty, List of suggested reviewers, Figures, Graphical abstract, Proposed cover picture, Appendix).

Step 5: Confirmation

- Final confirmation is required.

Article Types

Feature Articles are contributions that are written on Editor's invitation. They should be clear and concise summaries of the author's most recent work written with the broad scope of ACSi in mind. They are intended to be general overviews of the authors' subfield of research but should be written in a way that engages and informs scientists in other areas. They should contain the following (see also general guidelines for article structure below): (1) an introduction that acquaints readers with the authors' research field and outlines the important questions for which answers are being sought; (2) interesting, novel, and recent contributions of the author(s) to the field; and (3) a summary that presents possible future directions. Manuscripts should normally not exceed 40 pages of one column format (font size 12, 33 lines per page). Generally, experts who have made an important contribution to a specific field in recent years will be invited by the Editor to contribute a **Feature Article**. Individuals may, however, send a proposal (of no more than one page) for a **Feature Article** to the Editor-in-Chief for consideration.

Scientific articles should report significant and innovative achievements in chemistry and related sciences and should exhibit a high level of originality. They should have the following structure:

1. Title (max. 150 characters),
2. Authors and affiliations,
3. Abstract (max. 1000 characters),
4. Keywords (max. 6),
5. Introduction,
6. Experimental,
7. Results and Discussion,
8. Conclusions,
9. Acknowledgements,
10. References.

The sections should be arranged in the sequence generally accepted for publications in the respective fields and should be successively numbered.

Short communications generally follow the same order of sections as Scientific articles, but should be short (max. 2500 words) and report a significant aspect of research work meriting separate publication. Editors may decide that a Scientific paper is categorized as a Short Communication if its length is short.

Technical articles report applications of an already described innovation. Typically, technical articles are not based on new experiments.

Preparation of Submissions

Text of the submitted articles must be prepared with Microsoft Word. Normal style set to single column, 1.5 line spacing, and 12 pt Times New Roman font is recommended. Line numbering (continuous, for the whole document) must be enabled to simplify the reviewing process. For any other format, please consult the editor. Articles should be written in English. Correct spelling and grammar are the sole responsibility of the author(s). Papers should be written in a concise and succinct manner. The authors shall respect the ISO 80000 standard [1], and IUPAC Green Book [2] rules on the names and symbols of quantities and units. The Système International d'Unités (SI) must be used for all dimensional quantities.

Graphics (figures, graphs, illustrations, digital images, photographs) should be inserted in the text where appropriate. The captions should be self-explanatory. Lettering should be readable (suggested 8 point Arial font) with equal size in all figures. Use common programs such as MS Excel or similar to prepare figures (graphs) and ChemDraw to prepare structures in their final size. Width of graphs in the manuscript should be 8 cm. Only in special cases (in case of numerous data, visibility issues) graphs can be 17 cm wide. All graphs in the manuscript should be inserted in relevant places and **aligned left**. The same graphs should be provided separately as images of appropriate resolution (see below) and submitted together in a ZIP file (Graphics ZIP). Please do not submit figures as a Word file. In **graphs**, only the graph area determined by both axes should be in the frame, while a frame around the whole graph should be omitted. The graph area should be white. The legend should be inside the graph area. The style of all graphs should be the same. **Figures and illustrations** should be of sufficient quality for the printed version, i.e. 300 dpi minimum. **Digital images and photographs** should be of high quality (minimum

250 dpi resolution). On submission, figures should be of good enough resolution to be assessed by the referees, ideally as JPEGs. High-resolution figures (in JPEG, TIFF, or EPS format) might be required if the paper is accepted for publication.

Tables should be prepared in the Word file of the paper as usual Word tables. The captions should appear above the table and should be self-explanatory.

References should be numbered and ordered sequentially as they appear in the text, likewise methods, tables, figure captions. When cited in the text, reference numbers should be superscripted, following punctuation marks. It is the sole responsibility of authors to cite articles that have been submitted to a journal or were in print at the time of submission to ACSi. Formatting of references to published work should follow the journal style; please also consult a recent issue:

1. J. W. Smith, A. G. White, *Acta Chim. Slov.* **2008**, *55*, 1055–1059.
2. M. F. Kemmere, T. F. Keurentjes, in: S. P. Nunes, K. V. Peinemann (Ed.): *Membrane Technology in the Chemical Industry*, Wiley-VCH, Weinheim, Germany, **2008**, pp. 229–255.
3. J. Levec, Arrangement and process for oxidizing an aqueous medium, US Patent Number 5,928,521, date of patent July 27, **1999**.
4. L. A. Bursill, J. M. Thomas, in: R. Sersale, C. Collola, R. Aiello (Eds.), *Recent Progress Report and Discussions: 5th International Zeolite Conference*, Naples, Italy, 1980, Gianini, Naples, **1981**, pp. 25–30.
5. J. Szegezdi, F. Csizmadia, Prediction of dissociation constant using microconstants, http://www.chemaxon.com/conf/Prediction_of_dissociation_constant_using_microconstants.pdf, (assessed: March 31, 2008)

Titles of journals should be abbreviated according to Chemical Abstracts Service Source Index (CASSI).

Special Notes

- Complete characterization, **including crystal structure**, should be given when the synthesis of new compounds in crystal form is reported.
- Numerical **data should be reported with the number of significant digits corresponding to the magnitude** of experimental uncertainty.
- **The SI system of units and IUPAC recommendations** for nomenclature, symbols and abbreviations should be followed closely. Additionally, the authors should follow the general guidelines when citing spectral and analytical data, and depositing crystallographic data.
- **Characters** should be correctly represented throughout the manuscript: for example, 1 (one) and l (ell), 0 (zero) and O (oh), x (ex), D7 (times sign), B0 (degree sign). Use Symbol font for all Greek letters and mathematical symbols.
- The rules and recommendations of the **IUBMB** and the **International Union of Pure and Applied Chemistry (IUPAC)** should be used for abbreviation of chemical names, nomenclature of chemical compounds, enzyme nomenclature, isotopic compounds, optically active isomers, and spectroscopic data.
- **A conflict of interest** occurs when an individual (author, reviewer, editor) or its organization is in-

volved in multiple interests, one of which could possibly corrupt the motivation for an act in the other. Financial relationships are the most easily identifiable conflicts of interest, while conflicts can occur also as personal relationships, academic competition, etc. **The Editors** will make effort to ensure that conflicts of interest will not compromise the evaluation process; potential editors and reviewers will be asked to exempt themselves from review process when such conflict of interest exists. When the manuscript is submitted for publication, **the authors** are expected to disclose any relationships that might pose potential conflict of interest with respect to results reported in that manuscript. In the Acknowledgement section the source of funding support should be mentioned. The statement of disclosure must be provided as Comments to Editor during the submission process.

- **Published statement of Informed Consent.** Research described in papers submitted to ACSi must adhere to the principles of the Declaration of Helsinki (<http://www.wma.net/e/policy/b3.htm>). These studies must be approved by an appropriate institutional review board or committee, and informed consent must be obtained from subjects. The Methods section of the paper must include: 1) a statement of protocol approval from an institutional review board or committee and 2), a statement that informed consent was obtained from the human subjects or their representatives.
- **Published Statement of Human and Animal Rights.** When reporting experiments on human subjects, authors should indicate whether the procedures followed were in accordance with the ethical standards of the responsible committee on human experimentation (institutional and national) and with the Helsinki Declaration of 1975, as revised in 2008. If doubt exists whether the research was conducted in accordance with the Helsinki Declaration, the authors must explain the rationale for their approach and demonstrate that the institutional review body explicitly approved the doubtful aspects of the study. When reporting experiments on animals, authors should indicate whether the institutional and national guide for the care and use of laboratory animals was followed.
- To avoid conflict of interest between authors and referees we expect that not more than one referee is from the same country as the corresponding author(s), however, not from the same institution.
- Contributions authored by **Slovenian scientists** are evaluated by non-Slovenian referees.
- Papers describing **microwave-assisted reactions** performed in domestic microwave ovens are not considered for publication in *Acta Chimica Slovenica*.
- *Manuscripts that are **not prepared and submitted** in accord with the instructions for authors are not considered for publication.*

Appendices

Authors are encouraged to make use of supporting information for publication, which is supplementary material (appendices) that is submitted at the same time as the manuscript. It is made available on the Journal's

web site and is linked to the article in the Journal's Web edition. The use of supporting information is particularly appropriate for presenting additional graphs, spectra, tables and discussion and is more likely to be of interest to specialists than to general readers. When preparing supporting information, authors should keep in mind that the supporting information files will not be edited by the editorial staff. In addition, the files should be not too large (upper limit 10 MB) and should be provided in common widely known file formats to be accessible to readers without difficulty. All files of supplementary materials are loaded separately during the submission process as supplementary files.

Proposed Cover Picture and Graphical Abstract Image

Graphical content: an ideally full-colour illustration of resolution 300 dpi from the manuscript must be proposed with the submission. Graphical abstract pictures are printed in size 6.5 x 4 cm (hence minimal resolution of 770 x 470 pixels). Cover picture is printed in size 11 x 9.5 cm (hence minimal resolution of 1300 x 1130 pixels)

Authors are encouraged to submit illustrations as candidates for the journal Cover Picture*. The illustration must be related to the subject matter of the paper. Usually both proposed cover picture and graphical abstract are the same, but authors may provide different pictures as well.

* The authors will be asked to contribute to the costs of the cover picture production.

Statement of novelty

Statement of novelty is provided in a Word file and submitted as a supplementary file in step 4 of submission process. Authors should in no more than 100 words emphasize the scientific novelty of the presented research. Do not repeat for this purpose the content of your abstract.

List of suggested reviewers

List of suggested reviewers is a Word file submitted as a supplementary file in step 4 of submission process. Authors should propose the names, full affiliation (department, institution, city and country) and e-mail addresses of five potential referees. Field of expertise and at least two references relevant to the scientific field of the submitted manuscript must be provided for each of the suggested reviewers. The referees should be knowledgeable about the subject but have no close connection with any of the authors. In addition, referees should be from institutions other than (and countries other than) those of any of the authors. Authors declare no conflict of interest with suggested reviewers. Authors declare that suggested reviewers are experts in the field of submitted manuscript.

How to Submit

Users registered in the role of author can start submission by choosing USER HOME link on the top of the page, then choosing the role of the Author and follow the relevant link for starting the submission process.

Prior to submission we strongly recommend that you familiarize yourself with the ACSi style by browsing the journal, particularly if you have not submitted to the ACSi before or recently.

Correspondence

All correspondence with the ACSi editor regarding the paper goes through this web site and emails. Emails are sent and recorded in the web site database. In the correspondence with the editorial office please provide ID number of your manuscript. All emails you receive from the system contain relevant links. **Please do not answer the emails directly but use the embedded links in the emails for carrying out relevant actions.** Alternatively, you can carry out all the actions and correspondence through the online system by logging in and selecting relevant options.

Proofs

Proofs will be dispatched via e-mail and corrections should be returned to the editor by e-mail as quickly as possible, normally within 48 hours of receipt. Typing errors should be corrected; other changes of contents will be treated as new submissions.

Submission Preparation Checklist

As part of the submission process, authors are required to check off their submission's compliance with all of the following items, and submissions may be returned to authors that do not adhere to these guidelines.

1. The submission has not been previously published, nor is it under consideration for publication in any other journal (or an explanation has been provided in Comments to the Editor).
2. All the listed authors have agreed on the content and the corresponding (submitting) author is responsible for having ensured that this agreement has been reached.
3. The submission files are in the correct format: manuscript is created in MS Word but will be **submitted in PDF** (for reviewers) as well as in original MS Word format (as a supplementary file for technical editing); diagrams and graphs are created in Excel and saved in one of the file formats: TIFF, EPS or JPG; illustrations are also saved in one of these formats. The preferred position of graphic files in a document is to embed them close to the place where they are mentioned in the text (See **Author guidelines** for details).
4. The manuscript has been examined for spelling and grammar (spell checked).
5. The **title** (maximum 150 characters) briefly explains the contents of the manuscript.
6. Full names (first and last) of all authors together with the affiliation address are provided. Name of author(s) denoted as the corresponding author(s), together with their e-mail address, full postal address and telephone/fax numbers are given.
7. The **abstract** states the objective and conclusions of the research concisely in no more than 150 words.
8. Keywords (minimum three, maximum six) are provided.
9. **Statement of novelty** (maximum 100 words) clearly explaining new findings reported in the manuscript should be prepared as a separate Word file.
10. The text adheres to the stylistic and bibliographic requirements outlined in the **Author guidelines**.
11. Text in normal style is set to single column, 1.5 line spacing, and 12 pt. Times New Roman font is

recommended. All tables, figures and illustrations have appropriate captions and are placed within the text at the appropriate points.

12. Mathematical and chemical equations are provided in separate lines and numbered (Arabic numbers) consecutively in parenthesis at the end of the line. All equation numbers are (if necessary) appropriately included in the text. Corresponding numbers are checked.
13. Tables, Figures, illustrations, are prepared in correct format and resolution (see **Author guidelines**).
14. The lettering used in the figures and graphs do not vary greatly in size. The recommended lettering size is 8 point Arial.
15. Separate files for each figure and illustration are prepared. The names (numbers) of the separate files are the same as they appear in the text. All the figure files are packed for uploading in a single ZIP file.
16. Authors have read **special notes** and have accordingly prepared their manuscript (if necessary).
17. References in the text and in the References are correctly cited. (see **Author guidelines**). All references mentioned in the Reference list are cited in the text, and vice versa.
18. Permission has been obtained for use of copyrighted material from other sources (including the Web).
19. The names, full affiliation (department, institution, city and country), e-mail addresses and references of five potential referees from institutions other than (and countries other than) those of any of the authors are prepared in the word file. At least two relevant references (important recent papers with high impact factor, head positions of departments, labs, research groups, etc.) for each suggested reviewer must be provided. Authors declare no conflict of interest with suggested reviewers. Authors declare that suggested reviewers are experts in the field of submitted manuscript.
20. Full-colour illustration or graph from the manuscript is proposed for graphical abstract.
21. **Appendices** (if appropriate) as supplementary material are prepared and will be submitted at the same time as the manuscript.

Privacy Statement

The names and email addresses entered in this journal site will be used exclusively for the stated purposes of this journal and will not be made available for any other purpose or to any other party.

ISSN: 1580-3155

Koristni naslovi

Slovensko kemijsko društvo
Slovenian Chemical Society



Slovensko kemijsko društvo

www.chem-soc.si

e-mail: chem.soc@ki.si



Wessex Institute of Technology

www.wessex.ac.uk



SETAC

www.setac.org



European Water Association

<http://www.ewa-online.eu/>



European Science Foundation

www.esf.org



European Federation of Chemical Engineering

<https://efce.info/>



IUPAC

INTERNATIONAL UNION OF
PURE AND APPLIED CHEMISTRY

International Union of Pure and Applied Chemistry

<https://iupac.org/>

Novice evropske zveze kemijskih društev EuChemS najdete na:

 **EuChemS**
European Chemical Society

Brussels News Updates

<http://www.euchems.eu/newsletters/>



DONAU LAB Ljubljana
Member of LPPgroup

 **BINDER**

Best conditions for your success



Komore za testiranje baterij

Vakuumski sušilniki

Klimatske komore



Donau Lab d.o.o., Ljubljana
Tbilisjska 85
SI-1000 Ljubljana
www.donaulab.si
office-si@donaulab.com

Razvoj in inovacije za globalno uspešnost

Znanje, kreativnost zaposlenih in inovacije so ključnega pomena v okolju, kjer nastajajo pametni premazi skupine KANSAI HELIOS. Z rešitvami, ki zadostijo široki paleti potreb, kontinuiranim razvojem ter s kakovostnimi izdelki, Helios predstavlja evropski center za inovacije in poslovni razvoj skupine Kansai Paint.



Part of  **KANSAI
PAINT**



www.helios-group.eu

 **KANSAI
HELIOS**
Designing Excellence

MAGNEZIJ Krka



**VAŠA
PRVA
IZBIRA***

**MAGNEZIJ +
VITAMIN B₂**

**BODITE
NEUSTAVLJIVI**

- ✓ Manj utrujenosti
- ✓ Normalno delovanje mišic

www.magnezijkrka.si

Prehransko dopolnilo ni nadomestilo za uravnoteženo in raznovrstno prehrano. Skrbite za uravnoteženo in raznovrstno prehrano ter zdrav način življenja.

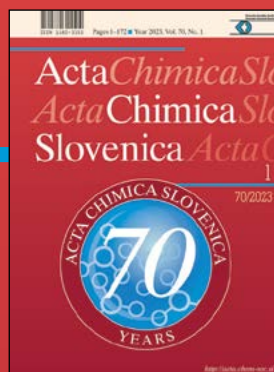
* Prodajni podatki ePharma Market Slovenija za leto 2022, prodaja v lekarnah, kategorija izdelki z magnezijem.

KRKA

ActaChimicaSlovenica

ActaChimicaSlovenica

The year 2023 marks the publication of the 70th volume of the Acta Chimica Slovenica issued by Slovenian Chemical Society. Volume 1 appeared in 1954 as Vestnik Slovenskega kemijskega društva (Bulletin of the Slovenian Chemical Society) and the name was changed into Acta Chimica Slovenica with vol 40 (1993). More details are presented in the Editorial.



Year 2023, Vol. 70, No. 1

